OXFORD

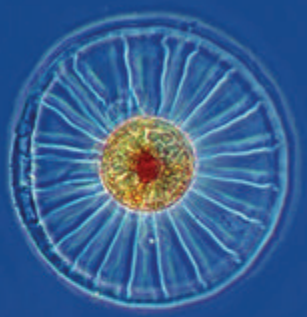

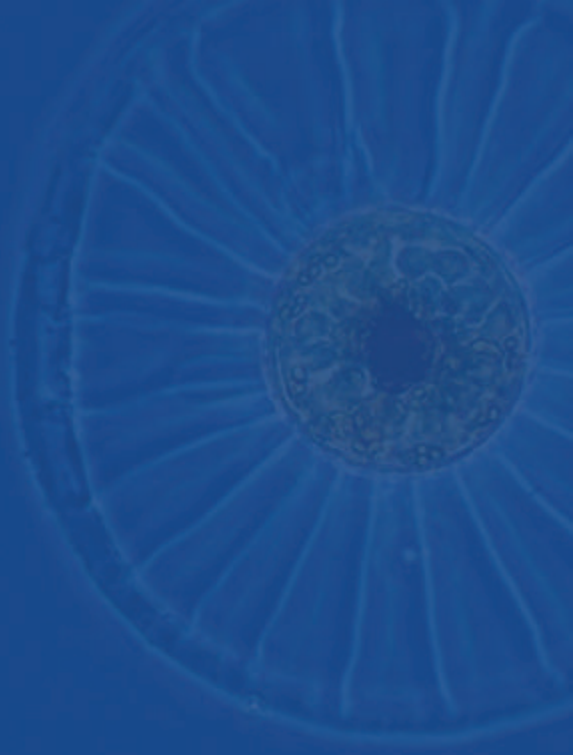

MARINE GEOCHEMISTRY

Ocean Circulation, Carbon Cycle and Climate Change

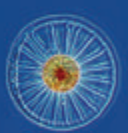

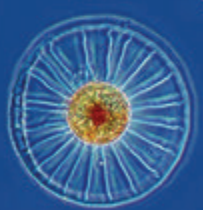

MATTHIEU ROY-BARMAN
AND CATHERINE JEANDEL

MARINE GEOCHEMISTRY

Marine Geochemistry

Ocean Circulation, Carbon Cycle and Climate Change

Matthieu Roy-Barman
and
Catherine Jeandel

OXFORD
UNIVERSITY PRESS

OXFORD
UNIVERSITY PRESS

Great Clarendon Street, Oxford, OX2 6DP,
United Kingdom

Oxford University Press is a department of the University of Oxford.
It furthers the University's objective of excellence in research, scholarship,
and education by publishing worldwide. Oxford is a registered trade mark of
Oxford University Press in the UK and in certain other countries

First Edition published in 2016

Impression: 1

Published in the United States of America by Oxford University Press
198 Madison Avenue, New York, NY 10016, United States of America

British Library Cataloguing in Publication Data
Data available

Library of Congress Control Number: 2016932193

ISBN 978–0–19–878749–5 (hbk.)
ISBN 978–0–19–878750–1 (pbk.)

Printed and bound by
CPI Group (UK) Ltd, Croydon, CR0 4YY

Contents

Foreword xi
Preface xv
Units, notation and abbreviations xix

1 A Few Bases of Descriptive and Physical Oceanography 1

1.1 The Size of the Ocean 1
1.2 Salinity, Temperature and Density: The Basic Parameters of the Oceanographer 2
1.2.1 Salinity 3
1.2.2 Temperature 4
1.2.3 Density 5
1.3 Vertical Structure of the Ocean 6
1.4 The Main Water Masses 9
1.5 Ocean Currents 13
1.5.1 Surface Circulation 13
1.5.2 The Physical Principles 15
1.5.3 The Wind-Driven Ocean Circulation 18
1.5.4 Ekman Pumping 21
1.5.5 Coastal Upwelling 25
1.5.6 Geostrophic Currents 26
1.6 Large-Scale Circulation 31
1.6.1 Vorticity 31
1.6.2 Sverdrup Balance 33
1.6.3 The Intensification of the Western Boundary Currents 37
1.6.4 Eddies and Recirculation 38
1.6.5 The Thermocline Ventilation 38
1.6.6 The Equatorial Circulation 40
1.6.7 The Deep Circulation 41
Appendix 1: The Atmospheric Forcing 43
Problems 44

2 Seawater Is More than Salted Water 49

2.1 Why Is Seawater Salty? 50
2.1.1 The Chemical Composition of Salt 50
2.1.2 Residence Time 51
2.1.3 Rivers and Estuaries 51

2.1.4 The Atmosphere 52
2.1.5 Volcanic and Hydrothermal Processes 52
2.1.6 The Removal of Chemical Elements 53
2.2 Concept of Conservative and Non-Conservative Tracers 54
2.3 The Nutrient Cycle and the Role of Biological Activity 55
2.3.1 Nutrient Profiles in Seawater 55
2.3.2 The Life Cycles in the Ocean 56
2.3.3 Influence of Deep Circulation on the Nutrient Distribution 60
2.4 Gases in Seawater 62
2.4.1 Definition of Apparent Oxygen Utilization 65
2.5 Relationships between the Different Tracers 65
2.5.1 Extracting the Conservative Fraction of a Tracer 65
2.5.2 Construction of Conservative Tracers 66
2.5.3 Horizontal and Vertical Changes of Tracers 68
2.6 Carbon Chemistry 70
2.6.1 The Carbonate System 70
2.6.2 Calcium Carbonate 73
2.6.3 Organic Carbon 74
2.7 The Redox Conditions in the Ocean 75
2.8 Behavior of Trace Metals 78
2.8.1 The Different Types of Profiles 78
2.8.2 Oxidation and Reduction of Manganese 79
2.8.3 Complexation of Iron 81
2.9 Many Open Questions 83
Appendix 1 83
Problems 87

3 Stable Isotopes 91

3.1 What Is an Isotope? 91
3.2 Notations 93
3.3 The Different Types of Fractionations: The Oxygen Example 95
3.3.1 Kinetic Fractionations 95
3.3.2 Thermodynamic Fractionations 95
3.3.3 Seaside Analogy 97
3.3.4 The "Biological" Fractionations 97
3.3.5 Mass-Dependent and Mass-Independent Fractionations 97
3.3.6 Clumped Isotopes 98
3.4 Oxygen Isotope Fractionation 100
3.4.1 The Fractionations in the Water Cycle 100
3.4.2 Isotope Exchange between Water and Solid 103
3.5 Hydrogen Isotope Fractionation 103
3.6 Carbon Isotope Fractionation 103
3.6.1 Fractionations in the Carbonate System 104

3.6.2 Biological Fractionations 106
3.6.3 The $\delta^{13}C$–PO_4^{3-} Relationship in Seawater 107
3.7 Nitrogen Isotope Fractionation 108
3.8 Sulfur Isotope Fractionation 110
3.9 Boron Isotope Fractionation 111
3.10 Silicon Isotope Fractionation 112
3.11 Iron Isotope Fractionation 112
3.12 Mixing of Isotopic Tracers 115
3.12.1 Conservative Mixing 116
3.12.2 Non-Conservative Mixing 119
3.13 Evolution of the Isotopic Signature during a Reaction 120
3.13.1 Example: Nitrate Assimilation by Phytoplankton 121
Appendix 1: Evolution of Isotopic Signatures during Fractionation Processes 122
Problems 125

4 Radioactive and Radiogenic Isotopes 129

4.1 Radioactivity 129
4.2 The Radioactive Decay Law and its Applications 130
4.2.1 The Radioactive Decay Law 130
4.2.2 Disintegration without Simultaneous Production 131
4.2.3 Disintegration with Simultaneous Production 133
4.2.4 Definition of the Activity 134
4.3 The Long-Lived Radioactive Decay Systems 136
4.3.1 Strontium 137
4.3.2 Neodymium 139
4.3.3 Lead 141
4.3.4 Helium 142
4.4 The Uranium and Thorium Decay Chains 143
4.5 Cosmogenic Isotopes 147
4.5.1 The ^{14}C Isotope 147
4.5.2 The ^{10}Be Isotope 150
4.6 Artificial Isotopes 151
Appendix 1 155
Integration of the Radioactivity Equation for a Closed System without Production Term 155
Integration of the Radioactivity Equation for a Closed System with Production Term 156
Calculation of the Mean Lifetime of an Isotope 158
Problems 159

5 Box Models 162

5.1 One-Box Model 162
5.1.1 The Conservation Equation 162

5.1.2 Case of Enzyme Kinetics 164
5.1.3 Steady State 165
5.1.4 Residence Time 165
5.2 Dynamic Behavior of a Reservoir 166
5.2.1 Constant Forcing 166
5.2.2 Temporal Evolution of the Forcings 168
5.3 Box Models and Isotopic Tracers 170
5.3.1 Use of U and Th Decay Chains 170
5.3.2 Using the Isotopic Composition of a Tracer 171
5.3.3 Application Exercise: Ventilation of the Deep Waters in the Red Sea 172
5.4 Dynamics of Coupled Boxes 175
5.5 Mean Age, Residence Time and Reservoir Age of a Tracer 177
Problems 179

6 Advection–Diffusion Models 183

6.1 An Infinitesimal Box 183
6.2 Advection 184
6.3 Molecular Diffusion 186
6.3.1 Random Walk 186
6.3.2 The Fick Law 187
6.3.3 Gas Diffusion at the Air–Sea Interface 189
6.4 Eddy Diffusion 191
6.5 The Full Conservation Equation 193
6.5.1 Example 1: Radium Transport in Coastal Waters 195
6.5.2 Example 2: Dispersion of SF_6 in the Thermocline 199
6.6 The Case of Sediment Transport 201
Problems 203

7 Development and Limitations of Biological Activity in Surface Waters 206

7.1 Life Cycle in the Ocean 206
7.2 Development of the Biological Production in Surface Waters 213
7.3 Estimating the Primary Production 217
7.4 Global Distribution of Photosynthesis and Ocean Color 221
7.5 Iron Limitation 223
7.6 Silica Limitation 225
7.7 A CO_2 Limitation? 227
7.8 The Long-Term Limitation of the Production 228
7.9 Anthropogenic Impacts 229
Problems 231

8 CO_2 Exchanges between the Ocean and the Atmosphere 235
8.1 The Global Carbon Cycle 235
8.2 The Partial Pressure of CO_2 in Seawater 235
8.2.1 Temperature Effect 236
8.2.2 Carbonate System Effect 236
8.2.3 Photosynthesis 239
8.2.4 Remineralization 239
8.2.5 The Formation of Calcium Carbonate ($CaCO_3$) 239
8.2.6 $CaCO_3$ Dissolution 240
8.2.7 Overall Effect on the Pumping of CO_2 241
8.3 The Carbon Storage Capacity of the Ocean 243
8.4 Rate of CO_2 Transfer at the Air–Sea Interface 245
8.5 Gas Equilibration Time between the Mixed Layer and the Atmosphere 248
8.5.1 Perturbation of Oxygen 248
8.5.2 Perturbation of the Carbonate System 248
8.5.3 Perturbation of the Isotopic Composition 249
8.6 Observation of the Anthropogenic Perturbation at the Ocean Surface 251
8.7 Global Estimate of the Ocean–Atmosphere Exchanges 251
8.8 Spread of the Anthropogenic Perturbation in the Deep Ocean 253
Problems 260

9 The Little World of Marine Particles 265
9.1 Origin and Nature of Marine Particles 265
9.2 Marine Particle Sampling 269
9.3 The Distribution of Particles 272
9.4 Particle Sinking 274
9.5 Changes of the Particle Flux with Depth 278
9.5.1 The Organic Matter Flux 278
9.5.2 The Mineral Phases 280
9.6 Estimation of the Particle Flux 280
9.6.1 ^{234}Th and Irreversible "Scavenging" Models 281
9.6.2 Relations between Small and Large Particles 284
9.6.3 ^{230}Th and Reversible Models 285
9.7 The Role of Margins 287
9.7.1 Boundary Scavenging 287
9.7.2 Boundary Exchange 289
9.8 The Distribution of Sediments on the Seafloor 291
9.9 The Diagenesis 292
9.10 Timescales and Sediment Fluxes 296
Problems 299

10 Thermohaline Circulation 302

10.1 The Long Path of Deep Waters 302
10.2 The Rapid Progression of Transient Tracers 308
10.2.1 Deep Current Dynamics 309
10.2.2 Intensity of the Recirculation 313
10.3 ^{14}C-Transient Tracer Comparison 314
10.4 The Contribution of ^{231}Pa–^{230}Th 317
10.5 The Origin of the AABW 320
10.6 Closure of the Meridional Overturning Circulation 323
Problems 325

11 Ocean History and Climate Evolution 331

11.1 The Origin of the Ocean 331
11.2 The First Traces of Life 333
11.3 The Rise of Oxygen 333
11.4 Geological Sequestration of CO_2 336
11.5 The Closure of the Panama Isthmus 339
11.6 The Last Glaciation 340
11.7 El Niño Exacerbated by Human Activity? 348
11.8 The Climate of the Future and the Ocean 350
11.9 The Expected Consequences 352
Problems 358

Problem solutions 363
Glossary 373
References 381
Index 395

Foreword

Marine chemistry, chemical oceanography, marine biogeochemistry—just a taste of the terminology encountered by a student upon their introduction to the field of oceanography. Faced with the proliferation of disciplinary terms, one can easily understand why such a student might imagine oceanography to be a highly fragmented field, where the focus of each subdiscipline is of limited interest to investigators in other subdisciplines. Nothing could be further from the truth!

As any successful oceanographer will confirm, marine science is a highly interdisciplinary field that relies on tight connectivity among its subdisciplines. For example, the interplay between physics and biology regulates the distributions of many dissolved chemicals in the ocean while the physical and chemical environment shapes ocean ecosystems. Physics, chemistry and biology each contribute to the amount and composition of sediment accumulating on the seafloor, while biological and chemical transformations within sediments just below the seabed generate a flux of chemicals back into the water column. Building upon an accurate knowledge of the processes that regulate chemical distributions in the modern ocean, one can derive a wealth of information about past environmental conditions from the abundance and isotopic composition of chemical "tracers" extracted from marine sediments. As indicated in its subtitle, *Marine Geochemistry* provides the student of oceanography, as well as interested professionals in other fields, with the essential interdisciplinary knowledge required to understand the ocean today, how it differed in the past, and what to expect under an evolving climate in the foreseeable future.

The authors, Matthieu Roy-Barman and Catherine Jeandel, are well known throughout the international oceanographic community. My own interaction with the authors illustrates how individual threads of the discipline interweave over time to form a cohesive fabric. I first met Catherine in the late 1980s when she was a visiting scientist at my institution, the Lamont-Doherty Earth Observatory of Columbia University. At that time we were both involved in the Joint Global Ocean Flux Study (JGOFS), an international program investigating the biological and chemical processes that regulate the distribution and fluxes of carbon in the ocean. Upon her return to France she led the implementation of a time-series station known as KERFIX near the Kerguelen Islands. This French contribution to JGOFS examined the processes that regulate fluxes of carbon in the Southern Ocean, the region in which the ocean is thought to exert the greatest control over natural changes in the CO_2 content of the atmosphere.

I first encountered Matthieu's work in the mid-1990s through the publication of one of the papers derived from his post-doctoral research with Gerald Wasserburg at the California Institute of Technology. His dissolved thorium profiles, measured near Hawaii, represented an impressive advance over my own work on the topic more than a

decade earlier. His data continue to serve as a standard against which new thorium results are compared today. Moreover, Matthieu's dissolved thorium profiles provided indisputable evidence in support of the reversible scavenging model that Michael Bacon and I proposed in the early 1980s. Matthieu is at the forefront of the field that uses thorium isotopes to derive rates of important processes in the ocean, including solid-solution chemical exchange and the physical transport of chemical species over basin-scale dimensions. This expertise is threaded throughout the textbook. In fact, the clear explanation of quantitative models to interpret thorium isotopes and other tracers sets *Marine Geochemistry* apart from other contemporary textbooks in the field.

Continuing with the metaphor of a fabric woven from individual threads, we can readily see how the interconnectivity of marine science advances our understanding about all aspects of the ocean if we consider the development of GEOTRACES. This international program, with contributors in more than 30 nations, studies the marine biogeochemical cycles of trace elements and their isotopes. Like any sound structure built on a solid foundation, the creation of GEOTRACES benefited from the experiences of the JGOFS program, mentioned above, while also emulating many of the successful principles exemplified by GEOSECS, the first global study of ocean geochemistry that is frequently cited by Roy-Barman and Jeandel.

How did this remarkable collaboration come about? The answer is revealed by following the threads of the fabric.

During a JGOFS meeting in 2000 (Bergen, Norway) Catherine Jeandel and I were commiserating about the slow rate of progress in the field of marine geochemistry. We felt that advances in understanding could be accelerated through greater coordination of international efforts and more active collaboration. We quickly discovered that marine geochemists worldwide shared this view, and that many were eager to devote time and energy to plan a coordinated global study that eventually adopted the name "GEOTRACES" to convey the value of tracers in understanding biogeochemical processes in the world ocean, much like the philosophical underpinnings of *Marine Geochemistry*. GEOTRACES promises not only to revolutionize our view of ocean trace element geochemistry but also to provide a template for coordinated research in other sub-disciplines of oceanography. Selected early results from GEOTRACES are included in this edition of Marine Geochemistry, reflecting the active leadership in the program by the authors.

Beyond GEOTRACES, *Marine Geochemistry* draws heavily from several other current programs. It is informed by, and brings applications from, all facets of oceanography. Results of the ARGO Array enable insights into ocean hydrography and circulation while the Tara Ocean Expeditions illustrate the distribution and diversity of ocean microbes. Complex interactions between Earth's climate and the ocean carbon cycle are explained using key points from the IPCC reports. The authors also present data from emerging fields such as proteomics, which can quantitatively inform on the ecosystem response to changing chemical environments. Informed by these new fields, marine geochemists are better prepared to assess how marine biogeochemical cycles will evolve under global change.

The ocean may be too expansive to manage, at least within our lifetime, but we need a more complete understanding of ocean processes and their interaction if society is

to sustainably maximize its use of ocean resources. Such an understanding begins with rigorous interdisciplinary training in all aspects of marine science. *Marine Geochemistry* introduces the reader to the range of tools and concepts inherent to marine geochemistry, embedded in the interdisciplinary context required to fully exploit that knowledge.

Their decades of combined experience as successful educators have enabled Roy-Barman and Jeandel to capture the essential interdisciplinary flavor of ocean science in *Marine Geochemistry*. Knowledge gained from the text can be applied to a broad spectrum of societal benefits including, but not limited to, maximizing the sustainable supply of food from the ocean while ensuring the health of marine ecosystems, minimizing the damage caused by submarine activities such as seabed mining, and unraveling the ocean's role in climate change. *Marine Geochemistry* provides an excellent foundation for students, teachers, policy makers and professionals in any field who wish to pursue these themes, and much more.

Bob Anderson
LDEO

Preface

Marine geochemistry has the dual objective of:

- understanding the behavior and distribution of chemical elements and their isotopes in the ocean to identify a priori their properties as tracers;
- using these same elements to study physical, chemical and biological ocean processes.

Marine geochemistry is a young discipline. Due to the importance of biological processes in the control of the cycles of the elements, the term "marine biogeochemistry" is also used. Sampling being very limited in time and space, oceanographers are often helpless in understanding how of a given system works. To help them, geochemists propose tools called "tracers." A "tracer" is an element or a parameter used to describe and quantify one (or more) processes which modifies the distribution of the chemical elements in the ocean or at its interfaces (with the atmosphere, the continent, the sediment ...) and therefore which controls the chemical composition of the "fluid and living environment" that is the ocean. The essential corollary question is to choose the best tracer suited for a given study. The geochemist then has two complementary approaches:

(1) The basic information given by the location of a chemical element in the periodic table. After the brilliant ideas of V. Goldschmidt (father of the fundamental geochemistry in the 1950s), the broad lines of a chemical element behavior in the environment can be predicted based on its ionic radius and its valence states.

(2) The description of the tracer cycle itself, in order to define its field of application.

It is difficult to deal with marine geochemistry without mentioning the huge contribution of a few pioneers of the discipline. The work of Harmon Craig on $^{13}C/^{12}C$—done in 1955 at the University of Chicago—is still used today. He was in the team of the Nobel Prize in Chemistry awarded to Harold C. Urey, who encouraged his students to explore the universe with the measurements permitted by the all new mass spectrometers. Craig was 29 y old when he moved to California ... the other universities of the coast being too timid to take a chance on a field as risky as geochemistry! Hired at Caltech, he was in contact with oceanographers such as Roger Revelle and proposed a theoretical explanation of the CO_2 cycle between ocean and atmosphere ... anticipating the implementation of famous time series of atmospheric CO_2 in Hawaii by G. Keeling. When in 1967, the physical oceanographer Henry Stommel proposed the first major exploration of the ocean by sections, he wished to have the first "tracer" measurements

that were mostly chronometers (^{14}C, ^{226}Ra, etc.). The names Harmon Craig but also Wally Broecker of the Lamont Doherty Geological Observatory (New York) and Derek Spencer of Woods Hole Oceanographic Institution (Massachusetts) appear naturally to refer to the leaders of the GEOSECS program, which would run until 1980. In 1969, Craig published a critical article which evaluated the "rate of overturning" of the ocean based on profiles of dissolved inorganic carbon and ^{14}C, and calculated the first estimate of the slow vertical speed of the deep waters, as yet never measured directly today. Also, the "GEOSECS" years saw the development of the early study of natural radionuclides in the ocean by Y. Nozaki and the first measurements of particles in suspension, with contributions from D. Lal from Scripps and his Indian colleagues S. Krishnaswami and B.L.K. Somayajulu. Meritorious efforts because they had to collect of the order of cubic meters of seawater for … one measurement!

W.S. Broecker, in the famous and seminal "Tracers in the Sea" in 1982, offers one of the best evaluations of what GEOSECS has brought to the knowledge of the ocean. With a more eclectic nature than Harmon, "Wally" is internationally recognized for his work on abrupt climate changes, his hypothesis of the "conveyor belt," his description of the "global warming," … The 1980s were the theater of many developments of marine geochemical tracers. Many studies since have focused on the description of the global cycle of some chemical elements … these works, which could look like some sort of "bet," were designed to identify the behavior of chemical elements in the ocean, in response to a number of their properties. These works had the merit to emphasize the first difficulty for the measurements of elements in natural environments: the risks of artifacts related to contamination during the analytical protocol. This period was also one of the advent of clean rooms with their specific material and reagents; in other words, the community learned to work properly.

Today, the progress made in the study of chemical and isotopic tracers—and in particular the improved sensitivity of new generations of mass spectrometers—and the scientific need to quantify poorly constrained fluxes of matter, led the marine geochemistry community to build the GEOTRACES international program (2010–2020). GEOTRACES aims to determine the distribution and the cycle of a series of tracers in the ocean in order to understand the response of these tracers to global change to improve the paleoreconstitutions and predict the evolution of the ocean under anthropogenic forcing. The strategy, coordinated worldwide, is based on an analysis of various tracers along the same oceanic sections, the multi-tracer approach being at the heart of GEOTRACES. Process studies in targeted areas will complement the global section approach.

In such a context of development of marine geochemistry, 35 y after the publication of "Tracers in the Sea" and 45 y after the seminal articles of Clair Patterson on isotopic measurements of lead in seawater, it is essential to propose a book giving the basis of marine geochemistry and providing an up to date view of our understanding of a series of selected tracers in the context of key questions of importance to contemporaneous oceanography.

This book presents the principles, methods and applications of marine geochemistry. Marine geochemistry is not an isolated discipline: the book offers numerous openings

on physical and biological oceanography, climatology, geology and ecology, allowing the reader to acquire a global vision of the functioning ocean. The book shows how marine geochemistry, with other disciplines, helps in the study of major issues such as the role of the ocean in climate regulation, the response of the ocean to climate changes or the impact of pollution, particularly through recent developments of isotope tracers.

Several application exercises within each chapter allow an immediate implementation of the principles learned in the course. Problems based on recent research articles are also proposed at the end of each chapter. They allow readers to test their knowledge, but also to present issues which have not been treated in the main body of the chapter. As such, they are an integral part of the course. Numerical results and elements of solutions are given at the end of the book.

This book is addressed to:

- advanced undergraduate and graduate students in oceanography, geochemistry or climatology as part of an earth or environmental science program;
- academics in earth or environmental sciences;
- professionals in the fields of coastal management and marine resources.

It is based on undergraduate and master courses that we have given during the last 20 y in the Paris-Saclay University, the University of Versailles-Saint Quentin, the University Paul Sabatier of Toulouse, at the University of the Mediterranean in Marseille and at the École Normale Supérieure of Paris to students mainly from the sectors of environmental science, physics, Earth sciences and biology. This diverse demographics pushed us to have an open and multidisciplinary approach of oceanography.

We have chosen to insist on the importance of isotopic tracers in oceanography. From the educational point of view, following chemical elements through their isotopic signature allows a simple and quantitative approach to the transport of the elements in the ocean. From the research point of view, isotopic tracers provide many fundamental results on the fluxes of material in the ocean.

The first chapter presents descriptive and physical oceanography basics essential to the understanding of the ocean. The physics of ocean circulation is discussed by combining an intuitive approach with the use of some fundamental equations. It may seem strange, even discouraging for some, to begin a geochemistry textbook with physics. In fact, the impact of currents on the biology and chemistry of the ocean is such that it is difficult to avoid this introduction. The presentation of the calculations in "boxes," however, facilitates reading "without equations," even if the equations are a good way to capture many non-intuitive phenomena. The deep circulation is merely touched upon here as Chapter 10 is entirely devoted to this subject. The reader who wants to go further will refer to Introduction to physical oceanography (Stewart, 2004) available online at: (http://oceanworld.tamu.edu/resources/ocng_textbook/contents.html).

The second chapter reviews the behavior of major chemical tracers and their biogeochemical cycles. We have assumed that the reader has already mastered the basics in chemistry (acid–base and redox reactions, precipitation dissolution, etc.). We have not reviewed exhaustively 92 elements of the periodic table, which also are not necessarily

"good" ocean tracers. We have not discussed in detail the equation of state and thermodynamic parameters of seawater that go beyond an undergraduate or master course in marine geochemistry and because it is very well developed elsewhere (IOC, 2010).

Chapters 3 and 4 describe the origins and causes of the changes in the isotopic ratios of the elements in the ocean: they reflect (1) the origin of the elements that have a specific isotopic signature when they arrive in the ocean, (2) the result of isotopic fractionations between stable isotopes within the ocean or (3) by decay of radioactive isotopes or accumulation of radiogenic isotopes. We present the principles of isotopic tracers in the context of ocean study. Many applications are proposed in later chapters.

Chapters 5 and 6 present the box models and advection–diffusion models which are important conceptual tools used to interpret the geochemical data in the ocean. The presentation is relatively detailed to allow the reader to use them in the following chapters.

Finally, we apply tracers to different objects that are at the heart of major current environmental issues: biological activity in the ocean (Chapter 7), the carbon cycle (Chapter 8), the flux of particles (Chapter 9), thermohaline circulation (Chapter 10) and the relationship between ocean and climate (Chapter 11).

We strongly thank Bob Anderson, François Baudin, Dominique Blamart, Damien Cardinal, Patrick Commeau, Jean-Claude Dutay, Nicolas Estrade, Norbert Frank, Jerome Gaillardet, François Lacan, Nicolas Metzl, Rosemary Morrow, Thierry Moutin, Christophe Rabouille and Claire Revillet for their careful proofreading of all or part of the book at various stages of advancement and their many suggestions. We also thank students who, willingly or unwillingly, have tested exercises in class or during exams. We warmly thank Bob Anderson who agreed to write a foreword to the book. Finally, we thank our families for their patience and indulgence while we have been preoccupied with the book!

Units, notation and abbreviations

Units

The units and the symbols used in this book are generally those of the international system. Common prefixes of the powers of 10 are:

G (giga): $10^9 = 1{,}000{,}000{,}000$
M (mega): $10^6 = 1{,}000{,}000$
k (kilo): $10^3 = 1000$
m (milli): $10^{-3} = 0.001$
μ (micro):$10^{-6} = 0.000001$
n (nano): $10^{-9} = 0.000000001$
p (pico): $10^{-12} = 0.000000000001$
f (femto): $10^{-15} = 0.000000000000001$

We have also used some common units not belonging to the international system.

Fraction and concentration (solid and liquid)	percent (%)	$1\% = 10^{-2}$ g g^{-1}
	per thousand (‰)	$1‰ = 10^{-3}$ g g^{-1}
	parts per million (ppm)	1 ppm = 10^{-6} g g^{-1}
	part per billion (ppb)	1 ppb = 10^{-9} g g^{-1}
	part per by trillion (ppt)	1 ppt = 10^{-12} g g^{-1}
	per meg (for "per mega")	per meg = 10^{-3}‰
Concentration (in the air)	part per million by volume (ppmv)	1 ppmv = 10^{-6} mol mol^{-1}
	part per billion by volume (ppbv)	1 ppbv = 10^{-9} mol mol^{-1}
	parts per trillion in volume (pptv)	1 pptv = 10^{-12} mol mol^{-1}
Water flux	Sverdrup (Sv)	1 Sv = 10^6 m^3 s^{-1}
Activity	Becquerel (Bq)	1 Bq = 1 disintegration per second
	disintegration per minute (dpm)	1 dpm = 0.01666 Bq
	Tritium Unit (TU)	1 TU = 1 ^{3}H atom for 10^{18} ^{1}H atoms

Notation

We have tried to use the most common notations found in the literature, but we had to face two limits: some variables are represented by different symbols depending on the authors and the same symbol is often used to represent different variables in the different fields covered in the book.

Variable	Description	Usual Unit
A	Atomic mass	g mol^{-1}
C	Concentration	mol kg^{-1}
d	Differential	
d	Distance	m
D	Molecular diffusion coefficient	cm^2 s^{-1}
D_{biot}	Diffusion coefficient during bioturbation	cm^2 y^{-1}
f	Fraction of a component in a mixture	%
f	Coriolis parameter	s^{-1}
F	Total flux Water flux Flux per unit area	quantity s^{-1} 1 Sv (Sverdrup) = 10^6 m^3 s^{-1} quantity m^{-2} s^{-1}
F	Remaining fraction of the reactant in a reaction	%
g	Acceleration of gravity of the Earth	m s^{-2}
G	Gibbs free energy	J kg^{-1}
h, H	Thickness	m
k	Ocean–atmosphere friction coefficient	dimensionless
k	Time constant	y^{-1}
K	Reaction equilibrium constant particulate/dissolved ratio	
k_p	Time constant of a sink term	y^{-1}
K_S	Half-saturation constant	mol L^{-1}
$K_{x,y}$	Horizontal turbulent diffusion coefficient	cm^2 s^{-1}
K_z	Vertical turbulent diffusion coefficient	cm^2 s^{-1}
l	Dynamic height	m
L	Distance	m

Variable	Description	Usual Unit
$\mathcal{N}$	Avogadro's number	6.02×10^{23} mol^{-1}
N	Number of atoms	mol
P	Pressure	N m^{-2}, atm
P_e	Péclet number	dimensionless
R	Isotope ratio	mol mol^{-1}
r	Radius	m
R	Ideal gas constant	J mol^{-1} K^{-1}
R_E	Radius of the Earth	km
s	Source term	mol m^{-3} s^{-1}
S	Salinity	dimensionless or g kg^{-1}
S	Surface	m^2
T	Temperature	°C
$T_{1/2}$	Half-life	y
u, v, w	East, north and vertical velocity components	m s^{-1}
U, V, W	East, north and vertical transport components	m^2 s^{-1}
U_a	Wind speed at 10 m above sea level	m s^{-1}
V	Volume	m^3
v_p	Piston speed	m s^{-1}
w_p	Particle settling speed	m s^{-1}
w_s	Sedimentation rate	m s^{-1}
[X], X	Concentration of the element X	mol kg^{-1}
[X]^{sat}	Concentration of a dissolved gas in equilibrium with the atmosphere	mol kg^{-1}
{X}	Activity of the radioactive element X	disintegration per second (Bq) or disintegration per minute (dpm)
x, y, z	Cartesian coordinates	m
Z	Atomic number	
α	Coefficient of solubility of a gas	mol kg^{-1} atm^{-1}
α_{A-B}	Coefficient of isotopic fractionation between compounds A and B.	dimensionless
β	Variation of the Coriolis parameter with latitude: df/dy	s^{-1} m^{-1}
β	Constant of complexation	

Variable	Description	Usual Unit
∂	partial derivative	
δ	Relative variation of an isotopic ratio with respect to a reference	‰ (in general) % for helium
Δ	Relative variation of an isotope ratio with respect to a reference corrected for mass dependent isotopic fractionation	‰ per meg (10^{-3}‰)
Δ_{A-B}	Difference of δ between compounds A and B.	‰
Δz	Thickness of the stagnant film	μm
ε_{Nd}	Relative variation of the $^{143}Nd/^{144}Nd$ ratio with respect to the bulk Earth	0.1‰ (epsilon unit)
Φ	Porosity	$m^3\ m^{-3}$
Γ	Radioactive production	fg $kg^{-1}\ y^{-1}$
η	kinematic viscosity	g $cm^{-1}\ s^{-1}$
φ	Latitude	°
κ	Time constant	y^{-1}
λ	Decay constant	y^{-1}
μ	Time constant	s^{-1}
Π	Potential vorticity	$s^{-1}\ m^{-1}$
θ	Potential temperature	°C
ρ	Density	kg m^{-3}
ρ_{rain}	Precipitation rate	mm y^{-1}
ρX	Speed of assimilation of X	mol $m^{-3}\ s^{-1}$
σ	Density anomaly	kg m^{-3}
τ	Friction force, wind stress	N m^{-2}, 1 kg $m^{-1}\ s^{-2}$
τ	Residence time	y
ω	Relative vorticity	s^{-1}
Ω	Angular velocity of rotation of the Earth	s^{-1}
Ω	Saturation index of carbonates in seawater	dimensionless
ζ	Revelle factor	dimensionless

Abbreviations

The following acronyms have been used in the book:

AABW	Antarctic Bottom Water
AAIW	Antarctic Intermediate Water
ACC	Antarctic Circumpolar Current
AOU	Apparent Oxygen Utilization
ASW	Antarctic Surface Water
CDW	Circumpolar Deep Water
CFC	Chlorofluorocarbon
DIC	Dissolved Inorganic Carbon
PIC	Particulate Inorganic Carbon
DOC	Dissolved Organic Carbon
POC	Particulate Organic Carbon
GEOSECS	Geochemical Ocean Sections Study
GISP	Greenland Ice Sheet Project
Gt C	Gigaton of carbon
HNLC	High nutrient low chlorophyll
ISW	Ice Shelf Water
MW	Mediterranean Water
NADW	North Atlantic Deep Water
NPDW	North Pacific Deep Water
GCP	Gross Community Production
GW	Glacial Water
NCP	Net Community Production
EP	Exported Production
NP	New production
PP	Primary production
RP	Regenerated production
RESP	Respiration
curl	curl (vertical component)
RSDW	Red Sea Deep Water
SAMW	Sub-Antarctic Mode Water
SeaWiFS	Sea-viewing Wide Field-of-view Sensor
TrOCA	Tracer combining oxygen, inorganic carbon and alkalinity
WDW	Warm Deep Water
WOCE	World Ocean Circulation Experiment
WSBW	Weddell Sea Bottom Water
WSDW	Weddell Sea Deep Water
WW	Winter Water

1

A Few Bases of Descriptive and Physical Oceanography

In this chapter, we present key concepts of descriptive and physical oceanography that are important for marine geochemistry.

1.1 The Size of the Ocean

The ocean covers 3.6×10^{14} m^2, which represents about 71% of the Earth's surface (see Table 1.1). Its depth is very variable: while **continental shelf** rarely exceeds 250 m depth, **continental slope** leads to **abyssal plains** at depths ranging from 3000 to 6000 m (Fig. 1.1). The extension of the continental shelf is variable: almost absent in the Mediterranean Sea, it reaches 300 km off the coast of Brittany. The shelf–slope limit is marked by a change of the seafloor slope (0.2% for the continental shelf against 5% for the continental slope). The different abyssal plains are separated by **ridges**. Ridges are mountain ranges, several thousands of meters high, which run over 60,000 km of ocean floor. Ridges are volcanic zones where oceanic crust is formed by partial melting of the mantle. They are segmented by fractures called **transform faults**. They are also areas of strong hydrothermal circulations, which generate spectacular phenomena: hot springs ($T > 350$°C) discovered in 1977, form huge underwater geysers also called black smokers located at certain points on the ridges. Cold sources (T ranging from 20 to 60°C) were discovered more recently, with a more diffuse distribution on the ocean floor but probably more abundant. The oceanic crust returns in the Earth's mantle in subduction zones, thus creating **abyssal trenches** with depth up to 11 km. Submarine landforms are more marked than those of the continents! However, it should be kept in mind that the ocean is only a thin film on the Earth's surface. Relatively speaking, the ocean on Earth has the thickness of a sheet of paper on the surface of a soccer ball. The average depth of the ocean is 3800 m. Seafloors deeper than 6000 m represent only 3% of the total ocean surface. The volume of the ocean is 1.36×10^{18} m^3. The ocean is by far the main reservoir of water at the Earth's surface (even if an amount of water of the same order of magnitude is stored deep in the Earth's mantle). The first $\sim$1000 m

Marine Geochemistry. First Edition. Matthieu Roy-Barman and Catherine Jeandel.

Table 1.1 *Essential characteristics of the ocean*

Surface	3.6×10^{14} m^2
Average depth	3800 m
Maximum depth	11,000 m
Total volume	1.36×10^{18} m^3
Average temperature	2.8°C
Average salinity	34.55 g kg^{-1}
Water flux from the rivers	10^6 m^3 s^{-1}

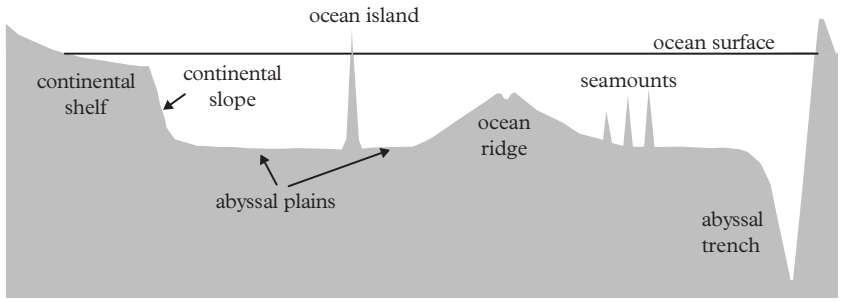

Figure 1.1 *Major oceanic landforms. The vertical scale is greatly exaggerated.*

of the ocean represents about 0.36×10^{18} m^3 and can be assimilated to the surface ocean in a broad sense (mixed layer + thermocline), while the deep ocean represents approximately 10^{18} m^3.

1.2 Salinity, Temperature and Density: The Basic Parameters of the Oceanographer

The salinity and the temperature of seawater play a fundamental role in oceanography. Together with pressure, they determine the **density** of seawater. Spatial variations of seawater density generate ocean currents. In addition, salinity and temperature are used as "ID card" of seawater. It is therefore fundamental to determine them with great precision. In practice, instruments such as the "CTD" probe (for Conductivity, Temperature and Depth) combine electronic sensors measuring seawater conductivity, temperature and pressure (to determine depth). Connected to the boat by an electric carrier cable, it allows the *in situ* determination of the temperature and salinity of seawater with depth.

1.2.1 Salinity

It is well known that seawater is salty. Historically, seawater **salinity** is defined as the weight of salt contained in 1 kg of water, when all carbonates have been converted into oxides, bromine and iodine have been replaced by chlorine and organic matter has been completely oxidized. Its average value in the ocean is 34.55 g kg^{-1}. This concentration is very high: the evaporation of 30 L of seawater produces about 1 kg of salt, while only a few grams of soluble elements are obtained by evaporating 30 L of river water. The salinity varies significantly from one point in the ocean to another (from around 32 g kg^{-1} in the Arctic Seas to more than 38 g kg^{-1} in the Mediterranean Sea). These variations are due to surface phenomena:

- evaporation;
- fresh water inputs (rain, rivers, ice);
- sea-ice formation in polar regions (when seawater freezes, ice is made of fresh water and the rejected salt-rich brine increases the salinity of the surrounding seawater).

Sea salt consists mainly of Na^+, K^+, Ca^{2+}, Cl^- and SO_4^{2-} ions. In Chapter 2, we will describe the origin of these ions. For now, we just have to know that the chemical composition of the salt is remarkably constant regardless of the seawater salinity (provided it is not too low). This was noted in the nineteenth century by Dittmar who analyzed 77 seawater samples from different depths in the world collected during the Challenger expedition (1873–1876). A practical consequence of this observation is that the determination of one of the major ions gives the content of other major ions and thus of salinity. For example, salinity is simply related to chlorinity

$$\text{Salinity (g kg}^{-1}) = 1.80655 \times \text{chlorinity (g kg}^{-1}).$$

Salinity measurements require a very high precision. The first chemical measurements of salinity were based on chlorinity measurement by precipitation of silver chloride. This technique is long and not very accurate (± 0.02). After having noticed that seawater conductivity varied with salinity and temperature at atmospheric pressure, Frank Wenner designed the first laboratory salinometer in 1930. The principle of the salinometer is to measure the ratio between the conductivity of a seawater sample and the conductivity of standard water. Precision obtained is of the order of 0.005. Today, salinity (S) is expressed by this dimensionless ratio between conductivities. This ratio is dimensionless, but its numerical value is equivalent to ‰ or g kg^{-1}. Later in the book, we adopt the "dimensionless" salinity convention.

The sea surface salinity map (Fig. 1.2) shows a distribution in latitudinal bands from the Equator to the poles (such distribution is called zonal): low salinity in equatorial waters, high salinity in tropical waters and low salinity in polar waters. This distribution reflects the balance between evaporation (which is maximal in the trade winds zone around 20–30°N and 20–30°S) and precipitations (which are maximum at the Equator and at high latitudes) at ocean surface (see Appendix 1). On average, the Atlantic Ocean

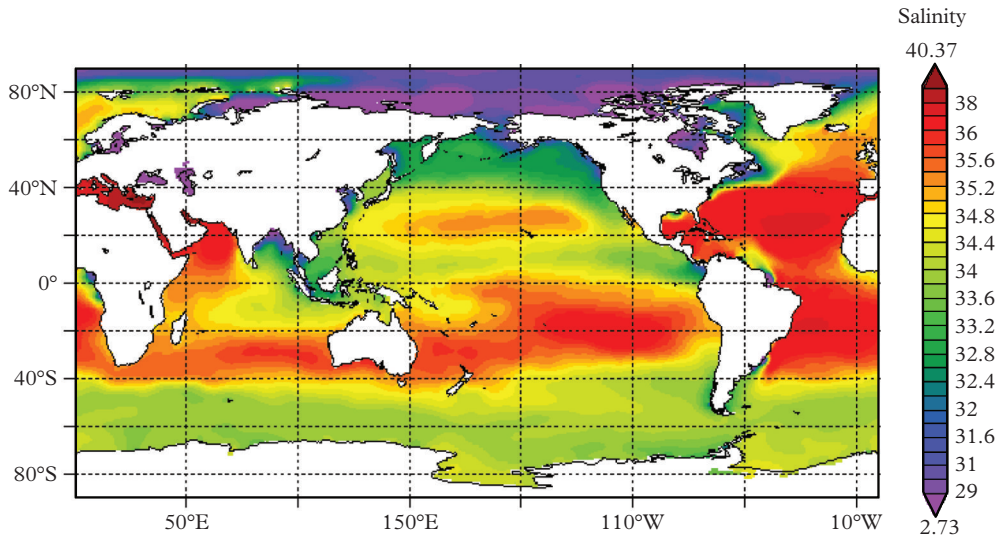

Figure 1.2 *Sea surface salinity map. Annual average on a grid of 1° × 1°. World ocean atlas 2001 (http://www.ferret.noaa.gov/NVODS/).*

is more salty than the Pacific Ocean. This is explained by (1) the input of very salty Mediterranean Water (MW), due to the very strong evaporation over the Mediterranean Sea, in the Atlantic Ocean and (2) the imbalance between the moist air transport by trade winds from the Atlantic to the Pacific across the thin Panama isthmus and the return of dry air at mid-latitudes (it loses its water vapor while crossing the American continent).

1.2.2 Temperature

Modern oceanographic thermometers use a platinum wire whose resistance is temperature dependent. They provide accuracy of the order of 0.0001°C. The thermometer of the CTD measures the *in situ* temperature, that is, at the depth where the probe is. This *in situ* temperature must be corrected for the effect of pressure: when seawater (or another body) is compressed, its temperature increases. To compare temperatures measured at different depths, oceanographers use the **potential temperature** (θ) which is the temperature of the water brought to atmospheric pressure, that is, when it was in contact with the atmosphere. It is estimated by correcting the *in situ* temperature from the effect of pressure: as compression heats the fluid, the potential temperature is always lower (of the order of 0.1°C km^{-1}) than the *in situ* temperature.

At the surface of the ocean, the temperature varies between –2 (seawater does not freeze at 0°C but at around –2°C due to the presence of salt) and 30°C (Fig. 1.3). The distribution of the temperature is grossly zonal: it is not surprising to find warm temperatures near the Equator and low temperatures in polar areas. However, there are many "anomalies." In the equatorial Pacific, water is much warmer in the west of the

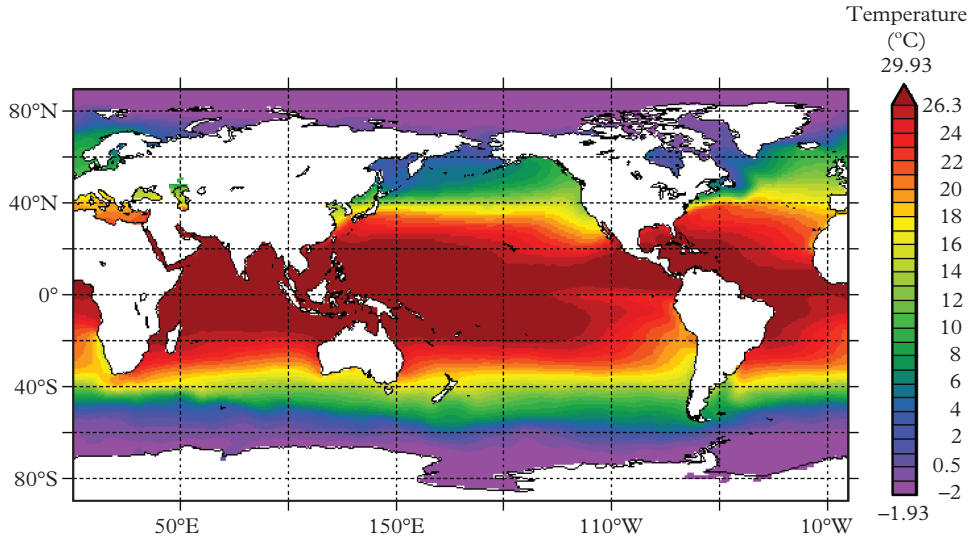

Figure 1.3 *Map of the sea surface temperature. Annual average on a grid of 1° × 1°. Word ocean atlas 2001 (http://www.ferret.noaa.gov/NVODS/).*

basin than in the east. Similarly, in the North Atlantic subtropical gyre, warm water flows northward in the west of the basin while cold water flows southward in the east of the basin. These anomalies reflect the occurrence of currents which will be described later in the chapter.

1.2.3 Density

Salinity, temperature and pressure determine the **density** of seawater (ρ). At 25°C and atmospheric pressure, seawater with a salinity of 35.0 has a density of $\rho = 1023$ kg m^{-3}. To simplify the writing of these density values, oceanographers use a term called "density anomaly" defined as $\sigma = \rho - 1000$.

For the previous example, $\sigma = 23$. For deep waters, the density anomaly is around $\sigma = 27$. A depth increase of 250 m, a temperature decrease of 4°C, or a salinity increase of 1.1 causes a density increase of approximately 1 kg m^{-3}. The influence of temperature, salinity and depth on density is not linear, especially at low temperatures. It is given by the "equations of state of seawater" (IOC et al., 2010). Since seawater salinity is relatively constant, it is mainly temperature variations that determine seawater density variations (particularly in the first 1000 m of the ocean). However, when temperature variations are small, salinity variations can significantly affect density (see Problem 1).

The potential density anomaly, σ_θ, of a water mass is the density anomaly of this water mass brought to atmospheric pressure; σ_θ allows comparison of the density of water masses at different depths. A surface along which the potential density is constant is called an "**isopycnal surface**." An isopycnal surface is represented by a constant

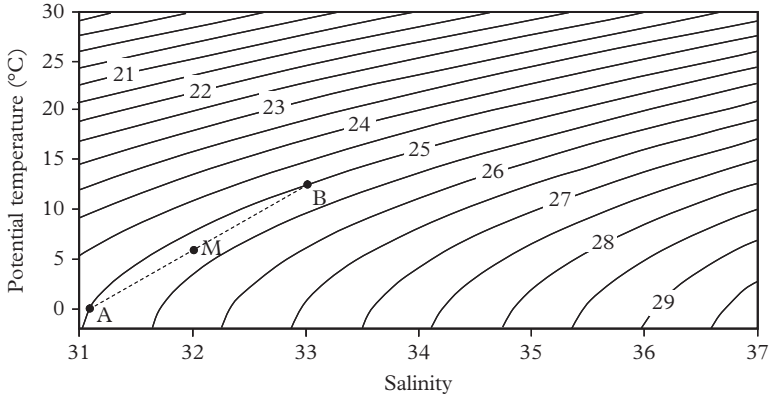

Figure 1.4 *Density anomaly as a function of potential temperature and salinity. Mixing of two water masses A and B of equal densities produces a denser water mass M.*

σ_θ curve in a θ–S diagram (Fig. 1.4). They are important because we will see in Section 1.3 that currents preferentially flow along these isopycnal surfaces. In most of the ocean, mixing occurs mainly along isopycnal surfaces. During isopycnal mixing, temperature and salinity of the water are modified, but density remains relatively constant.

We note that mixing of two water masses A and B with the same density creates a water mass M with a slightly higher density (Fig. 1.4). This mechanism is called "caballing." It is most significant for cold temperatures, in the area of nonlinearity of the equation of state of seawater. The caballing effect decreases for warm water masses.

Density is important because horizontal density gradients generate currents and vertical density gradients affect the vertical stability of water masses. In a "stable" ocean, the density increases with depth.

1.3 Vertical Structure of the Ocean

The solar radiation reaching the surface of the ocean is rapidly absorbed. The **euphotic layer** is the surface layer over which 99% of the solar radiation is absorbed. Its depth is generally of the order of 100–150 m. It is mainly determined by the seawater **turbidity**, that is, its contents in suspended solids. In biologically productive waters or close to a river mouth, the high particle load rapidly absorbs the sunlight, leading to a shallow euphotic layer. Conversely, algae-poor tropical waters let the sunlight penetrate very deeply, producing their indigo color. This warming of surface water causes a **stratification** of the ocean: in general, warm (heated by the Sun) and low density waters occur in the surface ocean, whereas colder and denser waters are at depth (Fig. 1.5). In view of the ranges of temperature (from –2 to 30°C) and salinity (from 32 to 38) of seawater,

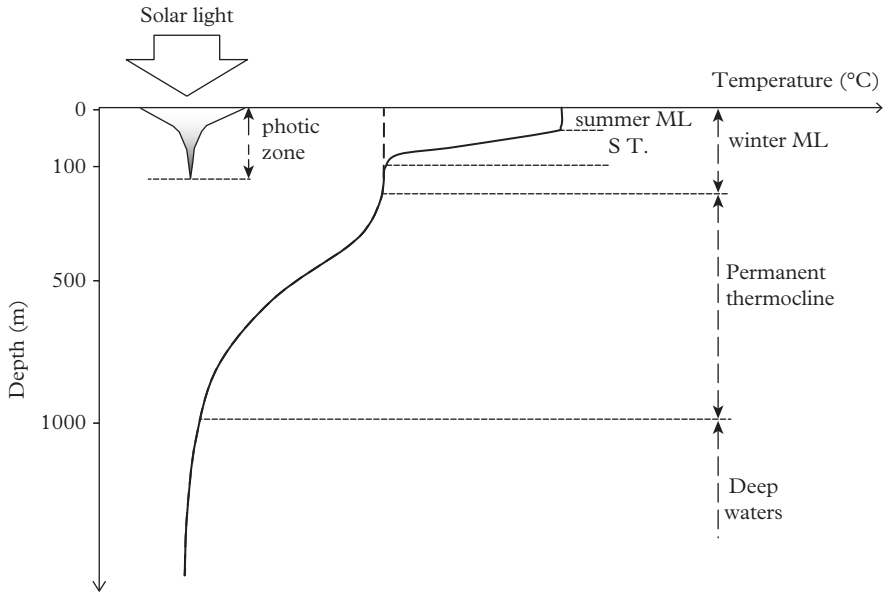

Figure 1.5 *Vertical temperature profile in the ocean at mid-latitudes. ML: mixed layer. ST: seasonal thermocline. The euphotic layer depth is usually different from the mixed layer depth.*

it is mainly temperature that controls density. At the ocean surface, there is the **mixed layer** with homogeneous temperature and salinity because it is stirred by the wind or subject to convection. It is isolated from deeper layers by the stratification, that is, a water layer in which the density increases rapidly with depth. The mixed layer thickness can vary from 20 m in summer when surface waters are very warm (as for example in the Mediterranean Sea) to several hundreds of meters in winter when surface waters cool and that they are stirred by strong winds: in the Mediterranean Sea, this vertical mixing can reach 2 km depth through convection. The mixed layer depth is generally different from the euphotic layer depth.

How Jules Verne has dressed Captain Nemo

During an underwater scuba excursion from the Nautilus in the company of Captain Nemo, Pierre Aronnax, Professor at the Museum of Natural History, describes the gradual disappearance of light with depth and its impact on the distribution of the algae species.

Innovation is often tortuous… and scuba is not the least surprising one. Indeed, its inventors are two French engineers, Auguste Denayrouze and

Benoit Rouquayrol who, 100 y before the "*the silent world*" and JY Cousteau's team, wanted to save the life of miners during firedamp explosion or mine flooding. In 1864, they submitted a patent for their "Rouquayrol–Denayrouze diver apparatus," first scuba providing air on demand ... tested, under the old bridge of Espalion—a small village in the center of France, far from the sea. This same year of 1864, the French Imperial Navy registered the apparatus. In 1867, the Rouquayrol–Denayrouze apparatus received the gold medal at the universal exhibition in Paris. Jules Verne attended the exhibition and discovered this invention with enthusiasm. In 1869, he chose it for Captain Nemo and the crew of the Nautilus in his novel *Twenty Thousand Leagues under the Sea*. He paid tribute to its creators by citing this diving equipment by the name Rouquayrol–Denayrouze apparatus.

The transition zone between warm surface waters and cold water deep (between 200 and 1000 m) in which the temperature varies most is called the **permanent thermocline**. In the mid and high latitudes, the surface water warming in spring and summer creates a seasonal thermocline that is later destroyed by the winter mixing. In the absence of marked seasons, the seasonal thermocline does not exist at lower latitudes. At high latitudes, strong winds and low temperatures result in very thick winter mixed layers (200–400 m). The deepest part of this winter mixed layer is not reheated in summer, so that it keeps its "winter water" characteristics.

Cold water being generally denser than warm waters, the thermocline is also a **pycnocline**, that is, a zone of strong density variation. This stratification makes difficult vertical mixing between water masses with different densities. Indeed, if a volume of water with a given density is raised in lighter waters or brought down in denser waters, buoyancy will tend to return to take it back to its equilibrium depth. When (temporary) dense waters are over lighter water, the situation is unstable and the dense water sinks. This is convection.

The stable ocean stratification therefore strongly opposes the "vertical" motion of water masses (it would be more accurate to speak of diapycnal motion which is perpendicular to isopycnal surfaces, as we will see later that isopycnal surfaces are not necessarily horizontal). On the contrary, flowing along isopycnal surfaces is easy because it does not need to work against the Archimedes (or buoyancy) force. Hence, isopycnal surfaces are surfaces of preferential water motion. On a meridian section of the Atlantic Ocean (Fig. 1.6), there is a strong correspondence between isotherms and isopycnal surfaces within the first 500 m (thermocline).

At the low latitudes, closely spaced isopycnal over the first hundreds of meters highlight a strong thermocline. At high latitudes, on the contrary, density hardly varies with depth (surface waters are already cold and dense) and the stratification is weak. It is essential to note that the isopycnal surfaces are frequently tilted and that they form an onion skin structure at low and middle latitudes (we will see why later in the chapter). Thus, a volume of water can change depth without difficulty when it moves along an isopycnal surface.

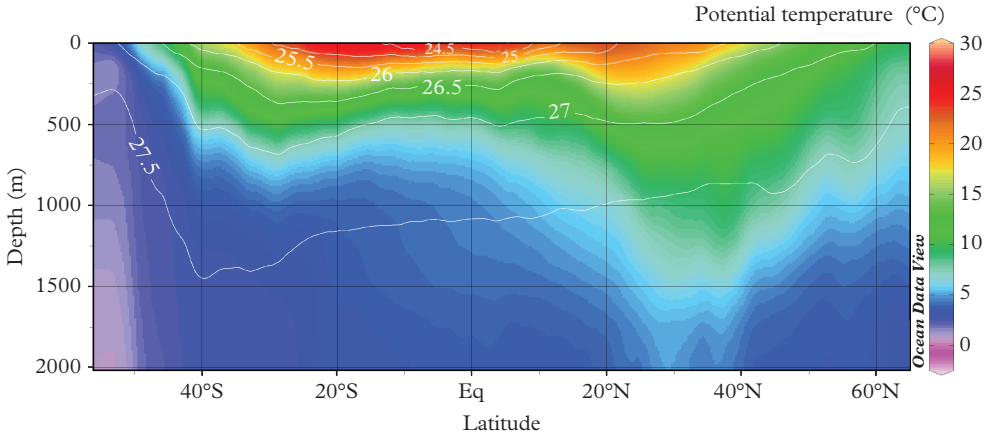

Figure 1.6 *Distribution of temperature (color scale) and of the potential density anomaly (**white contour lines**) on a meridian section of the Atlantic Ocean. The strong discrepancy between temperature and density around 1000 m depth is related to the presence of warm and salty (and therefore relatively dense) MW. The vertical scale is limited to the first 2000 m. Figure drawn with Ocean Data View from the e-WOCE database: http://odv.awi.de/.*

1.4 The Main Water Masses

In oceanography, temperature and salinity are the ID card of seawater. We saw earlier how to change seawater salinity at the ocean surface. Similarly, seawater temperature can be modified at the ocean surface by contact with air, by evaporation, or by radiation (heating by absorption of solar light or infrared, cooling by infrared emission). A seawater mass outcropping at the ocean surface can therefore change its physical properties. On the other hand, at depth, there are no direct exchanges with the atmosphere: potential temperature and salinity can no longer be changed by the processes cited above. Then, potential temperature and salinity can be modified only by mixing with seawater having different potential temperatures and salinities. Potential temperature and salinity are called **conservative tracers**.

Potential temperature and salinity are used to define **water masses** that have acquired given salinity and temperature characteristics and that keep these characteristics at depth unless they are modified by mixing with another water mass having different characteristics (Figs. 1.7–1.8 and Table 1.2). Conservative tracers are used to determine the origin of the water masses: for example, in the deep Atlantic (Fig. 1.7), the thick layer of salty and cold water, which occupies the 2–4 km depth range from the north to the south of the Atlantic is the North Atlantic Deep Water (NADW). Two water layers come from the south and are characterized by their low salinities: the Antarctic Intermediate Water (AAIW) is centered around 900 m; the Antarctic Bottom Water (AABW) flows at the bottom. MW bubbles occurring at 1000 m depth can be identified by their high salinity

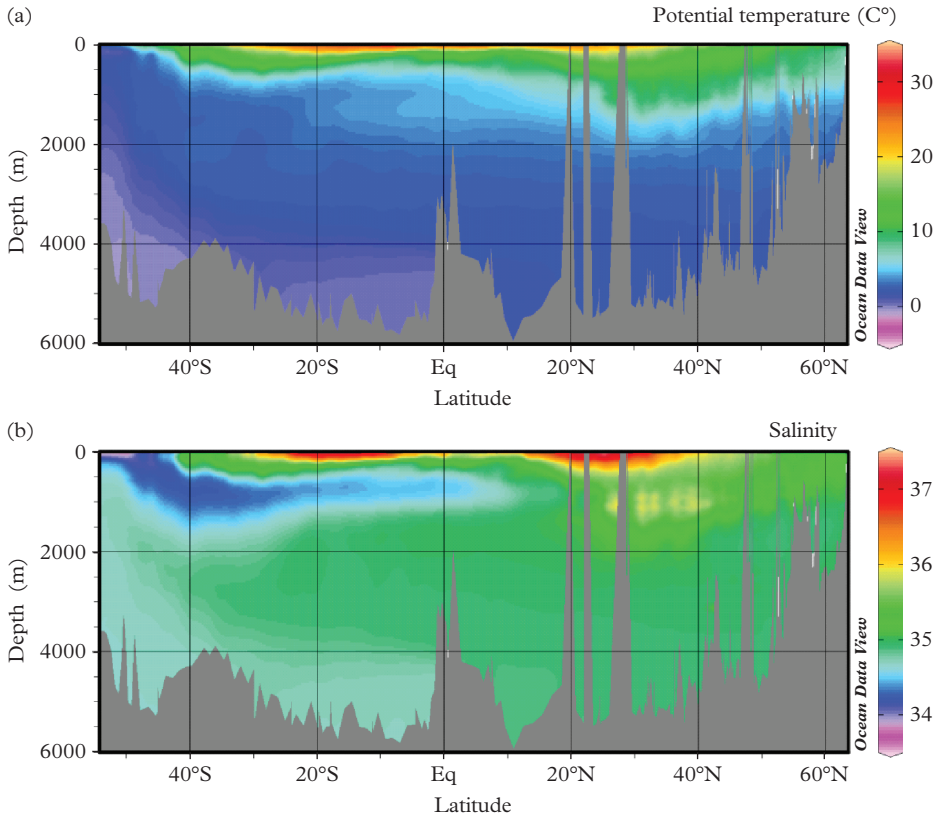

Figure 1.7 *North–south hydrographic section of the Atlantic Ocean. (a) Potential temperature; (b) Salinity. The topography is shown in dark gray. Figures drawn with Ocean Data View from the e-WOCE database: http://odv.AWI.de/.*

and high temperature (see Problem 2). In the Southern Ocean, the NADW gradually changes during its trip around Antarctica. It gradually mixes with the AAIW and AABW to produce the Circumpolar Deep Water (CDW). This water formed in the Southern Ocean "blender" spreads in the deep Pacific Ocean and the deep Indian Ocean. A comprehensive presentation of the water masses and their trajectories is available in the book by Tomczak and Godfrey (2003).

Let's consider the mixing of two water masses "1" and "2" of mass m_1 and m_2, of salinity S_1 and S_2 and of potential temperature θ_1 and θ_2. Here, the potential temperature (θ_m) and salinity (S_m) of the mixture are given by

$$\theta_m = f\theta_1 + (1-f)\theta_2, \tag{1.1a}$$

$$S_m = fS_1 + (1-f)S_2, \tag{1.1b}$$

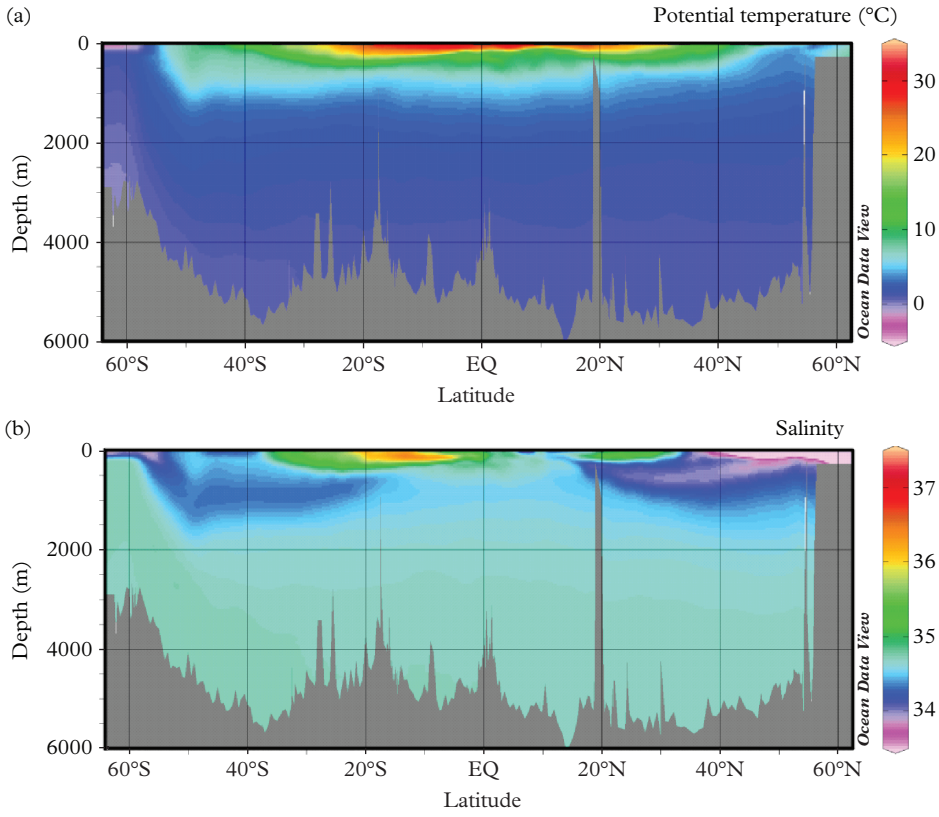

Figure 1.8 *N–S hydrographic section of the Pacific Ocean. (a) Potential temperature; (b) Salinity. Deep waters have very homogeneous temperature and salinity because there is only one deep water source in the south (CDW). Figures drawn with Ocean Data View from the e-WOCE database: http://odv.awi.de/.*

Table 1.2 *Potential temperature and salinity characteristics of the main water masses*

Water Mass	$\theta(°C)$	**S**
North Atlantic Deep Water (NADW)	2.4	34.9
Antarctic Intermediate Water (AAIW)	4	34.4
Antarctic Bottom Water (AABW)	0.2	34.7
Mediterranean Water (MW)	13	38.8
Circumpolar Deep Water (CDW)	1.45	34.7

where $f = m_1/(m_1+m_2)$ and $1-f = m_2/(m_1+m_2)$ are the mass fractions of water masses 1 and 2 in the mixture. There is a linear relationship between θ and S. Therefore samples aligned along a straight segment in a θ–S diagram indicate that they are produced by the mixing of two water masses. θ or S are used to determine the mixing proportions of the two water masses in the intermediate samples

$$f = (\theta_m - \theta_2)/(\theta_1 - \theta_2), \tag{1.2a}$$

$$f = (S_m - S_2)/(S_1 - S_2). \tag{1.2b}$$

Application exercise: water masses mixing

In the North Atlantic, water around 1000 m depth is the result of mixing between waters of Mediterranean origin and waters from the Labrador Sea. A sample collected at 1000 m depth has a salinity of 35.8. Estimate the proportion of MW and Labrador Sea water of the in this sample. Labrador Sea water has a salinity of 34.9.

Answer:

MW salinity is 38.8 (Table 1.2).

The mass fraction of MW in the sample is

$$f = (S_s - S_{\text{Labrador}})/(S_{\text{Mediterranean}} - S_{\text{Labrador}})$$
$$= 23\%.$$

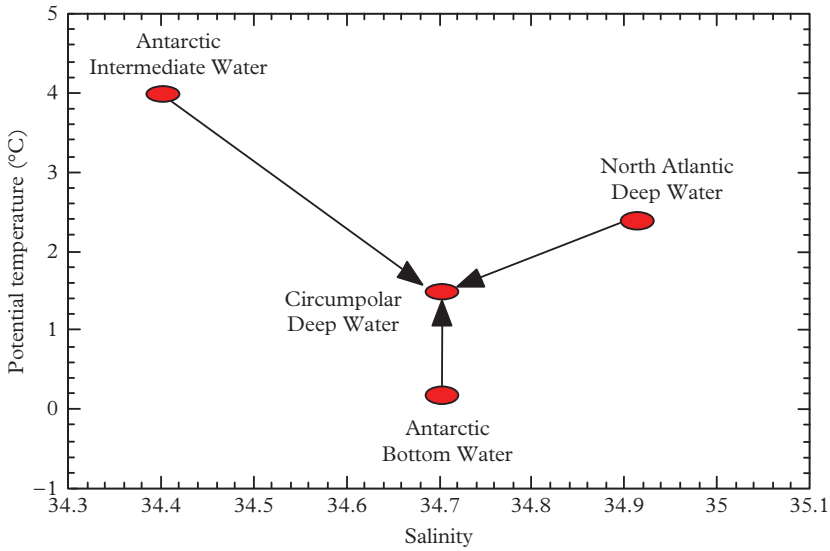

Figure 1.9 *Mixing of three water masses in a potential temperature–salinity diagram. The proportions of NADW, AAIW and AABW can be calculated with the lever rule.*

With one conservative tracer, we can determine the mixing proportions for two water masses. In order to determine the mixing fraction for the mixing of three water masses, two conservative tracers are required (Fig. 1.9) and for mixing of n water masses, $n-1$ conservative tracers are necessary. Hence, temperature and salinity are not sufficient to study complex mixings. This is why oceanographers use non-conservative tracers (oxygen, phosphate) that they combine to create conservative tracers. To do so, it is necessary to have some insight on biological activity as it strongly controls the behavior of these elements (see Chapter 2).

1.5 Ocean Currents

Water masses are constantly in motion: this is the ocean circulation. Large-scale movements of water masses are due to different phenomena:

- The wind drags surface waters, inducing surface currents.
- These surface currents, but also precipitation and evaporation, create "hills" and "valleys" at the ocean surface that induce pressure changes that generate currents over depths of hundreds or even thousands of meters.
- Density gradients due to differences in temperature and salinity may also cause horizontal and vertical water masses motions.
- Tidal currents, which are due to the gravitational fields of the Moon and the Sun. We will see in Chapter 10 that tides play an important role for the deep ocean mixing. The principle of the tides is not detailed here (the reader may refer to Stewart, 2004).

1.5.1 Surface Circulation

Figure 1.10 shows a map of surface currents. Most of these currents affect the first 1000 m of the ocean (we will see how, later in this chapter). Surface **circulation** is organized in large loops called **gyres**. Between 20° and 40°, anticyclonic subtropical gyres rotate clockwise in the northern hemisphere and counterclockwise in the southern hemisphere. These gyres are marked by intense currents on the western boundary of the basin: Gulf Stream and Brazil current in the Atlantic Ocean, Kuroshio in the North Pacific Ocean and Agulhas current in the southern Indian Ocean. At intermediate latitudes, currents leave the western boundary to cross the basins toward the east and the pole (e.g., North-Atlantic drift). Between 40 and 60°N, cyclonic subpolar gyres rotate counterclockwise in the northern hemisphere (and clockwise in the southern hemisphere). They are also marked by intense western boundary currents (like the Labrador Current in the North Atlantic and Oyashio in the Pacific). In the absence of continental mass around the Austral Ocean, the Circumpolar Current flows without interruption. Around the Equator, North and South Equatorial Currents (that can be seen as the westward branch of the subtropical gyres) flank the Equatorial Counter Current.

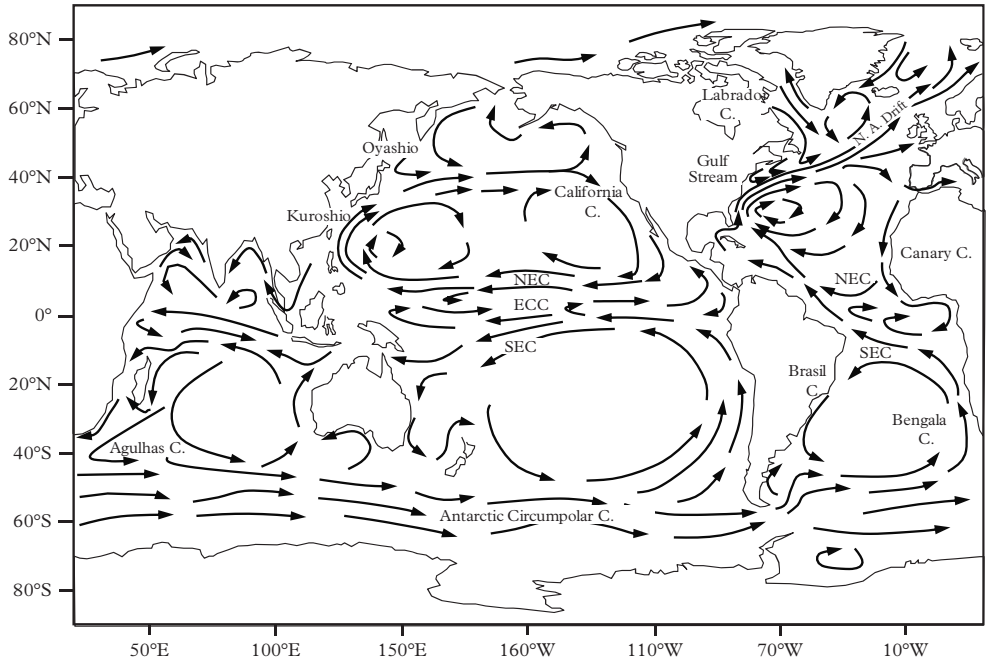

Figure 1.10 *Map of the surface currents. C: current; NEC: North Equatorial Current; SEC: South Equatorial Current; ECC: Equatorial Counter Current.*

In the fastest surface currents, speed can be as high as 1 m s^{-1}. These currents carry huge amounts of water. Current flux is expressed in millions of m^3 s^{-1} (Sverdrup: 1 Sv = 10^6 m^3 s^{-1}). To give an order of magnitude, the total water flux of rivers to the ocean is 1 Sv and all of the rain over the ocean represents 10 Sv. The Gulf Stream varies from 30 Sv in the Florida Strait to 90 Sv at 40°N. The Antarctic Circumpolar Current (ACC), which is the most powerful of the world, carries 130 Sv on average.

The Gulf Stream

The Old Man and the Sea, the last novel of Hemingway published during his lifetime, tells the battle of an old Cuban fisherman struggling with a huge swordfish between Cuba and Florida, on the edge of the Gulf Stream whose power in this area reinforces the danger and therefore the intensity of the story. This current has fascinated Europeans: it takes its name from its origin in the very warm Gulf of the Mexico, and carries such an amount of heat across the Atlantic, that it partly explains the mild climate of Europe up to the North of Norway (the Norwegian coast is never taken by the ice …) compared to the harsh climates in Greenland and Canada, yet at the same latitudes.

Noticed for the first time in 1513 by the Spanish navigator, Ponce de Leon, who found that off the coast of Florida his ships were constantly swept away by a warm current coming from the Caribbean Sea, this discovery was forgotten for more than 250 y. It is only after the work of Benjamin Franklin, consisting in a series of temperature measurements across the ocean, thus delimiting the boundaries of the current, that the existence of the Gulf Stream was officially recognized. He later established a hydrographic chart of this current, to indicate to sailors how to use it in their navigation. In 1849, Lieutenant Matthew Maury of the US Navy scientifically confirmed the theory of Benjamin Franklin. He established that at the exit of the Florida Strait, the Gulf Stream was 1000 m thick, 80 km wide and moving at the speed of 6–8 nautical miles per hour ... many early results which were confirmed later.

1.5.2 The Physical Principles

Here we describe the motion of water masses by applying the fundamental principle of dynamics (sum of forces = mass × acceleration). As we are mainly interested in permanent ocean circulation on a large scale (of the order of 1000 km or more), some simplifying assumptions are used: we consider motion in a mathematical plane tangent to the Earth (see box "The tangent plane") and we assume that the currents do not vary over time and that their spatial variations occurs over large distances. With these conditions fulfilled, equations (1.3a), (1.3b) and (1.3c) describe the motion of water.

The tangent plane

To simplify the geometry (which is justified for length scales less than or equal to 1000 km), the Ocean's surface is treated as its tangent plane (Fig. 1.11).

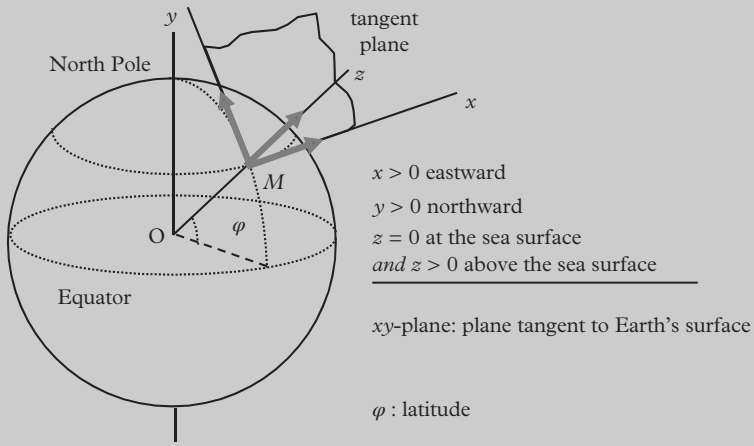

Figure 1.11 *The tangent plane.*

The position of a point M is given by its coordinates $M\begin{pmatrix} x \\ y \\ z \end{pmatrix}$ in a Cartesian coordinate system linked to the Earth. The vector $\vec{u}$ represents the speed of the water $\vec{u} = \begin{pmatrix} u \\ v \\ w \end{pmatrix}$.

Coriolis — pressure — friction

$$-fv = -\frac{1}{\rho}\frac{\partial P}{\partial x} + \frac{1}{\rho}\frac{\partial \tau_x}{\partial z}, \tag{1.3a}$$

$$+fu = -\frac{1}{\rho}\frac{\partial P}{\partial y} + \frac{1}{\rho}\frac{\partial \tau_y}{\partial z}, \tag{1.3b}$$

$$g = -\frac{1}{\rho}\frac{\partial P}{\partial z}. \tag{1.3c}$$

gravity — pressure

Three terms are important to describe the horizontal currents (equation (1.3)):

(1) The Coriolis force is due to the rotation of the Earth around its axis (see box "The Earth's rotation effects"). The Coriolis force depends on the Coriolis parameter "f",

$$f = 2\Omega \sin \varphi, \tag{1.4}$$

where Ω is the angular velocity of rotation of the Earth and φ is the latitude, and on the speed of the current. It is important to note that the east–west component of the Coriolis force ($-fv$) depends on the north–south component of the velocity (v) while the north–south component of the Coriolis force (fu) depends on the east–west component of the velocity (u).

(2) The forces related to horizontal change of pressure. Pressure (P) at a given depth (z) varies from one point of the ocean to another with the structure of overlying water masses. It produces horizontal pressure gradients ($\partial P/\partial x$ and $\partial P/\partial y$)

(3) The horizontal friction forces between the different ocean layers and at the ocean–atmosphere boundary. A moving volume of water tends to be slowed by friction forces against the surrounding waters (also called shear and noted τ). This is the case of surface waters dragged by the wind and that rub on deeper water layers. It creates vertical variations of friction forces ($\partial \tau/\partial z$).

(4) In the vertical direction, the acceleration of gravity is balanced by the increase of pressure (hydrostatic equilibrium).

The effects of Earth's rotation

The Earth's rotation around its axis has significant consequences for large-scale movements of air and water masses.

The Coriolis force

The Coriolis force represents the acceleration due to the rotation of the Earth around its axis in a fixed Cartesian reference frame with no motion relative to distant stars. The earth rotates on itself in 24 h, which corresponds to an angular speed $\Omega = 2\pi/(24 \times 60 \times 60) = 7.27 \times 10^{-5}$ s^{-1}. Thus, any motionless object on the Earth's surface has a tangential eastward speed due to Earth's rotation. This speed is maximum at the Equator where an object covers 40,000 km (the circumference of the Earth) in 24 h or $v = 463$ m s^{-1}. Toward the poles, parallels describe much smaller circles in 24 h, so that the tangential velocity decreases. On the pole of rotation, the distance traveled in 24 h being zero, the tangential speed is also zero.

Consider that Peter (P) located at the North Pole and Esther (E) located at the Equator want to play ball (Fig. 1.12). Esther threw the ball to Peter giving it a northward speed v_1. However, at the Equator, the ball also has an eastward tangential speed of 463 m s^{-1} due to the Earth's rotation. As the ball does not rub on the Earth's surface, it retains this tangential component moving northward over regions animated by lower tangential speeds. For someone on Earth observing the scene, the ball motion seems deflected eastward. Finally, the ball will not reach Peter and its movement appears to be deflected to the right. The Coriolis "force" thus seems to deflect the motion of large amplitude. In fact, this is not a real force.

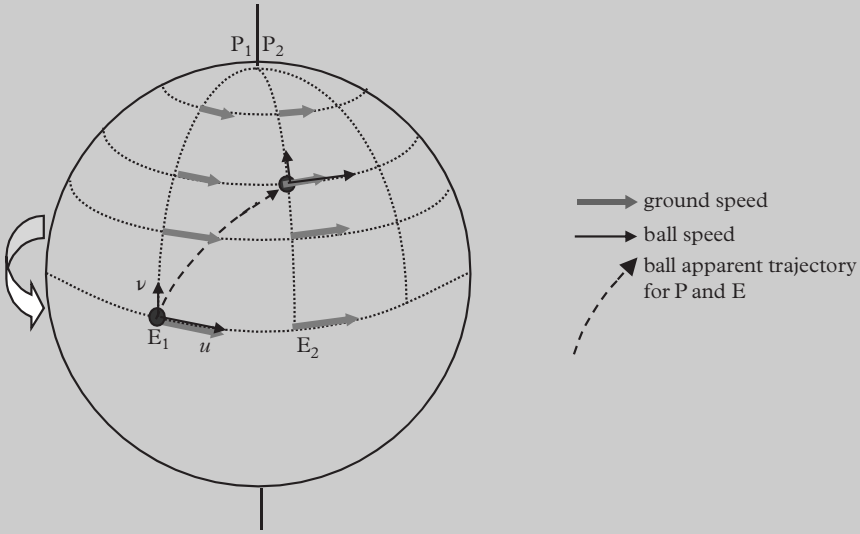

Figure 1.12 *Rotation of the Earth and Coriolis force.*

It is just an apparent deviation of air and water masse path for an observer on Earth who ignores that Earth rotates around its axis (as opposed to an observer looking at the Earth from space, and who sees the Earth's rotation).

The reader will check that the deviation is also to the right if Peter sends the ball from the North Pole. He will also check that the deviation is to the left of the movement in the southern hemisphere. How must Peter and Esther be placed to avoid the Coriolis force? If both of them are close to the Equator, their distance from the axis of the Earth hardly varies so the Coriolis force is low (it is maximum at the poles and zero at the Equator).

The Coriolis force is always perpendicular to the velocity: a current that flows northward in the northern hemisphere is deviated eastward by the Coriolis force, a current that flows eastward in the northern hemisphere is deviated southward by the Coriolis force.

1.5.3 The Wind-Driven Ocean Circulation

The wind blowing on the sea surface creates a friction force on the water called "wind stress" (τ, expressed in N m^{-2}) which is given by the empirical relationship

$$\tau = \rho_a k U_a^2, \tag{1.5}$$

where ρ_a is the air density (= 1.3 kg m^{-3}), k is a dimensionless coefficient of friction ($k = 1.3 \times 10^{-3}$) and U_a is the horizontal component of the wind speed measured at 10 m above the sea level. This wind stress on the surface water induces a surface current. The speed of this current is about 100 times lower than the wind speed.

Winds (annual average) at the surface of the ocean are represented in Fig. 1.13. Note here that the wind distribution is mainly zonal (with large north–south variations and little variation east–west) with the trade winds on both sides of the Equator, the westerlies (coming from the west and blowing eastward) that dominate at mid-latitudes (as in France) and easterlies (coming from the east and blowing westward) at high latitudes. A brief explanation of the distribution of this circulation is given in Appendix 1.

There are striking correspondences between the maps of winds and surface currents. In the North Atlantic for example, the Iceland depression corresponds to the Subpolar gyre and the Azores anticyclone corresponds to the Subtropical gyre (whose western branch is the Gulf Stream). In the Southern Ocean, westward winds (roaring forties, screaming fifties) correspond to the ACC. At lower latitudes, there is a correspondence between the trade winds and the North and South Equatorial Currents. A notable exception is the Equatorial Counter Current that moves in the opposite direction of the trade winds.

However, the current is usually not parallel to the wind. While exploring of the Arctic Ocean on board the Fram, Nansen noticed that during the ice-pack break-up, ice floes do not drift along the wind direction but at 45° to the right of the wind. Indeed, the surface current is deflected to the right (resp. left) in the northern hemisphere (resp. southern)

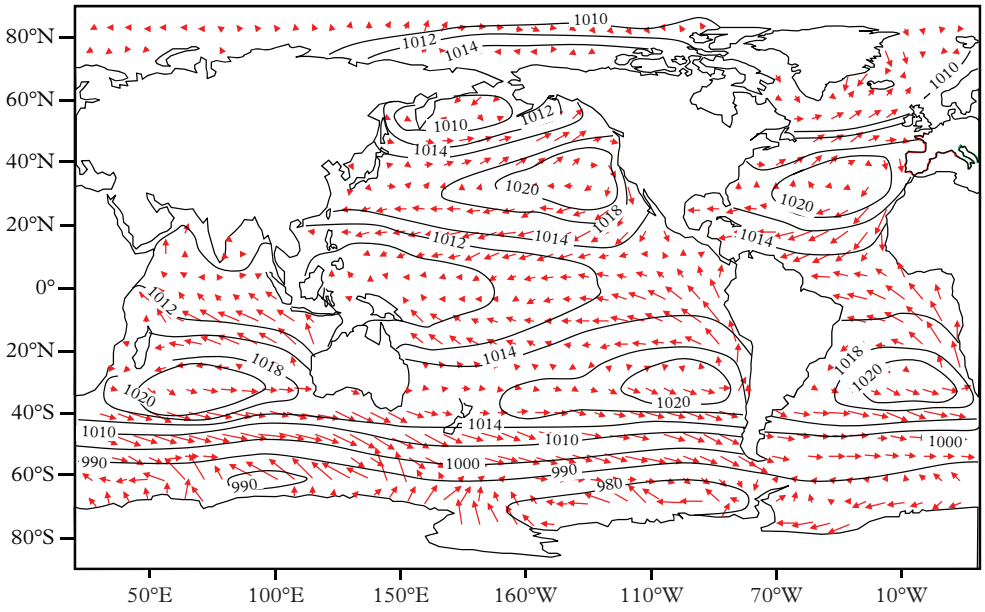

Figure 1.13 *Annual mean wind and atmospheric pressure (hPa) at the surface of the ocean. Modified from Stewart (2004).*

by the Coriolis force. Due to the friction of the surface water with the underlying water layer, the deviation from the wind direction is not 90° but approximately 45°. In turn, the surface layer drags the underlying layer, which is deviated by 45° to the right … As the current due to the wind spreads in depth, its direction changes and its intensity decreases rapidly: the speed vector describes a spiral called "Ekman spiral" (Fig. 1.14).

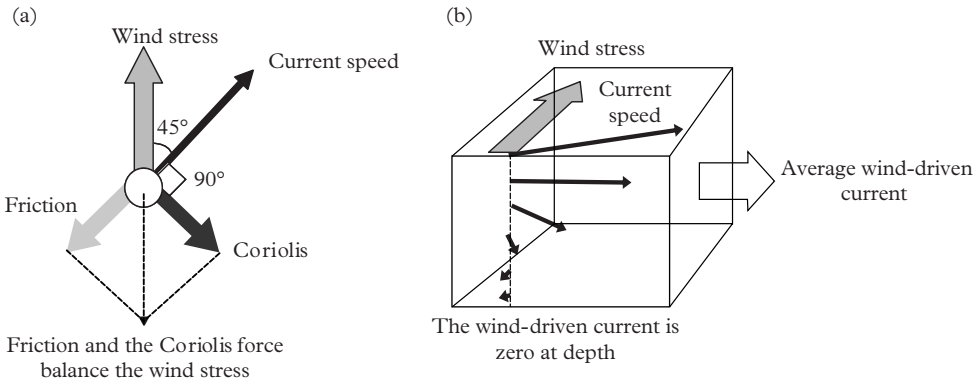

Figure 1.14 *Principle of the Ekman spiral. (a) Balance of forces at the ocean surface (top view). (b) Current propagation to depth in a seabird's eye view (after Open University, 1989).*

The effect of the wind is significant over an ~50 m thick layer: this is the **Ekman layer** (its depth is generally different from the mixed layer depth). At the base of the Ekman layer, the water velocity due to the wind is zero: the Ekman layer moves without friction on underlying water (friction is proportional to the current speed: if there is no current, there is no friction). It is submitted to the wind stress and the Coriolis force only, so that the average current speed is perpendicular to the wind (Fig. 1.14; see Problem 3).

Relationship between wind stress and current

To specifically assess the direct effect of the wind on the surface current, we neglect the effect of horizontal pressure gradients in equations (1.3a) and (1.3b). The equations are reduced to

$$\begin{cases} -fv = +\dfrac{1}{\rho}\dfrac{\partial \tau_x}{\partial z}, & \text{(1.6a)} \\ +fu = +\dfrac{1}{\rho}\dfrac{\partial \tau_y}{\partial z}. & \text{(1.6b)} \end{cases}$$

The Coriolis force balances the shear forces gradient. We want to determine the current created by the friction forces in the Ekman layer. The **transport** in the Ekman layer is calculated by integrating equations (1.6a) and (1.6b) between the base and the top (the ocean surface) of the Ekman layer

$$\begin{cases} V_E = \int_{\text{base}}^{\text{surf}} v \, dz = -\dfrac{1}{\rho f}\int_{base}^{\text{surf}} \dfrac{\partial \tau_x}{\partial z} dz = -\dfrac{1}{\rho f}\left(\tau_x^{\text{surf}} - \tau_x^{\text{base}}\right), & \text{(1.7a)} \\ U_E = \int_{\text{base}}^{\text{surf}} u \, dz = \dfrac{1}{\rho f}\int_{\text{base}}^{\text{surf}} \dfrac{\partial \tau_y}{\partial z} dz = +\dfrac{1}{\rho f}\left(\tau_y^{\text{surf}} - \tau_y^{\text{base}}\right). & \text{(1.7b)} \end{cases}$$

At the base of the Ekman layer, the current speed due to the wind is zero and therefore friction forces are zero $\left(\tau_x^{\text{base}} = \tau_y^{\text{base}} = 0\right)$, so that

$$\begin{cases} V_E = -\dfrac{\tau_x^{\text{surf}}}{\rho f}, & \text{(1.8a)} \\ U_E = +\dfrac{\tau_y^{\text{surf}}}{\rho f}. & \text{(1.8b)} \end{cases}$$

The transport of a current is defined as the water flux per unit of length perpendicular to the current. Transport simply represents the flow of the current divided by its width. It is expressed in $m^2\ s^{-1}$. This is not a common unit compared to the $m\ s^{-1}$ used for speed. The total current flow (expressed in $m^3\ s^{-1}$ or in Sv) is obtained by multiplying

the transport by the current width. Ekman transport is directly linked to the intensity of the wind stress (see box "Relationship between wind stress and current")

$$\begin{cases} V_{\mathrm{E}} = -\dfrac{\tau_x^{\mathrm{surf}}}{\rho f}, & \text{(1.8a)} \\ U_{\mathrm{E}} = +\dfrac{\tau_y^{\mathrm{surf}}}{\rho f}. & \text{(1.8b)} \end{cases}$$

Note that in the northern hemisphere ($f > 0$), northward wind ($\tau_y^{\mathrm{surf}} > 0$) produces an eastward water transport ($U_E > 0$). Similarly, an eastward wind ($\tau_x^{\mathrm{surf}} > 0$) produces a southward water transport ($V_E < 0$). Current is therefore deviated to the right of the wind in the northern hemisphere. In the Southern hemisphere ($f < 0$), water transport is at 90° to the left of the wind.

1.5.4 Ekman Pumping

In the subtropical gyres, the anticyclonic wind circulation creates a net water transport toward the center of the gyre (Fig. 1.15). This creates a pilling-up of water that results in a "hill" above the level of the sea at rest (i.e., in the absence of wind, evaporation, precipitation ... also known as the geoid). Conversely, in cyclonic gyres, the net water transport forced by the wind is outward from the gyre: water flows away from the center of the gyre producing a "valley" compared to the level of the sea at rest. Similarly, in the equatorial zone, the trade winds produce a northward water flow north of the Equator and a southward flow south of the Equator. There is divergence of water at the Equator and formation of a depression of the sea level. These "bumps and dips" or "hills and

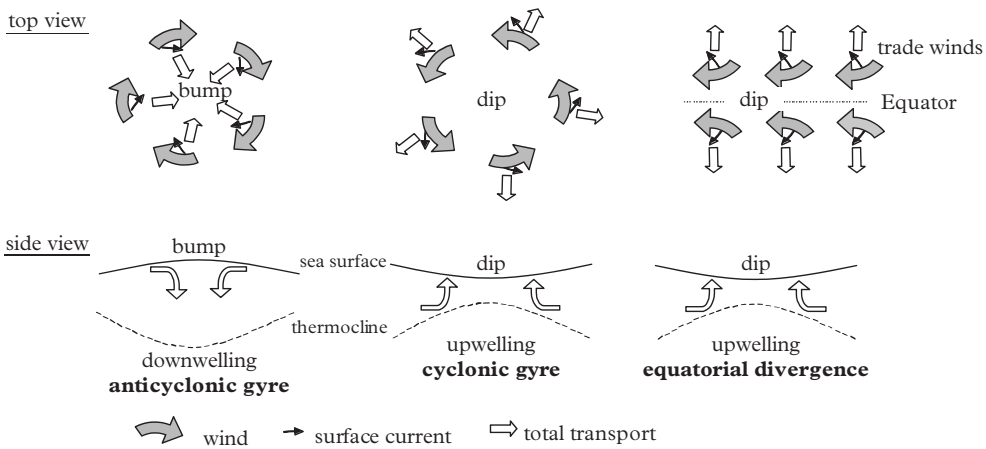

Figure 1.15 *Relationship between the wind and the surface currents. Modified from Open University (1989).*

valleys" are called the **dynamic height** of the ocean. They correspond to up to 1–2 m height difference compared to the level of the sea at rest. The ocean is not as flat as its reputation would suggest: in the center of the subtropical Atlantic, the dynamic height of the water is approximately 1.40 m higher than along the North American coast, off the coast of New York. If these heights seem modest, they have a critical impact on deep circulation: indeed, the water piled up in the center of the subtropical gyres cannot accumulate there forever. This water must escape downward, thereby generating deeper currents.

The horizontal convergence or divergence of water induces a vertical motion called "**Ekman pumping**." The water that accumulates in the anticyclonic gyres is pushed toward deeper layers, creating a downwelling (Ekman pumping is directed downward) resulting in a deepening of the thermocline. Instead, in areas of water divergence, water tends to rise to fill the "valley," creating an upwelling (Ekman pumping is directed upward), resulting in a rise of the thermocline. Changes of the thermocline level are easily seen on hydrographic sections (Figs. 1.7 and 1.8). The largest deepening of the thermocline is located in the subtropical latitudes at the vertical of the anticyclonic gyres. The thermocline is shallowest at the Equator and in subpolar gyres in the areas of current divergence. The upwelling of cold deep waters in the equatorial zone produces a minimum of temperature in the eastern equatorial Pacific and Atlantic (Fig. 1.3). The changes of the thermocline depth balance at depth the pressure variations induced by the hills and depressions of the ocean surface (see geostrophic current section). As the density difference between air and water is much higher than the density difference between the warm surface water and cold deep water, the depth of the thermocline varies much more (hundreds of meters) than the sea level (1 m).

We will see in Chapter 7 that Ekman pumping is fundamental to biological activity because it controls the nutrient inputs in surface waters.

The curl

The term $\frac{\partial_y()}{\partial x} - \frac{\partial_x()}{\partial y}$ is called the curl (specifically its vertical component). Curl quantifies the tendency of a flow to rotate in the horizontal plane. It can be interpreted as twice the angular velocity of a small turbine that wind or current would rotate around a vertical axis. In the northern hemisphere, a positive curl of the current causes the counter clockwise rotation of the turbine. On the contrary, a negative curl causes a clockwise rotation of the turbine. When the curl is zero, the turbine does not spin. The current does not have to describe a loop to have a significant curl. Figure 1.16 shows a wind with an eastward component that changes with the latitude and with no north–south component ($\partial v/\partial x = 0$). In case 1, the wind speed decreases northward ($\partial u/\partial y < 0$ because the wind speed is positive when the wind blows eastward): its curl ($\partial v/\partial x - \partial u/\partial y$) is positive and the turbine rotates counterclockwise. On the contrary in case 3, the wind speed (always counted positive eastward) increases northward ($\partial u/\partial y > 0$): its curl is negative. In case 2, the speed is constant with latitude: the wind curl is zero.

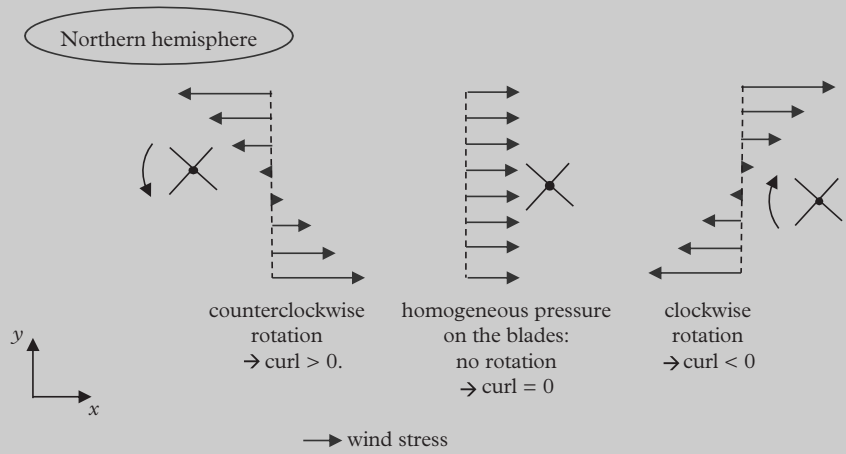

Figure 1.16 *Curl of the wind stress.*

In the case of gyres (Fig. 1.15), it is easy to understand that the rotating motion of the wind causes the convergence or divergence of the water. However, it is not necessary that the wind changes direction to produce a curl. It is sufficient that its intensity varies.

Let's consider the case of zonal easterly winds (Fig. 1.17). The wind has a zonal distribution. In zone 1, the wind intensity is lower in the South compared to the North (this is typically the case of the trade winds north of the Equator). It induces a positive curl (see box on the curl). As the trade wind intensity increases northward, the Ekman drift is stronger in the North than in the South. The water transported northward out of zone 1 by the Ekman drift is not balanced by the Ekman drift from the South of zone 1; therefore there is an upwelling of deep water (upward Ekman pumping). In zone 2, the intensity of the wind is constant with latitude, so that the wind curl is equal to zero. The water transported by the Ekman drift from the South is evacuated to the North. Therefore, there is no Ekman pumping. Finally, in zone 3, the intensity of the trade winds decreases northward, so that the wind curl is negative and water coming from the South cannot be evacuated in the North: it must sink and Ekman pumping is directed downward. It is thus the curl of wind that induces a horizontal divergence of water which must be balanced by a vertical flow of water (Ekman pumping).

The vertical velocity at the base of the Ekman layer is given by (see box "Ekman pumping")

$$\boxed{w^{\text{base}} = \text{curl}\left(\frac{\tau^{\text{surf}}}{\rho f}\right).} \tag{1.9}$$

At the scale of a gyre (~1000 km), f hardly varies, so that the vertical speed depends strongly of the wind stress curl. A positive wind curl (counterclockwise rotation) causes an upwelling of deep water at the base of the Ekman layer. On the contrary, a negative

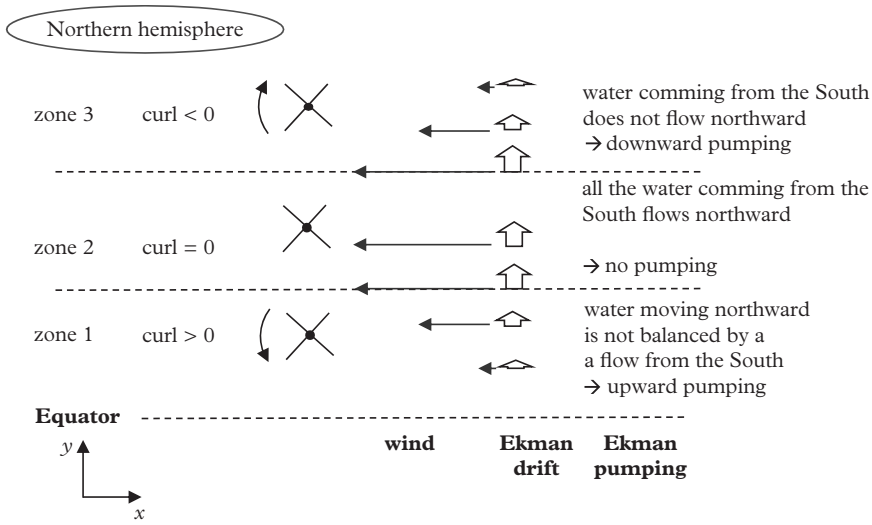

Figure 1.17 *Relationship between the wind curl and Ekman pumping.*

wind curl (clockwise rotation) leads to downwelling of surface water at the base of the Ekman layer. Equation (1.9) is extremely important in marine geochemistry because Ekman pumping largely determines the nutrient supply to the surface water by the upwelling of deep water. In particular, Ekman pumping depends of the meridian wind stress variation (Fig. 1.18; see Problem 4).

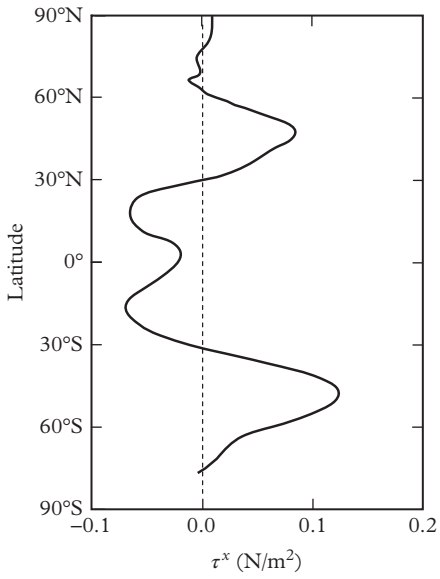

Figure 1.18 *Zonal average of the wind stress on the ocean surface. Modified from Hellerman and Rosenstein (1983).*

Ekman pumping

Water is an incompressible fluid: all the water that enters a fixed volume must be balanced by water that comes out. Mathematically, it is equivalent to

$$\frac{\partial u}{\partial x} + \frac{\partial v}{\partial y} + \frac{\partial w}{\partial z} = 0. \tag{1.10}$$

By integrating this equation between the base of the Ekman layer and the ocean surface, we obtain

$$\int_{\text{base}}^{\text{surf}} \left(\frac{\partial u}{\partial x} + \frac{\partial v}{\partial y} \right) \mathrm{d}z = - \int_{\text{base}}^{\text{surf}} \left(\frac{\partial w}{\partial z} \right) \mathrm{d}z \tag{1.11}$$

so that the components of Ekman transport (equations 1.7a and 1.7b) appear in the left member of the equation,

$$\left(\frac{\partial U_{\mathrm{E}}}{\partial x} + \frac{\partial V_{\mathrm{E}}}{\partial y} \right) = - \left(w^{\text{surf}} - w^{\text{base}} \right). \tag{1.12}$$

Noting that the water vertical velocity must be zero at the surface of the ocean ($w^{surf} = 0$) and replacing U_E and V_E by their expressions in equations (1.8a) and (1.8b), we obtain the vertical speed of the water at the base of the Ekman layer

$$w^{\text{base}} = \left(\frac{\partial \left(\tau_y^{\text{surf}} / \rho f \right)}{\partial x} - \frac{\partial \left(\tau_x^{\text{surf}} / \rho f \right)}{\partial y} \right), \tag{1.13}$$

which can be written as

$$w^{\text{base}} = \text{curl} \left(\frac{\tau^{\text{surf}}}{\rho f} \right),$$

where curl ( ) is the curl operator.

1.5.5 Coastal Upwelling

There are situations where Ekman pumping may be induced without a negative wind curl. Along the Western boundary of continents, relatively cold surface waters outcrop in the subtropical latitudes. This is the case along the coasts of Mauritania, Namibia, etc. (see Fig. 1.3).

For example, on the Mauritanian coast, the wind has a mean north–south direction parallel to the coast (Fig. 1.19). Therefore, the surface current is directed to the

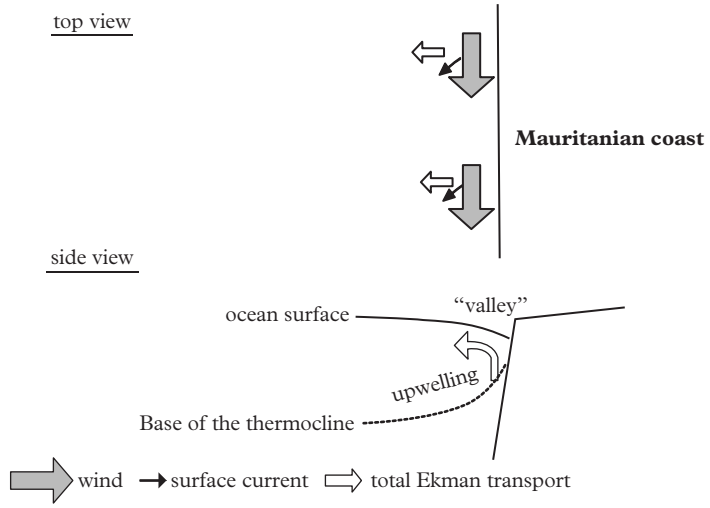

Figure 1.19 *Principle of the upwelling of deep water along the Mauritanian coast. Modified from Open University (1989).*

southwest and Ekman transport is westward, toward the open ocean. The African continent prevents an inflow of water from the east by the Ekman transport. Thus, there is a depression at the sea surface. The westward surface current is balanced by an upwelling of thermocline waters. Therefore, relatively cold waters are found at the surface. The case of the California upwelling is studied in Problem 5 using different tools presented in this chapter.

1.5.6 Geostrophic Currents

The presence of bumps and dips at the ocean surface causes horizontal pressure gradients: at a given depth the water pressure is stronger under a bump than under a dip. Water is pushed from high pressures to low pressures (Fig. 1.20). But, again, the water motion is deflected by the Coriolis force. Equilibrium is established between the pressure gradient and the Coriolis forces. The current speed must be at 90° (to the right in the northern hemisphere and to the left in the southern hemisphere) of pressure forces, that is, parallel to the line of equal pressure (isobar). This is the **geostrophic balance**.

The bumps and dips at the ocean surface (the dynamic topography) can be measured by satellite altimetry. An altimetric satellite is equipped with radar (also called an altimeter) that measures the return time of an electromagnetic wave emitted from the satellite and which reflects at the ocean surface. This time is used to determine the distance between the satellite and the ocean surface. As the position of the satellite is well known, the dynamic height of the ocean can be precisely deduced. Given the required precision, many corrections must be carried out for the signal propagation in the

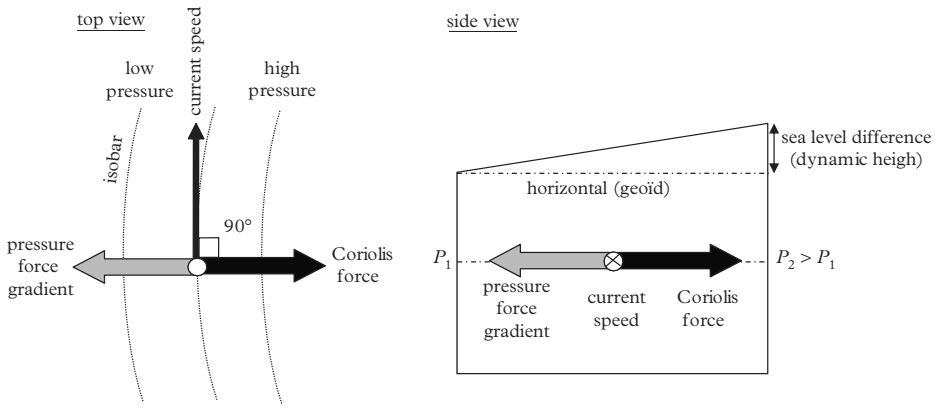

Figure 1.20 *Principle of the geostrophic balance. Modified from Open University (1989).*

atmosphere and for ocean phenomena (such as tides). The difference between the sea level and the level of the geoid (determined regardless of altimetric data) gives the dynamic topography which allows calculating the current speed (Rio et al., 2011). There is an excellent agreement between calculated currents (Fig. 1.21) and the surface current map (Fig. 1.10).

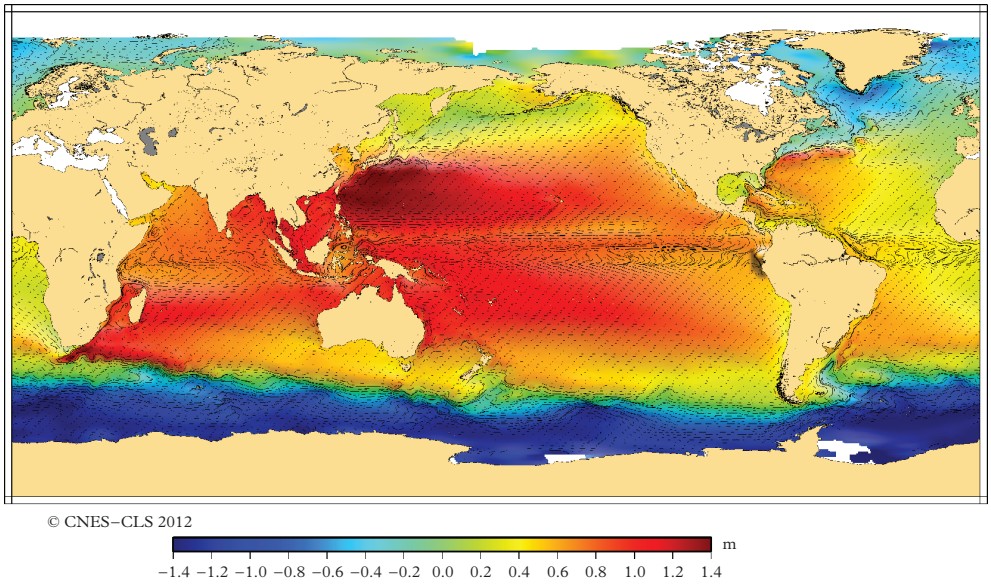

Figure 1.21 *Mean dynamic ocean topography. Black arrows represent the calculated current. Their length is proportional to the current speed. Credits CNES/CLS (http:www.aviso.altimetry.fr; see also Rio et al., 2011).*

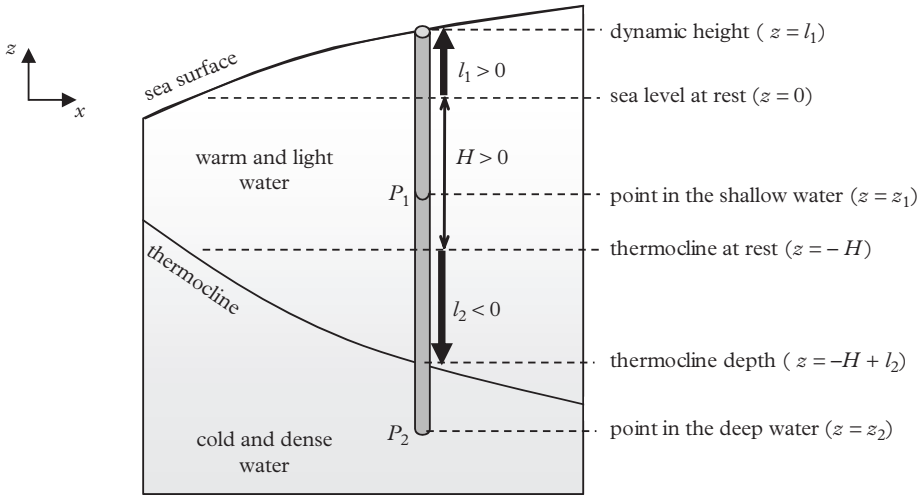

Figure 1.22 *A two-layer ocean. The slope of the sea surface is strongly exaggerated compared to the thermocline.*

Equations (1.3a) and (1.3b) make the link between the dynamic height variations and the current speed. Neglecting the friction terms, we get

$$\begin{cases} -fv = -\dfrac{1}{\rho}\dfrac{\partial P}{\partial x}, & \text{(1.14a)} \\ +fu = -\dfrac{1}{\rho}\dfrac{\partial P}{\partial y}. & \text{(1.14b)} \end{cases}$$

The Coriolis force and the pressure gradient forces are in balance. It appears immediately that the velocity is perpendicular to the pressure gradient. To simplify, we assume in the following that the pressure gradient is in the east–west direction: we will therefore use equation (1.14a) only. To represent the thermocline, we consider an ocean made of two layers: light and warm surface water above the cold, dense deep water (Fig. 1.22). The thermocline is the boundary between these two layers. The variation of the thermocline depth balances at depth the pressure gradient created by the dynamic topography at the surface of the ocean.

Geostrophic velocity in a two-layer ocean

To estimate the speed above and below the thermocline, we consider two points located at depths z_1 and z_2, above and below the thermocline. Remembering that the hydrostatic pressure at the base of a water column of density ρ and height h is $P = \rho gh$, P_1 and P_2 are

$$\begin{cases} P_1 = \rho_1 g\,(l_1 - z_1)\,, & (1.15a) \\ P_2 = \rho_1 g\,(l_1 + H - l_2) + \rho_2 g\,(-z_2 - H + l_2)\,. & (1.15b) \end{cases}$$

Combining equations (1.15a) and (1.15b) with equation (1.14a), we obtain

$$\begin{cases} v_1 = \dfrac{1}{f\rho_1}\rho_1 g \dfrac{\partial l_1}{\partial x}, & (1.16a) \\ v_2 = \dfrac{1}{f\rho_2}\left[\rho_1 g\left(\dfrac{\partial l_1}{\partial x} - \dfrac{\partial l_2}{\partial x}\right) + \rho_2 g \dfrac{\partial l_2}{\partial x}\right], & (1.16b) \end{cases}$$

$$\begin{cases} v_1 = \dfrac{g}{f}\dfrac{\partial l_1}{\partial x}, & (1.17a) \\ v_2 = \dfrac{g}{f}\dfrac{\rho_1}{\rho_2}\dfrac{\partial l_1}{\partial x} + \dfrac{g}{f\rho_2}(\rho_2 - \rho_1)\dfrac{\partial l_2}{\partial x}. & (1.17b) \end{cases}$$

The speed in the surface layer is directly given by the sea surface slope, which is measured by the altimetric satellites. If we assume that the current speed is equal to zero below the thermocline ($v_2 = 0$), then

$$\boxed{\frac{\partial l_1}{\partial x} = -\frac{\partial l_2}{\partial x}\left(\frac{\rho_2 - \rho_1}{\rho_1}\right).} \quad (1.18)$$

Taking for example $\rho_1 = 1025$ kg m^{-3} and $\rho_2 = 1027$ kg m^{-3}, we obtain $\left(\dfrac{\rho_2 - \rho_1}{\rho_1}\right) \approx 2 \times 10^{-3}$. The slope of the sea surface ($\partial l_1/\partial x$) is approximately 500 times lower than the slope of the thermocline ($\partial l_2/\partial x$) and in the opposite direction

$$\boxed{v_1 = -\frac{g}{f}\left(\frac{\rho_2 - \rho_1}{\rho_1}\right)\frac{\partial l_2}{\partial x}.} \quad (1.19)$$

The speed in surface waters, v_1, is then given by the slope of the thermocline which can be obtained by simple hydrographic measurements.

Note finally that in the absence of a thermocline (specifically when the isopycnal surfaces are parallel to the isobars), horizontal pressure gradients spread down to the sea floor and the speed given by equation (1.17a) is constant over the whole water column. This is partly the case in the Southern Ocean where the presence of cold surface waters strongly reduces the density gradient between the surface and deep waters.

Application exercise: the Gulf Stream (Halkin and Rossby, 1985)

Dynamic topography data show that there is about 1 m height difference over 100 km from the east coast of the United States and the center of the North Atlantic Subtropical gyre:

(a) Determine the speed of the surface current based on sea level measurements.

(b) Determine the slope of the thermocline in the high current zone on the hydrographic section made perpendicular to the Gulf Stream near 40°N (Fig. 1.23).

(c) Determine the surface current speed using the slope of the thermocline (assume that the salinity is 35.5).

(d) Compare the results of questions (a) and (c).

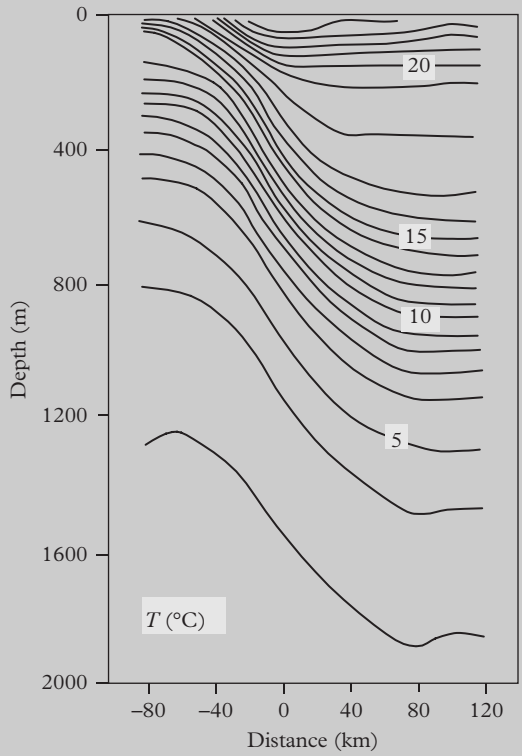

Figure 1.23 *Hydrographic section of the Gulf Stream. Modified from Halkin and Rossby (1985).*

Answers:

(a) Considering that $g = 10$ m s^{-2} and $f = 10^{-4}$ s^{-1},

$$\frac{\partial l_1}{\partial x} = \frac{1 \text{ m}}{100 \text{ km}} = 10^{-5}.$$

With equation (1.17a), we obtain $v_1 = \frac{10}{10^{-4}} \times 10^{-5} = 1$ m s^{-1}.
This is the current velocity in the Gulf Stream.

(b) In Fig. 1.23, from –40 to +40 km around the current maximum, isotherms deepen by about 500 m (e.g., in Fig. 1.23, isotherm 10°C goes from 330 to 800 m deep). The slope of the thermocline is (0.33 – 0.8 km) / 80 km = –0.0058.

(c) To evaluate roughly the density above and below the thermocline, we consider the 400 m depth level (this depth is taken as an example). From –40 to +40 km around the current maximum at 400 m, the temperature goes from 9 to 17°C. This temperature difference corresponds to a density difference of about 0.002 kg m^{-3} (see Fig. 1.4). From equation (1.19), we obtain

$$v_1 = -\frac{g}{f}\left(\frac{\rho_2 - \rho_1}{\rho_1}\right)\frac{\partial l_2}{\partial x} = -\frac{10}{10^{-4}} \times 0.002 \times (-0.0058) = 1.2 \text{ m s}^{-1}.$$

(d) In view of the large approximations, the agreement is satisfactory.

1.6 Large-Scale Circulation

We have seen that the wind creates bumps and depressions at the ocean surface that produce geostrophic currents. Therefore, there must be a relationship of water transport in the upper part of the ocean and the wind forcing. In addition, it is striking that the Subtropical North Atlantic gyre is very asymmetrical (Fig. 1.20) while the wind forcing over the basin is symmetrical (Fig. 1.13). To understand these phenomena that take place over great distances, we must take into account the effect of latitude on the Coriolis force and introduce a new concept: vorticity.

1.6.1 Vorticity

In addition to the translation movements seen previously, an object can rotate around the local vertical axis: it has a vorticity. Mathematically, vorticity is defined as the curl of the velocity. For a rotating solid, it is equal to twice its angular velocity. Vorticity is positive when the rotation is counterclockwise. Due to the Earth's rotation, objects at Earth's surface tend to spin around the local vertical axis (Fig. 1.24). It is the **planetary**

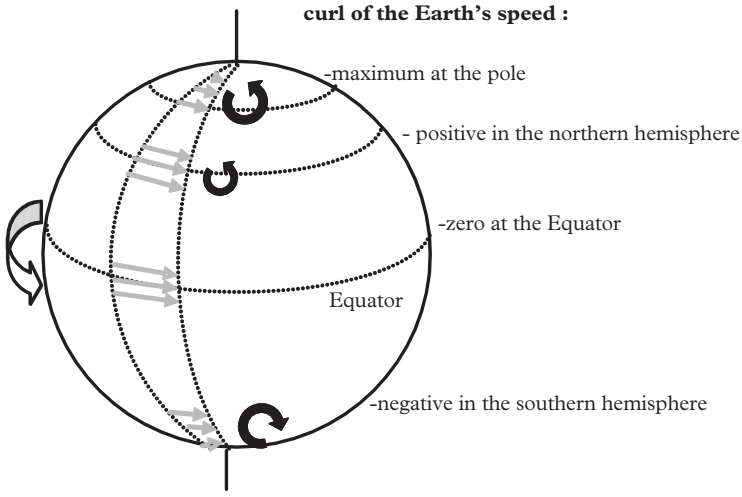

Figure 1.24 *Relationship between the planetary vorticity and latitude.*

vorticity. Planetary vorticity is equal to the Coriolis parameter $f = 2\ \Omega \sin \varphi$. Planetary vorticity is positive in the northern hemisphere and maximum at the North Pole because the tangential speed of the Earth's surface decreases rapidly close to the pole. On the contrary, at the Equator, the planetary vorticity is zero because the tangential speed of the Earth is practically constant around the Equator. Planetary vorticity is negative in the southern hemisphere.

A volume of water may also spin (relative to a reference frame linked to the Earth). It is the **relative vorticity** (noted ω). For example, relative vorticity can be induced by wind forcing or by friction along the coasts. It is important to understand that the planetary vorticity of any water mass that changes latitude is transformed into relative vorticity (Fig. 1.25). A water mass initially at the North Pole and moving (frictionless) toward the Equator retains its rotation motion. For an observer located at the Equator, this water mass spins counterclockwise when it arrives at the Equator. Its positive planetary vorticity has thus been transformed into positive relative vorticity. Conversely, water originally located at the Equator and heading to the North Pole acquires a negative relative vorticity (it seems to turn clockwise for an observer located on the sea ice).

A spinning ice-skater can decrease his rotation speed by opening his arms or increase it by bringing his arms back. In doing so, he uses what physicists call the conservation of angular momentum. A water column of height H in rotation obeys the same laws. When it stretches (water upwelling toward the surface), its diameter decreases and rotation accelerates (Fig. 1.26). On the contrary, if its diameter increases because it is pushed downward (sinking to the bottom), it decelerates. The **potential vorticity** (Π) is the ratio $(f+\omega)\ /h$. Far from the ocean surface and from coasts (two areas

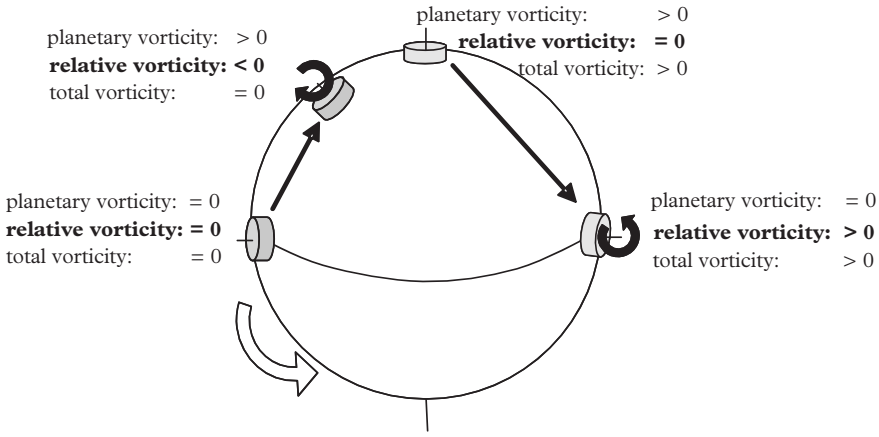

Figure 1.25 *Effect of latitude change on the relative vorticity.*

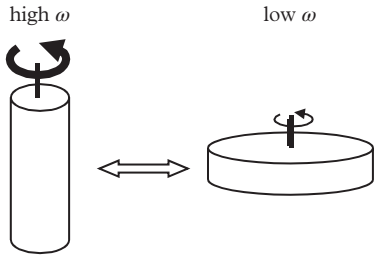

Figure 1.26 *Conservation of relative vorticity.*

where the vorticity can be modified), the potential vorticity must remain constant: therefore

$$(f + \omega)/h = \text{constant}.$$

In addition, the vorticity of water masses isolated from the surface (and thus from the wind forcing) is dominated by the planetary vorticity: $|f| \gg |\omega|$, so that

$$\boxed{(f/h) = \text{constant}.} \tag{1.20}$$

The consequence of this fundamental relationship is that a water column which stretches or is pressed down must change latitude to keep its potential vorticity constant.

1.6.2 Sverdrup Balance

In the center of the North Atlantic gyre, the surface current flows southward (Fig. 1.10 and 1.21). It is neither an anticyclonic flow, nor a flow toward the center of the gyre as we could have expected from the wind forcing (Fig. 1.15). This is due to vorticity.

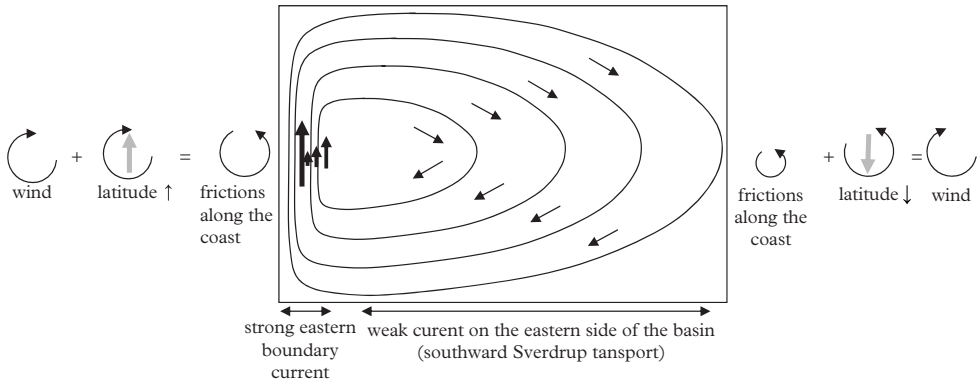

Figure 1.27 *Circulation in an anticyclonic gyre and vorticity balance. The Sverdrup transport explains the southward flow in the central and eastern parts of the basin. It is not relevant for the western boundary current discussed in Section 1.6.3. This east–west asymmetry is introduced by change of latitude which alters the vorticity balance. Modified from different sources.*

When surface waters transported toward the gyre center by the Ekman drift sink (downward Ekman pumping), they spread under the Ekman layer so that the height h of the water column decreases. We saw previously that far from the ocean–atmosphere boundary and from the coasts, the potential vorticity of a water mass $\Pi \approx f/h$ must remain constant. The water column that spreads must therefore move toward the Equator to reduce its planetary vorticity (f) and thus to slow down. In the case of the North Atlantic gyre, it thus creates a meridian southward current responsible for the **Sverdrup transport** V_S (see box "Sverdrup transport"). V_S intensity depends on the wind curl (equation (1.27)). Note that equation (1.27) does not imply that the current is strictly southward (Fig. 1.27). The current also has an east–west component U_s which can be calculated from equation (1.27). The Sverdrup transport explains the wide Canary Current which occupies most of the width of the gyre and flows southward. The water that sinks at the center of the gyre flows southward and upwells at the Equator. Surface current maps show mainly the Sverdrup transport which is more intense than the Ekman transport (see Application exercise: currents in a subtropical gyre).

Sverdrup transport

To take into account simultaneously the effect of the wind and of the pressure gradients, we calculate the curl of the acceleration, by differentiating equation (1.3a) by y and equation (1.3b) by x

$$\begin{cases} -\rho \dfrac{\partial f}{\partial y} v - \rho f \dfrac{\partial v}{\partial y} = -\dfrac{\partial^2 P}{\partial y \partial x} + \dfrac{\partial}{\partial y}\left(\dfrac{\partial \tau_x}{\partial z}\right), & \text{(1.21a)} \\ +\rho \dfrac{\partial f}{\partial x} u + \rho f \dfrac{\partial u}{\partial x} = -\dfrac{\partial^2 P}{\partial x \partial y} + \dfrac{\partial}{\partial x}\left(\dfrac{\partial \tau_y}{\partial z}\right). & \text{(1.21b)} \end{cases}$$

Note that according to equation (1.4) (see also Fig. 1.28)

$$\begin{cases} \dfrac{\partial f}{\partial x} = 0, \quad \text{because } f \text{ does not vary with longitude} \\ \dfrac{\partial f}{\partial y} = \left(\dfrac{\partial f}{\partial \varphi}\right) \times \left(\dfrac{\partial \varphi}{\partial y}\right) = \dfrac{2\,\Omega\,\cos\varphi}{R_E}. \end{cases} \tag{1.22}$$

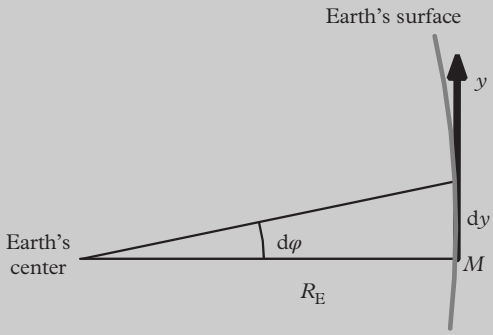

Figure 1.28 *Relationship between a change (φ) of latitude and the distance traveled.* R_E *is the radius of the Earth.*

We note $\partial f/\partial y = \beta$. β is different from zero because the Coriolis parameter depends on the latitude. β represents the change of the Coriolis force with latitude. We will see later that it is a fundamental parameter to understand the intensification of western boundary currents. Subtracting equation (1.21a) from equation (1.21b) and introducing β, we obtain

$$\rho\beta v + \rho f\left(\frac{\partial v}{\partial y} + \frac{\partial u}{\partial x}\right) = \frac{\partial}{\partial x}\left(\frac{\partial \tau_y}{\partial z}\right) - \frac{\partial}{\partial y}\left(\frac{\partial \tau_x}{\partial z}\right). \tag{1.23}$$

This equation is integrated between a depth ($z = -d$) sufficiently large for the current speed to be zero and the surface of the ocean ($z = 0$)

$$\rho\beta V_S + \rho f\left(\frac{\partial U_S}{\partial x} + \frac{\partial V_S}{\partial y}\right) = \frac{\partial\left[\tau_y^{\text{surf}} - \tau_y^{-d}\right]}{\partial x} - \frac{\partial\left[\tau_x^{\text{surf}} - \tau_x^{-d}\right]}{\partial y}, \tag{1.24}$$

where U_S and V_S represent the east–west and north–south components of the Sverdrup transport. If it is assumed that

horizontal transport is not divergent

$$\frac{\partial U_S}{\partial x} + \frac{\partial V_S}{\partial y} \approx 0; \tag{1.25}$$

friction forces at $z = -d$ are zero because the velocity is zero: $\tau_x^{-d} = \tau_y^{-d} = 0$.

Equation (1.24) is then reduced to

$$\rho\ \beta\ V_S = \left(\frac{\partial \tau_y^{\text{surf}}}{\partial x} - \frac{\partial \tau_x^{\text{surf}}}{\partial y} \right). \tag{1.26}$$

This can be written as

$$\boxed{\rho\beta V_S = \text{curl}\ \left(\tau^{\text{surf}}\right).} \tag{1.27}$$

The Sverdrup transport is important because it is responsible for the meridian heat transport in the ocean. It is balanced by a western boundary current (Fig. 1.27; see Problem 6). We will see in Chapter 7 that the Sverdrup transport is also responsible for the transport of nutrients in the thermocline. Ocean currents form cyclonic gyres when curl(τ^{surf}) is positive or anticyclonic gyres when curl(τ^{surf}) is negative (Fig. 1.18). In areas where curl(τ^{surf}) is zero, there is no meridian transport: these areas serve as natural barriers between the subpolar and subtropical gyres.

In the Southern Ocean, the lack of continental barrier does not allow to build up an east–west pressure gradient that would produce a meridian flow. Therefore, the current is zonal around Antarctica. Nevertheless, the westward winds produce a strong northward Ekman drift. It is balanced by a southward injection of warm eddies formed by instabilities of the ACC (Marshall and Speer, 2012). This southward injection of light water explains the tilting of the isopycnals in the ACC thermocline (Figs. 1.6 and 1.10).

Application exercise: currents in a subtropical gyre (Sudre et al., 2013)

We consider a subtropical gyre located between 25 and 40°N in which the zonal wind stress component evolves linearly from –0.05 N m^{-2} at 25° N to +0.08 N m^{-2} at 40°N (Fig. 1.18). It is assumed that the meridian wind component is zero.

(a) Determine the Ekman transport and the Sverdrup transport in the gyre. How are they oriented?

(b) Determine the total intensity of the southward transport. Comment on the result. It is assumed that the east–west length of the gyre is 6000 km.

(c) Determine the vertical speed at the base of the Ekman layer.

Solution:

(a) The wind is considered to be essentially zonal ($\tau_y = 0$).

Sverdrup transport:

$$\beta = 2 \times 7.28 \times 10^{-5}/(6400 \times 1000) \times \cos(40°) = 1.74 \times 10^{-11}\ \mathrm{m^{-1}s^{-1}}.$$
$$\rho \approx 1000\ \mathrm{kg\ m^{-3}}.$$
$$V_S = \mathrm{curl}(\tau)/\rho\beta$$
$$= -(\Delta\tau_x/\Delta y)/\rho\beta$$
$$= -(0.08 - (-0.05))/(1500 \times 1000)/1000/(1.74 \times 10^{-11})$$
$$= -4.98\ \mathrm{m^2 s^{-1}}.$$

$V_S < 0$, so the transport is southward.
Ekman transport:
at 40°N: $V_E = -\tau_x/\rho f = -0.08/1000/10^{-4} = -0.8\ \mathrm{m^2 s^{-1}}$;
at 25°N: $V_E = -\tau_x/\rho f = -0.05/1000/10^{-4} = -0.5\ \mathrm{m^2 s^{-1}}$.
We note that V_E is lower than V_S.
(b) The southward current.
We assume that the gyre covers $L = 6000$ km:

$$V_S \times L = -4.98 \times 6000 \times 1000\mathrm{m^3 s^{-1}}$$
$$= -30 \times 10^6\ \mathrm{m^3 s^{-1}} = -30\ \mathrm{Sv}.$$

(c) Ekman pumping.

$$w_E = -((0.08/(1000 \times 2 \times 7.28 \times 10^{-5} \times \sin(40))$$
$$-(-0.05/(1000 \times 2 \times 7.28 \times 10^{-5} \times \sin(25°)))/(1500 \times 1000)$$
$$= 1.1 \times 10^{-6}\ \mathrm{m\ s^{-1}}$$
$$= 35\ \mathrm{m\ y^{-1}}.$$

1.6.3 The Intensification of the Western Boundary Currents

In the following, we still focus on the example of the North Atlantic Subtropical gyre. Its western branch (the northward flowing Gulf Stream) is narrow and much faster than its wide and slow eastern branch (the southward flowing Canary Current; Fig. 1.21). This gyre is forced by an anticyclonic atmospheric circulation. Therefore, the curl of the wind stress is negative, which induces a southward thermocline water transport. How does this water return to the North despite the Sverdrup relation? The return is possible along the boundary of the basin, where the lateral friction cannot be neglected. Vorticity helps to understand the gyre asymmetry. The anticyclonic circulation of wind at subtropical latitudes gives the ocean a negative relative vorticity. If nothing was balancing this effect, the gyre would spin up indefinitely. This is not the case, because the

current slows down by friction along the coasts. In opposing the water movement, friction transmits a positive relative vorticity which tends to compensate the acceleration by the wind. However, the key to the problem lies here; the situation is not the same for the two sides of the basin. On the eastern boundary, the wind effect is largely balanced by the increase of the relative vorticity of the water flowing southward and to a lesser extent by friction on the boundary which can remain low. On the contrary, on the western boundary of the basin, the wind stress is reinforced by the decrease of the relative vorticity of the water that moves poleward, so that friction must be higher to slow down the movement. The friction is proportional to the velocity, so that velocity must be stronger in the west of the basin (the Gulf Stream) than in the east (the Canary Current). It is therefore the change of the Coriolis force with latitude which is responsible for the intensification of the currents on the Western boundary of the basin. This principle of current intensification on western boundary can be extended to cyclonic gyres (see Problem 7).

1.6.4 Eddies and Recirculation

The Gulf Stream is not fully explained by Sverdrup's theory. For example, the Sverdrup balance predicts a maximum meridian transport of 30 Sv which must be located 28° N. Yet the current is 90 Sv at 40° N. The cause of this disagreement is the presence of recirculation loops in the gyre, increased by the formation of eddies by the Gulf Stream. The Gulf Stream is so energetic that its trajectory is not stable: it forms meanders which are ejected from the current as eddies when they intersect themselves (Fig. 1.29).

Eddies ejected north of the Gulf Stream contain in their core the warm waters of the Subtropical gyre and they have an anticyclonic rotation. Eddies ejected south of the Gulf Stream contain in their core the cold waters of the Labrador current and they have a cyclonic rotation. As these cyclonic eddies head south, they allow the increase of the Gulf Stream intensity by creating a water recirculation loop. In addition, these eddies are in geostrophic equilibrium. At the center of the cyclonic eddies, the isopycnal surfaces are uplifted toward the surface, while in the center of anticyclonic eddies, the isopycnal surfaces deepen in the thermocline. As these eddies carry more kinetic energy than the average current, they have a particular importance in terms of vertical mixing through changes of the thermocline level that they induce.

1.6.5 The Thermocline Ventilation

We have noted earlier in the chapter that, on a north–south section of the ocean, the isopycnal surfaces form an onion-skin structure in the thermocline and that water masses move preferentially along isopycnal surfaces. At high latitudes, isopycnal surfaces outcrop at the ocean surface, allowing surface water to be carried at depth in the thermocline. As surface water is rich in oxygen, this phenomenon is called the **ventilation** of the thermocline. In the Atlantic at 42°N for example, winter mixed layer can be 200 m thick. It contains waters with homogeneous properties called **modal waters**. Spring warming of surface waters isolates modal waters from the atmosphere: this is

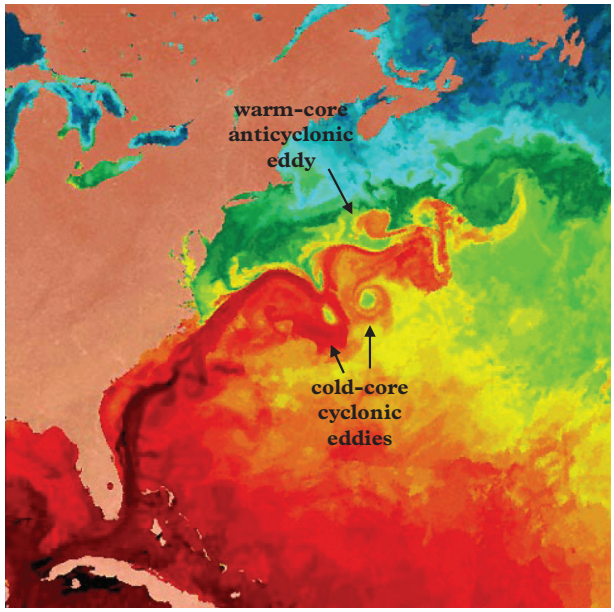

Figure 1.29 *The Gulf Stream seen in the infrared wavelength. It shows the presence of eddies. Color scale: orange-red: 24–28° C, green-yellow: 17–23° C, light blue: 10–16° C, dark blue 2–9° C. Credit: O. Brown, R. Evans and M. Carle, University of Miami, Rosenstiel School of Marine and Atmospheric Science, Miami, Florida.*

the beginning of the **subduction** of the modal waters along isopycnal surfaces. Modal water formed near 40°N is then led by Sverdrup transport at 400 m below the subtropical gyre, and then returned to the surface at the level of the equatorial divergence (Fig. 1.30). We will see later in this book that ventilation plays an essential role in the transport of chemical elements in the thermocline.

Non-ventilated **shadow areas** occur in the thermocline along the eastern boundary of the basins. We consider a volume of water transported to the Southeast in the thermocline (in the northern hemisphere). When it comes in contact with the eastern boundary of the basin, its east–west speed component must cancel ($u = 0$). For a geostrophic movement, this in turn means the absence of north–south pressure gradient (equation (1.14b)). As a consequence, the water mass height h must therefore remain constant (just use the principle of equation (1.19) applied to an east–west speed). But the volume of water must also keep its potential vorticity f/h. As h and f/h are constant, $f = 2\Omega \sin \varphi$ must also be constant and the water mass cannot change its latitude φ. The volume of water avoids this contradiction by not following the coast but by moving to the southwest. Therefore, it leaves to its left a part of the thermocline which is not easily ventilated called

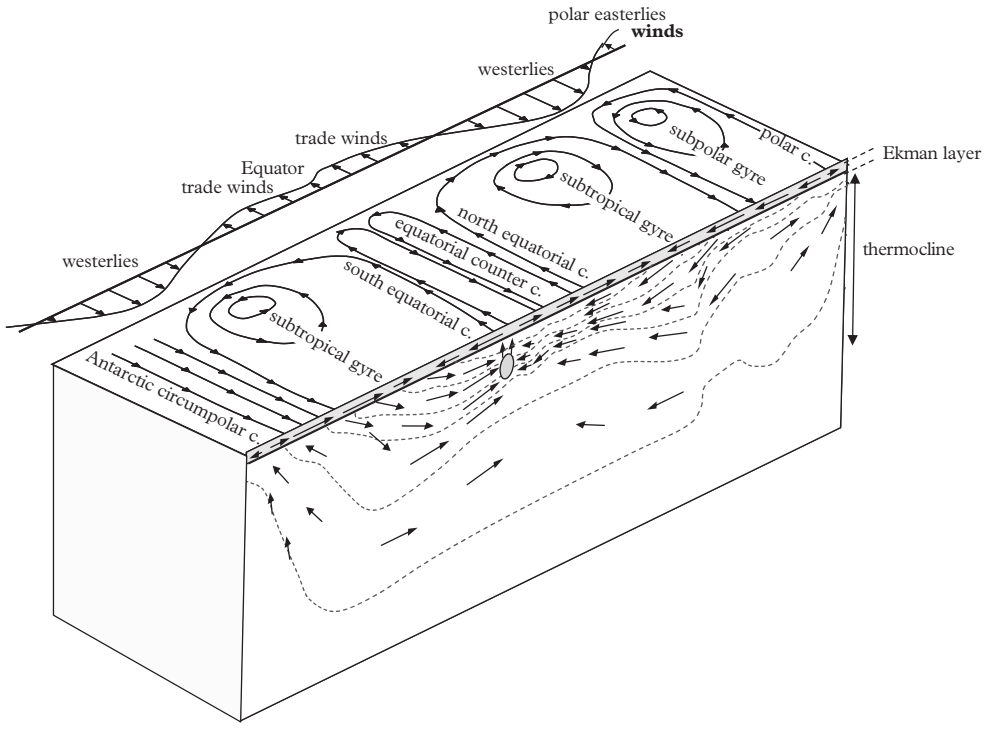

Figure 1.30 *Schematic diagram of the surface currents organization with wind stress (adapted from Munk, 1950) and motion of water masses in the thermocline. Black arrows in the Ekman layer: Ekman transport. Gray ellipse below the Ekman layer: Equatorial Under Current. Gray dashed curves: isopycnal surfaces.*

a shadow zone. This poorly ventilated shadow area can acquire specific geochemical properties, like a strong or total depletion in dissolved oxygen (see Chapter 2).

1.6.6 The Equatorial Circulation

The equatorial circulation is dominated by four large currents: the North Equatorial Current, the South Equatorial Current, the Equatorial Counter Current and Equatorial Undercurrent (Fig. 1.30). In the Pacific Ocean, the North (resp. South) Equatorial Current is the southern (resp. northern) branch of the North (resp. South) Pacific subtropical gyre (Fig. 1.10). Driven by the trade winds, they carry water westward. Water accumulates on the western edge of the basin and forms a sea level bump compared to the eastern part of the basin. The water that accumulates is very warm and forms the so-called warm pool.

The low wind intensity in the intertropical convergence zone (between 5 and 10°N) allows the water to flow eastward (in the opposite direction of the wind).

The Equatorial Undercurrent flows between 100 and 300 m in depth and is centered on the Equator, between –2° and +2° of latitude. At the surface, the South Equatorial

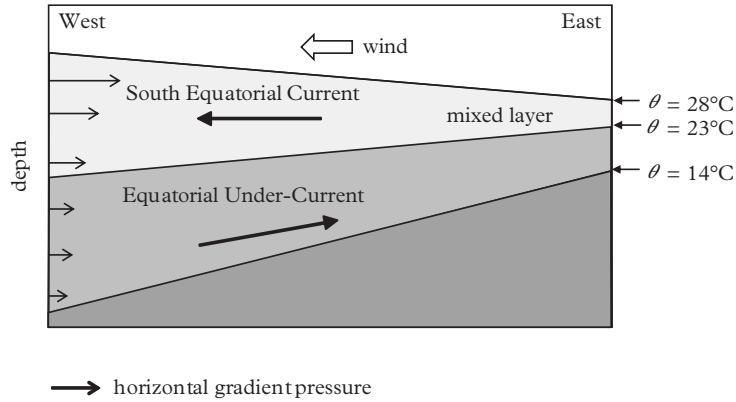

Figure 1.31 *Variation of dynamic height and of the thermocline depth on an east–west section of the equatorial Pacific Ocean. The 14° C isotherm is uplifted from 250 m deep in the west of the basin to 120 m deep east of the basin. Modified from Open University (1989).*

Current flows westward. At depth, the thermocline responds by upwelling in the eastern part of the basin (Fig. 1.31). We have already mentioned the east–west pressure gradient created by the South Equatorial Current. The pressure gradient is transmitted under the mixed layer to the thermocline. The very marked thermocline at the base of the mixed layer allows decoupling the westward flow of the South Equatorial Current from the eastward Equatorial Undercurrent in the thermocline. As there is no Coriolis force at the Equator, the Equatorial Undercurrent flows directly from the high pressures to the low pressure, that is, eastward. Should it depart from the Equator, the Coriolis force would bring it back to the Equator. However, we should not have a purely two-dimensional view of the Equatorial Undercurrent. Waters from the subtropical gyre flow through the thermocline to feed into the undercurrent (Fig. 1.30).

In the Pacific Ocean, the equatorial circulation undergoes large interannual variations known as the El Niño Southern Oscillation (ENSO). A decrease of the trade winds intensity can cause a shift of the warm pool from the western edge to the center of the basin and a slowdown of the equatorial upwelling in the east of the basin, which is at the origin of extreme climate events (see Chapter 11).

1.6.7 The Deep Circulation

Locally and temporarily, dense waters can form over less dense water: this is the case in the Norwegian Sea during winter when surface waters undergo a cooling and an increase in salinity by evaporation and brine rejection during sea-ice formation. They become denser than the underlying water and they sink toward the sea floor. Similarly, deep water formation takes place off the French Riviera in winter, when surface water, cooled to 12–13°C by the cold "mistral" wind, sinks down to 2500 m deep.

We can see on the map of surface currents (Fig. 1.10) that part of the Gulf Stream flows northward and that there is no equivalent in the North Pacific. Where does this water go? The North Atlantic drift transports warm and salty water to high latitudes. This water enters the Arctic Ocean and it can be found in the Norwegian Sea. In winter, the water is cooled by winds and its salinity increases due to the formation of sea ice (when water freezes at the ocean surface, it forms ice made of freshwater and very salty brines are rejected in seawater). The water becomes very dense and it sinks (Fig. 1.32). It is so dense that it can spread on the bottom of the North Atlantic. Pushed each year by new inflows, NADW moves to the South Atlantic. Approaching Antarctica, some of this water enters the Weddell Sea, where it goes back to the surface and where it is strongly cooled. This water contributes to the formation of the coldest and densest water of the deep ocean: AABW which spreads at the bottom of the equatorial Atlantic. Another fraction of the Weddell Sea Water is mixed with less salty (sea-ice melting, precipitation) surface water around 50–60°N. Transported northward by the Ekman drift, it feeds the AAIW which are exported down to a depth of 800 m in the southern subtropical gyres. A mixture of NADW, AABW and AAIW form the CDW that fills the deep Indian and deep Pacific Oceans. Applying the principles of ocean dynamics, we will see in Chapter 10 that there are intense currents existing in the deep ocean.

Paradoxically, dense water formation is not sufficient to establish a deep circulation. Dense water formation alone would produce a stable stratification of the ocean (warm and light surface waters above cold and dense deep waters). Deep water would have no reason to go back to the surface and deep circulation would stop. The key to thermohaline circulation is the upwelling of deep water, which is made possible by its mixing with warmer and lighter surface water. The upwelling of the cold deep waters must be

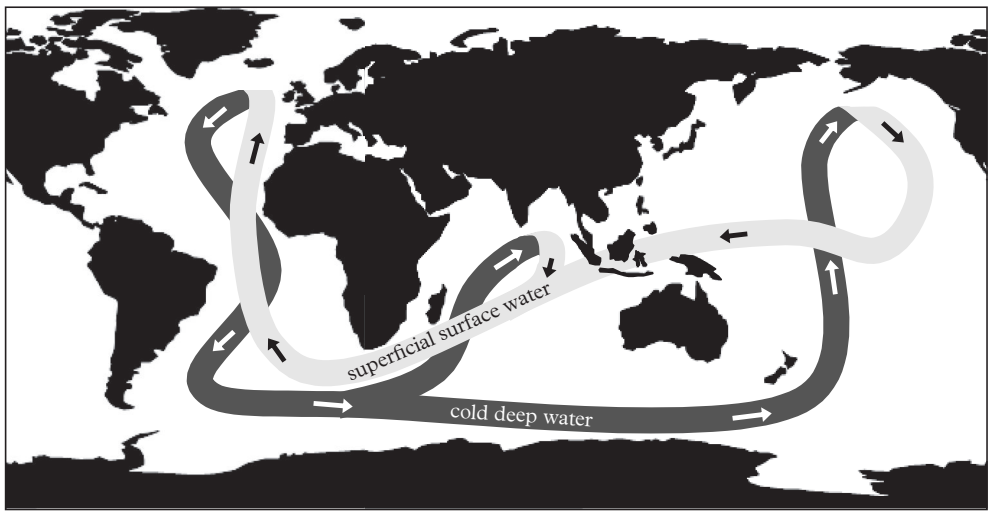

Figure 1.32 *The oceanic conveyor belt, a simplified vision of the thermohaline circulation. Adapted from Broecker and Peng (1982).*

balanced by the mixing of warm water diffusing toward the deep ocean (Munk, 1966). This principle will be developed in Chapters 6 and 10. Deep water upwelled back to the surface is then transported by currents (including the Gulf Stream) to high latitudes to refill areas of deep water formation. This circulation is called the thermohaline circulation or the conveyor belt or more recently the Meridional Overturning Circulation (or MOC). We will see in Chapter 10 that it still keeps many secrets.

Appendix 1

The Atmospheric Forcing

To understand the ocean circulation, we need to say a few words on atmospheric circulation. Atmospheric circulation is driven by two main factors: (1) the disparity of the solar flux at the Earth's surface and (2) the Earth's rotation. A given solar radiation flux intercepts a greater surface at the pole than at the Equator. Therefore, on average, lower latitudes receive more solar energy per square meter than the poles. This imbalance is amplified by the presence of ice in polar areas. This ice cover reflects most of the light that it receives. It is this imbalance that leads to the atmospheric and oceanic circulations whose "role," or rather whose effect, is to reduce the pole–Equator temperature gradient by transporting heat from the Equator toward the poles. If the Earth was not turning on its axis, atmospheric circulation would be reduced to two convection cells between the Equator and the poles: at the Equator the air heated by the ground is warm and less dense, so it rises and flows poleward in altitude. In Polar Regions, the air is cooled, it becomes denser and so it sinks to the ground and it flows back to the Equator at the Earth's surface.

In fact, Earth's rotation strongly complicates this scheme due to the Coriolis force. An air mass going from the Equator to the North Pole is deflected to the East, whereas an air mass going from the North Pole to the Equator is deflected to the West. Atmospheric circulation is organized in cells (Fig. 1.33):

- Hadley cell: at the Equator, the air heated by the ground rises and flows poleward. Leaving the Equator, it is deflected eastward by the Coriolis force (in the northern hemisphere). Around 30°N, it moves to the East. Therefore, it does not reach the pole directly because the Coriolis force brings it back toward the Equator. As it cools, it becomes denser and sinks toward the ground. As it returns to the Equator at the surface, it is deflected to the West: this is the origin of the trade winds. At the Equator (or more precisely in the Intertropical Convergence Zone where the trade winds meet and which is not always centered on the Equator), there is no wind and the permanent ascent of moist air causes precipitation: it is the doldrums where the sailors feared to be trapped due to the lack of wind.

- Polar cell: at the North Pole (resp. South), cold and dense air subsides and flows southward (resp. northward) at the Earth's surface while being deflected to the West (resp. East). During this journey, air warms and around 50°N, it rises to return to the pole in altitude and refill the polar subsidence.

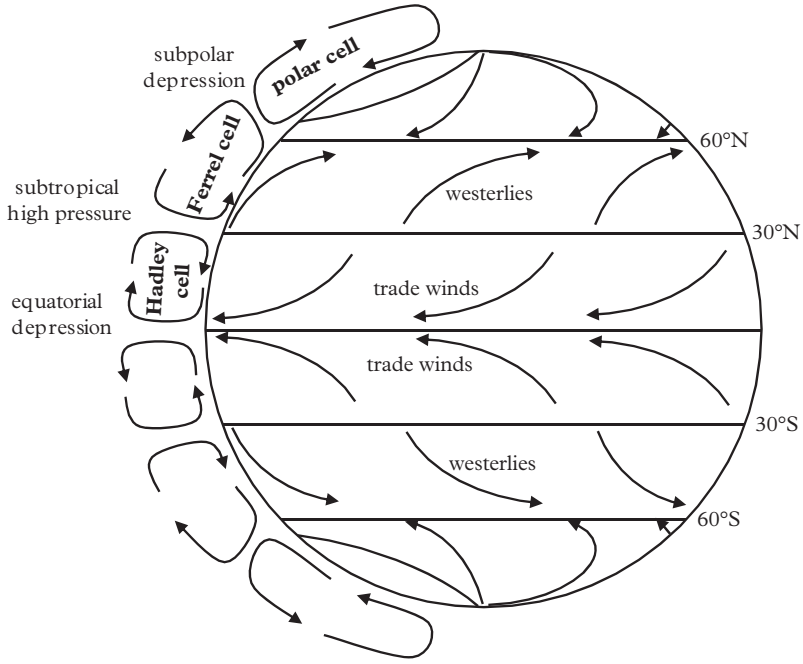

Figure 1.33 *Zonal distribution of winds.*

- Ferrel cell: between the Hadley and the polar cells, there is a more complex cell that controls the mid-latitudes climate. For example, France is under the double influence of the Azores anticyclone and of the Irish Sea depression. Confrontation of a cold air mass from the North and a warm air mass from the South creates a frontal zone (with strong temperature gradient) in which the warm air rises. As westerlies dominate, the air arrives from the ocean and it produces precipitations.

Between 30 and 60°N, the westerly winds dominate. This is true in Europe, but it is even truer in the southern hemisphere where there is no landmass to slow and deflect the wind: this is the origin of the roaring forties and the screaming fifties that are well known to Cape Horners.

For oceanographers, the important aspects of the atmospheric circulation are the surface component of wind at the base of these cells, and the heat, evaporation and precipitation fluxes caused by the convergence/divergence zones.

PROBLEMS

Problem 1: Stratification of the Arctic Ocean

The Arctic Ocean receives surface waters from the Atlantic Ocean through the Fram Strait.

(1) Use information in Table 1.3 and Fig. 1.4 to determine the density of the Arctic surface water and water of Atlantic origin.

Table 1.3 *Features of the Arctic waters*

Origin of Surface Water	Temperature (°C)	Salinity
Fram Strait	4.0	34.5
Arctic Ocean	−1.5	<33.5

(2) Explain why in the Arctic Ocean, very cold waters are found above warmer waters.

Problem 2: What is the Circumpolar Deep Water mix?

Using the data in Table 1.2, determine in what proportions NADW, AABW and AAIW mix to form Circumpolar Deep Water (CDW).

Problem 3: Surface current in the Eastern Pacific (Chereskin, 1995)

To study the surface current off the California coast, seven drifting buoys are deployed simultaneously at the same location and at depths of 8, 16, 24, 32, 40, 48 and 60 m. These buoys are followed during 7 months (Fig. 1.34).

(1) What is the point to represent the difference of trajectory between each buoy and the deepest one?
(2) Describe the evolution of the current with depth. Explain this evolution and the relationship between the current and the wind.

Problem 4: Effect of wind on the vertical motion of the ocean (Hellerman and Rosenstein, 1983)

Figure 1.17 shows changes of the average zonal wind stress with latitude. Determine upwelling and downwelling areas.

Problem 5: The California upwelling (Barth et al., 2000)

We study the California upwelling.

(1) Figure 1.35a represents the temperature of the ocean along the Oregon and California coast. Knowing that on average the wind blows southward, explain the distribution of the sea surface temperatures.
(2) How does the dynamic topography of the ocean (sea level) evolve from the open ocean to the coast? Same question for the thermocline.
(3) Figure 1.35b represents the map of the dynamic topography of the ocean. What is, according to you, the direction of geostrophic currents? Draw on the map the

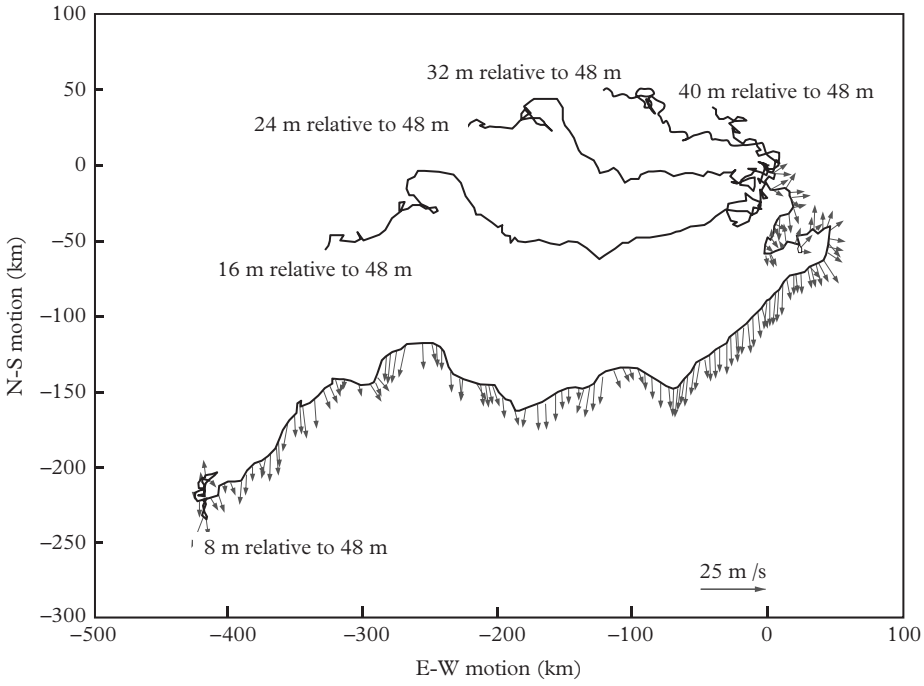

Figure 1.34 *Path of drifting buoys and wind. Each continuous line gives the difference of path between a given buoy and the reference buoy drifting at 60 m. The arrows associated with the trajectory of the buoy drifting at 8 m give the speed and direction of the wind along the way. Modified from Chereskin (1995).*

velocity vectors to show the direction and (relative) speed of the current. Where is the maximum velocity?

(4) Estimate the average speed of the geostrophic current at the point of coordinates: 124.9°W and 42.55°N.

(5) Around 43.2°N–125.4°E, the isopycnal surface outcropping at the ocean surface deepens westward down to 50 m deep over an east–west distance of 100 km. Is this consistent with the previous observations?

Problem 6: Is there a Sverdrup balance in the North Pacific? (Hautala et al., 1994)

A balance of the meridian transport of water with a density anomaly lower than 27.5 kg m^{-3} is established at 24°N in the Pacific (Table 1.4). Poleward currents are counted positive.

(1) Comment on the values in Table 1.4. What is the net transport of water at 24°N?

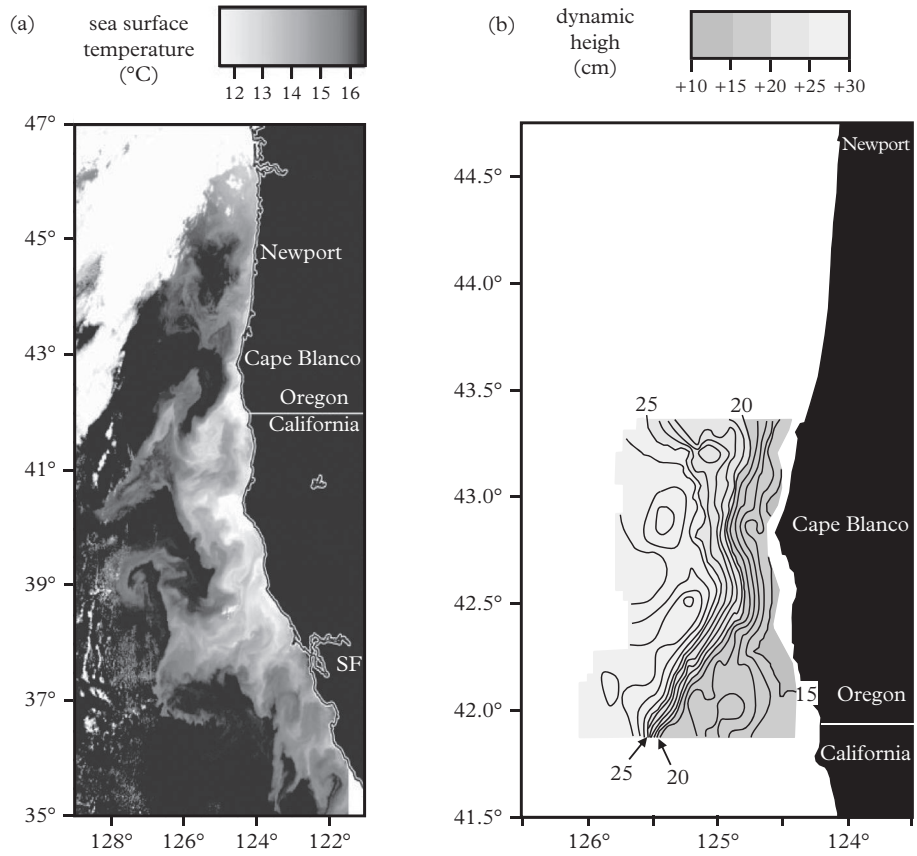

Figure 1.35 *The California upwelling. (a) Ocean surface temperature on the west coast of the United States. The temperature scale is given above the figure. The white area in the northwest corner is due to the presence of clouds. (b) Dynamic height of the ocean calculated by assuming that the velocity is zero at 100 m. Modified from Barth et al. (2000).*

Table 1.4 *Water flux of in the Pacific at 24°N*

	Current (Sv)	**Average Temperature (°C)**
Kuroshio and the Philippine Sea	+37	20.6
Ekman	+7	22.6
Geostrophic current within the basin	–41	15.9
North Pacific intermediate water	–3	7.0

(2) At 24°N, the average curl of the wind shear over the basin is -3.8×10^{-8} N m^{-3} and the width of the basin is 11,000 km. Determine the Sverdrup transport. Is the result consistent with the values in Table 1.4?

(3) In what direction is the net heat transport at 24°N?

Problem 7: Intensification of the Labrador Current

Use the rationale explaining the western boundary current in an anticyclonic gyres (like the Gulf Stream) and show that it also explains the intensification of the Labrador Current that is forced by a cyclonic wind circulation.

2

Seawater Is More than Salted Water

Marine geochemistry is the study of the behavior and distribution of chemical elements in the ocean. It does not cover only the chemical and biological reactions in which these elements are involved, but also the conditions in which these elements are introduced into the ocean, then transported and finally removed from the ocean. Thus, stocks and fluxes of chemical elements in the ocean are determined to establish budgets.

All the elements and chemical compounds, whether they are natural or anthropogenic (produced by humans, e.g., pesticides, or the products of thermonuclear explosions, for example), pass through the ocean. They are introduced by rivers, runoff, the atmosphere and the winds (for dust) as well as, for some of them, by volcanism and submarine hydrothermal fluids. Then, they stay in seawater for variable amounts of time. Indeed, depending on whether they are soluble and transported passively by currents or insoluble and transported quickly to the bottom by sinking particles, and on whether they enter the food chain or they have no nutritional value, the fates of the chemical elements in the ocean are very different (Appendix 1). All these chemical elements and the molecules that they form can potentially be used to highlight and quantify fluxes of matter in the ocean. While physical oceanographers measure currents and set water motion in equations, geochemists observe chemical elements spreading as dyes in the ocean. Thus, the study of some major, minor or trace elements and their isotopes can bring major constraints on the ocean motions. These elements and isotopes are called **tracers**. Geochemists are constantly going back and forth between the understanding of the chemical behavior of the tracers at the microscopic scale and their transport across the ocean.

The routes of the chemical elements in the ocean are described as **biogeochemical cycles** in which the tracers can undergo repeated chemical transformations (the prefix "bio" highlights the importance played by biological processes in certain transformations). However, these cycles are not closed circuits in the ocean: there are always exchanges with the outside that must be quantified to understand the exact role of each tracer and the effects of human activity on the chemical composition of the ocean.

Two tracers with very different cycles can still share a bit of the road together: their cycles are coupled. For example, to study the carbon cycle, geochemists are also interested in nitrate, phosphate and oxygen cycles and in cycles of elements so scarce that they are rarely discussed in everyday life, such as thorium or neodymium, to understand

Marine Geochemistry. First Edition. Matthieu Roy-Barman and Catherine Jeandel.

different aspects of the behavior of carbon in the ocean. Thus, biogeochemical cycle studies are always multidisciplinary.

The chemical composition of seawater is the result of all the biogeochemical cycles. Here we present a few cycles that will address many phenomena that regulate the chemical composition of seawater.

2.1 Why Is Seawater Salty?

2.1.1 The Chemical Composition of Salt

Salinity has been initially defined in Chapter 1 as the weight of salt contained in 1 kg of water. It is on average $S = 34.5$ g kg^{-1} in the ocean. Although all the elements of the periodic table can be detected in seawater, only those given in Table 2.1 contribute significantly to salinity. They are called the major elements, as opposed to the others which are quantitatively minor.

Salinity varies significantly throughout the ocean (see Chapter 1), but the chemical composition of the salt (i.e., the relative abundance of major ions) is remarkably constant from one point of the ocean to another. To understand this constancy, we must focus

Table 2.1 *Abundance of the major constituents of seawater*

Element	Seawater[a] (g kg^{-1})	Rivers[a] (g kg^{-1})	Hot Hydrothermal Fluids[b] (g kg^{-1})
H_2O	964.85	999.901	969–963
Na^+	10.77	0.00515	10–12
Mg^{2+}	1.290	0.0335	0
Ca^{2+}	0.4121	0.0134	0.47–0.83
K^+	0.399	0.0013	1.30–197
Sr^{2+}	0.0079		0.006–0.009
B_{total}	0.0045		0.0055–0.0061
Cl^-	19.354	0.00575	18–21
SO_4^{2-}	2.712	0.00825	H_2S: 0.22–0.29[c]
$HCO_3^- + CO_3^{2-}$	0.118–0.146	0.0520	CO_2: 0.25[c]
Br^-	0.0673		0.064–0.075
F^-	0.0013		
SiO_2	0.0013	0.0104	0.94–1.17

[a]After Coppin-Montégu (1996). [b]After Edmond et al. (1979). [c]Hydrothermal fluids are reducing (S as H_2S) and acidic (C as CO_2 mainly).

both on the *origin* and *fate* of salt in the ocean. The main source of dissolved ions in the ocean is river inflow. However, in contrast to seawater, river waters are enriched in Ca^{2+} compared to Na^+, depleted in Cl^- compared to Na^+ and the silica content is much higher in rivers than in seawater. This means that seawater is not simply river water enriched in salt by evaporation. We must therefore understand why the relative proportions of chemical elements change after their introduction into the ocean by rivers. If the Na of table salt is brought to the ocean by rivers, Cl is provided by submarine volcanism (see Section 2.1.5). Na^+ and Cl^- ions are very soluble and remain on average about 93 million y in the ocean before their removal as salt (NaCl) deposits in areas of very high evaporation, acting as natural salt marshes.

Other ions spend less time in the ocean. This is, for example, the case of calcium: Ca is brought by rivers and removed "faster" from seawater, on a timescale of 1 million y, by living organisms which make $CaCO_3$ shells that accumulate in limestones.

2.1.2 Residence Time

The first factor that determines the chemical composition of seawater is the average time spent by each chemical element in the ocean, called its **residence time**. The residence time of an element, $\tau_{element}$, is defined as the ratio between the quantity of this element in a given reservoir (quantity) and total inflow (or outflow) of this element to this reservoir (Σfluxes)

$$\tau_{element} = \frac{\text{Quantity}}{\Sigma\,(\text{Flux in})} = \frac{\text{Quantity}}{\Sigma\,(\text{Flux out})}. \tag{2.1}$$

In the case of the global ocean fed with ions by rivers, the total amount is the average concentration of the element multiplied by the volume of the ocean (1.36×10^{18} m^3, Table 1.2). The inflow is the total river water flux multiplied by the average element concentration in rivers (see Problem 1). The stocks of elements in the ocean are, in general, easier to determine than fluxes (sometimes also called source and sink terms). In the following, we present a first inventory of source and sink terms. It will be detailed and completed throughout this book.

2.1.3 Rivers and Estuaries

Rivers are the main vector of dissolved ions from the continents to the ocean. However, the mixing zone between fresh water and seawater (we will use hereafter the generic name of estuary) plays the role of chemical filter for the continental inputs. In fresh water, fine particles remain in suspension because their surface electrical charges keep them away from each other. The increase in salinity allows the neutralization of these electrical charges by ions in solution and allows flocculation of particles under the influence of van der Waals forces. Then, particles settle under the effect of their weight. During this flocculation–sedimentation, chemical elements are adsorbed on particles and transferred to the sediment (Fig. 2.1). In the sediment, a fraction of the chemical elements can be

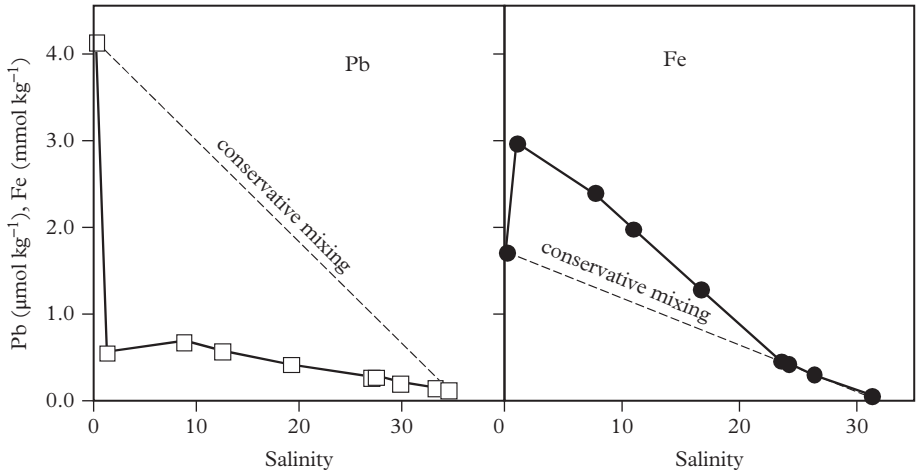

Figure 2.1 *Behavior of dissolved iron and lead in an estuary. As soon as fresh water arrives in the estuary, Pb is removed by adsorption on settling particles. On the contrary, iron is released in solution by the dissolution of minerals carried by the river or of sediment resuspended by tidal currents. Modified from Braungardt et al. (2003).*

dissolved. This does, however, concern the poorly soluble elements and not very soluble elements such as Na or Cl.

2.1.4 The Atmosphere

The wind transports over large distances particles blown over the continent or formed in the atmosphere. In contact with seawater, these particles are partially dissolved, releasing chemical elements. The impact of these inputs is globally low relative to rivers. However, it may be significant for insoluble metals which are efficiently removed in estuaries (see Chapter 9). Significant amounts of phosphate and nitrate can also be recovered from wind-blown particles transported from the continents to the open ocean.

The atmosphere exchanges large quantities of gas with the ocean. These fluxes will be discussed later in the chapter. Gases (with the notable exception of CO_2) are not taken into account to estimate salinity, which concerns only non-volatile species.

2.1.5 Volcanic and Hydrothermal Processes

Approximately 60,000 km of mid-ocean ridge runs through ocean basins. There are 2–3 km high submarine volcanic chains where intense volcanism occurs (it is one of the manifestations of the plate tectonics). Gases emitted during eruptions include chlorine (Cl_2) which is, in the long term, the main source of chloride ions (Cl^-) in the ocean. Rivers bring Cl^- ions, but this Cl^- comes essentially from sea sprays transported by wind and erosion of saline rocks of marine origin, so that it does not enrich seawater in Cl relative to Na.

Submarine volcanism is at the origin of another source of elements for the ocean: hydrothermal fluids. The origin of these fluids is seawater which infiltrates and circulates in the oceanic crust. When it approaches the active volcanic areas, it heats up and reacts with the surrounding rocks to form hydrothermal fluids. These fluids are ejected out of the oceanic crust at temperatures up to 350°C through chimneys called "black smokers" because the plumes that they eject are made black by precipitation of iron sulfides and hydroxides. During their journey in the oceanic crust, the chemical composition of the fluids varies significantly:

- When they are still cold, they lose part of their cations by reaction with the crust: Li^+, Ba^{2+}, Rb^+, K^+, Ca^{2+}, UO_2^{2+}, ... and particularly Mg^{2+} concentration is virtually zero in "pure" hydrothermal fluids (non-mixed with seawater).
- As fluid percolates, they are heated and become acidic and reducing. They then dissolve many chemical elements such as Li, Ba, Rb, K, Sr and many transition metals.

Overall, hydrothermal inputs are significant compared to rivers in the case of more soluble elements (Li, Sr ...). Metals (Cu, Ni, Co ...) are quickly precipitated during the mixing of hydrothermal fluids with oxidizing and cold seawater, thus creating metal deposits in the vicinity of black smokers. With their lower oxidation rates, Fe and Mn are transported over large distances and they precipitate to form crusts of Fe and Mn in areas of low sedimentation.

2.1.6 The Removal of Chemical Elements

The chemical composition of seawater depends not only on the inputs but also on the removal rate of each element from the ocean. We have already seen that dissolved elements are lost during hydrothermal circulations in the oceanic crust. Other elements are incorporated into volatile compounds and lost by diffusion to the atmosphere. This is the case, for example, of nitrogen compounds that can be transformed by bacteria into volatile N_2 and N_2O. This is also the case for dimethyl sulfate that is produced by phytoplankton, which use it as an "antifreeze," and which is volatile; in the atmosphere, it is oxidized and forms micron-size droplets of sulfuric acid that control the formation of clouds. However, the main sink of chemical elements is the deposition of particulate matter on the seafloor. The ions are incorporated into these particles by the biological activity (organic synthesis, formation of skeletons and shells for calcium and silica, formation of Mn oxides by bacteria ...) or abiotic chemical reactions (adsorption of chemical elements on Fe–Mn oxides, on clay ...). Finally, other elements are trapped directly in sediments (sulfates, pyrite) or at their surface in Mn nodules and Fe–Mn crusts. The role of marine particles and sediment will be detailed in Chapter 9. For each element, the equilibrium between inputs and losses determines the stock contained in the ocean (see Chapter 5).

The efficiency or the difficulty of removing an element from the ocean determines its residence time. This residence time must be compared to the mixing time of the ocean,

which is the water turnover time in the deep ocean (see Chapter 10) and which is of the order of 1000 y. The residence times of major ions range from millions to tens of millions of years. They are much longer than the mixing time of the ocean. Chemically inert ions are therefore very well "mixed" in the ocean. This is why the chemical elements that determine salinity are in constant proportions in the ocean. It is because major ions are chemically very inert that salinity is a water mass tracer: it is not affected by chemical or biological reactions in the ocean. Salinity is therefore, as potential temperature, a conservative tracer which can only be changed by mixing when water masses are isolated from the surface.

A story worth its salt . . .

The ocean contains a lot of salt and cooking salt is obtained by evaporating seawater. In Norse mythology, the salt of the ocean is from a salt mill, located at the bottom of the sea. Ancient humans believed that the salt from the oceans came from the sinking of a merchant vessel carrying large quantities of salt amphorae. In fact, the salt of the ocean is an honorable old man because it has been present in seawater for a very long time. It comes from the erosion of the continents which brings—via rivers to the yet little salty taste—of the order of 3.6 gigatons of salt in the ocean per year, which exceeds the capacity of a merchant ship! Its concentration remains stable as some salt disappears also every year: for example in the salt marshes, where it is precipitated.

Humans absolutely need salt in their food and, before the advent of the refrigerator, for food preservation. This is why taxes on salt were established. In France, this was based on the transport of salt and called the "gabelle," from a word of Arab origin, Kabala, which means tax. For four and a half centuries (from the middle of the fourteenth century to the aftermath of the French Revolution) the salt gabelle was applied in the kingdom of France. The king was considered as the owner of the soil and, thus, he could control the raw materials and at the same time the salty water. With taxes, the king of France wanted to establish his monopoly on the sale of salt. The sale of salt was controlled by royal officers known as "the grenetiers," and the taxpayers were required to annually consume the "salt of the duty," that is to say a certain quantity of salt. The rules becoming harsh and unequal, the gabelle became increasingly unpopular, and a parallel market developed. Who can imagine today that smuggling had developed around such a common product?

2.2 Concept of Conservative and Non-Conservative Tracers

What about the other chemical elements? There are only a dozen major elements in seawater, while the Mendeleev table contains 52 stable elements. Some minor compounds are chemically inert and their low abundance in the ocean simply reflects their low abundance on Earth. Other elements (such as aluminum, iron or phosphorus) are major

constituents of terrestrial rocks, but they occur only in trace amounts in the ocean. Their residence times are very short because they are actively removed from the ocean by chemical or biological reactions. Their behavior can be more or less decoupled from that of water masses.

This decoupling is observed on hydrographic sections (Figs. 2.2 and 2.3). At first glance, the main water masses (North Atlantic Deep Water (NADW), Antarctic Bottom Water (AABW), Antarctic Intermediate Water (AAIW) and Circumpolar Deep Water (CDW)) identified on θ and S sections can be recognized on the O_2 (dissolved oxygen) and PO_4^{3-} (dissolved phosphate) sections. Therefore, the distribution of O_2 and PO_4^{3-} is in part determined by water mass mixing. However, differences can be observed:

(1) In the North Pacific, the deep waters are very homogeneous in temperature and salinity because there is only one source of deep water lying in the South. Around 1000 m depth O_2-poor and phosphate-rich waters do not match the core of the North Pacific Intermediate Water, which can be recognized by extremes in temperature or salinity. Despite their low temperature, the deep waters are oxygen-depleted, which demonstrates that they have left the surface for a long time.

(2) In the surface waters of the Atlantic and Pacific oceans, PO_4^{3-} concentrations are low regardless of temperature and salinity.

PO_4^{3-} and O_2 content are therefore not only determined by mixing of water masses: biological activity plays an important role too.

When the concentration of an element can change when the water mass is not in contact with the atmosphere or is not mixing, this element is called a **non-conservative tracer**. Its distribution depends not only on addition and/or subtraction related to biological or chemical reactions, but also on currents and water mass mixing. The comparison between conservative and non-conservative tracers is used to quantify the influence of biological and chemical processes on the biogeochemical cycles of elements.

2.3 The Nutrient Cycle and the Role of Biological Activity

2.3.1 Nutrient Profiles in Seawater

To understand the effect of biological activity on the distribution of the chemical elements, we can study the vertical profiles of phosphate, silicate, dissolved inorganic carbon (DIC) and dissolved oxygen (Fig. 2.4). In the North Pacific, the phosphate concentration is zero at the surface, maximum at 1000 m depth (3 μmol kg^{-1}), and it remains high between 1000 m and the seafloor (between 2.5 and 3 μmol kg^{-1}). In the North Atlantic, trends are identical, even if concentrations in deep and intermediate levels are lower (1.8 and 1.5 μmol kg^{-1}, respectively). These profiles are the result of the simultaneous action of living beings and oceanic circulation.

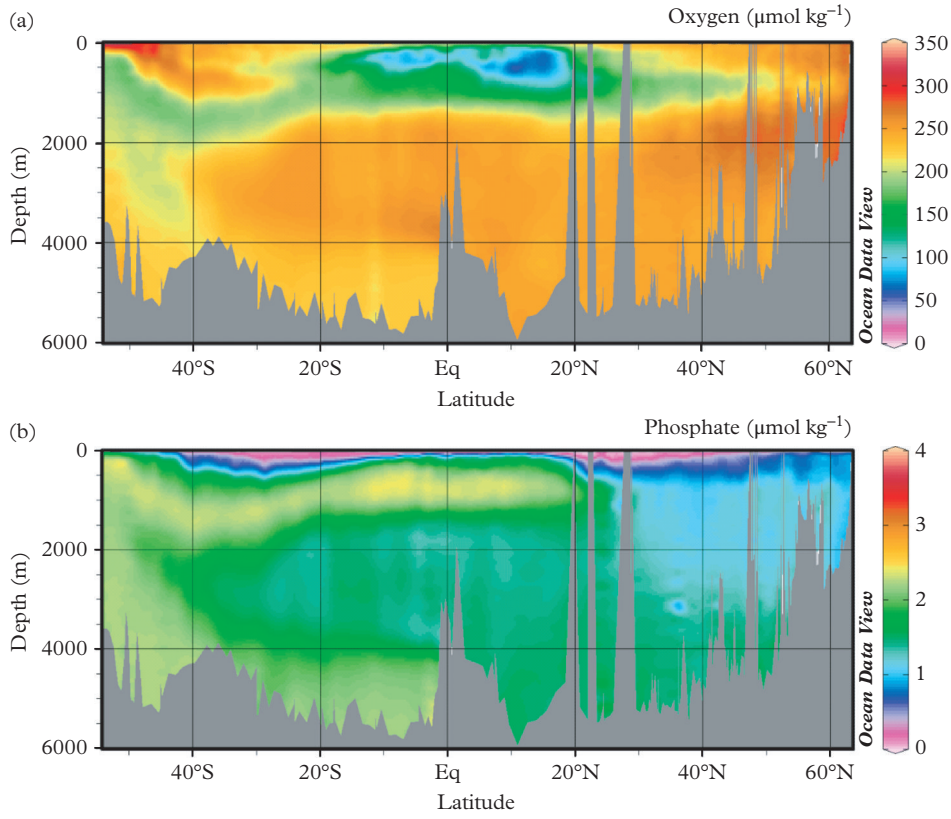

Figure 2.2 *North–south hydrographic section of the Atlantic Ocean. (a) Dissolved oxygen. (b) Phosphate. Figures drawn with Ocean Data View from the e-WOCE database: http://odv.awi.de/.*

2.3.2 The Life Cycles in the Ocean

At the base of marine ecosystems, there is **photosynthesis** (Fig. 2.5): micron-sized algae use the energy from the Sun and dissolved CO_2 to produce organic carbon that enters into the constitution of all organic molecules (sugars, lipids, proteins, etc.). Photosynthesis is often summarized by the reaction

$$CO_2 + H_2O + \text{light energy} \rightarrow CH_2O + O_2. \qquad (2.2)$$

As the energy from light is required, photosynthesis occurs at the surface of the ocean, in the photic zone that receives light. The depth of the photic zone varies from a few meters in very turbid waters to more than 150 m in very clear and plankton-poor waters. Elements other than carbon are essential to the constitution of living organisms: nitrogen supplied by nitrate (NO_3^-) allows the synthesis of amino acids and proteins; phosphate

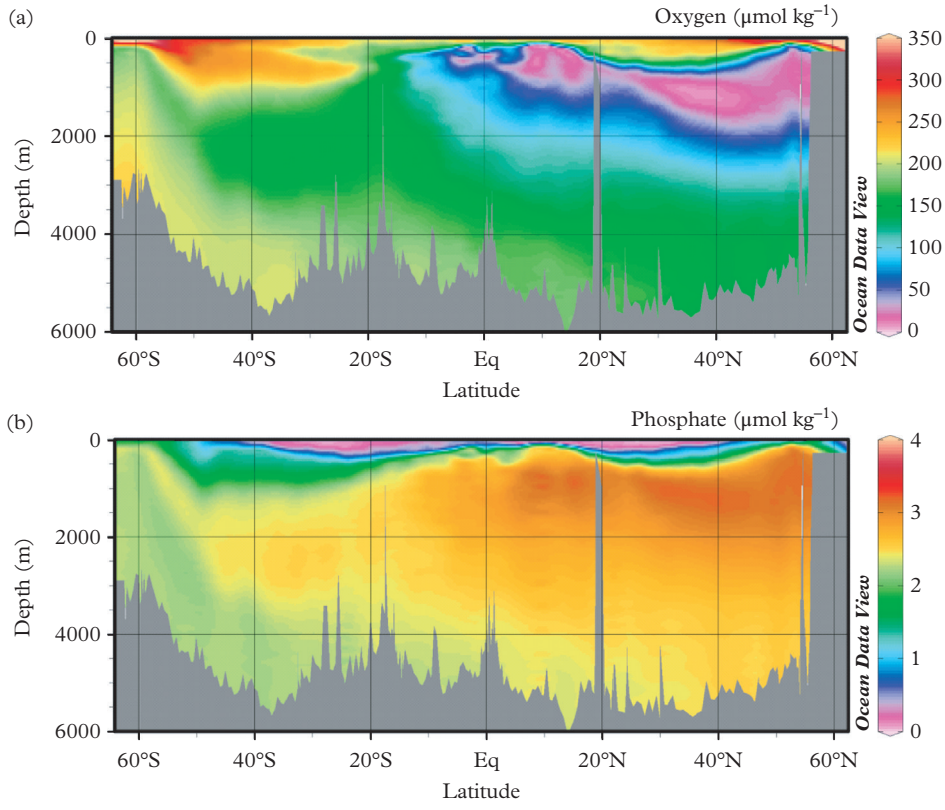

Figure 2.3 *North–south hydrographic section of the Pacific Ocean. (a) Dissolved oxygen. (b) Phosphate. Figures drawn with Ocean Data View from the e-WOCE database: http://odv.awi.de/.*

(PO_4^{3-}) enters the structure of DNA, RNA and molecules carrying energy (ATP); sulfate provides sulfur necessary for the synthesis of a particular amino acid (cysteine). The formation of organic matter can be described very schematically by the equation

$$106\ CO_2 + 16\ HNO_3 + 1\ H_3PO_4 + 122\ H_2O + \text{light energy} \rightarrow$$

$$(CH_2O)_{106}(NH_3)_{16}(H_3PO_4) + 138\ O_2. \qquad (2.3)$$

This reaction reflects the reduction of CO_2 and NO_3^- (represented here by nitric acid HNO_3 to simplify the electric charge balance) in carbon hydrates and amino acids (here represented by the ammonia) and the incorporation of phosphate for the synthesis of various molecules. The relationship between the different stoichiometric coefficients of this reaction are called the Redfield ratios (Redfield showed in 1934 that plankton

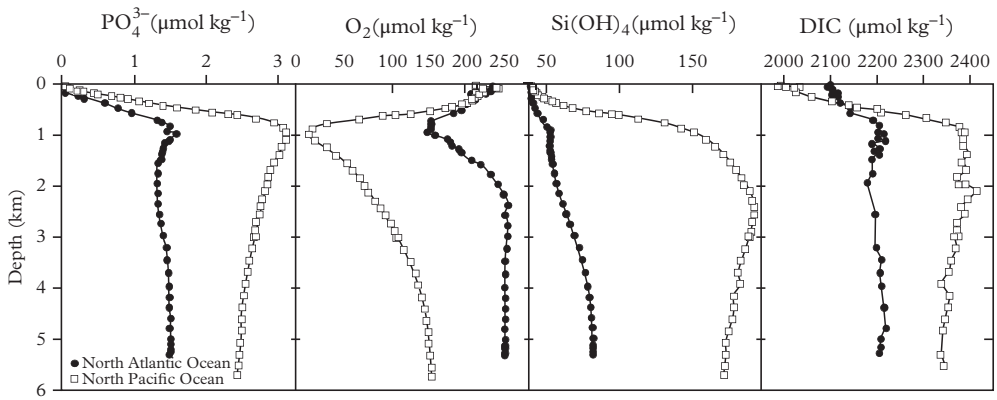

Figure 2.4 *Concentration profiles of different compounds in the North Atlantic and North Pacific. Black circles: North Atlantic. White squares: North Pacific. Figure drawn with Ocean Data View from the e-WOCE database: http://odv.awi.de/.*

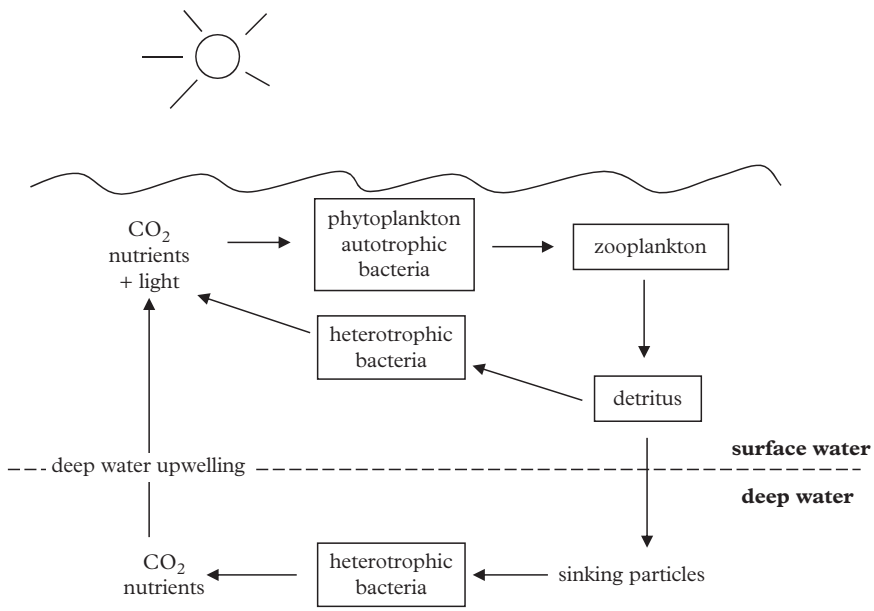

Figure 2.5 *Simplified nutrient cycle in surface and deep waters.*

are always more or less composed of the same proportions of carbon, nitrogen and phosphate). These ratios are written as

$$P/N/C/O = 1/16/106/-138. \quad (2.4)$$

There is a "minus" sign before the coefficient for oxygen because this element is produced by photosynthesis while P, N and C are consumed. It must be noted that these ratios characterize the proportions in which the elements are consumed by biological activity, but that they are not, in general, the ratios between the concentrations of elements in seawater. In fact, only the P/N ratio is approximately the same in organic matter and seawater (of the order of 1/15 to 1/16). The control that nitrate and phosphate exert on biological production is probably related to this similarity (see Chapter 7).

At the ocean surface, the concentrations of NO_3^-, PO_4^{3-} or $Si(OH)_4$ (dissolved silica used by algae (diatoms) or animals (radiolarians) to build up their silica skeletons) are often virtually zero: these nutrients are entirely consumed by the phytoplankton. They are called **limiting elements** because their absence limits the development of phytoplankton. The role of the limiting elements in the biological activity of surface waters will be detailed in Chapter 7.

Other nutrients such as DIC (or mineral carbon, which includes CO_2, carbonate and bicarbonate ions), calcium and barium (whose role in biological activity is not understood, even though its cycle seems clearly related to biological activity through the precipitation of strontium sulfate tests highly enriched in barium) are also present (their concentrations are lower in surface waters compared to deep waters, but they are never zero); these nutrients are non-limiting elements.

The organic matter produced by phytoplankton is consumed by heterotrophic bacteria and different species of zooplankton. If it is not quickly remineralized in surface waters, this organic matter leaves the surface water and falls toward the seafloor in different forms: aggregates of senescent or dead phytoplankton cells, feces, zooplankton bodies, etc. While falling, this organic matter is eaten by bacteria and animals. Organic matter is oxidized and transformed into mineral elements: at depth, nutrient concentrations increase and reach a maximum at around 1000 m. Overall, this produces the reverse reaction of photosynthesis with oxygen consumption and release of nutrients in seawater, called remineralization or respiration

$$(CH_2O)_{106}(NH_3)_{16}(H_3PO_4) + 138\ O_2 \rightarrow$$
$$106\ CO_2 + 16\ HNO_3 + 1\ H_3PO_4 + 122\ H_2O + \text{chemical energy}. \quad (2.5)$$

Now, we can easily explain the vertical distribution of phosphate (Fig. 2.4): the concentration is zero at the surface due to consumption by phytoplankton, while high concentrations at depth are due to the remineralization. The role of remineralization in the phosphate maximum at 1000 m is well illustrated by the oxygen minimum at the same depth. In the absence of light (and thus of photosynthesis), phosphate accumulates passively. The same process explains the profiles of DIC. In the case of silica, the dissolution of siliceous tests is a passive phenomenon: the ocean is undersaturated with amorphous silica that constitutes the skeleton of many planktonic species (see Chapter 9).

2.3.3 Influence of Deep Circulation on the Nutrient Distribution

We still have to explain why the deep phosphate, silica and inorganic carbon concentrations are higher in the Pacific than in the Atlantic (it can be checked in Figs. 2.2 and 2.3 that this is a systematic trend). It must be always kept in mind that the ocean is always in motion and that any vertical profile reflects the relative importance of transport by currents and of chemical or biological reactions. Let's have a look at the circulation. We have seen in Chapter 1 (see also Chapter 10 for more details) that the deep waters flow from the North Atlantic to the North Pacific over a time period of the order of 1000 y. During this journey, deep waters are progressively enriched in nutrients by the remineralization of organic matter (Fig. 2.6). Symmetrically, the dissolved oxygen concentration decreases from the Pacific to the Atlantic as remineralization goes along. All these changes reflect the "aging" of deep waters.

Nutrients undergo repeated chemical and/or biological transformations that define **"biogeochemical" cycles**. Let's take the relatively simple case of the phosphate cycle. Phosphate molecules are brought to the ocean by rivers. However, the direct contribution of rivers is significant in the coastal areas only. In general, PO_4^{3-} is supplied to surface waters mainly by an internal recycling of PO_4^{3-} in the ocean, that is, by upwelling of phosphate-rich deep waters during winter mixing and/or in upwelling areas (see Chapter 7). In surface waters, PO_4^{3-} is quickly consumed by biological activity to synthesize organic molecules. At the end of the food chain, PO_4^{3-} can be carried by sinking particles to the deep ocean. As this particulate matter is remineralized, PO_4^{3-} is released into the abyss. This remineralization is very efficient: according to a first-order model (Broecker and Peng, 1982) only 1% of the organic matter that falls from the surface is buried in the sediment in the open ocean (it will be further discussed in Chapter 9 that this proportion is highest in coastal areas). In deep waters, the PO_4^{3-} molecule is not consumed. Transported by currents, it remains approximately 1000 y in the abyss until

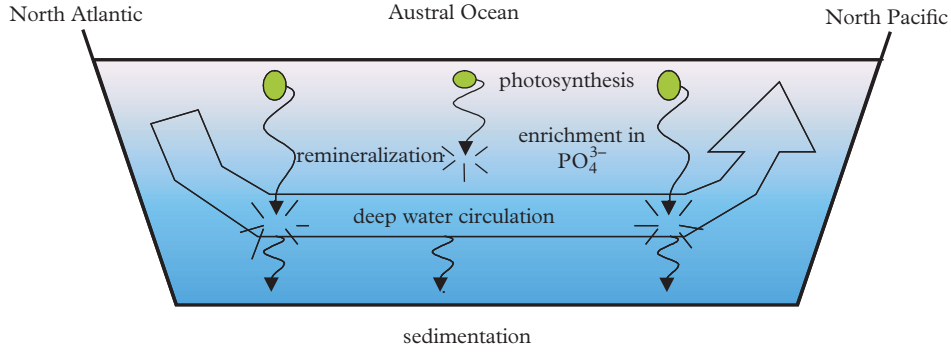

Figure 2.6 *Changes of the deep water chemical composition. During the thermohaline circulation, deep waters are enriched in nutrients by accumulation of the remineralization products due to biological activity.*

the deep water returns to the surface. There, it is again consumed by phytoplankton and the cycle is repeated. It takes between 20,000 and 80,000 y (or between 20 and 80 cycles) for this phosphate molecule to eventually leave the ocean by being permanently incorporated in the sediment on geological timescales.

The shapes of the profiles of dissolved elements depend on the interactions between dissolved and particulate matter (Fig. 2.7). The difference between the ocean mixing time (which reflects the thermohaline circulation dynamics) and the residence time of a chemical element determines its concentration profile:

- The residence time of conservative elements is much longer that the ocean mixing time and the concentration profiles of conservative elements are relatively homogeneous throughout the ocean.
- Nutrients (e.g., NO_3^-, PO_4, C, $Si(OH)_4$) have an overall residence time which is very long compared to the ocean mixing time because they are actively recycled before disappearing in the sediment. However, a concentration gradient is

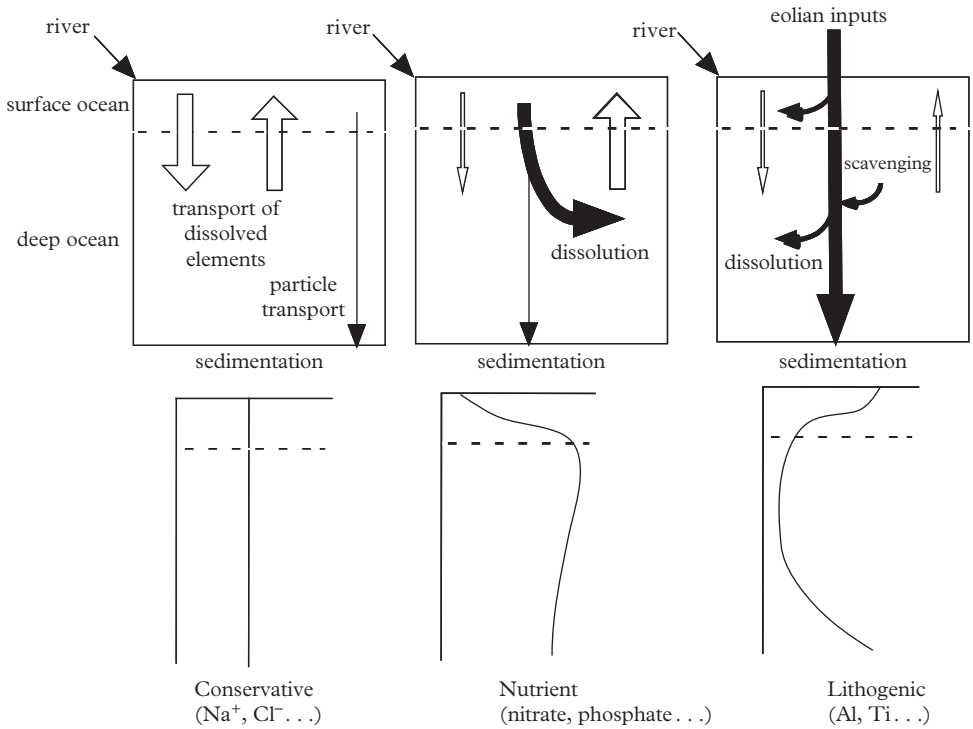

Figure 2.7 *Impact of the interactions between dissolved and particulate matter on concentration profiles. White arrows: flux of dissolved elements carried by the currents. Black arrows: particulate flux, adsorption to marine particles and remineralization. The arrow thickness gives a rough idea of the flux intensity.*

maintained between the surface and the deep waters, due to an active uptake of nutrients in surface waters and their recycling at depth.

– Elements with a residence time equal to or shorter than the ocean mixing time (e.g., Al, Th ...) are hardly soluble and quickly removed on particles. They do not have the time to be well mixed and their concentration distributions are very heterogeneous and strongly influenced by external inputs. Some of these elements have profiles with depletion at the surface and enrichment at depth without a clear involvement of the biological activity. This is the case of neodymium for example.

2.4 Gases in Seawater

In view of the role of gases such as O_2 or CO_2 in marine geochemistry, it is important to now introduce notions on their behavior (ocean–atmosphere gas exchange kinetics will be treated in Chapters 6 and 8). At the ocean surface, atmospheric gases dissolve in seawater. The chemical composition of the atmosphere is presented in Table 2.2. The abundance of gases is expressed as partial pressure, that is, by the contribution of the gas to the total atmospheric pressure. In usual conditions of temperature and pressure, the atmospheric gases behave as perfect gases. For O_2, for example, we can write $P_{O_2}^{\text{atmosphere}} = n_{O_2}RT/V$. If seawater is left long enough in contact with the atmosphere, the gas content in seawater is in equilibrium with the gas content in the atmosphere and the dissolved gas concentration is given by Henry's law

$$[O_2]^{\text{sat}} = \alpha P_{O_2}^{\text{atmosphere}}, \tag{2.6}$$

Table 2.2 *Solubility of gases in seawater*

Gas	Partial Pressure in Air[a] (atm)	α at 0°C[b] (10^{-3} mol kg^{-1} atm^{-1})	α at 25°C[b] (10^{-3}mol kg^{-1} atm^{-1})	Solubility at 25°C[c] (μmol kg^{-1})
He	0.00000524	0.349	0.332	1.68×10^{-3}
N_2	0.78084	0.794	0.507	383
O_2	0.20946	1.670	1.019	207
CFC-11	variable	26.61	7.30	Variable
Ar	0.00934	1.830	1.117	10.1
He	0.00000524			1.68×10^{-3}
CFC-12	–	65.0	20.7	–
CO_2	0.00036	62.9	28.4	9.6

[a]For a total pressure $P_{\text{total}} = 1$ atm. [b]For a salinity of 35.0. [c]For a salinity of 35.0 and at equilibrium with the atmosphere. After Coppin-Montégu (1996) and Warner and Weiss (1985).

where α is the solubility coefficient of O_2 and $[O_2]^{sat}$ is the concentration of O_2 in a seawater saturated relative to the atmosphere. $[O_2]^{sat}$ is called O_2 solubility in seawater (it has the dimensions of a concentration). Different parameters affect α:

- α depends strongly on temperature: α increases when the temperature decreases so that the gases are more soluble in cold water than in warm water (Fig. 2.8). For example, an open soda bottle better preserves its gas content in a fridge longer than in the heat.
- α also depends on the nature of the gas; small molecules are less soluble than heavy ones; a polar molecule like CO_2 is more soluble than a nonpolar molecule like O_2 (Table 2.2).
- Finally, α slightly decreases as salinity increases, but this effect will be neglected in this book. The solubility of different gases is presented in Table 2.2.

To compare the gas content of the atmosphere and seawater, the partial pressure of O_2 in seawater is defined as

$$P_{O_2}^{seawater} = \frac{[O_2]}{\alpha}, \tag{2.7}$$

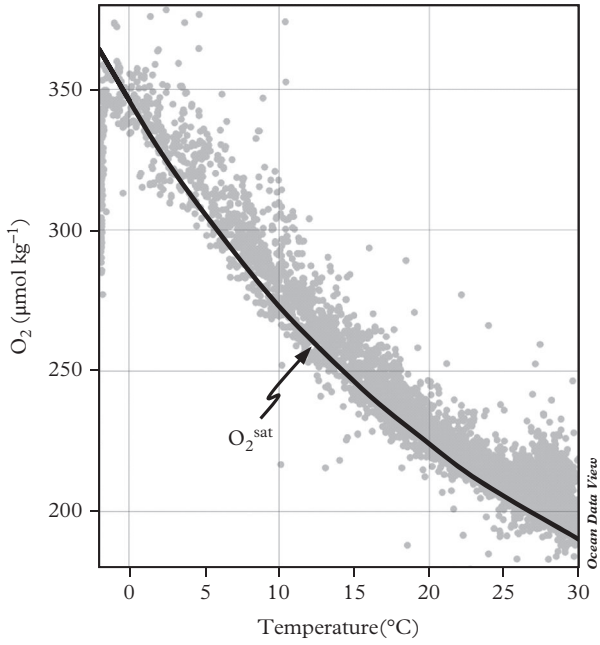

Figure 2.8 *Variation of O_2 content in surface waters. The black curve represents O_2 solubility. The points correspond to the O_2 measurements in surface waters (<10 m depth, $33.5 < S < 36.7$). Figure drawn with Ocean Data View from the e-WOCE database: http://odv.awi.de/.*

where $[O_2]$ represents the concentration of O_2 dissolved in seawater. $P_{O_2}^{seawater}$ is the partial pressure of O_2 of air in equilibrium with seawater.

The degree of O_2 saturation in seawater is defined as

$$O_2 \text{ saturation} = [O_2]/[O_2]^{sat} \times 100. \tag{2.8}$$

Note that the concentration of O_2 in seawater ($[O_2]$) is equal to the solubility of O_2 ($[O_2]^{sat}$) only when there is an equilibrium between water and air (thus when $P_{O_2}^{seawater} = P_{O_2}^{atmosphere}$). Seawater is then saturated with oxygen (% saturation = 100%). If percentage saturation is <100%, water is undersaturated in O_2, while if the percentage is >100% saturation, it is supersaturated in O_2.

An imbalance between the ocean and the atmosphere has different causes (see Problem 2). Oversaturation may come from:

- an increase in temperature;
- O_2 production by photosynthesis;
- to a lesser extent, transfer of air bubbles at a few meters of depth by breaking waves (effect of pressure on the solubility of the gas);
- mixing between water masses with different temperatures (it can be seen in Fig. 2.8 that the relationship between O_2 solubility and temperature is not linear, so that mixing of surface waters with different temperatures leads to a slight supersaturation).

On the contrary, undersaturation of O_2 can result from:

- a decrease of the temperature;
- O_2 consumption by respiration.

When water is in contact with the atmosphere, the imbalance tends to decrease by gas diffusion at the water/air interface (see Chapters 6 and 8). In the case of oxygen, it takes between 1 week and 1 month to equilibrate O_2 between the ocean mixed layer and the atmosphere. This is short compared to the season cycle so that the O_2 concentration of the mixed layer is generally close to equilibrium with the atmosphere. This is the same for most gases, with the notable exception of CO_2, which will be treated later in this chapter and in Chapter 8.

Application exercise: CFC-12 concentration

In 1980, the atmospheric partial pressure of the CFC-12 was 300×10^{-12} atm. Determine the concentration of CFC-12 in seawater at equilibrium with this atmosphere at 25°C.

$$[\text{CFC-12}]^{sat} = \alpha P_{O_2}^{atmosphere} = (20.7 \times 10^{-3}) \times (300 \times 10^{-12}) = 6.2 \times 10^{-12} \text{ mol kg}^{-1}.$$

2.4.1 Definition of Apparent Oxygen Utilization

The apparent oxygen utilization (AOU) of a water mass is the difference between the O_2 solubility and the O_2 concentration measured in this water mass

$$\mathrm{AOU} = [\mathrm{O_2}]^{\mathrm{sat}} - [\mathrm{O_2}]^{\mathrm{measured}}. \tag{2.9}$$

In surface waters, the O_2 concentration is close to saturation ($[O_2]^{sat}$), so that AOU represents the amount of oxygen used by respiration since the water mass is no longer in equilibrium with the atmosphere. The AOU of a water mass isolated from the atmosphere increases with time. During the thermohaline circulation, AOU evolves in a way that is opposite to that of the oxygen concentration. To determine $[O_2]^{sat}$ of a water mass, it is sufficient to know its potential temperature (Fig. 2.8), which is the temperature that it would have at atmospheric pressure, that is, its temperature when it was last in contact with the atmosphere.

2.5 Relationships between the Different Tracers

2.5.1 Extracting the Conservative Fraction of a Tracer

To illustrate quantitatively the influence of biology and water mass mixing on the distribution of nutrients, let's now look at samples collected in the North Atlantic between 1700 m and 4000 m deep for which θ, S, $[PO_4^{3-}]$ and AOU were analyzed (Fig. 2.9).

First, conservative elements are used to determine if there is a mixing relation between these samples. The linear relationship between θ and S (Fig. 2.10) indicates that samples are mixtures between a moderately salty and cold water (NADW, water mass 1) and a warmer and saltier water (water mass 2, influenced by the Mediterranean Water). The mixing proportions of water masses 1 in the intermediate samples are given by

$$f = (\theta_{\mathrm{m}} - \theta_2)/(\theta_1 - \theta_2). \tag{2.10}$$

Conversely, the relationship between θ (conservative) and AOU or PO_4^{3-} (non-conservative) is not linear, indicating that these parameters are not conservative. Indeed, AOU or PO_4^{3-} does not depend only on water mass mixing, but also on the remineralization of the particulate organic matter. In deep waters, bacteria and animals consume oxygen (which raises the AOU) and reject phosphate in the proportion of the O/P Redfield ratio. The O/P stoichiometric ratio can be calculated from the above data. Having found f with equation (2.10), we calculate $\mathrm{AOU}_{\mathrm{conservative}}$ and $PO_{4\ \mathrm{conservative}}^{3-}$, which are the concentrations that would be expected if AOU and PO_4^{3-} were conservative parameters

$$\mathrm{AOU}_{\mathrm{conservative}} = f \times \mathrm{AOU}_1 + (1-f)\mathrm{AOU}_2, \tag{2.11a}$$

$$[\mathrm{PO_4^{3-}}]_{\mathrm{conservative}} = f \times [\mathrm{PO_4^{3-}}]_1 + (1-f)[\mathrm{PO_4^{3-}}]_2. \tag{2.11b}$$

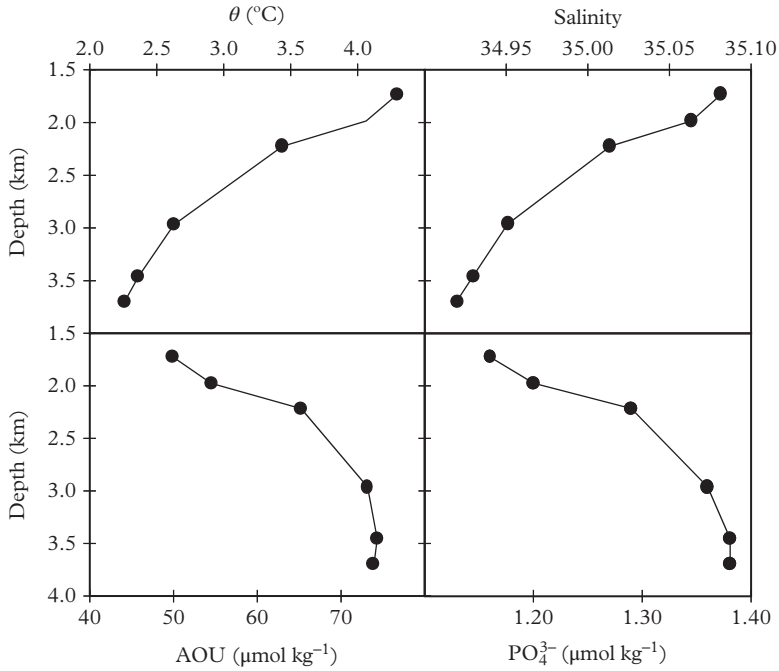

Figure 2.9 *Vertical variations of AOU, S, θ and* PO_4^{3-} *in the North Atlantic.*

We can then obtain the change in AOU and PO_4^{3-} produced by remineralization

$$\Delta AOU = AOU_{measured} - AOU_{conservative}, \tag{2.12a}$$

$$\Delta[PO_4^{3-}] = [PO_4^{3-}]_{measured} - [PO_4^{3-}]_{conservative}. \tag{2.12b}$$

Finally, we calculate the $\Delta AOU/\Delta[PO_4^{3-}]$ ratio, which is the ratio in which oxygen is used and PO_4^{3-} excreted during remineralization. Despite some dispersion, these values are relatively comparable to the value of Redfield, around 140 (Fig. 2.10).

It is therefore possible to separate the relative contribution of mixing and remineralization in the evolution of non-conservative tracer concentration in seawater (see Problems 3 and 4).

2.5.2 Construction of Conservative Tracers

The cycles of major nutrients are coupled together, as shown by equations (2.3) and (2.5). So, in principle, it is possible to reconstruct the evolution of the concentration of a nutrient based on the evolution of another nutrient. One of the applications

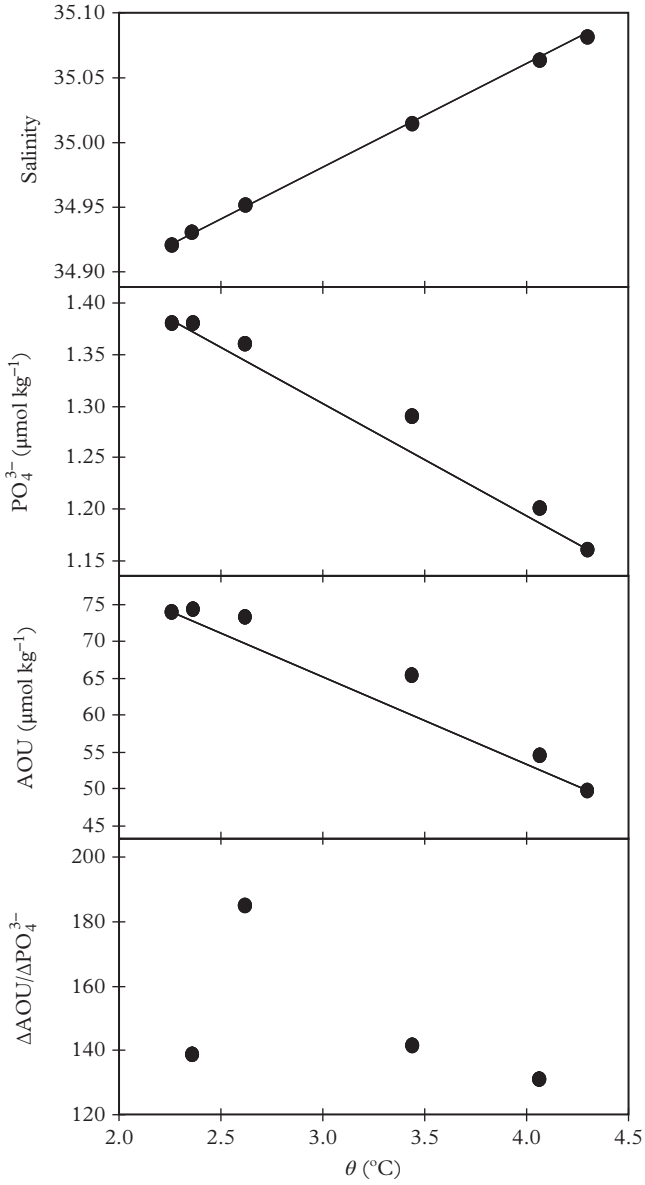

Figure 2.10 *Variations of S, $[PO_4^{3-}]$, AOU and $\Delta AOU/\Delta PO_4^{3-}$ with θ in the North Atlantic.*

of this principle is the construction of conservative tracers with nutrients. For example, preformed phosphate is defined as

$$\text{Preformed phosphate} = [PO_4^{3-}] + \text{AOU} \times (-1/138), \tag{2.13}$$

where PO_4^{3-} and AOU are the phosphate concentration and apparent oxygen utilization of the water mass. 1/138 is the Redfield ratio between PO_4^{3-} and O_2; it allows conversion of the amount of oxygen used into a quantity of remineralized PO_4^{3-}.

Preformed phosphate represents the concentration of PO_4^{3-} that the water mass should have had when it was in equilibrium with the atmosphere at the ocean surface. The term "preformed" is equivalent to "initial." This parameter is useful for discriminating between the NADW (preformed phosphate = 0.80 μmol kg^{-1}, low PO_4^{3-} concentration because there is PO_4^{3-} consumption in surface waters) and the AABW (preformed phosphate = 1.6 μmol kg^{-1}, high concentration because strong vertical mixing supplies PO_4^{3-}-rich waters and the lack of light limits photosynthesis and PO_4^{3-} consumption in the surface waters: therefore it leaves the surface waters with a high PO_4^{3-} concentration). However, this type of tracer must be used with caution because it depends on many assumptions, in particular on the Redfield ratio. The tracer PO_4^* (Broecker et al., 1991) is now preferred to preformed phosphate

$$PO_4^* = [PO_4^{3-}] + [O_2] \times 175 - 1.95\ \mu\text{mol kg}^{-1},$$

which corresponds to a P/O Redfield ratio of 1/–175 and a concentration of oxygen saturation independent of temperature. NADW and AABW are specifically identified on the basis of the tracer PO_4^* ($PO_4^* = 0.73 \pm 0.03$ μmol kg^{-1} in the NADW, $PO_4^* = 1.63 \pm 0.03$ μmol kg^{-1} in the AABW).

Similarly, the preformed nitrate of a water mass can also be defined. These new tracers increase the number of "conservative" parameters that can be used to determine the number and the proportions of water masses present in a given sample.

2.5.3 Horizontal and Vertical Changes of Tracers

In the example in Section 2.5.2, we have interpreted the changes in tracer concentration along a vertical profile as a result of the combination of water mass mixing and biological activity along this profile. However, we have seen in Chapter 1 that often water mass mixing is not vertical, but essentially occurs along isopycnal surfaces, particularly in the thermocline where density gradients are very strong. When an isopycnal surface outcrops at the surface of the ocean, its PO_4^{3-} concentration is low (surface water) and its O_2 concentration is in equilibrium with the atmosphere. As seawater moves downward along this isopycnal surface, its PO_4^{3-} concentration increases and its O_2 concentration decreases due to the remineralization (Fig. 2.11a and b).

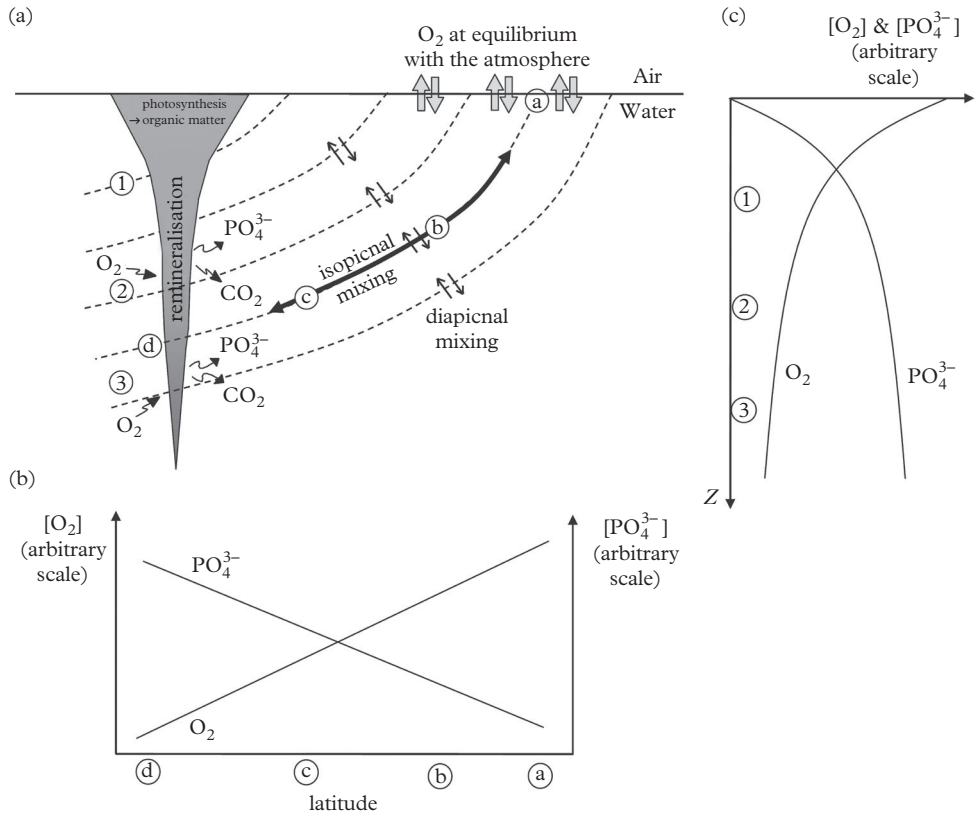

Figure 2.11 *Variations of PO_4^{3-} and O_2 in the thermocline. (a) Principle. (b) Evolution on an isopycnal surface. (c) Vertical profile.*

In fact, a vertical concentration profile is the result of the piling up of isopycnal surfaces. These surfaces are all the more isolated from the atmosphere and have experienced remineralization since they are located at depth (Fig. 2.11c). PO_4^{3-} and O_2 concentrations are expected to be correlated along an isopycnal surface (Fig. 2.12).

Application exercise: evolution of concentrations along an isopycnal surface

Figure 2.12 shows O_2 and PO_4^{3-} concentrations in the North Atlantic on the surface of density $\sigma = 27.0$.

(a) At which latitude does this surface outcrop? Down to which depth is it present?

(b) Determine the P/O Redfield ratio.

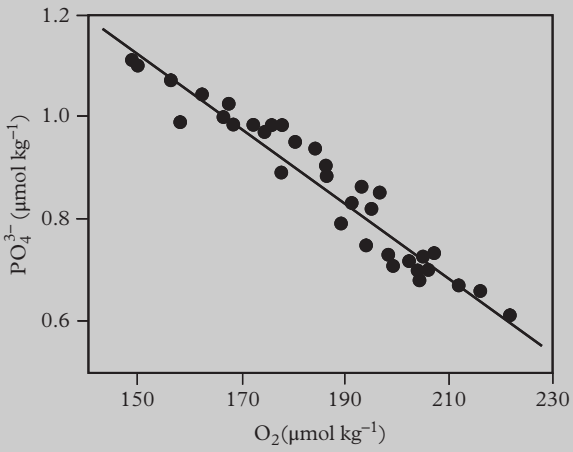

Figure 2.12 *PO_4^{3-} variations with O_2 in the North Atlantic with the surface density $\sigma = 27.0$. Changed according to Takahashi et al. (1985).*

Answers:

(a) In Fig. 1.6 of Chapter 1, this surface is in contact with the atmosphere at 65°N and it deepens down to 600 m at 30°N.

(b) O_2 and PO_4^{3-} concentrations are aligned on a straight line of slope: $\Delta[PO_4^{3-}]/\Delta[O_2] = -138$ mol mol^{-1}.

2.6 Carbon Chemistry

Carbon plays an important role in seawater chemistry for different reasons:

- It is the main component of the organic matter.
- The various species of DIC determine the pH of seawater.
- By its control on the atmospheric CO_2 content, the oceanic carbon cycle is at the heart of many oceanographic research programs. Chapter 8 being devoted to these questions, we describe here only a few basic principles.

2.6.1 The Carbonate System

Carbon dioxide (CO_2) is not like the other gases. While the oxygen concentration measured in a surface water is usually close to the solubility, $[O_2]^{sat}$, DIC concentrations in the surface waters are of the order of 2000 μmol kg^{-1} while the CO_2 solubility does not exceed 23 μmol kg^{-1} (Table 2.2). Where does such a difference come from? In seawater, dissolved CO_2 represents approximately 1% of the DIC. The most abundant species are the bicarbonate ion (HCO_3^-) and carbonate ion (CO_3^{2-}) which represent approximately

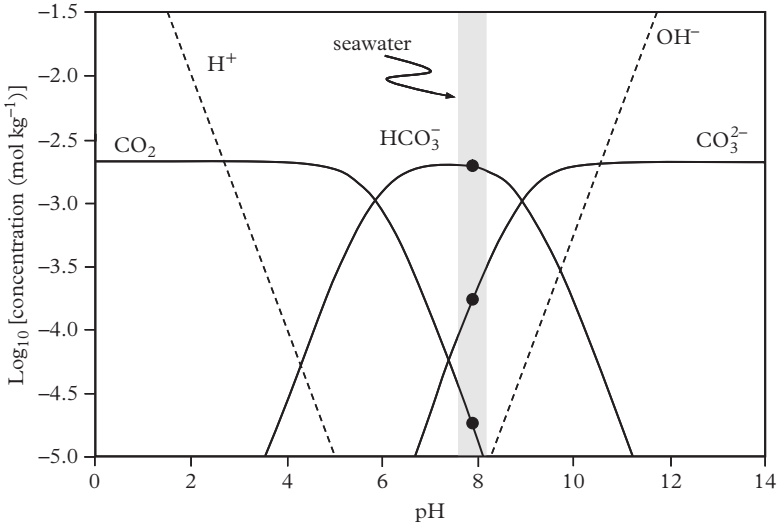

Figure 2.13 *Concentration of chemical species in the carbonate system. Gray band: range of pH in the ocean. Black points: concentration of* HCO_3^-, CO_3^{2-} *and* CO_2 *in seawater. Note that* $[HCO_3^-] \gg [CO_3^{2-}] \gg [CO_2]$. *Modified from Ridgwell and Zeebe (2005).*

89 and 10% of DIC in the ocean (Fig. 2.13). CO_2 is a diacid which dissociates following the reactions

$$CO_2 + H_2O \Leftrightarrow HCO_3^- + H^+ \qquad K_1 = \frac{[HCO_3^-][H^+]}{[CO_2]} \tag{2.14a}$$

$$HCO_3^- \Leftrightarrow CO_3^{2-} + H^+ \qquad K_2 = \frac{[CO_3^{2-}][H^+]}{[HCO_3^-]} \tag{2.14b}$$

where K_1 and K_2 are thermodynamic constants depending on temperature and pressure (at 25°C and atmospheric pressure, for a salinity of 35.0, $K_1 = 1.392 \times 10^{-6}$ and $K_2 = 1.189 \times 10^{-9}$).

The inventory of acids and bases present in seawater indicates that dissolved CO_2 and CO_3^{2-} are, respectively, the strongest acid and the strongest base in seawater. They react together according to the reaction

$$CO_2 + CO_3^{2-} + H_2O \Leftrightarrow 2\,HCO_3^-. \tag{2.15}$$

It is the equilibrium between carbonate species that determines the pH of seawater. From equations (2.14a) and (2.14b) and the relative proportions of dissolved CO_2, HCO_3^- and CO_3^{2-} given above, we calculate $[H^+] \approx 10^{-8}$ mol kg^{-1}. It follows that

$$pH_{seawater} = -\log_{10}[H^+] \approx 8. \tag{2.16}$$

Note that for an accurate calculation, it is necessary to also take into account the boron species. In seawater, 80–90% of the boron forms boric acid ($B(OH)_3$) and 10–20% forms borate ions ($B(OH)_4^-$). The boric acid/borate ion proportion is determined by the equilibrium

$$B(OH)_3 + H_2O \Leftrightarrow B(OH)_4^- + H^+ \tag{2.17}$$

which depends on the pH. At 25°C, atmospheric pressure and salinity of 35.0, $K_B = 2.526 \times 10^{-9}$.

The pH of seawater varies with temperature and the proportion of the carbonate ion and dissolved CO_2; at a given temperature, surface seawater is depleted in CO_2 by photosynthesis and is therefore a little less acidic than a deep water in which organic carbon remineralization has released CO_2 (Fig. 2.14).

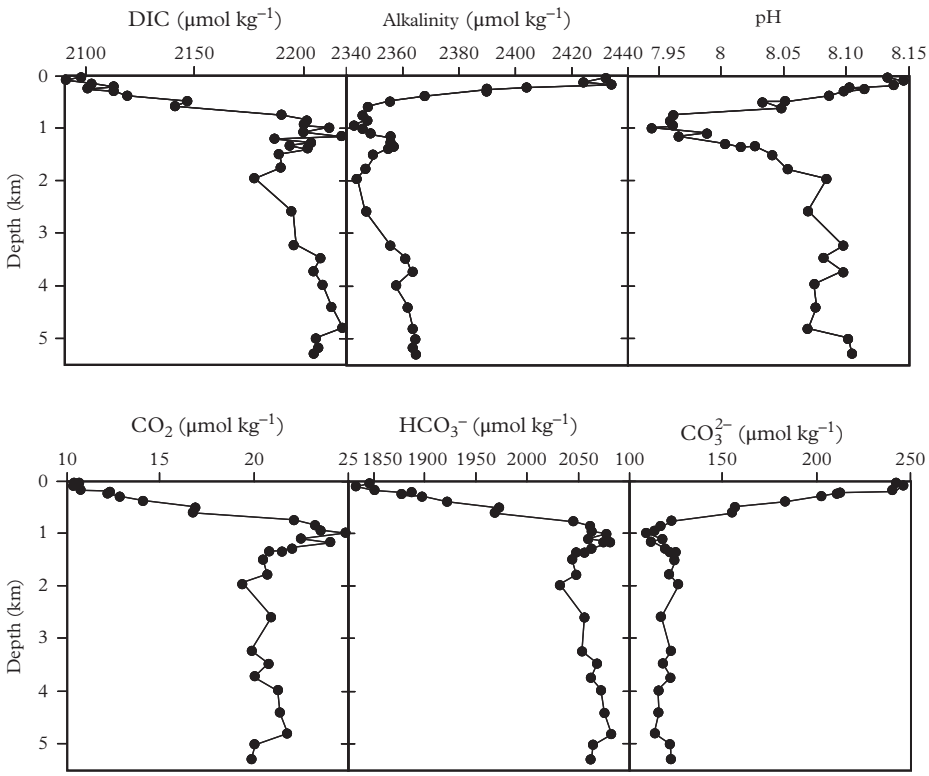

Figure 2.14 *The carbonate system on the Geosecs section 115 B (26° W, 27° N) in the North Atlantic.*

2.6.2 Calcium Carbonate

Carbonate ions are involved in the formation of a mineral, calcium carbonate ($CaCO_3$), according to the reaction

$$Ca^{2+} + CO_3^{2-} \Leftrightarrow CaCO_{3(solid)}. \qquad \text{precipitation of a solid}$$

$CaCO_3$ is a solid which can be precipitated with different crystallographic forms: the most common is calcite (rhombohedral form), but it also occurs as aragonite (orthorhombic form). $CaCO_3$ stability depends on the value of the product $[Ca^{2+}] \times [CO_3^{2-}]$ compared to the value of the solubility product K_s (at 25°C, atmospheric pressure and for a salinity of 35, $K_{s\text{-calcite}} = 4.47 \times 10^{-7}$ mol^2 kg^{-2} and $K_{s\text{-aragonite}} = 6.76 \times 10^{-7}$ mol^2 kg^{-2}). $K_{s\text{-calcite}}$ and $K_{s\text{-aragonite}}$ increase significantly with pressure (of the order of a factor of 2 between 0 and 5000 m). As the concentration of Ca^{2+} is fairly constant in the ocean, the stability of carbonates is mainly determined by the CO_3^{2-} concentration and depth (Fig. 2.15). The saturation state of seawater with respect to $CaCO_3$ is determined from

$$\Omega = [Ca^{2+}][CO_3^{2-}]/K_s.$$

- If $\Omega < 1$, seawater is undersaturated with respect to $CaCO_3$, which tends to dissolve spontaneously.
- If $\Omega = 1$, seawater is saturated (in equilibrium) with respect to $CaCO_3$, which is stable.
- If $\Omega > 1$, seawater is supersaturated with $CaCO_3$, which, in theory, could precipitate spontaneously.

Although $\Omega > 1$ in surface and intermediate waters, $CaCO_3$ precipitation is never spontaneous: it is always controlled by living beings that produce shells or skeletons also called "**tests**." Conversely, living organisms in CO_3^{2-}-poor deep water form shells although $\Omega \ll 1$. Nevertheless, there is no contradiction between the precipitation of $CaCO_3$ in an undersaturated seawater and thermodynamics: some living beings simply create microenvironments where chemical conditions ($\Omega \gg 1$) differ substantially from the surrounding seawater.

The depth of the **carbonate saturation horizon** is defined by $\Omega = 1$. A few hundred meters below this saturation horizon, the **lysocline** is the depth at which a mineral (here calcite or aragonite) starts to dissolve significantly because seawater is undersaturated with respect to this mineral. Etching marks of the carbonate tests are visible and the carbonate content of the sediment starts to decline. In the North Atlantic, the lysocline of aragonite occurs around 3500 m and that of calcite at 5000 m. In the North Pacific, the lysocline of calcite and aragonite are reached around 1000 m due to the low CO_3^{2-} concentration.

The **compensation depth** of calcite (CCD) and aragonite (ACD) is the depth at which these minerals disappear from the sediments. This depends both on the lysocline

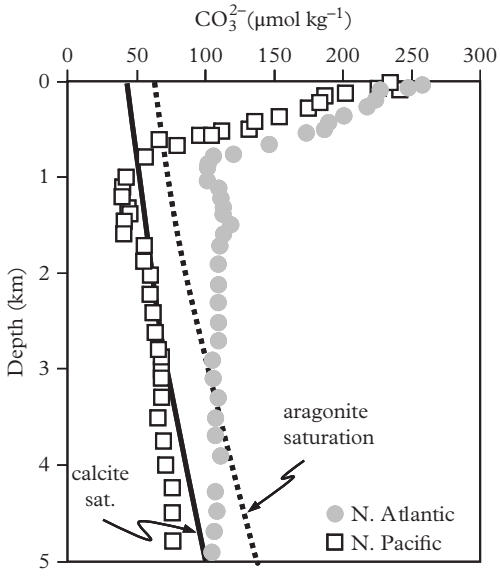

Figure 2.15 *Saturation of carbonates and CO_3^{2-} concentration. Saturation curves (sat.) show that aragonite starts to dissolve at shallower depth than calcite. Low CO_3^{2-} concentration in the deep Pacific implies a greater solubility of carbonates compared to the deep Atlantic.*

depth (the compensation point is necessarily below the lysocline) and on the rain rate of carbonate from the surface waters (it will be deeper when the flux of carbonate tests settling—"raining"—from the photic zone is large). The compensation depth is usually 500–1000 m below the lysocline.

2.6.3 Organic Carbon

Even if DIC represents most of the oceanic carbon, a small fraction of the oceanic carbon occurs in organic molecules. Dissolved organic carbon (DOC) represents only a few percent of the total oceanic carbon, but it is the main reservoir of organic carbon at the Earth's surface. DOC is made of a multitude of molecules produced by biological activity (molecules exuded by phytoplankton, excreted by zooplankton, produced by the degradation of organic matter by bacteria, etc.) and with very different chemical behaviors: sugars and proteins are called "labile" components because they are quickly recycled by biological activity, while lipids that are more resistant to bacterial activity are said to be "refractory." The DOC concentrations are higher in surface waters (60–80 μM), where DOC is formed, than in the deep ocean depth (34–48 μmol kg^{-1}), where DOC is only consumed by bacterial activity (Fig. 2.16). In deep water, there is a decrease of the DOC concentrations from the North Atlantic to the North Pacific that reflects the progressive oxidation of DOC during the circulation of the deep waters.

Particulate organic carbon (POC) represents the organic carbon contained in all living organisms and particulate organic detritus. The POC is much less abundant than the dissolved organic carbon. The POC concentration carried by small particles in suspension in seawater is of the order of 2–3 μmol kg^{-1} in surface waters and of the order of 0.04–0.01 μmol kg^{-1} in deep waters.

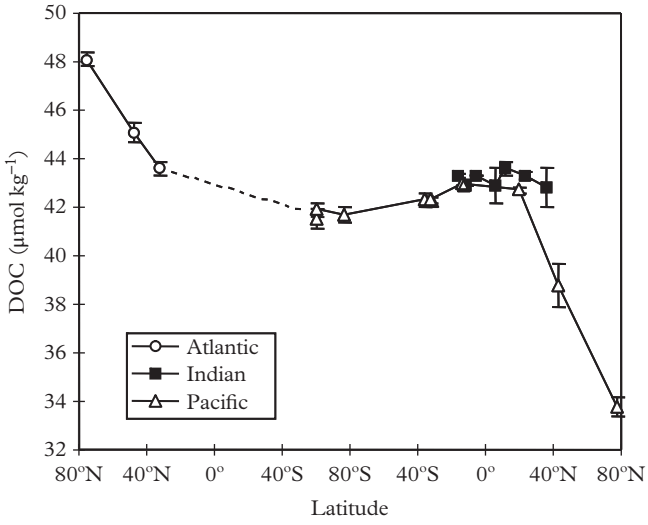

Figure 2.16 *Evolution of the DOC concentration in the deep ocean. Modified from Hansell and Carlson (1998).*

2.7 The Redox Conditions in the Ocean

Redox reactions are chemical reactions in which one or more electrons are transferred from one compound to another. The compound that gives electrons is oxidized while the compound receiving them is reduced. During photosynthesis, inorganic molecules such as CO_2, NO_3^- and SO_4^{2-} are reduced (they receive electrons) to organic carbon, organic nitrogen (or ammonia) and organic sulfur compounds. For example

$$CO_2 + H_2O \rightarrow O_2 + CH_2O$$

can be decomposed into

$$CO_2 + 4\ e^- + 4\ H^+ \rightarrow CH_2O + H_2O \text{ (carbon reduction)}$$

and

$$2\ H_2O \rightarrow O_2 + 4\ e^- + 4\ H^+. \text{ (water oxidation)}$$

Similarly, during remineralization, carbon and organic nitrogen are oxidized (they lose one or more electrons) to CO_2 and NO_3^-. Photosynthesis allows solar energy to be collected and to be stored as chemical energy, while respiration (remineralization) allows retrieval of this energy for the functioning of living cells. Generally, the redox reactions are often slow if they are not catalyzed by enzymes. Thus, organic matter produced by plankton contains an excess of energy, which makes it thermodynamically unstable

in seawater, but in the absence of bacterial activity, it is oxidized very slowly. This is called a metastable state. It allows organic compounds to store chemical energy that can be transported, for example, in the deep ocean and on the ocean floor to feed abyssal ecosystems.

Although there are no free electrons in solution, a virtual electron concentration is defined to quantify the oxidizing or reducing character of the environment. It is based on the reduction of water (H^+ represents water)

$$H^+ + e^- \rightarrow \tfrac{1}{2}\, H_2.$$

By setting arbitrarily that the change in Gibbs free energy (ΔG°) of this half-reaction is null, the law of mass action can be written as

$$P_{H_2}^{1/2}/([H^+][e^-]) = e^{-\Delta G^\circ/RT} = 10^0,$$

where $R = 8.314$ J mol^{-1} K^{-1} and T is the absolute temperature. This allows determination of the concentration of electrons

$$[e^-] = (P_{H_2})^{1/2}/[H^+].$$

A pe scale is defined like the pH scale: $pe = -\log_{10}[e^-]$.

A high pe corresponds to oxidizing environments. Redox couples tell us about the pe of seawater.

Dissolved oxygen is the primary electron acceptor in seawater. Surface waters are O_2-repleted (photosynthesis and equilibrium with the atmosphere), so that they contain O_2 and H_2O simultaneously

$$\tfrac{1}{2}\, H_2O \rightarrow \tfrac{1}{4}\, O_2 + e^- + H^+ \qquad \text{with } \Delta G^\circ = -118.6 \text{ kJ mol}^{-1}.$$

In applying the law of mass action, we obtain $[e^-][H^+](P_{O_2})^{1/4} = 10^{-20.75}$

The pe of seawater is then given by the relationship

$$pe = -20.75 + 1/4 \log_{10}(P_{O_2}) - pH.$$

In deep waters, respiration causes a decrease of the O_2 concentration. This depletion increases when waters remain at depth for a long time (Fig. 2.3). Sometimes, it produces anoxia, that is, of a total absence of O_2. This is the case in some isolated basins (Black Sea) or when waters isolated for a long time from the atmosphere are subject to intense remineralization in upwelling areas (Arabian Sea, Eastern Pacific). The biological conditions are then strongly modified. It is NO_3^- which is then used as electron acceptor

$$NO_3^- + 6\, H^+ + 5\, e^- \Leftrightarrow \tfrac{1}{2}\, N_2 + 3\, H_2O.$$

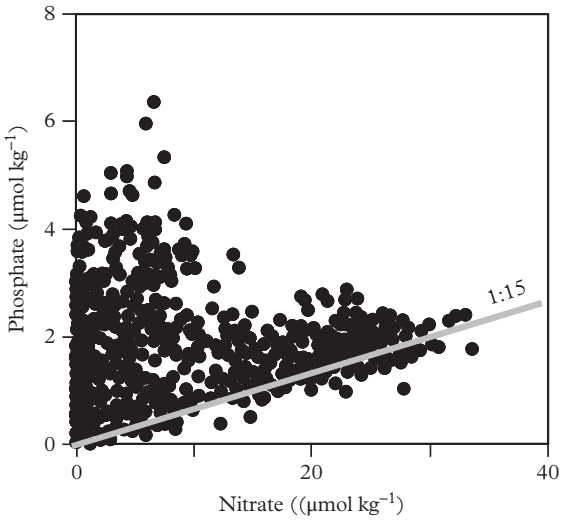

Figure 2.17 *Concentrations of dissolved inorganic nitrogen and dissolved inorganic phosphate in the Arabian Sea. The straight line corresponds to the P/N ratio of 1:15 generally measured in seawater. Samples located above this line have lost nitrogen by denitrification. In the absence of nitrogen, phosphate is not consumed by phytoplankton. Modified after Bange et al. (2005).*

This is **denitrification**. Denitrification is well known in organic-rich marine sediments (see Chapter 8) and anoxic waters (Fig. 2.17). More recently, denitrification has been observed in the thermocline through the variations of the P/N ratio that it induces in seawater. Denitrification is a sink for nitrate in the ocean.

In seawater and marine sediments, the environment is rarely reducing enough to produce hydrogen H_2 (this is sometimes the case around natural oil seeps, as in the Gulf of the Mexico). However, the reduction of sulfur from SO_4^{2-} to HS^- and then the reduction of CO_3^{2-} to CH_4 are frequently observed in sediments

$$SO_4^{2-} + 9\ H^+ + 8\ e^- \Leftrightarrow HS^- + 4\ H_2O$$

$$HCO_3^- + 9\ H^+ + 8\ e^- \Leftrightarrow CH_4 + 3\ H_2O.$$

This corresponds to the mass action laws

$$[HS^-]/([SO_4^{2-}][e^-]^8[H^+]^9) = 10^{-33.92}$$

$$[CH_4]/([HCO_3^-][e^-]^8[H^+]^9) = 10^{-27.2}.$$

The pe of seawater is then given by the relationships

$$pe = 1/8\ (33.92 + \log_{10}([HS^-]/([SO_4^{2-}]) - 9\ pH);$$

$$pe = 1/8\ (27.2 + \log_{10}([CH_4]\ /([HCO_3^-]) - 9\ pH).$$

As the H^+ ions are involved in redox half-reactions, pe–pH diagrams are used to determine the stability field of the chemical species (Fig. 2.18).

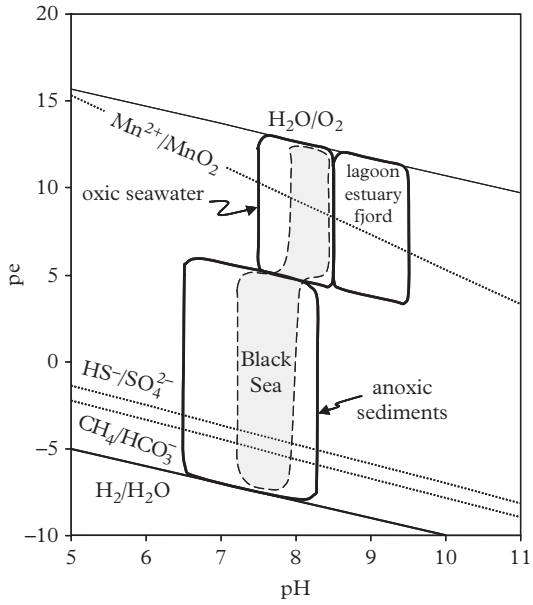

Figure 2.18 *pe–pH conditions encountered in the ocean. The theoretical stability limits of a few chemical species are identified. The presence of metastable species makes the use of this diagram delicate. Adapted from different sources.*

Given the reduced pH range in seawater, the diagram shows that the presence of O_2/H_2O, SO_4^{2-}/HS^-, CO_3^{2-}/CH_4 or Mn^{2+}/MnO_2 strongly constrains the pe in principle. Strongly reducing conditions occur in closed and very stratified basins as the Black Sea (see Problem 5). It is difficult, however, to use chemical equilibria between oxidized and reduced species to determine the redox condition (see Section 2.8.2 for the case of manganese).

2.8 Behavior of Trace Metals

In the ocean, trace elements are defined as any chemical species with a concentration of the order of 10^{-6} g g^{-1} (or 1 ppm, for parts per million, which corresponds to a piece of sugar in 6 tons of water) or less. Many metals fall into this category, with concentrations ranging from 10^{-8} g kg^{-1} (i.e., well below the ppm!) to less than 10^{-18} g kg^{-1} for some very scarce short-lived radioactive isotopes.

2.8.1 The Different Types of Profiles

Trace metals have a very wide range of behaviors: some are relatively conservative (rhenium, osmium and uranium, for example); others are used as enzyme cofactors by algae and have nutrient profiles (this is the case of cadmium and zinc, which are therefore called "micronutrients"); finally others have a behavior controlled by their uptake and release by particles (thorium, aluminum, manganese, neodymium, etc.) or

mixed biological/particulate behavior (iron). The behavior of metals in the ocean is strongly influenced by their chemical properties (complexation, oxidation state, precipitation of solid phases), which determine their speciation and thus their solubility and/or their availability for living beings. Metals with a high degree of oxidation (>V) often form very soluble oxyanions in oxygen-rich waters. For example, Re^{7+} forms ReO_4^- in seawater, so that rhenium has a generally conservative behavior, as shown by the good correlation between dissolved rhenium and salinity (Fig. 2.19). U^{6+} forms the extremely soluble UO_2^{2+} cation which is stabilized by the presence of carbonate ions, just like Ca^{2+}. These metals are soluble when they are oxidized, but they become insoluble in reducing environments. Thus, they are removed from anoxic waters and found in high concentration in organic-rich sediments. Many elements which have an oxidation state of IV (Th^{4+}, Ce^{4+}, Mn^{4+}) form extremely insoluble hydroxides ($Th(OH)_4$, $Ce(OH)_4$, $Mn(OH)_4$). This is also the case for elements with an oxidation degree III when they have a small ionic radius (Fe^{3+}, Al^{3+} and rare earth elements such as Nd^{3+}). Their concentration in seawater depends heavily on local inputs: high variations of dissolved Al concentration are due to very variable continental inputs between the Central Pacific and the Mediterranean Sea (Fig. 2.19(b)). The reduction of these metals causes an increase of their solubility ($Fe^{3+} \rightarrow Fe^{2+}$, $Mn^{4+} \rightarrow Mn^{2+}$, $Ce^{4+} \rightarrow Ce^{3+}$). Finally, some metals are enzyme cofactors so that they have nutrient-type profiles controlled by biological activity (Fe, Zn, Cd, etc.), which explains the similarity of dissolved Cd and phosphate profiles (Fig. 2.19(a)). Other examples will be considered in Problems 6 and 7.

2.8.2 Oxidation and Reduction of Manganese

In seawater, manganese occurs as dissolved Mn^{2+} (reduced) and particulate Mn^{4+} (oxidized) that precipitates as MnO_2 solid on marine particles. We can calculate the concentration of dissolved Mn^{2+} in equilibrium with solid MnO_2. The oxidation reaction is

$$Mn^{2+} + 2\,H_2O \Leftrightarrow MnO_{2(solid)} + 2\,e^- + 4\,H^+ \text{ with } \Delta G^\circ = -237.4 \text{ kJ mol}^{-1}.$$

Applying the law of mass action, we obtain

$$[e^-]^2[H^+]^4/[Mn^{2+}] = 10^{-41.6}.$$

At pH = 8 and pe = 12 (surface conditions) we can deduce

$$[Mn^{2+}] = [e^-]^2[H^+]^4/10^{-41.6} = 10^{(-2\times12-4\times8+41.6)} = 10^{-14.4} \text{ mol kg}^{-1}.$$

This extremely low value means that Mn must be fully oxidized and fixed on marine particles. However, concentrations observed in seawater are much higher: from 10^{-9} to 2.5×10^{-9} mol kg^{-1} (Fig. 2.20). In practice, the reaction rate is so slow that the

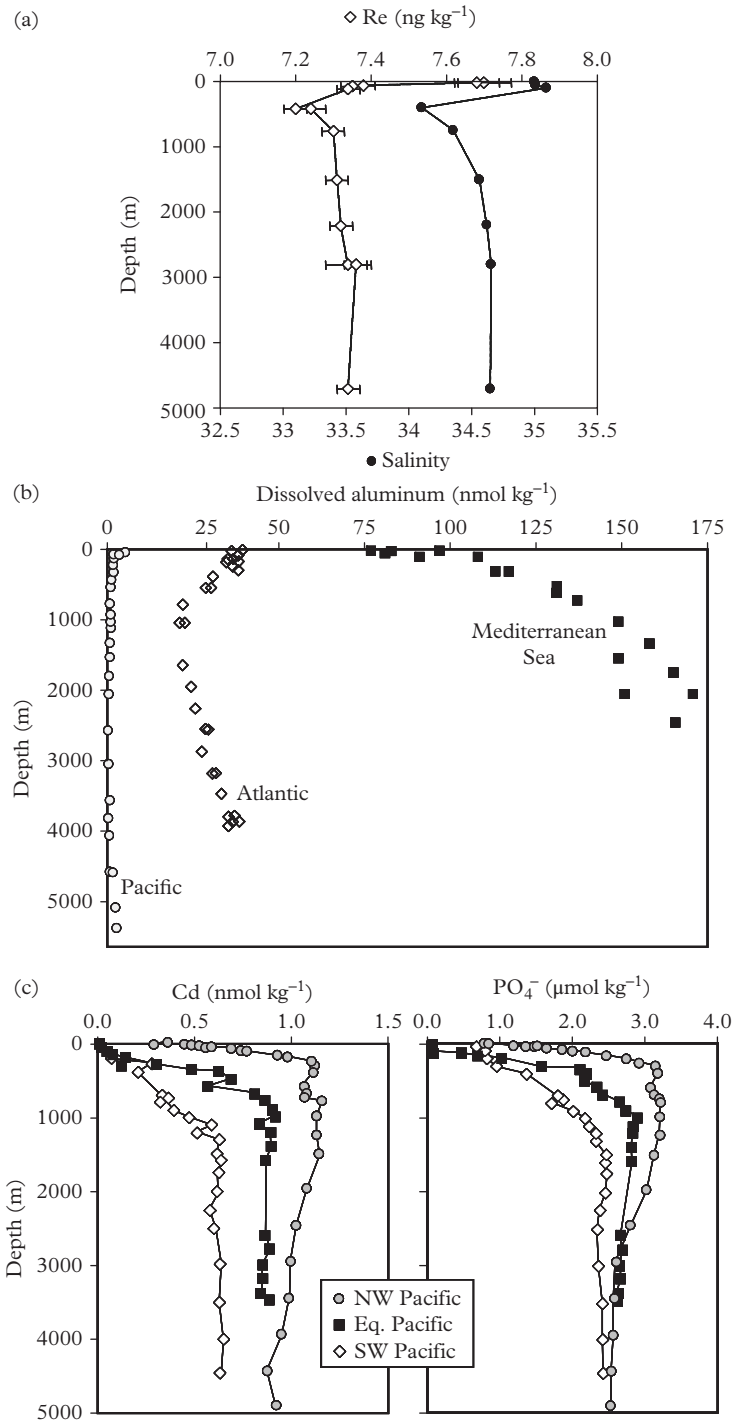

Figure 2.19 *Characteristic profiles of trace elements. (a) Dissolved rhenium and salinity with conservative behavior. (b) Dissolved aluminum showing the reactive behavior of an element with particles. (c) Cadmium and phosphate dissolve with a nutrient behavior. Modified from Anbar et al. (1992), Bruland and Lohan (2003) and Abe (2004).*

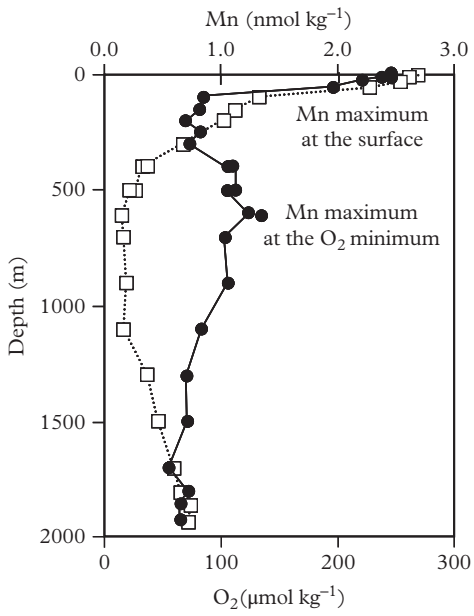

Figure 2.20 *Concentration of dissolved Mn and O_2 in the Pacific Ocean. Modified from Johnson et al. (1996).*

thermodynamic equilibrium is rarely reached. Moreover, in surface waters, the photochemical reactions (catalyzed by light) are important: the photo-reduction of Mn oxides explains the high concentrations in surface waters. During the oxidation of organic matter, Mn(IV) serves as an electron acceptor and it is reduced to Mn^{2+}. This reaction takes place in micro-environments created by the organic matter decomposition (fecal pellets). Mn^{2+} then diffuses into seawater. This explains the increase of the Mn concentration around 700 m deep in the O_2 minimum zone.

2.8.3 Complexation of Iron

In waters containing oxygen, iron is in its most oxidized form: Fe(III). Fe(III) forms insoluble hydroxides according to the reaction

$$Fe^{3+} + 3\ OH^- \leftrightarrow Fe(OH)_{3(solid)} \quad pK_s = 38.7$$

For seawater at pH = 8, we obtain a very low Fe^{3+} solubility

$$[Fe^{3+}] = 10^{-pK_s}/[OH^-]^3 = 10^{-38.7+3\times(14-8)} = 10^{-20.7} \text{mol kg}^{-1},$$

which is much less than the dissolved iron concentrations measured in seawater, which are of the order of 10^{-10}–10^{-9} mol kg^{-1}.

Iron, as other metals, form complexes with hydroxide ions

$$Fe^{3+} + H_2O \Leftrightarrow Fe(OH)^{2+} + H^+ \qquad p\beta_1 = 2.43$$
$$Fe^{3+} + 2\,H_2O \Leftrightarrow Fe(OH)_2^+ + 2\,H^+ \qquad p\beta_2 = 7.12$$
$$Fe^{3+} + 3\,H_2O \Leftrightarrow Fe(OH)_3 + 3\,H^+ \qquad p\beta_3 = 12.32$$
$$Fe^{3+} + 3\,H_2O \Leftrightarrow Fe(OH)_4^- + 4\,H^+ \qquad p\beta_4 = 21.6$$

The total iron in solution is given by

$$\begin{aligned} Fe_{total} &= [Fe^{3+}] + [Fe(OH)^{2+}] + [Fe(OH)_2^+] + [Fe(OH)_3] + [Fe(OH)_4^-] \\ &= [Fe^{3+}] + [Fe^{3+}] \times \beta_1/[H^+] + [Fe^{3+}] \times \beta_2/[H^+]^2 + [Fe^{3+}] \times \beta_3/[H^+]^3 \\ &\quad + [Fe^{3+}] \times \beta_4/[H^+]^4 \\ &= [Fe^{3+}](1 + \beta_1/[H^+] + \beta_2/[H^+]^2 + \beta_3/[H^+]^3 + \beta_4/[H^+]^4). \end{aligned}$$

Considering that pH = 8 and $[Fe^{3+}] = 10^{-20.7}$ mol kg^{-1}, we obtain (Fig. 2.21)

$$\begin{aligned} Fe_{total} &= 10^{-20.7}(1 + 10^{-2.43+8} + 10^{-7.12+16} + 10^{-12.32+24} + 10^{-21.6+32}) \\ &= 10^{-20.7}(1 + 10^{+5.57} + 10^{+8.88} + \boxed{10^{+11.68}} + 10^{+10.4}) \\ &\qquad\qquad\qquad\qquad\qquad\qquad \downarrow \\ &\qquad\qquad\qquad\qquad\qquad \text{Most abundant species} \\ &= 1.0 \times 10^{-9} \text{mol kg}^{-1}, \end{aligned}$$

which is close to the values measured in seawater. We see that the formation of complexes stabilizes Fe(III) in solution.

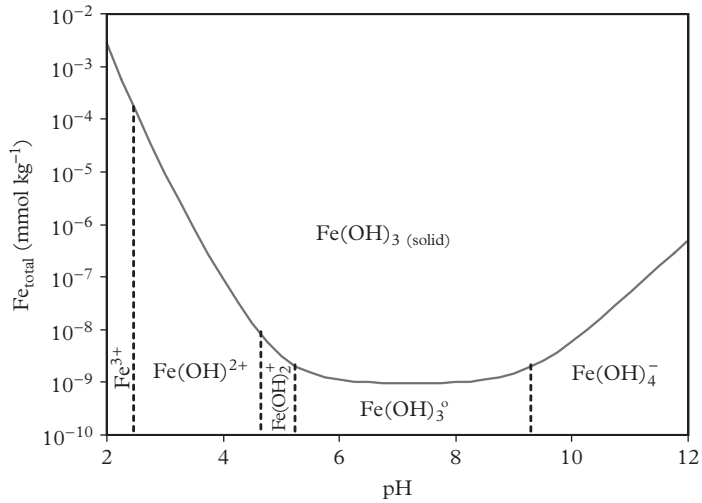

Figure 2.21 *Fe hydroxides solubility with pH. Fe solubility is lowest in the seawater pH range. Modified from Millero (1998).*

Limitation of Fe solubility by precipitation of solid iron hydroxides explains why this metal, which is the second most abundant metal in the Earth's crust, is dramatically depleted in the ocean. Hence, Fe can be a limiting element for biological activity. To prevent shortcomings, algae have developed different strategies. One of them is to produce siderophores, which are molecules with a very high affinity for the Fe(III) and that solubilize Fe by complexing it (see Problem 8). The study of thorium isotopes has allowed important progress on the geochemistry of trace metals and their interaction with marine particles. They will be detailed in Chapter 8.

2.9 Many Open Questions

One of the limitations inherent to most chemical tracers is that with few exceptions, their concentrations provide no information on their origin, or on their fluxes. Indeed, how can it be known if, at a given time, the nitrogen used by phytoplankton comes from the nitrogen stocks recycled in seawater or from the uptake of atmospheric N_2 by bacteria? How could we determine the flux of CO_2 actually absorbed by phytoplankton in the mixed layer while there is continuous remineralization and gas exchange with the atmosphere? What is the ventilation rate of the deep ocean? How can the settling rate of microscopic marine particles in the deep ocean be determined? How can the sediment accumulation rate be determined when it can be as low as a few millimeters per thousands of years? Isotopic tracers help to answer such questions because they carry information that are not recorded by the classical chemical tracers. This is the subject of Chapters 3 and 4.

Appendix 1

Atomic Number	Element	Symbol	Speciation	Type of Profile*	Average Concentration in Seawater (ng kg^{-1})**	Average Concentration in the Upper Continental Crust (% or ppm)***
1	Hydrogen	H	H_2O			
2	Helium	He	dissolved gas	c	7.6	
3	Lithium	Li	Li^+	c	180×10^3	
4	Beryllium	Be	$BeOH^+$, $Be(OH)_2$	s + n	0.21	20 ppm
5	Boron	B	H_3BO_2	c	4.5×10^6	3.0 ppm
6	Carbon	C	HCO_3^-, CO_3^{2-}	n	27.0×10^6	15 ppm
7	Nitrogen	N	Dissolved N_2	c	8.3×10^6	
			NO_3^-	n	0.42×10^6	

continued

Atomic Number	Element	Symbol	Speciation	Type of Profile*	Average Concentration in Seawater (ng kg^{-1})**	Average Concentration in the Upper Continental Crust (% or ppm)***
8	Oxygen	O	dissolved O_2	reverse n	2.8×10^6	
9	Fluorine	F	F^-	c	1.3×10^6	
10	Neon	Ne	dissolved gas	c	160	
11	Sodium	Na	Na^+	c	10.78×10^9	2.89%
12	Magnesium	Mg	Mg^{2+}	c	1.28×10^9	1.33%
13	Aluminum	Al	$Al(OH)_3$	s	30	8.04%
14	Silicon	Si	H_4SiO_4	n	2.8×10^6	30.8%
15	Phosphorus	P	HPO_4^{2-}, $NaHPO_4^-$, $MgHPO_4$	n	62×10^3	700 ppm
16	Sulfur	S	SO_4^{2-}, $NaSO_4^-$, $MgSO_4$	c	898×10^6	
17	Chlorine	Cl	Cl^-	c	19.35×10^9	
18	Argon	Ar	dissolved gas	c	0.62×10^6	
19	Potassium	K	K^+	c	399×10^6	2.8%
20	Calcium	Ca	Ca^{2+}	≈c	412×10^6	3.00%
21	Scandium	Sc	$Sc(OH)_3$	(s + n)	0.70	11 ppm
22	Titanium	Ti	$Ti(OH)_4$	s + n	6.5	0.30%
23	Vanadium	V	HVO_4^{2-}, $H_2VO_4^-$, $NaHVO_4^-$	≈c	2.0×10^3	60 ppm
24	Chromium	Cr	CrO_4^{2-}, $HCrO_4^-$	r + n	210	35 ppm
			Cr (III)	r + s	2	
25	Manganese	Mn	$MnCl^+$, Mn^{2+}	S	20	600 ppm
26	Iron	Fe	$Fe(OH)_3$	s + n	30	3.5%
27	Cobalt	Co	Co^{2+}, $CoCO_3$, $CoCl^+$	S	1.2	10 ppm
28	Nickel	Ni	Ni^{2+}, $NiCO_3$, $NiCl^+$	n	480	20 ppm
29	Copper	Cu	$CuCO_3$, $CuOH^+$, Cu^{2+}	s + n	150	25 ppm
30	Zinc	Zn	Zn^{2+}, $ZnOH^+$, $ZnCO_3$, $ZnCl^+$	n	350	71 ppm
31	Gallium	Ga	$Ga(OH)_4^-$	s + n	1.2	17 ppm
32	Germanium	Ge	H_4GeO_4, $H_3GeO_4^-$	n	5.5	1.6 ppm
33	Arsenic	As	$HAsO_4^-$	r + n	1.2×10^3	1.5 ppm
			As(III)	r + s	5.2	
34	Selenium	Se	SeO_4^{2-}, SeO_3^-, HSeO	r + n	100	50 ppm
35	Bromine	Br	Br^-	c	67×10^6	
36	Krypton	Kr	dissolved gas	c	310	

Atomic Number	Element	Symbol	Speciation	Type of Profile*	Average Concentration in Seawater (ng kg^{-1})**	Average Concentration in the Upper Continental Crust (% or ppm)***
37	Rubidium	Rb	Rb^+	c	0.12×10^6	112 ppm
38	Strontium	Sr	Sr^{2+}	almost c	7.8×10^6	350 ppm
39	Yttrium	Y	YCO_3^+, YOH^{2+}, Y^{3+}	n	17	22 ppm
40	Zirconium	Zr	$Zr(OH)_4$, $Zr(OH)_5^-$	s + n	15	190 ppm
41	Niobium	Nb	$Nb(OH)_6^-$, $Nb(OH)_5$	?	<5	25 ppm
42	Molybdenum	Mo	MoO_4^-	c	10×10^3	1.5 ppm
43	Technetium	Tc	TcO_4^-		no stable isotope	no stable isotope
44	Ruthenium	Ru		?	<0.005	
45	Rhodium	Rh		n	0.08	
46	Palladium	Pd		n	0.06	0.5 ppm
47	Silver	Ag	$AgCl_2^-$	n	2.0	50 ppm
48	Cadmium	Cd	$CdCl_2$	n	70	98 ppm
49	Indium	In	$In(OH)_3$	S	0.01	50 ppm
50	Tin	Sn	$SnO(OH)_3^-$	S	0.5	5.5 ppm
51	Antimony	Sb	$Sb(OH)_6^-$	≈c	200	0.2 ppb
52	Tellurium	Te	TeO_3^{2-}, $HTeO_3^-$	r + s	0.05	
53	Iodine	I	IO_3^-	≈c	58×10^3	
			I^-	(r + s)	4.4	
54	Xenon	Xe	dissolved gas	c	66	
55	Cesium	Cs	Cs^+	c	306	3.7 ppm
56	Barium	Ba	Ba^{2+}	n	15×10^3	550 ppm
57	Lanthanum	La	La^{3+}, $LaCl^{2+}$, $LaCO^{2+}$	p	5.6	30 ppm
58	Cerium	Ce	$CeCO_3^+$, Ce^{3+}, $CeCl^{2+}$	p	0.7	63 ppm
59	Praseodymium	Pr	$PrCO_3^+$, Pr^{3+}, $PrSO_4^+$	p	0.7	7.1 ppm
60	Neodymium	Nd	$NdCO_3^+$, Nd^{3+}, $NdSO_4^+$	p	3.3	26 ppm
61	Promethium	Pm			no stable isotope	no stable isotope
62	Samarium	Sm	$SmCO_3^+$, Sm^{3+}, $SmSO_4^+$	p	0.57	4.5 ppm
63	Europium	Eu	$EuCO_3^+$, Eu^{3+}, $EuOH^{2+}$	p	0.17	0.88 ppm
64	Gadolinium	Gd	$GdCO_3^+$, Gd^{3+}	p	0.9	3.8 ppm
65	Terbium	Tr	$TbCO_3^+$, Tb^{3+}, $TbOH^{2+}$	p	0.17	0.64 ppm

continued

Atomic Number	Element	Symbol	Speciation	Type of Profile*	Average Concentration in Seawater (ng kg^{-1})**	Average Concentration in the Upper Continental Crust (% or ppm)***
66	Dysprosium	Dy	$DyCO_3^+$, Dy^{3+}, $DyOH^{2+}$	p	1.1	3.5 ppm
67	Holmium	Ho	$HoCO_3^+$, Ho^{3+}, $HoOH^{2+}$	p	0.36	0.80 ppm
68	Erbium	Er	$ErCO_3^+$, $ErOH^{2+}$, Er^{3+}	p	1.2	2.3 ppm
69	Thulium	Tm	$TmCO_3^+$, $TmOH^{2+}$, Tm^{3+}, $TmOH^{2+}$	n	0.2	0.33 ppm
70	Ytterbium	Yb	$YbCO_3^+$, $YbOH^{2+}$	p	1.2	2.2 ppm
71	Lutetium	Lu	$LuCO_3^+$, $LuOH^{2+}$	p	0.23	0.32 ppm
72	Hafnium	Hf	$Hf(OH)_4$, $Hf(OH)_5^-$	p	3.4	5.8 ppm
73	Tantalum	Ta	$Ta(OH)_5$	?	<2.5	2.2 ppm
74	Tungsten	W	WO_4^-	c	10	2.0 ppm
75	Rhenium	Re	ReO_4^-	c	7.8	0.4 ppm
76	Osmium	Os		c	0.002	0.05 ppm
77	Iridium	Ir		c	0.00013	0.02 ppm
78	Platinum	Pt		c	0.05	
79	Gold	Au	$AuCl_2^-$	c	0.02	1.8 ppm
80	Mercury	Hg	$HgCl_4^-$	c	0.14	
81	Thallium	Tl	Tl^+, TlCl, $Tl(OH)_3$	almost c	13	750 ppm
82	Lead	Pb	$PbCO_3$, $Pb(CO_3)_2^{2-}$, $PbCl^+$	S	2.7	20 ppm
83	Bismuth	Bi	BiO^+, $Bi(OH)_2^+$	S	0.03	127 ppm
84	Polonium	Po		S		
85	Astatine	At				
86	Radon	Rn	dissolved gas	c		
87	Francium	Fr				
88	Radium	Ra	Ra^{2+}	n	0.00013	
89	Actinium	Ac		p		
90	Thorium	Th	$Th(OH)_4$	S	0.02	10.7 ppm
91	Protactinium	Pa		S		
92	Uranium	U	UO_2^{2+}	c	3.2×10^3	2.8 ppm
93	Neptunium	Np				
94	Plutonium	Pu		p + r		
95	Americium	Am		p		

*c = conservative, n = nutrient, p = particles reactive and r = redox properties. Modified after Li (1991).

**Estimated by following the methods of Quinby-Hunt and Turekian (1983).

***Taylor and McLennan (1995). http://www.agu.org/eos_elec/97025e-table.html.

PROBLEMS

Problem 1: Residence time of Na in the ocean

The main source of sodium (Na) in the ocean is the dissolved Na transported by rivers. The flux of river water to the ocean is of the order of ... (it was given in Chapter 1). The average Na concentration is 0.49 mol kg^{-1} in seawater and 2.3×10^{-4} mol kg^{-1} in river water. The volume of the ocean is of the order of ... (check again in Chapter 1). Calculate the residence time of Na in the ocean. Compare it to the ocean mixing time. What can you conclude about the distribution of Na in the ocean?

Problem 2: Over- and undersaturation of oxygen in the ocean (Craig and Hayward, 1987)

The degree of O_2 saturation of seawater has been determined in the North Pacific (Table 2.3). The mixed layer is 20 m deep. The depth of the photic zone is 100 m. Explain the O_2 saturation profile.

Table 2.3 *O_2 saturation profile*

Depth (m)	10	20	30	40	50	60	70	80	90	150
Saturation (%)	106	106	113	109	103	99	97	97	95	90

Problem 3: Chemical behavior of indium (Alibo et al.,, 1999)

An oceanographer who is interested in the geochemical behavior of indium (In) in the ocean measures an In vertical profile (Table 2.4). Assuming that the water mass at 1500 m is the result of the mixing between the water masses at 1000 and 2000 m, establish if indium is a conservative element?

Table 2.4 *Vertical distribution of dissolved indium*

Depth (m)	1000	1500	2000
Salinity	34.281	34.419	34.624
Indium dissolved (10^{-12} mol kg^{-1})	0.712	0.825	0.873

Problem 4: Behavior of strontium (De Villiers, 1999)

To characterize the chemical behavior of strontium (Sr) in the ocean, Sr and Ca concentrations are analyzed in seawater samples collected in the Pacific Ocean (Table 2.5).

(1) How many water masses mix between 1000 and 2000 m deep?
(2) Is strontium conservative during this mixing?

(3) The concentration of dissolved Sr can be affected by the dissolution of calcite or aragonite. Which mineral is more likely to dissolve at the sampling depths?

(4) Knowing that the Sr/Ca ratio of calcite is 1.5 mmol mol^{-1} and that it is 8.6 mmol mol^{-1} in aragonite, consider what should the Sr/Ca ratio of seawater be at 1600 m, if its enrichment in Sr is due to the dissolution of these minerals. Compare with the measured value and conclude.

(5) Similarly, what would be the effect of the dissolution of celestite, a highly soluble Sr sulfate, synthesized in surface water by acantharians. Celestite contains no calcium. Determine the nature and proportion of minerals whose dissolution accounts for the evolution of the chemical composition of the sample taken at 1600 m compared to those collected at 1000 and 2000 m.

Table 2.5 *Vertical distribution of Ca and Sr*

Depth (m)	Temperature (°C)	Salinity	Sr (μmol kg^{-1})	Sr/Ca (mmol mol^{-1})
1000	2.82	34.38	88.72	8.64
1200	2.51	34.44	88.94	8.64
1600	2.07	34.53	89.16	8.65
1800	1.90	34.56	89.14	8.64
2000	1.77	34.59	88.94	8.62

Problem 5: Profiles of metals in the Black Sea (Yemenicioglu S. et al., 2006)

Dissolved Fe^{2+}, Mn^{2+}, O_2 and H_2S profiles have been measured in the Black Sea (Fig. 2.22). The Black Sea is heavily stratified between 0 and 100 m deep. Explain the distribution of dissolved Fe and Mn with respect to redox conditions.

Problem 6: Vertical profiles of elements in the ocean (Nozaki, 1997)

Y. Nozaki compiled the vertical profiles of all the chemical elements dissolved in the Pacific Ocean in a periodic table. Here are a few examples:

- Tungsten: [W] $\approx$ 60 pmol kg^{-1} from the surface to the seafloor (water column depth: 5 km).
- Cobalt: [Co] = 50 pmol kg^{-1} in surface waters then [Co] decreases down to 2 km ([Co] = 15 pmol kg^{-1} to 2 km) and finally [Co] $\approx$ 10–15 pmol kg^{-1} down the seafloor.
- Nickel: [Ni] = 3 nmol kg^{-1} in surface waters, then [Ni] increases steadily down to 1 km depth ([Ni] = 9.5 nmol kg^{-1}), then [Ni] $\approx$ 10–11 pmol kg^{-1} down to the seafloor.

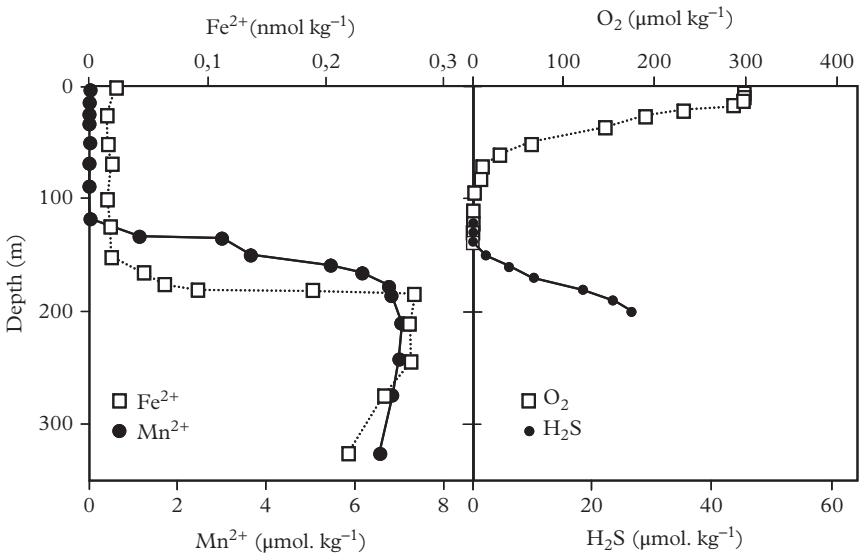

Figure 2.22 *Profiles of dissolved Fe, Mn, O_2 and H_2S in the Black Sea. Modified from Yemenicioglu S. et al. (2006).*

- Zinc: concentration is zero in surface waters, then [Zn] steadily increases down to 1.5 km ([Zn] = 8 pmol kg^{-1} at 1.5 km) and then [Zn] ≈ 8–9 pmol kg^{-1} down to the seafloor.
- Krypton: [Kr] = 2.5 nmol kg^{-1} in surface waters, then [Kr] increases regularly until [Kr] = 3.5 pmol kg^{-1} at 1.5 km and then [Kr] ≈ 3.5–4.0 pmol kg^{-1} down to the seafloor.

What is the behavior of each of these chemical elements?

Problem 7: Mn and Fe in the North Atlantic Ocean (Hatta et al., 2014)

During a GEOTRACES section through the North Atlantic from the west coast of the USA to the Mauritanian coast, dissolved Mn and Fe have been analyzed. Explain the main features appearing along this section:

- The Fe concentration generally increases with depth: [Fe] ⩽ 0.5 nmol kg^{-1} in surface waters then [Fe] steadily increases down to 1 km ([Fe] = 0.8–1 nmol kg^{-1} at 1.5 km) and then [Fe] ≈ 0.8 nmol kg^{-1} down to the seafloor. Between 20 and 30°N, there is a local surface maximum ([Fe] = 0.8 nmol kg^{-1} in surface waters).
- The Mn concentration generally decreases with depth: [Mn] > 1.0 in surface waters then [Mn] steadily decreases down to a depth of 300 m ([Mn] = 0.2 nmol kg^{-1} at 300 m) and then [Mn] ≈ 0.2 pmol kg^{-1} down to the seafloor.

Fe and Mn profiles deviate from this general shape at two locations:

- Midway between the American and the African coasts, there is a plume of Mn-rich and Fe-rich water extending from the seafloor to 1 km above it: [Mn] up to 20 nmol kg^{-1} and [Fe] up to 50 nmol kg^{-1} (whereas dissolved Al increases at most by a factor 2).
- A Mn-rich and Fe-rich water tongue extends horizontally from the Mauritanian coasts at a depth of about 200–400 m: [Mn] up to 0.6 nmol kg^{-1} and [Fe] up to 1.5 nmol kg^{-1} (whereas dissolved Al shows no particular enrichment).

Problem 8: Iron complexation by siderophores (Witter et al., 2000)

During their bloom, diatoms release siderophores in seawater to make Fe hydroxides bio-available. The complexation constant of Fe^{3+} by siderophores (Sid^{n-}) is determined experimentally

$$Fe^{3+} + Sid^{n-} \Leftrightarrow (SidFe)^{3-n} \qquad K = 10^{22}.$$

(1) For seawater at pH = 8 containing a total iron concentration of 10^{-9} mol kg^{-1}, siderophores are added to obtain a total siderophores concentration of 10^{-9} mol kg^{-1}. Determine the percentage of the total iron which is complexed by siderophores.

(2) What can happen if iron hydroxide precipitates are present on the marine particles of this seawater?

3

Stable Isotopes

When the chemical elements, particularly the light ones, are involved in physical, chemical or biological transformations, the relative abundance of their isotopes can change. This change is the trademark of these transformations. Measuring the isotopic composition of these elements allows their journey through the ocean to be traced.

3.1 What Is an Isotope?

Matter is made of atoms. In each atom, a central nucleus composed of protons and neutrons is surrounded by a cloud of electrons. Each atom X is characterized by two numbers, Z and A.

- Z is called the atomic number. It is the number of protons in its nucleus. It is also the number of electrons of the atom when it is not ionized.
- A is called the atomic mass and represents the sum of the number of protons plus the number of neutrons in the nucleus.

It can be written as ${}^{A}_{Z}\mathrm{X}$.

The **chemical properties** of an atom are determined by the structure of its electronic cloud. Indeed, chemical bonds are created by electrons that can be shared between the atoms. For example, atoms with the same atomic number Z are *chemically indistinguishable* and they are constituents of the same chemical element. Atoms of the same chemical element with different atomic masses A are called "**isotopes**" (from the Greek "iso" for "same" and "topos" for "place" because they occur at the same location in the Mendeleev table). Isotopes differ by their number of neutrons $(A-Z)$. The number of isotopes of the same chemical element is variable. For example, gold has only one isotope (${}^{197}_{79}\mathrm{Au}$), while tin has the largest number, that is, nine (${}^{112}_{50}\mathrm{Sn}$, ${}^{115}_{50}\mathrm{Sn}$, ${}^{116}_{50}\mathrm{Sn}$, ${}^{117}_{50}\mathrm{Sn}$, ${}^{118}_{50}\mathrm{Sn}$, ${}^{119}_{50}\mathrm{Sn}$, ${}^{120}_{50}\mathrm{Sn}$, ${}^{122}_{50}\mathrm{Sn}$ and ${}^{124}_{50}\mathrm{Sn}$).

Mass spectrometers can be used to measure very precisely the ratio between the abundances of the different isotopes of a chemical element. These ratios are called **isotopic ratios** or **isotopic compositions**. The isotopes of a chemical element having identical electronic clouds should have identical chemical properties. Thus, these isotopic

Marine Geochemistry. First Edition. Matthieu Roy-Barman and Catherine Jeandel.

ratios should be constant in nature since they are not modified by chemical reactions. This is largely true, but precise measurements of isotopic ratios show that there are two exceptions to this rule:

(1) The abundance of some isotopes varies due to radioactivity. These changes are the subject of Chapter 4.

(2) The isotopic compositions of some elements involved in physico-chemical or biological reactions vary systematically and independently of any radioactivity. These variations, which affect light elements more significantly than heavy ones, are the subject of this chapter.

Therefore we add to the Mendeleev table, which constitutes the basis of chemical tracers, a table of stable, radioactive and radiogenic isotopes that we can use to understand how the ocean works (Fig. 3.1).

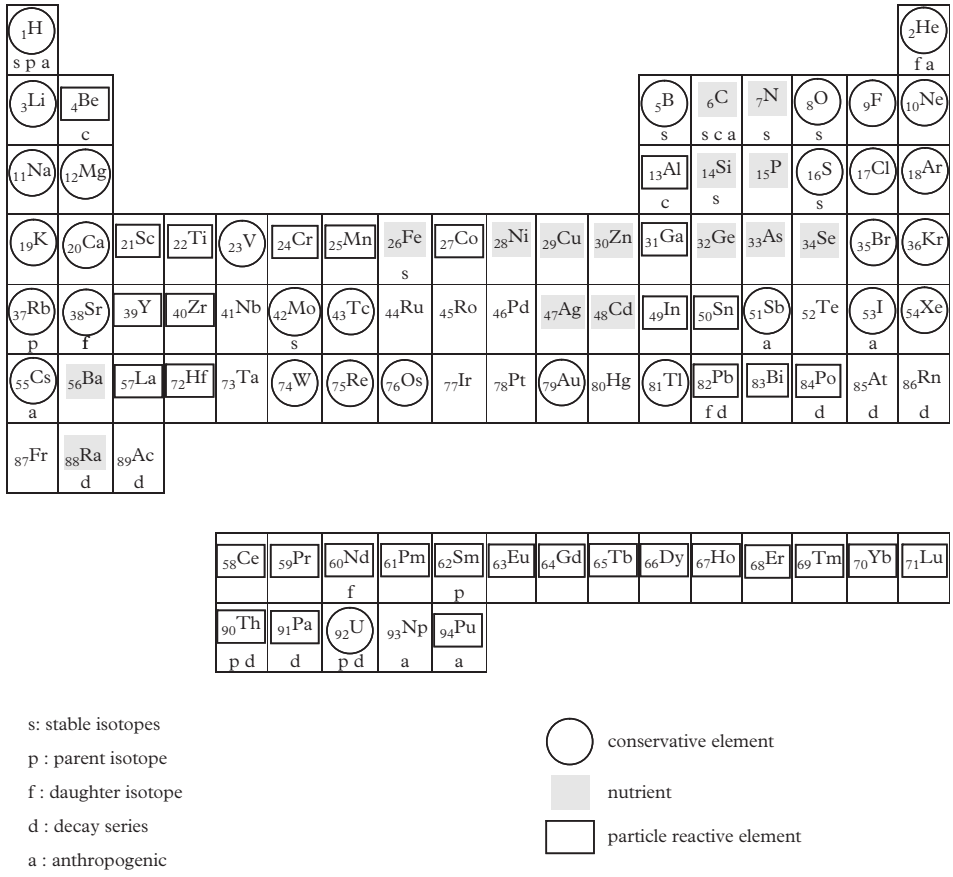

Figure 3.1 *Main stable and radioactive isotopic systems and their geochemical behaviors.*

While the isotopes of a light element have identical electronic clouds, they have very slightly different physico-chemical behaviors due to their different masses. Isotopic abundance variations are also called **isotopic fractionations.** These fractionations were first observed for elements with masses lower than 36. They have been extensively studied for hydrogen and oxygen, which are the constituents of water, as well as for carbon, nitrogen and sulfur, which are the major constituents of organic matter (with H and O). Analytical progress made in recent years now allows study of the isotopic fractionation of transition metals such as copper or iron (mass ≤ 60) and up to Cd (mass 123). The study of these metals as isotopic tracers is in its infancy, both from the analytical and geochemical point of view. Here we will mainly focus on iron isotopes. Examples of the application of molybdenum isotopic fractionation to the study of the oxygenation of the ocean will be presented in Chapter 11. Even if it is not new, silicon isotopes have strongly benefited from this analytical progress. Given the central role of dissolved silica in marine geochemistry, this opens up interesting applications.

3.2 Notations

Generally, isotopic fractionations are variations of the order of a few thousandths of the isotopic ratios. Rather than reasoning directly with the ratio "R", geochemists prefer to use the relative deviation δ (expressed as ‰) of the isotopic ratio R with respect to a reference ratio R_{ref} or standard value (Table 3.1)

$$\delta_{sample} = \left\{ \frac{R_{sample}}{R_{reference}} - 1 \right\} \times 1000. \tag{3.1}$$

When a physical, chemical or biological transformation causes an isotope fractionation, it is quantified using the fractionation coefficient α. For a chemical equilibrium $A \leftrightarrow B$ or an irreversible transformation $A \rightarrow B$, the isotope fractionation factor α_{A-B} is defined as follows:

$$\alpha_{A-B} = \frac{R_A}{R_B} = \frac{1000 + \delta_A}{1000 + \delta_B} \approx 1 + \frac{\delta_A - \delta_B}{1000}. \tag{3.2}$$

A coefficient Δ is also defined (this factor is also frequently denoted ε, but we will not use this notation to avoid ambiguity with the Nd isotopic composition):

$$\Delta_{A-B} = (\alpha_{A-B} - 1) \times 1000 \approx \delta_A - \delta_B. \tag{3.3}$$

Application exercise: fractionation of oxygen from the water

Consider water vapor with a $\delta^{18}O$ of –20‰ relative to the SMOW reference. If the fractionation coefficient of oxygen between liquid and vapor is $\alpha_{liquid-vapor} = 1.0092$ at 25°C, what is the $\delta^{18}O$ of liquid water at isotopic equilibrium with the vapor. Use exact and approximate methods.

Table 3.1 *The delta notation*

Notation	δD	$\delta^{11}B$	$\delta^{17}O$	$\delta^{18}O$	$\delta^{13}C$	$\delta^{15}N$	$\delta^{30}Si$	$\delta^{34}S$	$\delta^{98}Mo$(or $\delta^{98/95}Mo$)	$\delta^{56}Fe$
Ratio	$D/^{1}H$	$^{11}B/^{10}B$	$^{17}O/^{16}O$	$^{18}O/^{16}O$	$^{13}C/^{12}C$	$^{15}N/^{14}N$	$^{30}Si/^{28}Si$	$^{34}S/^{32}S$	$^{98}Mo/^{95}Mo$	$^{56}Fe/^{54}Fe$
Reference	SMOW[a]	NBS-951[b]	SMOWPDB[c]	SMOWPDB	PDB	atmosphere	NBS-28[b]	CDT[d]	Rochester[e] JMC	IRMM-14[f]
Reference ratio	0.0016	4.044	3.76×0^{-4}	0.00200	0.00112	0.00677	~0.033532[g]	0.0442	1.5157	15.698

[a]Standard Mean Ocean Water (synthetic seawater representing the average ocean). [b]National Bureau of Standards. [c]Pee Dee belemnite (for a fossil belemnite from the geological formation of Pee Dee.) [d]Canon Diablo troilite (FeS_2). [e]Standard of the University of Rochester, provided by Johnson Matthey Corporation. [f]Institute for Reference Materials and Measurements. [g]NBS-28 is not certified for Si isotopes yet due to the lack of sufficiently accurate measurements.

Solution:
Exact solution: $\delta^{18}O_{liquid} = \alpha_{liquid-vapor}(1000 + \delta^{18}O_{vapor}) - 1000 = -10.98‰$.
Approximate solution: $\delta^{18}O_{liquid} \approx \delta^{18}O_{vapor} + (\alpha_{liquid-vapor} - 1) \times 1000 = -10.80‰$.

Note that later in the chapter, we will also use $\alpha_{B-A} = \frac{R_B}{R_A} = \frac{1}{\alpha_{A-B}}$.

3.3 The Different Types of Fractionations: The Oxygen Example

3.3.1 Kinetic Fractionations

When a chemical reaction or a phase transition occurs irreversibly (i.e., the transformation occurs only in one direction for kinetic and/or thermodynamic reasons or because products are systematically separated from the reactants), the light isotopes react faster than the heavy isotopes. Intuitively, the chemical bond between two atoms can be seen as a spring between two oscillating masses. The lighter the masses, the larger their vibrational frequency and the weaker the chemical bond. Therefore, for a given chemical element, a light isotope forms less stable chemical bonds than a heavy one. A light isotope reacts faster, so that it is enriched in the reaction products. These kinetic effects decrease when the temperature increases (they vanish at high temperature).

Consider the transformation: liquid water → water vapor. In liquid water, the oxygen atom (negatively charged) of a water molecule often establishes one or two hydrogen bonds with (positively charged) hydrogen atoms of nearby water molecules. Thus, $H_2^{16}O$ evaporates more easily than $H_2^{18}O$ because it is more weakly bound to the liquid phase. Meanwhile $H_2^{18}O$ remains preferentially in the liquid. Similarly, for the ice → liquid water transition, $H_2^{16}O$ moves preferentially from ice to liquid water relative to $H_2^{18}O$.

The speed of the molecules must be also taken into account. The kinetic energy of a molecule ($E_c = ½mv^2$) is determined by the temperature of the environment. For a similar kinetic energy, the light isotope-containing molecules have higher speeds than those containing heavy isotopes. The collision frequency of light molecules with their neighbors is greater, increasing their probability of reaction. In addition, during molecular diffusion, the light molecules diffuse faster than heavy ones (see Chapter 6) producing an isotopic fractionation.

3.3.2 Thermodynamic Fractionations

In the previous section, we considered an irreversible reaction. When the reverse reaction also takes place, a chemical equilibrium is established when the two reactions balance each other so that the quantities of products and reactants remain constant. In this case, the isotopic compositions in the products and the reactants become constant and eventually an **isotopic equilibrium** is reached (Fig. 3.2). However, these isotopic

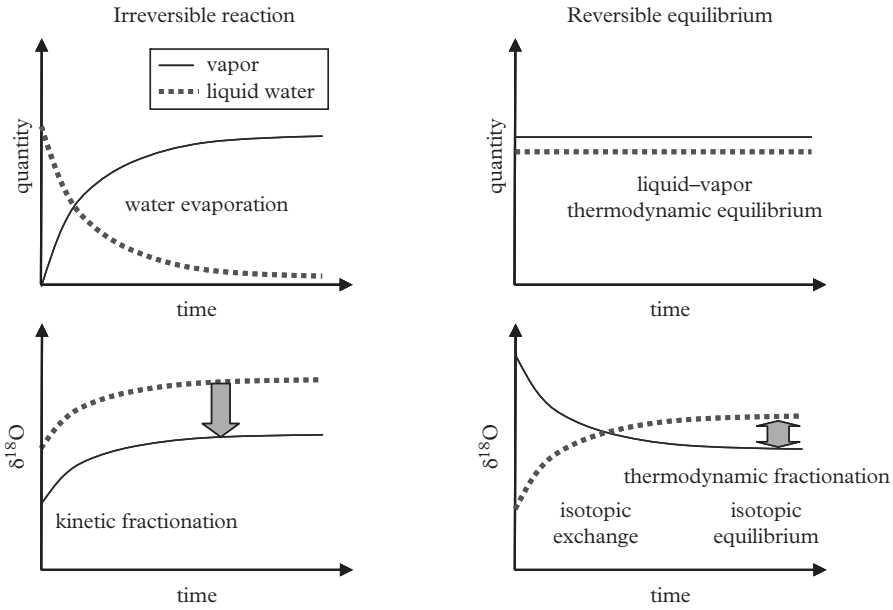

Figure 3.2 *Effect of reversibility on isotopic fractionations between liquid water and water vapor. During the irreversible evaporation of water, the liquid–vapor isotopic fractionations are due to kinetic effects. When water is put in contact with vapor (thermodynamic equilibrium), isotope exchange leads to an isotopic equilibrium determined by thermodynamic fractionations.*

compositions are not necessarily equal because the light isotope is not favored to the same extent in the two reactions.

Consider the liquid water ↔ vapor equilibrium. It is the result of two unidirectional reactions: liquid water → vapor and vapor → liquid water. We have seen that during liquid water evaporation ^{16}O is enriched in the vapor. In principle, the vapor condensation produces an enrichment of liquid water in ^{16}O, but as in the vapor most of hydrogen bonds are broken, the difference of behavior between $H_2^{16}O$ and $H_2^{18}O$ is small. Therefore, when the two reactions are balanced, the liquid water is enriched in ^{18}O whereas vapor is enriched in ^{16}O. Similarly, when ice is at equilibrium with liquid water, ^{18}O is enriched in the ice, where each water molecule established two hydrogen bonds with its neighbors while in the liquid, bonds are less regular. Generally, heavy isotopes are enriched in compounds in which they can form more stable bonds.

Now let's mix ^{18}O-depleted liquid water with ^{18}O-enriched water vapor in a closed container. We assume that liquid and vapor are in thermodynamic equilibrium (no change in the quantity of vapor and liquid). Although the quantities of vapor and liquid remain constant, there are constant and equal fluxes of molecules that condense into the liquid phase and evaporate into the vapor at the liquid–vapor interface: liquid water is gradually enriched in ^{18}O and water vapor is gradually depleted in ^{18}O. This is

an **isotopic exchange** that lasts until isotopic equilibrium is reached (Fig. 3.2). Isotopic fingerprinting allows us to follow the exchange of material between two phases, even if there is no net flux of material between them. Isotope exchange is a very general concept that also is used in the case of radiogenic isotopes (see Chapter 4).

3.3.3 Seaside Analogy

The behavior of vacationers (chemical element) at the seaside and their distribution between sunbathing and swimming (chemical speciation) obey the same principles. There are two types of vacationers: children (light isotopes) and their parents (heavy isotopes). At the opening of the beach, children are always the first in the water (kinetic fractionation). Then little by little, adults who have installed towels and umbrellas also go swimming. Children are quicker to get out of the water (always the kinetic effect) but they gladly return to swimming. After some time (during which isotope exchange occurs), things are stabilized:

- The average number of persons on the beach and in the water remains constant (chemical equilibrium is reached).
- Most children are in the water while most adults sunbathe on the beach: the isotopic equilibrium has also been reached.

3.3.4 The "Biological" Fractionations

Biological reactions can cause fractionations resulting essentially from kinetic processes because many biological reactions are not at equilibrium. For example, when they breathe, all living organisms preferentially use oxygen $^{16}O_2$ compared to $^{16}O^{18}O$ or $^{18}O_2$. On the other hand, photosynthesis does not generate isotopic fractionation between the $\delta^{18}O$ of the water and the $\delta^{18}O$ of the O_2 released in the atmosphere. It follows from these two processes that atmospheric oxygen (O_2, $\delta^{18}O = +20.8‰$) is enriched in ^{18}O compared with seawater ($\delta^{18}O = 0‰$). This is the Dole effect (Fig. 3.3). Biological fractionations are particularly important in the case of carbon and nitrogen. They are due to the preferential use of light isotopes by living beings.

3.3.5 Mass-Dependent and Mass-Independent Fractionations

Theoretical studies predict that, for a given element, fractionation between two isotopes increases when the mass difference between these isotopes increases: isotope fractionation depends on the mass (Urey, 1947). As the mass difference between ^{16}O and ^{17}O is half the mass difference between ^{16}O and ^{18}O, it is expected that for terrestrial samples: $\delta^{17}O \approx 0.5 \times \delta^{18}O$. Hence, in a $\delta^{17}O$ versus $\delta^{18}O$ diagram, terrestrial samples lie on a straight line with a slope of about 0.516. This implies that $\delta^{17}O$ contains *a priori* the same information as $\delta^{18}O$, so that it has long been of little interest.

However, there are a few cases where the dependency between the fractionation extent and the mass difference does not work. The first case was found in meteorites consisting of a mixture of materials formed by different nuclear reactions in stars. Such

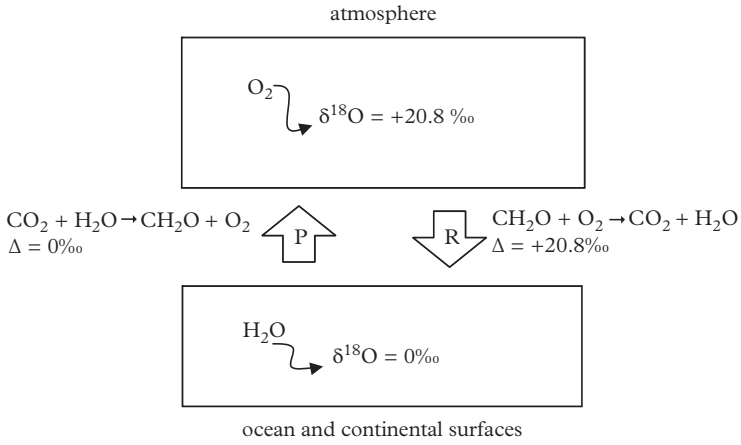

Figure 3.3 *Schematic representation of the Dole effect. "P": Photosynthesis; "R": Respiration.*

isotopic variations existed when the solar system was formed, but they were completely erased during the formation and evolution of the Earth. Recently, mass-independent isotope fractionation has been found in the stratosphere during the synthesis of ozone (O_3) from molecular oxygen (O_2) in the presence of ultraviolet radiation. During this reaction, O_2 is depleted identically in ^{17}O and ^{18}O relative to ^{16}O while O_3 is enriched identically in ^{17}O and ^{18}O. This mass-independent fractionation is still poorly understood, but it seems that the asymmetry of $^{16}O^{17}O$ and $^{16}O^{18}O$ molecules compared to $^{16}O^{16}O$ plays a key role.

In the troposphere, photosynthesis and respiration (see Chapter 2) produce mass-dependent fractionations only. Yet, in the $\delta^{17}O$ versus $\delta^{18}O$ diagram, atmospheric O_2 lies under the mass-dependent fractionation line, because it is a mixture between photosynthetic O_2 and ^{17}O-depleted stratospheric O_2 (Fig. 3.4).

To quantify the mass-independent fractionations, we use the deviation of $\delta^{17}O$ from the line of mass-dependent fractionation (also called the terrestrial fractionation line)

$$\Delta^{17}O = \delta^{17}O - 0.516 \times \delta^{18}O, \tag{3.4}$$

where 0.516 is the average slope of the mass-dependent fractionation line in the $\delta^{17}O$ versus $\delta^{18}O$ diagram. As these variations are very small, they are expressed in 10^{-3} ‰, usually called "per meg" (per mega).

3.3.6 Clumped Isotopes

We have seen in Section 3.3.1 that heavy isotopes form stronger bonds than light isotopes. Therefore, in carbonates, ^{13}C–^{18}O bonds occur slightly more frequently than what would be expected if the association of C and O isotopes was purely random. As a consequence, the CO_2 produced by dissolution of $CaCO_3$ in hydrochloric acid contains a

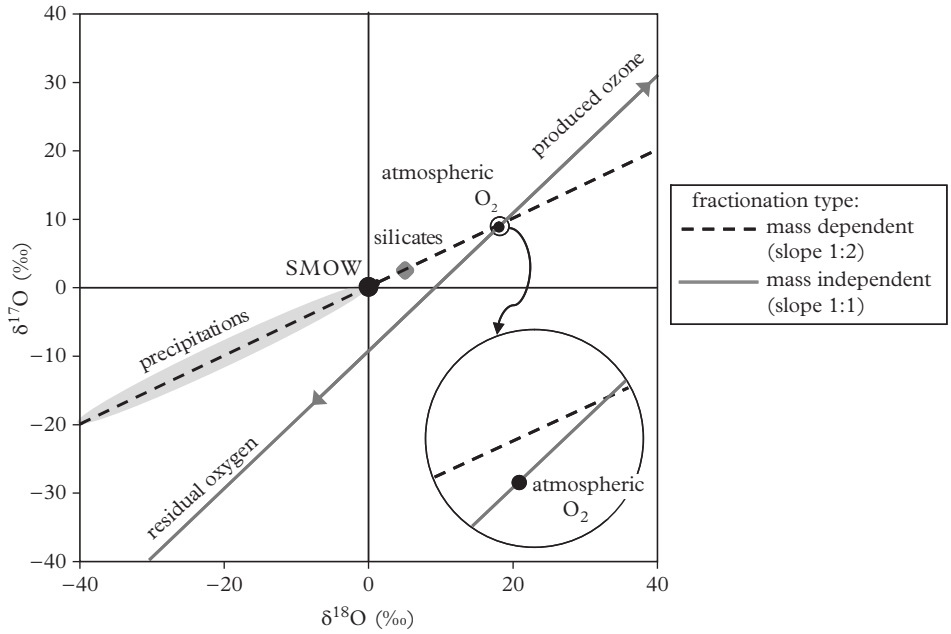

Figure 3.4 *Mass-dependent and mass-independent fractionations in a $\delta^{17}O$ versus $\delta^{18}O$ diagram. Most terrestrial samples are on a straight line of slope ≈ 0.516 (dashed lines) because their production is associated with mass-dependent fractionations. Atmospheric O_2 is slightly below this line. The O_3 production from O_2 in the stratosphere produces mass-independent fractionations leading to ^{17}O-rich ozone and ^{17}O-depleted O_2 (continuous line of slope 1). This dilution of ^{17}O-depleted O_2 in the atmosphere explains why atmospheric oxygen is below the mass-dependent fractionation line. Modified from Thiemens and Shaheen (2013).*

relative excess of $^{13}C^{18}O^{16}O$ compared to $^{12}C^{16}O^{16}O$. Molecules of the same chemical species but with different isotopes are called "isotopologs." $^{13}C^{18}O^{16}O$ has a molar mass of 47, so that the relative excess of ^{13}C–^{18}O bonds compared to a random distribution is called Δ_{47}. Δ_{47} is expressed in "per meg": 1 per meg corresponds to a relative excess of 10^{-6}. Just like the $\delta^{18}O$ of carbonates, the Δ_{47} of carbonates is temperature dependent, but unlike the $\delta^{18}O$ of carbonate it does not depend on the isotopic composition of seawater which has been highly variable during Earth's history. Much effort is put into the analysis of the Δ_{47} of ancient carbonates or phosphates because it should provide an absolute thermometer for ancient seawater (Cummins et al., 2014). For example, the combined analyses of clumped isotopes and $\delta^{18}O$ on tropical corals and brachiopods from the Silurian (≈ 433 My) indicate that the tropical surface water temperature was 33±7°C and that the $\delta^{18}O$ of seawater was about 1‰ lower than today, which could be due to the complete absence of ice sheets compared to today (ice sheet melting releases "light" water).

3.4 Oxygen Isotope Fractionation

The $^{18}O/^{16}O$ ratio of seawater is relatively constant (Fig. 3.5), so that the average isotopic ratio of the ocean (Standard Mean Ocean Water or SMOW) was chosen as the reference ratio for the calculation of $\delta^{18}O$ in water cycle studies. Marine carbonates are systematically enriched in ^{18}O compared to seawater so that their $\delta^{18}O$ is calculated by taking the isotopic composition of a belemnite fossil (PDB for Pee Dee belemnite, which is a Cretaceous belemnite fossil found in the formation of Pee Dee in the United States) as a reference. The $\delta^{18}O$ of the Pee Dee belemnite expressed relative to the SMOW as a reference is +30.4‰.

In recent studies on mass-independent fractionations, $\delta^{17}O$ and $\delta^{18}O$ are expressed relative to the isotopic composition of the atmospheric O_2.

We are now going to put the different fractionation processes back into the oceanic context of the water cycle and of solid–water interactions. We will not come back to mass-independent fractionations and clumped isotopes here, but examples will be presented in Chapters 7 and 11.

3.4.1 The Fractionations in the Water Cycle

When seawater evaporates ($\delta^{18}O = 0‰$), water vapor is enriched in ^{16}O and its $\delta^{18}O$ is therefore negative (Fig. 3.6). Similarly, raindrops are enriched in ^{18}O compared to the water vapor from which they condense. Most (90%) atmospheric water vapor is precipitated on the ocean, but condensation and precipitation do not take place on the spot. Very schematically, water evaporates at low latitudes, and then it is carried to high latitudes by atmospheric circulation. Flowing poleward, air masses cool. This triggers the formation of rain or snow. The formation of precipitation causes a rapid ^{18}O depletion of the water vapor. Its $\delta^{18}O$ becomes more negative and the new raindrops also have an increasingly negative $\delta^{18}O$ during transport. This is the **Rayleigh distillation** phenomenon (see Section 3.11). Thus, there is an inverse correlation between latitude and the $\delta^{18}O$ of precipitations.

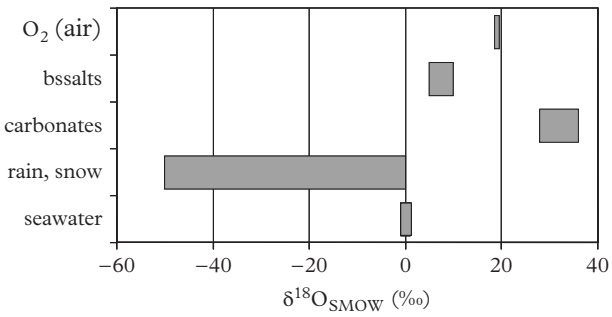

Figure 3.5 *Range of $\delta^{18}O$ (relative to the SMOW scale) in the ocean and the atmosphere.*

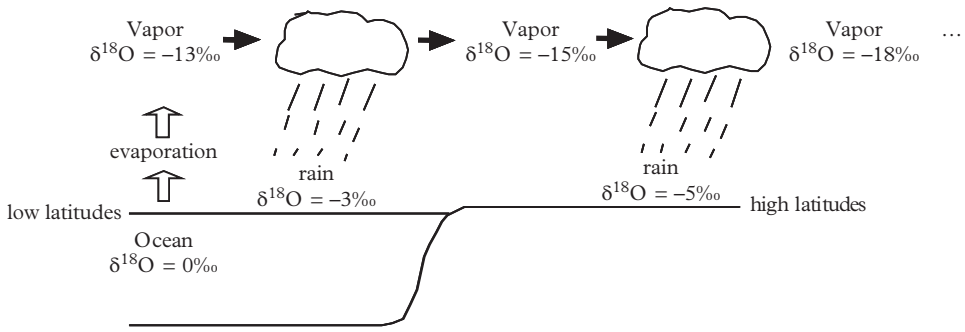

Figure 3.6 *Evolution of $\delta^{18}O$ in precipitations. The atmospheric circulation transports the water vapor from the low latitude to the high latitude.*

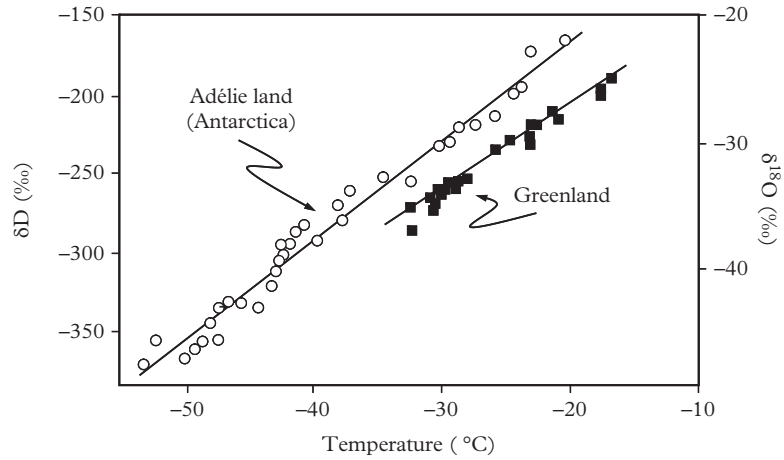

Figure 3.7 *Evolution of δD in of Adélie land snow and of $\delta^{18}O$ in Greenland snow with temperature. Modified from Jouzel et al. (1997).*

A fundamental consequence of this phenomenon is the occurrence, at the local scale, of a correlation between the $\delta^{18}O$ (or δD) of precipitations (rain or snow) and the ground temperature (Fig. 3.7). Indeed, cold air has a much lower equilibrium water vapor pressure than warm air. In winter, rainfall and snowfall come, therefore, from air masses that have lost much more water vapor (and therefore ^{18}O) than in summer. Winter precipitations have a more negative $\delta^{18}O$ than summer precipitations. This $\delta^{18}O$–temperature correlation is a real isotopic thermometer that records the temperature of polar ice. It will be used in Chapter 11 for the study of climate.

The $\delta^{18}O$ of seawater varies much less than the $\delta^{18}O$ of precipitations (Fig. 3.5). In surface waters, evaporation increases the salinity and the $\delta^{18}O$ of seawater. Precipitations

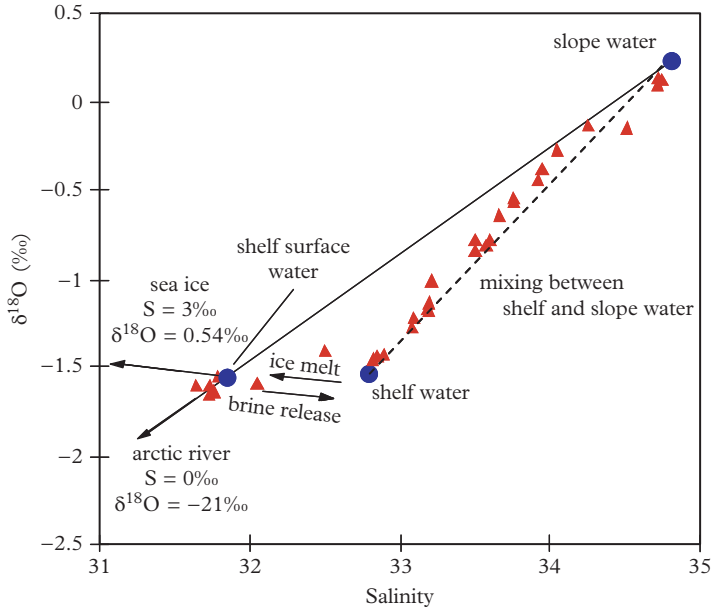

Figure 3.8 *Salinity–$\delta^{18}O$ relationship in the Labrador Sea. Without sea-ice formation, the points should be placed on the mixing line between the slope water and the Arctic rivers (solid line). Sea-ice formation causes the rejection of salt-rich brines that are very slightly depleted in ^{18}O. These brines account for the signatures of the continental shelf water. Most samples are the result of the mixing between the shelf water and the continental slope water (dashed line). Modified from Khatiwala et al. (1999).*

have the opposite effect. The $\delta^{18}O$ of seawater is strongly correlated with salinity (Fig. 3.8). However, since the $\delta^{18}O$ of rainfall becomes more negative as the latitude increases, the slope of the salinity–$\delta^{18}O$ correlation in seawater increases with latitude (this is called the local meteoritic water line). In deep waters, $\delta^{18}O$, like salinity, is a conservative tracer of water masses. However, $\delta^{18}O$ differs from the salinity in different ways:

* During sea-ice formation, the salinity of residual seawater increases strongly while its $\delta^{18}O$ hardly changes ($\alpha_{ice-water} = 1.0029$) and remains more or less conservative.
* Changes in salinity provide information on inputs of fresh water but say nothing about the origin of this water. However, different sources of fresh water (rain, river, melting ice) can be identified by their $\delta^{18}O$ (see also Chapter 10).
* Finally, the $\delta^{18}O$ of ice provides valuable information about its formation (see Problem 1).

3.4.2 Isotope Exchange between Water and Solid

When water is in contact with mineral-containing oxygen, there is reaction between the oxygen of the mineral and that of the water. For example

$$CaC^{18}O^{16}O_2 + H_2{}^{16}O \Leftrightarrow CaC^{16}O_3 + H_2{}^{18}O.$$

In the case of calcium carbonate, this reaction takes place during the formation of the mineral. For this isotope exchange reaction, the law of mass action is written as

$$K = \frac{[CaC^{16}O_3] \times [H_2{}^{18}O]}{[CaC^{18}O^{16}O_2] \times [H_2{}^{16}O]} = \frac{(^{18}O/^{16}O)_{H_2O}}{(^{18}O/^{16}O)_{CaCO_3}}. \quad (3.5)$$

Experience shows that $K < 1$, that is, calcium carbonate is enriched in ^{18}O. K is temperature dependent: the ^{18}O enrichment of carbonates increases when the temperature decreases. An empirical relationship between temperature and isotopic fractionation was established by precipitating calcite at equilibrium with seawater in controlled conditions (Epstein et al., 1953)

$$T(°C) = 16.9 - 4.2(\delta^{18}O_{calcite} - \delta^{18}O_{water}) + 0.13(\delta^{18}O_{calcite} - \delta^{18}O_{water})^2. \quad (3.6)$$

By analyzing $CaCO_3$ fossilized shells, it is possible to use this relationship to reconstruct the temperature of calcite formation, if $\delta^{18}O_{water}$ is known. This method is particularly applied to foraminifera, which are unicellular animals widespread in the ocean. Some foraminifera species live at well-defined depths. Thus, the $\delta^{18}O$ test of foraminifera living in surface or deep waters is used to determine paleotemperatures of these waters (see Chapter 11).

3.5 Hydrogen Isotope Fractionation

During the water cycle, the physico-chemical behavior of oxygen and hydrogen are coupled. Hydrogen isotopes (^1H and ^2H or D for deuterium) are therefore subject to the same fractionation processes as oxygen. Due to the large relative mass difference between H and D, δD variations are much larger than the $\delta^{18}O$ variations. δD is less frequently analyzed than $\delta^{18}O$ in oceanographic studies because it does not provide additional information on the water cycle. Notable differences in behavior and fractionation between δD and $\delta^{18}O$ appear in hydrothermal systems since volcanic rocks interacting with seawater are rich in oxygen and poor in hydrogen.

3.6 Carbon Isotope Fractionation

The main source of carbon isotope fractionation is photosynthesis. Indeed, the organic carbon produced during photosynthesis is systematically depleted in ^{13}C compared

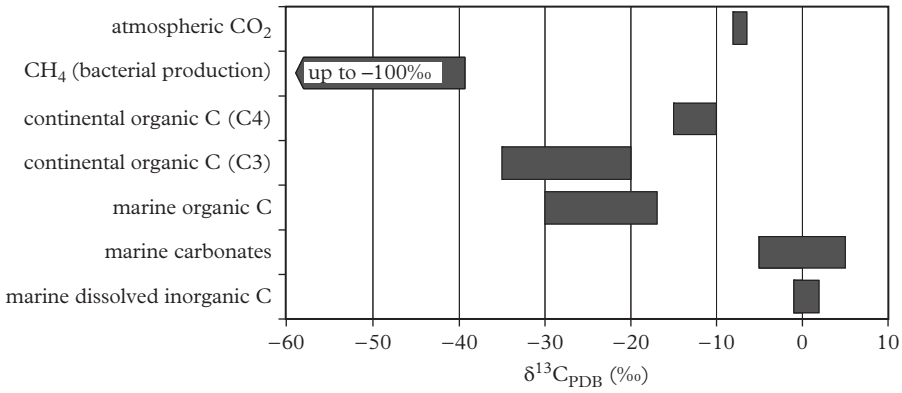

Figure 3.9 *Range of variation of $\delta^{13}C$ (relative to the PDB scale) in the ocean, the atmosphere and the biosphere.*

to inorganic carbon from which it is formed (Fig. 3.9). There are also significant fractionations between the different inorganic carbon species, but they are less important than fractionation during the photosynthesis. The fractionation mechanisms involved in photosynthesis will be detailed in Section 3.6.2, but since dissolved inorganic carbon (DIC) is used as raw material for the photosynthesis of organic carbon, we will first focus on fractionations between inorganic carbon species. Then, we will present fractionations linked to biological activity, their effects on organic and inorganic carbon, as well as their applications to the ocean.

The growing use of fossil fuels since the industrial revolution has led to the injection into the environment of CO_2 with the isotopic signature of organic matter since both oil and coal have a vegetal origin (see Problem 2). This is the **Suess effect** (Fig. 3.10). The use of $\delta^{13}C$ to quantify carbon fluxes in the ocean–atmosphere–biosphere system will be presented in Chapter 8.

3.6.1 Fractionations in the Carbonate System

There are isotopic fractionations between the different species of DIC (Fig. 3.11). The $\delta^{13}C$ of DIC is close to the $\delta^{13}C$ of HCO_3^- because HCO_3^- represents 90% of DIC in seawater. Fractionation coefficients between CO_2, HCO_3^- and CO_3^{2-} are temperature dependent. When an isotopic equilibrium is established between the seawater and the atmosphere, the overall isotopic fractionation between the DIC in seawater and atmospheric CO_2 depends on the temperature and on the relative abundance of CO_2, HCO_3^- and CO_3^{2-} in seawater. In addition, we will see in Chapter 7 that the isotopic equilibrium is far from being always reached between the ocean and the atmosphere.

Many marine organisms produce shells made of calcium carbonate ($CaCO_3$) as calcite or aragonite according to the reaction:

$$CO_3^{2-} + Ca^{2+} \Leftrightarrow CaCO_3(\text{solid}).$$

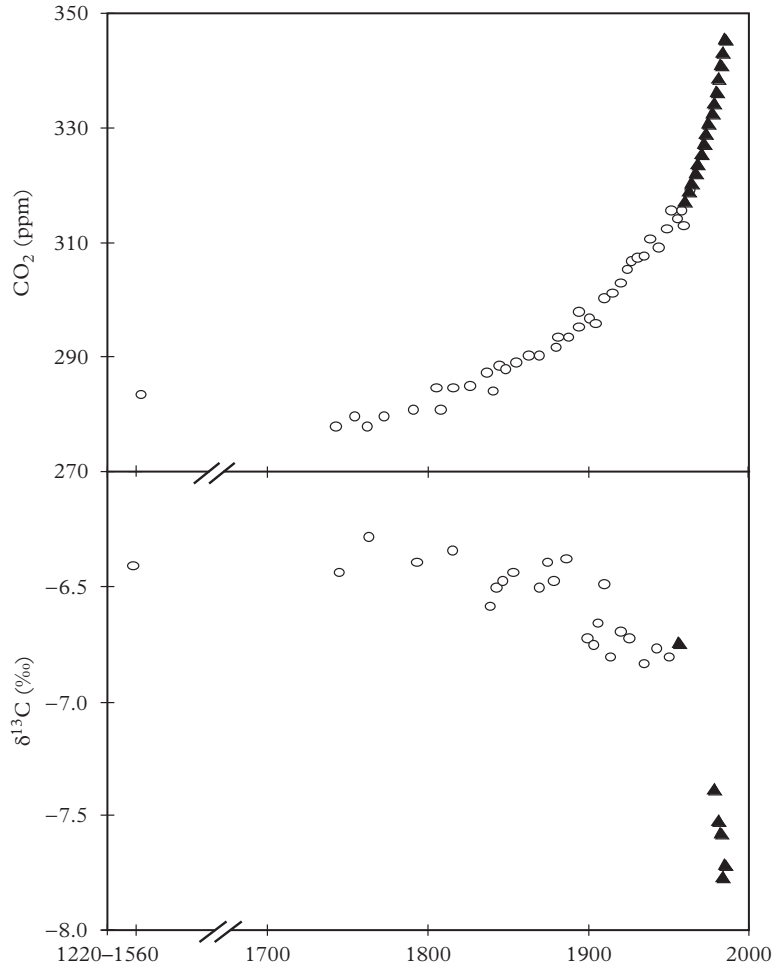

Figure 3.10 *Evolution of the atmospheric CO_2 concentration and isotopic composition since the Middle Ages. After 1954, data are direct measurements (black triangles). Previous data were obtained by analyzing air bubbles trapped in ice cores (white circles). The $\delta^{13}C$ shows that the increase in CO_2 concentration is due to the addition of ^{13}C-depleted photosynthetic carbon. Modified from Friedli et al. (1986).*

There is a small fractionation between $\delta^{13}C_{CaO_3}$ and $\delta^{13}C_{HCO_3^-}$ ($\Delta_{CaCO_3-HCO_3^-}$ = 1.85‰ at 20°C) and thus between $\delta^{13}C_{CaO_3}$ and $\delta^{13}C_{DIC}$. The $\delta^{13}C_{CaO_3}$ of marine carbonate is used to reconstruct the isotopic composition of DIC in the ocean (see Problem 3; see also Chapter 11). However, "vital effects" related to respiration of cells can alter this isotopic fractionation and complicate the use of the data.

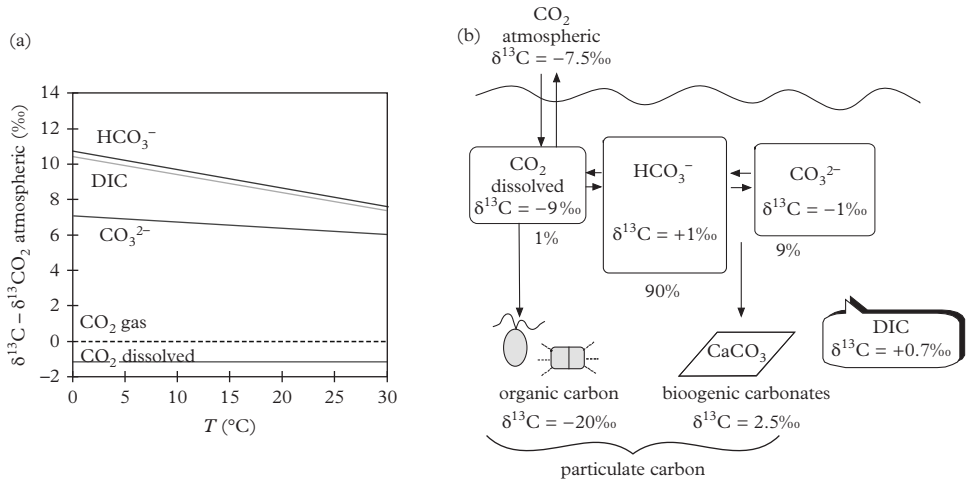

Figure 3.11 *Variation of $\delta^{13}C$ in the carbonate system at equilibrium with atmospheric CO_2. (a) Fractionation coefficient in the carbonate system as a function of the temperature. Modified from Lynch-Stieglitz et al. (1995). (b) $\delta^{13}C$ of the various reservoirs in the surface ocean. Photosynthesis by phytoplankton tends to increase the $\delta^{13}C$ of the surface waters, whereas the formation of calcium carbonate tends to decrease it. Overall, when algae with calcareous shells grow, the effect of photosynthesis dominates over the calcium carbonate formation, which leads to an increase of the $\delta^{13}C$ of seawater.*

3.6.2 Biological Fractionations

The $\delta^{13}C$ of organic matter is systematically lower than the $\delta^{13}C$ of the inorganic carbon from which it was photosynthesized. The fractionation occurs in two steps:

- The molecular diffusion (see Chapter 6) of $^{12}CO_2$ is faster than that of $^{13}CO_2$. For terrestrial plants, atmospheric CO_2 diffuses from air into leaves through small openings (called stomata), allowing the leaves to exchange gases with the atmosphere while limiting water loss. In the ocean, the renewal of CO_2 in the immediate vicinity (a few tens of microns) of algae is made by molecular diffusion in water. These steps lead to relatively low fractionations.
- The reduction of inorganic carbon to organic carbon is accompanied by a large kinetic fractionation. In most photosynthetic organisms (terrestrial and aquatic), reduction of CO_2 is catalyzed by Ribulose 1.5 bisphosphate carboxylase oxygenase (Rubisco), which favors the reduction of $^{12}CO_2$ compared to $^{13}CO_2$ ($\delta^{13}C_{\text{organic matter}} \approx -20$ to -30‰). In some terrestrial plants (called C4 plants), the reduction of HCO_3^- by the phosphoenolpyruvate carboxylase (PEP carboxylase) enzyme produces a lower fractionation ($\delta^{13}C_{\text{organic}} \approx -8$ to -18‰).

In general, the $\delta^{13}C$ of marine photosynthetic organisms (which have a C3 metabolism) is lower than in terrestrial plants. The slow rate of molecular diffusion around the

algae can limit the availability of CO_2. In CO_2-rich water, algae use preferentially ^{12}C and ^{13}C is left aside. In CO_2-poor water, the same algae begin by preferentially using ^{12}C, but as the environment becomes depleted in ^{12}C, it is forced to assimilate ^{13}C, the relative abundance of which has increased. This forms organic carbon with a less negative $\delta^{13}C$ than what it would be in a CO_2-repleted environment (see Chapter 7). There is little isotopic fractionation between an animal and its food (^{12}C enrichment is less than 1‰). Therefore, $\delta^{13}C$ is a good indicator of food sources through the food chain (see Section 3.8).

3.6.3 The $\delta^{13}C$–PO_4^{3-} Relationship in Seawater

In deep waters, the $\delta^{13}C$ of a water mass is no longer controlled by the equilibrium with the atmosphere. The DIC of seawater has a $\delta^{13}C$ that varies systematically with depth between +2 and –0.5‰ (Fig. 3.12). $\delta^{13}C$ mirrors the PO_4^{3-} concentration, indicating a relationship with biological activity. In surface water, phytoplankton take up CO_2 and PO_4^{3-} for photosynthesis. In doing so, they deplete seawater in PO_4^{3-} and change the $\delta^{13}C$ of DIC. The formation of marine organic matter depleted in ^{13}C relative to ^{12}C ($\delta^{13}C = -20‰$) produces an enrichment of seawater in ^{13}C relative to ^{12}C ($\delta^{13}C = 0$ to +2‰). Conversely, in deep waters, the remineralization of the organic matter produces an increase in the PO_4^{3-} and DIC concentration (Fig. 3.13). As the carbon released has a very negative $\delta^{13}C$, this leads to a decrease of the $\delta^{13}C$ of DIC (see Problem 4).

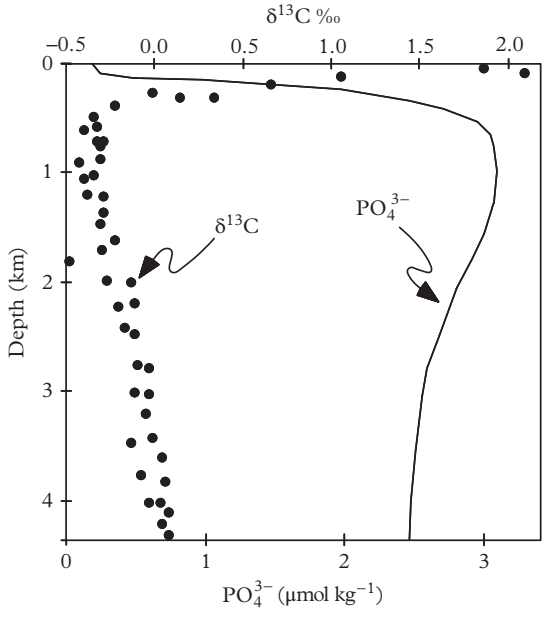

Figure 3.12 *Vertical profile of the PO_4^{3-} concentration and of the $\delta^{13}C$ of DIC in seawater in the North Pacific. These symmetrical curves reflect the formation of organic matter in surface water (PO_4^{3-} assimilation and enrichment of seawater in ^{13}C) and its remineralization at depth (dissolution of PO_4^{3-} and enrichment of seawater in ^{12}C). Modified from Broecker and Peng (1982).*

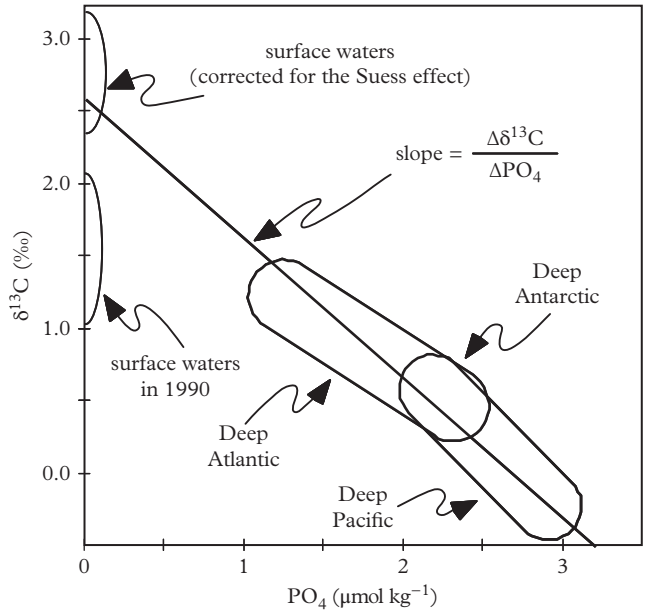

Figure 3.13 *Relationship between the PO_4^{3-} concentration and the $\delta^{13}C$ of DIC. When deep waters were formed, they were in contact with an atmosphere that had a less negative $\delta^{13}C$ than today (Suess effect). Present surface waters corrected for the Suess effect plot on the deep water correlation. The linear relationship between PO_4^{3-} and $\delta^{13}C$ is consistent with the theory. Modified from Broecker and Peng (1982).*

As a result, there is a linear relationship between PO_4^{3-} and $\delta^{13}C$ in today's ocean (see Problem 5) that is used to reconstruct paleo-currents (see Chapter 11).

3.7 Nitrogen Isotope Fractionation

The main source of nitrogen isotope fractionation is biological activity (Fig. 3.14). When phytoplankton convert NO_3^- or NH_4^+ into organic nitrogen, they preferentially assimilate ^{14}N which leads to a depletion of the organic matter in ^{15}N. However, the synthesis of organic nitrogen by N_2 reduction made by bacteria like *Trichodesmium* produces a negligible fractionation (see Problem 6). The fractionation of nitrogen isotopes by zooplankton is complex (Fig. 3.14).

Overall, the $\delta^{15}N$ increases of 3.5‰ at each new level of the food chain, which allows its use as a tracer of the position of the different animal species in this chain (Fig. 3.15). The $\delta^{15}N$ of seawater nitrate (the initial reservoir) and therefore the $\delta^{15}N$ of the phytoplankton and zooplankton that develop in this water strongly vary depending on the degree of nitrate exhaustion of the euphotic layer (see Appendix 1).

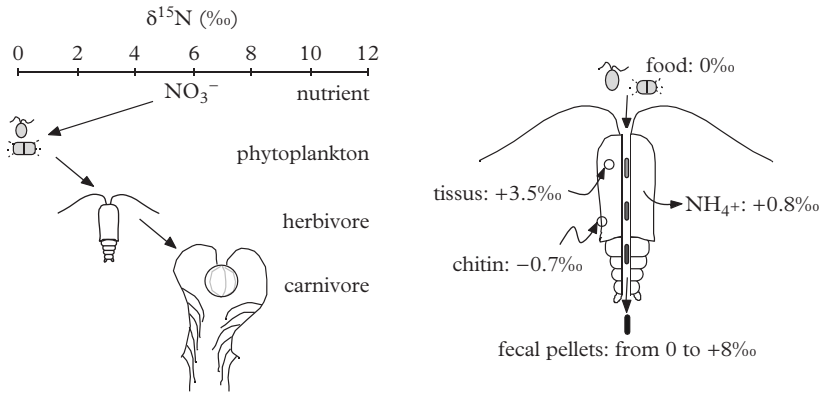

Figure 3.14 *Fractionation of the nitrogen isotopes through the food chain. (a) The $\delta^{15}N$ of nitrate of the deep waters that feed the euphotic layer is about +6‰. When nitrogen is not limiting, phytoplankton (here a diatom and a flagellate) preferentially assimilate ^{14}N. Then, at each level of the food chain (here an herbivorous copepod and a carnivorous ctenophore), the $\delta^{15}N$ of the zooplankton increases by about 3.5‰. (b) Variation of $\delta^{15}N$ in a copepod whose food has a $\delta^{15}N$ of 0‰. Modified from Montoya (1994).*

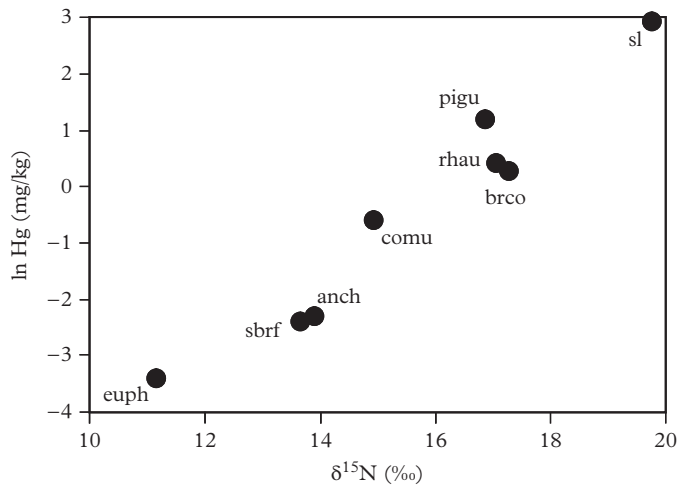

Figure 3.15 *Variation of the logarithm of the mercury (Hg) concentration as a function of $\delta^{15}N$ for different marine organisms in the Gulf of the Farallones (which borders San Francisco, California). Mercury undergoes a bioaccumulation through the food chain. euph: euphausiid (shrimp). sbfr: short-bellied rockfish. anch: anchovy. comu: common murre. brco: Brandt's cormorant. rhau: rhinoceros auklet. pigu: pigeon guillemot. sl: sea lion. Modified from Jarman et al. (1996).*

Denitrification also produces a large ^{15}N enrichment of the remaining nitrates. This enrichment can be used as a water tracer over more than 1000 km (Liu and Kaplan, 1989). Wastewaters are isotopically labeled by denitrification. It is possible to control their arrival in the coastal environment even before the effects of eutrophication linked to excessive nitrate releases become noticeable.

3.8 Sulfur Isotope Fractionation

The main source of fractionation of sulfur isotopes is the reduction of SO_4^{2-} to H_2S by bacteria, during which a fractionation up to 60‰ can exist between SO_4^{2-} and H_2S. This reduction is at the origin of the difference in isotopic composition between seawater ($\delta^{34}S = +20‰$) and sedimentary sulfides ($\delta^{34}S = -17‰$). These two reservoirs are complementary with regard to mantle/continental sulfur ($\delta^{34}S \approx 0‰$), which represents the source of sulfur in the ocean.

The synthesis of cysteine and the transfer of the sulfur in the food chain occur without significant fractionation, so $\delta^{34}S$ is a tracer for the origin of sulfur in the food chain (see Problem 7). Two isotopes being more informative than one, it is often used jointly with one or several other tracers (Fig. 3.16). Similarly, during precipitation of gypsum

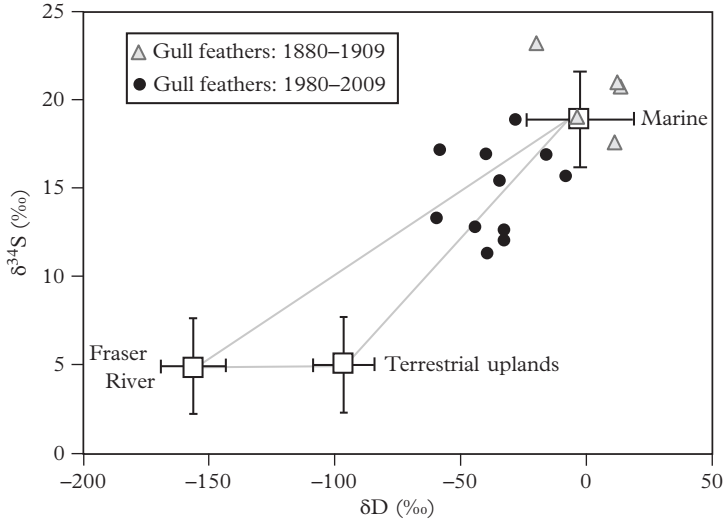

Figure 3.16 *Isotopic signature of a gull feather from British Columbia. Sulfur and hydrogen isotopes are only slightly fractionated through the food chain, so they retain the signature of primary producers in the gull feather. In the late nineteenth–early twentieth century, gulls fed mainly on marine resources. Today, they have incorporated a significant fraction of terrestrial/freshwater food in their diet, in response to the decline of forage fish availability. Modified from Hobson et al. (2015).*

($CaSO_4 \cdot 2H_2O$), isotopic fractionations are low (less than 2‰), so that the $\delta^{34}S$ of gypsum in evaporites can be used to study the evolution of the $\delta^{34}S$ of seawater. As for oxygen, mass-independent isotopic fractionations of sulfur exist in the environment (see Chapter 11).

3.9 Boron Isotope Fractionation

Boron is a conservative element in the ocean with a concentration of 4500 μg kg^{-1}. In seawater, 80–90% of the boron occurs as boric acid ($B(OH)_3$) and as borate ions ($B(OH)_4^-$) for the remaining 10–20%. The boric acid/borate ion ratio depends on the pH (Fig. 3.17) because it is determined by the equilibrium

$$B(OH)_3 + H_2O \Leftrightarrow B(OH)_4^- + H^+.$$

It is thought that only $B(OH)_4^-$ is taken up by solid phases (clays and carbonates).

The isotopic composition of boron in seawater is constant ($\delta^{11}B$ = 39.5‰). However, there is an isotope fractionation ($\alpha_{B(OH)_4^- - B(OH)_3} = 0.973$) between $B(OH)_3$, which is enriched in ^{11}B, and $B(OH)_4^-$, which is depleted in ^{11}B. As the $B(OH)_3/B(OH)_4^-$ ratio varies with pH, values of $\delta^{11}B_{B(OH)_3}$ and $\delta^{11}B_{B(OH)_4^-}$ are also pH dependent. At

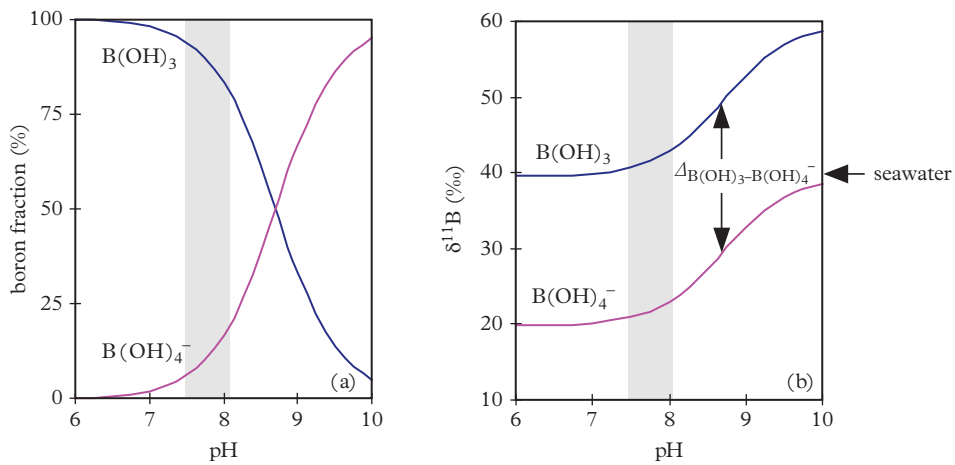

Figure 3.17 *pH effect on the abundance and the $\delta^{11}B$ of $B(OH)_3$ and $B(OH)_4^-$. The shaded band represents the range of the pH of seawater. (a) Variation of the $B(OH)_3/B(OH)_4^-$ ratio with pH. At the seawater pH, $B(OH)_3$ represents 80–90% of dissolved boron. (b) Variation of $\delta^{11}B$ of $B(OH)_3$ and $B(OH)_4^-$ with pH. At low pH, $\delta^{11}B_{B(OH)_3} \approx \delta^{11}B_{seawater}$ = 39.5‰ and $\delta^{11}B_{B(OH)_4^-}$ = (39.5 – 20) = 19.5‰. Conversely, at high pH, $\delta^{11}B_{B(OH)_4^-} \approx \delta^{11}B_{seawater}$ = 39.5‰ and $\delta^{11}B_{B(OH)_3}$ = 59.5‰.*

very low pH, boron is mostly in the form of boric acid so that $\delta^{11}B_{B(OH)_3} = 39.5‰$ and $\delta^{11}B_{B(OH)_4^-} = (39.5 - 20) = 19.5‰$. On the contrary, at high pH, boron is mostly borate, so that $\delta^{11}B_{B(OH)_3} = 59.5‰$ and $\delta^{11}B_{B(OH)_4^-} = 39.5‰$. For usual seawater pH, $\delta^{11}B_{B(OH)_3}$ varies from 43.3 to 45.6‰, while $\delta^{11}B_{B(OH)_4^-}$ varies between 23 and 25‰.

The adsorption of boron on clays ($\Delta_{clay-seawater} \approx -20‰$) and crust oceanic weathering ($\Delta_{altered\ crust-seawater} \approx -37‰$) occur with a ^{10}B depletion of seawater. During the incorporation of boron in carbonates, only borate ions are incorporated. Therefore, there is a global fractionation between carbonate and seawater. However, the boron isotopic composition of carbonates reflects the boron isotopic composition of borate ion in solution ($\delta^{11}B_{carbonate} = \delta^{11}B_{B(OH)_4^-}$). It is therefore possible to determine the paleo-pH of seawater from the $\delta^{11}B$ of foraminifera tests or corals if the $\delta^{11}B$ of seawater at the time of their formation is known (Sanyal et al., 1995).

3.10 Silicon Isotope Fractionation

Silicon is supplied to the ocean mainly by rivers ($\delta^{30}Si \sim +1.1‰$) and groundwaters ($\delta^{30}Si \sim 0.25‰$), and to a lower extent by volcanic activity ($\delta^{30}Si \sim -0.3‰$), but the impact of continental particle dissolution at ocean margins has to be quantified (Georg et al., 2009). During silicic acid ($Si(OH)_4$) consumption by diatoms, the lighter Si isotope (^{28}Si) is preferentially consumed and incorporated in biogenic silica (b-SiO_2), leaving the silicic acid pool enriched in heavy Si isotope (^{30}Si) (De La Rocha et al., 1997). The fractionation factor $\Delta_{b\text{-}SiO_2-Si(OH)_4} \sim -1.1 \pm 0.4‰$ seems to be independent of temperature and species, although a recent study on in vitro diatoms has challenged this consensus observed from ocean and fresh water (Sutton et al. 2013). The $\delta^{30}Si$ of silicic acid typically ranges from +1 to +3‰ (Fig. 3.18). The heaviest values are obtained when surface waters become exhausted in silicic acid (up to +4.4‰ in the Equatorial Pacific Ocean, Grasse et al., 2013). The same trend (with an offset due to isotope fractionation) is observed for biogenic silica with $\delta^{30}Si$ typically ranging from –0.4 to +2.3‰ (Fripiat et al., 2012). See Problem 10.5 to learn more on $\delta^{30}Si$ in the deep ocean.

The $\delta^{30}Si$ signature of biogenic silica strongly depends on the extent of Si depletion of the surface waters. Hence, the $\delta^{30}Si$ signature of biogenic silica is a proxy of Si-nutrient utilization in paleoceanography. Silicon stable-isotope measurements suggest that the percentage utilization of silicic acid by diatoms in the Southern Ocean during the last glacial period was strongly diminished relative to the present interglacial (De La Rocha et al., 1997).

3.11 Iron Isotope Fractionation

Iron distribution in the ocean results from its sources, sinks and internal cycling. Sinking particles constitute the only sink that removes Fe from the water column, whereas there are numerous Fe sources. Several Fe sources to the open ocean are currently being

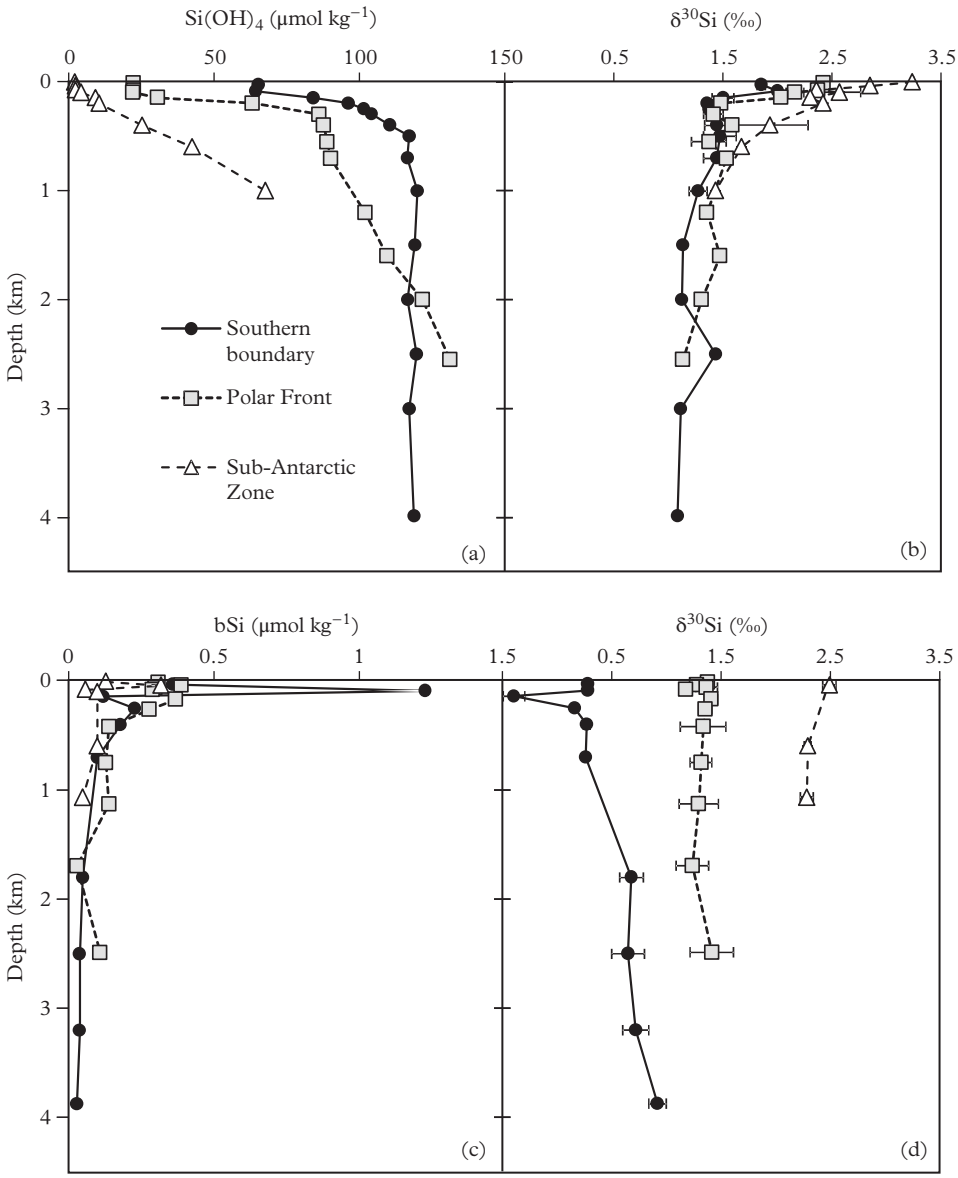

Figure 3.18 *Concentration and isotopic composition of dissolved and particulate silica in the Southern Ocean. (a) Dissolved silica (silicic acid). The dissolved silica concentration increases with depth. In the surface waters, the dissolved silica concentration decreases from the south (southern boundary) to the north (Subantarctic Zone) of the Antarctic Circumpolar Current (see Section 7.6 of Chapter 7 for details). (b) The $\delta^{30}Si$ of dissolved silica is relatively constant (~ +1.5‰) in the deep ocean. In contrast, the $\delta^{30}Si$ of the surface waters increases northward as the silica concentration decreases. (c) Particulate biogenic silica concentration. The highest biogenic silica concentrations occur in the surface water with available dissolved silica. (d) The $\delta^{30}Si$ of particulate biogenic silica is relatively constant with depth at a given station. It is shifted by ~ −1.5‰ compared to the $\delta^{30}Si$ of dissolved silica in the surface waters (isotopic fractionation). Modified after Fripiat et al. (2012).*

debated. Their distinct isotopic signature can help to disentangle them (Labatut et al., 2014 and references therein):

- The continental crust has a signature of $\delta^{56}Fe = 0.07 \pm 0.02‰$.
- Atmospheric dusts sampled close to arid regions have $\delta^{56}Fe$ (from 0.04 to 0.08‰) close to the continental crust value. Marine aerosols sampled in the open ocean exhibit more variability.
- In areas of high primary production, pore waters of organic-rich sediments deposited on continental shelves and upper slopes display a light dissolved Fe isotopic composition, $\delta^{56}Fe = -3.3‰$ to $-1.7‰$ that reflects the reduction of Fe(III) to Fe(II) in the sediments during diagenesis.
- Conversely, in organic-poor sediments, the positive Fe isotopic signature of pore waters corresponds to a "non-reductive" release of Fe from these sediments (Radic et al., 2011).
- Hydrothermal fluids are characterized by a slightly light composition ($\delta^{56}Fe$ values between –0.5 and –0.21‰, for dissolved Fe, and between –0.7 and –0.11‰ in the particulate fraction).
- For river inputs, $\delta^{56}Fe$ ranges from –1.4 to +0.2‰ for dissolved Fe. The suspended matter signature ranges from –0.87 to +0.4‰.

The effect of these sources is best illustrated by west–east Atlantic sections of dissolved Fe and $\delta^{56}Fe$ (Fig. 3.19), where each dissolved Fe maximum is tagged by its $\delta^{56}Fe$ signature, which persists throughout the water column (Conway and John, 2014). Taking the $\delta^{56}Fe$ of the surface water as reflecting dust dissolution only and assuming that dissolved Fe in the deep ocean is a mixture dust-derived Fe and a single local Fe source, such as hydrothermal fluids or sediments (strong hypotheses but one must start somewhere), it is possible to calculate the relative contribution to the dissolved phase from Saharan dust aerosols (71–87%), hydrothermal venting at the Mid-Atlantic Ridge (2–6%), reductive sedimentary dissolution on the African margin (1–4%) and non-reductive sedimentary dissolution from oxygenated sediments on the North American margin (10–19%). This highlights the fact that hydrothermal vents are a source of iron, which travels thousands of kilometers from vent sites, potentially influencing surface productivity.

In the open ocean, the $\delta^{56}Fe$ of dissolved Fe ranges from –0.74 to +0.80‰, while the $\delta^{56}Fe$ of particulate Fe ranges mostly from –0.10 to +0.46‰. The internal cycle of Fe isotopes in the open ocean is very poorly documented. Unlike $\delta^{13}C$ or $\delta^{30}Si$ isotopes, $\delta^{56}Fe$ does not increase systematically in surface waters. Although it is generally considered that there is a preferential uptake of light Fe isotopes by phytoplankton when dissolved Fe is assimilated (see Problem 8), the estimated fractionation factor is low: $\Delta_{\text{organic Fe–dissolved Fe}} \sim +0.1‰$. In surface waters, the particulate Fe fraction (with a significant lithogenic component) is often much more abundant than the dissolved Fe fraction. During particulate Fe dissolution/desorption, heavy Fe isotopes are preferentially released in the dissolved pool, in much the same way as non-reductive Fe is released from sediments (Labatut et al., 2014).

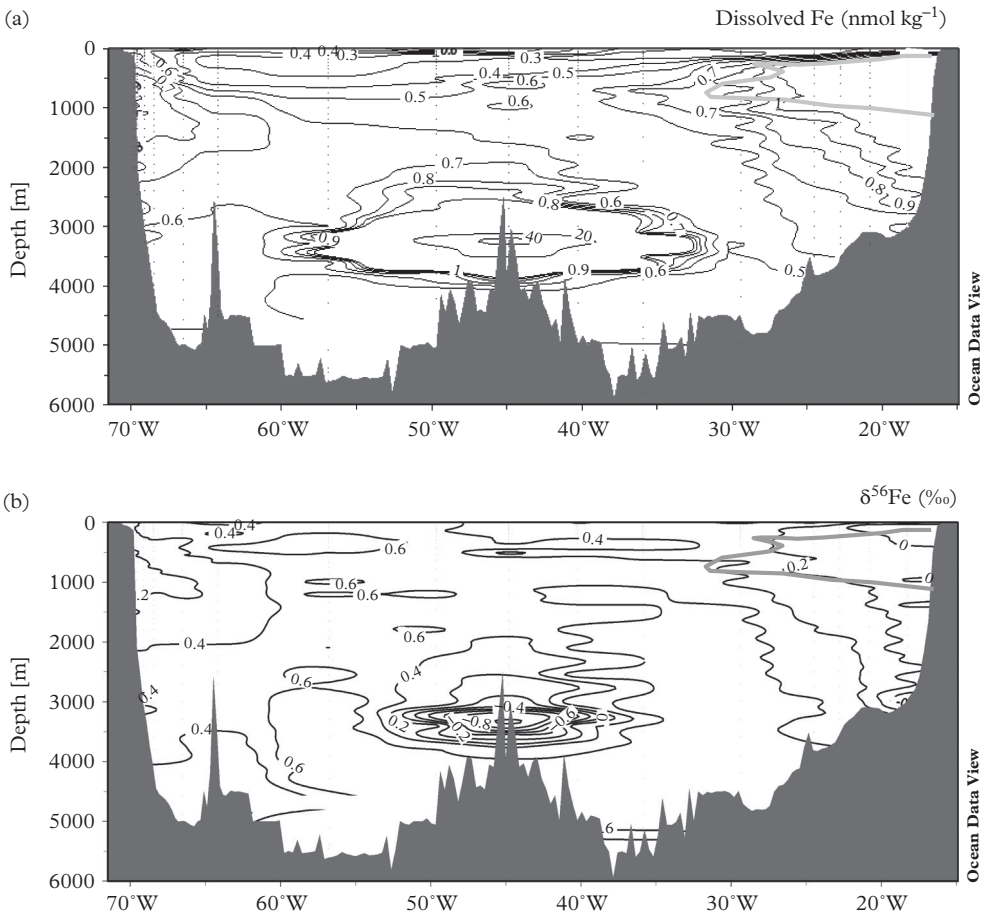

Figure 3.19 *Concentration and isotopic composition of dissolved Fe along a North Atlantic section from Cape Cod, Massachusetts in North America to the Cape Verde Islands off Africa. (a) Dissolved Fe concentration. High concentrations along the continental margins and very high concentrations at the mid-Atlantic ridge indicate Fe inputs. (b)* δ^{56}*Fe of dissolved Fe. Each source has its own* δ^{56}*Fe signature: null to negative for the reductive Fe release on the eastern side of the basin, slightly positive for the non-reductive Fe release on the western side, strongly negative in the hydrothermal plume and* $\approx$*0.6‰ for the general background released by Saharan dusts dissolution. Dotted gray line: oxygen-minimum zone. Modified after Conway and John (2014).*

3.12 Mixing of Isotopic Tracers

The ocean is an open environment in which compounds of various origins are mixed: water mass mixing, mixing of marine particles ingested by zooplankton, mixing between solid and dissolved compounds either by adsorption of the former on marine particles or by dissolution of the latter in seawater. Although the mechanisms are very different,

the isotopic composition of a tracer follows a relationship independent of the mixing mechanism itself. This mixing equation is also valid for the isotopic compositions of tracers related to radioactive pairs.

3.12.1 Conservative Mixing

Consider the mixing of two compounds A and B that are called the end-members of the mixing (Fig. 3.20). We mix a mass m_A of material from the end-member A with a mass m_B of material from the end-member B. We consider a tracer with a concentration C_A and an isotopic ratio isotope R_A in the A end-member and a concentration C_B and the isotopic ratio R_B in the B end-member. The conservation equations of the mass of the tracer and of the minor isotope are

$$\begin{cases} m_m = m_A + m_B \\ m_m C_m = m_A C_A + m_B C_B, \\ m_m C_m R_m = m_A C_A R_A + m_B C_B R_B. \end{cases} \tag{3.7}$$

If we call $f_A = m_A/(m_A + m_B)$ the mass fraction of material from the A end-member, the equations become

$$\begin{cases} C_m = f_A C_A + (1 - f_A) C_B, \\ R_m = \dfrac{f_A C_A R_A + (1 - f_A) C_B R_B}{f_A C_A + (1 - f_A) C_B}. \end{cases} \tag{3.8}$$

If the tracer is conservative during the mixing, there is a linear relationship between f_A and C_m. From equation (3.8), we obtain

$$f_A = \frac{C_m - C_B}{C_A - C_B}. \tag{3.9}$$

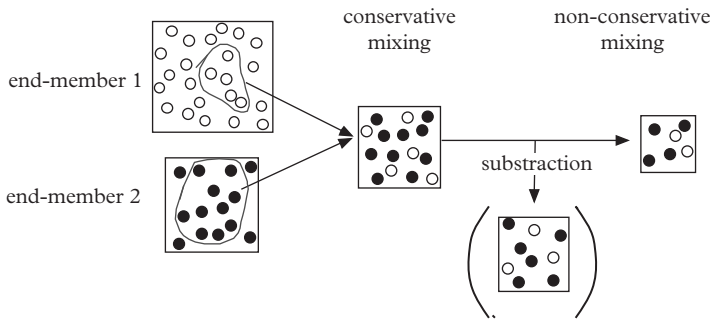

Figure 3.20 *Illustration of the behavior of an isotopic tracer during a conservative and a non-conservative mixing. The isotopic composition of the mixture allows determination of the proportions of tracers from the two end-members even if mixing is not conservative, providing that the fractionation coefficient is known (1 in the present illustration).*

There is a linear relationship between f_A and R_m only if $C_A = C_B$. If $C_A \neq C_B$, the denominator of equation (3.8b) is not constant and the relationship between f_A and R_m is not linear. Introducing equation (3.9) in equation (3.8b), it follows that

$$R_m = \frac{C_A R_A - C_B R_B}{C_A - C_B} + \frac{C_A C_B (R_B - R_A)}{C_A - C_B} \times \frac{1}{C_m}. \tag{3.10}$$

Equation (3.10) shows that in the case of a conservative mixing, there is a hyperbolic relationship between the isotopic composition and the concentration of samples for different mixing proportions. In this case, there is a linear relationship between the isotopic composition and the inverse of the concentration of the mixture.

Note 1: Sometimes, we do not consider f_A and $1 - f_A$ the fraction of end-member in the mixing, but rather "f_e" and "$1 - f_e$," the fractions of element of interest from the end-members A and B in the mixing. In this case, we obtain

$$f_e = \frac{m_A C_A}{m_A C_A + m_B C_B} = \frac{f_A C_A}{f_A C_A + (1 - f_A) C_B}, \tag{3.11a}$$

$$R_m = f_e R_A + (1 - f_e) R_B. \tag{3.11b}$$

Note 2: We have considered so far isotope ratios but these equations are also usable with the relative deviations (δ).

3.12.1.1 Example of mixing hyperbola: the $\delta^{11}B$ in the Elbe estuary

The brackish waters of the Elbe estuary are mixtures of fresh water from the Elbe River and of seawater from the North Sea (Barth, 1998). As the Elbe water salinity is negligible compared to seawater, the mass fraction of seawater in a sample of brackish water is proportional to its salinity (S) which is a conservative tracer ($f = S_{\text{brackish water}}/S_{\text{seawater}}$, equation 3.9). The linear relationship between S and [B] reflects the conservative behavior of boron (Fig. 3.21). The nonlinear relationship between [B] and $\delta^{11}B$ is due to the difference in boron concentration in the Elbe and the North Sea. In the estuary, adding very little seawater to the Elbe water brings a lot of boron. $\delta^{11}B$ changes quickly because most boron comes from seawater and it overwhelms the Elbe River signature. The linear relationship between 1/[B] and $\delta^{11}B$ indicates that this is a mixing between two end-members:

- the Elbe water, characterized by a low salinity ($S < 0.5$), a low boron content (0.25 μg kg^{-1}) and a low $\delta^{11}B$ (= 23.9‰);
- seawater, characterized by a high salinity ($S = 34.7$), a low boron content (4700 μg kg^{-1}) and a high $\delta^{11}B$ (= 40.9‰).

It is therefore a typical case of a conservative mixing between two end-members.

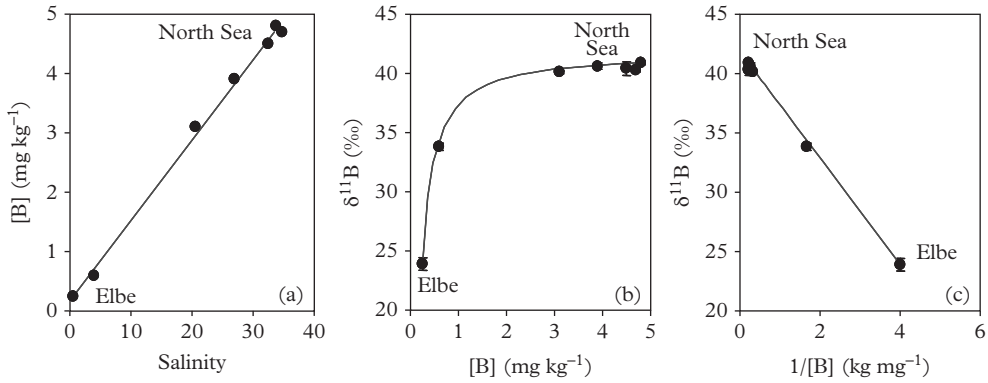

Figure 3.21 *Effect of mixing on the isotopic composition of boron in the Elbe River estuary. (a) Linear salinity–[B] relationship (see equation 3.8). (b) Relationship between [B] and $\delta^{11}B$. It is a mixing hyperbola (equation 3.10). (c) Relationship between 1/[B] and $\delta^{11}B$. The linear relationship (easier to identify than a hyperbola) confirms that there is a two end-member mixing. Modified from Barth (1998).*

Exercise: Water mixing in the Weddell Sea (Weiss et al., 1979)

On the western shelf of the Weddell Sea, a small fraction of very cold water of meteoritic origin produced by the melting of the Antarctic ice sheet ($\delta^{18}O_{glacier} = -50‰$) mixes with seawater ($\delta^{18}O_{seawater} = -0.35‰$). Knowing that the Western Shelf Water produced by this mixing has an isotopic signature $\delta^{18}O_m = -0.5‰$, determine the fraction of water coming from the glacier melting.

Solution:

The Western Shelf Water has an intermediate isotopic signature between the melt water and seawater, which are the two end-members of the mixing (Fig. 3.22).

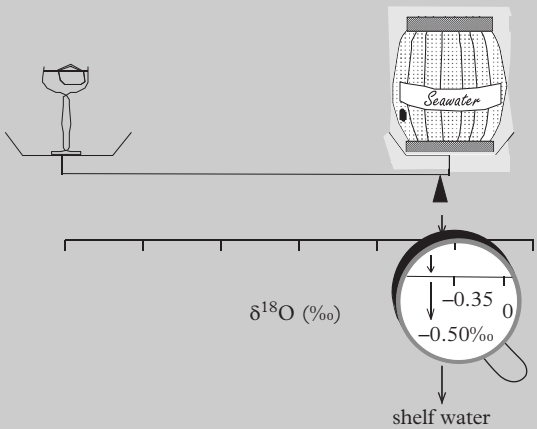

Figure 3.22 *Isotopic balance during the formation of the Western Shelf Water. The $\delta^{18}O$ of the shelf water is the barycenter of the $\delta^{18}O$ of water from glacier melting and seawater, weighted by the proportion of water in the mixture.*

The fraction of melted water from the glacier in the shelf water is given by equation (3.11b):

$$f_{\text{glacier}} = \frac{\delta^{18}O_m - \delta^{18}O_{\text{seawater}}}{\delta^{18}O_{\text{glacier}} - \delta^{18}O_{\text{seawater}}} = \frac{-0.5 - (-0.35)}{-50 - (-0.35)} = 0.003.$$

In this example, the fractions of water (f_m) and of oxygen (f_e) in the water coming from the melting of the glacier are identical because the amount of oxygen in H_2O is virtually the same in seawater and fresh water (it is in fact a little lower in seawater due to dilution by the salt). This result will be used in Chapter 10.

3.12.2 Non-Conservative Mixing

By using the mass conservation equation, we have implicitly assumed that mixing is conservative, that is, without subtraction or addition of tracer. In a non-conservative mixing, a fraction of the tracer and/or of the carrier phase is removed or added. The relationship between the inverse of the concentration and the isotopic composition is then no longer respected. Nevertheless, the isotopic composition records information on the source of the material.

3.12.2.1 Application: the diet of Magellan penguins

Magellan penguins live on the coast of Patagonia and feed on anchovies and squids (Forero et al., 2002). $\delta^{15}N$ is used to determine precisely the contributions of the prey to the nutrition of the penguins. Obviously a penguin is not a simple assemblage of anchovies and squids as, during digestion, it assimilates only a fraction of the food and rejects the rest. The mixing is therefore non-conservative. $\delta^{15}N$ of anchovies ($\delta^{15}N = +17‰$) is higher than $\delta^{15}N$ of the squid ($\delta^{15}N = +13.5‰$) because anchovies are at a higher trophic level than squids. The $\delta^{15}N$ of penguins depends on the $\delta^{15}N$ of their prey and on the isotope fractionation linked to the metabolism of penguins ($\Delta_{\text{prey–penguin}} = +3‰$ for penguins). By correcting the $\delta^{15}N$ of penguins from isotopic fractionation, we obtain the $\delta^{15}N$ of their food:

$$\delta^{15}N_{\text{prey}} = \delta^{15}N_{\text{penguin}} + \Delta_{\text{prey–penguin}}.$$

We then use equation (3.11b) to determine the proportion of nitrogen provided by anchovies in the food

$$f_{\text{anchovy}} = \frac{(\delta^{15}N_{\text{penguin}} + \Delta_{\text{prey–penguin}}) - \delta^{15}N_{\text{squid}}}{\delta^{15}N_{\text{anchovy}} - \delta^{15}N_{\text{squid}}} = \frac{(18.8 - 3.0) - 13.5}{17 - 13.5} = 0.67.$$

$\Delta^{15}N$ narrows ornithological observations suggesting that Magellan penguins feed primarily on anchovies. It also shows that the penguins give to their offspring ($\delta^{15}N$ =

+19.2‰) a larger proportion of anchovies than they eat themselves. Anchovies have a high nutritional value and they are easy to digest. Magellan penguins are loving parents!

3.13 Evolution of the Isotopic Signature during a Reaction

During a reaction that produces an isotopic fractionation, the fractionation factor α determines the relationship between the isotopic ratios of the products and reactants at a given time. However, this is not sufficient to predict the evolution of the isotopic signatures during the whole process. Indeed, this evolution also depends of the reaction extent, on the possible renewal of products and on the possible separation of products and reactants. Let's consider a transformation

$$A \rightarrow B,$$

which is associated with a fractionation factor $\alpha_{A\text{–}B}$ as defined by equation (3.2). However, in order to obtain simpler formulas and to be consistent with the oceanographic literature, we now introduce $\alpha_{B\text{–}A} = (\alpha_{A\text{–}B})^{-1} = \frac{R_B}{R_A} = \frac{1000+\delta_B}{1000+\delta_A} \approx 1 + \frac{\delta_B - \delta_A}{1000}$. Initially, only A is present and it has an isotopic ratio R_A^0 (the exponent 0 represents the initial state). We want to determine the final isotopic ratios (R_A and R_B) in three cases:

(1) The reaction is complete. Any compound A initially present has now turned into B:

$$R_B = R_A^0. \tag{3.12}$$

(2) The reaction is incomplete and an isotopic equilibrium is established between products and reactants that are in contact. If we call F the fraction of A that has not been transformed into B, the evolution of the ratios is given by (see Appendix 1)

$$R_A = \frac{R_A^0}{F + \alpha_{B\text{–}A}(1-F)}, \tag{3.13}$$

$$R_B = \frac{\alpha_{B\text{–}A} R_A^0}{F - \alpha_{B\text{–}A}(1-F)}. \tag{3.14}$$

(3) The reaction is incomplete and there is no bulk isotopic equilibrium between products and reactants because as soon as a new increment of B is formed, it is taken away from A. The systematic separation of products and reactants prevents isotopic exchange between the remaining reactants and all of the products.

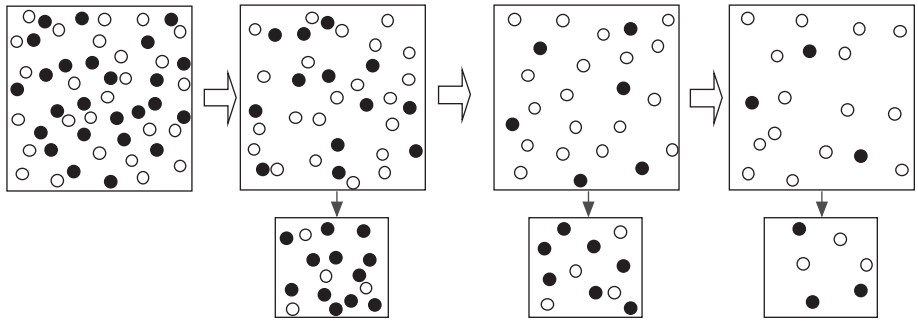

Figure 3.23 *Illustration of the Rayleigh process. A reservoir contains a tracer consisting of two isotopes (white and black). Initially, the white/black ratio in the reservoir is 1. Some tracer is progressively removed from the reservoir. At each step, the proportion of black is five times larger in the material extracted than in the residual material. The residual material is quickly depleted in black isotope and, as a result, the extracted material also becomes black-depleted.*

This causes stronger variations of R_A and R_B. Thus, for F, the remaining fraction of A, it is shown that (see Appendix 1)

$$R_A = R_A^0 F^{\alpha_{B-A}-1} \tag{3.15}$$

and that the increment of B formed at this time has an isotopic ratio

$$R_B = \alpha_{B-A} R_A^0 F^{\alpha_{B-A}-1}. \tag{3.16}$$

The cumulated quantity of B formed up to this point has an average isotopic ratio

$$R_B^{cumul} = R_A^0 \frac{1 - F^{\alpha_{B-A}}}{1 - F}. \tag{3.17}$$

This is the Rayleigh distillation. Extreme isotopic ratios are obtained when $F \to 0$ (Fig. 3.23). The difference between the equilibrium fractionation and Rayleigh process is therefore stronger when F is low (Fig. 3.24). Rayleigh distillation appears frequently in geochemistry ($\delta^{18}O$ of rain, $\delta^{15}N$ of nitrate in seawater, etc.).

3.13.1 Example: Nitrate Assimilation by Phytoplankton

In the euphotic layer, when a phytoplankton uses nitrate it preferentially assimilates ^{14}N relative to ^{15}N (Altabet and François, 1994). If the organic nitrogen is exported at depth as particulate matter (no remineralization) and there is no mixing between surface and deep waters (stratification), the euphotic layer is depleted in NO_3^- and the $\delta^{15}N_{NO_3^-}$ becomes higher and higher. This phenomenon is especially strong when NO_3^- becomes

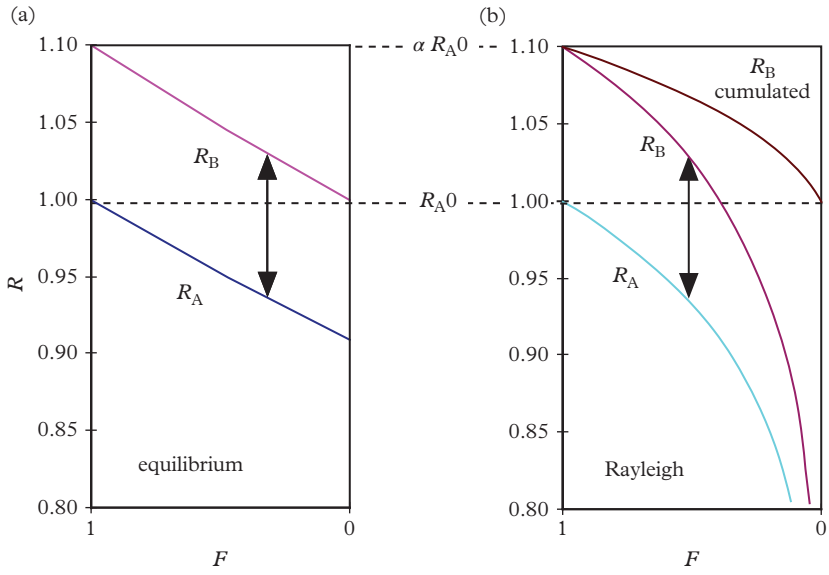

Figure 3.24 *Evolution of the isotopic ratio of products and reactants in the reaction $A \rightarrow B$ with the same fractionation coefficient $\alpha = 1.10$ (represented by the double arrow) under different conditions. (a) Reaction at equilibrium: R_A and R_B vary linearly with f. (b) Rayleigh processes: the evolution of ratios is faster and more important. The R_B cumulative curve represents the sum of all "b" increments already extracted from A.*

limiting. For small variations of the isotopic ratios, equation (3.15) is equivalent to (see Appendix 1)

$$\delta^{15}N_{NO_3^-} = \delta^{15}N^{initial}_{NO_3^-} + \Delta_{nitrate\text{–}phytoplankton}\{\ln([NO_3^-]) - \ln([NO_3^-]_{initial})\}. \qquad (3.18)$$

The analysis of nitrate concentration and $\delta^{15}N_{inorganic}$ in surface water reveals a linear relationship between $\ln([NO_3^-])$ and $\delta^{15}N_{NO_3^-}$ (Fig. 3.25).

The Rayleigh distillation model cannot always be applied due to water mass mixing (Problem 5) and the presence of microenvironments (Problem 9).

Appendix 1

Evolution of Isotopic Signatures during Fractionation Processes

Consider a transformation A→B associated with a fractionation factor $\alpha_{A\text{–}B}$ between a light major isotope "l" and a sparse heavy isotope "h." Initially, only A is present and it has an isotope ratio R_A^0 (the exponent 0 represents the initial state). We want to determine

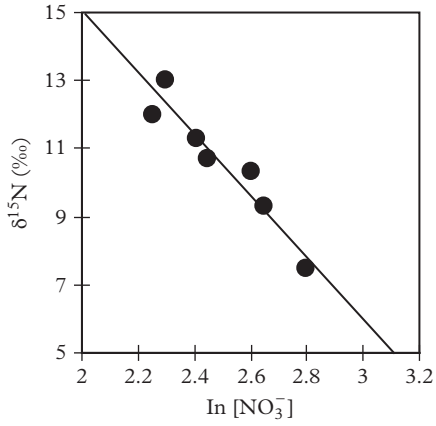

Figure 3.25 *Relationship between $\delta^{15}N$ and ln($[NO_3^-]$) in the subarctic Pacific. $[NO_3^-]$ is expressed in μmol kg^{-1}. The observed linear relationship is predicted by equation (3.18). The slope of the straight line gives a fractionation coefficient during nitrate assimilation by phytoplankton of $\Delta_{nitrate-phytoplankton}$ = 9.1 ‰. Modified from Altabet and François (1994).*

the final isotopic ratios $R_A = (h/l)_A$ and $R_B = (h/l)_B$ when the reaction is incomplete in the case where A and B are in isotopic equilibrium throughout the reaction and in the case where A and B are systematically separated (Raleigh distillation).

(1) There is an isotopic equilibrium between products and reactants. F is the fraction of A reactant that has not been transformed into B (remaining fraction of A). The product and the reactant remain in contact. In order to obtain simple formulas and to be consistent with the oceanographic literature, we introduce $\alpha_{B-A} = (\alpha_{A-B})^{-1} = \frac{R_B}{R_A} = \frac{1000+\delta_B}{1000+\delta_A} \approx 1 + \frac{\delta_B - \delta_A}{1000}$. The relationship between the R_A and R_B is

$$R_B = \alpha_{B-A}\, R_A. \tag{A1}$$

Equation (3.11b) is used (the initial reactant is equal to the mixture of the product formed and of the remaining reactant)

$$R_A^0 = FR_A + (1-F)R_B, \tag{A2}$$

or by using equation (A1):

$$R_A^0 = FR_A + (1-F)(\alpha_{B-A}R_A),$$

which leads to

$$R_A = \frac{R_A^0}{F + \alpha_{B-A}(1-F)}, \tag{A3a}$$

$$R_B = \frac{\alpha_{B-A}R_A^0}{F + \alpha_{B-A}(1-F)}. \tag{A3b}$$

(2) Many fractionation reactions (including biological reactions) are not at isotopic equilibrium due to a kinetic isotopic fractionation and/or continual separation of products and reactants.

In the case of a purely kinetic process, there is two parallel reactions, one affecting the light isotope "l" and the other the heavy isotope "h" with a different kinetic constants $k_l > k_h$. Therefore

$$\begin{cases} \dfrac{d[1]}{dt} = -k_1[1], \\ \dfrac{d[h]}{dt} = -k_h[L]. \end{cases} \tag{A4}$$

Taking the ratio of these two equations, we obtain

$$\frac{d[h]}{d[l]} = \frac{k_h}{k_l}\frac{[L]}{[l]}. \tag{A5}$$

Writing $k_h/k_l = \alpha_{B-A}$

$$\frac{d[h]}{d[l]} = \alpha_{B-A}\frac{[h]}{[l]}. \tag{A6}$$

Hence

$$\frac{[h]}{[h]_0} = \left(\frac{[l]}{[l]_0}\right)^{\alpha_{B-A}}, \tag{A7}$$

then

$$\frac{[h]}{[l]} = \left(\frac{[h]}{[l]}\right)_0 \left(\frac{[h]}{[l]}\right)^{\alpha_{B-A}-1}. \tag{A8}$$

Noting that $F = [l]/[l]_0$ is the remaining fraction of element which has not yet reacted (the light isotope is by far the most abundant) and that $R = [h]/[l]$, one finally obtains

$$R_A = R_A^0 F^{\alpha_{B-A}-1}. \tag{A9}$$

The increment of B formed when the remaining fraction is F has for its isotope ratio

$$R_B = \alpha_{B-A} R_A^0 F^{\alpha_{B-A}-1}. \tag{A10}$$

The cumulative quantity of B formed up to this point has an average isotopic ratio R_B^{cumul}.

Applying equation (3.11b), we obtain $R_A^0 \times (1) = R_A^0 F^{\alpha_{B-A}-1} \times F + R_B^{\text{cumul}} \times (1-F)$. It follows that

$$R_B^{cumul} = R_A^0 \frac{1 - F^{\alpha_{B-A}}}{1 - F}. \tag{A11}$$

Extreme isotopic ratios are obtained when $F \to 0$. Taking the logarithm of equation (A9), we obtain

$$\ln(R_A) = \ln\left(R_A^0\right) + (\alpha_{B-A} - 1)\ln(F) \tag{A12}$$

or

$$\ln\left((R_A/R_{ref})/(R_A^0/R_{ref})\right) = (\alpha_{B-A} - 1)\ln(F)\,. \tag{A13}$$

By introducing the δ notation (equation 3.1), we obtain

$$\ln\left((1 + \delta_A/1000)/(1 + \delta_A^0/1000)\right) = (\alpha_{B-A} - 1)\ln(F)\,. \tag{A14}$$

It follows that

$$\ln(1 + \delta_A/1000) - \ln\left(1 + \delta_A^0/1000\right) = (\alpha_{B-A} - 1)\ln(F)\,. \tag{A15}$$

As $\delta \ll 1000$

$$\delta_A - \delta_A^0 = 1000\,(\alpha_{B-A} - 1)\ln(F)\,. \tag{A16}$$

Introducing the Δ notation (equation 3.3), we obtain

$$\delta_A - \delta_A^0 = -\Delta_{A-B}\ln(F) = \Delta_{B-A}\ln(F)\,. \tag{A17}$$

PROBLEMS

Problem 1: Sea-ice formation (Jeffries et al., 1994)

The $\delta^{18}O$ of an ice core sampled on a floe in the Amundsen Sea is investigated to study ice growth processes. Over the first 5 m from the base of the core, ice has a $\delta^{18}O$ between 0 and +1‰. Above, the $\delta^{18}O$ decreases gradually over 2 m to reach a value of –15‰ at the top of the core. What does $\delta^{18}O$ tell you about floe formation?

Problem 2: The air of Paris (Widory and Javoy, 2003)

The CO_2 concentration and the $\delta^{13}C$ of air samples collected in 1998 in Paris and its suburb has been analyzed (Table 3.2).

Table 3.2 *Concentration and $\delta^{13}C$ of CO_2 in Paris*

	CO_2 (ppmv)	$\delta^{13}C$ (‰)
Place de la Concorde	508	– 12.7
Place de l'Étoile	517	– 13.5
Jardin des Plantes (botanical garden)	413	– 9.5
University of Jussieu (campus)	405	– 9.3
University of Jussieu (underground parking)	951	– 19.8
Essonne (non-urbanized area)	393	– 8.5

(1) Explain these variations of concentration and isotopic composition by specifying the $\delta^{13}C$ of the CO_2 sources involved (in 1998, the CO_2 concentration of oceanic air was 370 ppmv).

(2) At the end of a Geochemistry class at the University of Jussieu, the CO_2 concentration in the room is 4630 ppmv and its $\delta^{13}C$ is –24.5‰. What can you conclude?

Problem 3: The $\delta^{13}C$ of corals (Lindsley et al., 2000)

The average annual $\delta^{13}C$ of precisely dated coral from the Clipperton atoll in the Eastern Pacific has been determined. Between 1895 and 1950, the $\delta^{13}C$ value of coral remained in the range –2.5±0.25‰. After 1950, there was a decrease of $\delta^{13}C$ and a value of –3.25±0.25‰ was reached for the 1995–1997 period. Explain these results.

Problem 4: A "Prestigious" oil spill (Medina-Bellver et al., 2005)

During the oil spill of the "Prestige" tanker that affected the Spanish and French coast in 2002–2003, authorities and scientists wondered whether indigenous bacteria were able to degrade the heavy fuel sludge coating of the coast. To answer this question, the $\delta^{13}C$ of the dissolved inorganic carbon and the $\delta^{18}O$ of stagnant seawater collected between rocks contaminated by oil were analyzed (Table 3.3).

Table 3.3 *$\delta^{13}C$ and $\delta^{18}O$ of samples collected*

	$\delta^{13}C$ (‰)	$\delta^{18}O$ (‰)
Stagnant seawater in contaminated area	–6 to –8	0
Non-contaminated seawater	0	0
Oil from the Prestige	–30	not determined
Water fresh runoff to the ocean	–27	–10

Experience shows that when bacteria degrade organic matter (oil or continental vegetation), they produce dissolved inorganic carbon with the same $\delta^{13}C$ as the organic material.

(1) Explain the signature of the runoff water.

(2) According to you, do the indigenous bacteria degrade the oil? Justify your answer.

Problem 5: $\delta^{13}C$–PO_4^{3-} relationship in seawater (Broecker and Maier-Reimer, 1992)

We want to establish the relationship between the $\delta^{13}C$ and the phosphate concentration of seawater (see Fig. 3.11). We consider an initial seawater whose concentrations and isotopic compositions are DIC_i, $[PO_4^{3-}]_i$ and $\delta^{13}C_i$. The marine organic matter is characterized by an isotopic composition $\delta^{13}C_{org}$ and a C/P Redfield ratio.

(1) If biological activity adds or subtracts a quantity of carbon ΔDIC to average seawater, what should the $\delta^{13}C$ of this modified seawater be?

(2) Derive the relationship between the variations of $\delta^{13}C$ in seawater and $\Delta[PO_4^{3-}]$ (the change in $[PO_4^{3-}]$). Use the Redfield ratio of the organic matter and the isotopic fractionation between seawater and organic matter.

Problem 6: Origin of nitrogen in the subtropical Pacific (Karl et al., 1997)

The Subtropical North Pacific gyre surface water is characterized by a nitrate concentration close to zero and a very low abundance of phytoplankton. The thermocline waters that supply surface waters with nitrate during the winter convection have a $\delta^{15}N = +6‰$. Organic matter collected by sediment traps below the photic zone has a $\delta^{15}N$ which varies from +3.8‰ in winter to +1.5‰ in the summer. What can you infer about the origin of the nitrogen used to synthesize organic matter in this area? Estimate the fraction *f* provided by the fixation of atmospheric nitrogen (N_2)

Problem 7: Urban sewage in the deep ocean (Van Dover et al., 1992)

In the 1980s, wastewaters of New York City were detected in the Atlantic Ocean 185 km off the coast and 2000 m deep. Prior to release, it had been assumed that the currents would be sufficient to disperse sewage and avoid the accumulation on the seafloor of the organic matter that they carry. Four years later, sea urchins (which, naturally, feed on phyto-detritus) were collected upstream, in the vicinity and 70 km downstream of the discharge area and analyzed for S isotopes (Table 3.4).

Table 3.4 δ^{34} *S around the sewage disposal site*

Site	Sample	$\delta^{34}S$ (‰)
Upstream site	phyto-detritus	+17.4
Upstream site	sea urchin	+17.4
Area of releases	sea urchin	+12.2
Site downstream	sea urchin	+16
New York	wastewater	+3

(1) Estimate the fraction f of organic matter from wastewater in the sea urchin diet in upstream, downstream and on the sewage disposal site.

(2) Was it justified to stop this wastewater dumping in 1992?

(3) Was it reasonable to think that the current is high at 2000 m depth off the New York coast (*Hint:* see Chapter 10).

Problem 8: Iron fractionation during the bloom (Ellwood et al., 2015)

Dissolved and particulate Fe concentration and isotopes are measured before and during the bloom in the subtropical surface water off New Zealand.

	Pre-Bloom Period	**Bloom Period**
Primary production (μmol C L^{-1} d^{-1})	1	11
Dissolved Fe (nmol kg^{-1})	0.3	0.1
$\delta^{56}Fe_{dissolved}$ (‰)	–0.15	+0.15
Particulate Fe (nmol kg^{-1})	0.1	12
$\delta^{56}Fe_{particulate}$ (‰)	+0.15	–0.10
Fe/Al (mol mol^{-1})	0.1	2.5

(1) Compare the concentration and the δ^{56}Fe of the dissolved Fe before and during the bloom and explain their evolution.

(2) Compare the concentration, the Fe/Al ratio and the δ^{56}Fe of the particulate Fe before and during the bloom. What is the origin of the particulate Fe? *Hint:* learn about the Fe/Al ratio in section 9.1 of Chapter 9.

Problem 9: Isotopic fractionation in microenvironments (Bender, 1990)

Many biological reactions occur in microenvironments (organic aggregates in decomposition, fecal pellets, stomachs of zooplankton), which has a strong influence on the evolution of the isotopic composition of the tracers. Consider the case of oxygen. A liter of seawater contains initially 300 μmol kg^{-1} of O_2 with $\delta^{18}O = 0‰$. When the oxygen is used by bacteria (respiration), the isotopic fractionation coefficient is $\alpha_{O_2-CO_2} = 0.981$.

(1) Assuming that 50% of the dissolved oxygen is consumed by bacteria, calculate the δ^{18}O of the remaining oxygen if oxygen is gradually consumed by the bacteria living freely in seawater.

(2) Same question assuming that oxygen is consumed by bacteria in microenvironments isolated from the surrounding seawater. In these microenvironments, the O_2 consumption is complete.

(3) A seawater sample has lost 50% of its O_2 relative to saturation with the atmosphere and it has a δ^{18}O of +6‰. What can you conclude?

4

Radioactive and Radiogenic Isotopes

The main contribution of radioactivity to oceanography is to provide chronometers to time phenomena that are otherwise difficult to quantify and which will be developed in the following chapters (thermohaline circulation, particle flux). It also produces distinct isotopic ratios which provide traceability to seawater and marine particles.

4.1 Radioactivity

We have seen in Chapter 3 that a chemical element can have different isotopes with a given number of protons but different numbers of neutrons. The neutron number cannot be any number. Indeed, some isotopes are stable, whereas other isotopes which have an excess or a deficit of neutrons are unstable. For light elements (up to ^{56}Fe), stable nuclei have a neutron/proton ratio close to 1, while for heavier elements, this ratio tends toward 1.5. Beyond bismuth ($Z = 83$), there are no more elements with strictly stable isotopes.

An unstable isotope is called a **radioactive isotope** because it decays spontaneously by producing a new isotope and emitting various rays (α, β, γ). It is frequently referred to a **parent isotope** that decays into a **daughter isotope** or **radiogenic isotope**. The daughter isotope has a different chemical nature (different Z) to the parent isotope. When the daughter isotope is not radioactive itself, things stop. If it is radioactive, it decays and the decay chain continues until a stable nucleus is formed.

There are different forms of radioactivity:

* The α disintegration: an atom containing an excess of neutrons and protons decays to give an atom where two protons and two neutrons have been ejected as a helium-4 nucleus (called, in this case, an α particle).

$$\text{Example:} \quad {}^{238}_{92}\text{U} \rightarrow {}^{234}_{90}\text{Th} + {}^{4}_{2}\text{He}$$

* The β^- decay: an atom containing an excess of neutrons decays producing another atom in which one neutron has been converted to one proton. This decay produces the emission of an electron (e^-, also known as a β^- particle) and an antineutrino ($\bar{\nu}$).

Marine Geochemistry. First Edition. Matthieu Roy-Barman and Catherine Jeandel.

Examples: $^{3}_{1}\mathrm{H} \rightarrow {}^{3}_{2}\mathrm{He} + \mathrm{e}^{-} + \bar{\nu}$

$$^{14}_{6}\mathrm{C} \rightarrow {}^{14}_{7}\mathrm{N} + \mathrm{e}^{-} + \bar{\nu}$$

* β^{+} decay: an atom containing a deficit of neutrons decays by giving an atom in which a proton has been converted to a neutron. This decay occurs with the emission of a positron (e^{+}, also known as a β^{+} particle) and a neutrino (ν).

Example: $^{26}_{13}\mathrm{Al} \rightarrow {}^{26}_{12}\mathrm{Mg} + \mathrm{e}^{+} + \nu$

In these three forms of radioactivity, the new nucleuses are excited. They lose their excess energy by emitting very high energy photons: γ particles (or γ rays).

4.2 The Radioactive Decay Law and its Applications

4.2.1 The Radioactive Decay Law

Radioactivity concerns only the nucleus of the atom. The radioactive decay is independent of the electronic cloud and, therefore, of the environment of the atom. It does not depend on the chemical state of the atom, or on the temperature and pressure conditions. It is an absolute clock. A radioactive atom has a probability "$\lambda \mathrm{d}t$" of disintegrating during a time interval $\mathrm{d}t$. λ is called the decay constant of the isotope. Its dimension is the inverse of a time. λ is independent of the environment in which the atoms are and it does not vary with time (one says that the radioactive atoms do not "age" because they always keep the same probability of disintegration until ... their disintegration). Radioactive atoms decay independently of each other. Consider N identical radioactive atoms at time $t = 0$. The number of disintegrations during a time interval $\mathrm{d}t$ is $dN = -N\lambda \mathrm{d}t$. Therefore, the decay rate of N nuclides is

$$\frac{\mathrm{d}N}{\mathrm{d}t} = -\lambda N. \tag{4.1}$$

This is the well-known law of radioactive decay.

Application exercise: the radium decay rate

Determine the number of disintegrations per second produced by one gram of ^{226}Ra. The decay of ^{226}Ra constant is $\lambda = 1.37 \times 10^{-11}\ \mathrm{s}^{-1}$.

Solution:

$$1\mathrm{g\ of\ }^{226}\mathrm{Ra\ is\ equivalent\ to\ } \frac{1\mathrm{g}}{226\ \mathrm{g/mol}} = 0.00442\ \mathrm{mol\ of\ }^{226}\mathrm{Ra}.$$

One mole consists of $\mathcal{N} = 6.02 \times 10^{23}$ atoms (Avogadro number), 1 g of ^{226}Ra consists of $0.00442 \times 6.02 \times 10^{23} = 2.66 \times 10^{21}$ atoms.

The number of disintegrations produced by 1 g of ^{226}Ra is, therefore, $\lambda N = 2.66 \times 10^{21} \times 1.37 \times 10^{-11} = 3.7 \times 10^{10}$ disintegrations per second.

4.2.2 Disintegration without Simultaneous Production

If the system does not exchange matter with the outside world (it is called a **closed system**) and if the radioactive isotope is not produced in the system, the solution of equation (4.1) is (see demonstration in Appendix 1)

$$N_t = N_0 e^{-\lambda t}. \tag{4.2}$$

The abundance the radioactive isotope (N_t) decreases exponentially with time (Fig. 4.1). The **half-life** or period of the isotope (denoted $T_{1/2}$) can be deduced from equation (4.2). It is the time required for half of the original radioactive atoms decay.

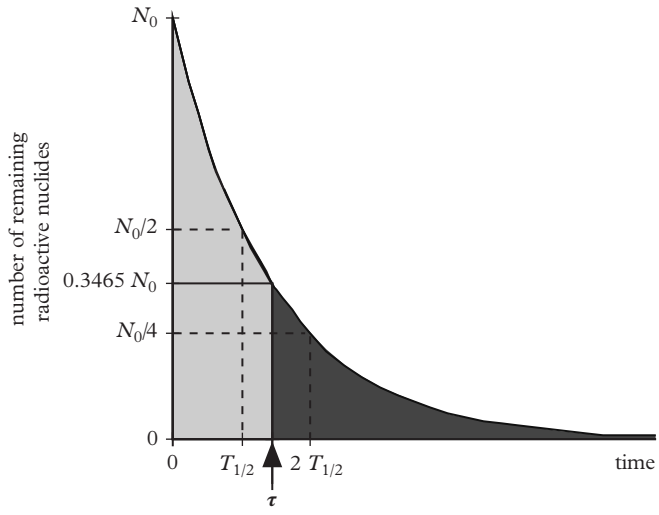

Figure 4.1 *Temporal evolution of the abundance of a radioactive isotope in the case of a closed system without simultaneous production: 50% of atoms disintegrate during the first half-life ($T_{1/2}$) so that after two half-lives, only 25% of the initial atoms remain. The vertical segment of x-axis at $t = \tau$ divides the area under the curve in two equal surfaces: τ is the average lifetime of the isotope.*

Setting $N/N_0 = ½$ at $t = T_{1/2}$, in equation (4.2), we obtain $\frac{N_0}{2} = N_0 e^{-\lambda T_{1/2}}$ and we rearrange to obtain the classic formula (see Appendix 1)

$$T_{1/2} = \frac{\ln 2}{\lambda}. \tag{4.3}$$

The **average life-time** τ of the isotope is defined as

$$\tau = \frac{1}{N_0} \int_{t=0}^{+\infty} t dN_t = \frac{1}{\lambda}. \tag{4.4}$$

Radioactive isotopes with half-lives comparable to or greater than the age of the Earth (4.55 billion y) are called **long-lived isotopes**. Radioactive isotopes with half-lives much smaller than the age of the Earth and called **short-lived isotopes**.

The most popular application of equation (4.2) is without doubt the dating of the charcoal, the paintings and the bones of prehistoric men with carbon-14 (^{14}C). Plants assimilate atmospheric ^{14}C through photosynthesis and then pass it to animals that eat them. After death, there is no more ^{14}C uptake by the remains of plants and animals. ^{14}C atoms disintegrate: the chronometer is running. As ^{12}C does not disintegrate, its concentration remains constant over time. By dividing the two parts of equation (4.2) by the ^{12}C concentration, we obtain

$$(^{14}C/^{12}C)_t = (^{14}C/^{12}C)_0 \times e^{-\lambda t}.$$

^{14}C and ^{12}C are incorporated by living beings in a ratio very close to the atmospheric ^{14}C /^{12}C ratio. As a gross approximation, $(^{14}C/^{12}C)_0$ is obtained by assuming that the $^{14}C/^{12}C$ ratio of the atmosphere has remained constant over time (*we will see later than this is not strictly true*). Dividing by ^{12}C, we do not have to know the absolute amount of ^{14}C in the sample. It should be noted that after seven half-lives, only 1/128th of the initial stock of ^{14}C remains, which sets a limit to the chronometer. Despite advances of particle accelerator analysis, ^{14}C ($T_{1/2} = 5730$ y) does not allow us to correctly date samples older than 50,000 y. For example, the several million years old first hominids are out of reach of ^{14}C.

Application exercise: disintegration of ^{233}Pa

A geochemist prepares a solution of ^{233}Pa (artificial isotope of protactinium) that he will use during his next oceanographic cruise. Knowing that the cruise will begin in 60 days and that then he will need 10^{-12} g of ^{233}Pa, how much ^{233}Pa must he prepare? The half-life of ^{233}Pa is 27 days.

Solution:

The ^{233}Pa decay constant is $\lambda = \frac{\ln 2}{T_{1/2}} = 0.026\ d^{-1}$.

In 60 days, the concentration in ^{233}Pa will therefore be reduced by a factor $e^{0.026\times60} = 4.76$.

Therefore, he must prepare 4.76×10^{-12} g of ^{233}Pa.

Problems 1 and 2 offer other applications.

4.2.3 Disintegration with Simultaneous Production

If the radioactive isotope is produced in the system (e.g., by the decay of a parent isotope), the evolution equation of N_t becomes

$$\frac{dN_t}{dt} = -\lambda N_t + \Gamma_t, \tag{4.5}$$

where Γ_t represents the decay rate of the radioactive isotope. The solution of this equation for a closed system is (see Appendix 1)

$$N_t = N_0 e^{-\lambda t} + \int_0^t e^{-\lambda(t-t')} \times \Gamma_{t'} dt'. \tag{4.6}$$

When Γ_t is constant with time (e.g., production of ^{234}Th and ^{230}Th by ^{238}U and ^{234}U, natural production of ^{14}C by the cosmic rays, etc.), we get

$$N_t = N_0 e^{-\lambda t} + \frac{\Gamma}{\lambda}\left(1 - e^{-\lambda t}\right). \tag{4.7}$$

The evolution of N over time is not necessarily an exponential decay any longer (Fig. 4.2). If $\lambda \times t \gg 1$, then $e^{-\lambda t}$ tends toward 0 and the quantity of radioactive isotopes becomes constant (asymptote on Fig. 4.2)

$$N_t = \frac{\Gamma}{\lambda}. \tag{4.8}$$

In this case, the system is at steady state or at **secular equilibrium**.

There is a radioactive "**disequilibrium**" when there is a difference between the number of radioactive atoms in the sample and the number expected at steady state (secular equilibrium). A positive disequilibrium is called an "**excess**" while a negative disequilibrium is called a "**deficiency**" (or is treated as a negative excess)

$$N_{t,\mathrm{xs}} = N_t - \frac{\Gamma}{\lambda} = \left(N_0 - \frac{\Gamma}{\lambda}\right) e^{-\lambda t}. \tag{4.9}$$

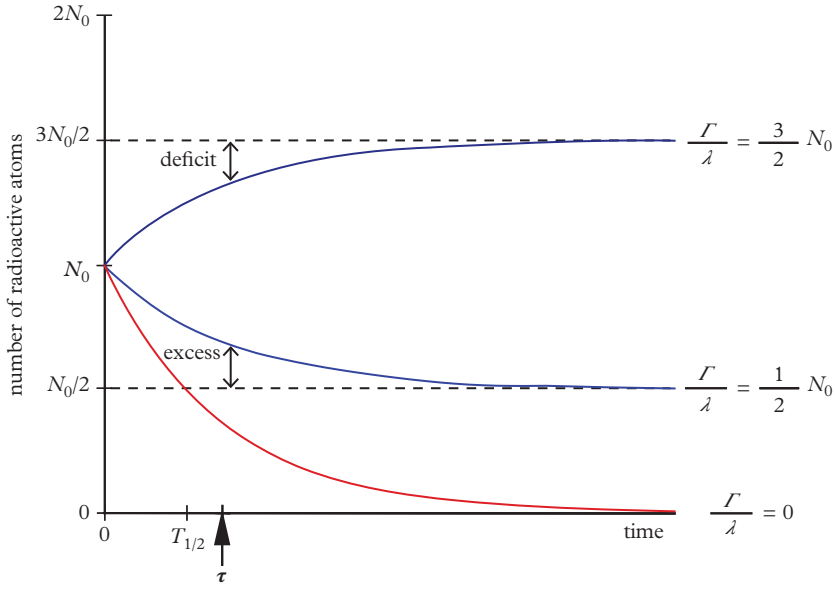

Figure 4.2 *Evolution over time of the abundance of a radioactive isotope with a constant production* Γ. *Cases of* $\Gamma/\lambda = 0$ *(no production),* $\Gamma/\lambda = N_0/2$ *and* $\Gamma/\lambda = 3N_0/2$ *are represented. When* $\Gamma \neq 0$, *the curves do not follow an exponential decay. However, the excess or the deficit relative to secular equilibrium decreases exponentially. The excess or the deficit is reduced by 50% during one half-life (*$T_{1/2}$*).*

In natural environments, the disequilibria are due to differences in chemical properties of the parent and the daughter isotopes.

4.2.4 Definition of the Activity

The law of radioactive decay ($dN/dt = -\lambda \times N$) indicates that the number of disintegrations per unit of time (dN/dt) in a sample (N) is proportional to the number of radioactive atoms in this sample. The "**activity**" is the number of disintegrations per unit time produced by a sample. The activity is expressed in Becquerel (1 Bq = 1 disintegration per second in the International System). Traditionally, the concentration of many isotopes is expressed as an activity per unit of mass or volume because the abundance of these isotopes is estimated by counting the radioactive decay that they produce, that is, their activity. In view of the generally low activities in seawater, the practical units are disintegration per minute and per liter (dpm L^{-1}) or disintegration per minute and per m^3 (dpm m^{-3}). Here and throughout the book, curly brackets are used to denote an activity or activity ratio rather than an atom ratio.

Consider the decay chain $^{238}U \rightarrow {}^{234}Th \rightarrow \ldots$. The activities of ^{238}U and ^{234}Th are $\{^{238}U\} = \lambda_{238}{}^{238}U$ and $\{^{234}Th\} = \lambda_{234}{}^{234}Th$. The ^{234}Th activity in excess is $\{^{234}Th_{xs}\} = \{^{234}Th\} - \{^{238}U\}$. This is the ^{234}Th activity corrected by the ^{238}U activity (the ^{238}U activity is activity of ^{234}Th at secular equilibrium with ^{238}U). ^{238}U is constant on the time scales relevant for the ocean (the half-life of ^{238}U is 4.5 billion y). Hence, we can use equation (4.9) to show that in a closed system, the activity in excess decays exponentially

$$\{^{234}Th_{xs,t}\} = \{^{234}Th_t\} - \{^{238}U\} = \{^{234}Th_{xs,0}\}e^{-\lambda t}. \tag{4.10}$$

Activities allow an easy comparison of the abundance of the nuclides of radioactive decay chains. At secular equilibrium, the activity of the parent and daughter isotopes are identical (although their concentrations can differ by several orders of magnitude) and the activity in excess is zero.

Application exercise: calculation of activity and disequilibrium

A seawater sample has been analyzed. Complete Table 4.1:

Table 4.1 *Radioactive decay chains in seawater*

	Unit	^{238}U	^{234}Th	^{234}U	^{230}Th
Half-life		4.47×10^9 y	24.1 d	248×10^5 y	7.57×10^4 y
Concentration	g L^{-1}	3.3×10^{-6}			
Total activity	dpm L^{-1}				2×10^{-4}
Activity in excess	dpm L^{-1}		–0.3		
Activity ratio	dpm X (dpm $^{238}U)^{-1}$			1.14	

In oceanography, a system is rarely completely closed. The general case is rather the open system. Then, the incoming and outgoing fluxes of material must be taken into account (see Chapters 5 and 6 and the following discussion). Nevertheless, equations (4.2) and (4.10) can be applied to sediment dating and to the determination of sedimentation rates (see Chapters 6 and 9).

Atoms forming the Earth were produced more than 4.55 billion y ago (the age of the Earth), during the Big Bang or later in now dead stars. During the nucleosynthesis, stable and unstable isotopes are formed. Today, only stable and long-lived radioactive isotopes remain on Earth. There are also short-lived isotopes on Earth: some are produced continuously by natural processes (radioactive decay chains, interaction between cosmic rays and the atmosphere). Others have been produced by human activities since 1954: these are artificial radioisotopes.

4.3 The Long-Lived Radioactive Decay Systems

The long-lived radioactive decay systems have considerable importance in understanding the evolution of the Earth on a geological timescale. Their comprehensive study is beyond the scope of this book (see Allègre, 2008 for an in-depth presentation). Here, we present the evolution of these isotopic systems very succinctly and by focusing on their use in oceanography.

We consider a radioactive parent isotope (P) with a radioactive decay constant λ. It decays and produces a daughter isotope (D) which is not radioactive itself. The daughter isotope is called radiogenic. This daughter isotope has a different chemical nature to the parent isotope. Finally, we also consider as a reference a stable isotope (S) that has the same chemical nature as the daughter isotope (same atomic number Z) but which is neither radioactive nor radiogenic. A given sample contains initially P_0 atoms of parent isotope, D_0 atoms of daughter isotope and S_0 atoms of stable isotope. We assume that the quantities of the different isotopes evolve in a closed system (i.e., that there is no input or loss of material with the external environment). In this case, changes in the number of parent (P) and daughter (D) atoms are only due to the radioactive decay of the parent. The evolution of the quantity of parent isotope in the sample is determined by equation (4.2). Noting that $D_t = D_0 + (P_0 - P_t)$ and that the amount of stable reference isotope remains constant, we obtain the evolution of the D/S ratio of the sample over time

$$\left(\frac{D}{S}\right)_t = \left(\frac{D}{S}\right)_0 + \left(\frac{P}{S}\right)_t \left(e^{\lambda t} - 1\right). \tag{4.11}$$

The D/S ratio of a sample depends on the P/S ratio, on the time elapsed since the sample formation and on the initial D/S ratio. Considering the low value of λ for long lived isotopes, the D/S ratio variations are small and they build up over very long periods ($> 10^8$ y). Therefore, to understand the functioning of the long-lived isotopic systems, we must say a few words on Earth's evolution. After having been formed 4.55 billion y ago by accretion of interstellar material, the Earth has undergone various phases of differentiation: formation of the core and of the primitive atmosphere very early in its history, and then more gradually, the partial melting of the mantle has led to the formation of light crustal material floating on the mantle and of residual material accumulating in the mantle. During these episodes, the P/S ratios of the different isotopic pairs were modified according to the chemical properties of the elements: the Rb/Sr ratio in the continental crust is higher than in the Earth's mantle, while the Nd/Sm of the crust is lower than in the mantle (Fig. 4.3). After the differentiation, the $^{87}Sr/^{86}Sr$ and $^{143}Nd/^{144}Nd$ ratios evolved differently in the mantle and in crust: the slow disintegrations of ^{87}Rb and ^{147}Sm (parents) induce an enrichment of the continental crust in daughter isotope ^{87}Sr, while the mantle is enriched in ^{143}Nd: Sr or Nd enriched in their radiogenic isotopes are said to be radiogenic themselves.

In marine geochemistry and the study of surface processes (erosion, transport, diagenesis, etc.), the timescales are much shorter ($< 10^7$ y) than the half-life of the parent isotopes. Accordingly, we follow the fate of materials injected into the ocean with the

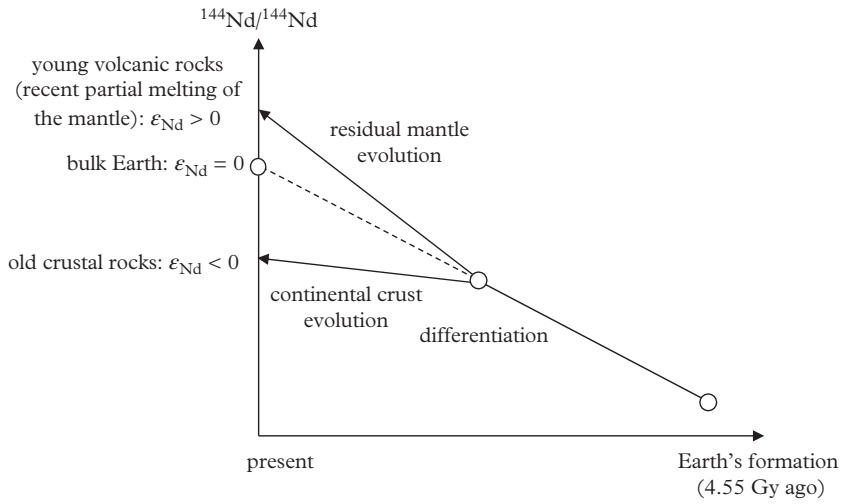

Figure 4.3 *Evolution over geological time of the Nd isotopic composition in the crust and the Earth's mantle.*

characteristic isotopic ratios of their sources (rivers, dust, hydrothermal inputs, etc.): the isotopic ratios are used as tracers with different sources and chemical behaviors (Table 4.2, Fig. 4.4).

4.3.1 Strontium

Strontium is soluble in seawater. It has a conservative behavior and its residence time is 2.7×10^6 y. Marine Sr has two main sources:

- Radiogenic Sr produced by continental erosion results from a mixing between very radiogenic Sr from silicate rocks and the less radiogenic Sr from marine limestones.
- When seawater circulates through newly formed oceanic crust, it heats up, leading to the dissolution of silicate minerals and the formation of authigenic minerals and of hydrothermal fluids. As a result, there is an isotopic exchange between seawater and the oceanic crust (Fig. 4.5). The hydrothermal fluids have an $^{87}Sr/^{86}Sr$ ratio (= 0.703) close to that of the unaltered oceanic crust ($^{87}Sr/^{86}Sr$ = 0.702).

Marine Sr has an intermediate isotopic signature ($^{87}Sr/^{86}Sr = 0.709236$) between the continental crust ($^{87}Sr/^{86}Sr = 0.7100–0.7400$) and the oceanic crust. Offshore and far from hydrothermal sources, this signature is extremely constant because the Sr residence time is very long (see Problem 3).

Despite the soluble nature of Sr, a small fraction of seawater Sr is found in particles because (1) Sr substitutes for Ca in $CaCO_3$ tests synthesized by marine organisms, (2)

Table 4.2 *The main characteristics of the long-lived isotopic systems*

Tracer	Strontium	Neodymium	Lead	Lead	Helium
Parent isotope	^{87}Rb	^{147}Sm	^{238}U	^{235}U	^{235}U, ^{238}U, ^{232}Th
Half-life (10^9 y)	45	109	4.47	0.704	4.75, 0.704, 14
Daughter isotope	^{87}Sr	^{143}Nd	^{206}Pb	^{207}Pb	^{4}He
Reference isotope	^{86}Sr	^{144}Nd	^{204}Pb	^{204}Pb	^{3}He
Notation	$^{87}Sr/^{86}Sr$	ε_{Nd} (see text)	$^{206}Pb/^{207}Pb$		$\delta^{3}He$
Signature of sources					
Average continental crust	0.7100–0.7400	–9 to –15	1.10–1.21		0.01
Old continental crust	0.7100–0.8000	–40			
Mantle	0.7024–0.706	+6 to +12			8–30
Meteorites					200
Atmosphere					1
Range for seawater	0.70925–0.70926	–17 to +4	1.145 to 1.205		
Chemical behavior	soluble	insoluble	insoluble		volatile
τ_{ocean} (y)	2.7×10^6	500	100		1000

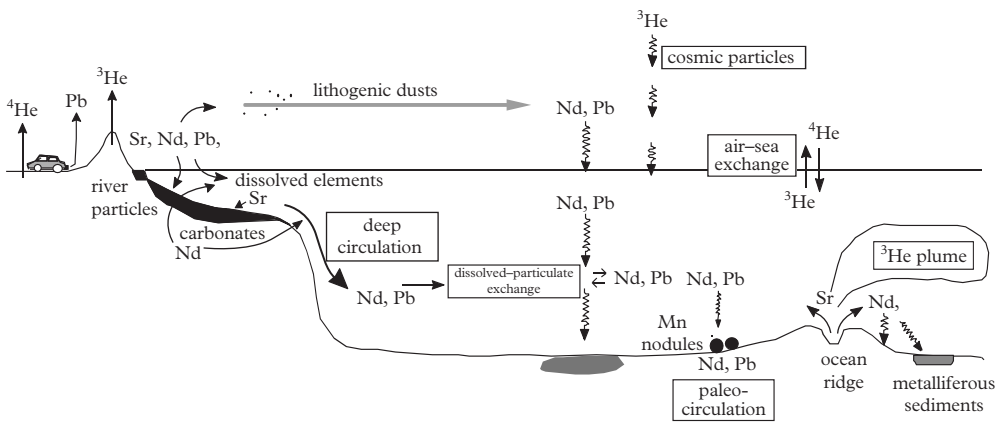

Figure 4.4 *Fluxes and processes studied with radiogenic isotopes of long-lived systems. Fine and straight arrows: transport as dissolved or gas form. Zigzag arrows: particulate transport. Gray arrow: transport by wind.*

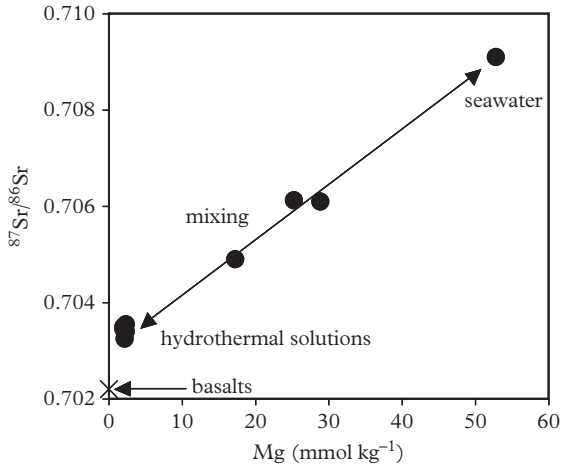

Figure 4.5 *Variation of the $^{87}Sr/^{86}Sr$ ratio during seawater/hydrothermal fluid mixing. The hydrothermal fluids being very Mg depleted compared to seawater, Mg is used as an index to estimate the ratio between seawater and hydrothermal solution. The $^{87}Sr/^{86}Sr$ ratio of hydrothermal solutions is strongly influenced by the circulation of fluids in contact with the oceanic crust. Modified from Piepgras and Wasserburg (1985).*

acantharians are unicellular animals with $SrSO_4$ tests and (3) particles of continental origin contain lithogenic Sr.

4.3.2 Neodymium

Neodymium is a rare earth element (REE or lanthanide family). It is a relatively insoluble element and therefore it tends to be absorbed on marine particles. Its concentration profile is depleted at the sea surface and enriched at depth (Fig. 4.6) which led to it being described sometimes as "bio-intermediate," although it does not enter in the biological cycle. Adsorbed on Fe–Mn oxides and hydroxides of iron, it tends to be removed from the ocean by adsorption on marine particles. This chemical reactivity gives a relatively short residence time (500–1000 y, Tachikawa et al., 1999). The variations of the $^{143}Nd/^{144}Nd$ ratio being very small, it is expressed as ε_{Nd}

$$\varepsilon_{Nd} = \left\{ \frac{\left(^{143}Nd/^{144}Nd\right)_{sample}}{\left(^{143}Nd/^{144}Nd\right)_{CHUR}} - 1 \right\} \times 10^4$$

where the "CHUR" (CHondritic Uniform Reservoir) represents the average isotopic composition of the Earth.

The flux of dissolved Nd transported by rivers is low. The main contribution of dissolved Nd into the ocean is the dissolution of a small fraction of particulate Nd transported by rivers and wind. The isotopic composition of Nd in a water mass depends on the geological history of the areas from which Nd comes from:

– Old cratons of the northern margin of the Atlantic (Canada, Greenland) are extremely non-radiogenic (very poor in ^{143}Nd) with negative ε_{Nd} (ε_{Nd} down to –50);

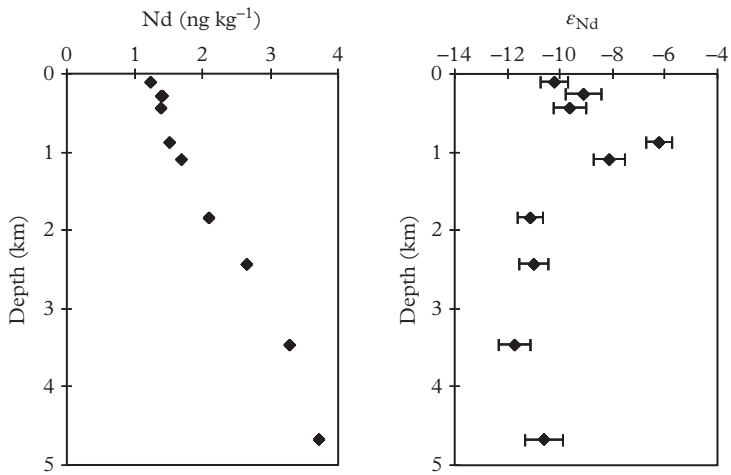

Figure 4.6 *Nd concentration and ε_{Nd} profiles in the South Atlantic. The less negative ε_{Nd} at 900 m marks a water of Pacific origin and suggests the presence of a return current of the thermohaline circulation by the "cold route" (see Chapter 11). Modified from Jeandel (1993).*

- The average continental crust is negative (ε_{Nd} is of the order of –10);
- Young volcanic rocks of the circum-Pacific Ring of Fire are radiogenic ($\varepsilon_{Nd} > 0$ and up to +8).

This distribution of geological provinces around the ocean leads to a progressive evolution of ε_{Nd} in seawater from the Atlantic Ocean to the Pacific Ocean in response to dissolved/particle isotopic exchanges, which are particularly marked at ocean margins (see Chapter 9). Variations of ε_{Nd} in water masses are explained by the ocean circulation (Fig. 4.7). Water sources of the North Atlantic deep and intermediate waters (Labrador Sea and Baffin Bay, Greenland Sea, Norwegian Sea) acquire very negative ε_{Nd} at the contact of very old continental masses. Flowing southward, the Atlantic waters receive Nd from the erosion of younger continents (Saharan inputs, Mississippi, Amazon, etc.), which leads to an increase of their ε_{Nd}. This trend is accentuated by mixing of the North Atlantic Deep Water with water containing Nd from the Pacific (Antarctic Bottom Water and Antarctic Intermediate Water). In the Pacific, ε_{Nd} values ranging between –10 and 0 reveal the influence of Nd inputs from young volcanic rocks of the Ring of Fire. The Indian Ocean is intermediate between the Atlantic and the Pacific. Offshore, the isotopic signature of the water masses evolve by mixing and it is used as a tracer of water mass trajectories (Figs. 4.6 and 4.7).

In seawater, around 1–5% of the Nd is carried by particles. Particles of continental origin and their Nd sink rapidly to the bottom of the ocean. Dissolved Nd is eliminated from seawater by uptake on marine particles that fall in the water column. Hence, there is a significant fraction of authigenic Nd on marine particles. ε_{Nd} in marine particles depends

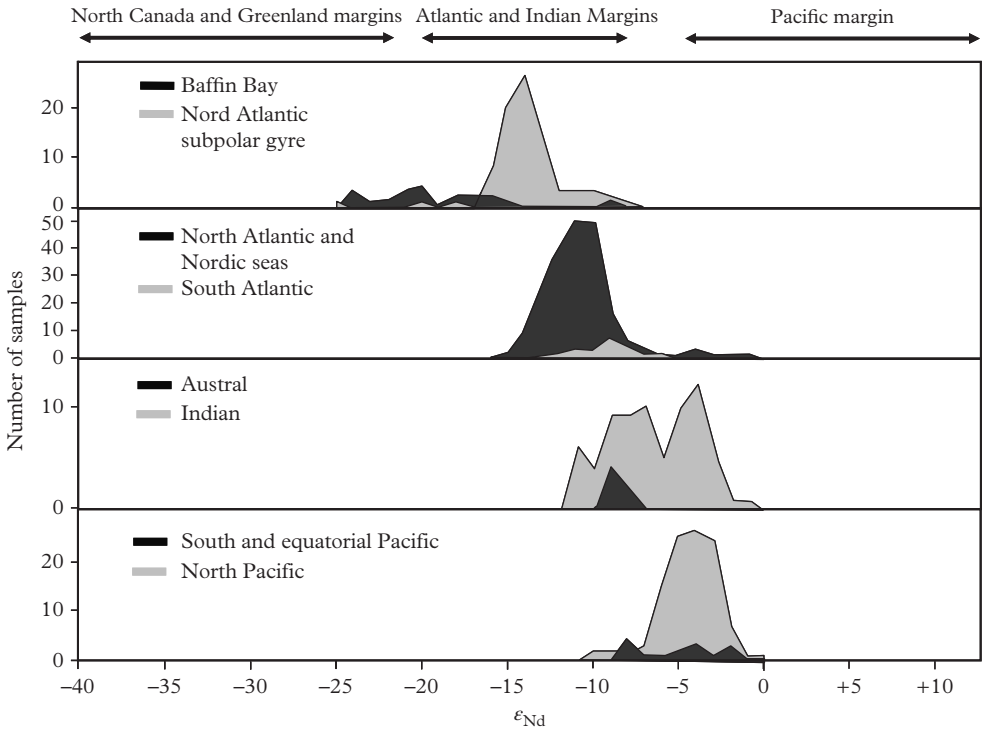

Figure 4.7 ε_{Nd} *values of ocean margins and seawater in different ocean basins. Modified from Jeandel et al. (2007) and Lacan and Jeandel (2005).*

on the ε_{Nd} of lithogenic particles brought to the ocean and of the ε_{Nd} of the authigenic Nd. As a result, authigenic and lithogenic Nd can be differentiated by their isotopic signatures. The Nd isotopic signature is an example of a tracer with multiple applications: water mass circulation tracer across ocean basins and tracer of seawater/particle interactions along the water column (see Problem 4). We will see that this is also the case for ^{230}Th, ^{231}Pa and many others. This underlines that the use of these tracers requires a thorough understanding of their biogeochemical cycles.

4.3.3 Lead

Lead is a rather insoluble heavy metal. As for Sr and Nd, it is naturally brought to the ocean by rivers and atmospheric dusts. However, Pb has had, since ancient times, a considerable importance in human activities, so that natural sources are often dominated by anthropogenic sources. Indeed, one of the main problems in Pb isotope studies in the environment is to avoid contamination by anthropogenic Pb during sampling and analytical work. The main source of anthropogenic Pb to the atmosphere (and thus the

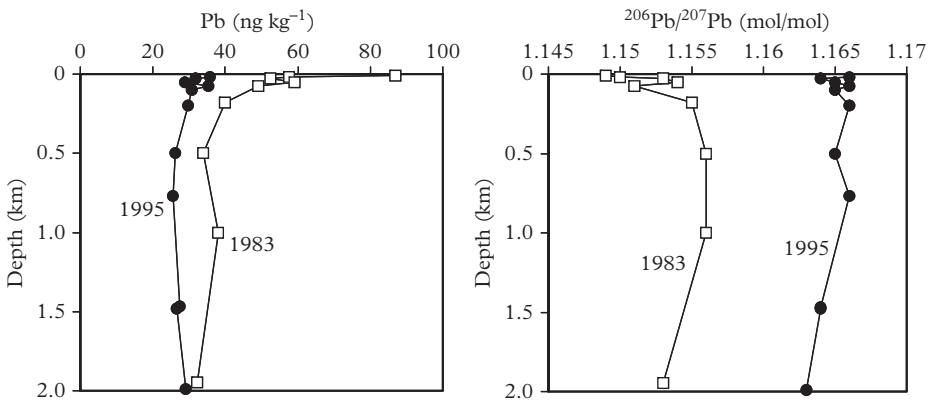

Figure 4.8 *Evolution of the concentration and isotopic composition of Pb in the Ligurian Sea between 1983 and 1995. The decline of concentration between 1983 and 1995 follows the progressive phasing out of lead emission by automobiles. The change in isotopic composition shows that while Pb was significantly influenced by leaded gasoline ($^{206}Pb/^{207}Pb \approx 1.08$ in France in the 1980s) in 1983, it was replaced in 1995 by lead of industrial origin ($^{206}Pb/^{206}Pb = 1.165–1.170$). Adapted from Alleman (1997).*

most likely to reach the open ocean) has long been leaded gasoline in which Pb was used an anti-knocking agent for combustion engines. By the end of the twentieth century, US and European laws made catalytic converters mandatory to reduce urban pollution. As these converters require the use of unleaded gasoline, it triggered the phasing out of leaded gasoline. Without being fully stopped, anthropogenic Pb emissions are therefore in sharp decline.

Pb has one stable and non-radiogenic isotope, ^{204}Pb (minor isotope), and also three radiogenic and stable isotopes: ^{206}Pb, ^{207}Pb and ^{208}Pb which are derived from the disintegration of ^{238}U, ^{235}U and ^{232}Th, respectively (see Section 4.4). Different Pb sources have distinct isotopic signatures (Fig. 4.8). As industrialized countries use lead extracted from ores with different isotopic compositions (according to their age and history), the Pb isotopic signature is used as a fingerprint to trace the origin of particles in air or water mass transport in the atmosphere and the ocean. For example, the Pb isotopic composition shows that anthropogenic Pb emitted on the east coast of the US crosses the Atlantic with the Gulf Stream and is removed from seawater by binding on marine particles at the level of the Mauritanian upwelling (Hamelin et al., 1997).

4.3.4 Helium

Helium is a noble gas. It is volatile and chemically inert. With its low mass, it is not retained by the Earth's gravity field and it escapes the Earth's atmosphere. Helium has two isotopes (^{3}He and ^{4}He) with different origins. "Primordial" ^{3}He has been trapped in the Earth's mantle since the Earth's formation and it outgases in the ocean and atmosphere

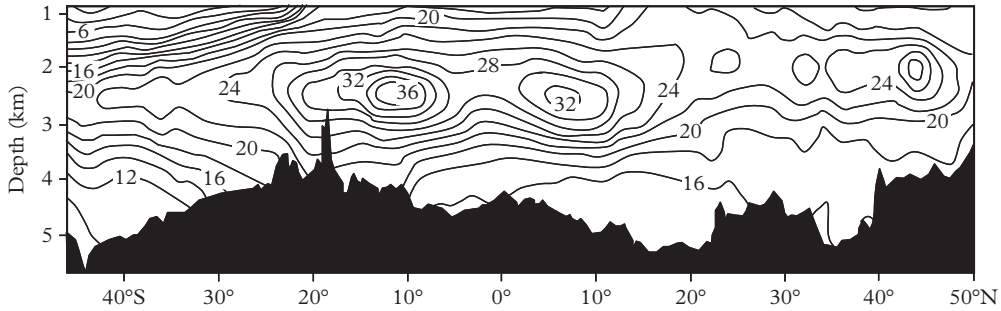

Figure 4.9 *δ^3He (%) on a North–South Pacific section (along 135° W). The ^{3}He plume emitted by the East Pacific rise is transported northward by currents. Modified from Siedler et al. (2001).*

during volcanic eruptions. ^{3}He is also brought to marine sediments by interplanetary dust (or IDP) that falls on the ocean surface and settles to the seafloor. These fine (< 10 μm) dusts are the result of the collisions between asteroids. They are enriched in ^{3}He implanted at their surface by solar winds until they fall on the Earth. Finally, we will see at the end of the chapter that ^{3}He is also produced by decay of anthropogenic tritium. ^{4}He is produced during the U and Th disequilibrium series as α particles (see Section 4.4). It is mainly produced in the Earth's crust, which is enriched in U and Th compared to the mantle. Geochemists express the (^{3}He/^{4}He) ratio of a sample normalized to the atmospheric ratio (R_a) or use the relative variation normalized to the atmospheric ratio (caution, here δ is expressed in % not in ‰ as for a stable isotope)

$$\delta^3\mathrm{He} = \left(\frac{\left(^3\mathrm{He}/^4\mathrm{He}\right)_{\mathrm{sample}}}{\left(^3\mathrm{He}/^4\mathrm{He}\right)_{\mathrm{atmosphere}}} - 1 \right) \times 100.$$

In seawater, there is a mixture of atmospheric He ($R/R_a = 1$ with $R_a = 1.384 \times 10^{-6}$ mol mol^{-1}) diffusing from the surface and of mantle He ($R/R_a = 8.5$) outgassed at the level of mid-ocean ridges and which is enriched in ^{3}He from the atmosphere. Analysis of ^{3}He enrichment of seawater allows the detection of hydrothermal plumes (Fig. 4.9).

4.4 The Uranium and Thorium Decay Chains

^{238}U, ^{235}U and ^{232}Th are long-lived radioactive isotopes present in all Earth's rock, from magmatic rocks to the abyssal ocean. Their slow disintegration produces a myriad of short-lived radioactive atoms that ends with the production of non-radioactive lead isotopes (Fig. 4.10). For example, ^{238}U decays to ^{234}Th, which itself decays to ^{234}Pa, which decays to ^{234}U that produces ^{230}Th and so on down to ^{206}Pb, stable at last! ^{238}U, which is at the beginning of the chain, has a much longer half-life than the following intermediate isotopes. At secular equilibrium, the activity of intermediate isotopes is equal to the

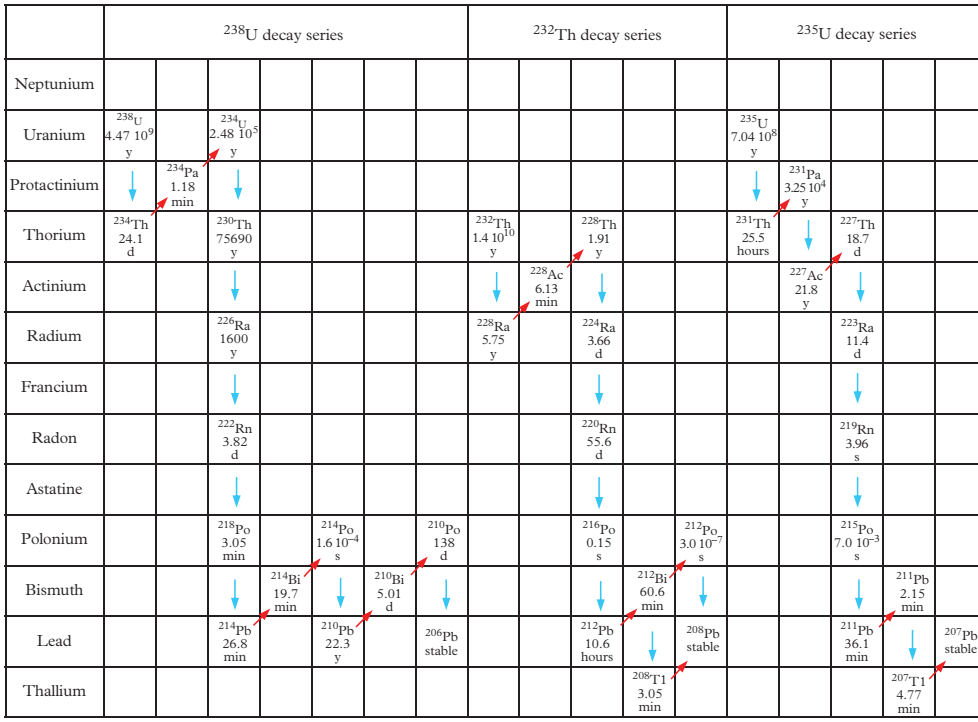

Figure 4.10 *Uranium and thorium decay chains. The vertical and tilted arrows represent* α *and* β *decays, respectively. Each line contains isotopes of a single element with the same chemical behavior but different half-lives.*

activity of the parent isotope with the slowest disintegration rate, that is, ^{238}U. However, the secular equilibrium is not always reached. In fact, geochemists are particularly interested in disequilibrium, because it reflects the removal or addition of a daughter isotope by a geochemical process that it is then possible to quantify.

Isotopes with very different chemical behaviors succeed each other along the decay chains (Fig. 4.11). For example, soluble ^{238}U decays to insoluble ^{234}Th. Soluble ^{226}Ra decays to ^{222}Rn, which is a volatile gas. There are also isotopes of the same element with widely varying half-lives. For example, the Th isotopes have half-lives ranging from 1 day (^{231}Th) to 1.4×10^{10} y (^{232}Th). These variations of chemical behavior and half-lives are used to study different oceanic processes.

The soluble or insoluble character of the elements is often evaluated by the fraction of the radionuclide which is located in the particles relative to the total quantity in seawater. There is generally: Th (∼15%) > Pb > Pa (∼1%)> Ac > Ra (∼0.3%) > U ($\sim 10^{-5}$%) > Rn (0%). Th is adsorbed on all the components of marine particles (organic matter, $CaCO_3$, biogenic silica, lithogenic particles, Fe and Mn oxides). The precise nature of the phases carrying Pb is not clearly established but it seems to have a strong affinity

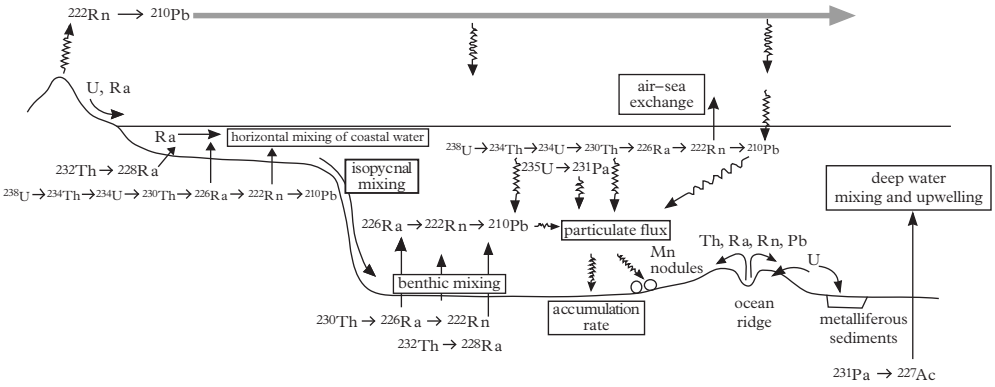

Figure 4.11 *Various sources of isotopes of the radioactive decay chains and different processes that can be studied.*

for organic matter. Pa has a high affinity for biogenic silica. Ra has very little affinity for particles except for barite ($BaSO_4$) in which it substitutes for Ba. UO_2^{2+} is stabilized in solution by complexation with carbonate ions and substitutes for Ca in aragonite, which allows coral dating by regrowth of ^{230}Th (see Problem 5). It is also adsorbed on Fe and Mn oxyhydroxides and it is highly enriched by reduction in organic-rich sediments in anoxic basins and during seawater circulation in the oceanic crust (hydrothermal). Rn, which is an inert gas, is not incorporated into particles

It is the chemical nature of the parent isotope that determines the daughter isotope input function. Soluble isotopes produced by radioactive decay of insoluble parents are injected into the ocean from continents or sediment. Insoluble isotopes produced by disintegration of soluble parents are injected throughout the ocean. The oceanic distribution of an isotope U and Th decay series depends on its chemical behavior, but also on its half-life and on its parent isotope distribution (Fig. 4.12). Thus, the isotopes of a single element can have very different horizontal and/or vertical distributions. It is then possible to use isotopic ratios as tracers of the origin of the material containing these isotopes.

The different chemical behaviors of parent and daughter isotopes create differences of activities between parent and daughter: these differences of activities are called **radioactive disequilibrium**. Some isotopes arrive in excess in the ocean:

- For example, rivers bring to the ocean an excess of soluble radium isotopes compared to their insoluble parent thorium isotopes (see Chapter 6).
- More surprisingly, ^{238}U and ^{234}U that belong to the same decay chain are not at secular equilibrium in continental waters. Indeed, in rocks, ^{238}U is well inserted in the mineral lattices, but the emission of an α particle during the decay of ^{238}U induces a recoil effect (in the sense of the recoil of the gun) on ^{234}Th which damages the crystal lattice. ^{234}U is then produced in a poorly crystalline area or even

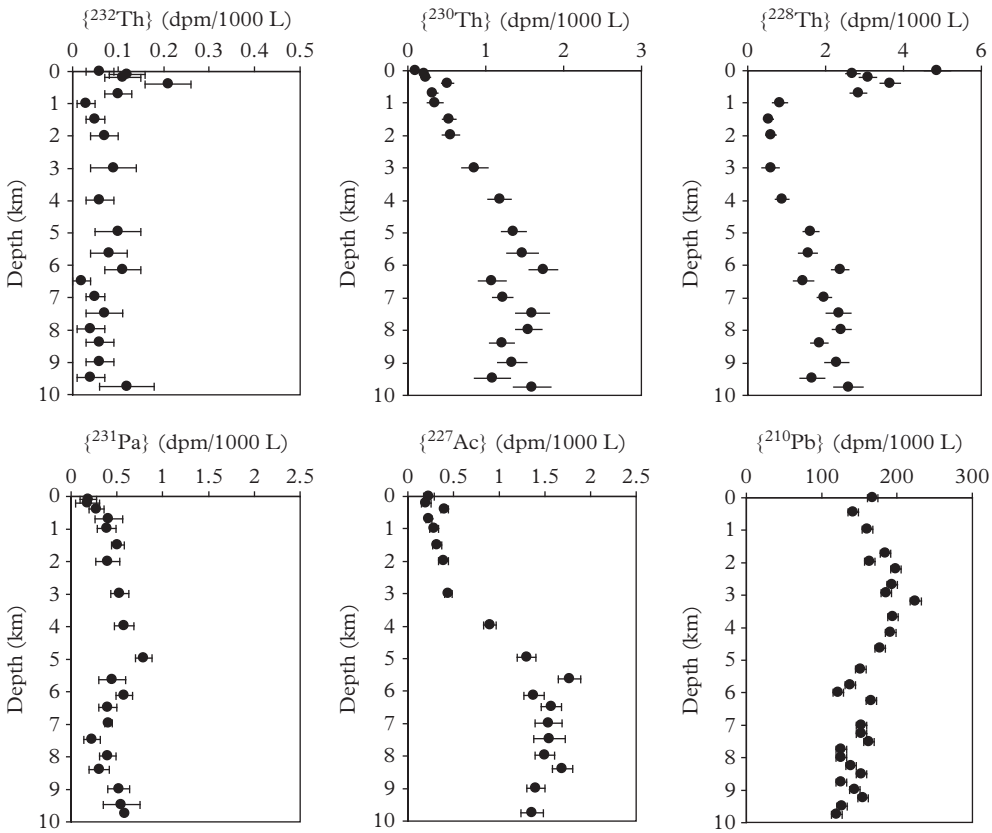

Figure 4.12 *Vertical profiles of isotopes of the U and Th decay chains (Bonin Island Trench, offshore Japan). Although ^{228}Th, ^{230}Th and ^{232}Th have a similar chemical behavior dominated by transport on marine particles, they have different profiles because they have different input functions in the ocean: ^{232}Th, which is at the head of a decay chain, is brought to the surface of the ocean by rivers and atmospheric dust, which explains the higher surface concentration; ^{230}Th is produced uniformly in the water column by the decay of ^{234}U; and ^{228}Th is produced by the decay of ^{228}Ra, which is enriched in surface waters (inputs from continents) and at the bottom of the ocean (diffusion from the sediments). As for ^{230}Th, ^{231}Pa is produced throughout the water column, but its lower affinity for marine particles limits the difference of concentration between surface and deep waters. The activities of ^{230}Th and ^{231}Pa are much lower than those of their respective parent isotopes ^{234}U ($(\{^{234}U\} = 2790$ dpm $m^{-3})$ and ^{235}U ($\{^{235}U\} = 114$ dpm m^{-3}), due to the removal of ^{230}Th and ^{231}Pa by marine particles. ^{227}Ac is at secular equilibrium with its parent ^{231}Pa between 0 and 3 km deep. Between 4 and 10 km, the diffusion of ^{227}Ac from the sediment release an excess of ^{227}Ac relative to ^{231}Pa. ^{210}Pb is in deficit compared to its parent ^{226}Ra, which has an activity that generally varies between 200 and 300 dpm m^{-3}. Despite the high affinity of ^{210}Pb for the marine particles, the ^{226}Ra–^{210}Pb imbalance is less important than the ^{234}U–^{230}Th or ^{235}U–^{231}Pa imbalance because the short half-life of ^{210}Pb allows a faster return to secular equilibrium. Modified from Nozaki et al. (1998).*

outside of the crystal where its grandparent ^{238}U was. Therefore, continental waters are generally enriched in ^{234}U compared to ^{238}U and disequilibrium also exists in the ocean (see Problem 5).

– ^{210}Pb is derived from the disintegration of ^{222}Rn: it is both produced *in situ* and brought by atmospheric deposition.

Disequilibrium can also be created in the ocean:

– With its short half-life, ^{222}Rn is usually at equilibrium with its parent ^{226}Ra, but as it is a gas, its diffusion to the atmosphere induces a deficit in surface waters (see Chapter 5).
– Insoluble isotopes produced by the decay of a soluble parent are in excess in marine particles and sediments and are in deficit in the dissolved phase. This is the case for Th, Pa, Pb and Po isotopes (see the examples of ^{234}Th, ^{230}Th and ^{231}Pa in Chapters 9, 10 and 11). In particular, these isotopes are used to date sediments (see Chapters 6 and 9). These isotopes are primarily marine particle tracers. Their removal from the water column occurs more efficiently where strong particle fluxes are able to scavenge them, as is the case at the ocean margins.
– The accumulation and radioactive decay of insoluble isotopes in marine sediments produces a source of soluble isotopes that diffuse in bottom waters where they are in excess (see the example of ^{227}Ac in Chapter 10).

4.5 Cosmogenic Isotopes

The Earth is permanently bombarded by particles (protons, helium nuclei) of very high energy produced by the Sun and the Galaxy: the cosmic rays. By deflecting charged particles, the Earth's magnetic field partially protects us from these radiations. Nevertheless, some particles collide with the atoms of the atmosphere and brake them to produce radioactive nuclei such as ^{10}Be (spallation of O and N) or ^{26}Al (spallation of Ar). Secondary neutrons produced during these spallation reactions may interact with other atoms to produce radioactive isotopes.

For example

$$^{14}_{7}N + n \rightarrow {}^{14}_{6}C + p,$$

where n and p are a neutron and a proton, respectively.

4.5.1 The ^{14}C Isotope

^{14}C has a half-life of 5730 y. In the atmosphere, ^{14}C is rapidly oxidized to $^{14}CO_2$. This carbon dioxide molecule then follows the carbon cycle as its $^{12}CO_2$ and $^{13}CO_2$ sisters: it is incorporated by living beings or by the ocean. In the absence of natural or

anthropogenic disturbance, the atmospheric production of ^{14}C is balanced by radioactive decay in the atmosphere, the ocean and the continental biosphere. In this case, the amount of ^{14}C and the $^{14}C/^{12}C$ ratio in the atmosphere are constant (see Problem 1 of Chapter 5). When a sample incorporates atmospheric carbon, it thus assimilates a given proportion of ^{12}C and ^{14}C. If this sample becomes isolated from the atmosphere and evolves in a closed system, the ^{14}C content and the $^{14}C/^{12}C$ ratio decrease exponentially (equation 4.2 for ^{14}C; ^{12}C being stable its concentration remains constant). The radioactive decay of ^{14}C is used to date objects over a period of about 50,000 y. These ages have considerable importance in both archaeology and in paleo-oceanography. The use of ^{14}C requires circumvention of some difficulties.

(a) First, ^{14}C undergoes isotopic fractionations just like ^{12}C and ^{13}C. As for the stable isotopes, $\delta^{14}C$ is defined as

$$\delta^{14}C_{sample} = \left\{ \frac{\left(^{14}C/^{12}C\right)_{sample}}{\left(^{14}C/^{12}C\right)_{reference}} - 1 \right\} \times 1000, \tag{4.12}$$

with $(^{14}C/^{12}C)_{reference} = 1.2 \times 10^{-12}$. This value corresponds roughly to the ratio in the atmosphere of 1954, just before the beginning of the nuclear tests.

Variations of the $^{14}C/^{12}C$ ratio are therefore due to both isotopic fractionations and radioactive decay of ^{14}C. To correct for isotopic fractionations (which depend on the mass difference) and keep only the information related to radioactivity, the $\Delta^{14}C$ of a sample is defined as

$$\Delta^{14}C_{sample} = \left(\left(1 + \frac{\delta^{14}C_{sample}}{1000} \right) \times \left(1 + 2 \times \frac{25 - \delta^{13}C_{sample}}{1000} \right) - 1 \right) \times 1000, \tag{4.13}$$

where $\delta^{13}C$ was defined in the previous chapter. $\delta^{14}C$ is the relative difference between the $^{14}C/^{12}C$ ratio of the sample and the average ratio of the atmosphere of 1954 (estimated from the study of tree rings) which serves as a reference. $\Delta^{14}C$ is the $\delta^{14}C$ that the sample would have if it had experienced a mass-dependent isotopic fractionation such as its $\delta^{13}C$ becomes –25‰ (this corresponds to the $\delta^{13}C$ average for C3 organic matter which is frequently used for dating).

(b) In addition, the ^{14}C production rate varies in space and time. It is higher toward the poles than at low latitude because the Earth's magnetic field is weaker at the poles and provides a reduced protection against cosmic rays. Nevertheless, atmospheric mixing is relatively fast (of the order of 1 y), so that the atmospheric abundance of ^{14}C is relatively uniform. The ^{14}C production rate also varies with time: rapid and periodic solar activity fluctuations have a relatively low impact on the cosmic ray flux. At the scale of a few thousand years, the fluctuations of the Earth's magnetic field intensity and its protective effect against cosmic rays have a significant impact on the production rate and the atmospheric abundance of ^{14}C. By analyzing the $^{14}C/^{12}C$ ratio of samples of known age (tree rings,

coral dated by the U–Th method (Problem 5), sediments dated by comparison with geochemical tracers of the GISP2 Greenland ice core that is dated by counting the annual layers), it is possible to reconstruct the atmospheric abundance of ^{14}C in the past: ^{14}C ages are consistently too low: the Earth's magnetic field was slightly less intense than today, allowing an increased production of ^{14}C (Fig. 4.13).

(c) Finally, the abundance of ^{12}C did not remain constant in the atmosphere over time. The study of air bubbles contained in the Antarctic ice sheet reveals that during the Last Glacial Maximum the atmospheric CO_2 concentration was about two times lower than today. Since the beginning of the industrial revolution in the nineteenth century, the combustion of fossil fuels has injected into the atmosphere ^{14}C-free CO_2 (coal and oil were formed millions of years ago, so they have lost all their initial ^{14}C) which artificially reduces the $^{14}C/^{12}C$ ratio of the atmosphere. In the future, the dating of objects that are contemporary to us will be made difficult by the artificial production of ^{14}C by human activity (see Section 4.6).

The most important application of ^{14}C in oceanography is the determination of the water renewal rate in the deep ocean, which is estimated from the decrease of $\Delta^{14}C$ in dissolved inorganic carbon (Fig. 4.14, see also Chapter 10).

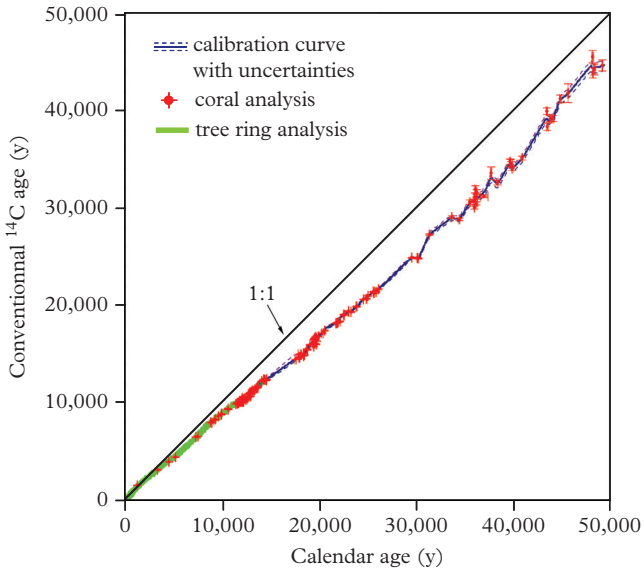

Figure 4.13 *Comparison of ^{14}C ages with other methods. Calendar ages are obtained by comparison of marine sediments with the GISP2 ice core, corals dated by the ^{238}U–^{230}Th method and tree ring counting. Modified from Fairbanks et al. (2005)*

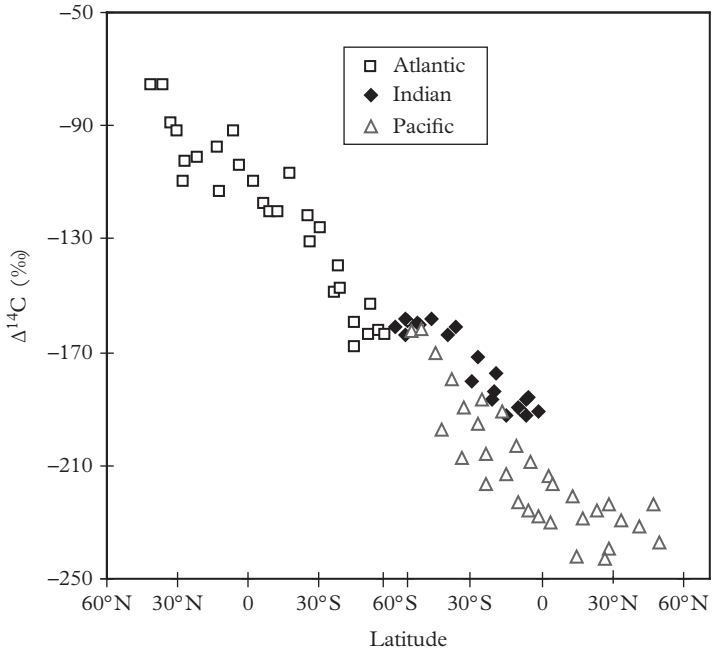

Figure 4.14 *Variation of $\Delta^{14}C$ in deep waters of the Atlantic, Indian and Pacific oceans with latitude. The regular decrease of $\Delta^{14}C$ reflects aging during the thermohaline circulation. Adapted from Broecker and Peng (1982).*

It also provides important information on the dissolved organic carbon cycle (Chapter 5) and on the age of sediments (Chapter 9).

4.5.2 The ^{10}Be Isotope

Beryllium has a stable isotope (^{9}Be) and a cosmogenic isotope (^{10}Be) whose half-life is 1.5×10^6 y. It is an element which is attached to marine particles, but which is nonetheless more soluble than thorium. It is removed from seawater by marine particles and it accumulates in sediments and manganese nodules. Thus ^{10}Be is used to determine sedimentation rates and growth rates of manganese nodules (equation 4.2). The ^{10}Be concentration archived in ice and sediment cores allows reconstruction of the fluctuations in the Earth's magnetic field that modulates its production as well as ^{14}C production. Beryllium-9 (^{9}Be) is not cosmogenic. It is found in continental materials and is brought to the ocean by rivers. The relative distribution of the ratio ^{9}Be/^{10}Be in the ocean allows us to quantify continent/ocean interface processes (Fig. 4.15).

^{32}P, ^{26}Al and ^{34}Si are cosmogenic isotopes of important chemical elements in marine geochemistry. Their use is, however, limited by their very low abundance in the environment.

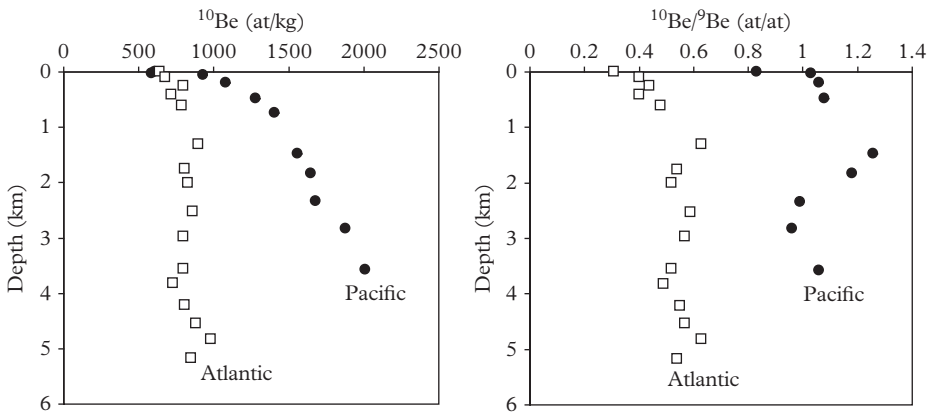

Figure 4.15 *^{10}Be concentration and ^{10}Be/^{9}Be ratio in seawater. ^{10}Be uptake by marine particles in surface water and its release at depth explain the evolution of the concentration of ^{10}Be with depth. The progressive accumulation of ^{10}Be during deep water circulation causes a progressive enrichment from the Atlantic to the Pacific, as for phosphate (Chapter 2). On each profile, the ^{10}Be/^{9}Be ratio is relatively constant because these two isotopes are introduced at the ocean surface. The high ratio in the Pacific reflects low inputs of lithogenic ^{9}Be far from continents. Modified from Kusakabe et al. (1987) and Ku et al. (1990).*

4.6 Artificial Isotopes

The use of nuclear energy for civilian and military purposes led to transient emissions of many radioactive isotopes in the environment. Some of these isotopes, such as ^{14}C or ^{3}H, were already naturally present in the environment because they are produced during spallation reactions. Others, such as ^{239}Pu, ^{231}Am, ^{90}Sr or ^{137}Cs, were absent from the environment before the nuclear era (Fig. 4.16).

Artificial isotopes cover a wide range of chemical behaviors: ^{3}H, ^{90}Sr and ^{137}Cs are soluble in seawater; ^{14}C is soluble but it is also involved in the cycle of organic matter; ^{239}Pu is highly particle reactive (Fig. 4.17) These isotopes can be followed as dyes transported by ocean currents, through the food chain or from the surface to the sediment by marine particles.

The main source of artificial nuclides in the environment has been atmospheric nuclear weapons tests. Between 1945 and 1980, there were 423 H-bomb explosions. Most of them were carried by the US and the USSR in the nuclear weapon race that accompanied the Cold War between 1954 and 1962. In 1963, a moratorium on atmospheric nuclear tests was signed by the USA, the United Kingdom and the Soviet Union. Free air tests were conducted after 1963 by France and China who had not signed the treaty, but their contribution is very small on a global scale. Most tests occurred in the northern hemisphere. During thermonuclear explosions, the nuclear mushroom cloud carries radioactive nuclides to the stratosphere where they can be transported over long distances. The fallout of ^{14}C, ^{3}H (also called **tritium**), ^{90}Sr, ^{137}Cs and ^{239}Pu produced

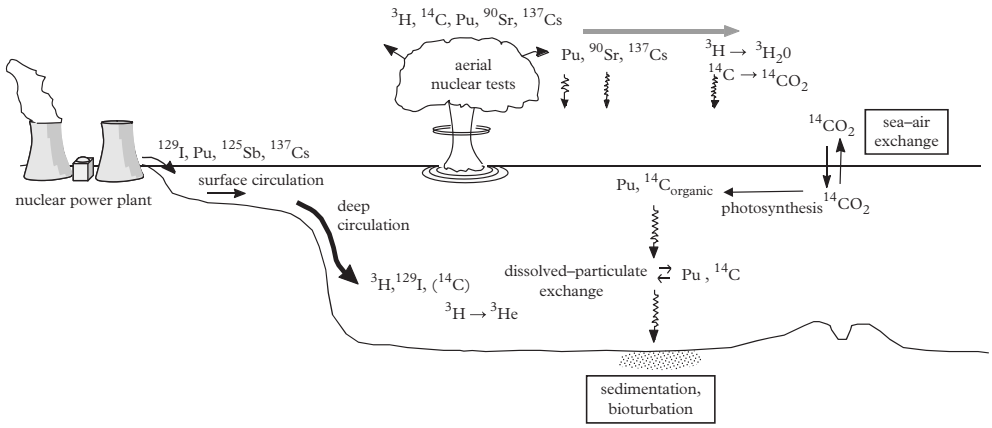

Figure 4.16 *Sources and fates of anthropogenic isotopes in the ocean. Some isotopes are introduced at the global scale (atmospheric tests of nuclear weapons). Others are injected locally (nuclear waste reprocessing plants). All are transient tracers.*

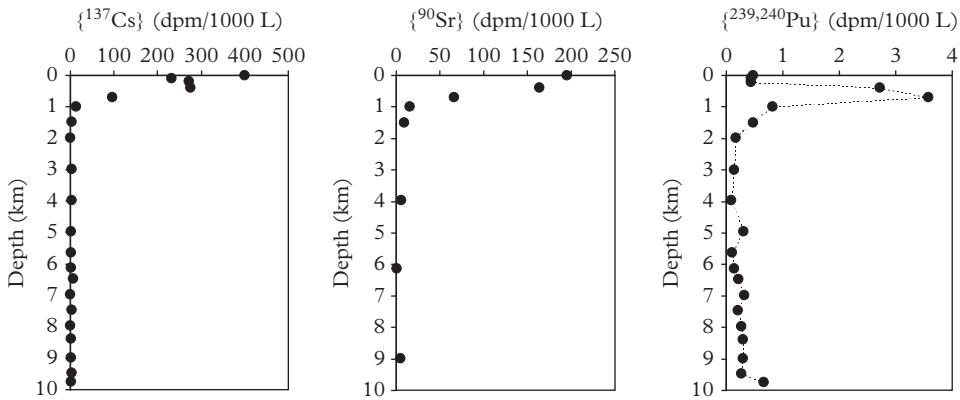

Figure 4.17 *Anthropogenic radionuclides in the Bonin Island Trench (Japanese archipelago of the Pacific). These isotopes are introduced at the ocean surface by rain and rivers. Soluble ^{137}Cs and ^{90}Sr have a concentration maximum in surface waters and are absent from the deep waters. On the contrary, the maximum concentration of Pu is located around 700 m and Pu is found down to the seafloor. This behavior mimics the ^{232}Th profile at the same site (Fig. 4.12) and reflects the reversible adsorption of Pu on sinking marine particles. Modified from Nozaki et al. (1998).*

during atmospheric tests therefore occurs across the planet. The extent of the fallout on the ocean surface depends on the chemical behavior of tracers in the atmosphere. ^{3}H is incorporated into water vapor, which has a residence in the atmosphere of few days only: most ^{3}H has been deposited in the northern hemisphere and there is much less ^{3}H in the southern hemisphere. On the other hand, ^{14}C incorporated into $^{14}CO_2$

remains long enough in the atmosphere to be carried to the southern hemisphere by atmospheric circulations. Therefore, similar anthropogenic ^{14}C concentrations are found in the northern and southern hemispheres.

The first studies of the impact of nuclear explosions in the ocean concerned ^{90}Sr and ^{239}Pu, which represented the highest radio-toxicological risks. However, in the 1970s, considerable efforts were produced for the analysis of ^{3}H and ^{14}C as tracers of the ocean circulation during the GEOSECS program. Anthropogenic ^{14}C injection resulted in a doubling of the amount of ^{14}C atmospheric ($\Delta^{14}C = +1000‰$) (Fig. 4.18). The ocean–atmosphere exchanges led to a ^{14}C enrichment of dissolved inorganic carbon in surface waters, which acquired a positive $\Delta^{14}C$ ($\Delta^{14}C \sim +100‰$), while deeper waters isolated from the atmosphere are still characterized by a negative $\Delta^{14}C$ (Fig. 4.19). A positive $\Delta^{14}C$ implies that atmospheric carbon has been incorporated since 1954. $\Delta^{14}C$ is therefore a powerful tool to trace the absorption of atmospheric carbon by the ocean. It is not always easy to distinguish between the anthropogenic and natural (cosmogenic) contributions because very few ^{14}C measurements in seawater existed before the start of the nuclear tests.

This difficulty does not exist for ^{3}H because its half-life (12.4 y) is short compared to the seawater residence time in the ocean so that cosmogenic ^{3}H is almost negligible compared to anthropogenic ^{3}H. The peak of ^{3}H emissions occurred in 1963 (Fig. 4.20). It is possible to follow the formation and circulation of "young" deep waters with ^{3}H (see Chapter 10). Tritium concentrations are given in "tritium units" (or TU): 1 TU

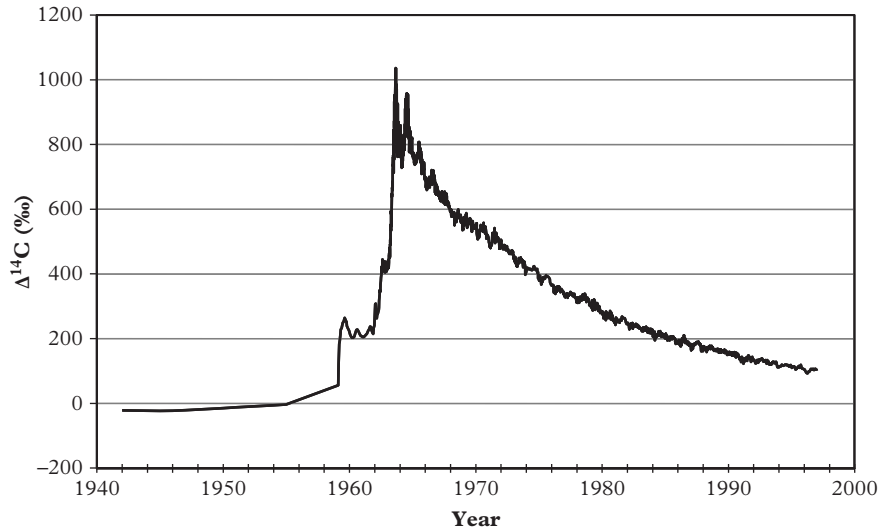

Figure 4.18 *Evolution of $\Delta^{14}C$ in the northern hemisphere atmosphere. The rapid increase of $\Delta^{14}C$ until 1963 is due to atmospheric nuclear testing. The slow decrease is due to the exchange of carbon between the ocean, the atmosphere and the biosphere, which dilutes anthropogenic ^{14}C. Modified from Stuiver et al. (1998).*

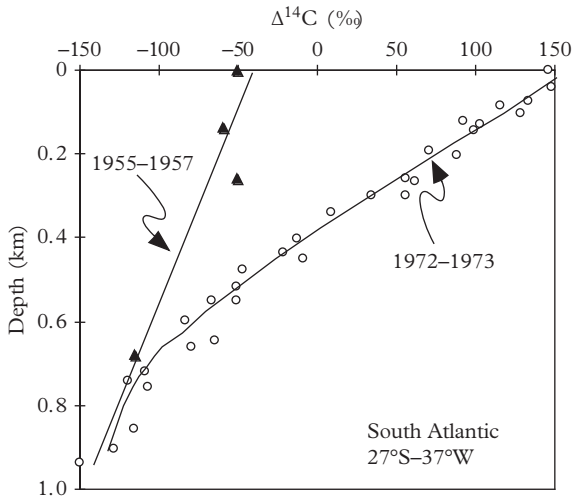

Figure 4.19 *Change of $\Delta^{14}C$ in the South Subtropical Atlantic. Sixteen years after the beginning of the atmospheric nuclear tests, anthropogenic ^{14}C was already at a depth of 600 m. Modified from Broecker and Peng (1982).*

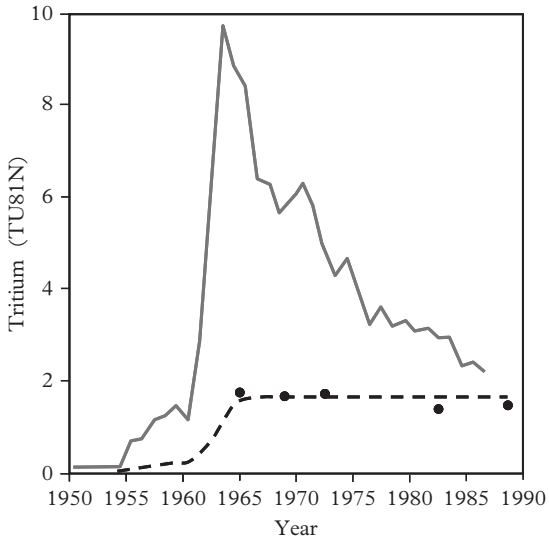

Figure 4.20 *Evolution of the tritium concentration in the tropical Atlantic. Gray curve: precipitation. Dashed curve: surface water (model). Black points: surface water (data). Modified from Doney et al. (1993).*

corresponds to 1 ^{3}H atom for 10^{18} ^{1}H atoms. The ^{3}H–^{3}He chronometer can be used to date the last contact of a water mass with the atmosphere (see Problem 6).

The civil nuclear industry has generated much smaller and more localized releases than atmospheric nuclear tests. Examples include European intentional discharges of nuclear fuels at Sellafield and La Hague reprocessing plants, or accidental releases due to the explosions of the Chernobyl and Fukushima reactors in 1986 and 2011 respectively (Fig. 4.21). These point sources allow local and regional studies. For example, ^{129}I is

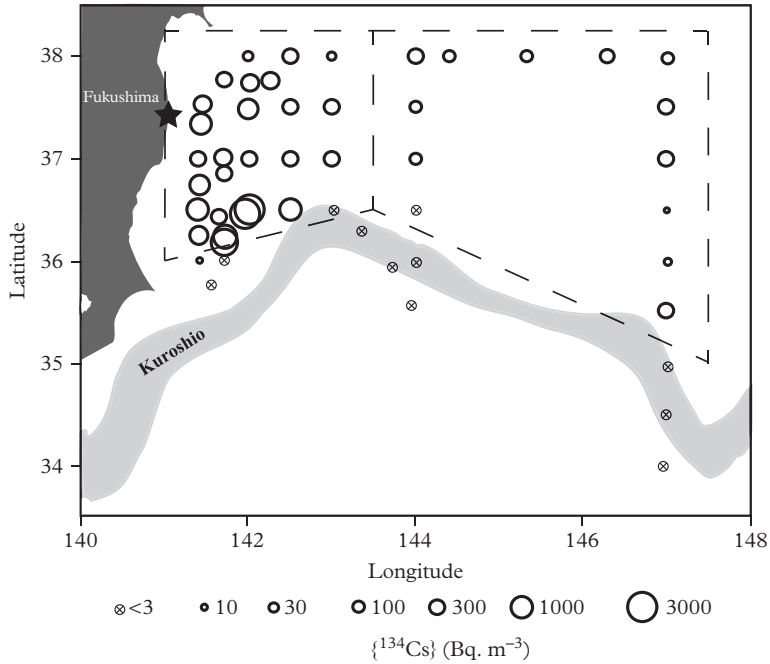

Figure 4.21 *^{134}Cs activity (Bq m^{-3}) in surface waters 3 months after the Fukushima accident. Fukushima-derived ^{134}Cs is detected throughout waters 30–600 km offshore, with the highest activities associated with near-shore eddies and the Kuroshio Current acting as a southern boundary for transport. Modified from Buesseler et al. (2012).*

specifically released by the nuclear waste reprocessing plant of La Hague. Its long half-life ($T_{1/2} = 17.3$ Ma) allows us to follow it into the deep ocean (see Chapter 10).

Finally, different point sources of man-made radioactive isotopes are due to the discharges of "preconditioned" radioactive waste by different countries, to the shipwrecks of nuclear propulsion submarines and to the dumping of nuclear reactors and their fuel (Kara Sea and Barents Sea bordering the Arctic coastal waters by the former USSR). To date, they have produced very localized and low contaminations (Problem 7).

Appendix 1

Integration of the Radioactivity Equation for a Closed System without Production Term

Since

$$\frac{dN}{dt} = -\lambda N,$$

it follows that

$$\frac{dN}{N} = -\lambda dt.$$

If we integrate between time $t' = 0$ and $t' = t$:

$$\int_0^t \frac{dN}{N} = -\int_0^t \lambda dt',$$

$$\ln\left(\frac{N_t}{N_0}\right) = -\lambda\,(t - t_0)\,,$$

$$N_t = N_0 e^{-\lambda t}.$$

Integration of the Radioactivity Equation for a Closed System with Production Term

In this instance

$$\frac{dN}{dt} = -\lambda N + \Gamma.$$

The method of variation of the constant is used. The solution of the equation without the second member $\left(\frac{dN}{dt} = -\lambda N\right)$ is of the form

$$N_t = A e^{-\lambda t},$$

where A is a constant.

The solution of the equation with the second member is also of the form

$$N_t = A_t e^{-\lambda t},$$

but A_t is now a function of time.

Under these conditions

$$dN_t/dt = (dA_t/dt)e^{-\lambda t} - \lambda A e^{-\lambda t}.$$

Replacing N_t in the full equation, the following is obtained

$$(dA_t/dt)e^{-\lambda t} - \lambda A_t e^{-\lambda t} = -\lambda A_t e^{-\lambda t} + \Gamma,$$

or

$$(\mathrm{d}A_t/\mathrm{d}t)\mathrm{e}^{-\lambda t} = \Gamma,$$

$$\mathrm{d}A_t/\mathrm{d}t = \Gamma\mathrm{e}^{\lambda t},$$

then

$$A_t = \int_0^t \Gamma_{t'}\mathrm{e}^{\lambda t'}\,dt' + B,$$

where B is a constant. It is then inferred that

$$N_t = \int_0^t \Gamma_{t'}\mathrm{e}^{\lambda(t'-t)}\,\mathrm{d}t' + B\mathrm{e}^{-\lambda t}.$$

B is determined by the initial conditions (at $t = 0$, $N_t = N_0$)

$$N_0 = B.$$

Hence

$$N_t = \int_0^t \Gamma_{t'}\mathrm{e}^{\lambda(t'-t)}\,dt + N_0\mathrm{e}^{-\lambda t}.$$

If $\Gamma_{t'}$ is constant over time (i.e., $\Gamma_{t'} = \Gamma$)

$$\begin{aligned} N_t &= N_0\mathrm{e}^{-\lambda t} + \int_0^t \Gamma\mathrm{e}^{\lambda(t'-t)}\,\mathrm{d}t' \\ &= N_0\mathrm{e}^{-\lambda t} + \Gamma\mathrm{e}^{-\lambda t}\int_{t'=0}^{t} \mathrm{e}^{\lambda t'}\,\mathrm{d}t' \\ &= N_0\mathrm{e}^{-\lambda t} + \Gamma\mathrm{e}^{-\lambda t}\left[\frac{\mathrm{e}^{\lambda t'}}{\lambda}\right]_0^t \\ &= N_0\mathrm{e}^{-\lambda t} + \frac{\Gamma}{\lambda}\left(1-\mathrm{e}^{\lambda t}\right). \end{aligned}$$

If Γ_t varies exponentially over time ($\Gamma_t = A\mathrm{e}^{\kappa t}$) and if $\kappa < 0$, Γ_t follows a radioactive-like exponential decay.

$$N_t = N_0 e^{-\lambda t} + \int_{t'=0}^{t} A e^{\kappa t'} e^{\lambda(t'-t)} dt'$$

$$= N_0 e^{-\lambda t} + A e^{-\lambda t} \int_{t'=0}^{t} e^{(\lambda+\kappa)t'} dt'$$

$$= N_0 e^{-\lambda t} + A\, e^{-\lambda t} \left[\frac{e^{(\lambda+\kappa)t'}}{\lambda+\kappa} \right]_0^t$$

$$= N_0 e^{-\lambda t} + \frac{A}{\lambda\kappa} \left(e^{\kappa t} - e^{-\lambda t} \right).$$

Calculation of the Mean Lifetime of an Isotope

$$\tau = \frac{1}{N_0} \int_{t=0}^{+\infty} t dN_t.$$

Using the radioactive decay law, we obtain

$$\tau = \frac{1}{N_0} \int_{t=0}^{+\infty} t\,(-\lambda N_t dt).$$

Since $N_t = N_0 e^{-\lambda t}$

$$\tau = -\lambda \int_{t=0}^{+\infty} t e^{-\lambda t} dt.$$

By integrating by parts

$$\tau = -\left[\frac{1+\lambda t}{\lambda} e^{-\lambda t} \right]_0^{+\infty}.$$

We obtain finally

$$\tau = \frac{1}{\lambda}.$$

PROBLEMS

Problem 1: Occupational hazards

Unfortunately for them, burglars stole a radioactive sample in a research center. It was the wrong move: they were found dead on their doorstep. The radioactive sample is in their house, but it may still be dangerous. The police contact you because you are a radioactivity expert. At the time of burglary, the sample contained N_0 radioactive atoms. It remains dangerous as long as the number of radioactive atoms is greater than $N_0/1000$. The half-life of the isotope is 1 day.

(1) If the sample was found 1 week after the burglary, is it still dangerous?

(2) If this is the case, how long must police wait before retrieving it without risk?

(3) At this time, what will be its activity?

Problem 2: Sedimentation rate with ^{14}C

In a sediment core from the Pacific, a foraminifer test sampled 100 cm below the core top has a $^{14}C/^{12}C$ ratio equal to 12.5% of the $^{14}C/^{12}C$ ratio of a foraminifer collected at the core top (it is assumed that the core top foraminifer is modern).

(1) What is the age difference between these two foraminifera?

(2) What is the sedimentation rate?
$\lambda_{^{14}C} = 1.22 \times 10^{-4}\ y^{-1}$.

Problem 3: Strontium in the Baltic Sea (Andersson et al., 1992)

The brackish waters of the Baltic Sea are the result of the mixing between North Atlantic seawater and fresh water from rivers draining old geological formations. Analyses of the Baltic seawater are given in Table 4.3.

Table 4.3 *Strontium in Baltic Sea brackish waters*

Sample no.	[Sr] (ppm)	$^{87}Sr/^{86}Sr$
1	0.566	0.70972
2	0.794	0.70954
3	2.56	0.70921

(1) Plot these data in an $^{87}Sr/^{86}Sr$ versus 1/Sr diagram. Conclude.

(2) Knowing that Sr concentration in the North Atlantic is 7.7 ppm, estimate the isotopic composition of North Atlantic water.

(3) Knowing that the land drained by the rivers have an average isotopic composition of 0.733, evaluate the river Sr concentration.

Problem 4: Neodymium in the Atlantic (Jeandel, 1993)

When the North Atlantic Deep Water (NADW) crosses the Equator, its Nd concentration and its Nd isotopic composition shift from $C^{\text{initial}} = 18\,\text{pmol}\,\text{kg}^{-1}$ and $\varepsilon_{\text{Nd}}^{\text{initial}} = -13.5$ to $C^{\text{final}} = 22\,\text{pmol}\,\text{kg}^{-1}$ and $\varepsilon_{\text{Nd}}^{\text{final}} = 11.5$.

(1) Assuming that this evolution is due solely to the dissolution of continental dusts, calculate the isotopic composition that these dusts must have. What do you think of this hypothesis, if you consider that the main surrounding landmasses have an ε_{Nd} between –8 and –13.

(2) We also test the hypothesis of a mixing between the NADW and a deep water coming from the South (Southern Component Water or SCW) whose characteristics are $C^{\text{SCW}} = 31\ \text{pmol}\ \text{kg}^{-1}$ and $\varepsilon_{\text{Nd}}^{\text{SCW}} = -8.5$. What fraction f of SCW should be added to the NADW to explain the isotopic evolution of the latter?

(3) What is the best assumption according to you?

(4) If isotopic data were not available, can you suggest a strategy for choosing between these two hypotheses.

Problem 5: Correction of ^{14}C ages by the U–Th method (Bard et al., 1990)

Corals collected on the Barbados Island have been dated by the ^{14}C method. To check these ages, the same corals are dated by the ^{238}U–^{230}Th method: when they grow, coral incorporate ^{238}U (there is a lot of ^{238}U in seawater) and no ^{230}Th (there is very little ^{230}Th in seawater, particularly in surface waters, as discussed in Chapter 9).

$^{238}\text{U} \rightarrow {}^{234}\text{Th} \rightarrow {}^{234}\text{U} \rightarrow {}^{230}\text{Th} \rightarrow \ldots$

^{238}U half-life = 4.47×10^9 y

^{234}Th half-life = 24.1 d

^{234}U half-life = 2.48×10^5 y

^{230}Th half-life = 7.54×10^4 y

^{238}U, ^{234}U and ^{230}Th activities have been analyzed in corals of different ages (Table 4.4).

Table 4.4 *Analyses of Barbados coral*

Sample No.	^{14}C Age (y)	$\{^{234}\text{U}/^{238}\text{U}\}$	$\{^{230}\text{Th}/^{234}\text{U}\}$	Earth's Magnetic Field Intensity (Relative to Present)
1	6586	1.141	0.0667	86 %
2	12,195	1.131	0.1190	90 %
3	17,186	1.136	0.1735	67 %

(1) In seawater, ^{234}U is not at secular equilibrium with ^{238}U: $\{^{234}\text{U}\} = 1.144\{^{238}\text{U}\}$. Determine the $\{^{234}\text{U}/^{238}\text{U}\}$ activity ratio of the coral 17,000 y after its formation. Knowing that this ratio is measured with an accuracy of the order of 1%,

does ^{234}U decay allow the dating of corals less than 30,000 y old with a relative accuracy of 1%?

(2) Determine the U–Th age of the coral. You may use the previous question to make an adequate approximation for corals under 17,000 y old.

(3) Compare the U–Th ages with ^{14}C ages, knowing that the precision of ^{230}Th measurements is of the order of 1%. Compare with the result of Problem 2.

(4) How do changes of the Earth's magnetic field intensity recorded in volcanic rocks help you to explain the age differences for a given sample?

Problem 6: Tritium–helium age

In a water mass located at a depth of 1000 m in the Atlantic Ocean, concentrations of 1.8 TU of ^{3}H and 2.0 TU of ^{3}He are determined. What is the ^{3}H–^{3}He age of this water mass? What does this age represents?

Problem 7: Plutonium in the Barents Sea (Holm et al., 1986)

Characteristic isotopic ratios of plutonium releases from the nuclear waste reprocessing plant from Sellafield (Great Britain), the atmospheric nuclear tests and military-grade plutonium are given in Table 4.5.

Table 4.5 *Pu analysis in Barents Sea and potential sources*

	Barents Sea Surface Waters (in 1980)	**Sellafield**	**Fallouts (in 1980)**	**Military-grade**
$\left\{\frac{^{238}Pu}{^{239+240}Pu}\right\}$	0.066	0.28	0.047	0.020
$\left\{\frac{^{241}Pu}{^{239+240}Pu}\right\}$	6.9	30	4	5

Determine the origin of the plutonium found in surface waters of the Barents Sea (in 1980).

5

Box Models

The ocean is such a vast and complex object that it would be illusory to claim to describe and understand it in detail. However, it is necessary to test the state of our knowledge with schematic representations, that is, models. These representations are deliberately simplified to study a particular aspect of the ocean. As a first step, a model allows us to check the status of our knowledge: is it possible to balance the tracer fluxes or is it necessary to call upon a new process to explain observations? Once the model is tuned with observations, it can be used to try to predict the evolution of the ocean in the future or to reconstruct it in the past.

Models represent the ocean as a chemical and biological plant receiving reagents of different origins (continent, atmosphere and submarine volcanism). These reagents are transported by currents and marine particles and they participate to chemical and biological reactions. The products leaving the plant are chemically different from the initial reactants. Beyond this image, we use the approach used to study industrial chemical reactor by representing the ocean as a box to which we apply the principle of matter conservation enunciated by Antoine Lavoisier two centuries ago: "nothing is lost, nothing is created, everything is transformed."

5.1 One-Box Model

5.1.1 The Conservation Equation

We consider the equation of conservation of matter in the general case of a tracer in a reservoir (the ocean, a sea, a water mass, a planktonic cell, etc.). The tracer is a chemical element, a molecule, an isotope which follows the movement in the ocean.

The reservoir of volume V contains an average tracer concentration C (Fig. 5.1). We assume that the reservoir is well mixed so that C is uniform in the reservoir. The reservoir is fed by a marine current at a flow rate F. For simplicity, we assume that water flow rates in and out of the reservoir are identical and constant over time, so that the volume of water in the reservoir is constant. The water flowing in the reservoir contains a tracer concentration C_i. The water flowing out of the reservoir has the tracer concentration of the reservoir $C_{out} = C.C$ may be different from C_i because of the reactions taking place

Marine Geochemistry. First Edition. Matthieu Roy-Barman and Catherine Jeandel.

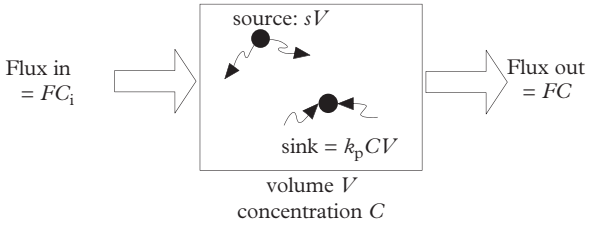

Figure 5.1 *Schematic representation of a model box.*

in the reservoir. During a time interval t, the amount of water entering the reservoir is $F \times dt$. During the same time interval dt, the amount of tracer flowing in the reservoir is $C_i \times F \times dt$, while the amount removed is $C \times F \times dt$. Fluxes (amount per unit time) of tracers into and out of the reservoir are $F \times C_i$ and $F \times C$, respectively.

In addition, in the box, the tracer can be created or destroyed by various processes (chemical reactions, biological activity, radioactivity . . .). A creation, referred as source term, corresponds to a positive flux $s \times V$ proportional to volume V of box but generally independent of the tracer concentration in the box. A loss, called a sink term, corresponds to a negative flux $-k_p \times V \times C$ proportional to the amount of tracer in the box. More generally, these terms are called "sources minus sinks."

The conservation equation simply says that the change of tracer amount in the box is equal to the amount of tracer flowing in or created in box minus the amount of tracer flowing out of the box or destroyed in the box

$$\underbrace{\frac{d(V \times C)}{dt}}_{\substack{\text{change of} \\ \text{tracer quantity} \\ \text{over time}}} = \underbrace{F \times C_i}_{\text{inflow}} \quad \underbrace{-F \times C}_{\text{outflow}} \quad + \quad \underbrace{sV}_{\text{source}} \quad - \quad \underbrace{pCV}_{\text{sink}}. \tag{5.1}$$

V is assumed constant, so it can be written out of the derivative. We note $k_w = F/V$, where k_w has dimensions of the inverse of a time

$$\frac{dC}{dt} = \underbrace{k_w (C_i - C)}_{\text{net current effect}} + s + k_p C. \tag{5.2}$$

The first term on the right-hand side of equation (5.2) represents the net effect of the current (what comes in minus what comes out) on the contents of the reservoir. Other physical processes creating an inflow and an outflow in a reservoir can be described in the same mathematical form (e.g., we will use it to describe gas exchange at the air–sea interface). Equation (5.2) can be rearranged to

$$\frac{dC}{dt} = -\left(k_w + k_p\right) C + s + k_w C_i.$$

This equation has the same form as the radioactivity equation with a production term. The $s + k_w C_i$ term is called "forcing." It corresponds to the constraints imposed on the system by tracer inputs. It is here independent of concentration in the reservoir (i.e., it exhibits zero-order kinetics: $dC/dt = \text{constant} \times C^0 = \text{constant}$). This term has the dimension of a concentration per unit of time.

The term $(k_w + k_p)C$ corresponds to the response of the system to the various inputs of tracer. This flux is proportional to the tracer concentration in the reservoir. It exhibits first-order kinetics: $dC/dt = \text{constant} \times C$. It is mathematically analogous to the radioactive decay. $(k_w + k_p)$ is the time constant associated with the loss of the tracer and its dimension is the inverse of a time.

5.1.2 Case of Enzyme Kinetics

Tracer fluxes do not always follow zero- or first-order kinetics. The biological reactions catalyzed by enzymes have Michaelis–Menten type kinetics giving rise to a "hybrid" behavior tending toward zero- or first-order kinetics depending on the environmental conditions (Fig. 5.2). For a reaction AB + enzyme → A + B + enzyme, the reaction rate is

$$\frac{d\,[AB]}{dt} = \frac{V_{max}\,[AB]}{K_s + [AB]}, \tag{5.3}$$

where V_{max} is the maximum reaction rate and K_s the half-saturation constant.

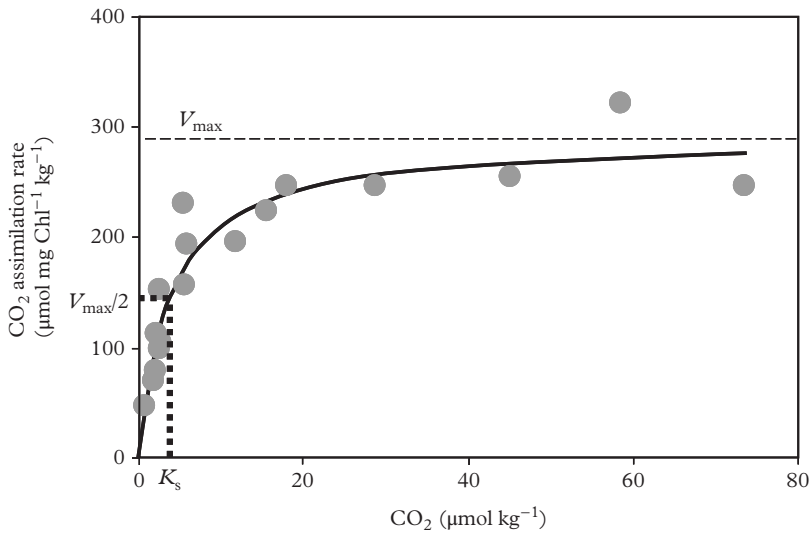

Figure 5.2 *Michaelis–Menten kinetics of CO_2 uptake by diatom Skeletonema costatum. Modified from Rost et al. (2003).*

When [AB] $\ll K_s$, then $\frac{d[AB]}{dt} \approx \frac{V_{max}}{K_s}[AB]$. The dissociation of each molecule of AB is quickly catalyzed by an enzyme. The more AB is abundant, the fastest the reaction is. It exhibits first-order kinetics. Its time constant is $\mu = V_{max}/K_s$.

When [AB] $\gg K_s$, then $\frac{d[AB]}{dt} \approx V_{max}$. Enzymes catalyzing the reaction are saturated by the abundance of AB. Increasing the AB concentration does not increase the reaction rate. It exhibits zero-order kinetics.

Between these two extreme cases, the relationship between [AB] and V_{max} is "non-linear." Nonlinear terms can introduce considerable difficulties in the resolution of equations.

5.1.3 Steady State

A system is at steady state when the concentration C is constant over time ($\frac{dC}{dt} = 0$). In this case

$$\underbrace{(k_w C_i + s)}_{\text{inputs}} - \underbrace{\left(k_w C + k_p C\right)}_{\text{removals}} = 0. \tag{5.4}$$

The tracer inputs are fully balanced by removals (see Problem 1). The concentration in the box is then

$$C_\infty = \frac{s + k_w C_i}{k_w + k_p}. \tag{5.5}$$

5.1.4 Residence Time

A tracer residence time in a box is the average time elapsing between entering and leaving the box. It is the time required to renew the tracer in the box. When a system is at steady state, the residence of a tracer is given simply by

$$\tau_{element} = \frac{Quantity}{\Sigma Flux\ in} = \frac{Quantity}{\Sigma Flux\ out}. \tag{5.6}$$

Note that

$$\tau_{element} = \frac{Quantity}{\Sigma Flux\ out} = \frac{VC}{FC + k_w CV} = \frac{1}{k_w + k_p}. \tag{5.7}$$

In equation (5.7), $k_w + k_p$ is equivalent to the decay constant in the radioactivity equation; $\tau_{element}$ is the characteristic response time of the system to a disturbance (it is called relaxation time in physics): an element having a very long residence time accumulates in the ocean and the cumulated stock is not sensitive to a transient change of the fluxes. Conversely, an element with a very short residence time is hardly or not stored in the ocean and a variation of the flux immediately causes a variation in the amount present in the ocean.

The residence time with respect to a given tracer flux is defined as the ratio between the quantity of tracer in the reservoir and this tracer flux at steady state

$$\tau_s = \frac{V \times C}{V \times s} = \frac{C}{s}; \text{ (residence time with respect to the source term)}$$

$$\tau_p = \frac{V \times C}{V \times C \times k_p} = \frac{1}{k_p}; \text{ (residence time with respect to the sink term)}$$

$$\tau_w = \frac{V \times C}{F \times C} = \frac{1}{k_w}. \text{ (residence time with respect to water transport)}$$

The residence times with respect to individual fluxes are greater or equal to the overall residence time. They represent the tracer residence time in the hypothetical case where there would be a single input or output flux in the reservoir. The shorter a residence time is, the more significant the control of the flux on the tracer quantity in the box is. The relative importance of the source and sink terms compared to *the transport terms* depends strongly on the chemical nature of the tracer: a soluble tracer that is not used by biological activity has a longer residence time τ_p than an insoluble element or a nutrient actively consumed by plankton. For soluble elements, τ is controlled by τ_w, while for more reactive elements, τ is controlled by τ_s and τ_p.

5.2 Dynamic Behavior of a Reservoir

Steady state is very often used as an *a priori* hypothesis of "common sense" as it allows solving the conservation equation simply. However, the relevance of this hypothesis may be difficult to check. In view of the uncertainties on the determination of the different fluxes, semi-quantitative agreement between the incoming and outgoing fluxes is often considered as a "proof" of the steady state. Some systems are clearly non-steady state: this is the case of the ocean carbon cycle, disrupted by the introduction of atmospheric CO_2, or transient tracers such as chlorofluorocarbons (CFCs), Pb, tritium and other nuclear tests products. Box models allow us to understand and predict the tracer dynamics that is strongly influenced by the inputs dynamics. We will consider several cases.

5.2.1 Constant Forcing

If inputs and outputs are not balanced in equation (5.2), the concentration C varies with time ($\frac{dC}{dt} \neq 0$) and the system is no longer in the steady state. When the tracer inputs ($s + k_w C_i$) are constant over time, the solution of the conservation equation is

$$C = C_0 \times e^{-[k_p + k_w] \times t} + \frac{s + k_w C_i}{k_p + k_w} \left(1 - e^{-[k_p + k_w] \times t}\right). \tag{5.8}$$

Introducing C_∞, we obtain

$$C = C_0 \times e^{-[k_P + k_W] \times t} + C_\infty \left(1 - e^{-[k_P + k_W] \times t}\right). \tag{5.9}$$

The concentration of the reservoir evolves between the initial concentration C_0 and the equilibrium concentration C_∞. The time constant associated with the return to equilibrium is

$$k_W + k_P = \frac{1}{\tau_{element}}. \tag{5.10}$$

In principle, steady state ($C = C_\infty$) is reached only after an infinite time. In practice, after a time equal to $3\tau_{element}$, the gap between C and C_∞ represents less than 5% of the initial difference between C_0 and C_∞: the system is close to steady state.

5.2.1.1 *Example: determining the scavenging rate of plutonium in surface waters*

Plutonium (Pu) was injected into the atmosphere during atmospheric nuclear tests. Pu concentrations in seawater (Fig. 5.3a) were analyzed after the ban of these tests, that is, when the external inputs of Pu became null ($s = 0$). Pu has a strong affinity for marine particles. The exponential decay of the Pu concentrations in Mediterranean

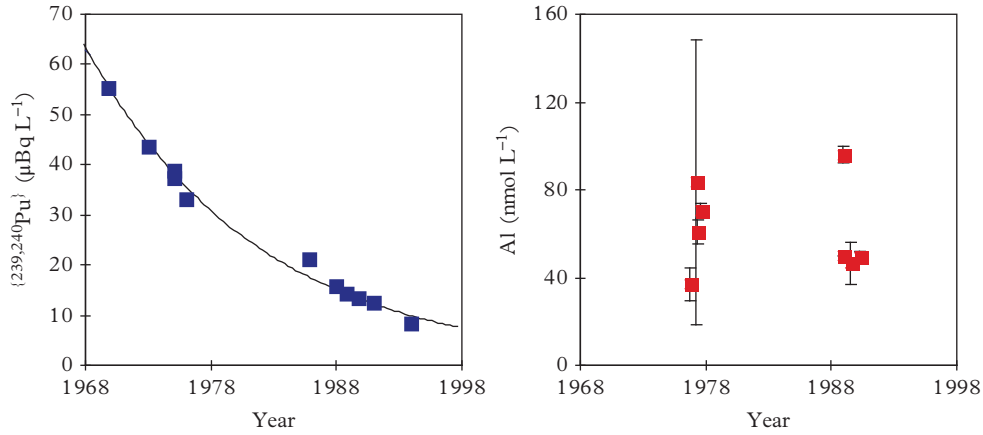

Figure 5.3 *Temporal evolution of the concentration of plutonium and aluminum in the surface waters of the Western Mediterranean Sea. (a) Plutonium (Papucci et al., 1996): in the 1950s and early 1960s atmospheric nuclear tests brought plutonium at the ocean surface, whereas it is normally absent. The temporal evolution of the Pu concentration in surface waters indicates a relaxation time of 14 y (continuous line). (b) Aluminum (data compiled from Caschetto and Wollast (1977) and Chou and Wollast (1997)).*

surface waters reflects the removal of Pu on marine particulate with first-order kinetics. Neglecting the effects of currents, we obtain $[\mathrm{Pu}] = [\mathrm{Pu}]_0 \times \mathrm{e}^{-k_\mathrm{p} \times t}$.

Aluminum is also eliminated by uptake on marine particles. However, the exponential decay is not seen as external inputs of Al compensate more or less regularly the scavenging effect, so that the system seems to be more or less at steady state on decades scale (Fig. 5.3b). Hence, Al residence time cannot be deduced from these data. Indeed, the long-term Al concentration is given by $[\mathrm{Al}] \approx [\mathrm{Al}]_\infty$.

Other examples are treated in Problems 2 and 3.

5.2.2 Temporal Evolution of the Forcings

The emission of industrial pollutants often increases more or less exponentially over time. This is the case of CO_2 and CFCs before their phasing out in 1996 (see Problem 4). We use equation (5.2), considering that the concentration C_i increases exponentially over time with a time constant κ: $C_\mathrm{i} \approx C_\mathrm{i}(0)\,\mathrm{e}^{\kappa t}$. If source and sink terms are zero in the reservoir, equation (5.2) becomes

$$\frac{\mathrm{d}C}{\mathrm{d}t} = -k_\mathrm{w} C + k_\mathrm{w} C_\mathrm{i}(0)\,\mathrm{e}^{\kappa t}. \tag{5.11}$$

The solution of this equation is (see the appendix to Chapter 4)

$$C = \left[C(0) - \frac{k_\mathrm{w} C_\mathrm{i}(0)}{k_\mathrm{w} + \kappa} \right] \mathrm{e}^{-k_\mathrm{w} t} + \frac{k_\mathrm{w} C_\mathrm{i}(0)}{k_\mathrm{w} + \kappa} \mathrm{e}^{\kappa t}. \tag{5.12a}$$

When $t \times k_\mathrm{w} \gg 1$, the first term of the right-hand side becomes negligible in equation (5.12a), so that

$$C = \frac{k_\mathrm{w} C_i(0)}{k_\mathrm{w} + \kappa} \mathrm{e}^{\kappa t} = \frac{k_\mathrm{w} C_\mathrm{i}}{k_\mathrm{w} + \kappa} \tag{5.12b}$$

and

$$k_\mathrm{w} = \frac{C/C_\mathrm{i}}{1 - C/C_\mathrm{i}} \kappa. \tag{5.12c}$$

The concentration evolves with a characteristic time of $1/\kappa$ imposed by anthropogenic inputs. The evolution of the system is located between two extreme cases:

- If $k_\mathrm{w} \gg \kappa$, then $C \approx C_\mathrm{i}$ (if water is renewed very quickly, the tracer concentration in the reservoir is identical to the concentration of the inflowing water).
- If $k_\mathrm{w} \ll \kappa$, then $C = \frac{k_\mathrm{w}}{\kappa} C_\mathrm{i}$ (if water is renewed slowly, the tracer-rich inflowing water is diluted by the tracer-poor water already present in the reservoir).

Example: determination of the NADW production rate in the Norwegian and Greenland Seas (Pickart et al., 1989)

CFCs (e.g., CFC-11) were used as coolants between 1950 and 1995. During this period, their use grew exponentially with a time constant of about 1/8.5 y^{-1}. These volatile molecules are transported in the atmosphere and then dissolved in the ocean so that surface waters have seen their concentration increase exponentially during this period. In the Norwegian and Greenland Seas, these CFCs are then transported by convection in intermediate water (Fig. 5.4). These intermediate waters flow over the Denmark and Iceland-Scotland Straits to form part of the North Atlantic Deep Waters (NADW).

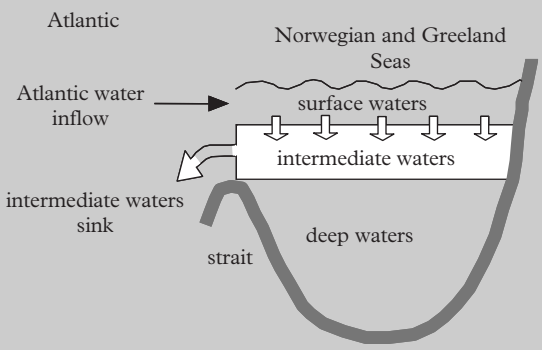

Figure 5.4 *Simplified representation of the formation of the North Atlantic deep water. In the Norwegian and Greenland Seas, CFC-rich surface water (0–200 m) from the Atlantic is mixed with CFC-poor intermediate waters. These intermediate waters flow over the Denmark and Iceland–Scotland Straits and they sink down to the seafloor in the North Atlantic. The effect of deep convection in the Norwegian and Greenland Seas is neglected because it has a relatively little effect on the CFC budget. After Pickart et al. (1989).*

In 1950, the CFC-11 surface and intermediate water concentrations were near zero. In 1983, the concentration in intermediate water was $C = 1.5$ pmol kg^{-1} while it was $C_i = 2.3$ pmol kg^{-1} in surface waters.

(a) Determine the residence time of the intermediate waters in Norwegians and Greenland Seas.

(b) Knowing that the intermediate waters cover a surface of 10^6 km^2 and are 400 m thick, determine their flux into the North Atlantic.

Answers:

(a) We assume that $t \times k_w \gg 1$. It can be inferred from equation (5.12c) that $k_w = \frac{C/C_i}{1-C/C_i}\kappa$

$= 0.22\ y^{-1}$

$= (4.5)^{-1}\ y^{-1}$.

The intermediate water residence time is $\tau_w = 4.5$ y.

Now, we must check that the assumption is well verified. CFC emissions have started around 1950 and measurements were made in 1983, so that $t = 33$ y. Therefore $t \times k_w = 5 \gg 1$.

(b) If the volume of the intermediate waters is $V = 4 \times 10^{14}$ m^3, their flux to the Atlantic $V/\tau_w = 2.8$ Sv (to be compared with the 30 Sv of the thermohaline circulation, see Chapter 10).

5.3 Box Models and Isotopic Tracers

The time constants associated with models are often poorly known. Radioactive tracers can be used to determine them.

5.3.1 Use of U and Th Decay Chains

The radioactive decay chains of U and Th have been presented in detail in Chapter 4. The source term is the radioactive production by the parent isotope ($\lambda_P C_P$), while the losses correspond to the radioactive decay of the daughter isotope ($\lambda_D C_D$) and another sink term ($k_p C_D$) for which the time constant must be estimated. The conservation equation reduces to

$$\lambda_P C_P - \lambda_D C_D - k_p C_D + k_w (C_{Di} - C_D) = 0. \tag{5.13}$$

Showing the activities

$$\{P\} - \{D\} + (-k_p \{D\} + k_w (\{D_i\} - \{D\}))/\lambda_D = 0. \tag{5.14}$$

For isotopes of short period, we neglect the water circulation term. k_p is then determined

$$k_p = \lambda_D \left(\frac{\{P\}}{\{D\}} - 1 \right). \tag{5.15}$$

5.3.1.1 Example: The rate of radon diffusion at the sea–air interface

Consider the transition $^{226}Ra \rightarrow {}^{222}Rn \rightarrow \ldots$. Ra is a soluble element while Rn is a gas. In deep waters, the ^{222}Rn activity is equal to the ^{226}Ra activity ($\{^{222}Rn\} = \{^{226}Ra\} = 6.7$ dpm/100 L) because all the gas produced disintegrates on the spot (Broecker and Peng, 1982). The only sink term is the radioactive decay; therefore $k_p = 0$. In mixed layer instead, the ^{222}Rn activity ($\{^{222}Rn\} = 4.7$ dpm/100 L) is lower than ^{226}Ra activity ($\{^{226}Ra\} = 6.7$ dpm/100 L): in surface waters, some ^{222}Rn is lost to the atmosphere. The time constant k_p associated with this sink is larger when the ^{226}Ra–^{222}Rn imbalance is stronger. According to equation (5.15), we obtain $k_p = 0.067$ d^{-1}, or a renewal time by diffusion of 15 d ($1/k_p$).

Note: in the case of gas diffusion, $k_p = v_p/h$ where h is the height of mixed layer and v_p is called the piston speed and it represents the speed of an imaginary piston pushing Rn to the atmosphere (see Chapter 5). We can then write

$$\lambda_{Rn-222} h(\{^{226}Ra\} - \{^{222}Rn\}) - v_p \times \{^{222}Rn\} = 0. \tag{5.16}$$

5.3.2 Using the Isotopic Composition of a Tracer

We apply the general model presented in Fig. 5.1 to the budget of a tracer with a major stable isotope (of concentration C) and a minor radioactive or stable isotope (of concentration C^*) characterized by an isotopic ratio $R = C^*/C$.

$$\begin{cases} \dfrac{dC}{dt} = k_w (C_i - C) + s - k_p C = 0, \\ \dfrac{dC^*}{dt} = k_w \left(C_i^* - C^*\right) + s^* - k_p C^* = \lambda \times C^*. \end{cases} \tag{5.17}$$

By introducing the isotopic ratio ($C^* = RC$), we get

$$\frac{d(RC)}{dt} = R\frac{dC}{dt} + C\frac{dR}{dt} = k_w (R_i C_i - RC) + R_s s - k_p RC - \lambda \times RC. \tag{5.18}$$

To simplify calculations, we assume that the major isotope is at steady state (C is constant) and that only the minor isotope evolves with time

$$k_w(C_i - C) + s - k_p C = 0. \tag{5.19}$$

Noting from equation (5.19) that $k_w C = k_p C + k_w C_i - s$, we obtain

$$\frac{dR}{dt} = \frac{1}{C}\left[k_w C_i (R_i - R) + s (R_s - R) - \lambda \times RC\right]. \tag{5.20}$$

If the minor isotope is also at steady state, equation (5.20) applied to a radioactive isotope becomes

$$k_w C_i (R_i - R) + s (R_s - R) - \lambda \times RC = 0, \tag{5.21a}$$

and for the stable isotopes

$$k_w C_i (R_i - R) + s (R_s - R) = 0. \tag{5.21b}$$

5.3.3 Application Exercise: Ventilation of the Deep Waters in the Red Sea

The Red Sea is an opening ocean characterized by an intense hydrothermal activity along the Red Sea ridge (Jean-Baptiste et al., 2004a). The circulation in the Red Sea is described in Fig. 5.5.

The deep waters are separated from the mixed layer by a very strong thermocline. In the Gulf of Suez, surface waters reach a sufficient density to sink to the bottom of the basin. It is also suspected that deep waters are renewed by diffusion /mixing at the base of the thermocline.

We want to determine the deep water residence time in the basin. Two tracers with very different sources are available: (1) anthropogenic ^{14}C is a transient tracer injected from surface and (2) mantle-derived ^{3}He is injected continuously from the seafloor by hydrothermal fluids. The confrontation of these two tracers should provide strong constraints on deep waters circulation.

5.3.3.1 The ^{3}He case

^{4}He concentrations are identical in surface and deep waters. However, hydrothermal fluids bring mantle-derived He that is strongly enriched in ^{3}He compared to atmospheric He. Surface waters contain atmospheric He. Therefore, there is strong ^{3}He enrichment in the deep waters compared to the surface waters. The 1000 km-long Red Sea ridge injects at the bottom of the basin a hydrothermal ^{3}He flux: $^{3}F_{\text{hydroth}} = 19$ mol y^{-1}.

Knowing that

- $\delta^{3}He_{\text{surface}} = 0$
- $\delta^{3}He_{\text{deep}} = +32\%$

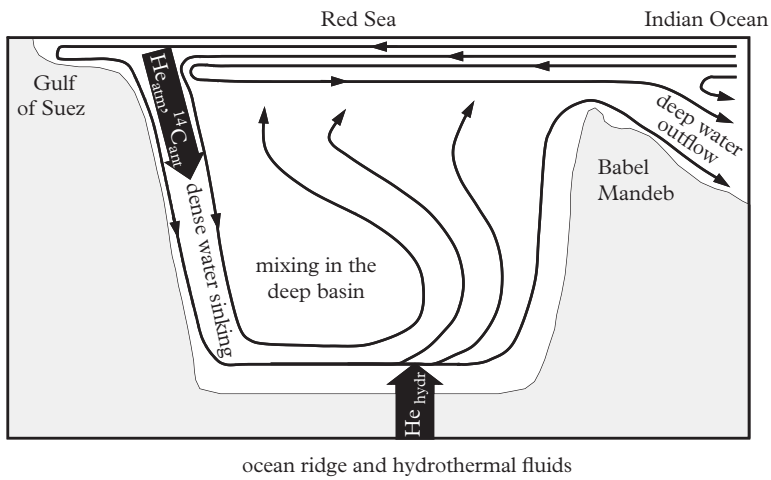

Figure 5.5 *Circulation and sources of tracers in the Red Sea.*

- $\delta^3He_{hydroth} = +750\%$
- $^4He_{surface} = {}^4He_{deep} = 1.7 \times 10^{-6}$ mol m^{-3}
- $(^3He/^4He)_{hydroth} = 1.18 \times 10^{-5}$ mol mol^{-1}
- hydrothermal ^{3}He flux: $^3F_{hydroth} = 19$ mol y^{-1}
- volume of the deep Red Sea: $V_d = 1.74 \times 10^5$ km^3

determine the residence time of the deep water in the Red Sea.

Answer:

^{4}He is the major helium isotope. There is a permanent hydrothermal activity in the Red Sea, so that the system is assumed to be at steady state. Therefore, equation (5.21b) is used. ^{3}He and ^{4}He are neither radioactive nor consumed by living beings, so that there is no He sink in the deep waters. The hydrothermal flux of helium is treated as a term source

$$s = \frac{^4F_{hydroth}}{V_d} = \frac{^3F_{hydroth}}{(^3He/^4He)_{hydroth} \times V_d}. \tag{5.22}$$

Equation (5.21b) reduces to

$$k_w \times \left[^4He\right]_{surf} \times \left(\delta^3He_{surf} - \delta^3He_{deep}\right) + \frac{^3F_{hydroth}}{\left(\frac{^3He}{^4He}\right)_{hydroth} \times V_d} \times \left(\delta^3He_{hydroth} - \delta^3He_{deep}\right) = 0. \tag{5.23}$$

Hence

$$k_w = -\frac{^3F_{hydroth}}{\left[^4He\right]_{deep} \times V_d \times \left(\frac{^3He}{^4He}\right)_{hydroth}} \times \frac{\delta^3He_{hydroth} - \delta^3He_{deep}}{\delta^3He_{surface} - \delta^3He_{deep}}. \tag{5.24}$$

Using numerical values: $k_w = \frac{1}{7y}$.

The deep water residence time estimated for helium is 7 y. Helium isotopes are not radioactive, so they do not allow determination of k_w directly. They only serve to compare the hydrothermal He flux, which is known, and the atmospheric He flux brought by the sinking surface waters.

5.3.3.2 The ^{14}C case

The temporal evolution of Δ^{14}C of surface waters in the region of deep water formation (Gulf of Suez) is determined by analyzing the Δ^{14}C of annual growth bands of corals living in surface waters (Fig. 5.6).

An oceanographic campaign shows that in 1977 the average Δ^{14}C in deep waters was $\Delta^{14}C^{final}_{deep} = -18.6$ ‰.

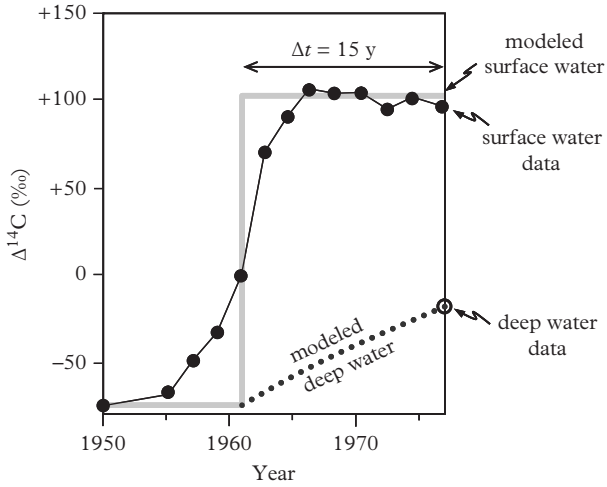

Figure 5.6 *Evolution of $\Delta^{14}C$ of surface waters. Black circles: analysis of coral of known age. Continuous gray curve: approximated evolution of $\Delta^{14}C$ used in the model. Black dotted curve: modeled evolution of $\Delta^{14}C$ in deep waters (equation 5.26).*

We assume that:

* The total inorganic carbon (DIC) is at steady state.
* Biological carbon fluxes are neglected.
* $(\Delta^{14}C_{\text{deep water}})_{1950} = (\Delta^{14}C_{\text{surface water}})_{1950} = -75‰$.

Answer:
We consider the following simplifications:

(1) Particulate organic carbon fluxes being negligible, $DIC_{deep} \approx DIC_{surface}$.

(2) Fifteen years after the peak of the atmospheric nuclear tests, the $\Delta^{14}C$ of deep water is significantly modified by anthropogenic ^{14}C. Water residence time must be of the order of a few decades. Therefore, we neglect the radioactive decay in the calculation.

(3) We approximate the time evolution of $\Delta^{14}C$ of surface waters by a staircase function (see dots on Fig. 5.6):
   - If $t < 1962$: $\Delta^{14}C^{\text{initial}}_{\text{surface}} = -75‰$.
   - If $t \geq 1962$: $\Delta^{14}C^{\text{final}}_{\text{surface}} = +100‰$.

(4) As radioactive decay is negligible, we assume that before the arrival of anthropogenic ^{14}C, $\Delta^{14}C^{\text{initial}}_{\text{surface}} = \Delta^{14}C^{\text{initial}}_{\text{deep}} = -75‰$.

The conservation of ^{14}C is given by equation (5.20) as

$$\frac{d\Delta^{14}C_{deep}}{dt} \approx k_w(\Delta^{14}C_{surface} - \Delta^{14}C_{deep}), \tag{5.25}$$

where k_w is the inverse of water residence time.

Hence

$$\Delta^{14}C_{deep}^{final} = \Delta^{14}C_{deep}^{initial} e^{-k_w t} + \frac{k_w \Delta^{14}C_{surface}^{final}}{k_w}\left(1 - e^{-k_w t}\right) \tag{5.26}$$

and

$$k_w = \ln\left(\frac{\Delta^{14}C_{deep}^{final} - \Delta^{14}C_{surface}^{final}}{\Delta^{14}C_{deep}^{initial} - \Delta^{14}C_{surface}^{final}}\right) \times \frac{1}{t}. \tag{5.27}$$

With $t = 15$ y, we obtain $k_w \approx (40y)^{-1}$.

The deep water residence time estimated with ^{14}C is 40 y.

5.3.3.3 Compare the two methods. What can you learn?

The ^{14}C residence time is 6.5 times higher than the He isotope residence time. Even if the hydrothermal He flux is not known with a great precision, it is unlikely that it is overestimated by a factor of 6.5!

How can the difference between these two residence time estimates be explained? It might be that direct sinking of dense surface water in the deep basin represents only a small fraction of the deep waters renewal. Most of the water from the surface could come from the base of the thermocline. The very strong increase in density between the top and the base of the thermocline results in a long transit time through the thermocline. We will see in Chapter 6 that it is typically of the order of a few decades. Anthropogenic ^{14}C is a transitory tracer: between 1954 and 1977, the thermocline waters had low anthropogenic ^{14}C concentration (anthropogenic ^{14}C had not yet time to diffuse downward), so that only convection in the Gulf of Suez area brought significant amounts of ^{14}C anthropogenic in the deep basin. On the contrary, helium is at steady state: the δ^3He balance reflects atmospheric helium transport through the thermocline waters (main water flux) and through convection (smaller water transport).

Other examples are treated in Problems 5 and 6.

5.4 Dynamics of Coupled Boxes

So far, we have studied the tracer behavior in a single box. When a system is described by several boxes, the same approach remains valid. However, features related to the box coupling appear. We consider the effect of this coupling on the simplest possible system: two reservoirs exchanging in a closed system. The ocean being generally an open system, we will consider here an *in vitro* experiment for which we know that the system is closed. We aim to determine the kinetics of manganese dissolution during degradation

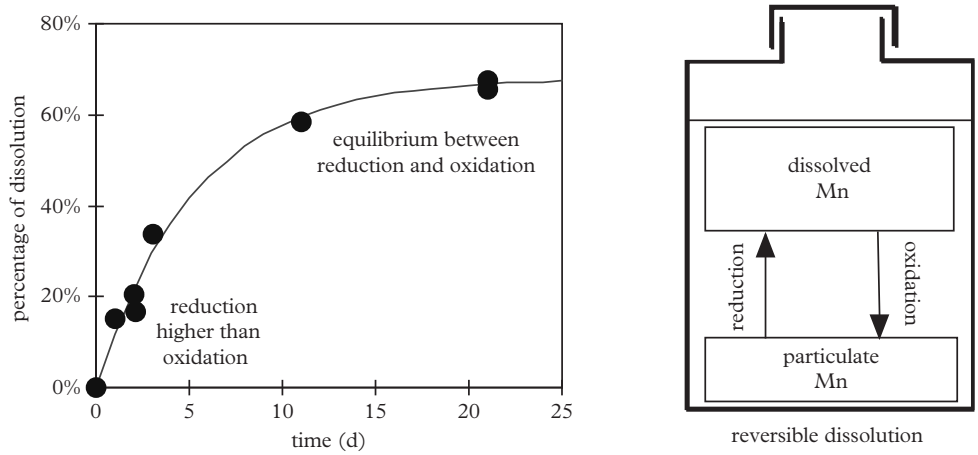

Figure 5.7 *Evolution of the percentage of Mn dissolution during an* in vitro *experiment of degradation of large marine particles and conceptual scheme of dissolution/precipitation. Marine particles are collected by filtration and then dispatched in different bottles of seawater. The bottles are left at constant temperature and in the dark to prevent photosynthesis. After different incubation times, the incubation solution and residual particles of a bottle are separated by filtration and analyzed. The evolution of the percentage of Mn dissolution with time is obtained with the concentrations of dissolved and particulate Mn (equation 5.28). By adjusting the values of* f^{max} *(= 68%) and* $k_{red} + k_{ox}$ *(= 5.3* d^{-1}*), a good agreement is obtained between experimental data and the model. Modified from Arraes-Mescoff et al. (2001).*

of large marine particles (fecal pellets, aggregates and detritus) under controlled conditions (constant temperature, no photosynthesis). This dissolution occurs by reduction of MnO_2 (solid) into soluble Mn^{2+} ion. In addition, some bacteria can oxidize Mn^{2+} into MnO_2 which lead to Mn precipitate on marine particles. The evolution of the fraction f of particulate Mn which dissolves over time is determined experimentally (Fig. 5.7)

$$f(t) = \frac{[\mathrm{Mn_d}](t) - [\mathrm{Mn_d}]^{\mathrm{initial}}}{[\mathrm{Mn_p}]^{\mathrm{initial}}}, \tag{5.28}$$

where $[\mathrm{Mn_d}]$ and $[\mathrm{Mn_p}]$ are the dissolved and particulate Mn concentrations both expressed relative to the total volume of solution.

Assuming that Mn dissolution and precipitation follow first-order kinetics, the conservation equations are

$$\begin{cases} \dfrac{\mathrm{d}[\mathrm{Mn_p}]}{\mathrm{dt}} = -k_{\mathrm{red}}[\mathrm{Mn_p}] + k_{\mathrm{ox}}[\mathrm{Mn_d}], \\ \dfrac{\mathrm{d}[\mathrm{Mn_d}]}{\mathrm{dt}} = +k_{\mathrm{red}}[\mathrm{Mn_p}] - k_{\mathrm{ox}}[\mathrm{Mn_d}]. \end{cases} \tag{5.29}$$

where k_{ox} and k_{red} are the time constants associated with the oxidation and reduction of manganese. At steady state, the Mn flux between two reservoirs is $k_{red}\left[Mn_p\right] = k_{ox}\,[Mn_d]$. It can be easily checked that the Mn residence time in the particulate and dissolved phases are $\tau_d = \frac{1}{k_{ox}}$ and $\tau_p = \frac{1}{k_{red}}$, respectively.

What is then the response time to a disturbance? As there is no input or removal of Mn in the system, the total amount of Mn in the system is constant: $[Mn_{total}] = [Mn_d] + [Mn_p] = [Mn_d]^{initial} + [Mn_p]^{initial}$.

It follows that

$$\begin{cases} [Mn_p](t) = [Mn_p]^{initial} e^{-(k_{red}+k_{ox})\times t} + \dfrac{k_{ox}}{k_{red}+k_{ox}}[Mn_{total}]\left(1 - e^{-(k_{red}+k_{ox})\times t}\right), \\ [Mn_d](t) = [Mn_d]^{initial} e^{-(k_{red}+k_{ox})\times t} + \dfrac{k_{red}}{k_{red}+k_{ox}}[Mn_{total}]\left(1 - e^{-(k_{red}+k_{ox})\times t}\right). \end{cases} \tag{5.30}$$

The characteristic time to return to equilibrium (relaxation time) of the coupled system is

$$\tau = \frac{1}{k_{red}+k_{ox}} = \frac{\tau_p \tau_d}{\tau_p + \tau_d}. \tag{5.31}$$

τ is smaller than the residence time of each box taken separately. If there were no oxidation, Mn particulates would dissolve completely and only τ_p would control the dynamical behavior of the system. In fact, a balance is established between the oxidation and reduction *before* the total dissolution of particulate Mn: therefore $\tau < \tau_p$. Similarly, the equilibrium is reached prior to the total oxidation of dissolved Mn. Therefore, $\tau < \tau_d$.

Combining equations (5.29) and (5.31), we obtain f, the fraction of dissolved Mn:

$$f(t) = f^{max}\left(1 - e^{-(k_{red}+k_{ox})\times t}\right) \text{ with } f^{max} = \frac{\frac{k_{red}}{k_{red}+k_{ox}}[Mn_{total}] - [Mn_d]^{initial}}{[Mn_p]^{initial}}. \tag{5.32}$$

Choosing $f^{max} = 68\%$ and $k_{red} + k_{ox} = 5.3\ d^{-1}$, a good agreement is obtained between the data and the model.

5.5 Mean Age, Residence Time and Reservoir Age of a Tracer

The mean age (τ_a) of a tracer in a reservoir that is the average time that a tracer has already spent in the reservoir since it arrived in the reservoir. It corresponds to questions such as: how long marine particles are suspended in the ocean mixed layer or how long a water mass is isolated from the atmosphere. The residence time (τ_r, also called transit time) and the mean age (τ_a) of a tracer in a box are two different concepts. The relationship between τ_a and τ_r depends on the type of transport of the tracer in the box (Fig. 5.8). Consider the analogy of people standing in the line at the Oceanographic Museum: every visitor is a tracer molecule and the reservoir is the queue. The residence

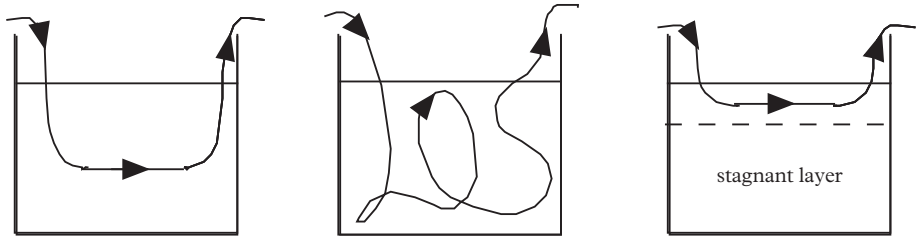

Figure 5.8 *Influence of transport processes on the relationship between residence time and the average age of the tracer in the reservoir.*

time is the average time that a person spends in the queue to buy his ticket while the average age is the average time that all of the people in the line have already passed in this line. Consider the behavior of different types of visitors:

- If visitors are disciplined, they wait their turn to buy their ticket. In this case, the visitor buying his ticket will have spent a time τ_r in the queue, whereas all the visitors still in the line have not yet waited for so long. Therefore, $\tau_a < \tau_r$. This is what happens when a water mass flows without being mixed by turbulence (we will return to this concept in Chapter 6) or when particle sinking in deep ocean away from turbulence.
- If visitors are very unruly, they constantly cut the line, so the order to buy tickets is independent of the order of starting in the line. In this case, $\tau_a = \tau_r$. This situation occurs whenever a reservoir is well mixed as, for example, in the surface mixed layer.
- Now consider a mix of disciplined and unruly visitors. Unruly visitors cut the line and buy quickly their tickets, whereas disciplined visitors remain for ages in the line. The average waiting time of those present in the line is much higher than the average time required to buy a ticket if you jump ahead people: $\tau_a > \tau_r$. For example, in the ocean most of particulate matter is quickly transported by large marine particles from the surface to the sediment and only very small particles that hardly settle are found in the water column.

Assimilating the age of a radioactive tracer to the renewal time of a reservoir can bias the results significantly (see Problem 7).

Finally, we note that the average time spent by visitors in the queue is *a priori* unrelated to the time elapsed since their birth. This means that the mean age of a tracer in a box is not necessarily its real age calculated from his birth date. This distinction is particularly important in the case of ^{14}C. The absolute age of the carbon in a given reservoir is called "reservoir age." It is calculated from the deficit in ^{14}C of the reservoir compared to

atmospheric ^{14}C. For example, the reservoir age of surface ocean water is the result of the production rate of ^{14}C in the atmosphere, exchange of carbon between the ocean and the atmosphere and upwelling of intermediate waters that contain old carbon. Before 1950, the reservoir age of carbon in the surface waters was of the order of 400 y ($\Delta^{14}C = -50‰$) while the average age of the carbon in the surface waters (equal to its residence time) was of the order of one year. Even taking into account the reservoir age, the apparent age of a radioactive tracer can be significantly different from residence time (Problem 6).

PROBLEMS

Problem 1: Abundance of ^{14}C in the atmosphere (Kovaltsov et al., 2012)

The production rate of ^{14}C in the atmosphere is estimated to be ~120 atoms cm^{-2} min^{-1}. Calculate the amount of ^{14}C present at the Earth's surface (expressed in number of atoms, in moles and in g). ^{14}C is mixed with atmospheric, biospheric and oceanic ^{12}C. These three reservoirs represent approximately 40,000 Gt of ^{12}C. Deduce the average $^{14}C/^{12}C$ ratio of the ocean–biosphere–atmosphere system.

Problem 2: Deep water formation in the Mediterranean Sea (Andrie and Merlivat, 1988)

In the Western Mediterranean Sea, the winter cooling of surface waters (0–450 m) leads to the formation of dense water that flow down in the deep basin (450–2000 m). It is assumed that the deep waters are fed by water from the base of the thermocline (~ 450 m depth) and that the formation of new deep water is balanced by deep water removal at the Gibraltar Strait. Between 1971 and 1981, the tritium concentration at the base of the thermocline remained constant (C_s = 3.3 TU). During the same period, the tritium concentration of water deeps (C_d) rises from 1.6 TU to 2.2 TU. Assuming that the deep reservoir is well mixed, what is the water residence time in the deep Western Mediterranean Sea?
Tritium's half-life is 12.4 y.

Problem 3: Artificial ocean fertilization (Abraham et al., 2000)

In HNLC (High Nutrients and Low Chlorophyll) areas, the development of the biomass areas is limited by the absence of iron (see Chapter 7). During an artificial fertilization experiment in the Southern Ocean, dissolved iron is injected in the surface waters to enhance the biological production. Then, the evolution of chlorophyll is monitored. In the iron-fertilized area, the chlorophyll concentration grows following first-order kinetics with respect to the chlorophyll concentration. The time constant μ ranges between 0.1 and 0.2 d^{-1}.

(1) Assuming that fertilized waters are not diluted by the surrounding waters and neglecting grazing by zooplankton, determine the evolution of the chlorophyll concentration over time as a function of μ.

(2) The loss of chlorophyll due to the phytoplankton grazing by zooplankton follows first-order kinetics with respect to chlorophyll concentration with a time constant $k = 0.01\ d^{-1}$. Is it reasonable to ignore its effect?

(3) In order to estimate the chlorophyll dilution by non-fertilized water, a known amount of SF_6 (a passive tracer) was injected together with iron. In the fertilized area, the SF_6 concentration is divided by two in 10 days. What is the value of k_w (time constant for the water renewal in the fertilized area)?

(4) Assuming that the initial chlorophyll concentrations in the fertilized and surrounding unfertilized area waters were identical and that the concentration of the non-fertilized surrounding waters has remained constant during the experiment, determine the conservation equation of chlorophyll in the fertilized zone.

(5) Deduce the evolution of the chlorophyll concentration over time as a function of μ.

(6) Knowing that during the experiment, the chlorophyll concentration has increased by a factor of six in 10 days, what is the value of μ?

Problem 4: CFCs and oxygen in the Marmara Sea (Lee et al., 2002)

The Marmara Sea is located between the Mediterranean Sea (Dardanelles Strait) and Black Sea (Bosphorus Strait). The deep basin of the Marmara Sea (100–500 m deep) is relatively isolated from surface waters (0–100 m). To determine the rate of oxygen consumption in the deep basin, O_2 and CFC were measured in 1988 (Table 5.1).

Table 5.1 *O_2 and CFC in the Marmara Sea*

	CFC-12 (pmol kg^{-1})	O_2 (μmol kg^{-1})
Surface waters	1.46 ± 0.01	244
Deep waters	0.74 ± 0.08	38

Until 1988, the CFC-12 concentration in the atmosphere (and therefore in surface waters) increased approximately exponentially with a time constant $\kappa_{CFC\text{-}12} = 1/14\ y^{-1}$.

(1) Determine the conservation equation of CFC-12 in deep waters and deduce the water residence time in the basin.

(2) Organic matter oxidation by bacteria is represented by a sink term p independent of the O_2 concentration. O_2 is assumed to be at steady state. Write the conservation equation of O_2 and determine the value of p.

Problem 5: Dissolved organic carbon in the ocean (Druffel et al., 1992)

The oceanic dissolved organic carbon (DOC) is the main reservoir of organic carbon on Earth. It is therefore important to constrain its cycle. The DOC is produced in surface water by biological activity and destroyed by bacterial respiration in the deep ocean.

(1) Knowing that the DOC concentration in the surface water is of the order of 50–60 μmol kg^{-1} while it is of the order of 40 μmol kg^{-1} in the deep ocean, determine the balance of DOC fluxes in the deep ocean. Determine DOC residence time with respect to bacterial respiration (use first-order kinetics). Consider that water residence time in the deep ocean is approximately 1000 y.

(2) ^{14}C has been analyzed in the DOC in North Atlantic deep waters ($\Delta^{14}C_{NA}$ = –300‰) and North Pacific deep waters ($\Delta^{14}C_{NP}$ = –500‰). Are these isotopic results consistent with results of question 1?

Problem 6: Deep mixing in the Andaman Basin (Dutta et al., 2007; Okubo et al., 2004)

The Andaman Basin is located in the North Indian Ocean. It is bordered to the North by Burma, to the East by Thailand and Malaysia and to the West by the Andaman and Nicobar Islands that separate them from the Gulf of Bengal. The basin average depth is about 1000 m, but it can be 4000 m deep locally. We want to determine the water renewal rate in the deep basin (depth greater than 1600 m) using these two tracers: ^{14}C and ^{230}Th.

(1) Seawater temperature and salinity are homogeneous in the deep basin and this water comes from 1400 m. The average $^{14}C/^{12}C$ ratio of seawater is given in Table 5.2. It is assumed that the total inorganic carbon concentration is identical at 1400 m and in deeper waters (particulate carbon remineralization is neglected). Write the conservation equation of ^{14}C in the deep basin and deduce water residence time. The half-life of ^{14}C is 5730 y.

(2) We want to test the previous result with ^{230}Th.^{230}Th is produced uniformly by disintegration of ^{234}U which has a constant concentration in seawater. The production rate of ^{230}Th is $\Gamma = 0.56 \times 10^{-15}$ g kg^{-1} y^{-1}.^{230}Th is radioactive and its half-life is 7.56×10^4 y. The concentration of ^{230}Th being constant in the deep basin, ^{230}Th transport by scavenging on marine particles is negligible (see Chapter 10). Write the conservation equation of ^{230}Th in the deep basin and determine the water residence time in the deep basin.

(3) Compare the two methods.

Table 5.2 *^{14}C and ^{230}Th in the Andaman Sea*

	1400 m	Deep Basin
$(^{14}C/^{12}C)_{sample}/(^{14}C/^{12}C)_{atm}$	0.832 ± 0.004	0.827 ± 0.004
^{230}Th (10^{-15} g kg^{-1})	12 ± 1	14 ± 1

Problem 7: Residence time and apparent age of radioactive tracers (Deleersnijder et al., 2001)

The apparent age of a radioactive tracer in a reservoir (like the deep ocean) is often used to estimate the water residence time in this reservoir. The purpose of the exercise is to show that it can induce errors.

We consider a chemically inert radioactive tracer in a well-mixed reservoir. The concentration of the tracer is C; λ is its disintegration constant. The volume of the reservoir is noted V. A constant water flux F renews the contents of the reservoir. The concentration of the incoming water is C_0.

(1) Assuming that the system is at steady state, determine the relationship between C and C_0.

(2) The apparent tracer age (Δt) is given by the relationship

$$C = C_0 \times \exp(-\lambda \times \Delta t\,).$$

Explain where does this formula come from? Determine the relationship between Δt and the water residence time in the reservoir ($\tau_w = 1/k_w$).

(3) What is the condition for $\Delta t \approx \tau_w$?

(4) Show that in certain conditions, $\Delta t \ll \tau_w$. What can you conclude?

6

Advection–Diffusion Models

The ocean is a turbulent environment in which waters are mixed continuously. This mixing yields tracer concentrations that evolve smoothly across the ocean. Box models studied in Chapter 5 divide the ocean into a few boxes with supposedly uniform concentrations, which does not allow a very accurate representation of the tracer distribution. This can be avoided by dividing the system in smaller and smaller boxes. Thus, in this chapter, we will consider the conservation equation for a very small box and describe more specifically transport processes and sources and sinks. This equation, called the advection–diffusion equation, can be solved to determine the changes of tracer concentration with space and time. We will use it for water mass and marine particle transport modeling and sediment diagenesis. The Green's theorem demonstrates that box models and advection–diffusion equations are two equivalent forms of the mass conservation equation.

6.1 An Infinitesimal Box

We present the advection–diffusion equation in an intuitive way by first considering the transport of matter in one direction, and then generalizing it to three dimensions. We consider a fixed and infinitely small ocean volume, $\mathrm{d}V = \mathrm{d}x\mathrm{d}y\mathrm{d}z$, containing a tracer concentration C (Fig. 6.1). This concentration can vary over time due to water or marine particle motion and the production or the destruction of the tracer within the considered volume.

The tracer flux F (of components F_x, F_y, F_z) flows across the volume. We want to determine the evolution of the amount of tracer in the volume $\mathrm{d}V$ over time. Considering the flux along the x-axis, the flux of tracer flowing into the box is

$$F_{\text{in}} = F_x \mathrm{d}y\mathrm{d}z. \tag{6.1a}$$

The flux of tracer flowing out of the box is

$$F_{\text{in}} = (F_{x+\mathrm{d}x})\,\mathrm{d}y\mathrm{d}z \approx \left(F_x + \left(\frac{\partial F_x}{\partial x}\right)\mathrm{d}x\right)\mathrm{d}y\mathrm{d}z. \tag{6.1b}$$

first-order Taylor's expansion

Marine Geochemistry. First Edition. Matthieu Roy-Barman and Catherine Jeandel.

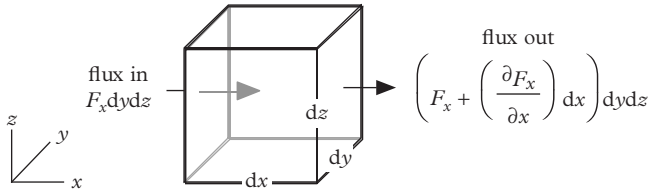

Figure 6.1 *Representation of a box of infinitesimal volume dV and of size dx, dy and dz, crossed by a water flux F_x along the x-axis.*

The net tracer flux is

$$F_{\text{in}} - F_{\text{out}} \approx F_x \mathrm{d}y\mathrm{d}z - \left(F_x + \left(\frac{\partial F_x}{\partial x}\right)\mathrm{d}x\right)\mathrm{d}y\mathrm{d}z = -\left(\frac{\partial F_x}{\partial x}\right)\mathrm{d}x\mathrm{d}y\mathrm{d}z. \tag{6.2}$$

If the tracer concentration in the box is C, the amount of tracer in the box is $C\mathrm{d}x\mathrm{d}y\mathrm{d}z$. Using the conservation equation, we write that the change of the amount of tracer with time is equal to what enters in the box minus what comes out of the box, that is, the net flux of tracer through the box

$$\frac{\mathrm{d}(C\mathrm{d}x\mathrm{d}y\mathrm{d}z)}{\mathrm{d}t} = F_{in} - F_{out} = -\left(\frac{\partial F_x}{\partial x}\right)\mathrm{d}x\mathrm{d}y\mathrm{d}z. \tag{6.3}$$

As the box size does not change over time, equation (6.3) can be divided by $\mathrm{d}x\mathrm{d}y\mathrm{d}z$:

$$\frac{\mathrm{d}C}{\mathrm{d}t} = -\left(\frac{\partial F_x}{\partial x}\right). \tag{6.4}$$

We now have to describe the physical nature of the fluxes. Thinking to water flow in the ocean, the first image that comes to mind is ocean currents. At first glance, one might consider these currents as "laminar" regular flows, where the speeds of nearby volumes of water are parallel. Looking closer, it appears that currents are full of eddies, so that directions and intensities of speeds are highly variable. This turbulence produces water stirring without a preferred direction of transport. Regular movements (called advection) and turbulent movements (called diffusion) induce transport of water and tracers that we are going to quantify.

6.2 Advection

The relationship between advection and the water flux is fairly intuitive. Consider water moving at a speed u along the x-axis. During the time interval $\mathrm{d}t$, the fluid moves through a distance $u\mathrm{d}t$ so that a volume $u\mathrm{d}t\mathrm{d}y\mathrm{d}z$ flows through the $\mathrm{d}y\mathrm{d}z$ surface which

is perpendicular to u. The amount of tracer flowing through this surface during the time interval $\mathrm{d}t$ is

$$\mathrm{d}q = Cu\mathrm{d}t\mathrm{d}y\mathrm{d}z. \tag{6.5}$$

The tracer flux is the amount of tracer passing per unit of time and surface

$$F = \mathrm{d}q/\mathrm{d}t/(\mathrm{d}y\mathrm{d}z) = Cu. \tag{6.6}$$

Hence,

$$\frac{\mathrm{d}C}{\mathrm{d}t} = -\frac{\mathrm{d}\,(uC)}{\mathrm{d}x}. \tag{6.7}$$

Water is an incompressible fluid, all the water that flows in the volume $\mathrm{d}V$ must be balanced by water flowing out of $\mathrm{d}V$. If advection occurs only along the x-axis, it implies that u is constant, so that

$$\frac{\mathrm{d}C}{\mathrm{d}t} = -u\frac{\mathrm{d}C}{\mathrm{d}x}. \tag{6.8}$$

$\mathrm{d}C/\mathrm{d}x$ is the gradient of concentration along the x-axis. If u and $\mathrm{d}C/\mathrm{d}x$ have the same sign (the concentration increases in the flow direction), it corresponds to a decrease of the tracer concentration in the box over time (Fig. 6.2).

This formulation of the flux is not specific to advection. It occurs when matter is transported along a preferential direction as in the case of the transport of elements by particle settling in the water column or accumulating in the sediment.

Consider particles in the water column. Their concentration (expressed in mass of particle per unit of volume of water, e.g., g m^{-3}) is m and their settling velocity is w_p (in m s^{-1}). The tracer concentration in the particles is c_p (expressed in mass of tracer per mass of particles, e.g., μg g^{-1}). C_p is the concentration of particulate tracer per volume of water $C_\mathrm{p} = mc_\mathrm{p}$ (in μg m^{-3}). The flux of tracer (in μg m^{-2} s^{-1}) due to particle settling is

$$F_\mathrm{p} = w_\mathrm{p}mc_\mathrm{p} = w_\mathrm{p}C_\mathrm{p}.$$

The conservation of mass equation is therefore written as

$$\frac{\mathrm{d}C_\mathrm{p}}{\mathrm{d}t} = -\frac{\mathrm{d}\left(w_\mathrm{p}C_\mathrm{p}\right)}{\mathrm{d}z}. \tag{6.9}$$

If the settling rate of particles is constant, it simplifies to

$$\frac{\mathrm{d}C_\mathrm{p}}{\mathrm{d}t} = -w_\mathrm{p}\frac{\mathrm{d}C_\mathrm{p}}{\mathrm{d}z}. \tag{6.10}$$

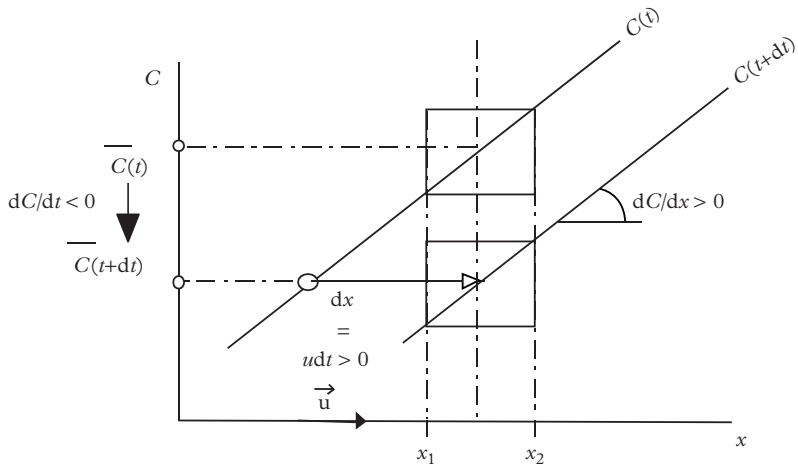

Figure 6.2 *Effect of advection on the evolution of the average tracer concentration C in a fixed volume. dC/dx is the concentration gradient and u is the velocity along the x-axis. During the time interval "dt" a small volume of water (white circle) is advected over a distance dx = u × dt (white arrow). Here, u and dC/dx are positive, which produces a decrease of the average concentration C between t and t + dt. This explains the "–" sign in the conservation equation.*

This last hypothesis is equivalent to the "u = constant" assumption made for the transport of dissolved tracers which reflects the water flux conservation. However, while the water flux is conservative because water is incompressible, the particle flux is not necessarily conservative. The transformations of marine particles (aggregation, disaggregation, dissolution, etc.) can lead to strong variations of the settling rate. It is, therefore, a very convenient hypothesis for calculations but not a necessarily verified one.

6.3 Molecular Diffusion

6.3.1 Random Walk

The path of a molecule in a liquid or a gas is unpredictable because it is frequently modified by shocks with other molecules. The movement of a given molecule is therefore "random." As shocks occur in all directions, overall they do not induce a preferential direction of motion. The random motion of each molecule of dissolved tracer in all directions has important consequences for the overall behavior of many tracers.

Consider a piece of sugar in a glass of water (Fig. 6.3). The sugar dissolves at the bottom of the glass to produce molecules of sugar. Initially, the concentration is high at the bottom of the glass while it is zero at the surface. After some time, even without stirring, water will become uniformly sweet. Once it is dissolved, sugar molecules move

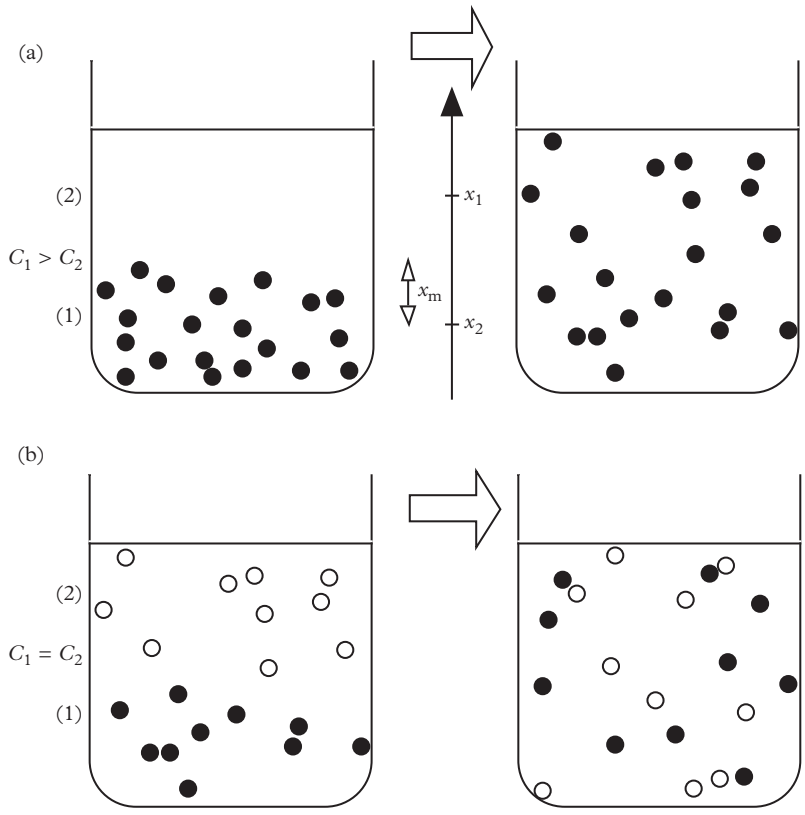

Figure 6.3 *Effect of molecular diffusion on the movement of sugar molecules in water. (a) System out of balance: the net flux across the dotted surface is non-zero, because there is a difference in concentration between the two parts of the glass* ($F_{1\to 2} = -D(C_2 - C_1)/\Delta x > 0$). *(b) System at equilibrium: molecules pass through the dashed line in their random walk but the net flux through the dashed line is null: as the concentration is homogeneous in the glass, the molecules going up balance descending ones* ($F_{1\to 2} = -D(C_2 - C_1)/\Delta x = 0$).

"randomly" and they spread in all the available space eventually. When the concentration has become uniform, molecules do not stop to move, but the motion of molecules going upward is balanced by molecules going downward, so the concentration remains uniform in the glass.

6.3.2 The Fick Law

The net flux across a surface separating two regions in the glass is proportional to the concentration difference between these two regions: when the concentration difference

Table 6.1 *Molecular diffusion coefficient of different gases in seawater*

Gas	Molar Mass	Diffusion Coefficient (10^{-5} cm^2 s^{-1})	
	(g mol^{-1})	at 0°C	at 25°C
He	4	3.0	5.8
O_2	32	1.2	2.3
CO_2	44	1.0	1.9
Rn	222	0.7	1.4

is large, the flux of molecules moving from the high concentration region toward the low concentration region is not balanced by a flux of molecule going from the low concentration region to the high concentration region. The flux is stronger when the distance between the two areas is smaller because the motion of molecules has quickly a significant effect. Net flux is given by

$$F = -D\frac{(C_2 - C_1)}{(x_2 - x_1)} = -D\frac{\mathrm{d}C}{\mathrm{d}x}. \tag{6.11}$$

This is the first Fick law. D is the molecular diffusion coefficient. It is expressed in cm^2 s^{-1}. For a given tracer, D is constant and identical in all directions (isotropic). The speed of the molecules increases with temperature (thermal agitation); D increases by a factor of 2 when the temperature goes from 0°C to 25°C (Table 6.1). D depends on the size and the chemical nature of the tracer. Small molecules move faster and more easily than large ones, so they have higher diffusion coefficients.

The unit of D is not familiar. However, $D/\Delta x$ has the unit of a speed. By analogy with the expression of the flux in the case of advection, we can write

$$F = -\frac{D}{(x_2 - x_1)}(C_2 - C_1) = -v_p(C_2 - C_1). \tag{6.12}$$

with

$$v_p = \frac{D}{(x_2 - x_1)}. \tag{6.13}$$

v_p is called the piston velocity, because we can imagine that molecules contained in the glass are mixed by the action of two pistons moving at a speed v_p in the opposite direction from the top to the bottom of the glass and vice versa. If the time required for the tracer diffusion from x_1 to x_2 is "t", we can write that $v_p = \frac{x_2 - x_1}{t}$. As v_p decreases when the distance increases (equation 6.13), diffusion is more efficient over short distances and

becomes negligible over large distances. Noting on Figure 6.3a that the average distance traveled by the molecules is $x_m = (x_2 - x_1)/2$, we obtain

$$x_m = \sqrt{2Dt}. \tag{6.14}$$

The average distance is a function of the square root of the time. As molecules move randomly, there is little chance that they always go in the same direction, which considerably reduces their net traveled distance. For example, the diffusion coefficient of sugar in water at 25°C is 0.5×10^{-5} cm^2 s^{-1}. For a distance of 10 μm, $v_p = 50$ μm s^{-1}: equilibrium is quickly reached. Over a distance of 10 cm, $v_p = 5 \times 10^{-7}$ cm s^{-1}: it will take 8 months to achieve equilibrium in the glass. In oceanography, the molecular diffusion plays a major role in the limitation of ocean–atmosphere gas exchanges and in the carbon isotope fractionation during CO_2 uptake by phytoplankton.

6.3.3 Gas Diffusion at the Air–Sea Interface

In the atmosphere and the ocean, the transport of matter is dominated by large-scale motions. However, at the ocean–atmosphere interface, material transfers occur by molecular diffusion through an extremely fine layer. Although the layer thickness is of a few tens of microns only, the slow rate of the molecular diffusion limits exchanges between the ocean and the atmosphere. Exchanges are modeled by considering that air and seawater are separated by a liquid "stagnant film" through which gas molecules must diffuse. There is also an atmospheric stagnant film in contact with seawater, but diffusion is much slower in water than in air, so that gas exchanges are limited by the stagnant film in seawater on which we will focus here (Fig. 6.4).

When the gas partial pressure at the surface ocean is different from gas partial pressure in the air, there is a gradient of dissolved gas concentration between the top and the base of the stagnant film. We consider the case of dissolved O_2. The conservation equation in the film is

$$\frac{\mathrm{d}[O_2]}{\mathrm{d}t} = -\frac{\mathrm{d}}{\mathrm{d}x}\left(-D_{O_2}\frac{\mathrm{d}[O_2]}{\mathrm{d}x}\right) = D_{O_2}\frac{\mathrm{d}^2[O_2]}{\mathrm{d}x^2}. \tag{6.15}$$

$[O_2]$ is the dissolved oxygen concentration. D being constant, it can be removed from the derivative term. At the stagnant film scale (approximately 30 μm), the travel time of an O_2 molecule by molecular diffusion is of the order of $t = \Delta z^2/(2D_{O_2}) = (3 \times 10^{-5})^2/(2 \times 2.3 \times 10^{-9}) = 0.2$ s. Steady state is therefore rapidly reached in the film, so that the concentration gradient in the film, $\mathrm{d}C/\mathrm{d}x$, is constant. The net O_2 flux is then given by the equation

$$F = -D_{O_2}/\Delta z([O_2] - [O_2]^{sat}), \tag{6.16}$$

$$F = -\alpha_{O_2} D_{O_2}/\Delta z(P_{O_2}^{seawater} - P_{O_2}^{atmosphere}),$$

where Δz is the thickness of the stagnant film and $[O_2]^{sat}$ corresponds to the dissolved O_2 concentration at equilibrium with the atmosphere. D_{O_2}, α_{O_2} and $[O_2]^{sat}$ being known,

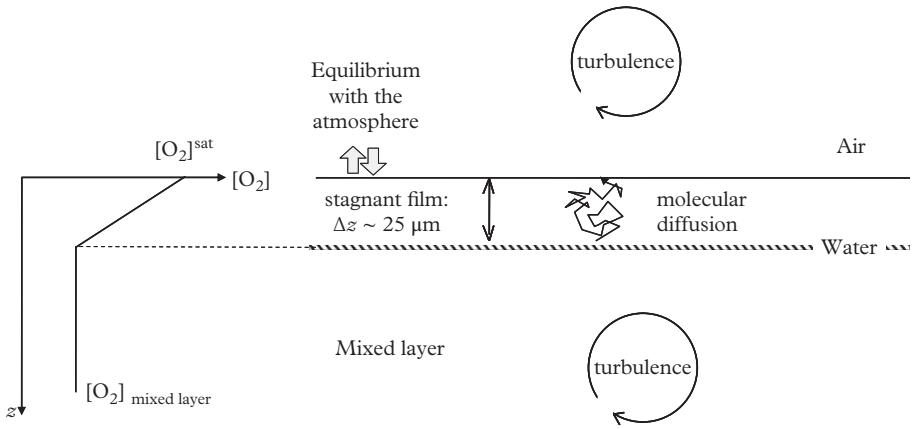

Figure 6.4 *Gas transfer at the ocean surface. At the basis of the stagnant film, the gas concentration is equal to the concentration in the mixed layer. At the top of the stagnant film, the concentration is in equilibrium with the atmosphere. If these two concentrations are different, there is a net gas flux by molecular diffusion through the film.*

the difficulty is to determine Δx. Different methods are used: some are based on the inventory of ^{222}Rn (see example in Section 5.3.1 in Chapter 5) or $^{14}CO_2$ penetration in the ocean (Chapter 8), other on wind tunnel measurements or on diffusion to the atmosphere of natural or artificial gases (Problem 1).

It must be noted that here F is a flux per unit area. For O_2 exchanges between the atmosphere and a water reservoir with a surface S and a height h without sources and sinks, the conservation equation becomes

$$Sh\frac{\mathrm{d}\,[O_2]}{\mathrm{d}t} = -S\frac{D_{O_2}}{\Delta z}\left([O_2] - [O_2]^{sat}\right). \tag{6.17}$$

This can be written as

$$\frac{\mathrm{d}\,[O_2]}{\mathrm{d}t} = -\frac{D_{O_2}}{h \times \Delta z}\left([O_2] - [O_2]^{sat}\right). \tag{6.18}$$

The time constant for gas exchange is $k_e = D_{O_2}/(h\ \Delta z)$. It has the same mathematical form as that of equation (5.2) in Chapter 5.

We emphasize that F is a *net* flux resulting from the difference between an inflow and an outflow:

$$\underset{\substack{\text{net flux}\\ \text{per unit area}}}{F} = \underset{\substack{\text{total flux diffusing}\\ \text{from the atmosphere}\\ \text{to the ocean}}}{D_{O_2}/\Delta z[O_2]^{sat}} - \underset{\substack{\text{total flux diffusing}\\ \text{from the ocean}\\ \text{to the atmosphere}}}{D_{O_2}/\Delta z[O_2]}. \tag{6.19}$$

If $[O_2] = [O_2]^{sat}$, then $F = 0$. However, O_2 molecules cross the stagnant film continuously by molecular diffusion and significant amounts of O_2 are exchanged between the ocean and the atmosphere.

Exercise: oxygen diffusion and ocean–atmosphere equilibrium

We consider the ocean mixed layer as a reservoir of seawater with a height h = 100 m and a surface S in contact with the atmosphere. The mixed layer is stirred permanently, so the O_2 concentration is uniform. Initially, the O_2 concentration in seawater is $[O_2]^0$ whereas O_2 solubility is $[O_2]^{sat} > [O_2]^0$. Determine the evolution of the O_2 concentration in the mixed layer with time.

Solution:

The net O_2 flux through the stagnant film is given by equation (6.17). The conservation equation of O_2 in the mixed layer is

$$\frac{d\,[O_2]}{dt} = -\frac{D_{O_2}}{h \times \Delta z}\left([O_2] - [O_2]^{sat}\right)$$

and the temporal evolution of $[O_2]$ is

$$[O_2] = [O_2]^{sat} + \left([O_2]^0 - [O_2]^{sat}\right) e^{-\frac{D_{O_2}}{h\Delta z}t}.$$

The piston velocity for O_2 is $\frac{D_{O_2}}{\Delta z}$, so that the time constant of O_2 diffusion is $k_{gas} = \frac{D_{O_2}}{h\Delta z} = (\tau_{gas})^{-1}$. τ_{gas} represents the time required for the piston to travel over the distance h. For a 100 m thick mixed layer, a stagnant film thickness Δz = 35 μm and $D_{O_2} = 2.3 \times 10^{-5}$ cm^2 s^{-1}, this corresponds to a residence time τ = 17 d. This relatively short time explains that O_2 in the mixed layer is generally close to equilibrium with the atmosphere.

Note: 17 days for a 100 m thick layer may seem short compared to the 8 months taken by sugar to diffuse in the glass of water. It is because in the mixed layer case, molecular diffusion limits transport only over the 35 μm thick stagnant film (transport within the mixed layer is provided by the turbulence), while sugar must diffuse throughout the glass (∼10 cm).

6.4 Eddy Diffusion

Molecular diffusion is rapidly inefficient when distance increase. Of course, it is possible to stir the water with a spoon to speed up sugar mixing. It is then water motion that

transports sugar over long distances. These movements being more or less random, they generate a flux that can be described in the same way as molecular diffusion:

$$F = -K\frac{(C_2 - C_1)}{(x_2 - x_1)} = -K\frac{\mathrm{d}C}{\mathrm{d}x}. \tag{6.20}$$

K is the eddy diffusion coefficient. It has the same units as D, but its value is much higher. For horizontal turbulent diffusion, $K_{x,y} \sim 10^6 - 10^7$ cm^2 s^{-1}, while for vertical turbulent diffusion, $K_z \sim 0.1 - 1$ cm^2 s^{-1}. We have seen in Chapter 1 that the horizontal movements of water masses are much easier than vertical ones, because the vertical stratification of the ocean prevents an efficient vertical mixing. This point will be illustrated below by the example of tracer diffusion in the thermocline. Vertical diffusion is strong in the wind-mixed surface layer (K_z up to 10^3 cm^2 s^{-1}); however, it is weak in the thermocline where density gradients are most important. When the density gradient is large, a volume of water moved vertically quickly returns to its equilibrium position by buoyancy (if it is forced to move upward, it is denser than the surrounding waters and therefore pushed downward, if the water volume is forced to move downward, it is less dense than the surrounding waters and therefore pushed upward). The displaced water mass returns to equilibrium by oscillating around its equilibrium position. The oscillation frequency (called the Brunt–Väisälä frequency) and therefore the return to equilibrium is faster when the density gradient is high. K_z can be estimated by measuring the microstructure of the vertical density gradient (which stabilizes the water masses vertically) and the speed of the currents (geostrophic currents, eddies, tides ...) which introduce perturbations in the environment.

Horizontal turbulence depends on the speed of the current and the size of the area considered (Problem 2). We have seen, for example, in Chapter 1 that the Gulf Stream generates many eddies that contribute to the mixing of the waters. These eddies exist also outside the areas of intense currents (Fig. 6.5).

Given the orders of magnitude of D and K, molecular diffusion plays a significant role only when the water flow is not turbulent, that is, at interfaces (ocean–atmosphere interface, seawater–cell interface) and over small distances. In the ocean, it is the turbulent diffusion that mixes the water masses.

Now let's go back to the conservation equation. In the case of diffusion, it is of the form

$$\frac{\mathrm{d}C}{\mathrm{d}t} = -\frac{\mathrm{d}}{\mathrm{d}x}\left(-K_x\frac{\mathrm{d}C}{\mathrm{d}x}\right) = K_x\frac{\mathrm{d}^2C}{\mathrm{d}x^2} + \frac{\mathrm{d}K_x}{\mathrm{d}x}\frac{\mathrm{d}C}{\mathrm{d}x}. \tag{6.21}$$

When K_x varies spatially, $\frac{\mathrm{d}K_x}{\mathrm{d}x}\frac{\mathrm{d}C}{\mathrm{d}x}$ is equivalent to an advection term. Assuming that K_x is constant on the x-axis, its derivative is zero and it can be inferred that

$$\frac{\mathrm{d}C}{\mathrm{d}t} = K_x\frac{\mathrm{d}^2C}{\mathrm{d}x^2}. \tag{6.22}$$

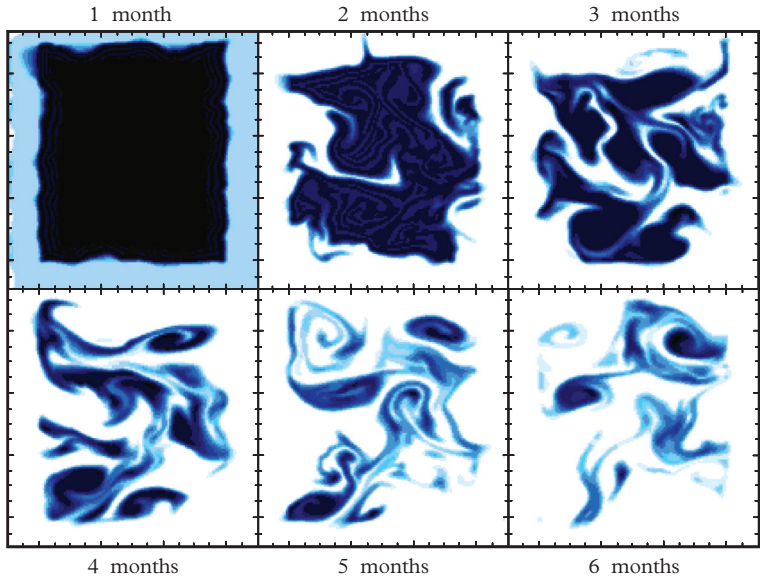

Figure 6.5 *Numerical simulation of the horizontal dispersion of a passive tracer in the Northeast Atlantic. The field size is of the order of 300 × 300 km. Initially the tracer is distributed uniformly in a rectangular field (dark color). Outside of the field, concentration is set to zero (light gray). The simulation lasts 6 months. The effect of eddies with a radius of several tens of kilometers (they are called mesoscale eddies) and the formation of filaments appear clearly. After 6 months, cores of tracer-rich eddies are still present (low advection), but most of the water of the domain was renewed (significant eddy diffusion). Adapted from an unpublished figure of M. Levy. See also Lehahn et al. (2007).*

This is the second Fick law. The temporal evolution of concentration in the box does not depend directly on the concentration gradient but on the change of the concentration gradient along the x-axis (Fig. 6.6).

If K_x is not constant along the x-axis, the term $\frac{\mathrm{d}K_x}{\mathrm{d}x}\frac{\mathrm{d}C}{\mathrm{d}x}$ is not null. It has the form of an advection term.

6.5 The Full Conservation Equation

The full conservation equation for transport along the x-axis is

$$\frac{\mathrm{d}C}{\mathrm{d}t} = \frac{\mathrm{d}}{\mathrm{d}x}\left(K_x\frac{\mathrm{d}C}{\mathrm{d}x}\right) - u\frac{\mathrm{d}C}{\mathrm{d}x} + s - p, \tag{6.23}$$

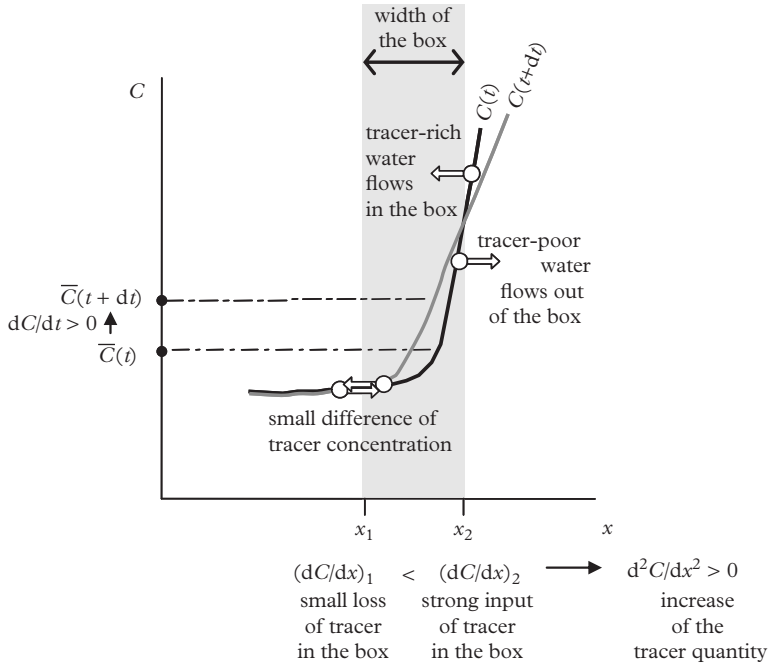

Figure 6.6 *Effect of diffusion on the evolution of the concentration C of a tracer in a box located between x_1 and x_2. If eddy diffusion occurs, small volumes of water (white circles) move (white arrows) across x_1 and x_2. At x_1 and x_2, the net flux of tracer goes from high concentrations to low concentrations. In the example, $(dC/dx)_1$ being positive, a net flux of tracer leaves the volume by side 1. As $(dC/dx)_2$ is positive and greater than $(dC/dx)_1$, the tracer enters the volume through side 2 faster that it is released through side 1. Overall, the average tracer concentration ($\overline{C}$) in the box increases with time.*

where s and p are the source and sink terms defined in Chapter 5. This conservation equation can be generalized to a transport in three dimensions

$$\frac{dC}{dt} = \frac{d}{dx}\left(K_x \frac{dC}{dx}\right) + \frac{d}{dy}\left(K_y \frac{dC}{dy}\right) + \frac{d}{dz}\left(K_z \frac{dC}{dz}\right) - u\frac{dC}{dx} - v\frac{dC}{dy} - w\frac{dC}{dz} + s - p. \quad (6.24)$$

Most of the time, this equation can only be solved by numerical methods (Albarède, 1995). Comparison of the orders of magnitude of the different terms frequently leads to simplifications (Problem 2). We will restrict ourselves to two one-dimensional examples, first with steady-state transport of radium in coastal waters which will allow comparing the influence of the various terms of the equation. Then, we will discuss the problem of solving this equation in non-steady-state conditions with the case of the release and

dispersal of a passive tracer in the ocean. Specific examples on the transport of chemical elements by marine particles and in sediments will be developed in Chapter 10.

6.5.1 Example 1: Radium Transport in Coastal Waters

Radium isotopes are used to characterize the mixing of coastal and open ocean waters on the continental shelf (Moore, 2000). We focus on the South Atlantic Bight on the East coast of the US (Fig. 6.7). The coast is separated from the Gulf Stream by the waters of the continental shelf. Shelf water residence time is of the order of a few tens of days, but the respective role of advection and diffusion is not clearly established.

Radium is a soluble element with four radioactive isotopes, all produced by radioactive decay of thorium isotopes: ^{223}Ra ($T_{1/2} = 11.4$ d), ^{224}Ra ($T_{1/2} = 3.66$ d), ^{226}Ra ($T_{1/2} = 1600$ y) and ^{228}Ra ($T_{1/2} = 5.75$ y). There is so little thorium in seawater that *in situ* production of Ra isotopes in seawater is low (or negligible). Radium is brought to the ocean at the contact with the thorium-rich "solid" reservoirs such as continents and sediments.

The four Ra isotopes are measured along four transects. For each isotope, the average of the four transects is considered (Fig. 6.8). What are the parameters controlling the evolution of concentrations? Concentration gradients between the coast and the open ocean show that the main source of radium is located at the coast. As sampling occurred in summer, a strong thermocline isolates surface waters from deeper waters. Therefore, we neglect vertical transport. Concentration gradients along the coast (between different transects are much lower than the gradients perpendicular to the coast, so that the effect of water circulation along the coast on the Ra isotopes is low. Finally, repeated sampling shows that the system is at steady state. Therefore, the transport of Ra isotopes is modeled as a one-dimensional process (along an x-axis perpendicular to the coast; it departs from the convention of the x-axis oriented eastward for the sake of simplicity) and at steady state. We first work on the distribution of ^{226}Ra–^{228}Ra isotopes which have

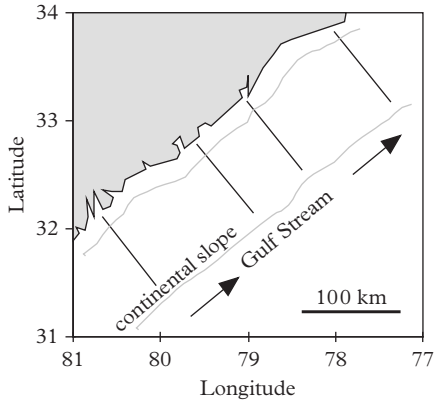

Figure 6.7 *Sampling area. The coast is bordered by continental shelf waters. Gulf Stream waters are found offshore. On each of four transects perpendicular to the coast, the four Ra isotopes have been measured in surface waters.*

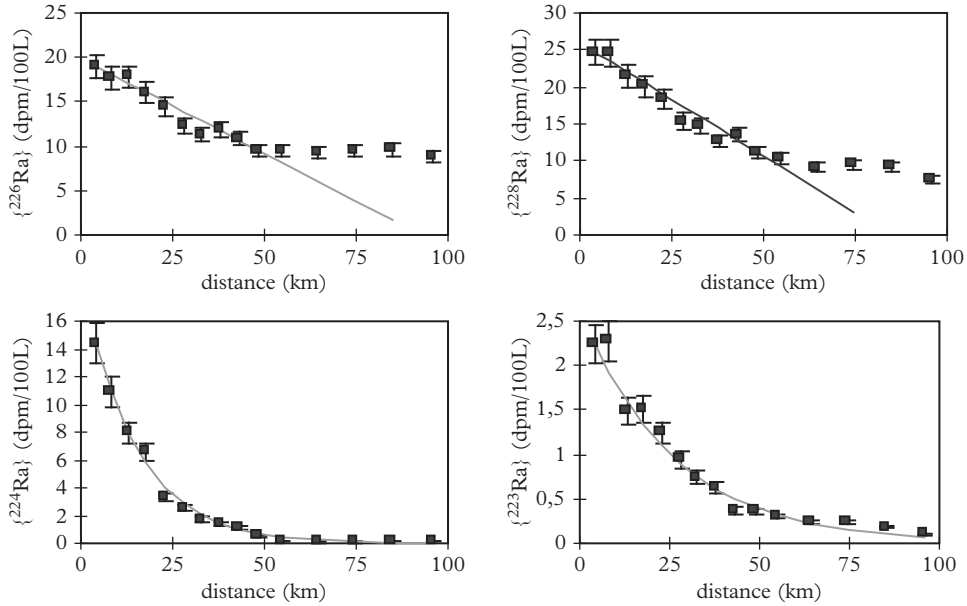

Figure 6.8 *Evolution of Ra isotopes with the distance to the coast. Each profile is the average of the four coast–open ocean transects. The continuous curves are obtained from equations (6.30) and (6.35).*

relatively long half-lives. Then we will see how the ^{223}Ra and ^{224}Ra isotopes provide additional information with their short periods.

Radium is soluble; it is not lost on marine particles and its only sink is radioactive decay. At steady state, the conservation equation for the activity of a radium isotope in solution is

$$K_x \frac{\mathrm{d}^2\{\mathrm{Ra}\}}{\mathrm{d}x^2} - u\frac{\mathrm{d}\{\mathrm{Ra}\}}{\mathrm{d}x} - \lambda\{\mathrm{Ra}\} = 0. \tag{6.25}$$

The half-lives of ^{226}Ra and ^{228}Ra are much larger than the water residence time on the shelf, so that their radioactive decay is negligible and they behave as conservative tracers. The equation simplifies to

$$K_x \frac{\mathrm{d}^2\{\mathrm{Ra}\}}{\mathrm{d}x^2} - u\frac{\mathrm{d}\{\mathrm{Ra}\}}{\mathrm{d}x} = 0. \tag{6.26}$$

This equation has a solution of the form

$$\{\mathrm{Ra}_x\} = B_1\, \mathrm{e}^{\left(\frac{u}{K_x} \times x\right)} + B_2. \tag{6.27}$$

To determine the values of the integration constants (B_1 and B_2), we set boundary conditions: at distances x_1 and x_2 from the coast, Ra activities are $\{\mathrm{Ra}_{x_1}\}$ and $\{\mathrm{Ra}_{x_2}\}$. This yields

$$\{\mathrm{Ra}_{x_1}\} = B_1\, \mathrm{e}^{\left(\frac{u}{K_x}\times x_1\right)} + B_2, \tag{6.28a}$$

$$\{\mathrm{Ra}_{x_2}\} = B_1\, \mathrm{e}^{\left(\frac{u}{K_x}\times x_2\right)} + B_2, \tag{6.28b}$$

B_1 and B_2 are deduced from equations (6.28a) and (6.28b), so we obtain the solution

$$\{\mathrm{Ra}_x\} = \left(\{\mathrm{Ra}_{x_2}\} - \{\mathrm{Ra}_{x_1}\}\right) \frac{\mathrm{e}^{\left(\frac{u}{K_x}\times(x-x_1)\right)} - 1}{\mathrm{e}^{\left(\frac{u}{K_x}\times(x_2-x_1)\right)} - 1} + \{\mathrm{Ra}_{x_1}\}. \tag{6.29}$$

The shape of the profile depends on the value of the Péclet number: $P_\mathrm{e} = \left|\dfrac{u\,(x_2 - x_1)}{K_x}\right|$. P_e is a dimensionless number characterizing the relative importance of advection and diffusion between x_1 and x_2 (Fig. 6.9).

When diffusion dominates over advection, $P_e \ll 1$ and equation (6.24) reduces to (remembering that $\mathrm{e}^x \approx 1 + x$ when $x \approx 0$)

$$\{\mathrm{Ra}_x\} = \left(\{\mathrm{Ra}_{x_2}\} - \{\mathrm{Ra}_{x_1}\}\right) \times \frac{x - x_1}{x_2 - x_1} + \{\mathrm{Ra}_{x_1}\}. \tag{6.30}$$

In this case (curve c on Fig 6.9), the profile is linear (constant concentration gradient between the coast and offshore) and it is independent of the value of K_x.

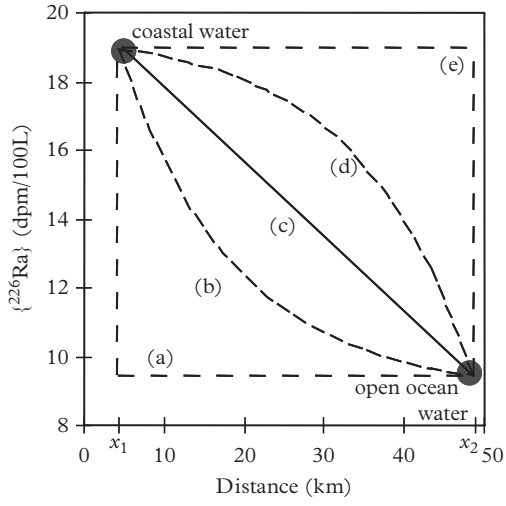

Figure 6.9 *Theoretical changes in $\{^{226}Ra\}$ or $\{^{228}Ra\}$ activity with the distance to the coast. (a) $P_e \gg 1$ and $u < 0$: offshore water is advected to the coast without affecting its concentration by mixing with the coastal water. (b) $P_e \approx 1$ and $u < 0$: open ocean water advected to the coast is mixed with coastal water by eddy diffusion; the profile becomes curved. (c) $P_e = 0$: diffusion is much stronger than advection and it mixes coastal and open ocean waters efficiently. (d) $P_e \approx 1$ and $u > 0$: advection carries coastal water offshore and mixing becomes significant away from the coast. (e) $P_e \gg 1$ and $u > 0$: advection is so strong that the coastal water invaded the plateau and it mixes only when it arrived in the open ocean.*

When advection is comparable to diffusion ($P_e \approx 1$), the profile becomes curved (equation 6.24). Indeed, advection of coastal water to the open ocean creates a strong concentration gradient offshore that eddy diffusion cannot fully homogenize (curve d). Conversely, the advection of offshore water toward the coast creates a strong concentration gradient near the coast that eddy diffusion cannot fully homogenize (curve b).

When advection dominates over diffusion ($P_e \gg 1$) and that water flows toward open ocean ($u > 0$), equation (6.29) is reduced to

$$\{\mathrm{Ra}_x\} = \{\mathrm{Ra}_{x_1}\}. \tag{6.31}$$

In this case (curve e), the Ra activity is constant and equal to the concentration of coastal water: coastal water is advected offshore without mixing and it loses its signature only beyond the plateau (which means implicitly that coastal water is infinitely diluted by open ocean water). Conversely, if the advection dominates ($P_e \gg 1$) but it is directed toward the coast ($u < 0$), equation (6.29) reduces to

$$\{\mathrm{Ra}_x\} = \{\mathrm{Ra}_{x_2}\}. \tag{6.32}$$

In this case (curve a), open ocean water is advected on the shelf and the coastal water signature is found only when the coast is reached.

Linear $\{^{226}\mathrm{Ra}\}$ and $\{^{228}\mathrm{Ra}\}$ profiles between the coast and 50 km offshore (Fig. 6.8) indicate that eddy diffusion transport dominates and advection is negligible. It is likely that the brake of slope observed beyond 50 km is due to lateral advection of Gulf Stream water: it corresponds to a different mixing scheme. We focus now on the 0–50 km zone.

As diffusion dominates, equation (6.31) shows that it is not possible to determine K_x with ^{226}Ra and ^{228}Ra. We can now use isotopes of shorter periods. $\{^{223}\mathrm{Ra}\}$ and $\{^{224}\mathrm{Ra}\}$ profiles allow us to neglect advection in equation (6.20). The conservation equation for $\{^{223}\mathrm{Ra}\}$ and $\{^{224}\mathrm{Ra}\}$ can be written as

$$K_x \frac{\mathrm{d}^2\{\mathrm{Ra}\}}{\mathrm{d}x^2} - \lambda\{\mathrm{Ra}\} = 0. \tag{6.33}$$

The solution of this equation is of the form

$$\{\mathrm{Ra}_x\} = B_3\, \mathrm{e}^{\left(-\sqrt{\frac{\lambda}{K_x}}\times x\right)} + B_4\, \mathrm{e}^{\left(\sqrt{\frac{\lambda}{K_x}}\times x\right)}. \tag{6.34}$$

Considering the very short half-life of ^{223}Ra and ^{224}Ra, their concentrations in the open ocean (away from any production area) must be zero. So, for $x = +\infty$, $\{\mathrm{Ra}_{+\infty}\} = 0$, which implies $B_4 = 0$ so that the term $B_4\mathrm{e}^{\left(\sqrt{\frac{\lambda}{K_x}}\times x\right)}$ in equation (6.34) does not becomes infinite. By setting the concentration at x_1, we obtain $B_3 = \{\mathrm{Ra}_{x_1}\}\mathrm{e}^{\left(\sqrt{\frac{\lambda}{K_x}}\times x_1\right)}$. It follows that

$$\{\mathrm{Ra}_x\} = \{\mathrm{Ra}_{x_1}\} \times \mathrm{e}^{\left(-\sqrt{\frac{\lambda}{K_x}}\times (x-x_1)\right)}. \tag{6.35}$$

By adjusting the curve given by equation (6.35) to the data (Fig. 6.8), we obtain $K_x = 400$ m^2 s^{-1}. By combining the information provided by the tracers of long and short half-lives, we have precisely determined the characteristic parameters of the physical transport. Depending on the length scale considered and on the dynamics of the ocean, the different Ra isotopes are more or less affected by the radioactive decay (see Problem 3).

Finally, we return to boundary conditions. K_x has been determined by adjusting the theoretical curve given by equation (6.35) to ^{223}Ra and ^{224}Ra data. This approach is common, but it is important to note that by fixing K_x, we impose a net seaward flux of the different Ra isotopes. We must check that these fluxes are realistic. In particular, for ^{226}Ra we obtained $F = K_x(\{^{226}\text{Ra}\}/\text{d}z) = 7.5 \times 10^{10}$ dpm km^{-2} d^{-1} (with $\text{d}\{^{226}\text{Ra}\}/\text{d}z = 0.22$ dpm/100 L/km). Considering that this flux is transported through a 10 m thick and 320 km long mixed layer, it corresponds to a total flux of 2.4×10^{11} dpm d^{-1} for the whole area. This is much more than the ^{226}Ra flux brought by rivers in this area (0.1×10^{10} dpm d^{-1}). Is the model unrealistic? No, it is more likely that there is an unforeseen source of Ra from the continent: it is probably the groundwater discharge in the coastal zone. This highlight of a new Ra flux is also important from the water balance point of view as submarine groundwater discharge could represent about 40% of the rivers flow.

6.5.2 Example 2: Dispersion of SF_6 in the Thermocline

Purposeful tracer release is increasingly used by oceanographers to study ocean circulation (Ledwell et al., 1998). They use sulfur hexafluoride (SF_6), which is normally absent from seawater, chemically inert and easy to analyze at very low levels. To estimate the horizontal and vertical diffusion coefficients in the thermocline, 139 kg of SF_6 was injected into a small volume of the North Atlantic at a depth of 300 m and the dispersal of the SF_6 was followed over 2.5 y.

6.5.2.1 Vertical Diffusion

Figure 6.10 shows the temporal evolution of the average vertical dispersion of SF_6. The thickness of the SF_6 layer grows from 2 m at the time of injection to 160 m after 1 y.

The vertical dispersion of SF_6 by the turbulent diffusion is governed by

$$\frac{\text{d}C}{\text{d}t} = K_z \frac{\text{d}^2 C}{\text{d}x^2}. \tag{6.36}$$

For an instantaneous injection of a quantity Q of tracer at depth z_0, its solution is (Turcotte and Schubert, 2014)

$$C(z,t) = \frac{Q}{2\sqrt{\pi K_z t}} \exp\left(-\frac{(z-z_0)^2}{4K_z t}\right). \tag{6.37}$$

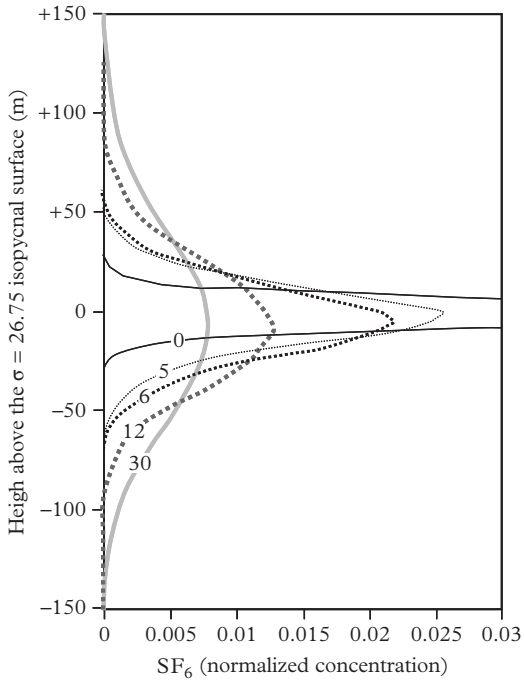

Figure 6.10 *Temporal evolution of the vertical distribution of SF_6 patch. The reference depth is located at 300 m. Concentrations are normalized to remove the effect of horizontal diffusion of the tracer distribution. Profile measured immediately after the tracer injection exceeds the scale and has a normalized concentration equal to 1. Profiles measured 5, 6, 12 and 30 months after the tracer injection show the effect of vertical diffusion. The vertical turbulent diffusion coefficient is $K_z = 0.17\ cm^2\ s^{-1}$. Modified from Ledwell et al. (1993).*

It is (except for the Q factor) a Gaussian curve of average z_0 (the tracer is centered on the depth z_0) and of standard deviation $\sigma = \sqrt{2K_z t}$ (70% of the tracer is located between the depths $z_o - \sigma$ and $z_o + \sigma$ and 95% of the tracer is located between the depths $z_o - 2\sigma$ and $z_o + 2\sigma$; this is to be compared with equation 6.14). By adjusting a curve corresponding to equation (6.37) to the data collected at each period, a K_z of the order of 0.17 $cm^2\ s^{-1}$ is obtained. This order of magnitude is easily found assuming that after 12 months (Fig 6.10), most ($\approx$ 95%) tracer spreads over $\approx$ 80 m ($\approx 2\sigma$) on both sides of the concentration maximum. It follows that $K_z = \frac{\sigma^2}{2t} = 0.25\ cm^2\ s^{-1}$. This low value reflects the strong density gradient in the thermocline which prevents vertical mixing. It is significantly less than the K_z measured in deep waters (Problem 4). We can finally note a slight deepening of the position of the maximum of concentration with time. This net displacement of the patch can be due to a transport of SF_6 by adsorption on marine particles (see equation 6.10) or to a slight increase of K_z with depth (see equation 6.21). Vertical eddy diffusion strongly increases in the vicinity of rough seafloor topography (Problem 5; see also Chapter 10).

6.5.2.2 Horizontal Diffusion

During the same period, the horizontal dispersion of the SF_6 patch has been much faster than vertical dispersion, but it is not reduced to the simple flattening of a Gaussian curve (Fig. 6.11). After a few months, the initial patch is stretched (by the mesoscale

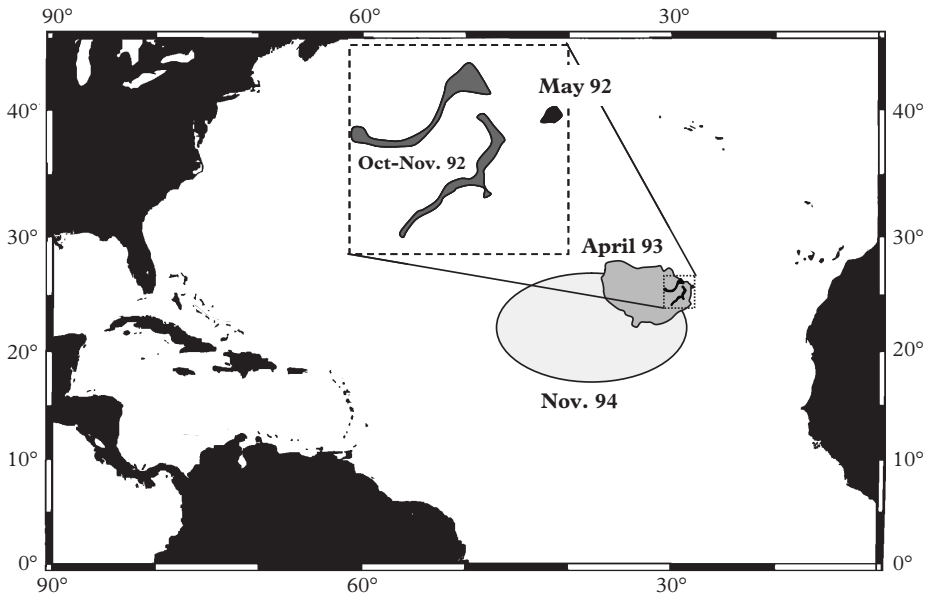

Figure 6.11 *Temporal evolution of the horizontal distribution of the SF_6 patch. Inset: zoom on the early evolution of the patch. Modified from Ledwell et al. (1998).*

eddies) in long filaments of several hundred km separated by tracer-free areas. After a year, turbulent mixing produced a continuous but heterogeneous patch of tracer. After 2.5 y, the SF_6 patch is stretched over 2000 km in the east–west direction and 1000 km in the north–south direction. This corresponds to a turbulent diffusion coefficient $K_x \approx 1.5 \times 10^7$ and $K_y \approx 6 \times 10^7$ cm^2 s^{-1}. $K_{x,y}$ increases when the length scale increases (Problem 6). Horizontal turbulent diffusion dominates in general compare to the much slower vertical diffusion.

6.6 The Case of Sediment Transport

The sediments that accumulate on the seafloor are made of two phases: solid grains and interstitial fluid. The relative abundance of the two phases is quantified by the porosity Φ

$$\Phi = \text{ interstitial fluid volume/volume of wet sediment.} \tag{6.38}$$

We write the advection–diffusion equation by considering the flux of solid particles or interstitial fluid through an infinitesimal volume at a constant depth z below ocean/sediment interface. The transport of particles is due to the gradual burial and compaction of sediments under their own weight (mathematically equivalent to the advection term) and bioturbation (mixing of grains by animals living and moving in the

sediment modeled as eddy diffusion). The transport of the interstitial fluid is due to the gradual burial (mathematically equivalent to the advection term) of the sediment (w_s is the sediment accumulation rate), bioturbation and molecular diffusion in the interstitial fluid. The general transport equations are as follows.

For the dissolved phase

$$\frac{\mathrm{d}\Phi C_s}{\mathrm{d}t} = \frac{\mathrm{d}}{\mathrm{d}z}\left(\Phi D \frac{\mathrm{d}C_s}{\mathrm{d}z}\right) - \frac{\mathrm{d}(\Phi w_s C_s)}{\mathrm{d}z} + s_s - p_s. \tag{6.39}$$

For the solid phase

$$\frac{\mathrm{d}((1-\Phi)C_p)}{\mathrm{d}t} = \frac{\mathrm{d}}{\mathrm{d}z}\left((1-\Phi)D \frac{\mathrm{d}C_p}{\mathrm{d}z}\right) - \frac{\mathrm{d}((1-\Phi)w_s C_p)}{\mathrm{d}z} + s_p - p_p. \tag{6.40}$$

Obviously these equations can be coupled through the source and sink terms. To simplify the equations, Φ and w_s are often assumed to be constant with depth. In some favorable cases (in the absence of s and p terms for example), the porosity disappears from the equations. It is wise to compare the importance of various processes to take into account those which are significant.

Application exercise: Sediment dating

We consider the concentration in excess of an insoluble isotope from the uranium decay series (^{234}Th, ^{230}Th, ^{210}Pb, ^{231}Pa) or of cosmogenic origin (^{10}Be). Determine the evolution of the depth profile in the extreme cases where sedimentation is negligible compared to bioturbation and in the case where bioturbation is negligible compared to sedimentation. Conclusion? Suggest a method to resolve the ambiguity.

Answer:

We use equation (6.40), assuming steady state and that porosity is constant. There is no source term (we are just interested in the excess). The radioactive decay term is written: $p_p = (1-\Phi)\,\lambda\, C_p$. Equation (6.40) reduces to

$$D\frac{\mathrm{d}^2 C_p}{\mathrm{d}^2 z} - w_s \frac{\mathrm{d}C_p}{\mathrm{d}z} - \lambda C_p = 0. \tag{6.41}$$

If bioturbation is negligible compared with the sedimentation, we obtain

$$-w_s \frac{\mathrm{d}C_p}{\mathrm{d}z} - \lambda C_p = 0. \tag{6.42}$$

By setting the surface concentration $C_p(0)$ as boundary condition, the solution is

$$C_p(z) = C_p(0)\mathrm{e}^{-\frac{\lambda}{w_s}z}. \tag{6.43}$$

If sedimentation is negligible compared to bioturbation, we obtain from equation (6.41)

$$D\frac{\mathrm{d}^2C_p}{\mathrm{d}^2z} - \lambda C_p = 0. \tag{6.44}$$

By setting the surface concentration $C_\mathrm{p}(0)$ as boundary conditions and a concentration equal to zero when $z \to +\infty$, the solution is (see the radium in coastal waters exercise)

$$C_p(z) = C_p(0)\mathrm{e}^{-\sqrt{\frac{\lambda}{D}}z}. \tag{6.45}$$

The two models predict an exponential decay of the concentration with depth. The agreement between model and data is not sufficient to choose a model. We need more information to decide. We can compare profiles of isotopes with different lifetimes or use man-made isotopes to have an independent estimate of the sedimentation rate.

PROBLEMS

Problem 1: Gas diffusion in the roaring forties (Jean-Baptiste and Poisson, 2000)

To estimate the thickness of the stagnant film which limits the exchange of gas between the water and the atmosphere in conditions of intense wind, known amounts of gas, SF_6 and ^3He, were injected in a lake on Kerguelen Island. The SF_6 and ^3He concentrations were monitored during several weeks. Concentrations decrease exponentially with time. ^3He concentration is divided by 2 every 6.5 days while the SF_6 concentration is divided by 2 every 15 days. At any moment, the gas concentrations are assumed to be homogeneous in the lake (due to vigorous water stirring by wind) and the concentrations of these gases are zero in the atmosphere.

(1) Why does the SF_6 concentration decrease more slowly than the ^3He concentration?

(2) Write the conservation equation of a gas in the lake.

(3) Deduce the stagnant film thickness and the corresponding piston speeds.

Useful data:

Lake depth: 47 m; surface area: 0.5 km^2.

Molecular diffusion coefficients: $D_{SF_6} = 2.5 \times 10^{-5}$ cm^2 s^{-1} and $D_{^3He} = 5.8 \times 10^{-5}$ cm^2 s^{-1}.

Problem 2: Nitrate transport in the subtropical gyre (Palter et al., 2005)

We want to determine the origin of the nitrate contained in subsurface water from the subtropical North Atlantic gyre. To do so, the characteristic time of the various transport and remineralization processes must be compared:

- Characteristic length of the gyre: 2000 km
- Thickness of the nitracline below subsurface waters: 500 m
- Characteristic speed of vertical advection: 10 cm s^{-1}
- Horizontal diffusion coefficient: 10^7 cm^2 s^{-1}
- Vertical diffusion coefficient: 10^{-1} cm^2 s^{-1}
- Nitrate production by remineralization of organic matter: 1 mmol $m^{-3}a^{-1}$
- Nitrate concentration in surface waters: 1 mmol m^{-3}
- Vertical nitrate concentration gradient in the nitracline: 20 mmol m^{-3}
- Horizontal nitrate concentration gradient between coastal and open ocean waters: 10 mmol m^{-3}

What are the dominant terms?

Problem 3: Coastal–open ocean diffusion in the Arctic Ocean (Smith et al., 2003)

We want to determine the horizontal eddy diffusion coefficient (K_x) between the northern coast of Canada and the Beaufort Sea. For this purpose, dissolved ^{228}Ra was measured. Near the coast, the ^{228}Ra activity is 0.09 dpm L^{-1} and 260 km offshore it is 0.06 dpm L^{-1}. Farther away in the center of the Arctic basin the concentration becomes very low.

(1) Assuming that the transport is only due to horizontal eddy diffusion, determine the conservation equation of $\{^{228}\text{Ra}\}$ and deduce K_x.

(2) Show that it is also possible to explain the distribution of the ^{228}Ra activity if transport is dominated by advection.

Problem 4: Vertical diffusion in the deep ocean (Munk, 1966)

Table 6.2 presents the potential temperature (θ) of the deep Pacific Ocean southwest of Hawaii.

Table 6.2 *Temperature in the deep Pacific Ocean*

Depth (m)	1000	2034	3046	4062	5078
θ(°C)	4.00	2.07	1.59	1.46	1.44

(1) Using these data, draw the θ–depth profile.

(2) Assuming that the vertical advection (vertical speed: w) and vertical diffusion (vertical eddy diffusion coefficient: K_z) are the only processes controlling mixing between the thermocline and the deep ocean, determine the advection–diffusion equation for θ (*Hint:* treat θ as a concentration).

(3) Deduce the relationship between θ and the depth z.

(4) By comparing with data, determine the K_z/w ratio.

(5) By taking the average w value obtained from the ^{14}C ($w = 3$ m y^{-1}), determine the value of K_z.

Problem 5: Vertical diffusion in the Southern Ocean (Watson et al., 2013)

A patch of artificial tracer is released in the Pacific sector of the Antarctic Circumpolar Current at a depth of about 1400 m. One year later, the patch has drifted eastward and 95% of the initial tracer has diffused vertically 60 m above and below the initial patch depth.

(1) Determine the vertical eddy diffusion coefficient around 1400 m in the Pacific sector of the Antarctic Circumpolar Current.

Eight months later, the patch has reached the Drake Passage. Upstream of the Drake Passage, 95% of the tracer is found between 1300 and 1500 m deep, whereas downstream of the Drake passage 95% of the tracer is found between 1200 and 1600 m.

(2) Assuming that the transit time of the water through the Drake Passage at a depth of 1400 m takes about 1 month, determine roughly the vertical eddy diffusion coefficient around 1400 m in the Drake Passage.

(3) Compare the two results. *Hint:* See Chapter 10.

Problem 6: Dispersion of chlorophyll (Abraham et al., 2000)

During an experiment of artificial fertilization in the Southern Ocean, the injection of dissolved iron in the water causes a large increase of the chlorophyll concentration. The size of the chlorophyll patch is determined first by measurements at sea, then by satellite observations. During the 12 days following the fertilization, the size of the patch increases from 10 to 30 km. 42 days after fertilization, the chlorophyll patch spans across 150 km.

(1) Determine the average value of the eddy diffusion coefficient in the first 12 days and over the next month.

(2) Plot these results and those obtained in the examples treated during this chapter in a log(K) diagram versus log(distance). What does this diagram tell you?

7

Development and Limitations of Biological Activity in Surface Waters

About half of the photosynthesis on Earth occurs in the oceans while the other half takes place on continents. As the biomass turnover time is much shorter in the ocean (of the order of a few weeks) than on continents (of the order of a decade), the oceanic biomass is very sensitive to environmental stresses. Understanding the factors controlling the development of the oceanic biomass has applications ranging from the carbon cycle and its consequences for climate change to environmental management and fisheries resources. We saw in Chapter 2 that the distribution of nutrients is strongly influenced by the biological activity. We will now examine how, in return, the distribution of nutrients and their transport by ocean currents control the development of the biological activity and its distribution at the ocean surface. Therefore this chapter will also deal with surface and thermocline circulation. We will also see how marine ecosystems respond to nutrient inputs or nutrient deficiency periods.

7.1 Life Cycle in the Ocean

The ocean is home to a multitude of living beings ranging from the tiniest micron-sized bacteria to blue whales, the largest living animal on Earth. These living beings are organized in ecosystems. Although these ecosystems have a great diversity, especially in coastal areas, the vast majority of the ocean is dominated by a more limited number of species. The majority of oceanic biomass is formed by the **plankton** that include all living beings transported more or less passively by the currents. Plankton include bacterial (**bacterioplankton**), vegetal (**phytoplankton**) and animal (**zooplankton**) species. They are defined by contrast to free-swimming animals (**nekton**) and those on the seafloor (**benthos**).

Living beings able to convert CO_2 into organic carbon are called **autotrophs**. The vast majority of autotrophic beings use light as an energy source to perform this conversion during photosynthesis

$CO_2 + H_2O + \text{sunlight energy} \rightarrow CH_2O + O_2$.

Marine Geochemistry. First Edition. Matthieu Roy-Barman and Catherine Jeandel.

They are sometimes called phototrophic beings. By language stretching, phototrophic organisms are assimilated to phytoplankton, thus including phototrophic bacteria in phytoplankton. They convert sunlight energy into chemical energy through pigments. The main pigment is **chlorophyll**. In the ocean, autotrophic beings include some families of bacteria and algae. Bacteria were the first photosynthetic beings on Earth (see Chapter 11). Their study is difficult due to their small size. For example, *Prochlorococcus*, which is the smallest (0.6 μm) and most abundant (up to 7×10^7 cellules cm^{-3}) photosynthetic being existing on Earth, was discovered only a few decades ago (Fig. 7.1a). This cyanobacterium is present in all waters of the globe between 40°S and 40°N down to 200 m deep, to the ultimate limits of light penetration (99% of sunlight is generally absorbed in the first 100–150 m of the ocean). *Prochlorococcus* occupies this gloomy environment thanks to a unique pigment with an enhanced absorption of blue light that dominates in deep waters (Biller et al., 2015). By contrast, *Synechococcus*, another cyanobacterium closely related to *Prochlorococcus*, is not restricted to oligotrophic environments but is found in nutrient-rich environments.

Trichodesmium is another species of phototrophic bacteria that lives in colonies. These colonies are formed of aggregates of filaments made themselves by hundreds of bacteria (Fig. 7.1b). Through aggregation, these colonies can form plurikilometric masses visible from space. *Trichodesmium* is able to convert the dinitrogen (N_2) dissolved in seawater into organic nitrogen. We will see the importance of this reaction later in this chapter.

Archaea (also called archaebacteria) have long been considered as unusual bacteria, if considered at all. In fact, archaea form the third kingdom of life, beside bacteria and eukaryotes. Until recently, oceanic archaea were thought to be confined to extreme environments such as hydrothermal vents. In fact, they seem ubiquitous in the world's

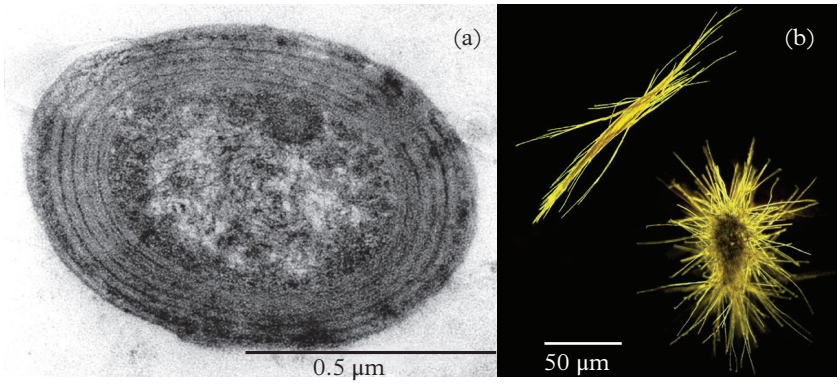

Figure 7.1 *Bacteria. (a) Longitudinal section of* Prochlorococcus *bacteria seen by transmission electron microscopy. Thylakoids (circulars bands), where photosynthesis occurs, are concentrated on the rim to collect a maximum of light. Reproduced with the kind permission of W. Li and F. Partensky. (b)* Trichodesmium *colonies seen by optical microscopy. Photo by Abigail Heithoff, Woods Hole Oceanographic Institution.*

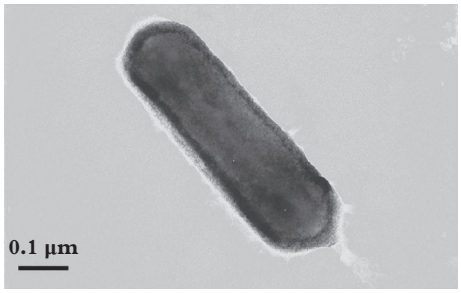

Figure 7.2 *Archaea (Crenarchaeota) seen by transmission electron microscopy. Modified from Könneke et al. (2005).*

ocean and could represent up ~30% of the free-living prokaryotic community (Fig. 7.2). They play an important role in the nitrification process. The trophic status of these archaea is not clear and could include both autotrophic and heterotrophic examples (Karner et al., 2001).

The most numerous algae of the ocean are microscopic (Not et al., 2012). Among them, common examples are the following:

- **Coccolithophorids** whose diameter is typically of the order of 5–10 µm. Their membrane is covered with tiny calcium carbonate shields called coccoliths (Fig. 7.3a). They live in warm to temperate waters. These microscopic algae have a considerable impact on the carbon cycle; the Normandy and southern England chalk cliffs are accumulations of coccoliths!
- **Diatoms** are larger algae (typically 10–50 µm) living in a protective capsule made of amorphous silica and sometimes richly ornamented called frustule (Fig. 7.3b). They frequently live in colonies and are particularly abundant in cold water.

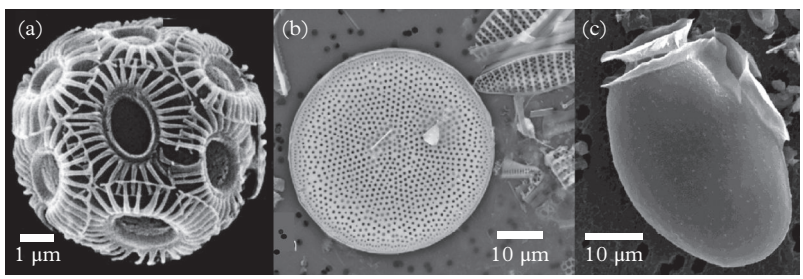

Figure 7.3 *Unicellular eukaryotic algae. (a) Calcareous test that protects the cell of* Emiliana Huxley, *a coccolithophorid. Modified after Young J. R. et al. (1999). (b) Siliceous frustule of centrix-type diatom (in the middle of the figure) and penade-type diatom (in the right-top corner of the figure). Modified after Salter et al. (2007). (c) Cellulose capsule of* Dynophisis. *Modified after Hattenrath-Lehmann et al. (2013).*

– **Dinoflagellates** (typically 10–50 μm) also have a protective capsule called amphiesma that can be armored with cellulose plates (Fig. 7.3c). They are often phototrophs, but some of them also ingest prey. *Dynophisis* does not digest all of its prey: it keeps the plastids safe and uses them for its own photosynthesis (klepto-phototrophy).

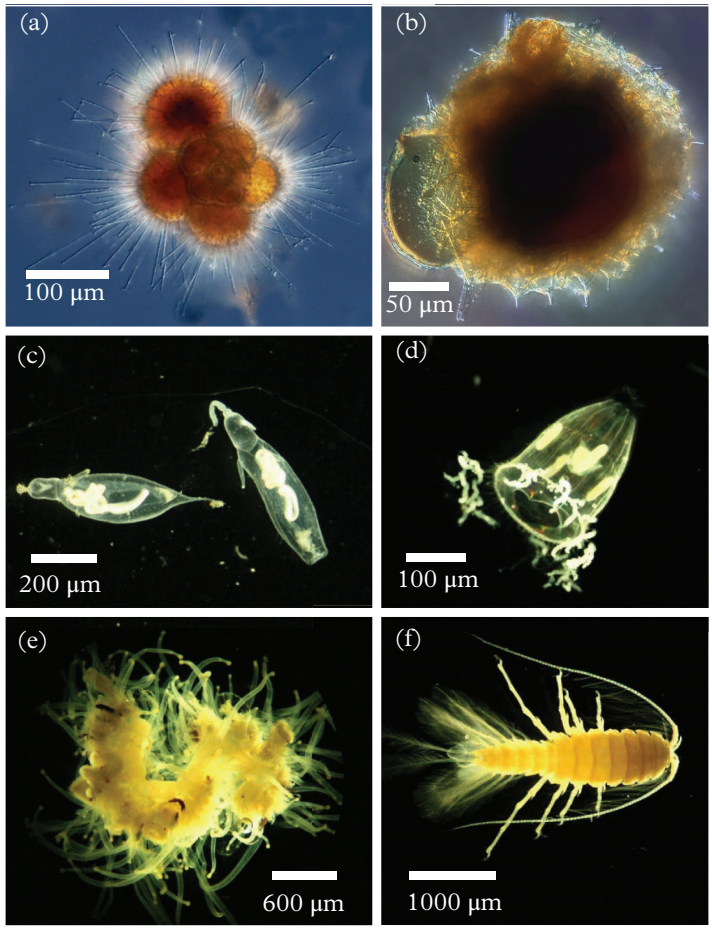

Figure 7.4 *Different types of zooplankton. (a) Foraminifera. (b) Radiolarian (in the center) eating a tintinnid (left). (c) Gymnosome pteropods. (d) Trachymedusae. (e) Colony of physonect siphonophore. (f) Isopod (crustacean). Photos (a) and (b): J.R. Dolan, Laboratoire d'océanographie de Villefranche-sur-Mer. Photos (c–e): Nathalie Leblond, Laboratoire d'océanographie de Villefranche-sur-Mer.*

Some very small photosynthetic eukaryotes were discovered only 20 y ago because they were too small to be caught by regular nets. *Ostreococcus*, the smallest known eukaryote, is only 1 or 2 μm large. Like all eukaryotes, it contains a single nucleus, but to fit in its tiny cell, it also contains a single chloroplast and a single mitochondrion!

Living beings that cannot convert CO_2 into organic carbon are called **heterotrophs**. They are heterotrophic bacteria, protozoans, adult animals or larval forms. To obtain organic matter, they eat other living or dead organisms (Fig. 7.4). Grazers are small animals that eat phytoplankton (like cows graze grass). They can be unicellular animals such as foraminifera, which are recognizable through their calcium carbonate external skeleton (called "test"), or small crustaceans such as copepods that filter large volumes of water to collect their food. Grazers are themselves eaten by carnivores. Finally, at all stages of the food chain, bacteria eat dead organic matter, thus playing a major role in recycling. The organic matter that escapes recycling in surface waters is not lost anyway. Most of this organic matter is remineralized as it sinks in the water column or when it reaches the sediment (see Chapter 9).

Viruses are important players in life cycles (Fig. 7.5): in surface waters, viral infection and subsequent cell lysis could roughly equal grazing as a source of microbial mortality (Suttle, 2007). Viruses are by far the most abundant biological entities in the oceans. However, because of their small size, they comprise only approximately 5% of the biomass. By contrast, prokaryotes (bacteria and archaea) generally represent up to more than 90% of the biomass. Protists (unicellular eukaryotes like foraminifera) can represent as much as half the biomass in surface waters, but in the deep ocean they only comprise a few percent or less of the biomass. Consequently, their biomass probably represents even less than that of the viruses (Fig. 7.6).

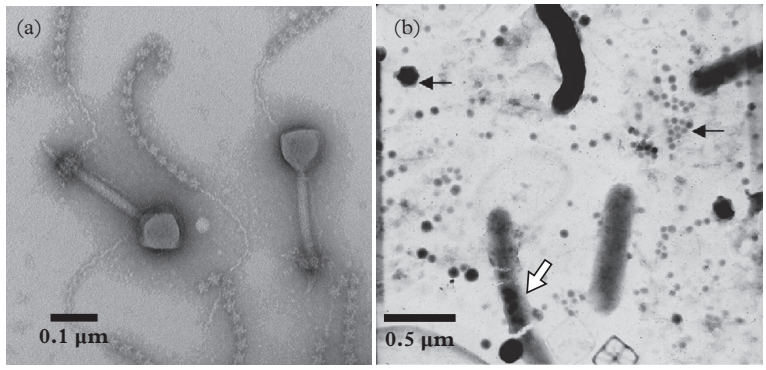

Figure 7.5 *Viruses and bacteria from Mediterranean seawater. (a) Viruses observed during the Tara Ocean Program. The nature of the "stars on strings" is unknown. Photo reproduced courtesy of Jennifer Brum, Sullivan Lab, Ohio State University. See also Brum et al. (2013). (b) Viruses and bacteria. Black arrows point to viruses of different size. The white arrow points to a bacteria obviously infected by viruses. Adapted from Weinbauer et al. (2004).*

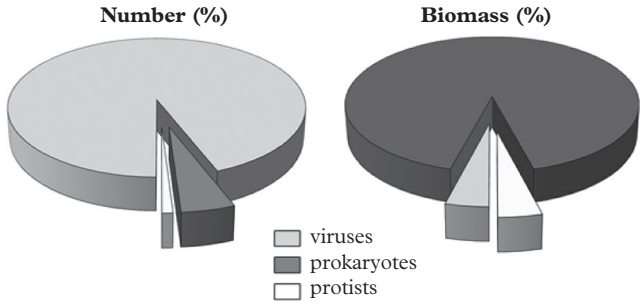

Figure 7.6 *Average number and mass distribution of prokaryotes, protists and viruses in the ocean. Viruses are most numerous, but due to their very low mass they represent a small fraction of the biomass. Adapted from Suttle (2007).*

Plankton are categorized operationally by their size, although they do not strictly correspond to the main taxonomic groups (Yamaguchi et al., 2002). The picoplankton (0.2–2 μm) consist of bacteria and picoeukaryotes. Nanoplankton (2–20 μm) include coccolithophorids and the smallest diatoms, while larger diatoms are part of microplankton (20–200 μm). Microplankton also include small protozoan zooplankton, such as foraminifera and radiolarians. Mesoplankton (200–2000 μm) are made of small metazoans, such as copepods. Larger metazoans, such as cnidarians (jelly fish), constitute the macroplankton (> 2000 μm).

Plankton chowder!

Alain Bombard, physician and researcher at the Oceanographic Museum of Monaco, has dedicated a part of his life to improve survival after shipwrecks. He argued that a human can survive many days in a lifeboat by eating marine plankton and by drinking rain water or water pressed out of raw fish (because the internal liquid of sea fishes is less salty than seawater). He became famous by testing his theory on himself. He left Monaco on a day in 1952 with an English volunteer, Jack Palmer, in a rubber lifeboat *The Heretic*, equipped with a sail and limited equipment (sextant, plankton net and fishing wire, maps, . . .). When they reached Tangier (Morocco), his teammate abandoned him. Bombard then sailed alone to the Atlantic. After several weeks without rain, he had to drink seawater. A freighter rescued him, but he refused to give up and returned to *The Heretic*. He eventually reached Barbados after 113 days at sea. Today, after the publication of a book and despite his detractors, the derivatives of *The Heretic* are mandatory on ships. Until his death, Bombard received letters from people who survived shipwrecks thanks to his experience . . . and the vitamins and proteins of plankton!

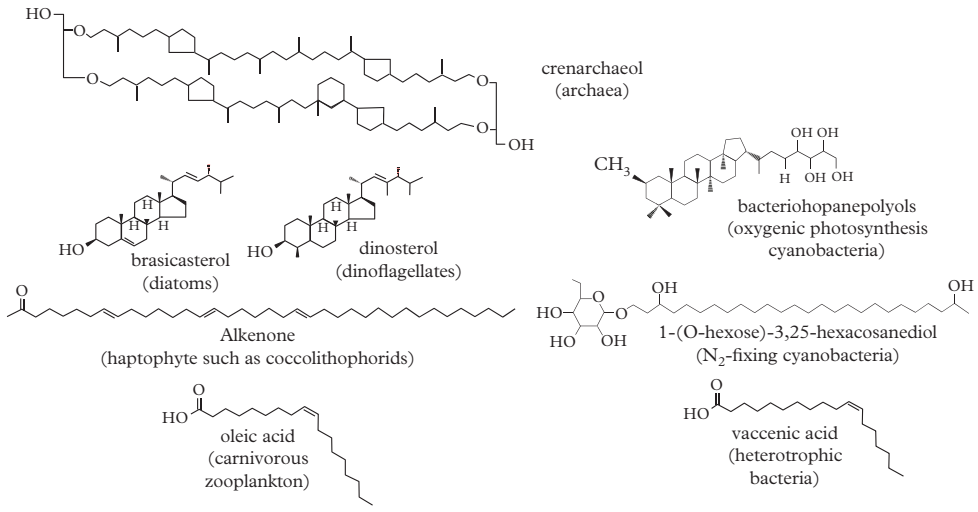

Figure 7.7 *Biomarkers of different plankton groups.*

Very roughly speaking, the average plankton collected with towed nets is made of 50% protein, 15% lipid, 15% carbohydrate and 20% nucleic acids (Hedges et al., 2002). However, there is huge variability depending on the types of plankton present: for example, phytoplankton have a higher carbohydrate/protein ratio than zooplankton. It is not the scope here to detail all the synthetized molecules, but it is worth noting that each plankton group produces specific molecules called biomarkers. They allow the original organic matter and the trophic relations in the ecosystem to be traced (Fig. 7.7). Lipid biomarkers are particularly useful for paleoreconstructions because they are relatively stable so that they (or their derivatives) can be identified in sediments or sedimentary rocks. The exact composition of some of these lipid molecules is temperature dependent (e.g., number of double carbon bonds in alkenones or number of cyclic groups in crenarchaeol) so that they can be used also as paleothermometers.

Life without photosynthesis

During the late 1970s, oases of life full of colonies of mollusks, crabs and tubiform animals called "riftia" were discovered around hot springs that line up along ocean ridges. The question of the sources of energy and nutrients in these ecosystems quickly arose. At a depth of several kilometers, in total absence of light, photosynthesis is indeed impossible. In addition, the amount of organic particulate material falling from the ocean surface is much too low to feed such oases. In fact, the riftia and shellfish live in symbiosis with bacteria that get their energy by oxidizing hydrogen sulfide (H_2S). These bacteria are called **chemotrophic** as opposed to phototrophic bacteria and algae that obtain their energy from sunlight.

Ten years later, other oases of life comparable to the vent communities have been discovered on the Gulf of Mexico seafloor, away from any hydrothermal activity. There, the ecosystem lives from chemical energy that bacteria recover by oxidizing methane (CH_4). This gas escapes from oil fields and diffuses through sediments to the chemotrophic communities that consume it. As hydrocarbons were produced by transformation of marine organic matter, sunlight is still the distant and ultimate source of this energy.

7.2 Development of the Biological Production in Surface Waters

Although organic matter is mostly made up of carbohydrates, the discussion of this chapter will focus in large part on nutrients such as nitrate, phosphate, silica or iron, which have a key role although less abundant than carbon. We saw in Chapter 2 that nutrients can limit organic matter production when they come to exhaustion. We therefore start the discussion with nitrogen, which is recognized as the main limiting factor for biological production in today's ocean.

Phytoplankton live in a paradoxical situation: they must remain at the sea surface to have light, but their development leads to nutrient depletion in surface water and therefore ultimately to a limitation of photosynthesis. In Chapter 2, the trip of the PO_4^{3-} molecule has introduced an important concept: the main source of nutrients for phytoplankton is the upwelling of deep water. This upwelling is difficult in summer as warm and light surface waters do not mix easily with cooler and denser underlying waters (Fig. 7.8). Vertical mixing is favored in winter because surface water temperature drops and wind stirs water more than 100 m deep. Surface waters are then enriched by the upwelling of nutrients. These nutrients are not consumed immediately: phytoplankton brought below the photic zone by the winter mixing is not in favorable conditions

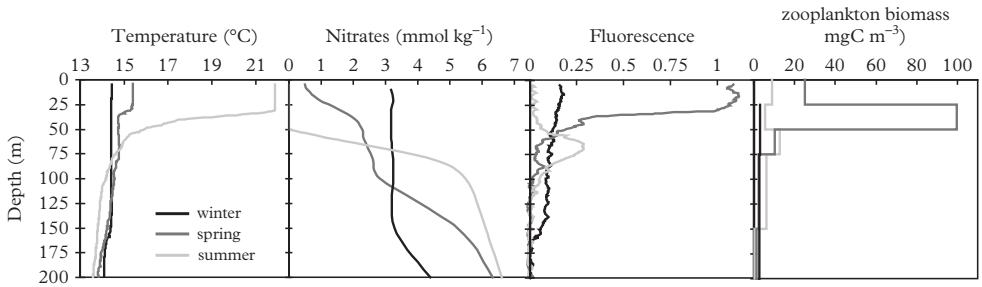

Figure 7.8 *Seasonal variations in the eastern North Atlantic (POMME project): in the mixed layer, the temperature is equal to the surface temperature. The fluorescence is due to the presence of chlorophyll and therefore it provides information on the abundance of phytoplankton.*

for photosynthesis. The biological production is then limited by the lack of light. In spring, surface waters warm up, become less dense and stabilize. With light and nutrients, phytoplankton then develop rapidly: this is the spring bloom. The phytoplankton growth is then limited by the nutrient depletion and zooplankton grazing. In summer, warm and light surface waters do not mix (or very little) with the nutrient-rich deep waters: in the absence of nutrients, the biomass is low in surface waters. There is, however, a maximum of chlorophyll beneath the surface where phytoplankton have both sunlight and nutrients (around 75 m of depth; Fig. 7.8). It is not until the following winter that the surface layer is effectively refilled with nutrients by winter mixing. The seasonal cycle described above is common in the ocean (Problem 1).

However, even in the absence of nitrate, phytoplankton activity can still continue. The dead particulate organic matter is actively recycled by bacteria before it has time to sink below the surface layer. Thus, particulate organic nitrogen is transformed into dissolved organic nitrogen and ammonium ions (NH_4^+), which can be used by phytoplankton. NH_4^+ being rapidly assimilated by phytoplankton, it does not have time to be oxidized to nitrate, as in the deep ocean (Fig. 7.9). Dissolved organic nitrogen is less easily assimilated than NH_4^+: it can be transported over long distances and supply nitrogen-deficient areas. In general, the lateral inputs should not be neglected (see Problem 5 of Chapter 5).

All the photosynthesized organic matter represents the **primary production (PP)**. During the year, the origin of nitrogen assimilated by phytoplankton evolves. When organic matter is photosynthesized with NO_3^- (or N_2 when it occurs) as a nitrogen source, it is called **new production (NP)** of organic matter. On the contrary, if the organic matter is formed from NH_4^+, it is called **regenerated production (RP)**. Therefore,

$$PP = NP + RP. \tag{7.1}$$

The distinction between new and regenerated production is important. Over a year, the organic nitrogen exported by sinking particles to the deep waters—the **exported production (EP)**—cannot exceed the amount of nitrate coming from the deep waters. As a general rule, if all available nitrate is consumed, the new production should be equal to the exported production *on average over a year*. At a given moment, these two fluxes can be different depending on the change of the biomass stock. Building of a comprehensive budget of the fluxes is difficult (Problem 3). The exported production represents a net loss of assimilable nitrogen for the ecosystem. It is therefore "in the interest" of the ecosystem to recycle organic matter. When the environment is low in nitrate (no NP), there is a closed loop between regenerated production and remineralization in surface waters. If this loop "leaks" because remineralization is ineffective, surface water becomes depleted in available nitrogen and the whole ecosystem is condemned.

Viral lysis short circuits the flow of carbon and nutrients from phytoplankton and bacteria to higher trophic levels (Suttle, 2007). The net effect of viruses on the biological pump is poorly constrained. At first sight, dissolved carbon released by cell lysis sinks slowly and is retained in surface waters, where much of it is converted by respiration to dissolved inorganic carbon (DIC), thereby reducing carbon export. However, compared to grazing, viral lysis releases directly labile cellular components, such as amino acids,

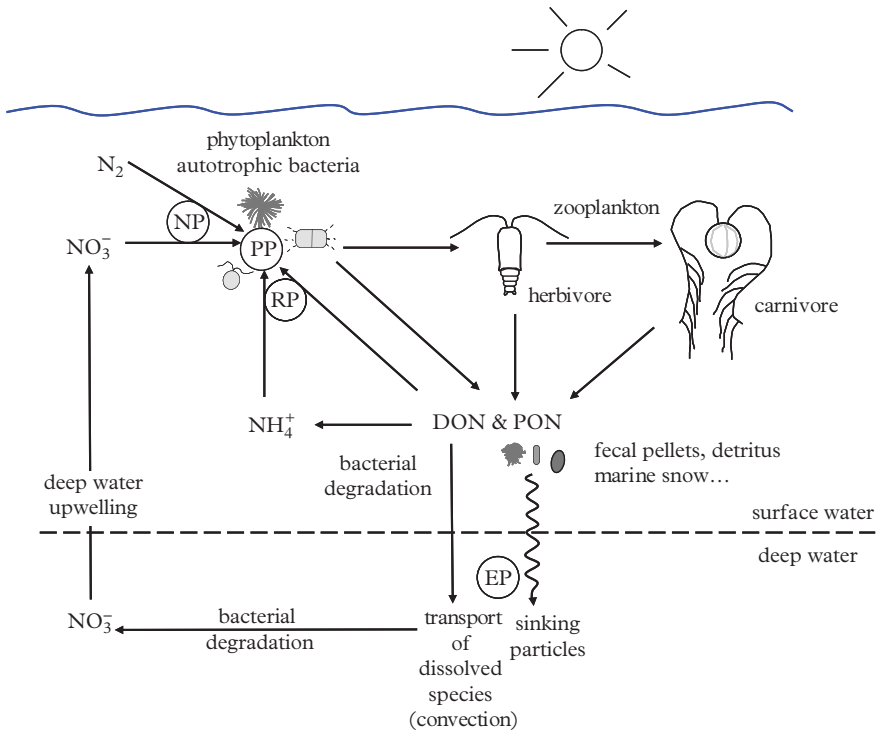

Figure 7.9 *Schematic representation of nitrogen fluxes through the marine ecosystem. DON: dissolved organic nitrogen; PON: particulate organic nitrogen. NP, RP, PP and EP labels indicate the fluxes corresponding to new production, regenerated production, primary production and export production.*

nucleic acids and complexed Fe, that can be rapidly incorporated by living organisms, thereby retaining more nutrients in the photic zone, whereas more recalcitrant carbon-rich material, such as cell walls, is probably exported to deeper waters. This "viral shunt" could increase the efficiency of the biological pump. Comparison of metagenomic data and particle flux estimates (obtained by underwater videoprofiler images of marine particles, see Chapter 9) suggests that *Synechococcus* and its viral phage assemblage (but not *Prochlorococcus*) are strongly correlated to the exported production throughout the oligotrophic ocean (Guidi et al., 2016). The causal link remains to be established, but it is suggested that the viral lysis of *Synechococcus* could produce colloids that favor particle aggregation and rapid sinking.

The concept of new and regenerated production entirely controlled by mineral nitrogen evolved with the discovery of the importance of the organic forms of dissolved nitrogen, carbon and phosphate as a source of nutrients for the synthesis of organic matter in surface waters. The role of bacteria in surface cycles becomes essential. More recently, the picture has become even more complicated. In very oligotrophic areas,

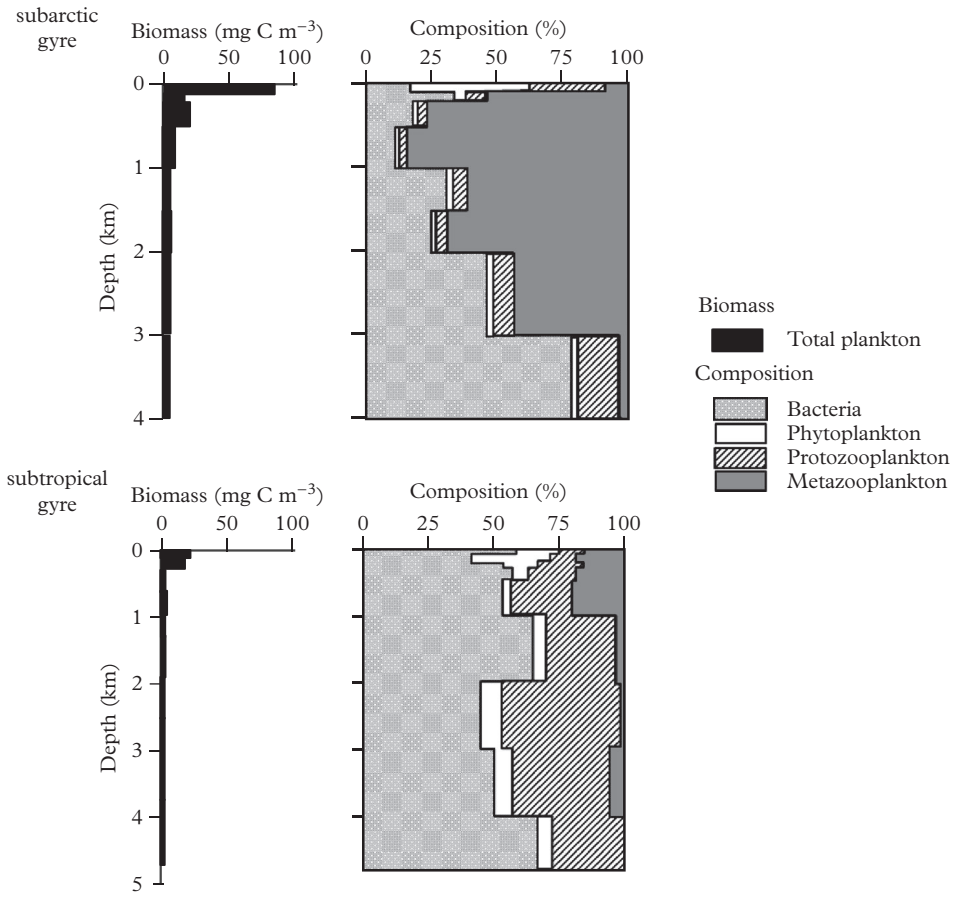

Figure 7.10 *Vertical distribution of total plankton biomass and its major taxonomic composition in two stations of the western North Pacific Ocean. The productive station is located in the subarctic gyre and the oligotrophic station is in the subtropical gyre. Subarctic gyre: nitrate-rich surface waters, associated with a weak thermocline, support a large phyto- and zooplanktonic biomass. The biomass is dominated by metazoan (crustacean, cnidarian, mollusks . . .). Subtropical gyre: nitrate-depleted surface waters, associated with a strong thermocline, result in a reduced biomass dominated by bacteria and support mainly small zooplankton (protists like foraminifera or radiolarians). Living phytoplankton cells are transported in the deep ocean embedded in sinking aggregates. Adapted from Yamaguchi et al. (2002).*

the uptake of molecular nitrogen (N_2) by certain types of algae and bacteria (such as *Trichodesmium*) provides a substantial amount of nitrogen to the ecosystem. The importance of N_2 fixation in the ocean was really understood only since the mid-1990s, with the impossibility of balancing the nitrogen budget and of explaining deviations from the Redfield ratio on the one hand and with the constraints brought by the nitrogen isotopes

(see Chapter 5) in the oligotrophic to areas on the other hand. When N_2 fixation is sufficient, nitrogen is not limiting any longer and as phosphate comes to exhaustion, it limits the biological production.

The behavior of the ecosystem can be characterized by the ratio between new production and primary production. This is the *f*-ratio

$$f = \mathrm{NP/PP}. \tag{7.2}$$

The new production reaches up to 50% of the primary production in spring when nitrate is abundant (eutrophic conditions), but it can be less than 5% in summer when surface waters are short on nutrients (oligotrophic conditions). Shifting from eutrophic to oligotrophic conditions causes an important evolution of the marine ecosystem: for example, in spring, phytoplankton are dominated by species of large sizes such as diatoms that form aggregates that quickly leave the surface by sedimentation, while in summer there are essentially nano- and picoplankton which are easily grazed and remineralized by bacteria and small zooplankton. Nutrient availability also controls the plankton community structure in the surface and deep waters of the gyres (Fig. 7.10).

DNA sequencing allows the adaptation of different types of plankton to environmental conditions to be understood. For example, *Prochlorococcus*, which is the smallest photosynthetic being on Earth, has a reduced genome that allows only NH_4^+ uptake as a nitrogen source. However, this reduced genome allows *Prochlorococcus* to be relatively insensitive to nutrient shortage thanks to a reduced nutrient requirement to synthetize DNA and to an efficient photoreceptor system that requires little nitrogen and iron. Metaproteomic studies have demonstrated that *Prochlorococcus* also responds to nutrient limitation by tuning the abundance of specific proteins promoting the uptake of P, N or Fe (Saito et al., 2014). Its small size gives a decisive advantage to absorb nutrients across its membrane with its very high surface/volume ratio compared to larger algae. Thus, *Prochlorococcus* is very abundant in the oligotrophic regions. Being small and having no mineral test, *Prochlorococcus* does not sink out of the photic zone and its death provides nitrogen assimilable by photosynthetic organisms even when nitrate is absent (oligotrophic conditions).

7.3 Estimating the Primary Production

Primary production is typically measured by incubation experiments, during which a solution strongly enriched in ^{14}C of artificial origin is added to seawater (with its living organisms) in a closed container. Enough ^{14}C is added so that the ^{14}C naturally occurring in seawater becomes negligible. However, the amount of added ^{14}C remains far below the amount of DIC naturally present in the sample, so that it does not alter the chemical composition of the environment. During the incubation, ^{14}C is taken up by phytoplankton. Plankton are then filtered and the amount of radioactivity of assimilated ^{14}C is measured. It is then easy to deduce the amount of DIC consumed by the plankton. To obtain results as close as possible to the natural conditions, simple and clever systems

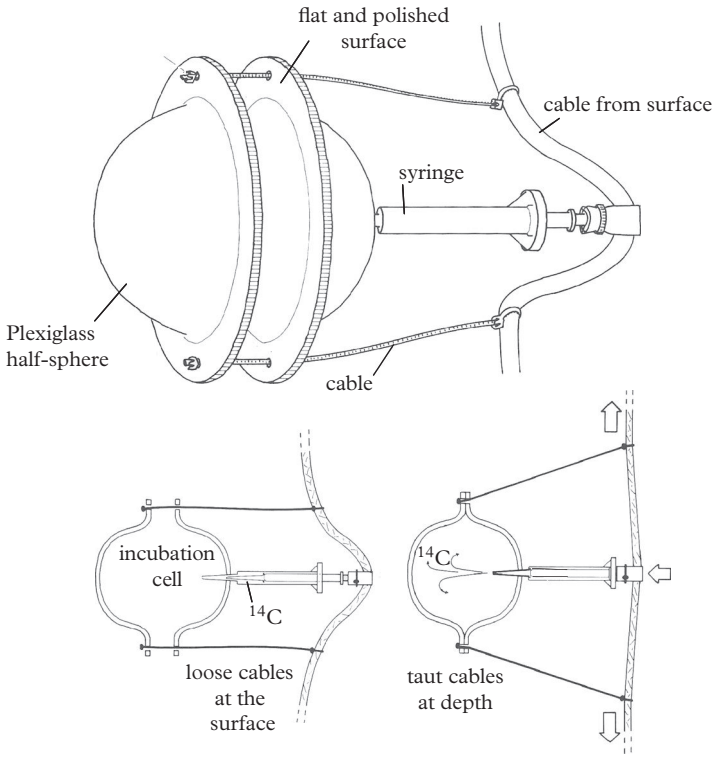

Figure 7.11 In situ *incubation system. The half-spheres are lowered open. When they arrive at the targeted depth, the nylon cable stretches out. It closes the half-spheres which trap seawater and it injects ^{14}C. The system remains closed when it's pulled back to the surface. Modified from Dandonneau and Le Bouteillier (1992).*

allow *in situ* incubations on mooring lines at different depths from the surface down to the base of the photic zone (Fig. 7.11). The new production can be determined by replacing ^{14}C by isotopically (^{15}N) labeled nitrate. If instead of nitrate, isotopically (^{15}N) labeled ammonium ions are added, the regenerated production can be determined.

Application exercise: Biological production in the NE Atlantic

During the POMME oceanographic program, the assimilation rates of carbon (ρcarbon), NO_3^- (ρNO_3^-) and NH_4^+ (ρNH_4^+) were measured in spring and summer (Table 7.1).

Table 7.1 *Biological production in surface waters*

	Spring	**Summer**
Mixed layer depth (m)	93	28
$(C/N)_{organic\ matter}$ (mol mol^{-1})	11	11
ρcarbon (mg C m^{-3} d^{-1})	42 ± 16	9 ± 3
ρNO_3^- (nmol kg^{-1} d^{-1})	130 ± 62	18 ± 19
ρNH_4^+ (nmol kg^{-1} d^{-1})	97 ± 39	63 ± 12

Calculate the primary production, the new production, the regenerated production of carbon and the *f*-ratio. Discuss the trophic status in spring and summer. Compare with the spring and summer data shown in Fig. 7.7, which were collected during the same program.

Solution:

Primary production is equal to the rate of carbon assimilation (therefore there is no calculation to do). The rates of nitrogen assimilation must be converted into carbon equivalent to be compared to the PP. For example,

$$\underset{mgC\,m^{-3}\,d^{-1}}{NP} = \rho NO_3^- \times \underset{kg\,m^{-3}}{10^3} \times \underset{nmol\,mmol^{-1}}{10^{-6}} \times \underset{(C/N)_{organic\,matter}}{11} \times \underset{g\,mol^{-1}}{12.}$$

The following results are obtained (Table 7.2):

Table 7.2 *Organic production in surface waters*

	Spring	**Summer**
PP (mg m^{-3} d^{-1})	42 ± 16	9 ± 3
NP (mg m^{-3} d^{-1})	17 ± 8	2.4 ± 2.5
RP (mg m^{-3} d^{-1})	12 ± 5	8.3 ± 2
NP + RP (mg m^{-3} d^{-1})	29 ± 13	10 ± 4
f = NP/(NP + RP)	57%	22%

NP + RP is not significantly different from PP, which is consistent with equation (7.1). The PP is stronger in spring, when nitrate is abundant (eutrophic conditions), than in summer when there is no more nitrate in surface waters (oligotrophic conditions). In summer, the new production is not significantly different from 0.

Another method is to measure the O_2 production by photosynthesis (Problem 2). The change of O_2 concentration is measured in seawater samples incubated with light (net community production, or NCP) and other samples incubated in the dark (respiration). The difference between the two is the gross community production

$$GCP = NCP - RESP. \tag{7.3}$$

These estimates are based on incubations in closed systems that may be biased. If zooplankton are undersampled in the small volume of seawater, the grazing pressure on algae is reduced and the primary production is overestimated. Similarly, the accidental contamination of the incubation system by a limiting element may also lead to overestimation of primary production. This is why a method based on the analysis of $\Delta^{17}O$ in non-incubated samples has been developed. It uses the unique signature given to atmospheric oxygen by mass-independent fractionations (see Chapter 3 for details). Atmospheric oxygen is preferentially depleted in ^{17}O during the formation of stratospheric ozone ($\Delta^{17}O = 0$ per meg, because the atmosphere is the reference) while photosynthetic oxygen ($\Delta^{17}O = 249$ per meg) is not. The $\Delta^{17}O$ of dissolved O_2 in seawater depends of the proportion of photosynthetic O_2 and of atmospheric O_2. As the net O_2 flux diffusing from the atmosphere is known (Chapter 6), the photosynthetic oxygen flux (GCP) can be determined. In addition, the degree of over- or under-saturation of O_2 in seawater allows estimating the ratio between primary production and regenerated production.

Application exercise: Estimation of biological production from $\Delta^{17}O$ (Hendricks et al., 2004)

In the polar front zone of the Southern Ocean, the following values are measured in the mixed layer:

$\Delta^{17}O = +51.0$ per meg;
$[O_2]/[O_2]^{sat} = 1.03$.

Based on the wind speed (see Chapter 8), the piston velocity is estimated as $v_p = 5.0$ m d^{-1}. The surface water temperature is 4.7°C. The mixed layer depth is $h = 50$ m.

Determine the primary production and net production of organic matter in the mixed layer. Assume that the $\Delta^{17}O$ of the O_2 of atmospheric origin is +8 per meg due to fractionation during diffusion in the stagnant film. The mass dependent isotopic fractionations related to photosynthesis and respirations are neglected because they do not affect $\Delta^{17}O$.

Solution:

Gross community production

$\Delta^{17}O$ of dissolved oxygen is intermediate between the photosynthetic O_2 and atmospheric O_2. Photosynthetic O_2 and atmospheric O_2 flux are roughly equivalent.

The balance equation for the isotopic composition is used in a steady-state system (Chapter 5, equation 5.21b), but the water transport term ($k_w C_w(R_w - R)$) is replaced by the atmospheric diffusion term ($v_p/h[O_2]^{sat}(R_{atm} - R_{ml})$) and the source term ($s(R_s - R)$) is the gross community production ($GCP(R_{phot} - R_{ml})$). The subscripts atm, phot and ml stand for the atmospheric, the photosynthetic and the mixed layer O_2. Replacing R by the $\Delta^{17}O$, this yields

$$v_p/h\,[O_2]^{sat}(\Delta^{17}O_{atm} - \Delta^{17}O_{ml})\rho_w + GCP(\Delta^{17}O_{phot} - \Delta^{17}O_{ml}) = 0.$$

It follows that

$$GCP = k_{O_2} \times [O_2]^{sat} \times \frac{\Delta^{17}O_{cm} - \Delta^{17}O_{atm}}{\Delta^{17}O_{phot} - \Delta^{17}O_{cm}} \times \rho_w.$$

The term ρ_w (density of water = 1027 kg m^{-3}) is here to convert the flux integrated over the mixed layer expressed in mmol m^{-2}. At 4.7°C, $[O_2]^{sat}$ = 320 μmol kg^{-1} (see Fig. 2.8 in Chapter 2). Using other values given above, we obtain GCP = 320 mmol m^{-2} d^{-1}.

Net community production

$O_2 > O_2^{sat}$: there is a net production of O_2 (photosynthesis dominates over remineralization). At steady state, this net production is balanced by an O_2 flux leaving the mixed layer

$$NCP = k_{O_2}(O_2 - O_2^{sat})\rho_w.$$

Using the values of the exercise, we obtain NCP = 48 mmol m^{-2} d^{-1}.

Finally, the primary production can be estimated from the chlorophyll content and the amount of light available for photosynthesis (photosynthetically available radiation or PAR). For this type of estimate it is particularly important to use the "ocean color" satellite data (see Section 7.4).

Other methods exist for estimating the organic matter production.

- In a well-stratified system, the decrease on the nutrient concentration (NO_3^-, PO_4^{3-}) in the photic zone between winter and summer is due to their consumption by phytoplankton. This allows calculation of new production of carbon by using the Redfield ratios (see Chapter 1).
- Sediment traps measure directly the production exported below the photic zone. We will see in Chapter 9 that trap data must to be used with caution.

7.4 Global Distribution of Photosynthesis and Ocean Color

We have seen in Chapter 1 that the winds at the surface of the ocean induce vertical movements of water called "Ekman pumping." The water that accumulates in the anticyclonic gyres moves downward (downward Ekman pumping), which leads to a deepening of the thermocline. On the contrary, in areas of horizontal current divergence, water has an upward motion (upward Ekman pumping), resulting in a rise of

the thermocline. It is the Ekman pumping which enables or inhibits the refilling of the oceanic mixed layer by nutrients. An upward Ekman pumping allows an upwelling of nutrient-rich deep water to the surface (upwelling area). Instead, with a downward Ekman pumping nutrient-poor surface waters sink and it is impossible for the deeper waters to feed the photic zone with nutrients. The intensity of photosynthesis is therefore directly related to the vertical movement.

A global picture of photosynthesis in the ocean is obtained by measuring the ocean color from satellites. On these satellites, sensors observe the ocean surface lit by the Sun and analyze the reflected light. In the absence of algae, the ocean surface is blue. Algae change the ocean color because they contain pigments (including chlorophyll) that absorb blue and red solar radiations, giving a green color to the ocean. The amount of chlorophyll present at the ocean surface can be retrieved from these data (the sensor does not see beyond a few meters deep.) By carefully selecting the wavelengths, it is possible to identify the types of pigments and thus the phytoplankton groups present. Algorithms taking into account the amount of chlorophyll and the amount of available light allow estimation of the primary production.

Figure 7.12 shows annual average concentration of chlorophyll from the SeaWiFS satellite. The most remarkable features are as follows:

– Around the Equator, the trade winds cause surface waters to flow away from the Equator, which causes upwelling of nutrient-rich deep waters and a development of phytoplankton.

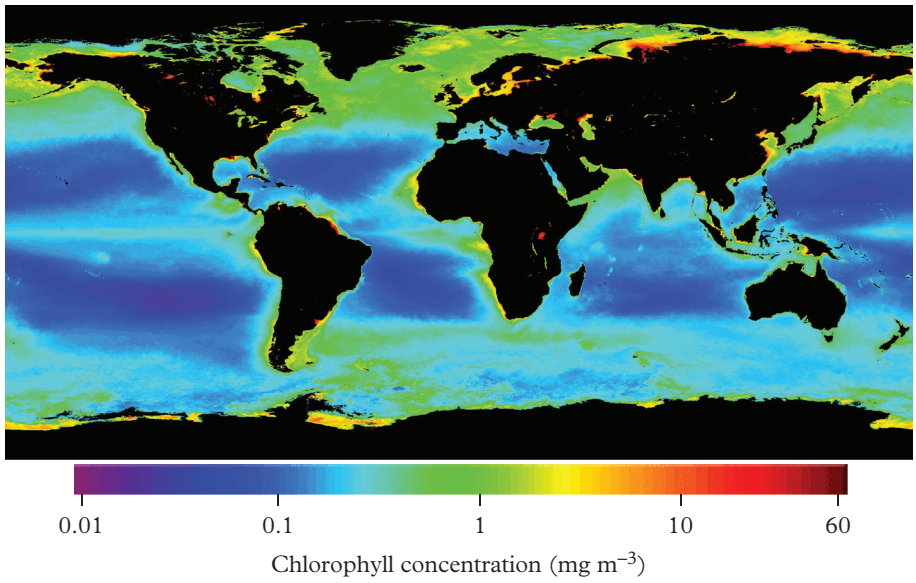

Figure 7.12 *Estimation of the concentration of chlorophyll in the ocean surface waters from SeaWIFS satellite measurements (annual average). After http://oceancolor.gsfc.nasa.gov/cgi/image_archive.cgi?c=CHLOROPHYLL.*

- Subtropical gyres are chlorophyll-poor because (1) the anticyclonic wind circulation induces a sinking of the surface waters in the center of the gyre, preventing the upwelling of nutrient-rich water, and (2) in the absence of marked seasons, there is little winter mixing;
- Cyclonic subpolar gyres are rich in chlorophyll because the cyclonic wind circulation induces an upwelling of deep water all year long and in winter, strong and cold winds mix surface waters over hundreds of meters.
- Coastal regions are rich in chlorophyll along the eastern edges of ocean basins such as off Mauritania: trade winds blow southward and the Ekman drift is westward, that is, the water is driven off the coast (see Chapter 1). The westward drift of surface water is balanced by an upwelling of cold and nutrient-rich thermocline waters. These nutrients allow the development of a significant biomass. An analogous process occurs along the Peruvian coast. However, there, the trade winds can slow down or even be reversed during the El Niño years: surface waters are then pushed toward the continent and they block the deep water upwelling: phytoplankton can no longer develop and fish catches are very bad.
- The mouths of the Amazon and the Orinoco rivers bring nutrients in large quantities to the ocean, so plankton develop easily.

More details on the information provided by ocean surface color are explored in Problem 3.

Large-scale circulation structures described in Chapter 1 and the winter mixed layer formation are not the only causes for upwelling of nutrients in surface water. Eddies with a radius of the order of 50 km (they are called "mesoscale eddies") cause changes of the mixed layer and thermocline depths, which allows new inputs of nutrient in the surface waters. These fine structures have long remained out of reach of modeling. The arrival of a model with spatial resolution in 1/9 of a degree or less allows them to be taken into account at the level of an ocean basin. Coupled physics/biology simulations suggest that the mesoscale activity supplies 30% of the nutrients required to support the primary production in the oligotrophic areas (Problem 4).

In some areas, Ekman pumping produces deep water upwelling, but the chlorophyll concentration of surface waters remains low. This includes areas with an upward Ekman pumping such as the north and equatorial Pacific, where productivity is much lower than in the Atlantic at the same latitudes. In the Southern Ocean, despite a positive wind curl that causes major upwelling of deep water in the polar front area (see Chapter 1), chlorophyll is scarce. In addition, measurements made at sea during oceanographic campaigns show that nutrients are abundant in these surface waters. These features are responsible for their acronym: HNLC (high nutrient, low chlorophyll). These features will be explained in Section 7.5.

7.5 Iron Limitation

It is sufficient to add just a very small amount of iron to surface water freshly collected in an HNLC area to stimulate the growth of algae and the consumption of nitrate.

Therefore, iron is the limiting element of HNLC areas. Why iron and why in these areas? Iron is a micronutrient used in many proteins involved in the carbon (including photosynthesis) and nitrogen (for N_2 assimilation) cycles. It is therefore essential for biological activity. Iron is the fourth most abundant element in continental rocks, but the very low solubility of Fe^{3+} (which is the stable form in water containing O_2) makes it in fact one of the least abundant elements of the ocean (Chapter 1). The HNLC zones are areas in which the inputs of continental material are very low. The crucial role of these inputs can be seen in the vicinity of volcanic islands such as the Kerguelen archipelago in the Indian sector of the Southern Ocean, where iron released by the weathering of lavas and volcanic sediments produces a chlorophyll plume in the midst of an HNLC zone (Fig. 7.13).

This limitation has a particular importance for the evolution of the climate. Based on the inverse correlation found in the Vostok ice core (Antarctica) between the desert dust content and the CO_2 concentration trapped in air bubbles (see Chapter 11), it was proposed that the low CO_2 concentrations observed during glacial periods are due to fertilization of currently HNLC areas by enhanced eolian deposition of iron-rich continental dusts. This enhanced dust flux would result from more arid conditions during

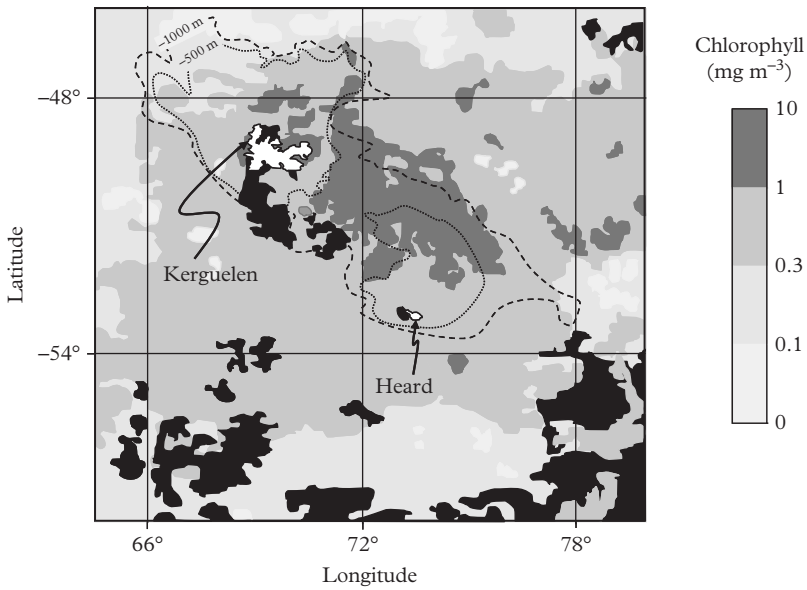

Figure 7.13 *Chlorophyll concentrations above and around the Kerguelen plateau. This SeaWiFS image obtained during the austral spring shows a chlorophyll plume associated with the Kerguelen and Heard Islands plateau (in white). Dotted line: 500 m isobath. Dashed line: 1000 m isobath. The Southern Ocean receives very little eolian dusts from continental areas, so that erosion of the Kerguelen Islands and the shelf sediments provide most of the iron that supports biological production. The black areas are hidden by clouds. Modified after Blain et al. (2001).*

the ice ages. To confirm the role of iron and to test its impact on full-scale ecosystems, half a dozen experiments of fertilization over areas of the order of hundreds of square kilometers have been achieved. They confirmed the limiting role of iron, but they did not demonstrate that they lead to a long-term sequestration of CO_2.

To prevent Fe shortcomings, algae have developed different strategies. One of them is to produce siderophores, which are molecules with a very high affinity for Fe(III). By complexing to Fe(III), siderophores stabilize Fe(III) in solution, whereas it would remain as insoluble Fe(III) hydroxides otherwise. In addition, some phytoplankton species create "private" stocks of bioavailable iron by releasing specific siderophores that are not recognized by their competing species. The *Prochlorococcus* bacteria have another strategy: its photosystem responsible for photon collection is so efficient that *Prochlorococcus* needs very little Fe for its photosynthesis.

Iron limitation does not only act on photosynthesis. It also affects the assimilation ratio of major nutrients (Problem 5). As iron is also involved in the reduction of N_2 to NH_3, cyanobacteria such as *Trichodesmium* may be limited by an iron deficiency. This also gives iron a limiting role in "non-HNLC" oligotrophic areas.

7.6 Silica Limitation

Silica also plays an important role in the control of biological production (Fig. 7.14). Indeed, the lack of silica limits diatom development, because they cannot synthesize their frustules made of amorphous silica. When nutrients are available, diatoms develop quickly. At the end of the bloom, they aggregate to each other and sink below the photic zone. They are therefore very efficient players of the export production (see Chapter 9). Diatoms dominate the Southern Ocean due to upwelling of silica-rich deep waters south of the Polar Front. Elsewhere, diatoms develop at the beginning of the bloom but they are rapidly limited by the lack of dissolved silica. To understand this limitation, we must return to the ocean circulation. We have seen above that surface waters are fed with nutrients to varying degrees by thermocline waters. However, the motion of these waters is not only vertical. The thermocline is largely ventilated by modal Subantarctic waters which originated around 45°S in the Southern Ocean. These modal waters were depleted in silica at the level of the polar region but they have kept a high nitrate concentration (remember that it is a HNLC zone). Under the effect of wind forcing, these waters downwell in the thermocline around 45°S.

These waters can be followed through the tracer "Si*" which is defined as follows

$$Si^* = [Si] - [NO_3^-]. \tag{7.4}$$

This tracer is quasi-conservative because the Si/N ratio of diatom production and remineralization is usually Si/N = 1/1. Subantarctic Mode Waters have the lowest Si* of the entire ocean, which allows us to follow them easily through the thermocline. Numerical simulations suggest that Subantarctic modal waters provide *ultimately* about 75% of the nutrients consumed by biological activity north of 30°S (Sarmiento et al., 2004).

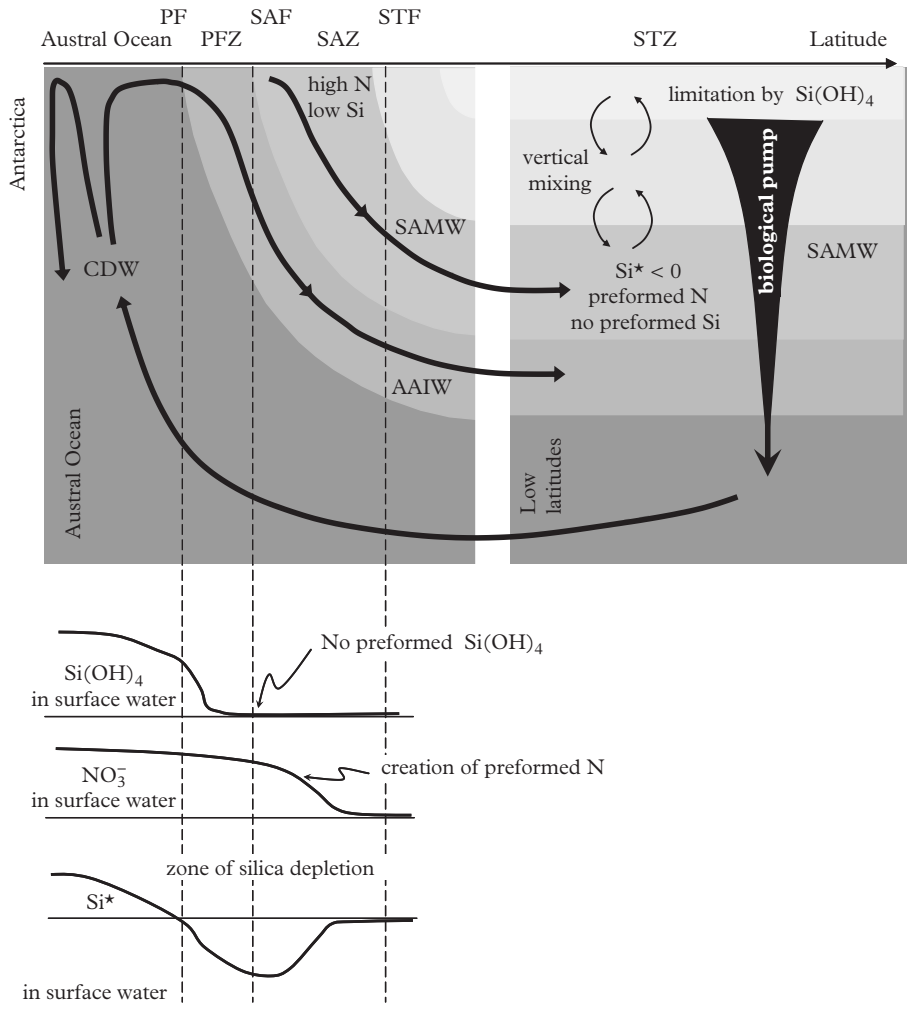

Figure 7.14 *Origin of the low dissolved silica content of thermocline waters. Top part of the figure: water mass circulation. Bottom part of the figure: tracer concentration in surface waters. Circumpolar Deep Water (CDW) upwells to the surface throughout the Southern Ocean. It is transported northward through the Antarctic Polar Front (APF) in the Polar Front Zone (PFZ) where Antarctic Intermediate Waters (AAIW) are formed, and then through the Subantarctic Front (SAF) in the Subantarctic Zone (SAZ) which is bounded to the north by the Subtropical Front (STF). Flowing northward, surface waters are depleted in dissolved silica faster than in nitrate giving Subantarctic Modal Water (SAMW) a very low* Si* *signature. The SAMW then sinks into the base of the thermocline and supplies nutrients to lower latitude waters. Modified from Sarmiento et al. (2004).*

7.7 A CO_2 Limitation?

We saw in Chapter 2 that the total inorganic carbon concentration is not strongly depleted in surface waters compared to deep waters, which means that inorganic carbon is not a limiting element of the biological production. However, photosynthesis specifically uses CO_2 that represents approximately 1% of DIC (see also Chapter 8). For many phytoplankton species, the half-saturation constant of CO_2 for photosynthesis is lower than CO_2 solubility (see Chapter 5, Fig. 5.2), which argues against a limitation by CO_2. However, it must be kept in mind that due to photosynthesis, the CO_2 concentration within and around a phytoplankton cell may be significantly lower than the average CO_2 concentration of seawater. In fact, isotopic data suggest that a limitation by CO_2 is possible.

Indeed, there is a decrease of the $\delta^{13}C$ of plankton when the CO_2 concentration of seawater decreases (Fig. 7.13). CO_2 being less soluble in warm water than in cold water, there is less CO_2 available in the former than in the latter. There is also a negative correlation between the $\delta^{13}C$ of organic matter and the sea surface temperature. (Note that

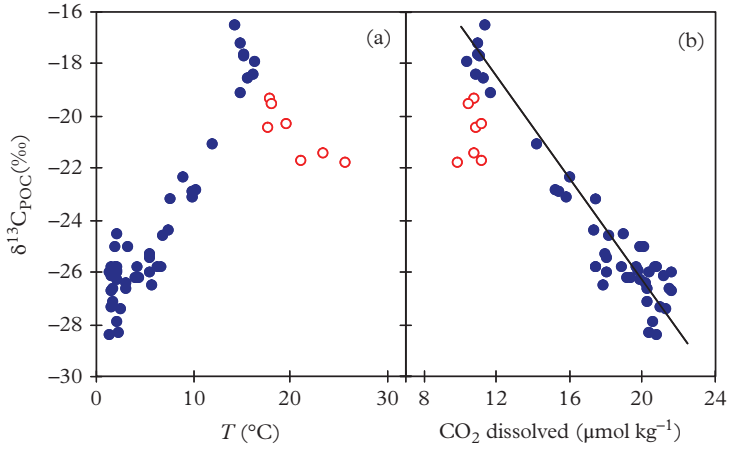

Figure 7.15 *Evolution of $\delta^{13}C_{POC}$, T and CO_2 in the surface water of the South Indian Ocean. Dots: samples collected south of the subtropical convergence (45° S). Empty circles: samples collected north of the subtropical convergence. A positive correlation exists between the $\delta^{13}C_{POC}$ and the seawater temperature below 15° C. Above 15° C, the $\delta^{13}C_{POC}$ decreases when temperature increases. (b) For CO_2 levels greater than 11 µmol kg^{-1}, the increase in fractionation with the CO_2 concentration is observed. The decrease of the CO_2 solubility when temperature increases explains the $\delta^{13}C_{org}$–temperature relationship between 0 and 15° C. When the CO_2 content is < 11 µmol kg^{-1}, isotopic fractionation becomes independent of the CO_2 concentration, suggesting that phytoplankton adapts to the low CO_2 content of warm seawaters. Modified from François et al. (1993).*

the direct influence of temperature on fractionation between DIC and atmospheric CO_2 is relatively weak. See Chapter 3.)

Algae have different strategies to avoid a growth limitation by a lack of dissolved CO_2: (i) catalysis of the conversion of HCO_3^- into CO_2 by the carbonic anhydrase enzyme that acts in and around the cell while the overall CO_2 concentration of seawater remains unaffected (Burkhardt et al., 2001) or (ii) in the case of coccolithophorids, by the use of CO_2 produced during the formation of $CaCO_3$ (see Chapter 8). These processes affect the $\delta^{13}C$ of the organic matter. Thus, there is not a simple and unique relationship between the $\delta^{13}C$ and $[CO_{2dissolved}]$ and the proposed relationship in Fig. 7.15 has a limited range of validity to reconstruct the CO_2 paleo-concentration of seawater.

7.8 The Long-Term Limitation of the Production

Which element limits the biological production on long timescales? In this chapter, we introduced nitrogen as the main limiting factor of today's ocean. However, in the long term, phosphate could take over. We have already mentioned that in very oligotrophic areas, dissolved nitrogen (N_2) fixation by *Trichodesmium* is sufficient for shifting from a nitrogen limitation to a limitation by phosphate which comes to exhaustion.

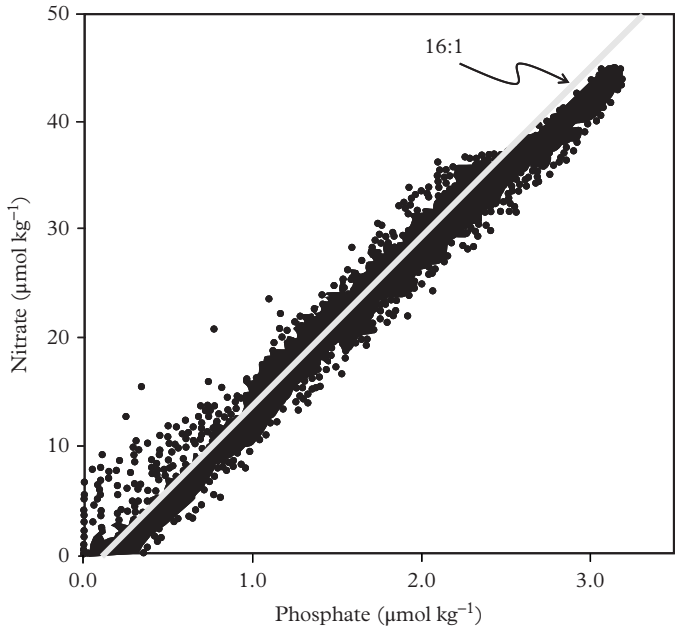

Figure 7.16 *Concentrations of nitrate and phosphate in the ocean. Adapted from Tyrell (1999).*

However, this is not the most common situation and it seems that in general the limiting nutrient is NO_3^- rather than PO_4^{3-}, because the vast majority of surface waters which contain no NO_3^- still contain some PO_4^{3-} (Fig. 7.16). In fact, nitrogen and phosphate cycles differ significantly. N_2 fixation and denitrification represent large nitrogen fluxes which cause a fast turnover of assimilable nitrogen across the ocean. Thus, the nitrate residence time in the ocean (about 3000 y) is much shorter than the phosphate residence time (20,000–80,000 y). The productivity of the ocean is therefore controlled in the long term by phosphate and in the short term by nitrate. It seems that the conflicting effects of N_2 fixation and denitrification maintain an N/P ratio of 16/1 in seawater across the ocean, similar to the N/P Redfield ratio of organic matter (Fig. 7.14). But how can these two processes that do not occur in the same areas of the ocean be coupled? A hypothesis involves dissolved oxygen. An increase of the nitrate stock due to a strong N_2 fixation would lead to an increase of organic matter production in surface waters and remineralization in the deep ocean. This enhanced remineralization would result in a decrease of the O_2 concentration in intermediate and deep waters. This follows an extension of anoxic zones and denitrification, which would reduce the nitrate concentration. Conversely, a global decrease in N_2 uptake would be compensated by a decrease of denitrification. Ultimately, N_2 fixation is limited by the availability of PO_4^{3-}, so that the N/P ratio of seawater adjusts to the N/P ratio of the organic matter mineralized in the deep waters. This would explain the similarity between the N/P ratio of organic matter and seawater (Tyrell, 1999).

7.9 Anthropogenic Impacts

Away from oligotrophic area, the ocean receives increasing nutrient inputs of anthropogenic origin. These effects are particularly marked in coastal areas with restricted communication with the open ocean. For example, the increase in nitrate emissions by agriculture results in fertilization of seawater, which triggers more and more "green tides" on the beaches of Brittany (France). In the Gulf of Mexico, the increase of nitrogenous compound inputs by the Mississippi River induces a strong organic matter production and a strong oxygen consumption to remineralize it at depth. The decrease of the dissolved oxygen content of seawater leads to the death of many animals and compromises the local fishing industry.

Eutrophication, that is, the overall increase in organic production, is not the only consequence of the increase in anthropogenic inputs. By modifying the P/N/Si ratio of coastal waters, these inputs change the structure of ecosystems. In the North Sea, for example, the N:P ratio of the Rhine increased from 30 in 1950 to 50 in 1985. Efforts to reduce releases of phosphate and the more modest decrease in nitrate releases have led to an N:P ratio greater than 100. At the same time the flux of silica, which is controlled by the alteration of minerals, has remained stable. In the North Sea, diatoms have declined and were replaced by flagellates like *Phaeocystis*, a toxic alga with an abundance that has increased by a factor of five. The reduction of phosphate releases in the 1990s does not

appear to have affected *Phaeocystis*. Its development is all the more important in that it is not grazed by zooplankton. In addition, overfishing may lead to significant changes in ecosystems. Climate change can have highly variable effects on the biological production (Problems 6 and 7).

Green or Red Adverse Opportunists

In August 2009, a horse died after getting stuck in rotten algae in an area which had been a large and beautiful beach in Brittany. Its rider fainted before being rescued by a backhoe that . . . just picked up these algae. Both were victims of poisoning by hydrogen sulfide (H_2S which gives the smell to stink balls) produced by the algae decomposition. These algae were *ulvea*. Their development is opportunistic, that is, they take advantage of an imbalance in the natural environment to proliferate. Over 50 y, the nitrate concentration in the French Brittany rivers has been multiplied by 10 due to of intensive agriculture (livestock, but also consolidation of fields removing any barrier to the water). *Ulvea* love nitrate. With spring warming and the return of the Sun, they use these riverine inputs and grow in the estuaries and sea, are carried by currents and just die on the beaches where they form huge green deposits called "green tides," which quickly decompose and become mushy and smelly, with the danger of associated toxic gases.

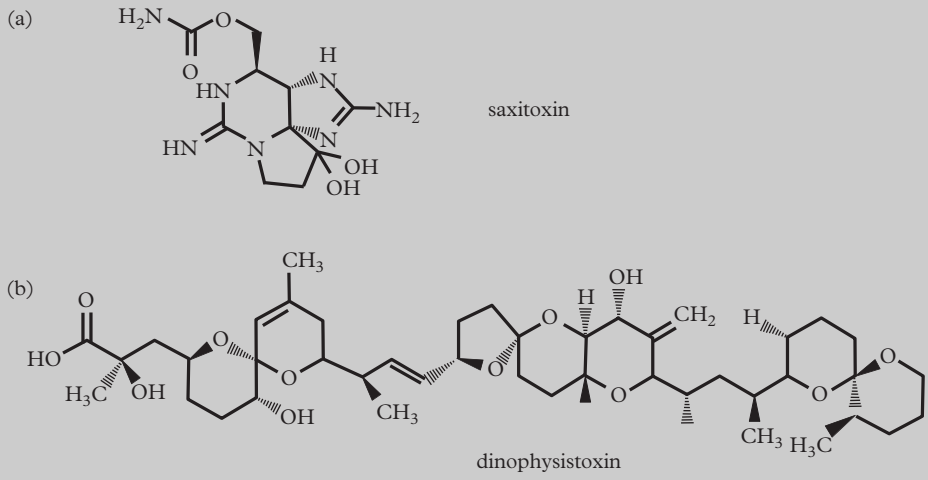

Figure 7.17 *Toxins produced by dinoflagellates and concentrated in shellfish. (a) Saxitoxin is produced by* Alexendrium *and causes the paralytic shellfish poisoning. (b) Dynophysistoxin-2 is produced by* Dynophysis *and causes the diarrhetic shellfish poisoning.*

Another color . . . but also undesirable, "red tides" are more and more frequent on the coasts. They are produced by dinoflagellates. Some dinoflagellates produce paralyzing poisons: the toxins responsible for paralytic shellfish poisoning (PSP) are so powerful that a quantity of the head of a pin (about 500 micrograms), easily present in 100 g of seafood, can be fatal to humans (Fig. 7.17). The first literary references (ca. 1000 BC) to harmful algal blooms are found in the Bible. "LORD: . . . I will strike the water of the Nile, and it will be changed into blood. The fish in the Nile will die, and the river will stink and thus the Egyptians will not be able to drink its water." (Exodus 7: 20–21). In 1793 one of the first fatal cases of food poisoning after eating contaminated shellfish was reported when British explorer Captain George Vancouver and his crew landed in British Colombia (Canada) in an area called, since then, Poison Cove.

PROBLEMS

Problem 1: Seasonal evolution of the biological production (Beauvais et al., 2003)

To evaluate the intensity of the biological production in the Mediterranean Sea, temperature, nitrate concentration and chlorophyll concentration were measured over a year in surface waters at the DYFAMED site (off the coast of Nice, France) (Fig. 7.18).

(1) Explain the causal relationships between these three parameters.

(2) How many bloom events occur? Do they have identical characteristics?

Problem 2: Community oxygen production

During the POMME program already described in this chapter, the net community production (NCP), the ecosystem respiration and the percentage of the various types of plankton were measured (Table 7.3).

Table 7.3 *Biological production in surface waters*

Season	Spring	Summer
NCP (mmol O_2 m^{-3} d^{-1})	1.6 ± 0.8	-1.1 ± 1.2
Respiration (mmol O_2 m^{-3} d^{-1})	-1.3 ± 0.5	-1.7 ± 0.9
Microplankton (%)	15	2
Nanoplankton (%)	66	20
Picoplankton (%)	20	77

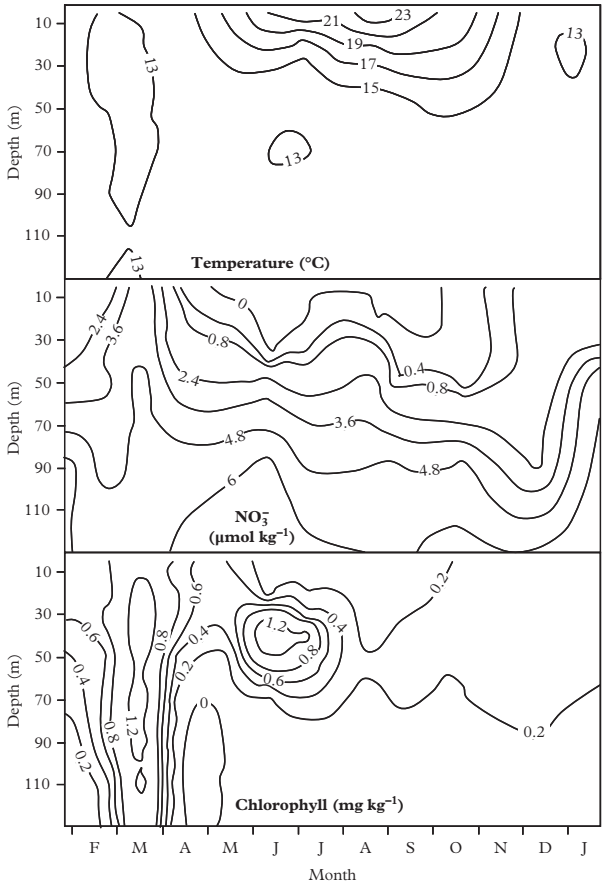

Figure 7.18 *Temporal evolution of temperature, nitrate concentration and chlorophyll concentration between 0 and 130 m in the western Mediterranean Sea. Modified from Beauvais et al. (2003).*

(1) Determine the gross community production.

(2) Compare these results with the primary production and new production based on the rates of carbon and nitrogen assimilation (see Application exercise: Estimation of biological production in the NE Atlantic).

(3) Based on these results and on the types of plankton, discuss the functioning of the ecosystem during spring and summer.

Problem 3: Questions about the SeaWIFS data

Referring to the Fig. 7.8, answer the following questions.

(1) Why is the Mediterranean Sea particularly oligotrophic, whereas surface water entering through the Strait of Gibraltar forms a cyclonic gyre?

(2) Why is the Black Sea very rich in chlorophyll although it is connected to the Mediterranean Sea?

(3) The Arabian Sea is moderately productive on average over the year. In fact, the production along the Arabian coast is low from autumn to spring, but is very high in summer. Explain why.

(4) Where are the most chlorophyll-poor waters in the ocean? Explain why.

(5) Why is there no visible upwelling effect along the west coast of Australia, unlike other western continental boundaries?

Problem 4: *Trichodesmium* in eddies (Davis and McGillicuddy, 2006)

During an east–west transect of the Subtropical North Atlantic gyre, the abundance of the *Trichodesmium* bacteria is measured continuously by a video-profiler towed by the vessel. Explain why *Trichodesmium* is consistently more abundant in anticyclonic eddies than in cyclonic eddies.

Problem 5: Effect of iron on diatoms (Hutchins and Bruland, 1998)

A small amount of iron is injected in the surface water of the California upwelling. Other surface water sample remains without iron addition as a control. Enriched samples and control samples are left for incubation during 4 hours and we note the following results (Table 7.4):

Table 7.4 *Biological production and nutrient*

	Enriched Samples		**Controls**	
	early	**end**	**early**	**end**
Chlorophyll ($\mu g\ kg^{-1}$)	0.5	9.2	0.5	2.4
Nitrate ($\mu mol\ kg^{-1}$)	8.1	0.13	8.1	6.5
Silica ($\mu mol\ kg^{-1}$)	8.2	0	8.2	3.4

(1) Comment the results.

(2) Knowing that the biomass is composed of diatoms, estimate the Si:N assimilation ratio for diatoms stressed and non-stressed by iron limitation.

(3) What can you conclude on the role of iron on the limitation of the diatoms by Si or N.

(4) What is the effect of iron on the f-ratio and the exported production?

Problem 6: Evolution of the Mauritanian upwelling (Stramma et al., 2010)

Climate change models predict a strengthening of the land–ocean thermal gradient along the Mauritanian coast.

(1) What effect should it have on the wind evolution? The data collected over the past 40 y appear to confirm these predictions.

(2) What is the consequence of this evolution on the surface current and vertical movements of water masses?

(3) What is the consequence of this evolution on organic production?

(4) Between 1960 and 2005, the concentration of dissolved oxygen in the thermocline waters below the Mauritanian upwelling decreased from 80 to 60 μmol kg^{-1}. Is there a connection between the wind strengthening and this decline of the O_2 concentration at depth?

Problem 7: Changes of the Bering Sea ecosystem (Schell, 2000)

The Bering Sea has long been an extremely rich ecosystem, but for two decades, the populations of birds and marine mammals have declined significantly. Is this related to the increasing pressure of fishing on the prey of these animals or a climate-related phenomenon that makes the ecosystem less productive? Researchers propose to use the $\delta^{13}C$ of bowhead whale bones to reconstruct the past biological productivity. Indeed, some whale bones shows annual growth layers in which the $\delta^{13}C$ depends on the $\delta^{13}C$ of their food. The $\delta^{13}C$ of the heterotrophic organisms is identical to the $\delta^{13}C$ of their prey, so that the $\delta^{13}C$ of whales reflects the $\delta^{13}C$ of the prey they eat, which itself reflects the $\delta^{13}C$ of the phytoplankton.

Experimental studies suggest that if algae growth rate is fast, their $\delta^{13}C$ is moderately negative, whereas if their growth rate is low their $\delta^{13}C$ becomes very negative. As the rate of algal growth increases with the availability of nutrients, there must therefore be a relationship between the $\delta^{13}C$ of the bones of the whales and the productivity in the Bering Sea

(1) Propose a mechanism linking the growth rate of algae and their $\delta^{13}C$.

(2) Between 1965 and 1995, the $\delta^{13}C$ of the whale bones decreased from –17 to –19.9‰. What can you conclude on the biological production trend in the Bering Sea over the last decades?

(3) From 1976 to 1995, the sea surface temperature of the Bering Sea has increased. Could it influence the evolution of productivity in the Bering Sea?

Following the publication of these results, other researchers have challenged the validity of the approach, because between 1965 and 1995 the CO_2 content of the atmosphere has increased by approximately 15% while the $\delta^{13}C$ of the atmospheric CO_2 has decreased by 0.3% (Cullen et al., 2001).

(4) Explain the origin of these variations. *Hint:* Look at Chapters 3 and 8.

(5) If these atmospheric variations are fully transferred to the dissolved CO_2 and $\delta^{13}C$ of surface waters, estimate qualitatively their impact on the assessment of biological productivity. *Hint:* Refer to Fig. 7.8 for an order of magnitude.

(6) In the Bering Sea, the mixed layers are very deep in the winter. What impact could it have on the evaluation of the biological productivity (Schell, 2001)?

8

CO_2 Exchanges between the Ocean and the Atmosphere

8.1 The Global Carbon Cycle

The exponential increase of greenhouse gas concentrations and, in particular, of the CO_2 concentration in the atmosphere since the industrial revolution is a source of concern (Fig. 8.1). It is mainly due to the combustion of fossil fuels and to a lesser extent to forest fires in tropical areas. This rise of greenhouse gases is likely to cause significant changes of the Earth's climate. Already, climate models undoubtedly attribute most of the 0.6°C of Earth's average surface temperature increase during the twentieth century to the accumulation of anthropogenic greenhouse gases in the atmosphere (see Chapter 11).

However, the accumulation rate of CO_2 in the atmosphere represents only half of the anthropogenic emissions (Fig. 8.2). The other half has already been absorbed by the ocean or the continental biosphere. The ocean plays a major role in the regulation of the CO_2 concentration in the atmosphere. The box-model representation of the carbon cycle highlights clearly that the main carbon reservoir at the surface of the Earth is the ocean. It contains 50 times more CO_2 than the atmosphere and 16 times more than the continental biosphere. Thus, the ocean regulates the carbon cycle at the Earth's surface. CO_2 fluxes between the ocean and the atmosphere cover different aspects:

- thermodynamics, with the differences of CO_2 partial pressure between the ocean and the atmosphere;
- diffusion kinetics, with the transfer of CO_2 at the ocean–atmosphere interface;
- a dynamic ocean, with the renewal of surface water and its transfer at depth.

8.2 The Partial Pressure of CO_2 in Seawater

We consider the ocean in contact with the atmosphere. The net CO_2 flux between the ocean and the atmosphere depends on the difference of CO_2 partial pressures between the atmosphere ($P_{CO_2}^{atmosphere}$) and seawater ($P_{CO_2}^{seawater}$). As the atmosphere is mixed quickly,

Marine Geochemistry. First Edition. Matthieu Roy-Barman and Catherine Jeandel.

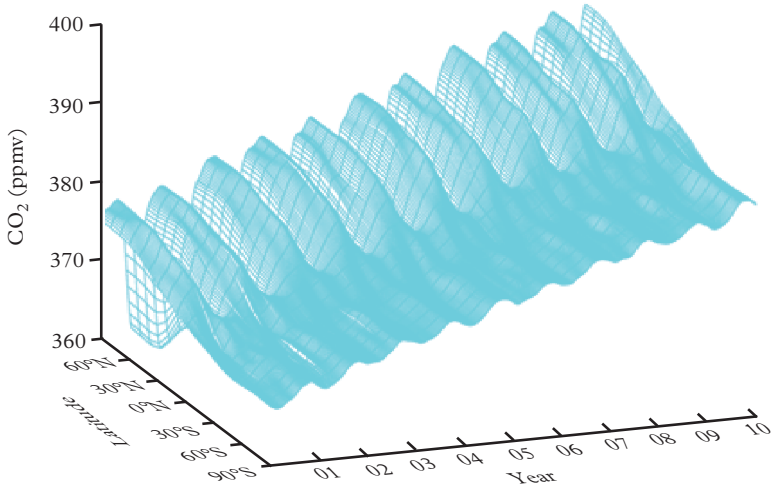

Figure 8.1 *Variation in time and space of the atmospheric concentration of CO_2. There is a concentration gradient between the two hemispheres. CO_2 seasonality is very marked in the northern hemisphere due to the strong seasonal variation of the continental biomass. There is also a long-term increase of the CO_2 concentration due to fossil fuel combustion. (Credit: NOAA/ESRL, http://www.esrl.noaa.gov/gmd/ccgg/).*

$P_{CO_2}^{atmosphere}$ varies much less than $P_{CO_2}^{seawater}$ either in time or in space (Fig. 8.3 and Problem 2). To understand the fluxes of CO_2 between the ocean and the atmosphere, we must first of all understand how $P_{CO_2}^{seawater}$ varies. The partial pressure of CO_2 in seawater is related to the concentration of dissolved CO_2 by the following relationship

$$P_{CO_2}^{seawater} = [CO_2]/\alpha_{CO_2}, \tag{8.1}$$

where α_{CO_2} is the solubility of CO_2 (Chapter 2).

8.2.1 Temperature Effect

The temperature strongly influences the CO_2 solubility, which drops by a factor of two between 0 and 25°C. Thus, for a given concentration of dissolved CO_2, $P_{CO_2}^{seawater}$ doubles between 0 and 25°C due to this decrease in solubility (Table 1.2 of Chapter 1).

8.2.2 Carbonate System Effect

We have seen in Chapter 1 that in seawater, dissolved CO_2 represents only roughly 1% of the dissolved inorganic carbon (DIC). Major DIC species are bicarbonate (HCO_3^-) and carbonate (CO_3^{2-}) ions that represent, respectively, 89 and 10% of the inorganic carbon.

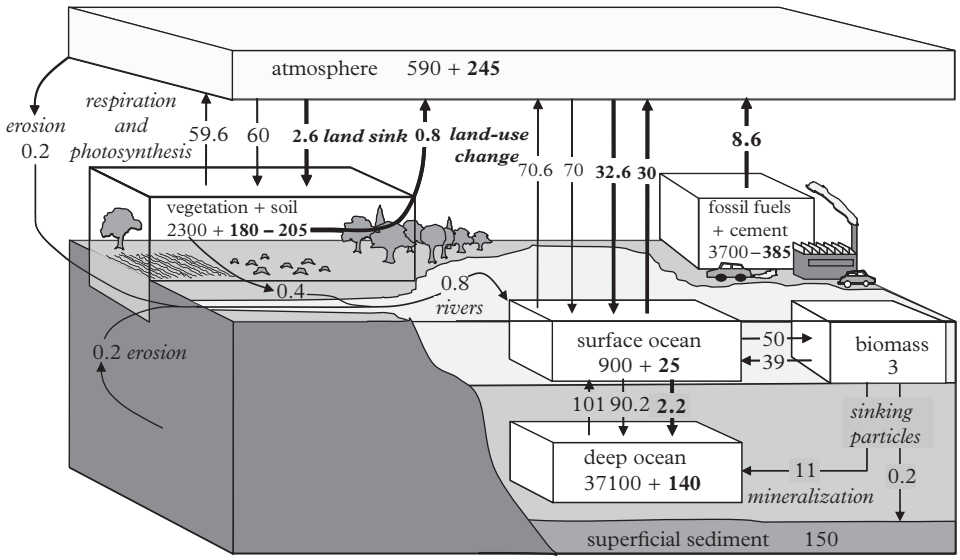

Figure 8.2 *Schematic representation of the carbon cycle in the 2000s. The reservoir contents (1 Pg C = 10^{15} g of carbon) are given for the pre-industrial period (normal characters), and for the content rise due to anthropogenic activities (bold characters). The arrows represent fluxes (1 Pg C y^{-1}: 10^{15} g of carbon per year) between different reservoirs (thin arrows: natural fluxes; thick arrows: anthropogenic fluxes). The difference between natural fluxes into and out of a box is zero (steady state). This is not the case for the anthropogenic fluxes: the C content of the atmosphere, the ocean and biosphere increases. After Sarmiento and Gruber (2002) and updated with LeQuere et al. (2013).*

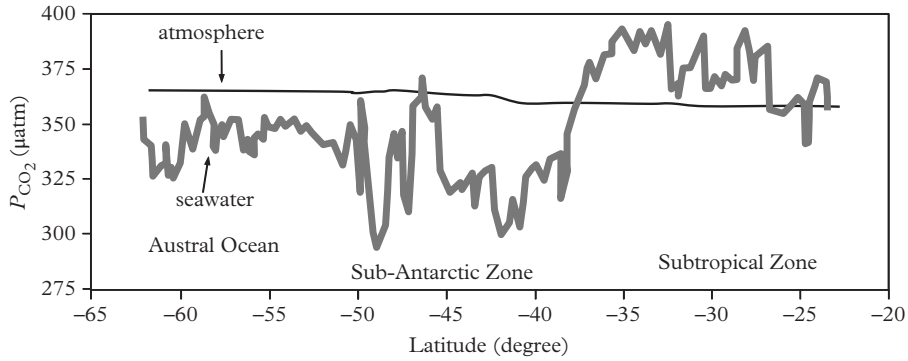

Figure 8.3 *P_{CO_2} along a transect between 63° S and 21° S (La Réunion Island) during the austral summer. Measurement in surface waters (thick line) and air (thin line). During the austral summer, the Subantarctic zones and part of the Southern Ocean act as a CO_2 sink while the subtropical zone is a source of CO_2. See Problem 2 for the winter section. Modified after Metzl et al. (2006).*

Dissolved CO_2 concentrations are dependent on all the chemical species involved in the diacid dissociation reactions

$$CO_2 + H_2O \Leftrightarrow HCO_3^- + H^+ \qquad K_1 = \frac{[HCO_3^-][H^+]}{[CO_2]} \tag{8.2}$$

$$HCO_3^- \Leftrightarrow CO_3^{2-} + H^+ \qquad K_2 = \frac{[CO_3^{2-}][H^+]}{[HCO_3^-]}. \tag{8.3}$$

K_1 and K_2 are constants depending only on temperature and pressure. By listing chemical species present in seawater (CO_2 gas, dissolved CO_2, HCO_3^-, CO_3^{2-}, H^+, H_2O) and the equations relating the concentrations of these species (equations 8.1, 8.2 and 8.3 and $[H_2O]$ = constant), we see that there are $6 - 4 = 2$ parameters that can be set freely. All the other parameters are then determined by the relations listed above. Familiar parameters such as $[CO_2]$ or $[H^+]$ are not practical because they are not conservative during the mixing of water masses. The concentration of DIC and alkalinity are therefore preferred. DIC is given by the equation

$$DIC = [CO_2] + [HCO_3^-] + [CO_3^{2-}]. \tag{8.4}$$

Alkalinity (Alk) is the concentration of negative charges that could neutralize H^+. It is calculated by the algebraic sum of the charges carried by weak acids and weak bases that can neutralize H^+

$$Alk = [HCO_3^-] + 2[CO_3^{2-}] + [B(OH)_4^-] + [OH^-] - [H^+], \tag{8.5}$$

or by the algebraic sum of charges carried by conjugated acids of strong bases (Na^+ is the conjugate acid of the strong base NaOH) and by the conjugate bases of strong acids (Cl^- is the conjugate base of the strong acid HCl)

$$Alk = [Na^+] + [K^+] + 2[Ca^{2+}] \ldots - [Cl^-] - [Br^-] - [NO_3^-] - 2[SO_4^{2-}]. \tag{8.6}$$

Electrical neutrality of water implies that the negative charge given by equation (8.5) equilibrates with the positive charge given by equation (8.6). Considering the most abundant species in seawater, equations (8.4) and (8.5) can be simplified as a first approximation to

$$\begin{cases} DIC \approx [HCO_3^-] + [CO_3^{2-}], & \text{(8.7a)} \\ Alk \approx [HCO_3^-] + 2[CO_3^{2-}]. & \text{(8.7b)} \end{cases}$$

It follows that

$$[CO_3^{2-}] \approx Alk - DIC, \tag{8.8a}$$

$$[HCO_3^-] \approx 2DIC - Alk. \tag{8.8b}$$

CO_2 is a diacid. When it dissolves in seawater, it reacts with the strongest available base in seawater: CO_3^{2-}. The reaction is therefore

$$CO_2 + CO_3^{2-} + H_2O \Leftrightarrow HCO_3^- \qquad \frac{K_1}{K_2} = \frac{\left[HCO_3^-\right]^2}{[CO_2]\left[CO_3^{2-}\right]}. \tag{8.9}$$

Combining equations (8.8) and (8.9), we obtain

$$[CO_2] = \frac{K_2}{K_1} \times \frac{(2DIC - Alk)^2}{Alk - DIC} \tag{8.10a}$$

or

$$P_{CO_2}^{seawater} = \frac{K_2}{\alpha_{CO_2} K_1} \frac{(2DIC - Alk)^2}{Alk - DIC}. \tag{8.10b}$$

These equations relate the concentration of dissolved CO_2 or $P_{CO_2}^{seawater}$ with the control variables of the system (DIC and Alk). We are now going to see which chemical processes can potentially change $P_{CO_2}^{seawater}$.

8.2.3 Photosynthesis

The uptake of dissolved CO_2 by phytoplankton and its conversion into organic carbon leads to a decrease of DIC without changing the alkalinity. The transformation of NO_3^- into amino acid slightly increases the alkalinity. Considering that the N/C Redfield ratio is N/C = 16/106, the effect of this change of alkalinity on $P_{CO_2}^{seawater}$ is low compared to the effect of DIC decrease. The DIC decrease and the alkalinity increase both contribute to the decrease of $[CO_2]$ (equation 8.10). Therefore, photosynthesis produces a decrease of $P_{CO_2}^{seawater}$.

8.2.4 Remineralization

Conversely, when organic matter is consumed by heterotrophic organisms, organic carbon and nitrogen are transformed into CO_2 and NO_3^-, which induces the DIC increase and decrease of alkalinity. This produces an increase of dissolved CO_2 and $P_{CO_2}^{seawater}$ as soon as respiration takes over from photosynthesis, as is the case in deep water (Fig. 8.4).

8.2.5 The Formation of Calcium Carbonate ($CaCO_3$)

Some organisms produce calcium carbonate ($CaCO_3$) shells or tests following the reaction:

$$Ca^{2+} + CO_3^{2-} \rightarrow CaCO_{3(solid)} \quad \text{precipitation of a solid}$$

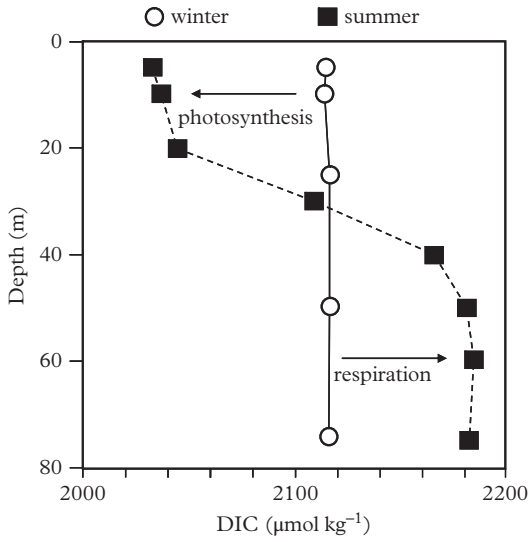

Figure 8.4 *Seasonal change of DIC in the North Sea. Photosynthesis produces the low DIC concentration in surface waters and remineralization produces a high DIC at depth. The winter mixing restores a constant DIC in the water column. Modified from Thomas et al. (2004).*

$CaCO_3$ precipitation decreases both alkalinity and DIC, but alkalinity decreases two times faster than DIC (1 CO_3^{2-} ion carries 2 negative charges for a single atom of carbon). Hence, the numerator of equation (8.10) is constant while the denominator decreases, so that there is an increase of dissolved CO_2 and $P_{CO_2}^{seawater}$. Despite the decrease of DIC, $CaCO_3$ precipitation produces a CO_2 increase because the consumption of CO_3^{2-} (a base) makes seawater more acid. This can be highlighted by rewriting the formation of calcium carbonate in the form

$$Ca^{2+} + 2\,HCO_3^- \rightarrow CaCO_{3(solid)} + CO_2 + H_2O.$$

8.2.6 $CaCO_3$ Dissolution

Conversely, $CaCO_3$ dissolves in the deep ocean below the lysocline in deep waters enriched in the CO_2 by remineralization. $CaCO_3$ dissolution causes a decrease of dissolved CO_2 and of $P_{CO_2}^{seawater}$ produced by the increase of alkalinity (Fig. 8.5)

In surface waters, there is antagonism between photosynthesis which reduces $P_{CO_2}^{seawater}$ and the $CaCO_3$ formation that increases $P_{CO_2}^{seawater}$. In deep waters, the remineralization of the organic matter and the dissolution of $CaCO_3$ have opposed effects on $P_{CO_2}^{seawater}$. On average, plankton use four times less carbon to make calcified tests than to synthesize organic matter (with a huge variability between calcifying and non-calcifying species. So, the effect of photosynthesis dominates. It is all the more important that algae without $CaCO_3$ test (for example, diatoms that have SiO_2 tests) induce only an effect of CO_2 pumping by photosynthesis.

The processes described previously can be studied during the seasonal changes of the carbonate system (Problems 1 and 2).

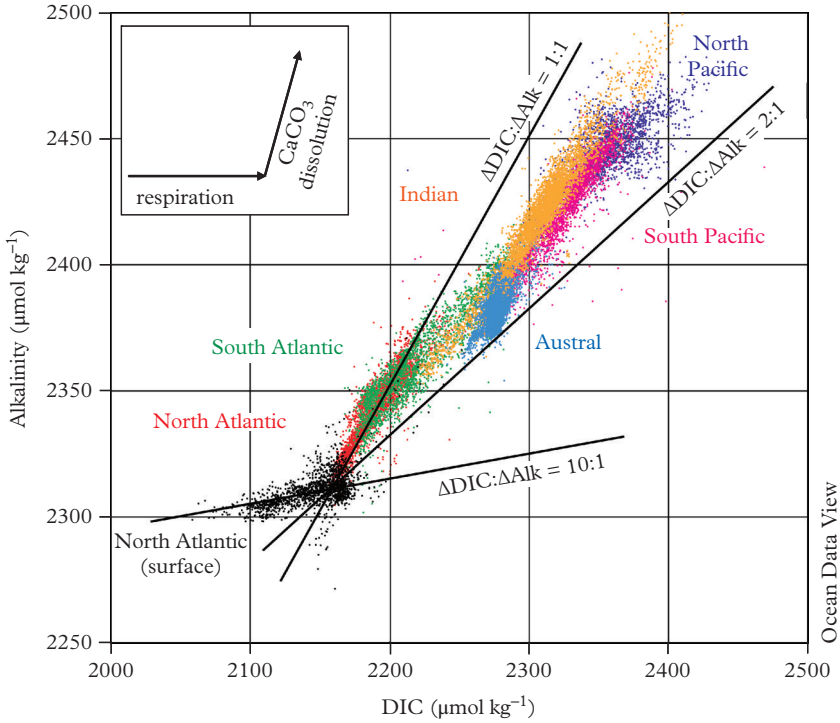

Figure 8.5 *Evolution of DIC and alkalinity (Alk) during the thermohaline circulation. Inset: influence of the remineralization and of the carbonate dissolution on DIC and Alk. Adapted from Emerson and Hedges (2008).*

8.2.7 Overall Effect on the Pumping of CO_2

The solubility of CO_2 in seawater increases when the temperature decreases: cold water absorbs more CO_2 than warm water. Atmospheric CO_2 is therefore absorbed by the ocean at high latitudes: this uptake is referred to as the **thermodynamic pump**. In addition to the temperature effect, the biological activity must be considered: photosynthesis converts dissolved CO_2 into particulate organic carbon which is quickly isolated from the atmosphere by sinking into the deep ocean. This is the **biological pump**. Finally, the **carbonate counter-pump** corresponds to the formation of $CaCO_3$. It slightly reduces the biological pump. A simple model of the carbon cycle in the deep ocean shows that the thermodynamic pump represents 90% of the carbon flux to the deep ocean, while the biological pump is responsible for only 10% of the flux to the deep ocean (see Chapter 10).

The CO_2 pumping is particularly efficient in the cold surface waters that sink to form deep waters. During their journey in the abyss, the deep waters are further enriched in CO_2 by the degradation of the organic carbon by bacteria. So, when these waters upwell

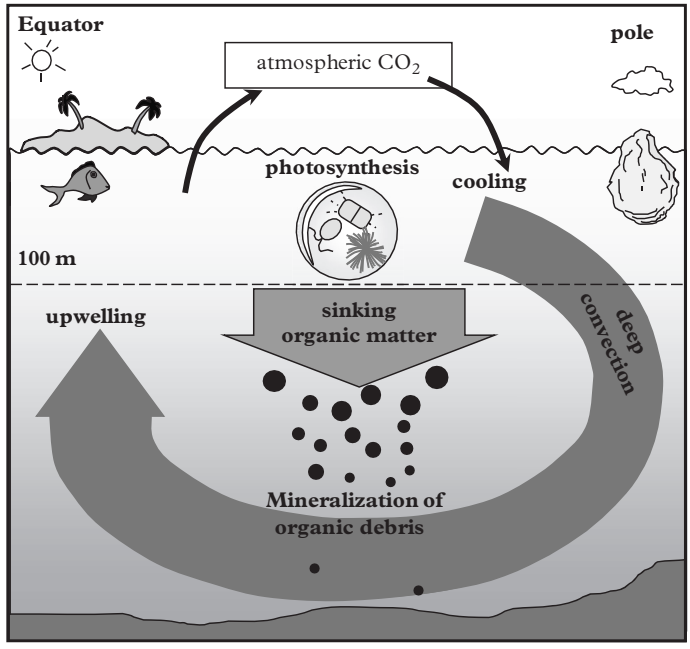

Figure 8.6 *Thermodynamic and biological pumps. Modified from Dandonneau and Jeandel (1998)*

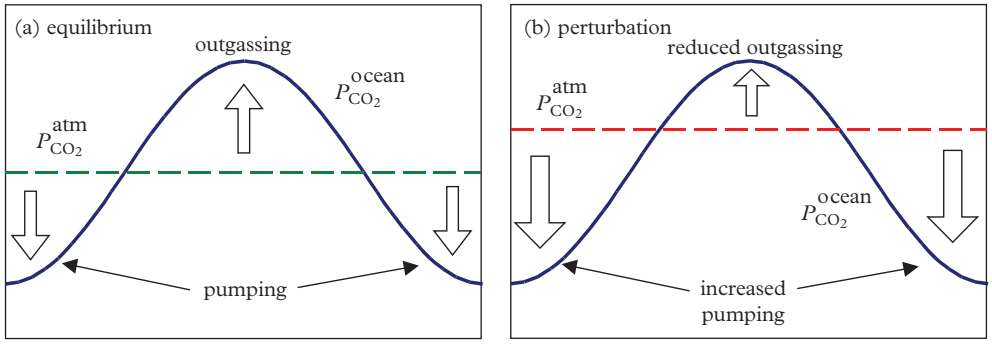

Figure 8.7 *Effect of variations of P_{CO_2} on CO_2 fluxes between the ocean and the atmosphere with latitude. At low latitudes (Equ: Equator), $P^{seawater}_{CO_2} > P^{atmosphere}_{CO_2}$ (warm water) induces a degassing at the Equator. At high latitudes, $P^{seawater}_{CO_2} < P^{atmosphere}_{CO_2}$ (cold water) causes atmospheric CO_2 pumping. The atmosphere is quickly mixed, so $P^{atmosphere}_{CO_2}$ remains relatively uniform. (a) In a system at equilibrium (steady state before the industrial revolution), pumping and outgassing were perfectly balanced and $P^{atmosphere}_{CO_2}$ and $P^{seawater}_{CO_2}$ remained constant. (b) if $P^{atmosphere}_{CO_2}$ grow rapidly, pumping increases at high latitudes ($P^{atmosphere}_{CO_2} - P^{seawater}_{CO_2}$ increases) while outgassing decreases at the Equator ($P^{seawater}_{CO_2} - P^{atmosphere}_{CO_2}$ decreases). There is a net flux of CO_2 into the ocean.*

at the surface, they are very rich in CO_2 and DIC. At low latitudes, due to the warming effect, they outgas CO_2 to the atmosphere. Thus, there is a constant CO_2 flux in the atmosphere between the poles where the CO_2 is absorbed by the ocean and the Equator where CO_2 is outgassed to the atmosphere (Fig. 8.6).

What is the effect of the rise of the CO_2 concentration in the atmosphere? At high latitudes, the atmospheric CO_2 increase promotes diffusion of atmospheric CO_2 into the ocean. At lower latitudes, it hinders CO_2 outgassing from the ocean to the atmosphere. So overall, there is an increase of the net flux of atmospheric CO_2 toward the ocean. It is the regulatory role of the ocean (Fig. 8.7).

8.3 The Carbon Storage Capacity of the Ocean

What is the change of DIC in the ocean induced by the increase of $P_{CO_2}^{\text{atmosphere}}$? By differentiating the logarithm of equation (8.10), we obtain

$$2\frac{\mathrm{d}\left[HCO_3^-\right]}{\left[HCO_3^-\right]} - \frac{\mathrm{d}\left[CO_2\right]}{\left[CO_2\right]} - \frac{\mathrm{d}\left[CO_3^{2-}\right]}{\left[CO_3^{2-}\right]} = 0. \tag{8.11}$$

HCO_3^- is by far the most abundant species; we can (for an approximate calculation) neglect its relative variation. It follows that

$$\frac{\mathrm{d}\left[CO_2\right]}{\left[CO_2\right]} \approx -\frac{\mathrm{d}\left[CO_3^{2-}\right]}{\left[CO_3^{2-}\right]}. \tag{8.12}$$

A relative increase of CO_2 is nearly balanced by a relative decrease of CO_3^{2-}. In addition, an increase of dissolved CO_2 does not affect alkalinity. By differentiating equation (8.8a) at constant alkalinity, we obtain

$$\mathrm{d}\left[CO_3^{2-}\right] \approx -\,\mathrm{d}\left[DIC\right]. \tag{8.13}$$

By combining equations (8.12) and (8.13), it follows that

$$\frac{\mathrm{d}\left[CO_2\right]}{\left[CO_2\right]} \approx \frac{\mathrm{d}\left[DIC\right]}{\left[CO_3^{2-}\right]} = \frac{\left[DIC\right]}{\left[CO_3^{2-}\right]} \times \frac{\mathrm{d}[DIC]}{[DIC]}. \tag{8.14}$$

Combining with equation (8.1), we obtain an expression of the form

$$\frac{\mathrm{d}P_{CO_2}^{\text{atmosphere}}}{P_{CO_2}^{\text{atmosphere}}} \approx \zeta \frac{\mathrm{d}\left[DIC\right]}{\left[DIC\right]}, \tag{8.15}$$

with

$$\zeta \approx \frac{[\mathrm{DIC}]}{\left[\mathrm{CO_3^{2-}}\right]} . \tag{8.16}$$

ζ is called the Revelle factor. With the approximations made above we obtain $\zeta \approx 10$ because carbonate ions account for about 10% of the total inorganic carbon. This value of 10 corresponds to the average ocean.

Application exercise

How does the Revelle factor of seawater in equilibrium with the atmosphere vary with temperature? Which water has the largest anthropogenic CO_2 storage capacity?

Solution:

Cold water has a higher dissolved CO_2 concentration than warm water (equation 8.10). The CO_3^{2-} concentration is therefore lower in cold water than in warm water. It follows that the Revelle factor is higher in cold water than in warm water (equation 8.16 taking into account that DIC varies very little).

In practice, ζ varies between 8 in warm waters and 16 in cold waters. The water with the highest storage capacity is the water with the lowest Revelle factor: it is warm water.

Note that even if the **relative** variation of the DIC (d[DIC]/[DIC]) is 10 times lower than that of dissolved CO_2 (d[CO_2]/[CO_2]), the increase of the **absolute** quantity of DIC (dDIC) is 10 times greater than that of dissolved CO_2 (d[CO_2]). Indeed, when atmospheric CO_2 enters the ocean, it is neutralized by CO_3^{2-}. Due to the equilibrium with bicarbonate and carbonate ions, seawater is able to absorb 10 times more atmospheric CO_2 than if seawater contained only CO_2. Thus, a small variation of the DIC in the ocean can have very strong impact on atmospheric CO_2. For example, what would happen if the biological pump was completely eliminated in the surface ocean? Today, the biological pump is responsible for the decrease of ~10% of the surface DIC compared to the DIC in the deep ocean. Thus, suppressing the biological pump would restore a 10% higher DIC concentration in the surface ocean. This DIC increase of ~10% would lead to a doubling of the partial pressure of CO_2 in the atmosphere ($+10\% \times \zeta = 100\%$).

The anthropogenic CO_2 absorption by the ocean can be seen as a titration of a base (CO_3^{2-}) by an acid (CO_2). The result of this reaction is a gradual decrease of the seawater pH at the surface of the ocean: it is called **ocean acidification**. Even if changes in pH are lower than what the term "acidification" could suggests (Problem 3), it remains that it can have very significant effects on calcifying organisms (Problem 4).

Before the beginning of the industrial revolution, the ocean contained 60 times more carbon than the atmosphere. The ocean is thus able to absorb six ($60/\zeta$) times more carbon dioxide than the atmosphere in response to the anthropogenic disturbance. So,

imagine that after having doubled the amount of atmospheric CO_2, all anthropogenic CO_2 emissions are stopped until ocean equilibrates with the atmosphere. When the ocean–atmosphere balance is restored, only $1/(6+1) = 4\%$ of the CO_2 excess will remain in the atmosphere. The rest $(6/(6 + 1) = 86\%)$ will have been absorbed by the ocean.

In this calculation, it was assumed that the thermodynamic equilibrium between the whole ocean and the atmosphere was reached. We will now study how fast this equilibrium can be established. To do this, we must consider different scales of space and time related to:

- the transfer of gas between the atmosphere and the ocean;
- the equilibration of the mixed layer with the atmosphere;
- the transport of surface waters to the thermocline and to the deep ocean.

8.4 Rate of CO_2 Transfer at the Air–Sea Interface

In the atmosphere and the ocean, fluid transport is dominated by turbulence. However, there is at the ocean–atmosphere interface a boundary layer in which the movements are laminar. Transfer of material across this layer occurs by molecular diffusion only (see molecular diffusion in Chapter 6). The thickness of this layer is of the order of a few tens of microns. The slow rate of molecular diffusion over this distance limits exchanges

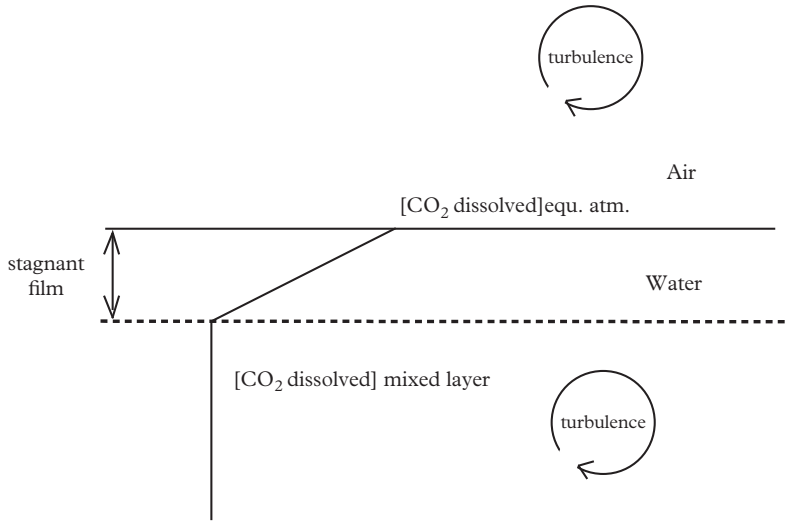

Figure 8.8 *Transfer of CO_2 at the surface of the ocean. At the basis of the stagnant film, the CO_2 concentration is equal to the CO_2 concentration in the mixed layer. At the top of the stagnant film, the CO_2 concentration is in equilibrium with the atmosphere. If these two concentrations are different, there is a net flux of CO_2 by diffusion of molecules through the film.*

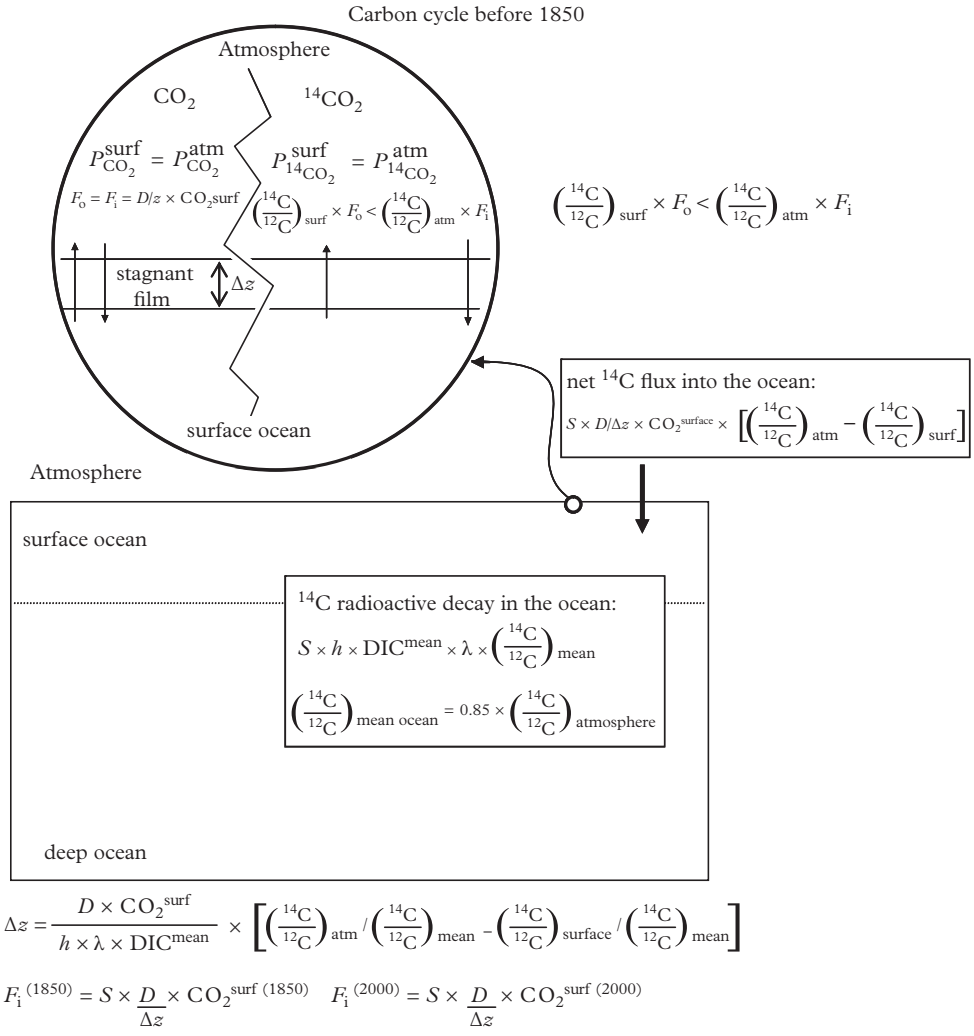

Figure 8.9 *Estimation of the CO_2 fluxes between the ocean and the atmosphere and the thickness of the stagnant film with natural ^{14}C. We consider the carbon cycle before the industrial revolution (the net flux of CO_2 between the ocean and the atmosphere is zero). ^{14}C exchanges between the ocean and atmosphere compensate the radioactive decay in the ocean. (S, h and λ are the ocean surface, ocean mean depth and ^{14}C half-life). The conservation equation of ^{14}C in the ocean gives an average thickness of the stagnant film of 35 μm. Using this value, it is possible to estimate the total flux of CO_2 exchanged between the ocean and atmosphere before 1850 and today. Modified from Broecker and Peng (1998).*

between the ocean and the atmosphere. One of the parameterizations of these exchanges assumes that air and seawater are separated by a "stagnant film" of liquid of a few tens of μm thick (Fig. 8.8) through which the CO_2 molecules move only by molecular diffusion (see Chapter 6).

When $P_{CO_2}^{seawater}$ in the surface ocean is different from $P_{CO_2}^{atmosphere}$, there is a difference in the CO_2 concentration gradient of the dissolved gas between the top and the base of the stagnant film. At steady state, the gradient of concentration in the film is constant. The net flux of CO_2 is due to molecular diffusion. It is given by the equation (Chapter 6, equation 6.16)

$$F = -\frac{D_{CO_2}}{\Delta z}\left([CO_2] - [CO_2]^{sat}\right), \tag{8.17}$$

$$F = -\alpha_{CO_2}\frac{D_{CO_2}}{\Delta z}\left(P_{CO_2}^{seawater} - P_{CO_2}^{atmosphere}\right), \tag{8.18}$$

where D_{CO_2} is the molecular diffusion coefficient of CO_2, α_{CO_2} the solubility coefficient, Δz the thickness of the stagnant film, $[CO_2]$ the concentration of dissolved gases and $[CO_2]^{sat}$ corresponds to its value at equilibrium with the atmosphere. D_{CO_2} and $[CO_2]^{sat}$ are known. The difficulty is to determine Δz. Different methods are used: some are based on the budget of ^{222}Rn, a natural radioactive gas (Chapter 5), whereas others are based on measurements in wind tunnels or release to the atmosphere of volatile compounds injected artificially in water (see Problem 1 of Chapter 6). Balancing the fluxes of natural ^{14}C at the ocean–atmosphere interface gives an estimate of the average thickness of the stagnant film at the surface of the ocean (Fig. 8.9), while the penetration of anthropogenic ^{14}C in the ocean allows studies at the local scale.

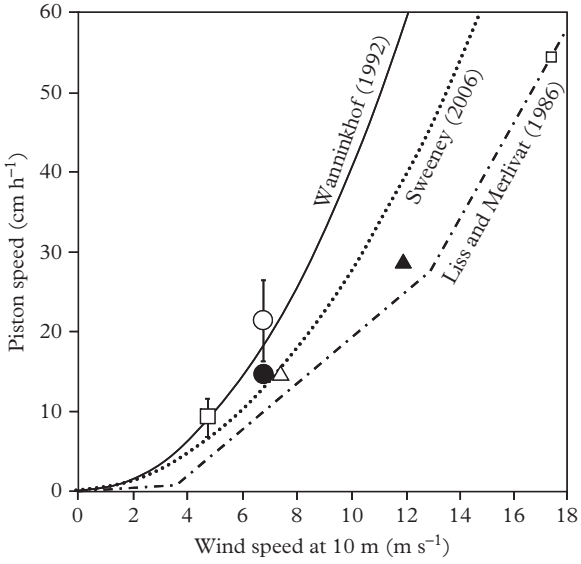

Figure 8.10 *Relationship between wind speed and the piston speed (v_p). White triangle: v_p average measured in the Atlantic with ^{222}Rn (see Chapter 5). Black triangle: measures in the North Pacific with ^{222}Rn. White circle: natural ^{14}C (see Fig. 8.9) overall. Black circle: global anthropogenic ^{14}C (Sweeney et al., 2007). Large white square: anthropogenic ^{14}C diffusion in the Red Sea. Small white square: measured by strong wind in the Irish Sea. The lines represent different theoretical relationships. Modified from Sweeney et al. (2007).*

There is a positive correlation between wind speed at the sea surface and the rate of gas transfer (Fig. 8.10). Indeed, by creating froth waves the wind increases the ocean–atmosphere interface. In addition, "waves" trap gas bubbles and bring them at depth, which facilitates gas exchange. For high wind speeds, there is a systematic bias between isotopic and wind tunnel results. The origin of this bias is not known but its existence contributes to the uncertainty on the CO_2 flux between the ocean and the atmosphere.

8.5 Gas Equilibration Time between the Mixed Layer and the Atmosphere

Gas exchanges between the ocean and the atmosphere are not instantaneous. When the partial pressure of a gas is different in the ocean and in the atmosphere, how long does it take to restore the equilibrium between these two reservoirs? The answer is not the same when considering a gas that does not react with water (like O_2) or CO_2 that is in chemical equilibrium with carbonates and bicarbonates ions or even $^{14}CO_2$ that represents a minor fraction of CO_2.

We consider a reservoir (height h and surface S) containing seawater in contact with the atmosphere (Fig. 8.11). Initially, seawater is in equilibrium with the atmosphere. The equilibrium is disrupted by imposing a permanent increase of the atmospheric partial pressure of the gas. We will compare the time that seawater takes to equilibrates with the atmosphere in the case of O_2, CO_2 and $^{14}CO_2$.

8.5.1 Perturbation of Oxygen

We have seen in Chapter 6 that the time constant to balance the partial pressure of the surface ocean with the atmosphere is $k_{O_2} = D_{O_2}/(h\Delta z)$. In this case, this corresponds to a relaxation time of 17 days.

8.5.2 Perturbation of the Carbonate System

At time $t = 0$, the CO_2 concentration in seawater is $[CO_2]^0$ whereas CO_2 solubility is $[CO_2]^{sat}$ ($> [CO_2]^0$) and the DIC concentration is DIC^0. If DIC changes only by

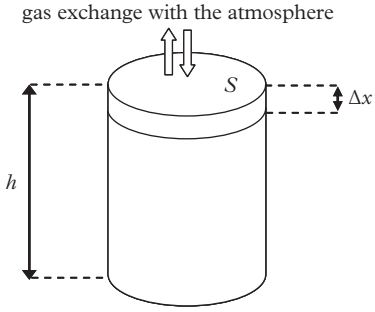

Figure 8.11 *Schematic representation of the reservoir considered (e.g., the oceanic mixed layer).*

diffusion of CO_2 from the atmosphere, the conservation equation of DIC in the mixed layer is

$$Sh\,\frac{\mathrm{dDIC}}{\mathrm{d}t} = -S\frac{D_{CO_2}}{\Delta z}\left([CO_2] - [CO_2]^{sat}\right). \tag{8.19}$$

Since $[CO_2] = K \times (2 \times DIC - Alk)^2/(Alk - DIC)$, equation (8.19) is not linear and it has no simple solution. To understand the dynamics of the system, we linearize this equation with an approximation. By introducing the Revelle factor (equation 8.16), we obtain

$$\frac{\left([CO_2] - [CO_2]^0\right)}{[CO_2]^0} = \zeta\,\frac{\left(DIC - DIC^0\right)}{DIC^0} \qquad \text{with } \zeta = 10. \tag{8.20}$$

From equation (8.20), we obtain an expression of CO_2 that is inserted into equation (8.19) to obtain

$$\frac{\mathrm{dDIC}}{\mathrm{d}t} = -\left(\frac{D_{CO_2}}{h\Delta z}\zeta\frac{[CO_2]^0}{DIC^0}\right)DIC \quad + \quad \frac{D_{CO_2}}{h\Delta z}\left([CO_2]^{sat} - (\zeta - 1)\,[CO_2]^0\right). \tag{8.21}$$

The second term on the right-hand side of equation (8.21) is constant. This linear differential equation has a time constant $k_{carbonate} = \frac{D_{CO_2}}{h\Delta z}\zeta\frac{[CO_2]^0}{DIC^0}$.

Since $\zeta\frac{[CO_2]^0}{DIC^0} \approx 0.1$, the equilibration of carbonates is therefore approximately 10 times longer than for oxygen: it is of the order of 6 months.

8.5.3 Perturbation of the Isotopic Composition

Suppose now that we double the atmospheric abundance of $^{14}CO_2$ and that we maintain indefinitely this concentration in the atmosphere. In view of the very low abundance of ^{14}C, this does not change $P_{CO_2}^{atmosphere}$ or the carbonate equilibrium in seawater. We can therefore calculate the evolution of the ($^{14}C/^{12}C$) isotopic ratio of seawater using equation (5.20) established in Chapter 5

$$\frac{\mathrm{d}R}{\mathrm{d}t} = \frac{1}{C}\left[k_w C_i\,(R_i - R) + s\,(R_s - R) - \lambda \times RC\right]. \tag{8.22}$$

In the present case, the concentration C is the concentration of DIC, $k_w = 0$ (no water mass mixing) and s is the source term of atmospheric carbon. Neglecting the effect of decay ($\lambda = 0$), we obtain

$$\frac{\mathrm{d}R}{\mathrm{d}t} = \frac{1}{DIC}\left[s\,(R_s - R)\right]. \tag{8.23}$$

The inflow of atmospheric carbon is

$$s = \frac{D_{CO_2}}{h\Delta z}\,[CO_2]^{sat}\,. \tag{8.24}$$

By combining equations (8.23) and (8.24), we obtain

$$\frac{dR}{dt} = \frac{D_{CO_2}}{h\Delta z}\,\frac{[CO_2]^{sat}}{DIC}\,(R_s - R)\,. \tag{8.25}$$

Therefore, the time constant for ^{14}C is $k_{^{14}C} \approx k_{carbonate}/\zeta$, that is, it is ten times lower than the time constant characteristic of the chemical equilibration of carbonates. About 5 y are required to restore the isotopic equilibrium.

Why do these three perturbations have different relaxation times (Fig. 8.12)?

- In the case of O_2 (which is a typical gas), the net flux of O_2 must exactly balance the initial deficit of O_2 in the mixed layer.
- CO_2 equilibrium is reached more slowly because the inflow of CO_2 must compensate the initial CO_2 depletion in the mixed layer **and** the CO_2 neutralized by reacting with CO_3^{2-} ions and which represents approximately $\zeta - 1$ (≈ 9) times the initial CO_2 deficit. In total, the balance is restored when an amount of CO_2 equivalent to 10 times the initial deficit has entered seawater. It is 10 times longer to achieve ocean–atmosphere equilibration for the carbonate system than for O_2.
- $^{14}CO_2$ being a minor isotope, a change of the partial pressure of $^{14}CO_2$ does not change the chemical balance of the carbonates and does not produces a significant

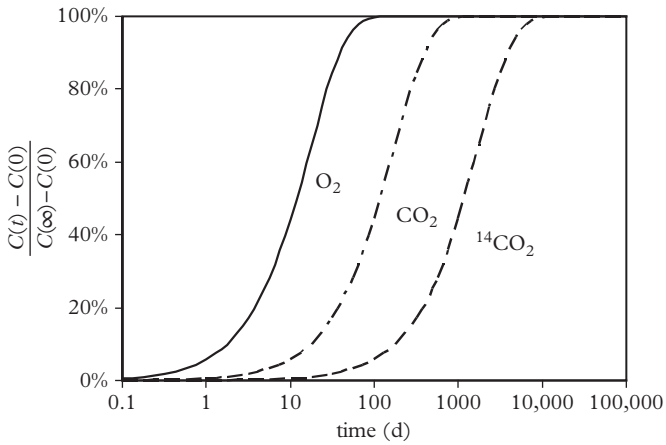

Figure 8.12 *Return to equilibrium after a disruption of the ocean–atmosphere equilibrium for a 100 m thick mixed layer.*

net flux of CO_2. However, as long as $P^{seawater}_{^{14}CO_2} < P^{atmosphere}_{^{14}CO_2}$, there is a net flux of $^{14}CO_2$ from the atmosphere to the ocean. Isotope equilibrium is reached when the $^{14}C/^{12}C$ ratio of DIC ($^{14}CO_2$ but also $H^{14}CO_3^-$ and $^{14}CO_3^{2-}$) is identical to that of the atmosphere (we neglect isotopic fractionations). The net $^{14}CO_2$ flux from the atmosphere to the ocean must compensate the initial deficit of $^{14}CO_2$ in the mixed layer **and** the deficit in $H^{14}CO_3^-$ and $^{14}CO_3^{2-}$. The isotopic equilibrium is restored when an amount equivalent to 100 times the initial $^{14}CO_2$ deficit has entered seawater. It is 100 times to achieve the ocean–atmosphere equilibration of ^{14}C than for O_2 and 10 times longer than for CO_2.

8.6 Observation of the Anthropogenic Perturbation at the Ocean Surface

While the effect of anthropogenic emissions on the CO_2 concentration in the atmosphere has been measured since a half-century by D. Keeling in Hawaii, the effect of these emissions on ocean carbon concentration was much more difficult to detect. Indeed, the seasonal variations of $P^{seawater}_{CO_2}$ and DIC are much larger that the increase of the DIC due to the long-term increase of $P^{atmosphere}_{CO_2}$. The establishment of several permanent marine stations allowed the first direct estimate of anthropogenic CO_2 uptake by the ocean surface waters. Data from the BATS station in Bermuda confirm that the anthropogenic effect is small relative to seasonal variations (Fig. 8.13, Bates et al., 2012). In 28 y, the DIC has increased on average by 1% while $P^{atmosphere}_{CO_2}$ and $P^{seawater}_{CO_2}$ increased by 10% (here we find the Revelle factor!). On the contrary, alkalinity shows no long-term variations. In this area, the ocean absorbs CO_2 from autumn to spring ($P^{atmosphere}_{CO_2} > P^{seawater}_{CO_2}$) and weakly outgases CO_2 in summer ($P^{atmosphere}_{CO_2} < P^{seawater}_{CO_2}$). On average, the Bermuda area behaves as a CO_2 sink.

The DIC concentration is highest in winter because the deepening of the mixed layer brings DIC-rich deep water and the low temperature promotes CO_2 pumping. On the contrary, the DIC concentration is lowest at the end of the summer, when a large amount of dissolved CO_2 has been consumed by the biological activity or outgassed from the warm surface waters. $P^{seawater}_{CO_2}$ is not in phase with the DIC. $P^{seawater}_{CO_2}$ is lowest in winter when surface waters are cold (although vertical mixing brings of CO_2-rich deeper waters at the surface) and $P^{seawater}_{CO_2}$ is high in summer when the surface waters are warm. In this oligotrophic area, the biological production is weak in summer: photosynthesis cannot balance the temperature effect. As a consequence of the increasing CO_2, the seawater pH and the calcite saturation index ($\Omega_{calcite}$) decrease.

8.7 Global Estimate of the Ocean–Atmosphere Exchanges

One of the challenges for the future evolution of the climate is to be able to quantify the atmospheric absorption of CO_2 by the ocean and to model the evolution of this

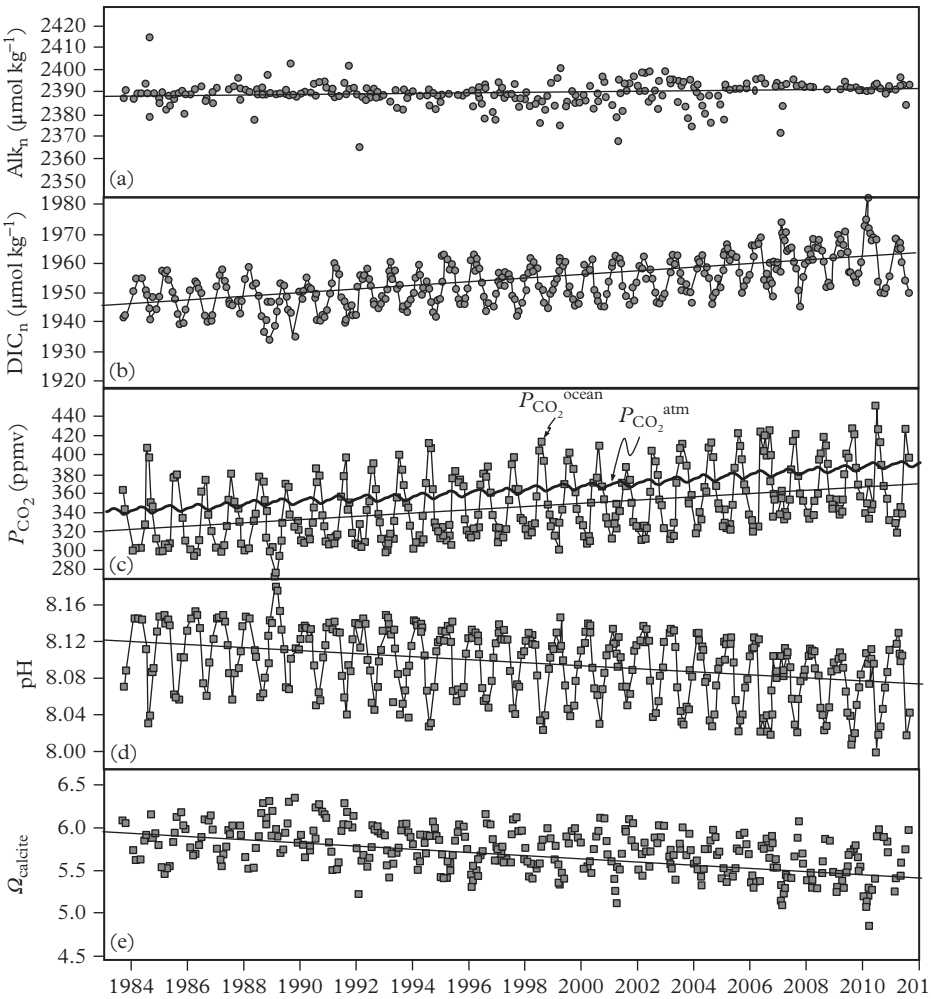

Figure 8.13 *Seasonal and long-term evolution of the carbonate system in the surface water of the Bermuda Time Series station (BATS) from 1984 to 2012. (a) Alkalinity normalized to a salinity of 35.0. (b) DIC normalized to a salinity of 35.0. (c) Atmospheric and seawater CO_2 partial pressure. (d) pH. (e) Calcite saturation index. Modified from Bates et al. (2012).*

flux in the future. The synthesis of several millions of $P_{CO_2}^{seawater}$ measurements in the surface ocean since the 1960s obtained by many groups allows the determination of seasonal variations of $P_{CO_2}^{seawater}$ in all ocean basins. To determine the CO_2 flux at the ocean–atmosphere interface, we must also know the speed of the piston which depends itself on wind speed (Fig. 8.10). Wind speed is obtained with meteorological models fed by satellites data.

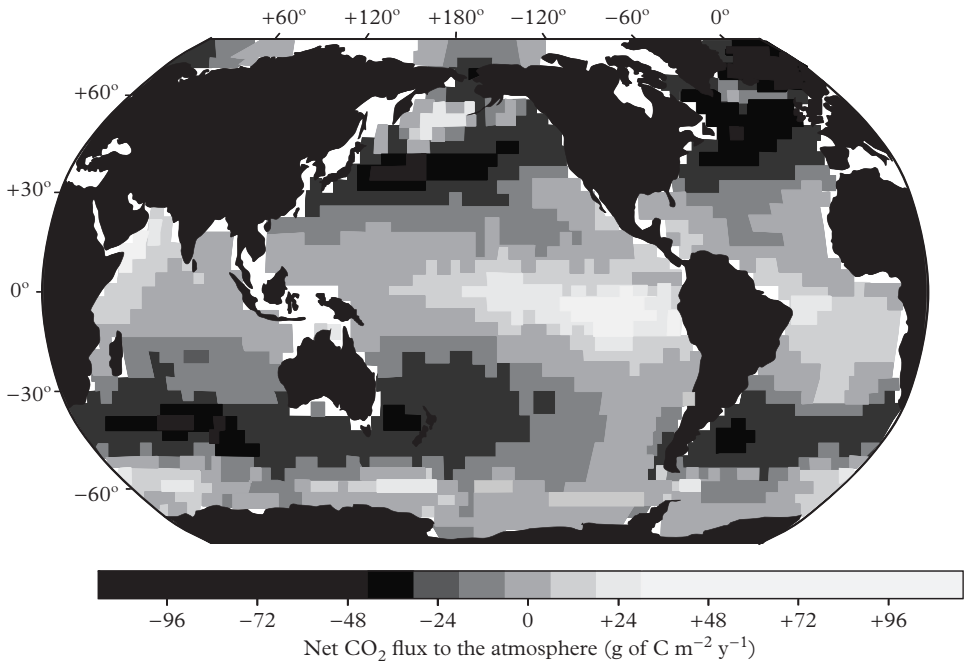

Figure 8.14 *Annual net CO_2 flux between the ocean and the atmosphere. The spatial resolution is 5° × 5°. Modified from Takahashi et al. (2009).*

All these data are combined to obtain the net annual ocean–atmosphere CO_2 flux (Fig. 8.14). Pumping of atmospheric CO_2 takes place mainly between latitudes 40° and 60° in both hemispheres (Fig. 8.14). Here warm waters flow poleward and mix with cold and nutrient-rich subpolar waters. The decrease of $P_{CO_2}^{seawater}$ in surface water is then due both to the cooling and the biological pump. The intensity of the winds in these areas further strengthens CO_2 pumping. In the equatorial band, upwelling of deep water bring to the surface cold and CO_2-rich waters that outgas strongly as they warm up. In addition, in the equatorial Pacific, the biological pump is limited by iron (HNLC zone, see Chapter 7). The net annual flux of anthropogenic CO_2 pumped by the ocean is 2 ± 1 Gt C y^{-1}, based on the compilation of $P_{CO_2}^{seawater}$ data.

8.8 Spread of the Anthropogenic Perturbation in the Deep Ocean

The efficiency of the $P_{CO_2}^{atmosphere}$ regulation by the ocean depends strongly on the speed at which anthropogenic CO_2 dissolved in surface waters is transported and stored in the deep ocean. Direct evaluation of the DIC change in the deep ocean over time is difficult. The anthropogenic perturbations have resulted in significant variation of the

$\delta^{13}C$ and $\Delta^{14}C$ of atmospheric CO_2 (Problem 5). These isotopic signatures are used to track the spreading of the anthropogenic carbon in the ocean.

The combustion of fossil fuels injects some very ^{13}C-depleted CO_2 into the atmosphere. Measurements in the Pacific Ocean between 1970 and 1990 show a decline of the $\delta^{13}C$ down to 300 m at the Equator and down to 700–1000 m at high latitudes and in subtropical gyres. This reflects the arrival of anthropogenic carbon in 20 y at these depths (Fig. 8.15). These data, associated with the evolution of the $\delta^{13}C$ in the atmosphere and the biosphere, allows determination of the relative contributions of the ocean and of the atmosphere in the uptake of anthropogenic carbon.

Similarly, the perturbation of $\Delta^{14}C$ by atmospheric nuclear tests is visible down to depths of 300 m at the Equator and down to approximately 600–1000 m in subtropical areas, just 20 y after the beginning of the tests (see Fig. 4.18). However, we have seen in Chapter 6 that the coefficient of vertical diffusion in the thermocline is of the order of 0.17 $cm^2\ s^{-1}$, which allows diffusion of ~300 m in 20 y. This difference is explained by isopycnal motion of water, as shown in the meridional distribution of the $\Delta^{14}C$ in the surface ocean (Fig. 8.16).

The anthropogenic signal is more or less visible in the water depending on the latitude (Fig. 8.17). In the 1970s, $\Delta^{14}C$ was around +170‰ in the Pacific subtropical gyres, while it was +100‰ at the Equator and –70‰ south of 60°S. These variations reflect significant features of the ocean circulation. The piling up and downward Ekman pumping of surface water in the subtropical gyres contributes to the spread of anthropogenic ^{14}C at depth. On the contrary, at the Equator, the upwelling of deep water (rich in "old" DIC) dilutes the anthropogenic signature. This mixing effect is most visible in the South Pacific where vertical mixing is such that the anthropogenic signal is not visible.

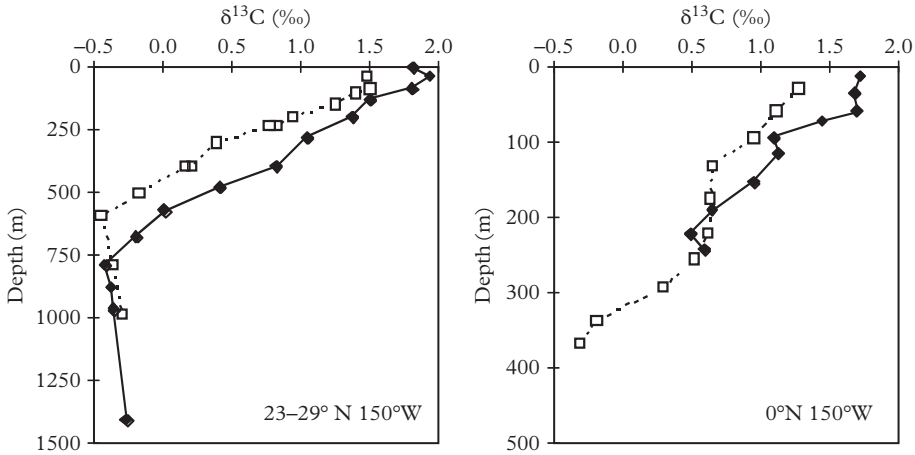

Figure 8.15 *Evolution of $\delta^{13}C$ of seawater between 1970 (black diamond) and 1990 (white squares) with depth. Note the difference of penetration depth between the tropic and Equator. The data were obtained in the Pacific Ocean. Modified from Quay et al. (1992)*

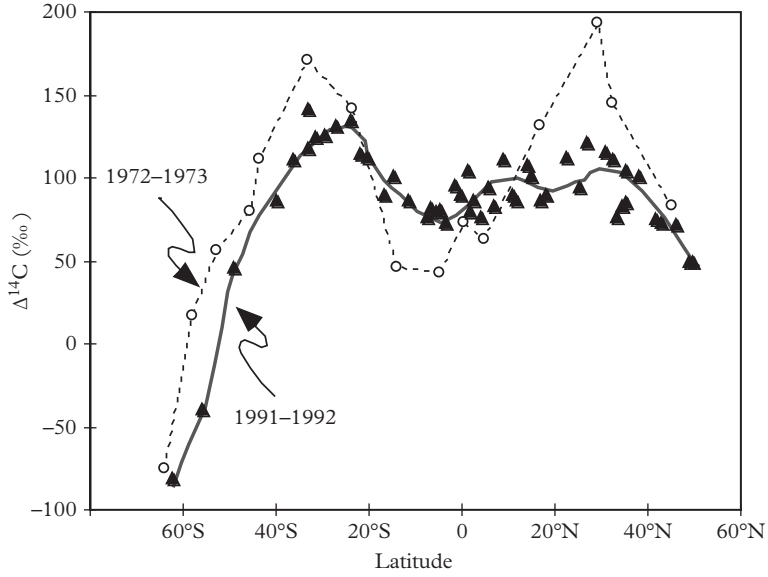

Figure 8.16 *The thermocline ventilation as seen from the anthropogenic $\Delta^{14}C$. The penetration of the signal occurs along surfaces of constant density slightly inclined to the horizontal rather than by vertical mixing made difficult by the density gradient. Water with positive $\Delta^{14}C$ is transported laterally from the gyres toward the Equator. Modified from Broecker and Peng (1982).*

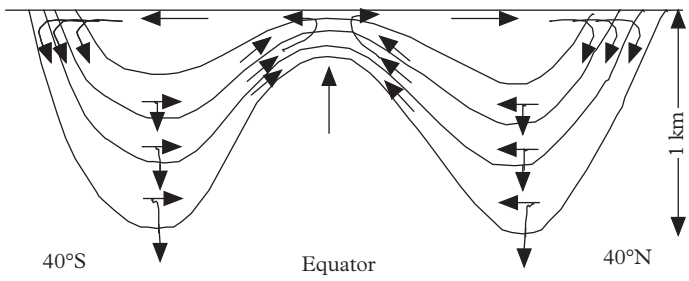

Figure 8.17 *Variation of $\Delta^{14}C$ in the surface waters of the Pacific with latitude in the 1970s and the 1990s. Modified after Key et al. (1996).*

Measurements in the 1990s show that changes visible in the 1970s have been partially erased. The $\Delta^{14}C$ decrease of the subtropical gyres is explained by a decrease of the atmospheric inputs and the dilution of the anthropogenic signal in the "old" carbon from deep waters. Curiously, there is an increase of $\Delta^{14}C$ at the Equator: it is due to the lateral transport of thermocline water that left the subtropical gyres in the 1970s and

which upwells at the Equator in the 1990s. This is consistent with an onion skin structure of the thermocline in which the carbon is transported along surfaces of constant density (isopycnal surfaces) which are in contact with the atmosphere at approximately 40°N and 40°S (Fig. 8.17 and Chapter 1). These isopycnal surfaces sink under the subtropical gyres and then they go back to the surface at the Equator. This structure is perfectly visible on the sections presented in Fig. 10.1 of Chapter 10.

$\Delta^{14}C$ and $\delta^{13}C$ allow the quantification of the anthropogenic CO_2 flux pumped by ocean. This is illustrated below using the example of $\delta^{13}C$.

A balance of carbon fluxes between the ocean, the atmosphere and the continental biosphere from 1970 to 1990 is established to determine the relative roles of the ocean and the continental biosphere in the absorption of anthropogenic CO_2 (Quay et al., 1992).

Between 1970 and 1990, 102 gigatons of carbon (Gt C) were injected into the atmosphere by human activities (Fig. 8.18). The $\delta^{13}C$ of fossil fuels and burned forests is –27‰. During the same period, the amount of CO_2 in the atmosphere increased from 696 to 754 Gt C and its $\delta^{13}C$ has fallen from –7.36 to –7.76‰. Out of the 102 Gt C emitted, only 58 Gt C have accumulated in the atmosphere. The remaining 44 Gt C have been already absorbed by the ocean and the continental biosphere.

The combustion of fossil fuels is not the only source of CO_2 for the atmosphere: ocean outgassing and carbon emitted by natural biomass destruction must also be considered.

Between 1970 and 1990, the penetration of the anthropogenic carbon in the ocean is marked by $\delta^{13}C$ down to 1000 m deep, with an average change in $\delta^{13}C$ of –0.2‰ (Fig. 8.15). It is less than the change of –0.4‰ observed in the atmosphere, because the thermocline ventilation is not instantaneous. The first 1000 m of the ocean contain C_o = 10,000 Gt C with an average $\delta^{13}C$ of the order of +1‰.

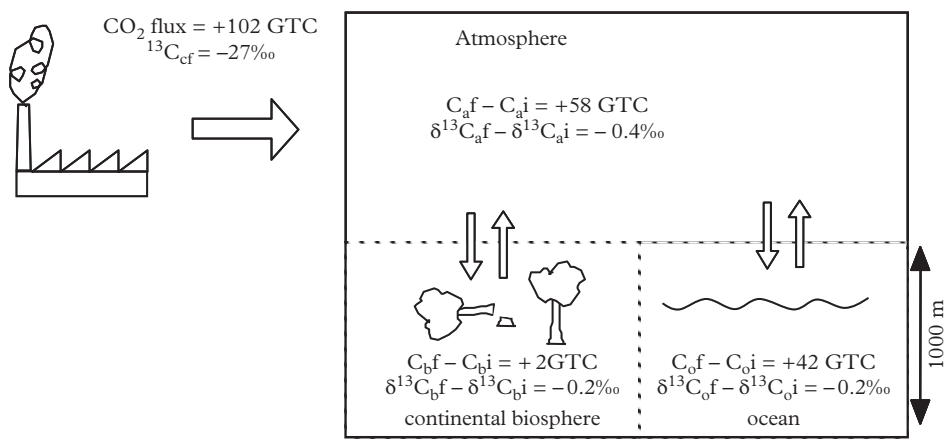

Figure 8.18 *Fluxes of anthropogenic CO_2 between the atmosphere, the ocean surface and the continental biosphere between 1970 and 1990.*

The continental biosphere emits carbon to the atmosphere via the degradation of organic matter and biomass fires. The biosphere does not have a uniform $\delta^{13}C$: the $\delta^{13}C$ of tree leaves and annual plants is determined by the $\delta^{13}C$ of the recent atmosphere, while the $\delta^{13}C$ of tree trunks is less negative because during their growth (tens or hundreds of years ago) the atmosphere had a less negative $\delta^{13}C$. It is assumed that the quantity of carbon emitted into the atmosphere annually approximately compensates for photosynthesis (60 Gt C y^{-1}). The average $\delta^{13}C$ of the continental biosphere is –27‰.

The conservation equations of CO_2 and $^{13}CO_2$ are applied to the "atmosphere + surface ocean + continental biosphere" system. In the following, the total quantity and the isotopic composition of the carbon contained in a reservoir are denoted C and $\delta^{13}C$. The reservoirs are denoted by the indices a, o and b which correspond, respectively, to the atmosphere, the ocean and the biosphere. We refer to 1970 and 1990 by the exponents i (initial) and f (final).

Conservation equation for total carbon

$$\underbrace{\left(C_a^f + C_o^f + C_b^f\right)}_{\text{final reservoir}} - \underbrace{\left(C_a^i + C_o^i + C_b^i\right)}_{\text{initial reservoir}} = \underbrace{C_{ff}}_{\text{fossil fuel input}}. \tag{8.26}$$

Conservation equation for carbon-13

$$\underbrace{\left(C_a^f \times \delta^{13}C_a^f + C_o^f \times \delta^{13}C_o^f + C_b^f \times \delta^{13}C_b^f\right)}_{\text{final reservoir}} - \underbrace{\left(C_a^i \times \delta^{13}C_a^i + C_o^i \times \delta^{13}C_o^i + C_b^i \times \delta^{13}C_b^i\right)}_{\text{initial reservoir}} = \underbrace{C_{ff} \times \delta^{13}C_{ff}}_{\text{flux of fossil fuels}}. \tag{8.27}$$

highlighting of the net flux of total carbon for each reservoir

$$\underbrace{\left(C_a^f - C_a^i\right)}_{\text{atmosphere}} + \underbrace{\left(C_o^f - C_o^i\right)}_{\text{ocean}} + \underbrace{\left(C_b^f - C_b^i\right)}_{\text{biosphere}} = \underbrace{C_{cf}}_{\text{fossil fuel}}. \tag{8.28}$$

highlighting of the net flux of carbon-13 for each reservoir

$$\underbrace{\left(C_a^f \times \delta^{13}C_a^f - C_a^i \times \delta^{13}C_a^i\right)}_{\text{atmosphere}} + \underbrace{\left(C_o^f \times \delta^{13}C_o^f - C_o^i \times \delta^{13}C_o^i\right)}_{\text{ocean}} + \underbrace{\left(C_b^f \times \delta^{13}C_b^f - C_b^i \times \delta^{13}C_b^i\right)}_{\text{biosphere}} = \underbrace{C_{cf} \times \delta^{13}C_{cf}}_{\text{fossil fuels}}. \tag{8.29}$$

We note that

$$\left(C_o^f \times \delta^{13}C_o^f - C_o^i \times \delta^{13}C_o^i\right) = \left\{C_o^f \times \left(\delta^{13}C_o^f - \delta^{13}C_o^i\right) - \left(C_o^f - C_o^i\right) \times \delta^{13}C_o^i\right\}, \tag{8.30a}$$

$$\left(C_b^f \times \delta^{13}C_b^f - C_b^i \times \delta^{13}C_b^i\right) = \left\{C_b^f \times \left(\delta^{13}C_b^f - \delta^{13}C_b^i\right) - \left(C_b^f - C_b^i\right) \times \delta^{13}C_b^i\right\}. \tag{8.30b}$$

Substituting and rearranging the previous equations, we obtain

$$\left(C_o^f - C_o^i\right) + \left(C_b^f - C_b^i\right) = C_{ff} - \left(C_a^f - C_a^i\right), \tag{8.31}$$

$$\delta^{13}C_o^i\left(C_o^f - C_o^i\right) + \delta^{13}C_b^i\left(C_b^f - C_b^i\right) = C_{ff} \times \delta^{13}C_{ff} - \left(C_a^f \times \delta^{13}C_a^f - C_a^i \times \delta^{13}C_a^i\right) - C_o^f \times \left(\delta^{13}C_o^f - \delta^{13}C_o^i\right) - C_b^f \times \left(\delta^{13}C_b^f - \delta^{13}C_b^i\right). \tag{8.32}$$

We obtain a system of two equations (equations 8.31 and 8.32) where the two unknowns are the net ocean–atmosphere ($C_o^f - C_o^i$) and continental biosphere–atmosphere ($C_b^f - C_b^i$) carbon fluxes. These two equations are independent because ocean, atmosphere and continental biosphere have different ^{13}C. Solving, we obtain

$C_o^f - C_o^i$ = 42 Gt C in 20 y, corresponding to a net carbon flux from the atmosphere to the ocean of 2.1 Gt C y^{-1}.

$C_b^f - C_b^i$ = 2 Gt C in 20 y, corresponding to a net flux of carbon from the atmosphere to the biosphere of 0.1 Gt C y^{-1} (or relatively little, finally the continental biosphere seems to remain relatively constant over the period). Another approach to evaluate the ocean sink is to compare the evolution of the CO_2 and O_2 concentration in the atmosphere (Problem 6). Note that in recent years, the continental biosphere appears to play an increasing role as it could absorb as much CO_2 as the ocean (Fig. 8.1). Today the ocean would absorb approximately 25% of the anthropogenic emissions of CO_2.

Methods using hydrological data (temperature, salinity, alkalinity, nutrient concentration, chlorofluorocarbons (CFCs), etc.) allow recalculation of the DIC concentration that a water mass would contain if it had been formed at equilibrium with an atmosphere containing 280 ppmv of CO_2. The difference between the DIC concentration measured in a seawater sample and the concentration that would be in equilibrium with an atmosphere containing 280 ppmv CO_2 represents the amount of anthropogenic carbon in the sample. An estimate made for the whole ocean from the calculation method named C^* suggests that between 1800 and 1994, the ocean has absorbed 48% of anthropogenic emissions (Fig. 8.19). To balance the atmospheric CO_2 budget over the same period, this would imply that the continental biosphere has been a net source of CO_2 due to deforestation. Not surprisingly, the North Atlantic is a zone of high penetration and storage of anthropogenic CO_2 (the North Atlantic Deep Water (NADW) formation). This is also the case to a lesser extent of the Subantarctic zone of the ocean on (30°S to 50°S), which corresponds to the area of the Antarctic Intermediate Water formation.

The low carbon accumulation in the south of the Southern Ocean (where deep waters are formed) is somewhat surprising. Other approaches for the calculation of anthropogenic carbon have been proposed. One of the criteria for the evaluation of these methods is the consistency between the anthropogenic carbon distribution and our knowledge of the water mass circulation. For example, the method "TrOCA" (Problem 7) shows a downwelling of the anthropogenic carbon in the South Atlantic associated with the formation of the Antarctic Bottom Water (AABW) (Fig. 8.20). This is all the more remarkable that unlike C^*, TrOCA does not include CFCs in its parameterization.

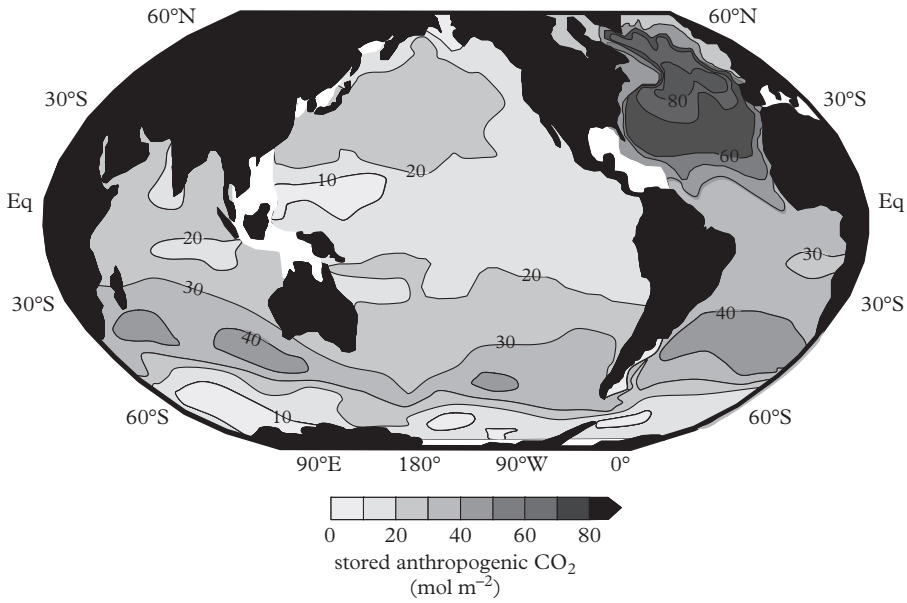

Figure 8.19 *Penetration of anthropogenic CO_2 in the ocean. Modified from Sabine et al. (2004).*

Comparison of different methods of anthropogenic carbon calculation gives an idea of the uncertainty of this type of approach.

Anthropogenic carbon is transported quickly down to a depth of 1000 m in the thermocline, but there is transient storage because this carbon is upwelled and outgassed at the Equator within a few decades. For the anthropogenic carbon to be isolated in the long term from the atmosphere, it must be transported below the thermocline, in deep waters. This transport occurs by two ways: the thermohaline circulation (Chapter 9) and the sinking of marine particles (Chapter 10), which represent respectively 90 and 10% of the flux of carbon to the deep ocean. Thermohaline circulation occurs on the century to millennium timescale, so it hardly allows rapid storage of anthropogenic CO_2. In view of the settling speed of marine particles, particulate transport is likely to respond much more quickly. An increase in the export of particulate carbon into deep waters has a direct impact on $P_{CO_2}^{seawater}$.

Currently, the biological pump is mainly limited by the lack of nutrients such as nitrate or phosphate in surface waters. However, in HNLC areas, large quantities of nitrate and phosphate available to the algae remain unused. It is now accepted that in regions remote from continental dust inputs, the organic production is limited by the absence of iron (see Chapter 7). Is it possible to fertilize them artificially with iron? Field experiments at the kilometer scale have given ambiguous results. The addition of iron stimulates photosynthesis and induces a decrease of $P_{CO_2}^{seawater}$, but this is not necessarily followed by an export of particulate carbon. Notwithstanding the environmental impacts which

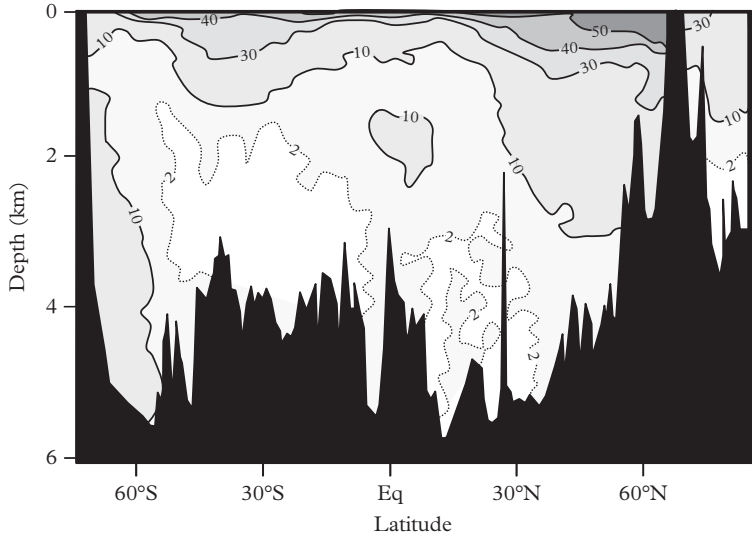

Figure 8.20 *Penetration of anthropogenic carbon in the Atlantic Ocean estimated by the TrOCA method. The thermocline is rich in anthropogenic carbon. The NADW in the North and the AABW in the South transport anthropogenic carbon in the deep ocean. Compare this figure with the temperature and salinity sections of the Atlantic (Chapter 1), and with the distribution of anthropogenic tracer in the deep ocean (Chapter 10). Modified from Vazquez-Rodriguez et al. (2009).*

are impossible to predict, fertilization on a large scale in the Southern Ocean is likely to have only a limited impact on the level of CO_2 in the atmosphere (see Problem 5 in Chapter 11).

PROBLEMS

Problem 1: Seasonal variations of the carbon cycle (Tsurushima et al., 2002)

The permanent station KNOT is located in the Northern Pacific (44°N, 155°E) off the coast of Japan. Temperature, phosphate, alkalinity and DIC profiles were measured at the end of the summer and in winter (Fig. 8.21) and the partial pressure of CO_2 is regularly monitored (Fig. 8.22). What important information can you deduce concerning seasonal changes in the carbon cycle (*Hint*: assume that they are representative of an annual cycle and that the conditions of January–February 1999 were identical to those of January–February 2000)?

Problem 2: Evolution of $P_{CO_2}^{seawater}$ during the austral winter (Metzl et al., 2006)

P_{CO_2} is measured on a transect between 58°S and La Réunion island during the austral winter (Fig. 8.23). During this period, which areas act as source or sink of CO_2.

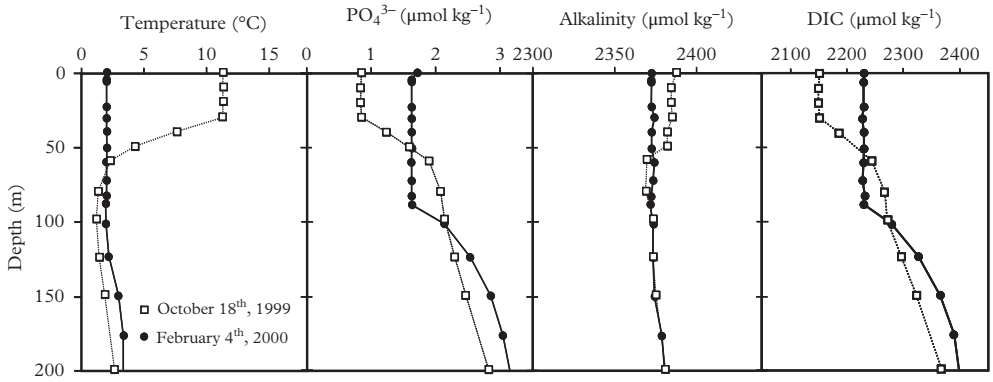

Figure 8.21 *Seasonal variation of the carbon cycle in the North Pacific. Modified from Tsurushima et al. (2002).*

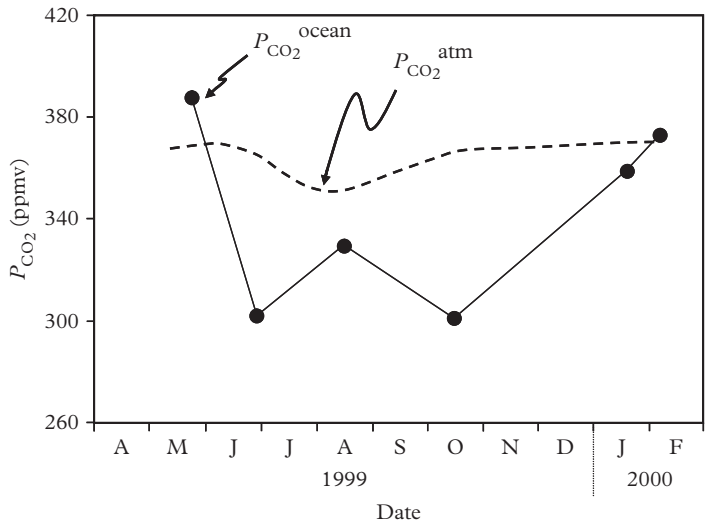

Figure 8.22 *Seasonal evolution of P_{CO_2} in the surface waters of the North Pacific. Modified from Tsurushima et al. (2002).*

Compare these observations with those made during the austral summer (Fig. 8.3) and explain them.

Problem 3: Ocean acidification (Caldeira et al., 2007)

Surface seawater at equilibrium with an atmosphere in which $P_{CO_2}^{atmosphere}$ = 280 ppm has a pH of the order of 8. Estimate the change of pH induced if this same seawater equilibrates with an atmosphere which $P_{CO_2}^{atmosphere}$ = 560 ppmv. Assume that seawater alkalinity remains constant and that the Revelle factor, ζ = 10. Do not try to obtain an

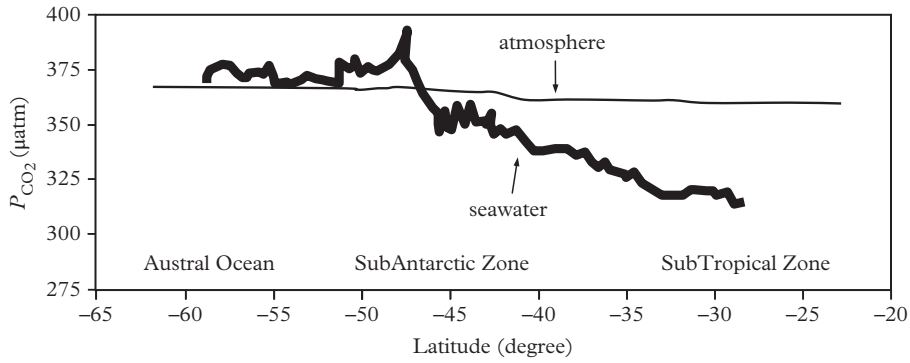

Figure 8.23 *P_{CO_2} along a transect between 63° S and 21° S (La Réunion Island) during the austral winter. Measurement in surface waters (thick line) and air (thin line). Modified after Metzl et al. (2006).*

exact result and use instead the approximate calculations. *Hint:* You can estimate the change in concentration of the H^+ ions by deriving equation (8.2) and of the HCO_3^- ions by deriving equation (8.8).

Problem 4: Impact of the ocean acidification on calcifying organisms (Orr et al., 2005)

The increase of the CO_2 concentration in the atmosphere causes the acidification of the oceans. You want to determine the impact of this acidification on calcifying organisms living in cold water and warm water. Table 8.1 gives the properties of North Atlantic and tropical Atlantic seawaters.

Table 8.1 *Two seawater properties*

	N. Atl.	**Trop. Atl.**
S	33	35
θ (°C)	4	25
DIC (µmol kg^{-1})	2049	2003
HCO_3^- (µmol kg^{-1})	1889	1772
CO_3^{2-} (µmol kg^{-1})	147	221
CO_2 (µmol.kg^{-1})	13	10
P_{CO_2} (atm)	0.00036	0.00036

(1) Assuming that seawaters of Table 8.1 become equilibrated with a P_{CO_2} of 560 ppmv, what will be their respective CO_3^{2-} concentrations? Alkalinity is assumed to be constant.

(2) Table 8.2 gives the CO_3^{2-} concentration needed to saturate seawater with respect to carbonates at 4 and 25°C.

Table 8.2 *Carbonate saturation conditions*

Temperature	**4°C**	**25°C**
CO_3^{2-} at saturation with calcite (μmol kg^{-1})	41.8	41.4
CO_3^{2-} at saturation with aragonite (μmol kg^{-1})	66.2	66.2

What can you infer about the impact of ocean acidification on pteropods (small mollusks building an aragonitic shell and often living in cold waters), coral (aragonite reef built in warm waters) and the coccolithophorids (cells with calcite test living mainly in warm water).

Hint: Seek inspiration from the calculations of the previous problem.

Problem 5: CO_2–$\delta^{13}C$ correlations in the atmosphere

Air samples collected at the Mona Loa Observatory (Hawaii) are analyzed to track the evolution of the concentration of CO_2 and its $\delta^{13}C$ in response to the emission of fossil fuels. For example in 1990, the CO_2 concentration was 354 ppmv and $\delta^{13}C$ was –7.76‰. In 2000, the concentration was 369 ppmv and $\delta^{13}C$ was –8.03‰.

Study of the Parisian air (see Problem 3 of Chapter 3) shows that CO_2 emissions from the combustion of fossil fuels produce a correlation of the form

$$\delta^{13}C = 7579/CO_2 - 27.9.$$

Does an increase of the atmospheric CO_2 concentration of 10 ppm give the same change of $\delta^{13}C$ in Paris and Hawaii? Why?

Problem 6: O_2 and CO_2 in the air (Battle et al., 2000)

Between 1991 and 1997, the combustion of fossil fuels has injected 6.2 Gt C y^{-1} and the cement manufactures produced 0.2 Gt C y^{-1}. If this carbon was fully accumulated as CO_2 into the atmosphere, an increase of the atmospheric CO_2 concentration of 2.75 ppmv y^{-1} would be observed. In fact, during the same period, the CO_2 content of the atmosphere has increased by only 1.24 ppmv y^{-1} as a result of the growth of the continental biosphere and pumping by the ocean. During the same period, very precise measurements show that the atmospheric O_2 concentration has decreased by 3.34 ppmv y^{-1}. It is interesting to combine CO_2 and O_2 data because photosynthesis and respiration affect both CO_2 and O_2, while pumping of anthropogenic CO_2 by the ocean thermodynamic pump does not affect O_2. Photosynthesis of 1 mole of biospheric carbon produces 1.1 mole of O_2. The combustion of 1 mole of fossil carbon consumes 1.43 mole of O_2. Cement production uses no oxygen.

(1) From the above data, determine the anthropogenic CO_2 flux absorbed by the ocean and the atmosphere (calculation or graphical method).

(2) It was assumed implicitly in the foregoing that there is no net annual flux of O_2 between the ocean and the atmosphere. What do you think of this hypothesis?

Problem 7: The anthropogenic carbon in the Atlantic Ocean (Touratier and Goyet, 2004)

To determine the amount of anthropogenic carbon in a water mass, a new tracer "TrOCA" (tracer combining oxygen, inorganic carbon and alkalinity) is defined as

$$\mathrm{TrOCA} = \mathrm{O_2} - \mathrm{R_{O/C}}(\mathrm{DIC} - 0.5\mathrm{Alk}),$$

where $R_{O/C}$ represents the Redfield ratio (see Chapter 2) between oxygen and carbon. By choosing slightly different numerical values than those given in Chapter 2, we have

$$\mathrm{TrOCA} = \mathrm{O_2} + (1/1.2)(\mathrm{DIC} - 0.5\mathrm{Alk}).$$

(1) Explain the principle of construction of this tracer. What does it represent? According to you, is it a conservative tracer?

(2) TrOCA^0 is defined as the value of TrOCA in an ocean in equilibrium with an atmosphere containing 280 ppmv of CO_2. On what type of samples can TrOCA^0 be directly measured?

(3) Using seawater samples from the deep South Atlantic (between 0 and 20°S) and the relationship between the O_2 and CO_2 solubilities with temperature, the following relationship is determined:

$$\mathrm{TrOCA}^0 = 1505 \times \mathrm{e}^{-(\theta/89)},$$

where θ is the potential temperature. Assuming that until now, the alkalinity of the ocean is not affected by the invasion of anthropogenic CO_2, show that the amount of anthropogenic carbon (C_{ant}) absorbed by a water mass is given by

$$\mathrm{C_{ant}} = 1.2(\mathrm{TrOCA} - \mathrm{TrOCA}^0).$$

(4) Calculate TrOCA for samples collected on a vertical profile in the North Atlantic Ocean (20°N, 66°W). Justify the choice of the profile location and determine C_{ant} along the profile (Table 8.3). Compare C_{ant} and CFC concentrations.

Table 8.3 *Analyses of seawater in the Northwest Atlantic*

Depth (m)	**50**	**894**	**1487**	**2956**	**3939**
θ (°C)	28.74	7.29	4.02	2.78	2.36
$[O_2]$ (μmol kg^{-1})	205	140	250	265	267
Alkalinity (μmol kg^{-1})	2353	2320	2317	2322	2327
DIC (μmol kg^{-1})	1989	2200	2161	2162	2168
CFC-11 (pmol kg^{-1})	1.612	0.141	0.781	0.371	0.407

9

The Little World of Marine Particles

The ocean contains 1.36 billion cubic meters of seawater that contains about 10 billion tons of solid particulate matter, or an average of 10 mg of particles per ton of water. Although scarce, marine particles play a key role in the control of marine chemistry. However, due to their low concentration, but also because the particle fluxes are irregular in time as in space (seasonal and interannual variability, pulses, variable geographic distribution . . .), they are difficult to sample, to characterize and it is often risky (and even not advised!) to extrapolate local information obtained on a single cruise to deduce what is happening at the scale of the year and/or at the ocean basin scale. The description of the particle dynamics and chemistry for an oceanic province and extension to the global ocean is a major issue which relies both on basic measurements (hydrology of the region, mineralogical, chemical and biological composition of particles) and also on tracer data (chemical elements capable of helping us to reconstruct the particle's history), and on models that take into account both the water and particle transport as well as chemical and isotopic exchange. The model outputs are compared to data, to validate or not the proposed parameterizations.

This chapter first presents the origin and the nature of marine particles and then outlines their regulatory role in marine chemistry. The main particle sampling methods are described, because they strongly influence information that oceanographers will deduce from their analysis. Finally, a few selected examples are presented to highlight some recent progress of our understanding of the particle flux dynamics and of dissolved/particulate exchanges.

9.1 Origin and Nature of Marine Particles

Marine particles have different origins: continental, marine and extraterrestrial (Fig. 9.1).

The first origin is external to the marine system: through erosion, the continents bring particles (natural or anthropogenic, mineral or organic) to the ocean. They reach the ocean primarily transported by rivers (sediment discharge, Fig. 9.2). It is estimated that before the establishment of large dams, the total flux of particulate material transported by rivers to the oceans was of the order of 20×10^{15} g y^{-1} (Milliman and Meade, 1983).

Marine Geochemistry. First Edition. Matthieu Roy-Barman and Catherine Jeandel.

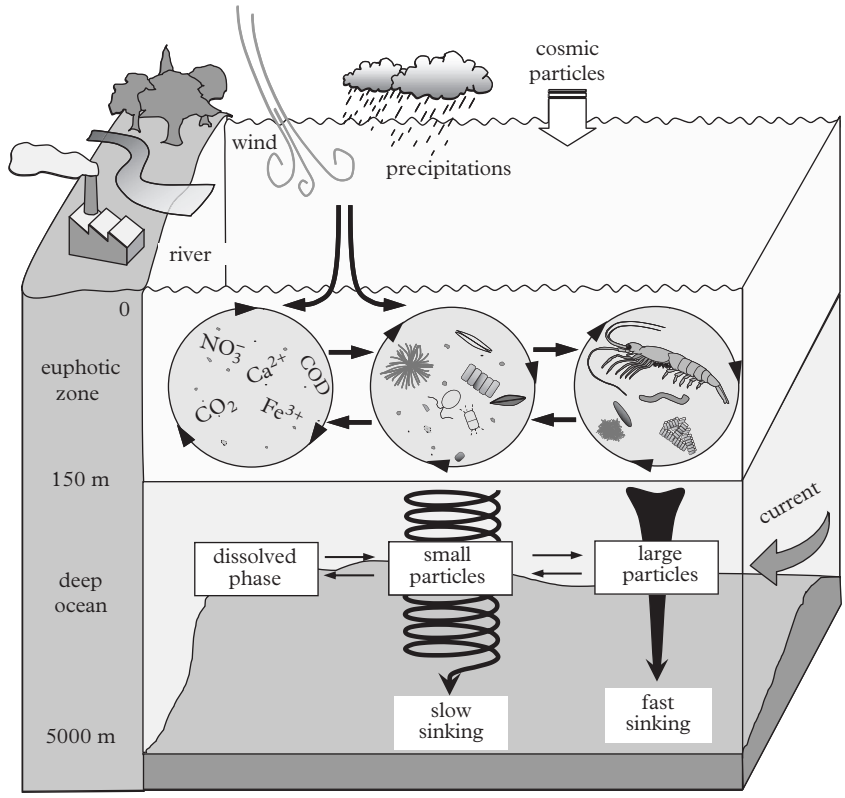

Figure 9.1 *Origin and fate of the particles in the ocean. Modified from Jeandel (1998).*

As we have already noted in Chapter 1, estuaries and margins act as filters of the particle discharge: 90% of particles transported by rivers settle in estuaries and margins and only 10% of the river particles reach the open ocean (Problem 1).

The flux of atmospheric dust reaching the ocean is 20 times lower than the discharge of river particles, with a value of 0.91×10^{15} g (Rea, 1994), but it plays a key role in remote ocean areas, away from continents (Fig. 9.3).

Particles of continental origin (also called terrigenous particles) consist of mineral and organic matter. The mineral (or lithogenic) fraction is essentially made up of silicate minerals (such as clays) and carbonates. These particles are rich in Si, Al and Fe, which are three major components of the continental crust. Depending on the nature of the rocks exposed on the continents, the proportions of major and minor components of the particles discharged to the ocean vary.

The organic fraction of terrigenous particles comes from the erosion of soils, covered by plant debris and furrowed by rain. It consists of organic carbon, amino acids and sulfur and phosphate compounds. According to the origin and history of the particle,

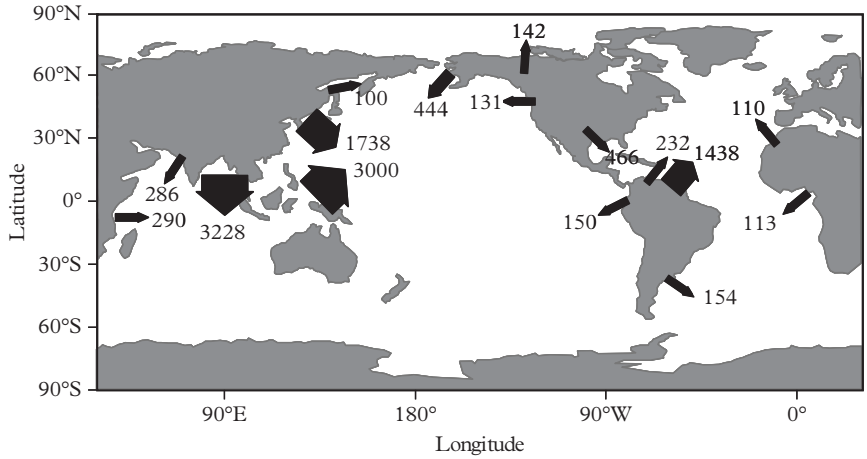

Figure 9.2 *Contribution of continental particles by the rivers. Particle flux in* 10^{12} *g* y^{-1}. *Modified from Milliman and Meade (1983).*

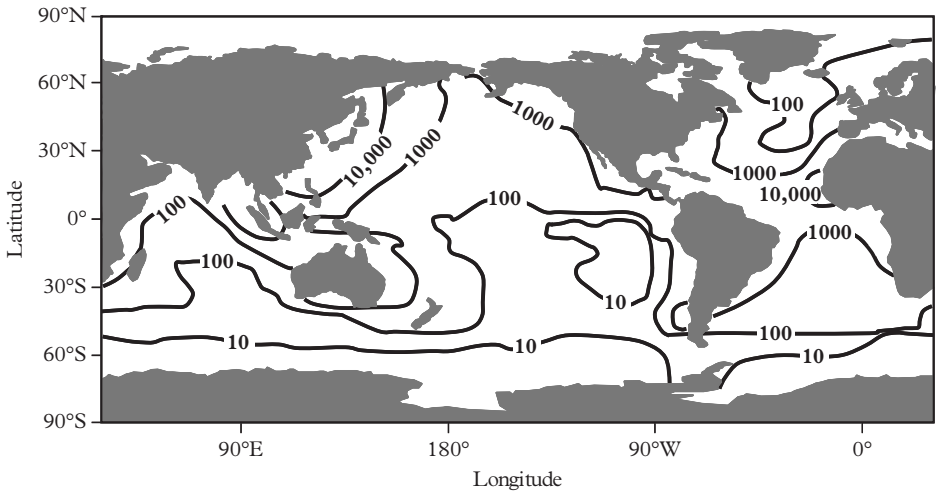

Figure 9.3 *Contribution of detrital particles by wind. Flux in mg* m^{-2} y^{-1}. *Modified from Duce et al. (1991).*

the organic material is more or less degraded when it arrives in the ocean. If it is still relatively fresh, organic material is said to be labile. In this case, it is easily remineralized by bacteria and it can be used by phytoplankton. Otherwise, it is designated as refractory. In this case, it is hardly degradable and it is transported to the sediment. Anthropogenic contaminants can be organic (e.g., hydrocarbons, pesticides or fertilizers molecules adsorbed on particles conveyed by rivers) or inorganic (e.g., heavy metals,

nuclear products, etc.). Since the 1950s, tens of kilotons of micro- and nanoplastic particles have been accumulated at the ocean surface, particularly in the gyres (Cózar et al., 2014). Their ecological impact is still unknown.

The second source of material is internal to the ocean and produced by marine biological activity. As we saw in Chapters 2 and 6, autotrophic phytoplankton species assimilate dissolved nutrients (C, N, P, Si, Ca) and use solar energy to produce organic matter mainly consisting of C, H, O, N, P (also called "soft matter"). Many of these species also produce a skeleton, consisting of amorphous silica or calcium carbonate ("hard" materials or biominerals). The sedimentation of these skeletons can produce large deposits of opal or chalk, such as those that make up the cliffs of Dover or Calais, made of coccoliths. Some autotrophic species, like cyanobacteria, have no skeleton. Biomarkers and their alteration products are powerful tools to reconstruct the origin of organic matter in the ocean (Fig. 9.4; see also Fig. 7.5).

In addition to the specific contribution of the biogenic elements, the chemical composition of marine particles is also modified by the incorporation of poorly soluble trace metals (Fe, Mn, Nd, Th ...) in **authigenic phases** (Fe and Mn hydroxides, for example). To distinguish the external contributions (lithogenic) and the internal production (biogenic and authigenic) of particles, the lithogenic content of marine particles is estimated with specific tracers. Assuming that (1) very insoluble elements such as Al, Ti or ^{232}Th are essentially carried by the lithogenic material and that (2) this lithogenic material has the chemical composition of the average continental crust (see appendix to Chapter 2), the lithogenic and authigenic/biogenic contributions of a chemical component (X) can be deduced

$$X_{litho} = Al \times (X/Al)_{cc}, \tag{9.1}$$

$$X_{bio\text{-}auth} = X_{total} - Al \times (X/Al)_{cc}. \tag{9.2}$$

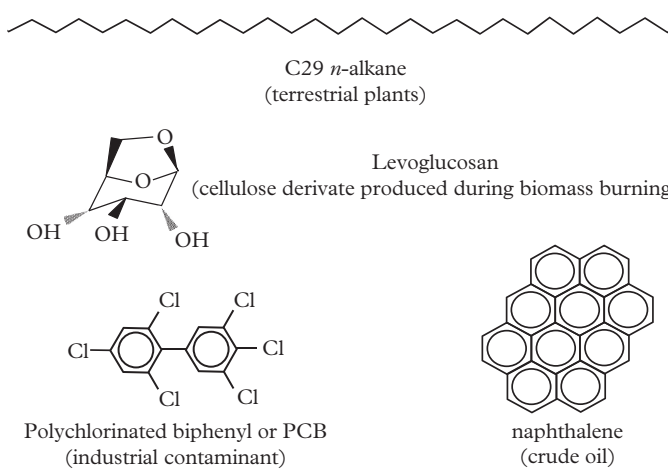

Figure 9.4 *Terrestrial and anthropogenic biomarkers.*

Sometimes a partial dissolution of the particles with diluted acids (also called "leaching") is used to determine the fraction of elements weakly bound to particles, also called the labile fraction. The labile fraction is *a priori* different from the authigenic fraction even if some authigenic phases are probably dissolved and if lithogenic phases are probably hardly attacked.

Application: Enrichment of Marine Particles in Fe and Zn

Marine particles are filtered in the Ross Sea (Antarctica). Half of the filter undergoes a total attack. The other half is attacked in a light manner. The result of the analysis is reported in ng of element per kg of filtered water (Table 9.1).

Table 9.1 *Analysis of particles*

	Al (ng kg^{-1})	Fe (ng kg^{-1})	Zn (ng kg^{-1})
Total dissolution	45	60	120
Leaching	3.2	12.3	101

What is the fraction of authigenic Fe and Zn? Compare with the labile fraction. We obtain Table 9.2:

Table 9.2 *Calculation of labile and authigenic fractions*

	Fe	Zn
$(X/Al)_{CC}$ (see appendix in Chapter 2)	0.44	0.00089
Authigenic concentration (ng kg^{-1})	40	119.96
Authigenic fraction	67%	100%
Labile fraction	20%	84%

Fe has a significant authigenic fraction although Fe is abundant in continental rocks (there are little continental inputs in the Ross Sea). Zn is entirely authigenic. The very light attack does not dissolve the authigenic fraction completely. It can be noted that Al is not completely insoluble.

Finally, extraterrestrial particles fall in the ocean: micrometeorites (10–100 μm) and interplanetary dust particles (IDP, particles not exceeding a few μm). Their flux is very low, but they bring elements that are rare on Earth such as Ir and ^{3}He in significant quantities. The relatively steady flux of Ir and ^{3}He is useful to determine the accumulation rate of ancient sediments.

9.2 Marine Particle Sampling

The role of marine particles in oceanography has been foreseen only recently (1970s). This is largely due to sampling difficulties (Fig. 9.5): particles are often at great depths,

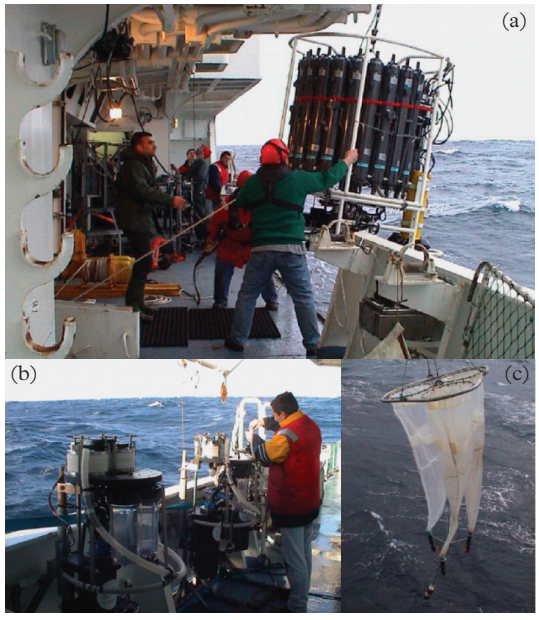

Figure 9.5 *Collection tools. (a) Rosette of Niskin bottles. (c) In situ pumps. (c) Zooplankton net.*

scarce and fragile. Zooplankton are collected by nets which are long silk (or nylon) cones with a PVC collector at their base and a mesh adapted to the size of the "catch": 50 μm for aggregates of phytoplankton, 200 μm for zooplankton. The fine suspended solids are filtered from water collected by Niskin bottles if a small amount of particles is sufficient.

In situ pumps are used when extraction of particles from several hundreds or thousands of liters of water is necessary. These pumps are lowered to the desired depths on a cable and they collect particles on filters of different meshes arranged in series in the pump head. *In situ* pumping also limits contamination issues. Cartridges containing Mn oxide-bearing fibers can be mounted downstream of the filters. Mn oxides scavenge efficiently many radionuclides dissolved in seawater. Despite the large volumes filtered, the masses of collected particles are so low that it is difficult to weigh them: therefore, particulate matter concentrations are often expressed in terms of quantity of chemical element carried by particles by volume of filtered seawater. This concentration reflects both the abundance of the chemical element in the particles and the abundance of particles in seawater.

The larger particles that fall in the water column are collected by sediment traps (Fig. 9.6). A sediment trap is a cylinder or a funnel at the base of which collection vials are mounted successively on a carousel. The sampling time of each vial is preprogrammed. The vials are poisoned with formalin to prevent their content being eaten by zooplankton (or fish) or degraded by bacteria. Despite this precaution, it is necessary, once the trap has been recovered, to hand pick under a microscope swimming organisms that tried to feed into the trap (Fig. 9.7). Finally, the traps do not necessarily collect 100% of the falling particles and we will see later how to estimate their efficiency. Traps can

Figure 9.6 *Sediment trap. (a) General view (collection surface is 1 m^2). (b) The carousel with the vials. (c) Vials after sample collection.*

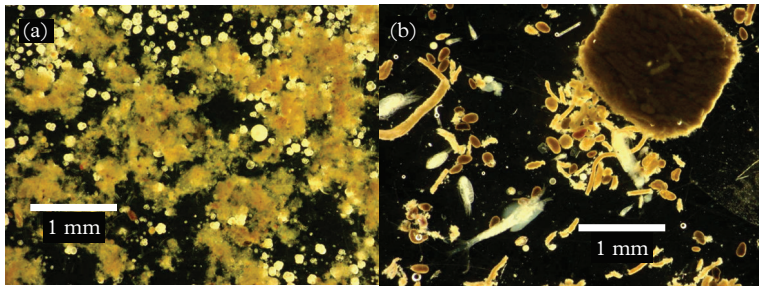

Figure 9.7 *Material collected in sediment traps. (a) Marine snow (brown) and foraminifera tests (white). (b) Accumulation of fecal pellets (brown) and swimmers (white). Observed field ≈ 5 mm (N. Leblond, Cellule piège INSU).*

be fixed (they are linked to a mooring anchored on the seafloor for periods of the order of 1 y) or drifting (they drift with the currents, followed by the oceanographic vessel which puts them in the water and get them back after one or two days).

Marine particles can be studied without necessarily sampling them. At the ocean surface, satellites that measure the "ocean color" allow evaluation of the algal production in the first meters of the ocean (see Chapter 7). By comparing the absorption of solar light at different wavelengths, it is possible to characterize the pigments and therefore the various algae groups. The sampling bottle rosettes are frequently equipped with sensors

that measure the fluorescence (which allows estimation of the chlorophyll content) as well as light absorption and backscattering (which allows estimation of the abundance of suspended particles and the biogenic/lithogenic ratio). Finally, the *in situ* observation of large particles is growing rapidly with the development of underwater video systems that determine in nearly real-time the vertical distribution of particles, their size distribution and their sinking velocity as well as the dominant zooplankton species (see Section 9.3).

With the deployment of these tools, it becomes possible to decipher the "particle message." Given the small size of the studied areas during oceanographic campaigns compared to the size of the ocean, it is essential to select well *a priori* the areas to study. This has led the researchers to combine their efforts in internationally coordinated actions.

The ocean star

There are not only scientists who film the ocean. Hundreds of movies have the sea and the oceans as their main subject . . . From "Jaws" by S. Spielberg to "Oceans" by J. Perrin, the abyss, their inhabitants, but also pirates, treasure hunters or various Robinsons have always inspired filmmakers. The most famous of all remains "The World of Silence" by Jacques-Yves Cousteau and Louis Malle, filmed in the early 1950s with scuba diving equipment and underwater cameras in the waters of the Mediterranean Sea, the Persian Gulf, the Red Sea and the Indian Ocean. It received the "Palme d'Or" at the Cannes festival in 1956 and an Academy Award in 1957. Still today, the film is number one at the box office of the documentary films with 4,600,000 spectators . . . and it probably triggered many oceanographer vocations.

9.3 The Distribution of Particles

Particle sampling methods allow us to distinguish different types of particles: small particles collected on filters having a pore size of $\approx$0.5 μm and large particles collected on filters having a pore size of $\approx$50 μm or collected with sediment traps. These size limits are somewhat arbitrary, but nevertheless they are used to characterize two very different behaviors.

Small particles (and colloids) have no or very low sinking velocities (of the order of 300 m y^{-1}; we will see later in the chapter how such a low speed is determined). As they sink very slowly, they tend to accumulate in the water column where they constitute most of the particle stock in the ocean. As particles are produced or introduced into surface waters, their abundance is highest there. Then, it decreases with depth (Fig. 9.8). There are also high particle concentrations in bottom nepheloid layers where strong bottom currents suspend and disperse particles. Finally, particles can be transported laterally from the shelf or slope areas in intermediate nepheloid layers.

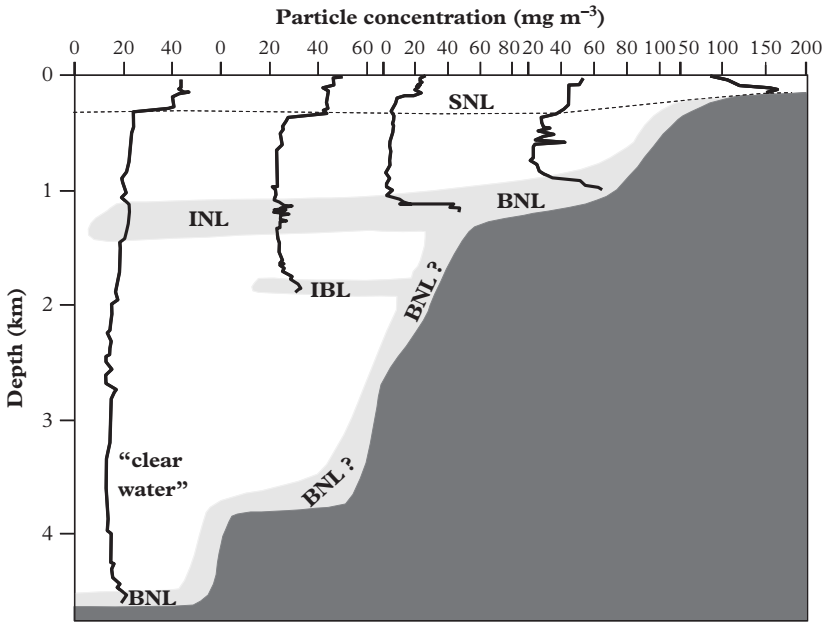

Figure 9.8 *Abundance of suspended particles on the Irish margin estimated by transmissometry (transmission of light in water). The transect extends over 300 km. SNL: surface nepheloid layer. INL: intermediate nepheloid layer. BNL: bottom nepheloid layer. Between the nepheloid layers are "clear waters." Modified from McCave et al. (2001).*

Large particles (Fig. 9.9) have very high sinking velocities of the order of 100–1000 m per day. These particles therefore constitute most of the sinking particle flux collected by sediment traps. They represent only about 1% of the stock of particulate matter in the water column because they do not have the time to accumulate. Their abundance is also much more variable in space and time than for small particles. As might be expected, there is a good correlation between the abundance of large particles in the water column measured by video profiler and the mass flux collected in sediment traps (Fig. 9.9). However, "particles" observed by video profiler do not always fall: some zooplankton species spend the daytime at depth away from predators and go back to the surface at night to feed.

Small particles and large particles are not isolated pools (Fig. 9.1). Small particles are aggregated together by filter feeding animals which graze phytoplankton and produce fecal pellets. Algae such as diatoms exude sticky organic molecules that allow the formation of aggregates (Fig. 9.7). During their fall, large particles sweep and aggregate slower particles on their way. Conversely, large particles can disaggregate: the most fragile of them like marine snow may be broken by current shearing. Fecal pellets can be destroyed by animals that eat them (Fig. 9.10) and rebuilt by the same animals.

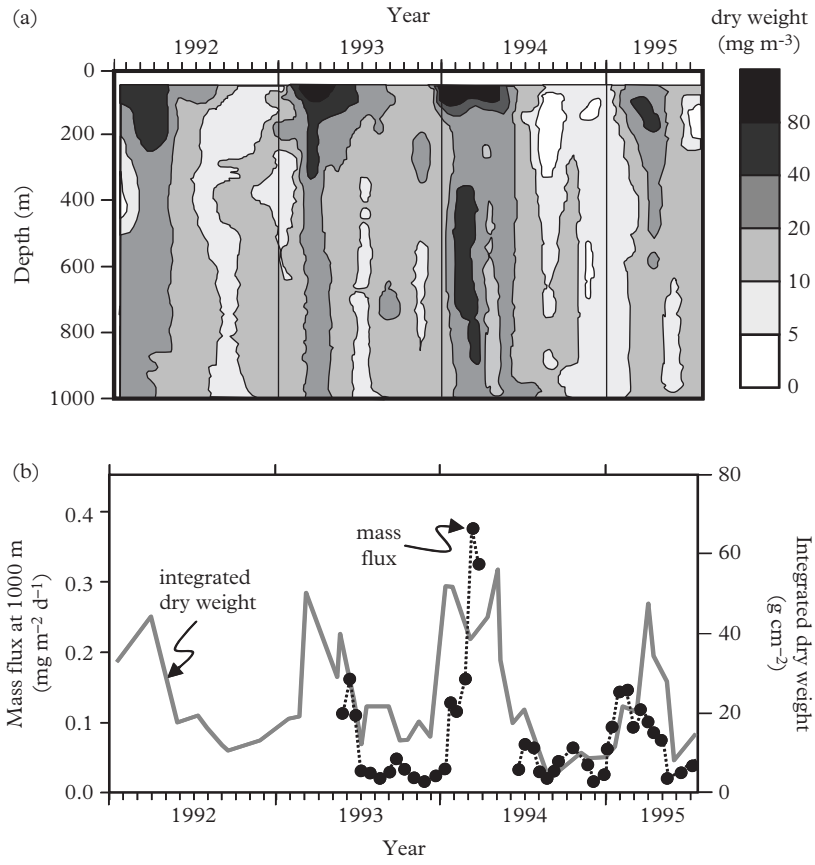

Figure 9.9 *Abundance and flux of large particles in the Mediterranean Sea (DYFAMED site located off Nice). (a) Evolution of the dry weight of particles measured by video profiler. (b) The integrated particle stock comparison between 0 and 1000 m (video profiler) and the flux collected at 1000 m by a sediment trap. Modified from Stemmann et al. (2002).*

9.4 Particle Sinking

How can we compare the primary production at the ocean surface with particles collected at 1000 or 2000 m when they may have been produced several weeks ago? The sinking speed of particles is the critical parameter that determines the degree of coupling between the ocean surface and the deep waters. A rapid fall causes important coupling and promotes the preservation of organic matter against remineralization. It also limits the horizontal transport of particles by currents, because particles collected in a trap were not necessarily produced just above it (Problem 2).

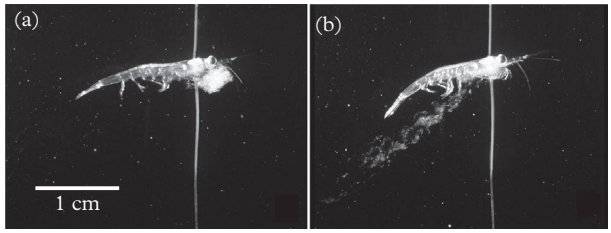

Figure 9.10 *Fragmentation of an aggregate of marine snow by a euphausiid. (a) A diatom aggregate sinking past the side of the animal's head. (b) The aggregate has been entrained, struck by the legs and ejected as a stream of fragments. Modified from Dilling and Alldredge (2000).*

The Stokes law gives the sinking speed w_p of a spherical particle, assuming that the acceleration of gravity is balanced by the friction of the particle on water

$$w_p = 2\,g \times (\rho_p - \rho_w)/(9\,\eta) \times r^2, \tag{9.3}$$

where g (9.81 m s^{-2}) is the acceleration of gravity, ρ_p and ρ_w are the densities of the particle and water, η is the kinematic viscosity of water and r is the radius of the particle.

Application exercise: Particles of the Baltic Sea (Neretin et al., 2003)

In the surface waters of the Baltic Sea, there is an intense formation of manganese oxide particles (MnO_2). The observation of particles with a secondary electron microscope reveals that 90% (in number) of the MnO_2 particles have a diameter of the order of 3.5 μm while the remaining 10 % have a diameter of the order of 8.5 μm.

(1) What is the settling speed the two types of particles and their relative contributions to the vertical flux of MnO_2?

(2) What happens if each large particle is in fact made up of 50% in volume of MnO_2 aggregated by 50% in volume of organic matter? The density of MnO_2 is 3.0 g cm^{-3}. Organic matter and water of the Baltic Sea are identical densities: 1.0 g cm^{-3}. The kinematic viscosity of water is $\eta = 0.015$ g cm^{-1} s^{-1}.

Answer:

(1) From equation (9.3), we obtain

For 3.5 μm particles: w_p = 0.00089 cm s^{-1} = 0.77 m d^{-1}.
For 8.5 μm particles: w_p = 0.0052 cm s^{-1} = 4.5 m d^{-1}.

The mass of a particle being proportional to its volume, an 8.5 μm particle contains $(8.5/3.5)^3 = 14$ times more Mn than a 3.5 μm particle.

Large particles are nine times less numerous than small ones but as they fall six times faster and as each large particle contains 14 times more MnO_2 than a small particle, they produce a flux that is $14 \times 6/9 = 9.4$ times larger than the MnO_2 flux of small particles. Thus large particles represent 90% of the MnO_2 particulate flux.

(2) A "mixed" particle whose volume is made up to half of MnO_2 and half of organic matter has a density of 2.0 g cm^{-3}. For an 8.5 μm "mixed" particle, the speed is 2.2 m d^{-1} or two times less than that of a particle of the same size made up entirely of MnO_2. As the "mixed" particles contain two times less MnO_2 than pure ones, the MnO_2 flux becomes four times lower. Mixed 8.5 μm particles produce a flux that is $9.4/4 = 2.3$ times higher than 3.5 μm particles entirely made of MnO_2 (or 70% of the MnO_2 flux still).

For large particles, the Stokes law no longer applies because turbulence appears around the particles and because large particles are rarely spherical (Fig. 9.11). Some of them are millimeter-size fragile assemblages called "marine snow." Marine snow has a settling velocity of the order of 100–1000 m d^{-1}. It can travel down the few kilometers separating the surface from the seafloor in a few days or a few weeks.

Marine particles are composite products, made of organic and mineral material (algae skeletons as well as continental dust). Equation (9.3) shows that the excess of density relative to water ensures the sinking of particles. The density of organic matter is close to that of seawater, which does not favor the sinking of particles. The presence of dense mineral phases (lithogenic particles, calcium carbonate or silica tests) is therefore essential to ensure the ballasting of the aggregates and to facilitate their preservation during their fall (Lombard et al., 2013). Biological activity allows the aggregation of small particles through grazing by filter-feeding animals and organic molecules produced by the biomass allow particles to stick to each other.

Finally, the mineral and organic phases have a role of mutual protection: cell membranes and organic films avoid unstable mineral phases to dissolve in seawater and dense mineral phases allow rapid transfer to the seafloor, avoiding particulate matter to be remineralized. Since aggregation and disaggregation phenomena are ubiquitous in the water column, a particle can be subject to very different fall speeds during its trip between the surface and the seafloor: slow speeds when the particle falls under its own weight and fast speeds when it is carried in a large aggregate before being left again to its own fate by the breakup of the aggregate. Determining the path of the particulate matter therefore requires a great reinforcement of tracers.

In view of the difficulty in the use of Stokes law for real particles, an estimate of the speed of the fastest particles can be obtained by comparing the mass flux peaks at different depths (Fig. 9.12).

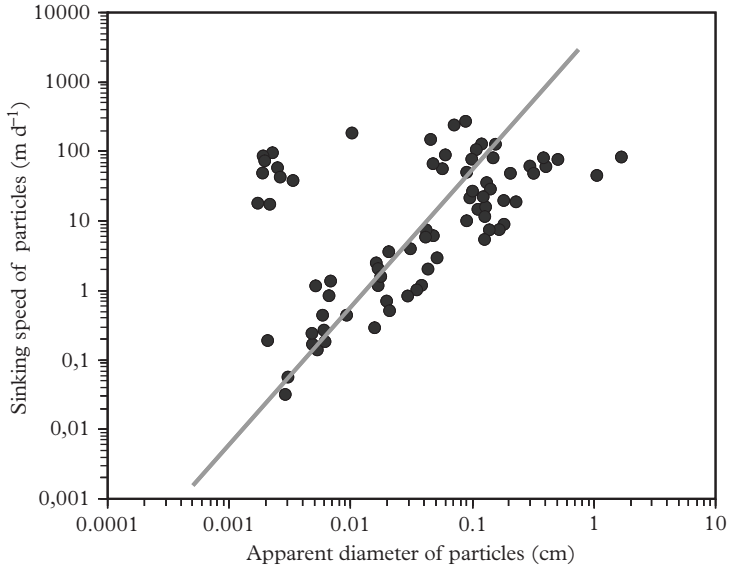

Figure 9.11 *Sinking speed of particles as a function of their diameter. The straight line corresponds to the Stokes law for a density difference of 0.0015 g cm^{-3} between the particles and the seawater. Modified from Stemmann et al. (2004).*

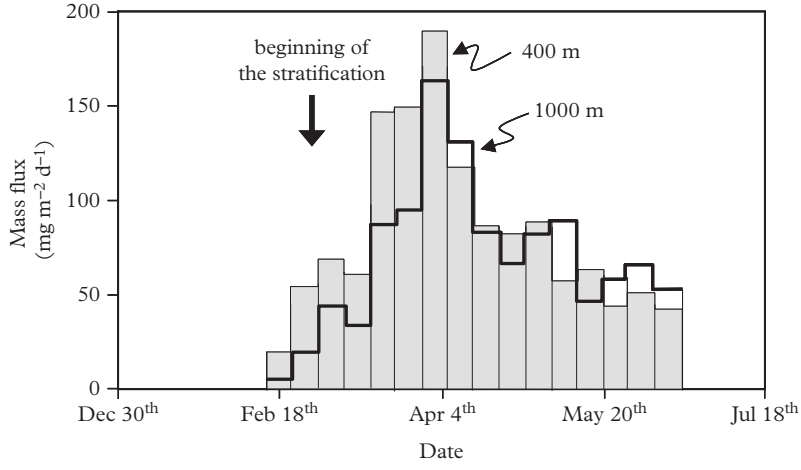

Figure 9.12 *Temporal evolution of the particle flux in the NE Atlantic. The highest particle flux occurs during the same collection interval of 8 days at 400 and 1000 m, which implies that the sinking rate of particles is at least 75 m d^{-1}. The maximum flux occurs 1 month after the beginning of the surface water stratification. Modified from Guieu et al. (2005).*

9.5 Changes of the Particle Flux with Depth

9.5.1 The Organic Matter Flux

Photosynthesis is the starting point of the food chain, including the life/death cycle that induces the sinking of organic matter in the water column. Expressed in terms of carbon fluxes, the quantity of organic material produced annually is of the order of 60×10^{15} g of carbon per year. However, only about 10% of all the photosynthesized organic matter (primary production) escapes remineralization in surface waters and falls into the deep ocean (exported production). In this section, we will not describe the production of these particles (see Chapters 2 and 8) but we will focus on their dynamics and their evolution in the water column.

Below the photic zone, there is no photosynthesis. The flux of particulate organic carbon (or POC) in the water column is therefore controlled by the production of organic matter in the photic zone and remineralization below. In the North Eastern Pacific, for example, the POC flux collected by sediment traps is lower in the center of the gyre, where oligotrophic conditions prevail, than in the California upwelling, where there is intense biological production (Fig. 9.13a). Whatever the biological production in the photic zone, the POC flux decreases exponentially with depth due to remineralization (Fig. 9.13b).

Organic matter is made up of a variety of compounds which are degraded at different rates (Benner and Amon, 2015). Carbohydrates (sugars) are most easily usable by heterotrophic organisms: they represent the labile fraction of organic matter. Proteins are degraded more slowly. Lipids are most resistant: they are the refractory portion of

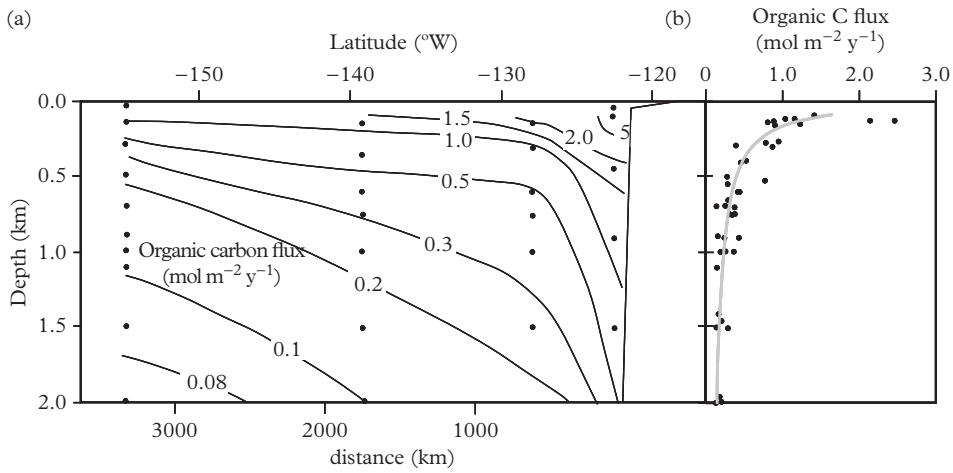

Figure 9.13 *POC fluxes collected by sediment traps in the Eastern North Pacific. (a) Hawaii–California transect. (b) Average evolution of the POC flux with depth obtained by excluding the results of the station closest to the coast. Modified after Martin et al. (1987).*

organic matter and they even survive to remineralization in the sediment. Dissolution rates are characterized with incubation experiments, assuming that remineralization follows first-order kinetics. Thus, the degradation rate of organic compounds by bacteria decreases by a factor of two when temperature deceases by 10°C (Arrhenius law). As organic matter produced in the euphotic zone sinks through the water column, its composition changes from one that is easily characterized by standard chromatographic techniques to one that is not identified at the molecular level and is therefore called "uncharacterized" (Lee et al., 2004a).

The study of the $\Delta^{14}C$ in particles shows that the remineralization is not the only factor affecting the carbon of marine particles (Fig. 9.14). In the photic zone, POC is photosynthesized using dissolved CO_2, so that its $\Delta^{14}C$ is similar to the $\Delta^{14}C$ of dissolved inorganic carbon (DIC), which is marked by the anthropogenic ^{14}C. Below the photic zone, the $\Delta^{14}C$ of POC in small particles decreases with depth and becomes intermediate between the DOC and the surface POC signatures. It is not surprising to find small particles with an anthropogenic $\Delta^{14}C$ because ^{230}Th shows that the residence time of these particle in the water column is of a few years (see Section 9.6). The most negative $\Delta^{14}C$ of POC in small particles does not result from *in situ* aging: it simply marks the recent incorporation of old carbon from the DOC (which can be fixed on small particles by bacteria) or from old sediment resuspension. The POC analyzed in deep traps has a variable $\Delta^{14}C$ (Problem 3): the most positive values indicate that this material contains recently photosynthesized POC and that it represents a source of positive $\Delta^{14}C$ for small particles in the deep ocean. Less positive $\Delta^{14}C$ result from an aggregation of ^{14}C-depleted small particles on large particles.

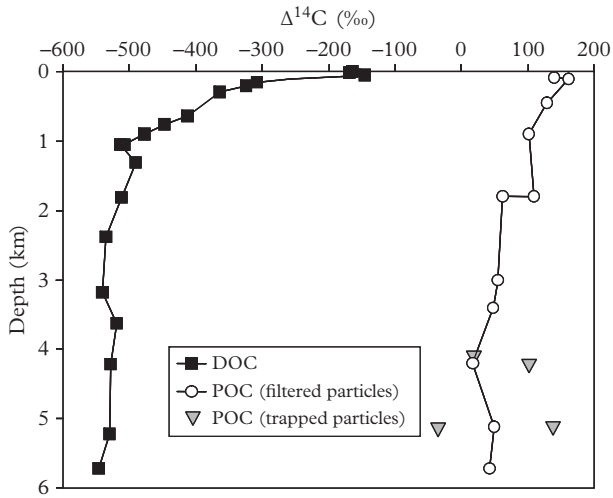

Figure 9.14 *$\Delta^{14}C$ of dissolved and particulate (small filtered particles and trapped particles) organic carbon in the Pacific Ocean. Modified from Druffel et al. (1992).*

Due to remineralization, only about 1% of carbon product reaches surface sediment in the open ocean. In surface sediments, organic C is still mineralized during biological and chemical reactions grouped under the name of **diagenesis**. Eventually, only about 0.1% of carbon produced in the photic zone is permanently buried in the sediment.

9.5.2 The Mineral Phases

Lithogenic material does not evolve much during its fall through the water column. However, some elements brought by lithogenic material may be partially dissolved in seawater. This is, for example, the case for Mn. Conversely, insoluble elements such as Al, Ti or ^{232}Th remain essentially associated with the mineral phases. Relatively complex exchange processes highlighted with Nd isotopes will be presented later in the chapter.

The biogenic phases may have varying fates. As long as seawater is saturated with respect to $CaCO_3$, planktonic tests formed in shallow waters are stable. Their dissolution becomes significant under the lysocline and they disappear from the sediments below the carbonate compensation depth when their dissolution in the sediment is faster than their supply from the surface waters (see Chapter 2). In practice, there is frequently an increase of the dissolved Ca^{2+} concentration and alkalinity above the lysocline. This may be due to the dissolution of carbonate in fecal pellets (the remineralization of organic matter produces CO_2 which acidifies the environment) or in the sediments of ocean margins (with then horizontal advection toward the open ocean).

Seawater is always undersaturated with regards to biogenic silica. Diatom frustules always tend to dissolve. The dissolution rate increases with temperature and the gradual remineralization of the organic protection of the frustule.

Certain phases, such as barite ($BaSO_4$), are not formed at the ocean surface but around 200–400 m deep in response to the degradation of organic matter (Problem 4).

9.6 Estimation of the Particle Flux

Sediment traps provide a first estimation of particle flux. However, there are limits to their use. First, the currents create turbulence around the trap, which affects the trajectory of the particle and which may artificially reduce the quantity of particles collected by the trap. This introduces a bias on the total particulate flux measurement but also on the composition of the flux because it is likely that slow particles are more easily lost. On the other hand, the implementation of sediment traps requires complicated and costly logistics. It is therefore important to quantify the particle flux by an independent method to validate sediment trap measurements and when necessary to obtain particle flux without sediment traps.

The disintegration series of ^{238}U are used to calibrate the flux of material through the water column. Uranium has a conservative behavior in the ocean. ^{238}U and ^{234}U therefore have constant concentrations and they are homogeneous sources of ^{234}Th and ^{230}Th in the ocean. Thorium is extremely insoluble in seawater. ^{234}Th and ^{230}Th are therefore produced in solution but they attach quickly to marine particles and they then become tracers of particulate matter.

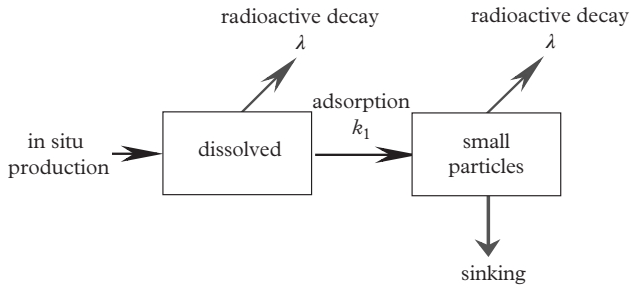

Figure 9.15 *Conceptual diagram of the thorium flux in the irreversible adsorption case.*

9.6.1 ^{234}Th and Irreversible "Scavenging" Models

We assume first that this uptake on particles or "scavenging" is irreversible (Fig. 9.15).

According to equation (5.15) in Chapter 5 (see Chapter 5 for the definition of activity)

$$k_1 = \lambda_{^{234}\mathrm{Th}} \left(\frac{\{^{238}\mathrm{U}\}}{\{^{234}\mathrm{Th_d}\}} - 1 \right). \tag{9.4}$$

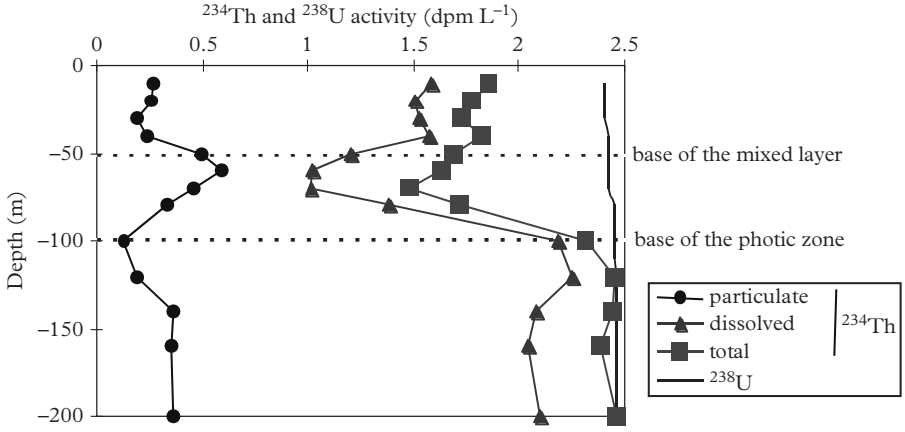

Figure 9.16 *Depth profile of dissolved, particulate and total ^{234}Th activity. The total ^{234}Th activity is lower than the ^{238}U activity in the photic zone, reflecting the removal of the particles produced by photosynthesis. The highest particle concentration is found in the chlorophyll maximum. Deeper, the total ^{234}Th activity becomes equal to the ^{238}U activity (this does not mean that particles do not fall, but that the particles that fall toward the seafloor are replaced by particles from the surface). Modified from Coale and Bruland (1987).*

If the activity of ^{238}U is equal to the dissolved ^{234}Th activity ($\{^{238}U\} = \lambda_{^{238}U}\ ^{238}U = \{^{234}Th_d\} = \lambda_{^{234}Th}\ ^{234}Th_d$), all the ^{234}Th produced by decay of ^{238}U is lost by the disintegration of dissolved ^{234}Th. The scavenging rate of ^{234}Th by particle binding is therefore equal to zero, resulting in $k_1 = 0$ and $\tau_1 = +\infty$. On the contrary, if $\{^{234}Th_d\}$ is very low, the disintegration of ^{234}Th is also very low and all the ^{234}Th produced by decay of ^{238}U is lost by scavenging on particles. The rate of ^{234}Th uptake by particles is very high, resulting in $k_1 = +\infty$ and $\tau_1 = 0$ (as soon as it is produced, dissolved ^{234}Th is fixed on marine particles).

If k_1 is constant in the water column, $\{^{234}Th_d\}$ is constant

$$\left\{^{234}Th_d\right\} = \frac{\lambda_{^{234}Th}}{\lambda_{^{234}Th} + k_1} \left\{^{238}U\right\}. \tag{9.5}$$

In general, k_1 varies with the particle concentration: k_1 is high in the particle-rich surface waters and smaller in the deep ocean when particle concentration decreases (Fig. 9.16).

Application: ^{234}Th in the surface waters of the Pacific Ocean (Coale and Bruland, 1987)

Based on the depth profiles of Fig. 9.16, determine the residence time of dissolved ^{234}Th in the mixed layer, at 70 m and at 200 m of depth.

Answer:

The U and dissolved ^{234}Th activities ($\{^{238}U\}$ and $\{^{234}Th_d\}$) read on Fig. 9.16 are reported in Table 9.3 and used to compute k_1 (equation 9.4) and the residence time $\tau_1 = 1/k_1$.

Table 9.3 *Dissolved ^{234}Th residence time calculation*

Depth	Mixed Layer	70 m	200 m
$\{^{238}U\}$ (dpm L^{-1})	2.4	2.43	2.46
$\{^{234}Th_d\}$ (dpm L^{-1})	1.5	1.0	2.1
k_1 (d^{-1})	0.017	0.042	0.0048
τ_1 (d)	58	24	209

The residence time of dissolved ^{234}Th is the lowest at 70 m (it corresponds to the maximum particle concentration capable of fixing the dissolved ^{234}Th) and the highest at 200 m where the particles are least abundant.

The uptake rate of dissolved ^{234}Th on particles has been also estimated in the range of a few hours with *in vitro* experiments. This is much lower than in the natural environment (Honeyman and Santchi, 1989). In fact, these experiments using particles with well-defined sizes are not representative of seawater in which very small particles

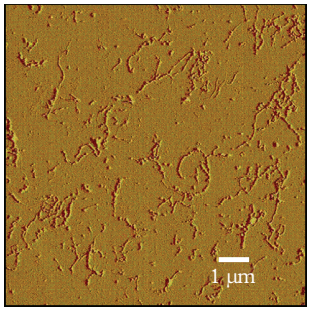

Figure 9.17 *Marine colloids observed by atomic force microscopy. They are made of organic fibers that often have a diameter less than 0.1 µm and that can form networks. They are rich in organic molecules that strongly bind metals such as thorium. Modified from Verdugo et al. (2004).*

(< 1 µm) called colloids are present. These colloids fix thorium because they represent a much larger specific surface area than small particles. Because of their small size, colloids pass through conventional filters and they are then analyzed with the filtered solution (Fig. 9.17). Thus, a significant fraction of "dissolved" thorium (and other metals) is not actually in solution but rapidly fixed on colloids that takes several weeks to be fixed on the small particles (Baskaran et al., 2004).

Similarly, the residence time of particulate ^{234}Th, and by the way the residence time of particles, can be determined in the surface waters. The activity of particulate ^{234}Th ($\{^{234}\mathrm{Th_p}\}$) is defined as the activity of ^{234}Th retained on the filter divided by the volume of filtered water. We obtain k_p, which is the removal rate (or scavenging rate) of particulate ^{234}Th from the surface layer by sinking in the water column, by replacing in equation (5.15) of Chapter 5 the activity of the parent isotope by the production of particulate ^{234}Th (Fig. 9.16)

$$\begin{aligned} k_p &= \lambda_{^{234}\mathrm{Th}} \left(\frac{\left(k_1/\lambda_{^{234}\mathrm{Th}}\right)\left\{^{234}\mathrm{Th_d}\right\}}{\left\{^{234}\mathrm{Th_p}\right\}} - 1 \right) \\ &= \lambda_{^{234}\mathrm{Th}} \left(\frac{\left\{^{238}\mathrm{U}\right\} - \left\{^{234}\mathrm{Th_d}\right\}}{\left\{^{234}\mathrm{Th_p}\right\}} - 1 \right). \end{aligned} \tag{9.6}$$

Application: Particulate ^{234}Th export from the surface waters (Coale and Bruland, 1987)

Still using Fig. 9.16, determine the residence time of particulate ^{234}Th in the mixed layer, in the 0–70 m layer and in the 0–200 m layer. Deduce the settling speed of the particles.

Answer:

On Fig. 9.16, we read the activities $\{^{238}\mathrm{U}\}$, $\{^{234}\mathrm{Th}_d\}$ and $\{^{234}\mathrm{Th}_p\}$ averaged between the surface and the maximum depth. As shown in Table 9.4, k_p and τ_p (= $1/k_\mathrm{p}$) are calculated from these values and equation (9.6).

Table 9.4 *Particulate thorium residence time calculation*

Depth	Mixed Layer	0–70 m	0–200 m
$\{^{234}Th_p\}$ (dpm L^{-1})	0.25	0.35	0.32
$\{^{234}Th_d\}$ (dpm L^{-1})	1.6	1.4	1.8
k_p (d^{-1})	0.063	0.058	0.030
τ_p (d)	16	17	34

The residence time of particulate ^{234}Th increases with the thickness, z, of the surface layer. If the particles are just formed at the ocean surface, their sinking velocity over the surface layer of thickness z is

$$w_p = z/\tau_p.$$

We infer that between 0 and 200 m, the settling speed of particles is 6 m d^{-1}.

Equation (9.6) allows calculation of the flux of particulate ^{234}Th or ^{230}Th from surface water as a function of depth and of the average U and Th isotope concentrations in the overlying water column. It is used to evaluate the sediment trap efficiency by comparing the calculated and measured ^{230}Th or ^{234}Th fluxes. ^{234}Th, which has a short half-life, is used for the validation of drifting traps (Problem 5). With its long half-life, ^{230}Th is adapted to evaluate the efficiency of moored traps by comparing the calculated ^{230}Th flux and the mean ^{230}Th flux collected during 1 y to average the seasonal variations of the flux. One of the limitation of this method is that the phases which carry Th isotopes are not known with certainty. Are sediment trap yields calculated with Th isotopes applicable to all the compounds of the particulate matter? The question remains open and requires case by case studies. It remains that the yields of moored and drifting traps collecting particles above a depth of 1000 m are frequently lower than 100%. It is indeed in this depth range that currents are the strongest and that they are more likely to create turbulence that prevents particles from falling into the trap.

9.6.2 Relations between Small and Large Particles

There is a paradox in the description of particle fluxes based on thorium isotopes. Sinking speeds given by thorium isotopes are generally low compared to sinking speeds of particles collected in sediment traps although they constitute most of the particulate matter flux.

A particle time series collected by a sediment trap moored at 3200 m in the Sargasso Sea (in the Atlantic Ocean, NE of the Caribbean) provides an answer (Fig. 9.18). The mass flux recorded in the particulate sediment trap is driven by the production of particles in the surface water and the rapid fall of these particles. ^{230}Th is produced in the whole water column and at 3200 m the contribution of the ^{230}Th produced in the surface

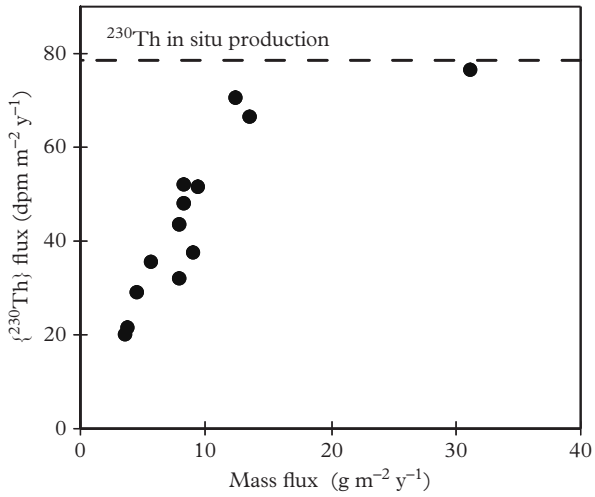

Figure 9.18 *^{230}Th flux and mass flux measured in a sediment trap moored at a depth of 3200 m in the Sargasso Sea. The linear relationship between the ^{230}Th flux and the mass flux indicates that the concentration of ^{230}Th is constant in the trapped material. This is no longer true for high fluxes because ^{230}Th-poor surface-derived material dilutes ^{230}Th-rich particles aggregated at depth. We note that the measured ^{230}Th flux is always lower than the ^{230}Th radioactive production in the overlying water column. It reflects the low efficiency of the trap or the lateral transport of particles. Modified from Bacon et al. (1985).*

waters is low. If the $^{230}Th_p$ flux was dominated by the slow sinking of small particles, this flux should be relatively constant and it should not be correlated with the mass flux. The good correlation between mass flux and $^{230}Th_p$ flux suggests that large particles from the surface aggregate ^{230}Th-rich small particles located at depth. The particulate transport scheme becomes still a little bit more complicated with the uptake of small particles on large ones (Fig. 9.1), a phenomenon already seen with carbon isotopes (Problem 3).

9.6.3 ^{230}Th and Reversible Models

Although it allows calibration of the traps, the irreversible scavenging model has its limits. In particular, it predicted that the dissolved ^{230}Th concentration should be constant with depth (equation 9.4), which is in complete contradiction with observations that generally show a linear increase of the dissolved ^{230}Th concentration with depth (Fig. 9.19).

To reconcile theory with observations, we assume that there is a rapid and reversible equilibrium (Fig. 9.20) between solution and particles ($[^{230}Th_p] = K[^{230}Th_d]$). Noting that Γ_{230} is the ^{230}Th production rate by ^{234}U decay, neglecting ^{230}Th decay because ^{230}Th has a long half-life and assuming steady state, we obtain

$$\frac{d\left[^{230}Th_d\right] + \left[^{230}Th_p\right]}{dt} = \Gamma_{230} - w_p \frac{\partial\left[^{230}Th_p\right]}{\partial z} = 0. \tag{9.7}$$

It follows that

$$\begin{aligned}\left[^{230}Th_p\right] &= \frac{\Gamma_{230}}{w_p} z,\\ \left[^{230}Th_s\right] &= \frac{\Gamma_{230}}{K w_p} z.\end{aligned} \tag{9.8}$$

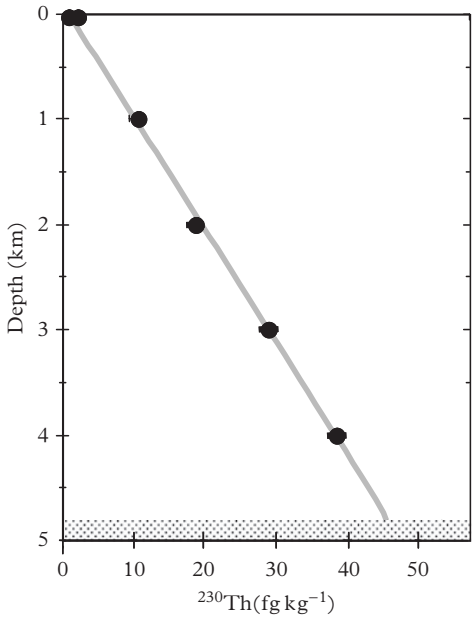

Figure 9.19 *^{230}Th depth profile measured in filtered samples in the tropical North Pacific. The curve is obtained from equation (9.8b). Adapted from Roy-Barman et al. (1996).*

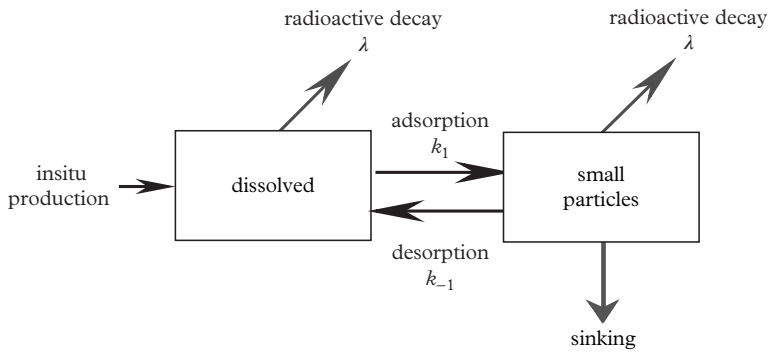

Figure 9.20 *Conceptual diagram of the thorium fluxes in the reversible adsorption case.*

The $^{230}Th_p$ profile is linear because, at a given depth, the flux of particulate ^{230}Th is only determined by the amount of ^{230}Th produced in the overlying water column. Therefore, the $^{230}Th_p$ profile alone tells us nothing on the dissolved particulate exchanges. As there is a rapid equilibrium between dissolved and particulate phases, dissolved and particulate ^{230}Th profiles must look the same. The reversible model explains the linear increase of $^{230}Th_d(z)$ by the stripping in the deep water a small fraction

of the ^{230}Th accumulated by the particles during their fall. The residence time of total ^{230}Th in a water column of depth h is then

$$\tau_s = \frac{\int_0^h \left[^{230}\mathrm{Th}_{\mathrm{d+p}}\right] dz}{w_p^{230}\mathrm{Th}_{\mathrm{p}}\,(h)} = \frac{1+K}{K}\frac{h}{2w_{\mathrm{p}}}. \tag{9.9}$$

Application exercise: ^{230}Th in the waters of the Pacific (Roy-Barman et al., 1996)

From Fig. 9.19, and knowing that particulate ^{230}Th is approximately 15% of dissolved ^{230}Th (K = 0.15), determine the settling speed of the particles and the ^{230}Th residence time in the water column.

Answer:

From the surface to 4000 m of depth, the $^{230}\mathrm{Th}_{\mathrm{d}}$ concentration increases linearly from 0 to 40 fg kg^{-1}. The slope of the $^{230}\mathrm{Th}_d$ profile is thus (40 – 0)/(4000 – 0) = 0.001 fg m^{-4}. From equation (9.8b) and taking K = 0.15, we obtain a sinking speed of particles w_{p} = 0.54/0.15/0.001 = 360 m y^{-1}. This is the average settling speed of particles larger than 0.2 μm (the pore size used for sample filtration).

From equation (9.9), we obtain the ^{230}Th residence time:

$\tau = (1 + 0.15) / 0.15 \times 4000 / (2 \times 540) = 43$ y.

The high ^{230}Th residence time in the water column and the low sinking speed of the particles reflect a low scavenging, in agreement with the low biological productivity and low detrital inputs of this area.

As ^{230}Th and ^{234}Th are two isotopes of a same element introduced in the seawater in the same chemical form, they must have the same chemical behavior and reversible exchange must apply also to ^{234}Th. However, the irreversible scavenging equations (equations 9.4 and 9.5) are used frequently to estimate POC flux based on ^{238}U–^{234}Th disequilibrium because in this case, only the net flux sinking of particulate ^{234}Th is used.

With the improvement of analytical techniques, it becomes clear that ^{230}Th profiles are rarely perfectly linear in deep waters because ^{230}Th transport by currents becomes more important than ^{230}Th transport by sinking particles. It becomes possible to use ^{230}Th to study deep circulations (see Chapter 10).

9.7 The Role of Margins

9.7.1 Boundary Scavenging

The continental margins (or continental boundaries) of the ocean are areas of high primary biological production and they receive strong continental inputs. The particle

fluxes are therefore much more intense than in the rest of the ocean. The chemical properties of water masses are preferentially modified at the continental margins. Since the vertical particulate flux of nuclides such as ^{230}Th, ^{231}Pa, ^{210}Pb and ^{10}Be (see Chapter 4) is more or less proportional to the mass flux, these nuclides are preferentially removed at the continental margins where nuclide flux in sediment traps and on the seafloor, in general, largely exceed the local *in situ* production (Fig. 9.21). In addition, the relative behavior of two nuclides such as ^{231}Pa and ^{230}Th may be different in continental margins (where both nuclides are efficiently scavenged) compared to the open ocean (where ^{230}Th is generally scavenged preferentially compared to ^{231}Pa; see Chapter 4).

In the Pacific Ocean, ^{230}Th and ^{231}Pa are preferentially removed from the water column at the ocean margins and in the subarctic Pacific where strong diatom fluxes efficiently scavenge ^{231}Pa (Hayes et al., 2014). There, the vertical fluxes of ^{230}Th and ^{231}Pa exceed their production in the overlying water column. The {^{231}Pa/^{230}Th} activity ratio in the margin sediments is much higher than the production ratio in seawater. This

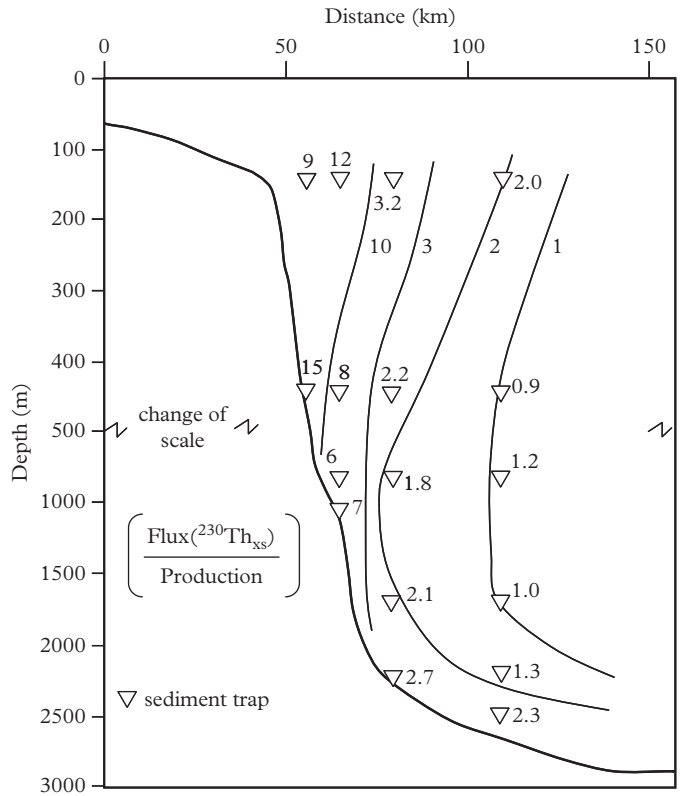

Figure 9.21 *Flux of $^{230}Th_{xs}$ normalized to* in situ *production rate on the Western Atlantic continental margin. Modified from Anderson et al. (1994).*

reflects the contribution of dissolved ^{231}Pa transported from the open ocean, where sediments have a $\{^{231}Pa/^{230}Th\}$ activity ratio lower than the production ratio. In the Atlantic Ocean, there is also a strong Th flux to the continental margins, but Pa–Th fractionation seems controlled by the export of Pa to the Southern Ocean. A recent high resolution GEOTRACES section of the Atlantic Ocean demonstrates the clear occurrence of ^{230}Th and ^{231}Pa depletion in the deep waters due to boundary scavenging, complicating the use of ^{230}Th and ^{231}Pa as tracers of the deep circulation described in Chapter 10 (Hayes et al., 2015).

Continental margins play an important role in the removal of anthropogenic contaminants. For example, sediments deposited at the bottom of the Okinawa trench (East of Taiwan) contain ^{210}Pb and ^{240,239}Pu inventories 20 times greater than the local atmospheric deposition (Fig. 9.22). The ^{240}Pu/^{239}Pu ratio in the sediment is higher than the ^{240}Pu /^{239}Pu ratio of atmospheric deposits and it is identical to the ^{240}Pu/^{239}Pu ratio of the direct contamination from the American nuclear test sites of the Pacific (Bikini and Enewetak islands). This Pu could therefore have been carried over 5000 km by the North Equatorial Current and the Kuroshio before being removed from the water column on the Taiwanese margin.

9.7.2 Boundary Exchange

Ocean margins are a sink for trace metals, but they are also a source of metals with the continental contributions that they receive (Fig. 9.23). Let's take the example of neodymium in the Pacific Intermediate Water and which flows along Papua New Guinea and through the Vitiaz Strait, around 850 m deep. Before flowing along the Papua New Guinea margin, the Pacific Intermediate Water has a concentration of 10 pmol kg^{-1} Nd and $\varepsilon_{Nd} = -8.0 \pm 0.3$. After passing along Papua New Guinea and through the Vitiaz Strait, the Pacific Intermediate Water has a Nd concentration of 9.5 pmol kg^{-1} and $\varepsilon_{Nd} = -2.0 \pm 0.3$. During the transit along Papua New Guinea, the potential temperature

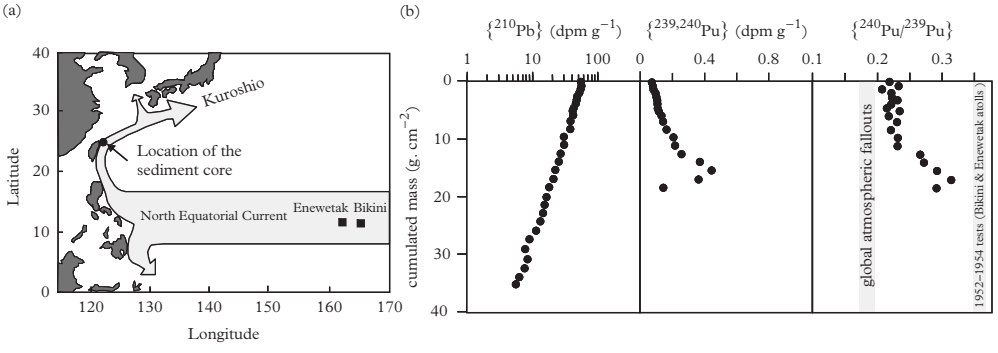

Figure 9.22 *Pu removal on the western margin of the Pacific Ocean. (a) Sampling site and surface currents. (b) $\{^{210}Pb\}$, $\{^{239,240}Pu\}$ and $\{^{240}Pu/^{239}Pu\}$ in the Okinawa trough sediments. Modified from Lee et al. (2004b).*

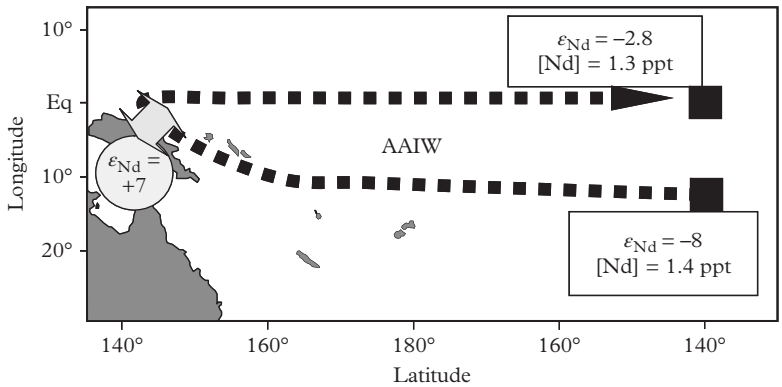

Figure 9.23 *Isotopic exchange along the Papua New Guinea margin. Modified from Lacan and Jeandel (2005).*

and salinity of the water mass do not change: therefore, there is no mixing with another water mass.

In this volcanic area, land weathering brings radiogenic Nd: $\varepsilon_{Nd} = +7$, a suitable source to explain the increase of ε_{Nd} of the water mass. However, the Nd concentration of the intermediate water hardly changes between its arrival along the Papua New Guinea margin and its exit through the Vitiaz Strait. The Pacific Intermediate Water flux is 3 Sv, so that the Nd flux is $F_{water} \times C_{Nd} = 132 \times 10^3$ kg y^{-1}. Using equation (5.21b) (Chapter 5), we find that 88×10^3 kg y^{-1} of land-derived Nd ($\varepsilon_{Nd} = +7$) has been added to intermediate waters, whereas 97×10^3 kg y^{-1} of the intermediate water Nd has been scavenged to the sediment. There is an exchange of about half of the Nd coming from the ocean with Nd freshly brought from continents that escaped the same trapping. It is likely that this boundary exchange occurs through the partial dissolution of continental particles deposited on the margin and the removal of dissolved Nd by adsorption on mineral phases such as Mn oxides. Boundary exchange has been long ignored because coast–open ocean concentration gradients only reflect the net effect of the margins (i.e., if they behave globally as a source or a sink for any given chemical element) but not the total fluxes exchanged. The ocean can receive strong Nd fluxes in areas where concentrations of Nd are not particularly high. This observation is crucial for the calculation of the Nd residence time in seawater. While the contributions of dissolved Nd by the rivers and the dissolution of the aerosols gives an oceanic Nd residence time $\geq$1000 y, ε_{Nd} data suggest that the Nd residence time is of the order of a few hundred years to maintain the isotopic composition gradient between the Atlantic and the Pacific. The paradox is resolved when we know that the main flux of Nd to the ocean is by boundary exchange and not by the direct contribution of the rivers or aerosol dissolution. What is valid for Nd is certainly true for other metals but is undetectable without isotopic signatures. This view could be supported by the difficulty of balancing the budget of Zn isotopes in the ocean (Little et al., 2014).

9.8 The Distribution of Sediments on the Seafloor

Marine particles that settle on the seafloor form sediments. The nature of the sediments depends on contributions from the ocean surface and the transformations undergone by particles in the water column and in the sediment itself (Fig. 9.24). In the ocean margins (in river deltas, coasts and on the continental shelf), organic-rich and lithogenic-rich sediments accumulate quickly (sedimentation rates can exceed 1 cm y^{-1}). After transit in deltas and on continental shelfs, sediments brought by large rivers flow into submarine canyons. They are transported as turbidity currents to the abyssal plain where they form deep submarine cones.

In the open ocean, the carbonate sediments dominate in marginal areas where the seafloor is shallower than 4000 m, that is, above the carbonate compensation depth. At great depths, carbonate and silica tests reaching the seafloor dissolve so rapidly that they cannot accumulate. Organic matter is efficiently remineralized at all depths. Below the carbonate compensation depth and away from diatom and radiolarian production areas, sediments are made of lithogenic particles carried by the wind. Sedimentation rates are

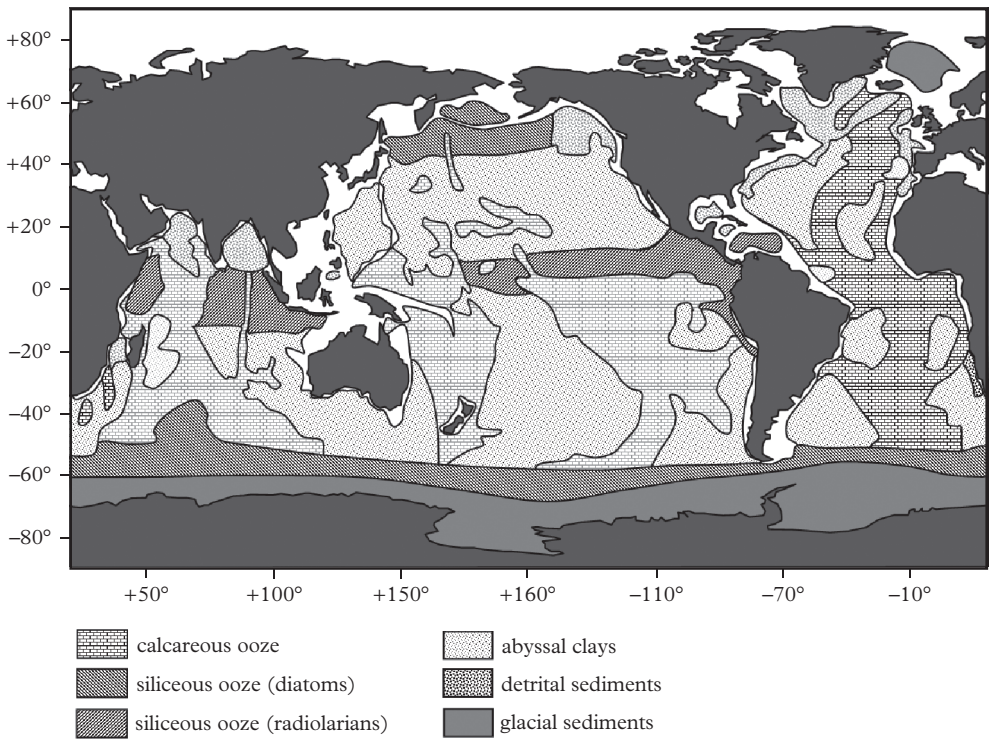

Figure 9.24 *Distribution of the main types of sediments at the bottom of the ocean. Adapted from different sources.*

extremely low (of the order of a few millimeters in 1000 y) so that these sediments are relatively rich in cosmic particles. Below upwelling areas (as in the equatorial Pacific or in the Antarctic polar front), sedimentation is dominated by diatoms in the Southern Ocean (creating an "opal belt" of diatom-rich sediments) or Radiolaria in the equatorial zone. Unlike calcium carbonate, seawater is always undersaturated with regard to amorphous silica, but in areas dominated by high diatom production and/or radiolarian production, siliceous tests accumulate in sediment so quickly that they cannot dissolve. In polar areas, the continental erosion by glaciers produces coarse lithogenic particles that are transported and dropped by icebergs to form glacial sediments.

9.9 The Diagenesis

Degradation of particles in the water column continues in the sediment during the early diagenesis. As particles stay in the surface sediments much longer than in the water column, the transformations are more important. In addition, the sediment forms a relatively confined environment in which extreme chemical and biological conditions that do not occur in the water column may develop. However, it is not a closed system: sediment particles receive and reject dissolved elements in the water column. Indeed, the sediment consists of two phases: the solid particles and the interstitial fluid. The volume of interstitial fluid depends on the porosity Φ

$$\Phi = \text{interstitial fluid volume / total volume of wet sediment.} \qquad (9.10)$$

The surface sediment porosity is frequently 60–90%. As the sediment settles under its own weight, porosity decreases with depth to values of the order of 40% in the sediment (at about 4 m of depth).

The evolution of the chemical composition of these two phases is coupled, even if they each have their own dynamics (Fig. 9.25). Organic matter is degraded by bacteria and burrowing animals. These animals have a particular importance because of mixing of surface sediment (a process called bioturbation); they allow the penetration of dissolved oxygen and fresh organic matter at depth in the sediment. The bioturbation layer typically has a depth of 5–15 cm. The degradation of organic matter in oxic sediment is described as remineralization in the water column

$$(CH_2O)_{106}(NH_3)_{16}(H_3PO_4) + 138\ O_2 \rightarrow 106\ CO_2 + 16\ HNO_3 + 1\ H_3PO_4 + 122\ H_2O + \text{chemical energy}$$

The degradation of organic matter produces an acidification of the environment, which promotes the dissolution of $CaCO_3$ (Fig. 9.26). The DIC concentration is higher in the interstitial fluid than in seawater, so that there is a DIC flux toward the water column. Organic matter oxidation also leads to a decrease of the O_2 concentration that can

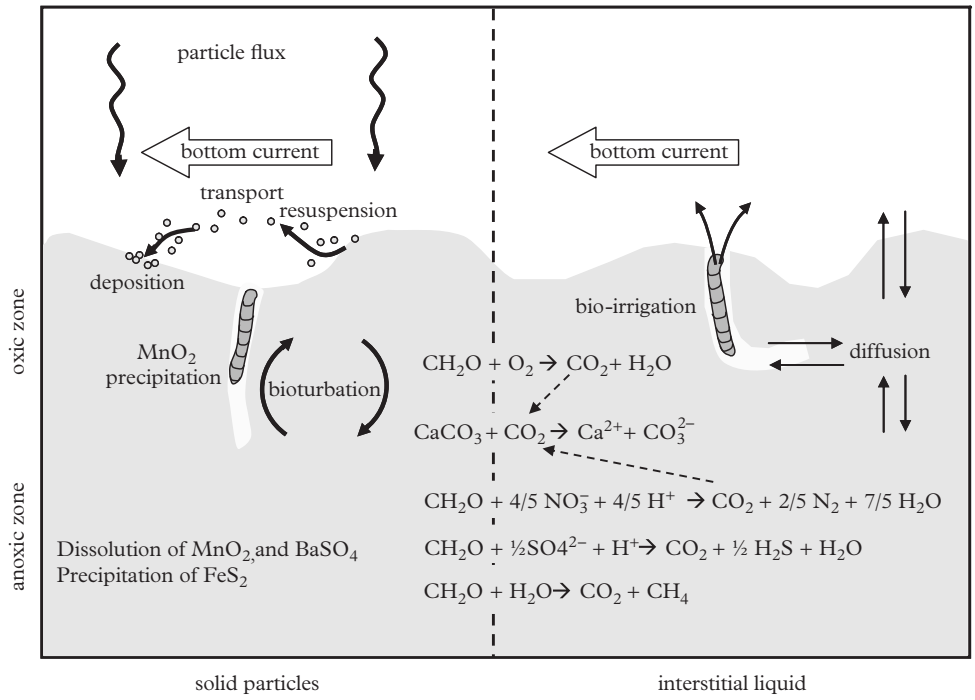

Figure 9.25 *Simplified scheme of diagenesis.*

end up in anoxia. Then molecules such as NO_3^- or SO_4^{2-} replace O_2 as electron acceptor for the anaerobic degradation of organic carbon by the bacteria

$$NO_3^- + 5\,e^- + 6\,H^+ \rightarrow ½\ N_2 + 3\ H_2O$$

$$SO_4^{2-} + 8\,e^- + 10\,H^+ \rightarrow H_2S + 4\ H_2O$$

With the decline of the SO_4^{2-} ion concentration, the interstitial fluid is no longer saturated with respect to barite ($BaSO_4$) which can dissolve. Iron and Mn oxides, which are unstable in a reducing environment, can also be used as electron acceptors, which leads to the release of Mn^{2+} and Fe^{2+} in the pore fluid. These ions diffuse into the interstitial fluid and precipitate when they arrive at the water–sediment interface because the bottom waters are O_2-rich. In areas with very low sedimentation rates, this can lead to the formation of MnO_2 crusts or nodules which are used for the paleoreconstitutions. Ultimately, organic matter is used as an electron acceptor. Incomplete oxidation of organic carbon by bacteria then produces methane (fermentation)

$$CH_2O + 4\,e^- + 4\,H^+ \rightarrow CH_4 + H_2O.$$

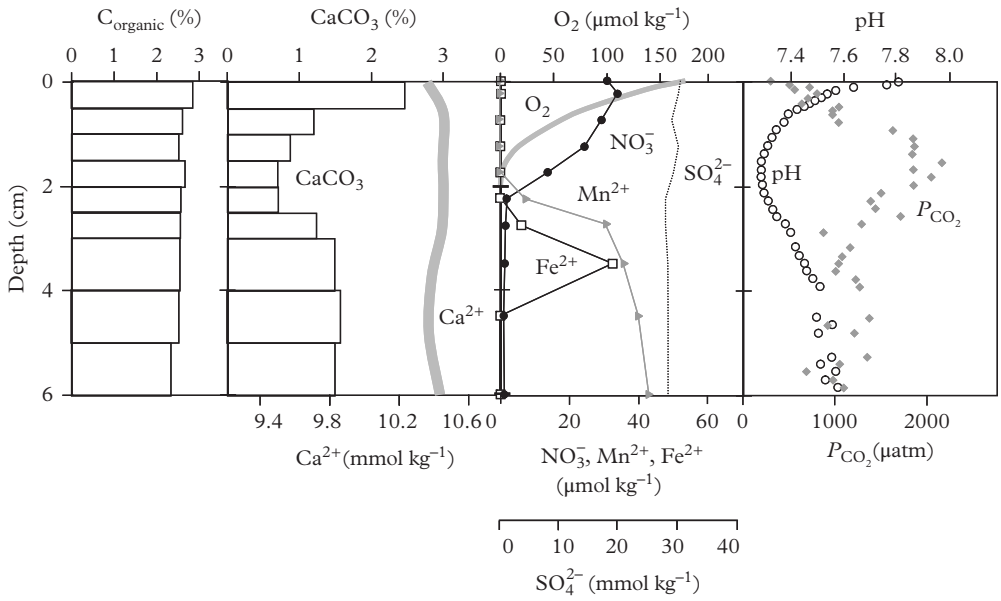

Figure 9.26 *Composition of pore fluid and solid phase in sediments of the equatorial Atlantic (upwelling of Gabon). Modified from Pfeifer et al. (2002).*

There may even be production of hydrogen (H_2) in areas of natural oil seep. In practice, there are many couplings between these cycles: for example, the reduction of MnO_2 allows denitrification. The effect of some of the reactions described above on the composition of the interstitial fluid and the solid phase is well visible on the analyses of sediment collected under the equatorial upwelling off the Gabon coast (Fig. 9.26). In the interstitial fluid, note in particular:

- the decay of dissolved electron donor species like O_2, NO_3^- and SO_4^{2-};
- the appearance of Mn^{2+} and Fe^{2+} when the sediment becomes anoxic (the decline of Fe^{2+} deeper in the sediment is due to the formation of pyrite—FeS_2—which is an iron sulfide) and which precipitates through (H_2S) hydrogen sulfide produced by the reduction of SO_4^{2-};
- the pH decrease and P_{CO_2} increase in the area of maximum remineralization which results in a slight increase of Ca^{2+} by the dissolution of carbonates.

In the solid phase, POC concentration decreases gradually. The sharp decline of the $CaCO_3$ concentration in the low pH depth confirms what was observed with the Ca^{2+} ions.

Application: Estimation of O_2 fluxes by different methods

From Fig. 9.25, evaluate the O_2 flux diffusing from bottom water to the sediment. Take $\Phi = 90\%$ and $D_{O_2} = 1.4 \times 10^{-5}$ cm^2 s^{-1}. Incubation in a benthic chamber deployed in the same area gives an O_2 consumption rate of 2 mmol m^{-2} d^{-1}. Compare these two values.

The O_2 diffusion flux in the sediment is given by the Fick law taking into account porosity (Chapter 6, equations 6.11 and 6.42): $F = -\Phi D_{O_2}(d[O_2]/dz)$. Over the first 5 mm of the sediment, the O_2 concentration decreases linearly from 180 to 90 nmol cm^{-3}. The concentration gradient is therefore $(d[O_2]/dz) = (90-180)/0.5 = -180$ nmol cm^{-4}. So, we obtain a flux $F = 2.3 \times 10^{-3}$ nmol cm^{-2} s^{-1} or 2.0 mmol m^{-2} d^{-1}.

There is a good match between the flux of O_2 diffusing into the sediment and the O_2 consumption rate measured in the benthic chamber. Most O_2 is therefore supplied to the sediment by diffusion rather than by bioturbation or bio-irrigation.

When conditions are very reductive in the sediment, the release of chemical species such as H_2S or CH_4 in seawater can induce anoxia in the bottom waters. This is the case in isolated basins such as the Black Sea or the Cariaco Basin (off the coast of Venezuela) where mixing between surface and bottom waters is very weak. A major discovery is the presence of methane hydrate crystals in these sediments. The stability of these minerals is very sensitive to a temperature increase in the bottom waters. Destabilization of these methane hydrates can trigger eruptions of mud volcanoes on the seafloor of these basins. Methane hydrates are a considerable reserve of CH_4 which could be reinjected in the ocean and the atmosphere relatively quickly at the geological timescale and with a strong climate impact in view of the strong greenhouse effect induced by methane (about 20 times more than the CO_2).

There is generally a good agreement between the productivity of surface water and the intensity of the remineralization in the underlying sediment (Fig 9.27). Margin areas represent 10% of the surface of oceans, but they support 20% of the ocean primary production and about 50% of the carbon burial. Most ocean sedimentation occurs in continental margin areas. This is also where diagenesis is most active: chemical elements mineralized in sediments of margin areas can diffuse to seawater and then be advected in the open ocean.

Some of the biogeochemical transformations observed in the water column are in fact the result of exchange with coastal areas. For example, Fig. 9.28 shows the evolution of concentrations in a benthic chamber deployed over sediments of the western margin of the North Atlantic at a depth of 750 m. Ions diffusing out of the sediment can be advected away from the coast and be interpreted (incorrectly) as a result of the remineralization of marine particles in the water column of the open ocean. Significant fluxes of calcium and alkalinity are particularly notable because they may affect waters above the lysocline and so oversaturated with $CaCO_3$ (unlike the sediment acidified by the decomposition of organic matter).

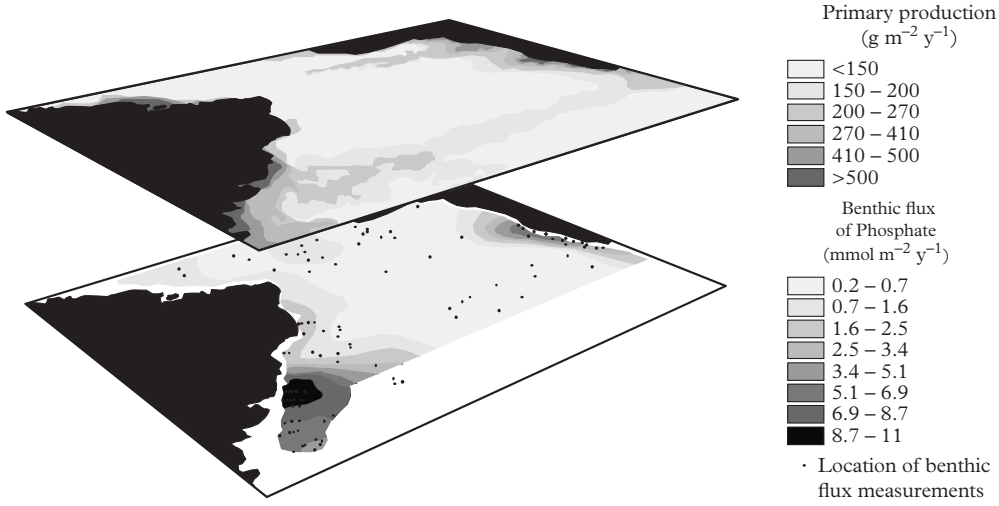

Figure 9.27 *Primary production and benthic flux of phosphate in the Atlantic. Modified from Hensen et al. (2004)*

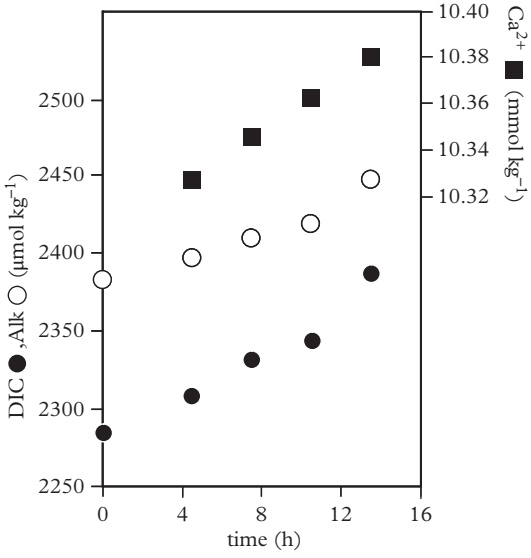

Figure 9.28 *Evolution of concentrations in a benthic chamber. Modified from Jahnke and Jahnke (2000).*

9.10 Timescales and Sediment Fluxes

The evolution of a sediment depends on the balance between the particle flux to the sediments, the diagenetic reactions and the transport by diffusion of the dissolved species in or out of the sediment. To constrain this dynamics, the rates of accumulation and

bioturbation of sediment, the rates of reaction and diffusion and the possible redistribution of sediment must be determined. Particles reaching the sediments have been highly enriched in insoluble nuclides such as ^{230}Th, ^{234}Th, ^{231}Pa and ^{210}Pb during their fall in the water column. These nuclides, which are in excess in the sediments compared to their soluble parents, are then used as chronometers. The rapid mixing of the surface sediment (generally from a few cm to 15 cm) by bioturbation is a ubiquitous phenomenon in marine sediments: it results in the presence of excess of short-lived isotopes (^{234}Th, ^{210}Pb) and man-made isotopes (Pu, ^{137}Cs) deep in sediments (Problem 6). Below the bioturbation layer, sediments are dated by isotopes of longer half-lives: ^{14}C allows dating sediments up to 50,000 y providing that they contain biogenic carbonates or organic matter (Problem 7). The disintegration of the ^{230}Th excess of marine sediments allows determination of sedimentation rates on timescales of a few hundreds of thousand years even in the absence of carbonates (Fig. 9.29). Beyond, dating of marine sediments is frequently done indirectly:

- by measuring the δ^{18}O of benthic foraminifera and comparing the age of already dated cores;
- by measuring the natural magnetization that they acquired during their formation, the sediment can be located on the Earth's magnetic field reversal scale (0–160 million y);
- by identifying the characteristic fossils present in other dated layers (0–600 million y);
- by measuring the ^{87}Sr/^{86}Sr ratio of carbonates and comparing it to the seawater evolution curve (0–600 million y; see Chapter 11);

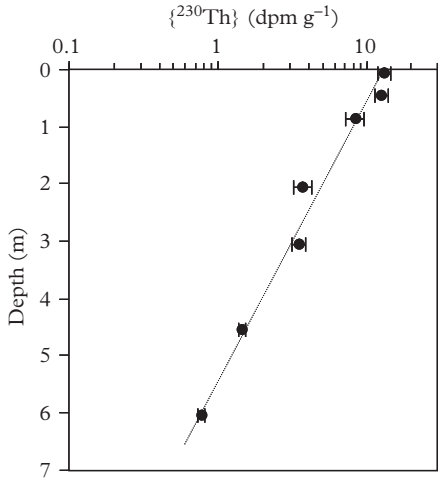

Figure 9.29 *Determination of the sedimentation rate by the decay of* $\{^{230}Th_{xs}\}$. *The* $\{^{230}Th_{xs}\}$ *activity is calculated relative to the* $\{^{238}U\}$ *activity which remains constant over time (neglecting changes in* ^{234}Th *and* ^{234}U *activities whose half-lives are relatively short compared to* ^{238}U). $\{^{230}Th_{xs}\}$ *is plotted versus depth on a semi-logarithmic graph. Assuming that the sedimentation rate* w_s *is constant and taking the logarithm of equation (6.43), we expect that the points must align along a line of equation* $ln(\{^{230}Th_{xs}\}) = ln(\{^{230}Th_{xs,0}\}) - \lambda/w_s \times z$. *The slope of the line is used to determine that the sedimentation rate is* $w_s = 1.9$ *cm* ky^{-1}. *Modified from Van Beek and Reyss (2001).*

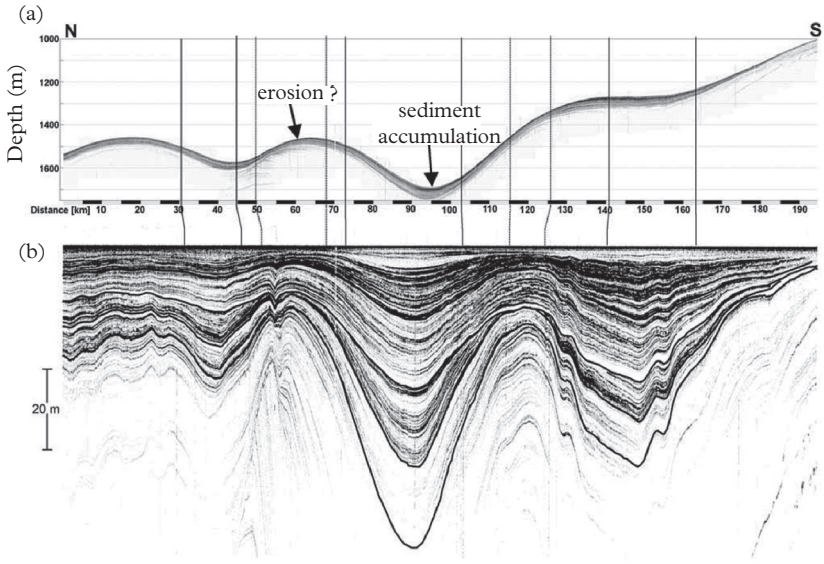

Figure 9.30 *Acoustic survey showing the redistribution of sediments along the Namibia coast. (a) Topographic profile in the Namibia basin. (b) Structure of the reflectors showing a preferential accumulation of sediments in depressions. Modified according Mollenhauer et al. (2002).*

- by radioactive dating of volcanic rocks or ash layers associated to sediments (0–4 billion y; see Chapter 11)

The determination of sediment ages and sedimentation rates gives a time-integrated value of the flux of material exported from the ocean surface and which accumulate in the sediment. This flux can be in principle compared to the particle flux in the overlying water column. However, this comparison has meaning only when considering the redistribution of sediments by bottom currents (Fig. 9.30). This redistribution occurs at the time of the particle deposition and it is often difficult to detect directly. It is necessary to quantify sediment focusing and winnowing to reconstruct the changes of carbon export over time. We have seen that when lateral transport is low, the ^{230}Th in the water column is transported vertically to the sediment. The flux of ^{230}Th preserved in the sediment (corrected for radioactive decay in the sediment) is compared to the ^{230}Th flux produced in the overlying water column. If they are different, it means that there was sediment redistribution on the seafloor. We can then normalize the flux of other chemical elements to the flux of ^{230}Th. For sediments too old to contain an excess of ^{230}Th, elements such as ^{3}He, Ir or Os are used because their main source in marine sediments are interplanetary dusts which are expected to have a more or less constant flux over time.

PROBLEMS

Problem 1: Sedimentation of particles in the Rhône River plume (Thill et al., 2001)

The Rhône River waters are very rich in particles. When the Rhône River flows into the Mediterranean Sea, it forms a freshwater plume confined at the sea surface. In the plume, the particle concentration decreases rapidly, due to its dilution by seawater and particle sedimentation. We consider a volume V of the plume moving at constant speed u ($= 0.6$ m s^{-1}) from the coast to the open sea and we assume that the thickness ($h = 0.1$ m) of the plume is constant. The water residence time in the plume is τ_w. We assume that the particle concentration in seawater is negligible compared to the plume water. The sinking speed of particles is w_p.

(1) Hydrological measurements show that the salinity of the plume water evolves according to the equation

$$S_{plume} = S_{seawater}(1 - e^{-0.33d}),$$

where d is the distance from the mouth of the Rhône (expressed in km). What is the value of τ_w?

(2) Write the conservation equation for particles and deduce the relationship between the concentration of particles and the distance from the shore.

(3) Table 9.5 gives the distance for which the particle concentration is divided by two for different size classes. Estimate the settling speed of the different class of particles. Which particles reach the open sea which is 30 km from the coast?

Table 9.5 *Distance required to reduce the particle concentration by 50%*

Particle Size (μm)	$d_{1/2}$ (km)
5–10	1.9
10–50	1.6
50–100	1.4

Problem 2: Where do particles come from? (Siegel et al., 2008)

Determine the maximum horizontal distance traveled by marine particles when they sink from the sea surface to a sediment trap in which they are collected at 1000 m assuming that their sinking speed is 100 m d^{-1} and that:

- they are advected by an horizontal current whose speed is 30 cm s^{-1};
- they are transported by horizontal eddy diffusion characterized by $K_x = 10^7$ cm^2 s^{-1}.

Same question if the trap is located at 5000 m.

Problem 3: The origin of particulate carbon

An oceanographer wants to determine the origin of the organic carbon in marine particles in a sediment trap located at 1000 m. Possible sources of carbon are: (1) the particulate organic carbon (POC) formed in the euphotic layer by phytoplankton, (2) the dissolved organic carbon (DOC) in the water column (which can be fixed on the particles by bacteria) and (3) POC brought from the continent which is close to the area studied. The oceanographer measures the $\delta^{13}C$ and $\Delta^{14}C$ of organic carbon present in the trap and the potential carbon sources (Table 9.6).

Table 9.6 *Isotopic composition of the particles*

	Material Trapped at 1000 m	DOC	Phytoplankton	Continental POC
$\delta^{13}C$ (‰)	–22.4	–22.0	–22.0	–29.0
$\Delta^{14}C$ (‰)	+85	–250	+100	+150

What percentages of carbon from phytoplankton, DOC and continental carbon contribute to the carbon of the trapped material?

Problem 4: Barite formation (Legeleux and Reyss, 1996)

We want to determine the depth of barite ($BaSO_4$) formation in the ocean. In the ocean, radium is essentially in the dissolved form. However, a small fraction of radium also occurs in barite crystals. The $\{^{228}Ra/^{226}Ra\}$ activity ratio in seawater decreases between 0 and 1000 m ($\{^{228}Ra/^{226}Ra\}$ is equal to 0.23 ± 0.05 dpm/dpm in surface waters, 0.13 ± 0.02 dpm/dpm at 200 m and 0.02 ± 0.01 dpm/dpm at 1000 m), and it remains relatively constant below 1000 m. The $\{^{228}Ra/^{226}Ra\}$ activity ratio of sinking particles trapped at 1, 2.5 and 4.5 km of depth is 0.12 ± 0.02 dpm/dpm. What is the depth of incorporation of radium in the marine particles (and by extension the depth of barite formation)?

Problem 5: Carbon flux under the ice (Coppola et al., 2002)

In early summer, the Barents Sea is still partially covered by sea ice. An oceanographer wants to determine the influence of sea ice on the amount of particulate organic carbon (POC) exported to the sediment. Drifting sediment traps are deployed to measure the exported POC flux. A trap drifting at a depth of 120 m in an ice-covered area collects a POC flux of 7 mmol m^{-2} d^{-1}. Another trap drifting at a depth of 200 m in an ice-free area collects a POC flux of 22 mmol m^{-2} d^{-1}.

(1) How can you explain the difference between the two traps?

(2) In order to check that the trap in the ice-covered area works correctly, the trapping efficiency is determined with the ^{234}Th method. In the water column of the ice-covered area, the average ^{234}Th activity is 1.75 dpm kg^{-1}, whereas the average ^{238}U activity is 2.45 dpm kg^{-1}. The trap drifting at 120 m in this area has collected a ^{234}Th flux of 2118 dpm m^{-2} d^{-1}.

Determine the trapping efficiency.

(3) The POC flux is sometime estimated based on the POC/^{234}Th ratio of the small particles filtered flux and ^{234}Th data in the water column. In the ice-covered zone, the average POC/^{234}Th ratio in small filtered particles is 55 μmol/dpm. What POC flux do you get from this ratio and U–Th data in the water column? Conclusion?

Hint: ^{234}Th radioactive decay constant = 0.0288 d^{-1}.

Problem 6: Bioturbation rate of sediments (Schmidt et al., 2002)

The ^{234}Th activity ($\{^{234}Th\}$) in marine sediments from the Iberian margin is measured to determine the intensity of bioturbation. The sedimentation rate is of the order of 1 mm y^{-1}. There is an excess of ^{234}Th compared to ^{238}U down to a depth of 1 cm.

(1) What is the depth of the bioturbated layer?

(2) Starting from the top of the sediment, $\{^{234}Th_{xs}\}$ is divided by 2 every 2 mm. If bioturbation is represented by a diffusion term characterized by the diffusion coefficient D_{biot}, what is the value of D_{biot}?

Hint: ^{234}Th radioactive decay constant = 0.0288 d^{-1}.

Problem 7: Dating of sediment (from Thomson et al., 2006)

A sediment core has been collected in the Atlantic Ocean at a depth of 1754 m. ^{14}C age are measured at different depths below the water–sediment interface (Table 9.7). Explain the distribution of the ages and determine the sedimentation rate?

Table 9.7 *Age of the sediment with depth*

Depth (cm)	**0.5**	**5**	**10**	**15**	**20**	**25**	**30**	**35**
Age (y)	3000	3100	3000	3900	4700	5800	6900	8000

10

Thermohaline Circulation

The deep ocean stores huge amounts of carbon brought by currents and released by remineralization. It appears from Chapter 9 that the ultimate fate of the anthropogenic carbon released in the atmosphere rests largely upon the buffering capacity of the deep ocean. By storing huge amounts of heat, the deep ocean also delays Earth's global warming. Thus, it is now time to learn more about the abyss. In Chapter 1, we described the main water masses filling the deep ocean, but we said little about the deep circulation, its dynamics and its interaction with the surface ocean. We focused on surface and intermediate water circulation, because they are most accessible to observation. Deep currents are not only poorly accessible to observation but also often extremely slow and overprinted by turbulence. This is why we have built up a toolbox of geochemical tracers and models through the preceding chapters that will provide fundamental information on deep water circulations for timescales ranging from decades to a millennium. In this chapter we will review some of these tracers and we will focus on the comparison and possible contradictions between different tracers and between tracers and physical models.

10.1 The Long Path of Deep Waters

Natural ^{14}C of dissolved inorganic carbon (DIC) in seawater highlights the main features of the thermohaline circulation. ^{14}C is formed in the atmosphere and absorbed by seawater at the ocean surface (see Chapter 7). If this water leaves the surface and sinks into the abyss, it is isolated from the atmosphere and the amount of ^{14}C decreases by radioactive decay or by mixing with ^{14}C-depleted older waters. The fundamental observation is that in the deep ocean, the $\Delta^{14}C$ age of DIC relative to the pre-bomb atmospheric carbon ($t = -1/\lambda \ln(1 - \Delta^{14}C)$) increases from the North Atlantic, where it is ~600 y old, to the North Pacific where it is ~2000 y old (Fig. 10.1). This corresponds to a decrease of the $\Delta^{14}C$ of the DIC of approximately 200‰ (see Fig. 10.2).

Meridian sections of the $\Delta^{14}C$ distribution in the Atlantic, Indian and Pacific oceans give an accurate illustration of the thermohaline circulation (Fig. 10.2). The youngest deep water (tagged by the least negative $\Delta^{14}C$) is the North Atlantic Deep Water (NADW). The North Atlantic is the first gateway of the waters to the abyss: warm and

Marine Geochemistry. First Edition. Matthieu Roy-Barman and Catherine Jeandel.

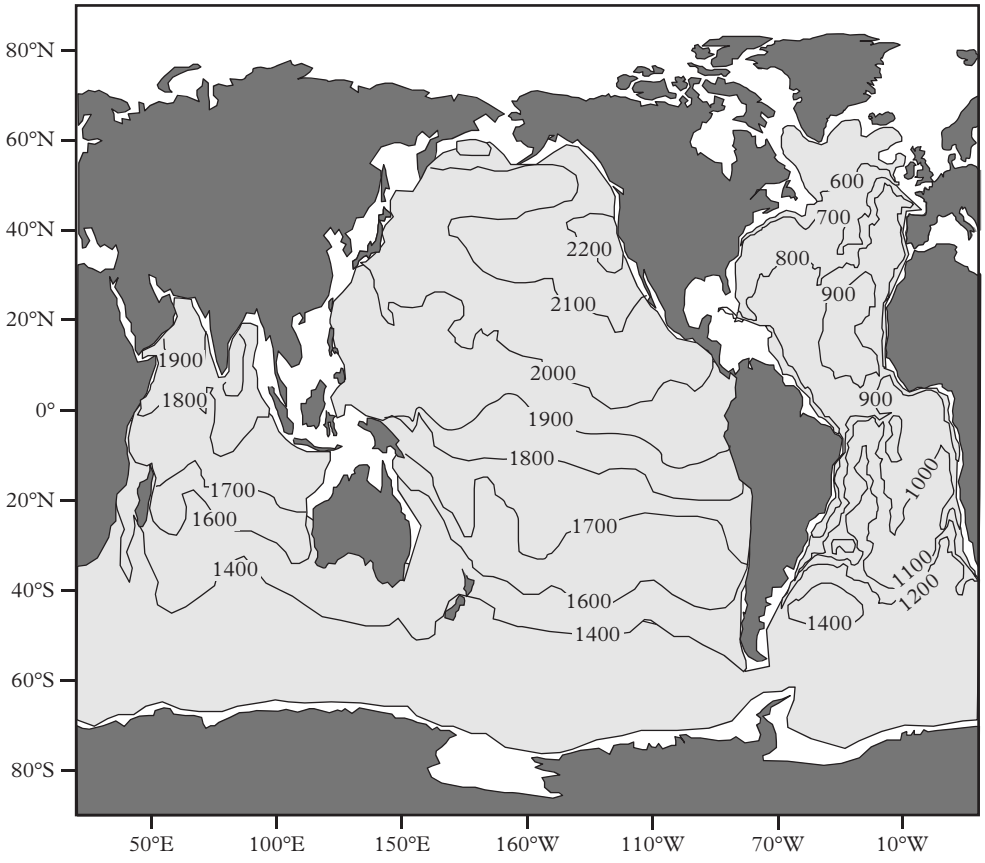

Figure 10.1 *Conventional age (in years) of deep (>1500 m) waters estimated from the $\Delta^{14}C$ of seawater. Modified from Matsumoto and Key (2004).*

salty surface waters transported from the Gulf of Mexico by the Gulf Stream and the North Atlantic drift enter the Nordic seas, the Norwegian, Greenland and Labrador Seas (Fig. 10.3). In winter, this water loses buoyancy by cooling, evaporation and sea-ice formation (sea-ice is made of fresh water, so brine rejection increases the salinity of the residual water; see Fig. 3.8 in Chapter 3). These dense waters accumulate in the Norwegian and Greenland seas and then they overflow above the sills separating these seas from the Atlantic Ocean. Cold waters are also formed in the Labrador Sea.

In the Atlantic Ocean, NADW is sandwiched between the Antarctic Bottom Water (AABW) below and the Antarctic Intermediate Water (AAIW) which flow northward and are associated with more negative $\Delta^{14}C$. The AABW comes from the edge of the Antarctic continent (we will return to that later) while the AAIW is formed in the northern part of the Southern Ocean. Figure 10.2 highlights the key role of the Southern Ocean that links the Atlantic, Indian and Pacific oceans. In the Atlantic sector of the

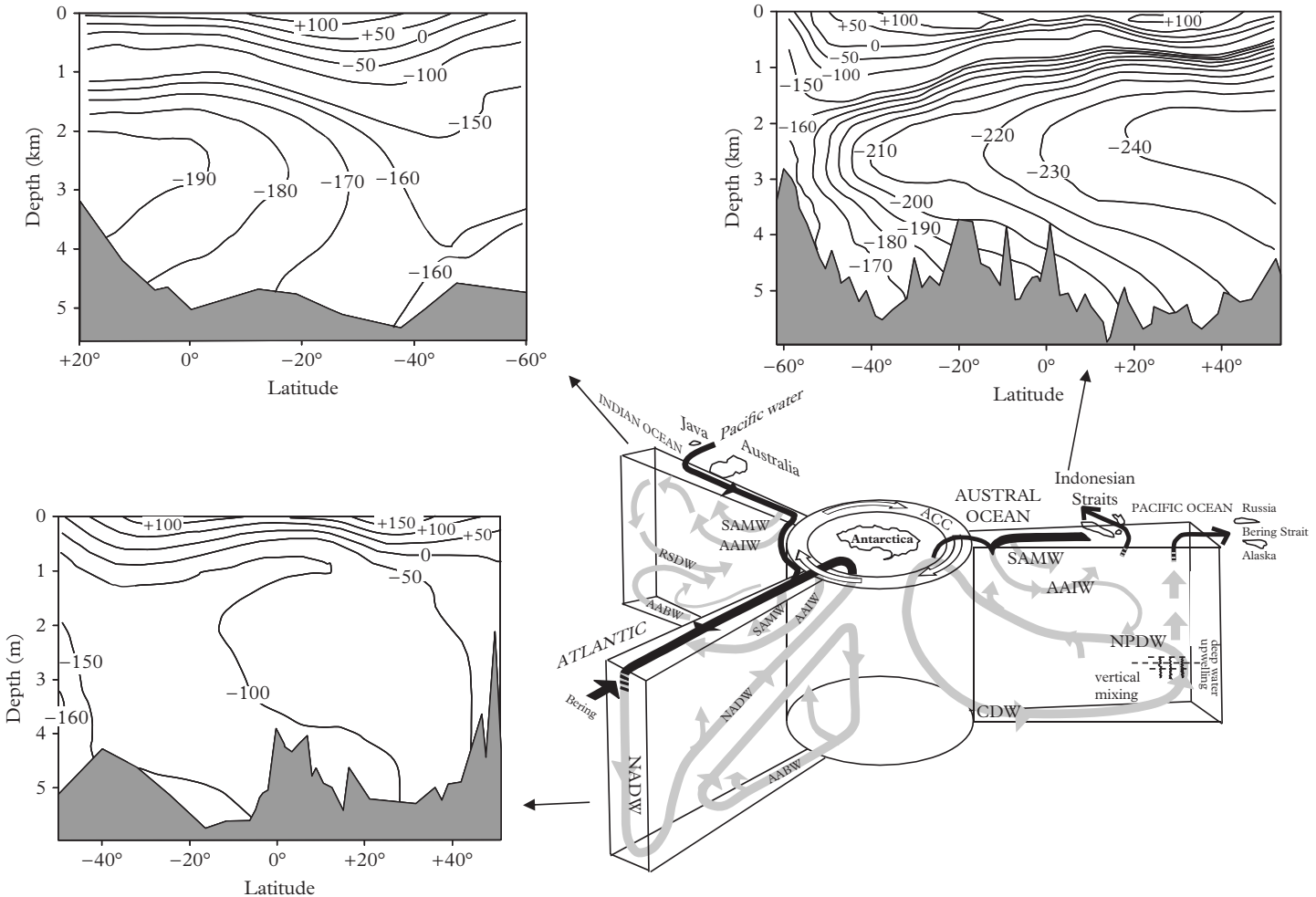

Figure 10.2 *Three-dimensional views of the thermohaline circulation and $\Delta^{14}C$ on meridian sections of Atlantic, Indian and Pacific oceans. Modified from Schmitz (1995).*

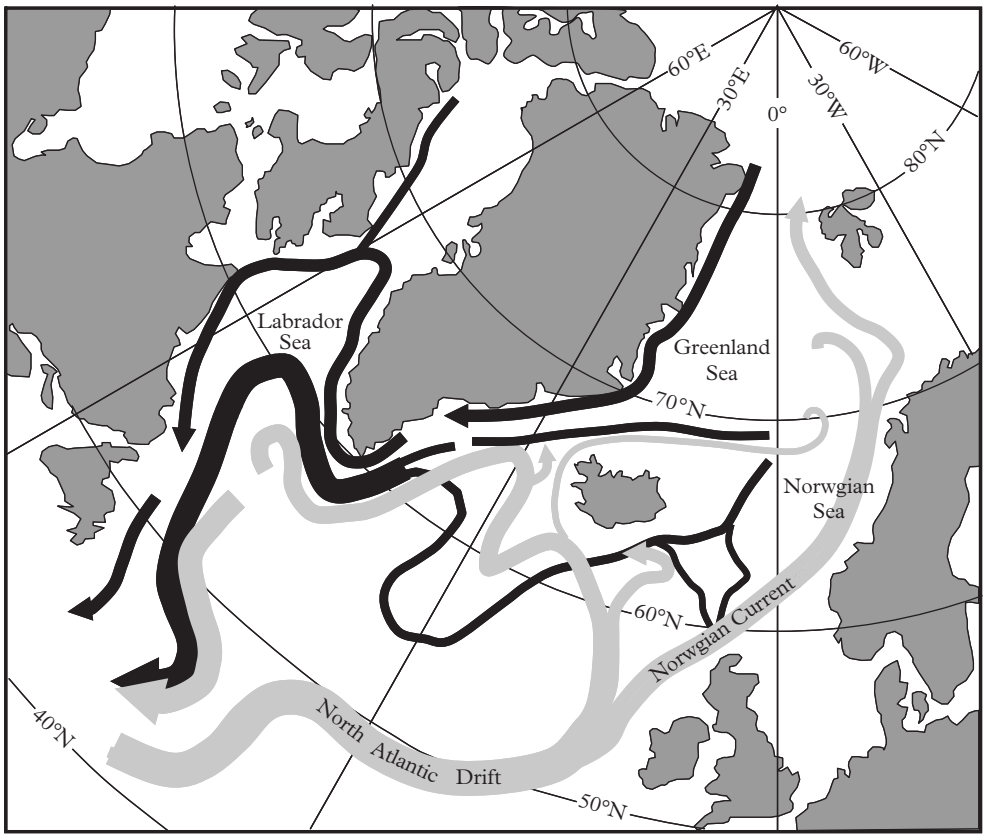

Figure 10.3 *Main currents and deep water formation areas in the North Atlantic. Surface currents are shown in gray. Deep currents are represented in black. Modified from a figure of the Woods Hole Oceanographic Institution.*

Southern Ocean, mixing of NADW, AABW and AAIW produces a blend called the Circumpolar Deep Water (CDW, see Chapter 1). As CDW is transported around Antarctica by the Circumpolar Current, it receives the contribution of other deep waters from the Indian and Pacific areas. The Circumpolar Current blender is so efficient that CDW has the same $\Delta^{14}C$ (–160‰) in the three sectors of the Southern Ocean.

CDW invades the deep Indian and Pacific oceans. In these oceans, there is no formation of deep water equivalent to those of the NADW: tropical conditions in the northern Indian Ocean do not allow water cooling and North Pacific surface water cooling does not raise the density sufficiently for them to sink in the deep ocean because the North Pacific waters are less saline and thus less dense than Atlantic waters. Figure 10.2 shows the gradual aging of the deep water to the north of the Indian and Pacific basins. The compilation of the GEOSECS and WOCE data collected in the Pacific Ocean provides

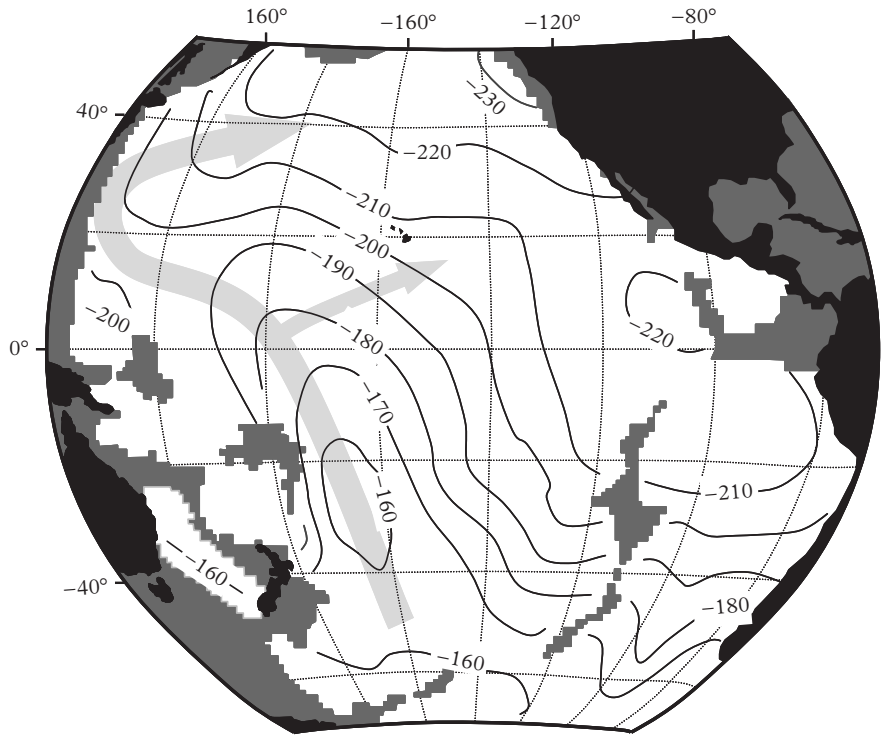

Figure 10.4 *Evolution of $\Delta^{14}C$ of bottom waters (depth >3500 m) in the Pacific Ocean. Water flows northward along the western edge of the basin. After crossing the Equator it turns eastward. Dark gray areas: oceanic landforms. Light gray arrows: possible trajectory of water. After Schlosser et al. (2001).*

a very detailed view of the deep circulation (Fig. 10.4). A tongue of CDW enters in the southwest of the basin and flows along the western edge of the basin. Water ages gradually as it moves northward. After passing the Equator, there is a change of direction toward the east of the basin. When it arrives in the North Pacific dead-end, deep water upwells slowly back to the surface. The oldest ocean waters are in the North Pacific at 2200 m deep: their $\Delta^{14}C = -240‰$ gives a reservoir age of 2250 y (see Chapter 5).

Exercise: The speed of the thermohaline circulation

We can use the evolution of $\Delta^{14}C$ in the deep waters to determine their average circulation speed (Fig. 10.5). The deep ocean has a volume $V_d = 3 \times 10^{18}$ m^3 and it is ventilated by a water flux F that we want to determine. The deep ocean is fueled in DIC by the sinking of surface water ($DIC_{surf} = 2000\,\mu M$) and the remineralization of particulate organic carbon. These two sources of deep DIC are

characterized by the same $^{14}C/^{12}C$ isotopic ratio $R_{surf} = 0.93\,R_{atm}$, where R_{atm} is the pre-bomb $^{14}C/^{12}C$ ratio of the atmosphere. Deep waters are isolated from the atmosphere for a time $\tau_w = V_d/F = 1/k_w$. They are characterized by a concentration $DIC_{deep} = 2300\,\mu M$ and an isotopic ratio $R_{deep} = 0.83\,R_{atm}$. The deep DIC leaves the deep ocean when waters upwell toward the surface: there is no sink term ($k_d = 0$) because in the deep ocean there is no photosynthesis. The loss of particulate carbon by sedimentation is not taken into account as we consider only a DIC balance here.

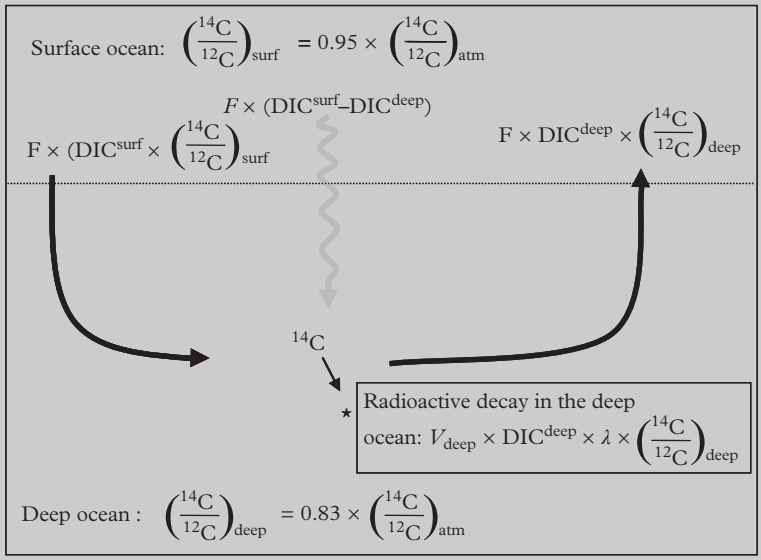

Figure 10.5 *Evaluation of the water residence time in the deep ocean. After Broecker and Peng (1982).*

Answer:
From equations (5.19) and (5.21) in Chapter 5 (see Fig. 10.5), we obtain

$$\begin{cases} k_w = \dfrac{\lambda}{\frac{R_{surf}}{R_{deep}} - 1}, \\ s = \dfrac{\lambda}{\frac{R_{surf}}{R_{deep}} - 1} \left(DIC_{surf} - DIC_{deep}\right). \end{cases} \tag{10.1}$$

It follows that $k_w = 0.00101\ y^{-1}$ and $s = 0.3\ \mu mol\ kg^{-1}\ y^{-1}$.

Hence it follows that:

- The average residence time of water in the deep ocean is $\tau_w = 1/k_w = 990$ y.
- The POC flux to the deep ocean is $s \times V_d = 11$ Gt y^{-1}.
- The DIC flux to the ocean deep is $k_w \times V_d \times DIC_{surf} = 72$ Gt y^{-1}.

87% of the carbon is brought into the deep ocean by current and only 13% by remineralization of sinking particles.

Knowing that the volume the deep ocean is $V_d = 10^{18}$ m^3, we infer that the thermohaline circulation flux F is

$F = V_d/\tau = 30 \times 10^6$ m^3 s^{-1} = 30 Sv.

10.2 The Rapid Progression of Transient Tracers

The presence in the deep ocean of anthropogenic tracers emitted to the atmosphere since the 1950s indicates that some deep waters have been in contact with the atmosphere during the past decades. These tracers can be followed as dyes injected on a large scale in the ocean or in smaller basins such as the Mediterranean Sea. They allow dating of the ventilation of deep waters, that is, the renewal of these waters by inflow of water that were recently in contact with the atmosphere. It is called ventilation because these inflowing surface waters are rich in dissolved oxygen (Problem 1). These tracers mainly include chlorofluorocarbons (CFCs) and tritium (^{3}H, see Chapter 4).

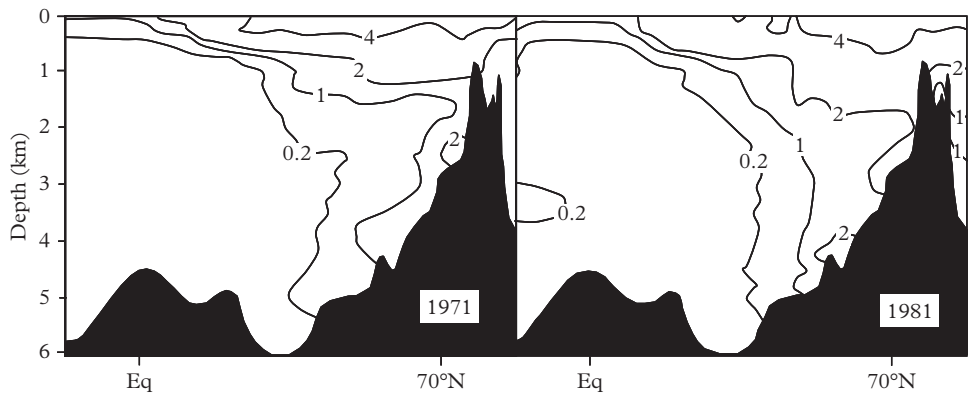

Figure 10.6 *Tritium measured on the same North Atlantic section in 1971 and 1981. Concentrations in TU units and corrected for the radioactive decay of tritium. Adapted from Östlund and Rooth (1990).*

In deep waters, the concentration of natural ^{3}H is so low that it is possible to follow the formation and circulation of deep water with the progression of anthropogenic ^{3}H. A section of the Atlantic gives a snapshot of the ^{3}H inflow in the deep ocean from the north along the seafloor, while in the equatorial and subtropical area, ^{3}H remains in surface waters (Fig. 10.6). The same section repeated 10 y later shows that the ^{3}H penetration has continued, but that the deep tropical Atlantic remains ^{3}H free. There is however a ^{3}H-rich water blob popping up at 3500 m depth in the equatorial zone (see below for explanation).

However, this section is not representative of the whole North Atlantic. East–west sections show that ^{3}H and CFCs flow preferentially along the western edge of the Atlantic: the deep waters are pushed southward and they are maintained against the continental slope by the Coriolis force gradient. Therefore, most of the ^{3}H and CFC transport occurs through a vein about 200 km wide. This confirms the occurrence of the deep western boundary currents predicted by Stommel and Aaron (see Section 10.2.1)

10.2.1 Deep Current Dynamics

We now apply equations (1.3a) and (1.3b) seen in Chapter 1 to the deep circulation. We assume that we are away from the coasts and from the ocean's surface, so that we can neglect the lateral frictions on margins and the wind stress. The equations of motion reduce then to the geostrophic balance

$$\begin{cases} -fv = -\dfrac{1}{\rho}\dfrac{\partial P}{\partial x}, \\ fu = -\dfrac{1}{\rho}\dfrac{\partial P}{\partial y}. \end{cases} \tag{10.2}$$

As in the case of the Sverdrup balance, we take the derivative of the first equation with respect to y and of the second with respect to x

$$\begin{cases} -\dfrac{\partial f}{\partial y} v - f\dfrac{\partial v}{\partial y} = -\dfrac{1}{\rho}\dfrac{\partial^2 P}{\partial x\,\partial y}, \\ f\dfrac{\partial u}{\partial x} = -\dfrac{1}{\rho}\dfrac{\partial^2 P}{\partial x\,\partial y}. \end{cases} \tag{10.3}$$

By subtracting the first equation from the second, we obtain

$$\frac{\partial f}{\partial y} v + \left(\frac{\partial u}{\partial x} + \frac{\partial v}{\partial y}\right) f = 0, \tag{10.4}$$

so that

$$\frac{\partial f}{\partial y} v = -\left(\frac{\partial u}{\partial x} + \frac{\partial v}{\partial y}\right) f. \tag{10.5}$$

Using the continuity equation, $\frac{\partial u}{\partial x} + \frac{\partial v}{\partial y} + \frac{\partial w}{\partial z} = 0$,
we obtain

$$\beta v = f \frac{\partial w}{\partial z}. \tag{10.6}$$

$$v = \frac{2\Omega \sin\varphi}{\frac{2\Omega\cos\varphi}{R_E}} \frac{\partial w}{\partial z} \qquad \varphi \text{ is the latitude}$$

$$= R_E \tan\varphi \frac{\partial w}{\partial z}. \tag{10.7}$$

If the seafloor is flat, the vertical speed (w_{sf}) must be zero at the seafloor level. We note w_{bt}, the vertical velocity at the base of the thermocline, and H, the thickness of the deep ocean (from the seafloor to the base of the thermocline). We can then write

$$\frac{\partial w}{\partial z} = \frac{w_{bt} - w_{sf}}{H} = \frac{w_{bt}}{H}, \tag{10.8}$$

where so that

$$\boxed{v = \frac{R_E \tan\varphi}{H} w_{bt}.} \tag{10.9}$$

Here we consider the simple case of a flat ocean in which deep circulation is controlled by a slow and homogeneous upwelling toward the base of the thermocline. Therefore, $w_{bt} > 0$ everywhere except in the areas of convection. A water column which stretches to the top ($w_{bt} > 0$ in equation 10.9) must move northward in the northern hemisphere and southward in the southern hemisphere. This is again the principle of the ice-skater who keeps his angular momentum constant (see Chapter 1). But if deep water upwelling implies a poleward advection, how can high latitude water masses spread toward the Equator? The previous calculation neglected friction because it was supposed to be away from the ocean boundaries. By contrast, along basin margins, deep waters can move toward the Equator and even cross the Equator. Deep water moving toward the Equator is deflected by the Coriolis force against the western boundary of the basin. Thus, Stommel et al. (1958) predicted the existence of intense deep currents on the western boundary of the ocean basins. In 1961, the first observation confirming this theory was published. In the center of the basin, speeds are slower and more difficult to measure (Problem 2). Like the surface circulation, the deep circulation has strong western boundary currents (see Chapter 1).

The analysis of CFCs has improved the picture of the deep western boundary current. CFCs were used as refrigerants between 1950 and 1995. During this period, their production increased more or less exponentially over a few decades (Fig. 10.7). These volatile molecules are transported in the atmosphere and then dissolved in the ocean. They are chemically inert and behave as passive tracers. The presence of CFCs in a water mass indicates that it has been in contact with the atmosphere less than 50–60 y ago.

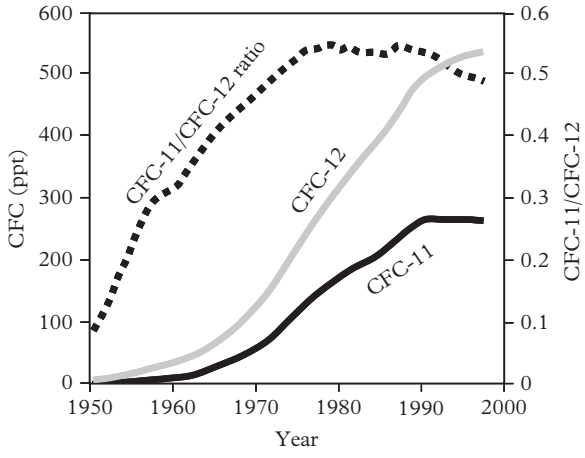

Figure 10.7 *Evolution of CFC-11 and CFC-12 concentrations and of the CFC-11/CFC-12 ratio in the atmosphere. Adapted from Beining and Roether (1996).*

The ratio between different CFC abundances can provide an estimate of the ventilation age (Problem 3).

Until the mid-1990s (Fig. 10.8), CFCs were found in the equatorial Atlantic in the lower NADW (which is produced by deep convection in the Greenland and Norwegian Seas) around 3500 m depth and the upper NADW (which finds its origin in the South

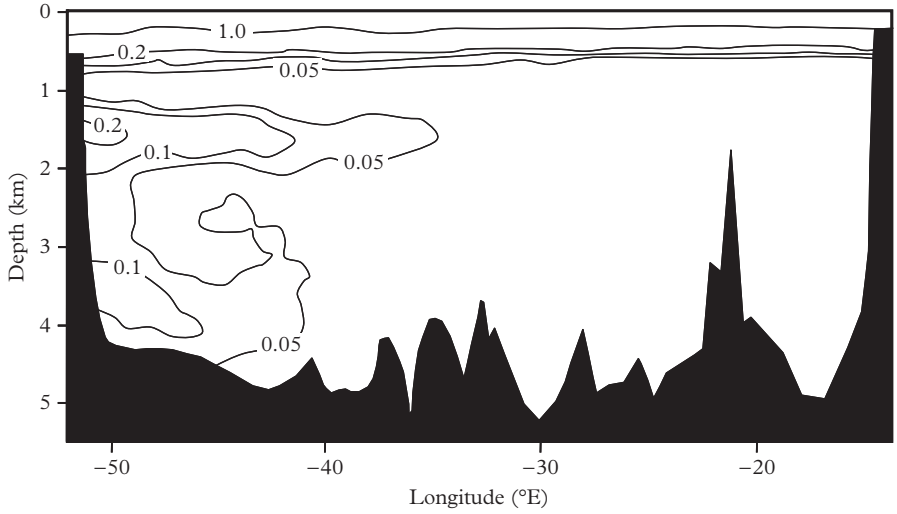

Figure 10.8 *Distribution of CFC-11 along an east–west section from the Atlantic at 10° N. CFC-11 concentration in pmol kg^{-1}. The surface waters in contact with the atmosphere are CFC rich. At depth, the upper NADW and lower NADW are marked by high CFC concentrations. The east of the basin is free of CFCs, because it has not been ventilated for at least 60 y. Adapted from Andrié (1998).*

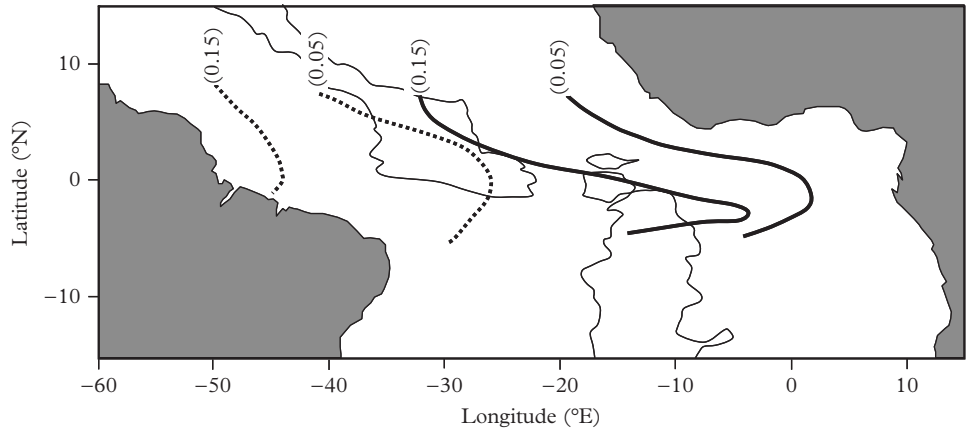

Figure 10.9 *Evolution of the CFC-11 concentration in the deep equatorial Atlantic. Concentrations are in pmol kg^{-1}. The campaigns conducted in 1983 (dotted lines) and 1993 (continuous lines) highlight the progress of the upper NADW (around 1500 m depth.) Because there is no Coriolis force at the Equator, the current is no longer maintained against the western boundary: therefore it extends to the east of the basin. Adapted from Andrié et al., 1998.*

of the Labrador Sea) located about 1500 m depth (Andrié et al., 2002). Between these two layers, the intermediate NADW is around 2500 m depth and it is produced by the deep convection in the Labrador Sea: it contained no CFCs, because, in the absence of deep convection over the previous 60 y, the Labrador Sea had not been ventilated deeply enough (Dickson, 1997). Since 1996, the arrival at the Equator of CFCs was observed in the intermediate NADW shortly after the resumption of the deep convection in the Labrador Sea (Freudenthal and Andrié, 2002). This increase of convection in the Labrador Sea and the simultaneous decline of convection in Greenland Sea are directly related to the decadal variations of the North Atlantic Oscillation (NAO).

Beyond their use as "dye," CFCs and ^{3}H are used to determine the rate of deep water formation over the past decades (Fig. 10.9). In Chapter 4, for example, we determined the flux of water passing the Iceland–Scotland Straits to produce part of the NADW. By extending this approach across the deep North Atlantic (including recirculation), a total flux of 17 Sv is obtained that takes into account water dragged by the deep current along its way. Thus, transient tracers are important tools to validate circulation models.

Application exercise: Evaluate the speed of the upper NADW

Answer: From Fig. 10.8, the "0.015 pmol kg^{-1}" concentration curve progresses by 28° eastward in 10 y. At the Equator, 1° of meridian corresponds to 110 km (40,000 km of Earth circumference corresponds to 360°). The speed is therefore of 308 km y^{-1} or 1 cm s^{-1}).

The speed of the western boundary current estimated from CFCs or ^{3}H is of the order of 1–2 cm s^{-1}. It is significantly less than average velocities of the order of 10 cm s^{-1} measured by **current meters** and the fleet of Argo drifting floats launched recently throughout the oceans (Gary et al., 2012). This difference is explained by the presence of **recirculation** loops that divert part of the western boundary current toward the interior of the basin and re-inject it upstream. The current meters measure the current increase caused by the recirculation. Anthropogenic tracers underestimate the speed of the water because recirculated water is not yet contaminated by ^{3}H and CFCs (effect of dilution of tracers by re-circulated water).

10.2.2 Intensity of the Recirculation

Recirculation represents water circulating in the deep ocean without having previously been involved in convection. Consider, for simplicity, a flat and rectangular ocean with its base at the Equator (a similar result is obtained if the curvature of the Earth is taken into account, as in Stommel and Arons, 1960). The east–west length is Δx, the north–south length is Δy and deep ocean thickness is H (Fig. 10.10). A source of deep water with an intensity S lies just north of the basin. We assume that w_{bt} is uniform throughout the basin. The vertical flux of water is $w_{\mathrm{bt}} \times \Delta x \times \Delta y$, and the horizontal northward flux is $v \times \Delta x \times H$. Noting that $\tan \varphi = \Delta y / R_E$, we can write equation (10.9) in the form

$$v = \frac{R_E \frac{\Delta y}{R_E}}{H} w_{bt}. \tag{10.10}$$

This yields

$$v \times \Delta x \times H = w_{\mathrm{bt}} \times \Delta x \times \Delta y. \tag{10.11}$$

The horizontal deep water flux to the North Atlantic is therefore equal to the upward water flux which goes back to the surface through the thermocline. When they reach the surface, these upwelled waters are then transported by currents (including the Gulf Stream) to high latitudes to feed the areas of deep water formation. As deep water upwells, it moves poleward (equation 10.9). To maintain potential vorticity, this poleward flux of deep water must be equal to the water flux upwelling through the thermocline (equation 10.11). This poleward flux of deep water then returns (dotted arrow on Fig. 10.10) in the deep western boundary current where it adds to the water flux produced by convection. Therefore, at high latitudes, the western boundary current is two times higher than the deep water flux strictly due to convection. This explains an important feature of the deep circulation: recirculation.

The limits of this model include the strong assumption of a uniform upwelling speed of the deep water over the whole basin (Problem 4). We already mentioned that vertical mixing through the thermocline is difficult (see Chapter 6). We will see in Section 10.6 that the Southern Ocean plays an important role in the deep upwelling.

CFCs and ^{3}H are not specific to a particular source of deep water in the North Atlantic. Conversely, ^{129}I marks specific convection areas. Indeed, ^{129}I is injected into

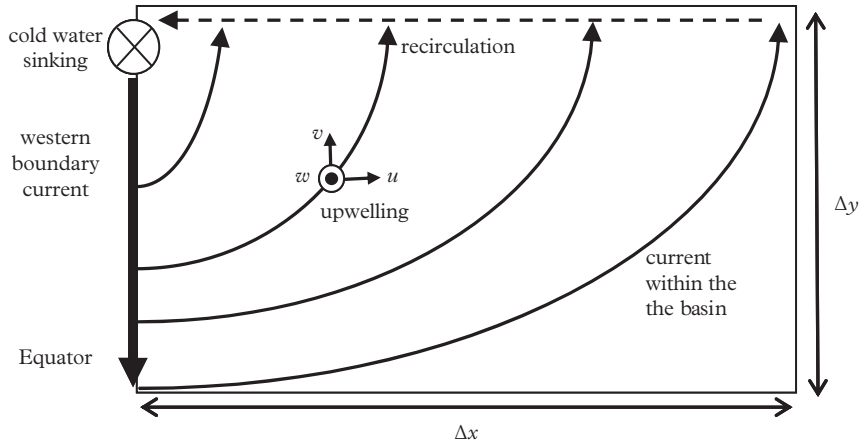

Figure 10.10 *Representation of the deep circulation in the Stommel–Arons model (view from top).*

the Atlantic by the nuclear waste reprocessing plants of Sellafield (UK) and La Hague (France), located along the coast of Wales for the first and north of the Cotentin Peninsula for the second: at the global ocean scale, they represent a point source of ^{129}I which is quickly advected in the North Sea. ^{129}I is then transported along the Norwegian coast and then, after passing the Fram Strait (located between Spitsbergen and Greenland), it enters the Arctic Ocean. After circulating around the Arctic, it returns to the Greenland and Norwegian Seas where it is transported at depth by convection. Then, ^{129}I passes the Iceland–Scotland and Denmark overflows to enter the Deep North Atlantic. ^{129}I is therefore a specific tracer of deep waters formed in the Greenland Sea and Norwegian Sea. The ^{129}I concentration is much lower in the deep waters formed in the Labrador Sea.

Transient tracers provide no information on the circulation in areas that have not been ventilated recently. In a longer term perspective, the ban of ^{3}H emissions combined with the short half-life of this isotope and the ban of CFC emissions will make these tracers more and more difficult to use in the coming decades. Natural tracers therefore have an important role to play in the study of the rapid ventilation of the ocean.

10.3 ^{14}C-Transient Tracer Comparison

The Δ^{14}C of the deep Atlantic waters varies between –70‰ in the North Atlantic and –170‰ in the South Atlantic (Fig. 10.11), which corresponds to an age difference of 930 y. This old age seems at odds with the presence in some of these old waters of CFCs which reflect ventilation less than 60 y old.

In fact, this variation of Δ^{14}C does not only reflect the effect of the radioactive decay in the Atlantic. It is first and foremost the result of the mixing of waters having different Δ^{14}C: NADW (Δ^{14}C = –70‰) and AABW (Δ^{14}C = from 160 to –170‰).

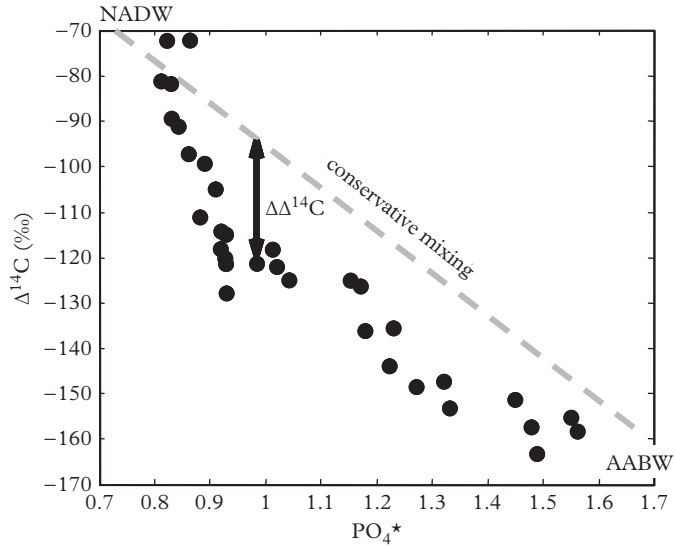

Figure 10.11 *Variation of $\Delta^{14}C$ versus PO_4^* for samples from the deep Atlantic Ocean. The dashed line represents the conservative mixing between NADW and AABW without aging effect. The dots represent the data. The vertical offset ($\Delta\Delta^{14}C$) between the conservative mixing line and the measured data is due to aging. After Broecker et al. (1991).*

Note that this mixing affects other nutrients and isotopic tracers (Problem 5). To decipher between aging and mixing effects, we must estimate the proportions of NADW and AABW present in a sample of deep water. The mixing proportions of water masses are usually identified by θ and S. However, the range of θ and S in the NADW and AABW are quite variable, resulting in significant uncertainties on the mixing proportions. The NADW and the AABW are well identified on the basis of the tracer PO_4^* ($PO_4^* = PO_4^{3-} + O_2/175 - 1.95$ μmol kg^{-1}; $PO_4^* = 0.73 \pm 0.03$ μmol kg^{-1} in the NADW, $PO_4^* = 1.63 \pm 0.03$ μmol kg^{-1} in the AABW; Broecker et al., 1991). $\Delta^{14}C$ is a conservative tracer if water mass mixing is very fast compared to its radioactive decay. If it was the case, we should observe a linear correlation (the mixing hyperbola—see Section 3.10—is almost a straight line, because the DIC concentration hardly changes between the different water masses) between $\Delta^{14}C$ and PO_4^* (Fig. 10.11). However, this is not the case: there is a variable vertical offset ($\Delta\Delta^{14}C$) between the data and the theoretical straight line. $\Delta\Delta^{14}C$ reflects the aging of water during mixing. The average time spent to achieve water mass mixing (circulation age) is: $t_{circ} = 1/\lambda \ln(1 - \Delta\Delta^{14}C)$.

The distribution of t_{circ} (Fig. 10.12) differs significantly from the distribution of the conventional ^{14}C ages (Fig. 10.1). While conventional ages increase steadily from the North Atlantic to the North Pacific, t_{circ} is minimal in the North Atlantic and the Weddell Sea, which clearly highlights the role of these two areas as deep water sources. We find

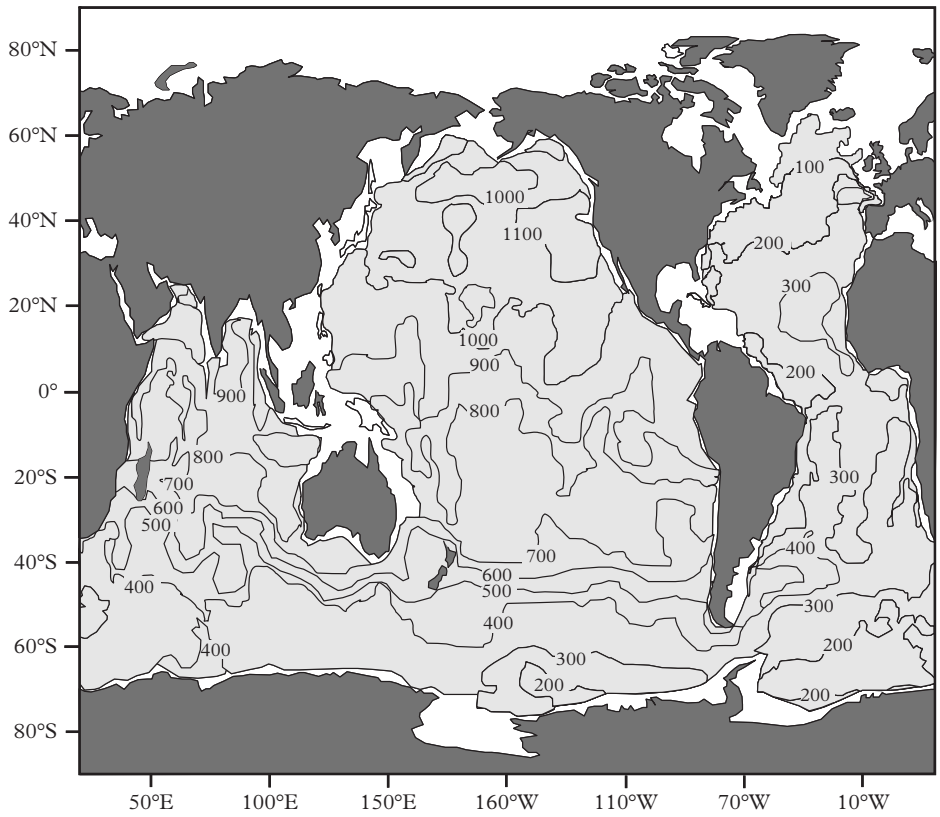

Figure 10.12 *Circulation age (in years) of the deep waters (z > 1500 m). Adapted from Matsumoto (2007).*

again an impact of circulation of western boundary currents already highlighted by the transient tracers: as it moves southward, NADW is maintained on the western edge of the Atlantic basin by the Coriolis force. Similarly, AABW is also diverted to the West as it flows northward (the Coriolis force deviates to the left in the southern hemisphere). So, water moves quickly along the western boundaries in narrow veins. The ventilation is much slower eastward: it takes approximately 300 y for the water to spread completely in the eastern basin. In the Pacific Ocean, CDW takes about 1000 y to reach the North Pacific from the Southern Ocean along the western boundary of the basin.

The circulation ages calculated on the western boundary of the Atlantic basin are still longer than those obtained based on recent injections of CFCs. In fact there is no contradiction. About 100–200 y are needed to renew *all* the water to the west of the basin while the presence of CFC indicates just that *part* of the water in the basin has recently been in contact with the atmosphere. Natural ^{14}C integrates information on long time scales whereas tritium and CFCs show transient phenomena (Problem 6).

10.4 The Contribution of ^{231}Pa–^{230}Th

In the recent years, the use of ^{230}Th and ^{231}Pa as tracers of the deep circulation has emerged. These two isotopes are produced in the ocean by decay of uranium and eliminated by scavenging on marine particles (see Chapter 4). When ^{230}Th and ^{231}Pa transport is dominated by marine particles, there is a balance between production and particle transport and their concentrations increase linearly with depth (see Chapter 9). If the transport by currents is significant, this balance is disrupted and the profiles are no longer linear (Fig. 10.13). During the NADW formation, ^{230}Th- and ^{231}Pa-poor surface waters sink to depth and then move southward along the North America continental slope. During this trip, these waters are slowly enriched in ^{230}Th and ^{231}Pa by the decay of uranium isotopes. This progressive return of Pa and Th toward the production/scavenging equilibrium allows estimation of the age of the water masses. As ^{230}Th and ^{231}Pa have different scavenging residence times (20–40 y for Th and 200–400 y for Pa), they allow study of different timescales. The phenomenon is more marked for ^{231}Pa, which is 10 times more soluble than ^{230}Th. Hence, currents take over more easily than particle transport, producing widespread "nonlinear" ^{231}Pa profiles.

To interpret Pa and Th depth profiles simply, we consider the model of vertical transport by particles in the water column (see Chapter 9) and we assume that, in addition, the water is renewed by a horizontal current which brings ^{230}Th and ^{231}Pa from outside and that carries away some of the ^{230}Th and the ^{231}Pa of the water column. We use the reversible scavenging model (equations 9.7 and 9.9) to which we add a term for water renewal: $1\tau_w \times (C_i - C)$ (see Chapter 4). The conservation equation is

$$-\frac{2h}{\tau_s} \times \frac{dC}{dz} + \frac{1}{\tau_w}(C_i - C) + \Gamma = 0, \tag{10.12}$$

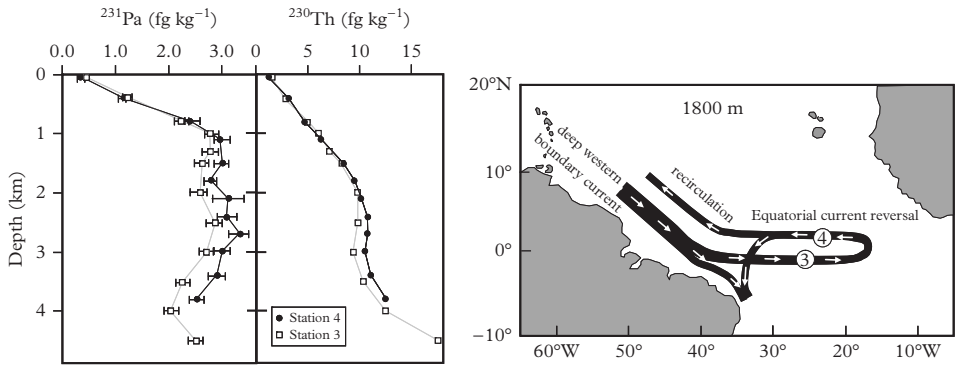

Figure 10.13 *Evolution of ^{231}Pa and ^{230}Th along the recirculation loop of the deep Equatorial Atlantic Current. There is no production–scavenging equilibrium below 1000 m deep for Pa and 2000 m deep for Th, reflecting the longer residence time of Pa. Evolution toward the equilibrium between the two stations allows estimation of the circulation time of the water masses. After Choi et al. (2001).*

where Γ, h, τ_s and τ_w are respectively, the radionuclide production, the height of the water column, the residence time of the element with respect to scavenging on particles and the water residence time. Assuming steady state, equation (10.12) is integrated to give (see the appendix to Chapter 4 for solution of the equation)

$$C(z) = (C_i - \Gamma\tau_w) \times \left[1 - e^{\left(-\frac{2\tau_s}{\tau_w} \times \frac{z}{h}\right)}\right]. \tag{10.13}$$

Equation (10.13) indicates that ^{230}Th and ^{231}Pa concentrations in surface waters increase linearly with depth because particulate transport outweighs advection (particulate transport is proportional to the vertical concentration gradient, which is not zero because the concentration increases with depth, whereas advection is proportional to the concentration which is very low in the surface waters). At depth, ^{230}Th and ^{231}Pa concentrations increase due to the reversible scavenging, so that the removal of ^{230}Th and ^{231}Pa by advection becomes significant. As the effect of advection increases, ^{230}Th and ^{231}Pa concentrations become constant: ^{230}Th and ^{231}Pa are advected so rapidly that they do not have time to accumulate in the water column and their concentration profiles become constant with depth.

Application exercise: Circulation of the NADW at the Equator

Consider Fig. 10.13. Knowing that the production rates of ^{230}Th and ^{231}Pa are $\Gamma_{230} = 0.56$ and $\Gamma_{231} = 0.025$ fg kg^{-1} y^{-1}, respectively,

(a) from equation (10.3), derive the expression of $C(z)$ in the deep ocean when $\tau_s \gg \tau_w$;
(b) estimate the time necessary for the NADW to flow from station 3 to station 4 at ≈3000 m deep.

Answers:

(a) If $\tau_s \gg \tau_w$, then, at depth

$$-\frac{2\tau_s}{\tau_w} \times \frac{z}{h} \to -\infty \text{ and } e^{\left(-\frac{2\tau_s}{\tau_w} \times \frac{z}{h}\right)} \to 0. \tag{10.14}$$

It follows that

$$C(z) \approx (C_i + \Gamma_{231} \times \tau_w). \tag{10.15}$$

This value is indeed independent of depth.

(b) The concentration of ^{231}Pa is constant at each station between 2000 and 4000 m, which suggests that the effect of the particle transport is negligible

over this depth range. If so, ^{231}Pa increases by *in situ* radioactive decay of ^{235}U and we have an age difference

$$\Delta t = ([^{231}\text{Pa}]_{\text{station 4}} - [^{231}\text{Pa}]_{\text{station 3}})/\Gamma_{231} \approx 0.4/0.025 = 16\,\text{y}.$$

^{230}Th profiles being dominated by particulate transport (mostly linear increase of concentrations with depth), it is risky to use it to calculate a circulation age.

Hence, part of the ^{230}Th and ^{231}Pa produced in areas of low particulate flux can be transported laterally and scavenged from the water column in areas of high sedimentation rate, such as continental margins and oceanic front zones where biological productivity is very high (Fig. 10.14). The chemical composition of marine particles controls the distinct behavior of Pa and Th: Th has a very high affinity for marine particulates in general, while Pa has specifically a high affinity for biogenic silica.

In the Atlantic, ^{230}Th is removed by marine particles mainly "on-site," while almost half of the ^{231}Pa produced in the North Atlantic is transported by the thermohaline circulation in the South Atlantic where it is eliminated from the water column in the

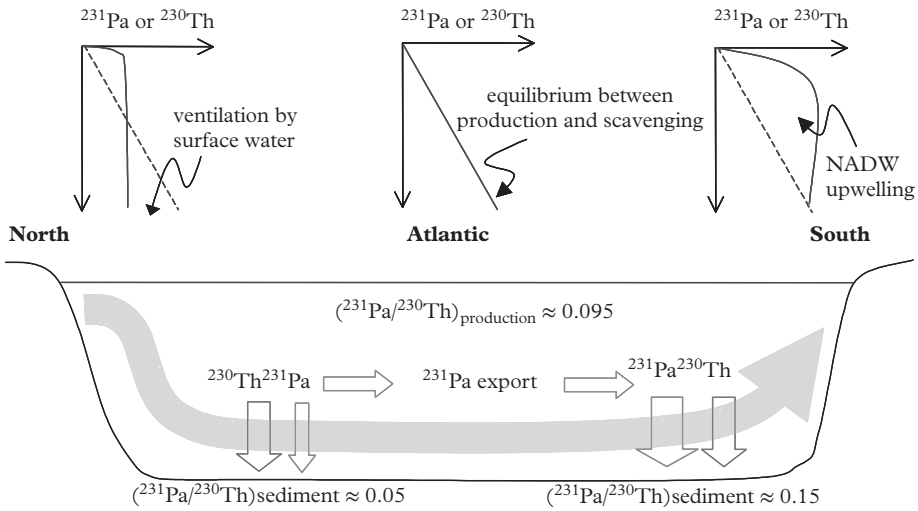

Figure 10.14 *Behavior of ^{230}Th and ^{231}Pa in the Atlantic Ocean. The shape of the ^{230}Th and ^{231}Pa profiles depends on the intensity of ventilation and upwelling of deep water. Today, about 50% of the ^{231}Pa produced in the North Atlantic is exported to the south by the NADW, while only 10% of the ^{230}Th is exported, which explains why the ^{231}Pa/^{230}Th ratios in sediments are different from the production rate ratio. Modified from François et al. (2004).*

polar front zone where there is a high production of diatoms with siliceous tests that have a strong affinity for ^{231}Pa. There is, therefore, a fractionation between ^{231}Pa and ^{230}Th in sediments associated with the competition between the transport by particle transport and by currents (Fig. 10.14). We will see in Chapter 11 that this differential transport of ^{231}Pa compared to ^{230}Th opens opportunities to reconstruct deep paleocirculations.

10.5 The Origin of the AABW

How is the AABW formed? At what rate? Why is it colder than the NADW? The answers to these questions lie in the Weddell Sea along the coast of Antarctica.

In the Weddell Sea, very cold and dense waters are formed (Fig. 10.15): the Weddell Sea Deep Water (WSDW) and the Weddell Sea Bottom Water (WSBW). The origin of this water is controversial. Some propose that sea-ice formation on the western plateau of the Weddell Sea allows cooling and an increase of the salinity of surface waters. As this plateau is wide and shallow, the water is blocked and not able to sink immediately,

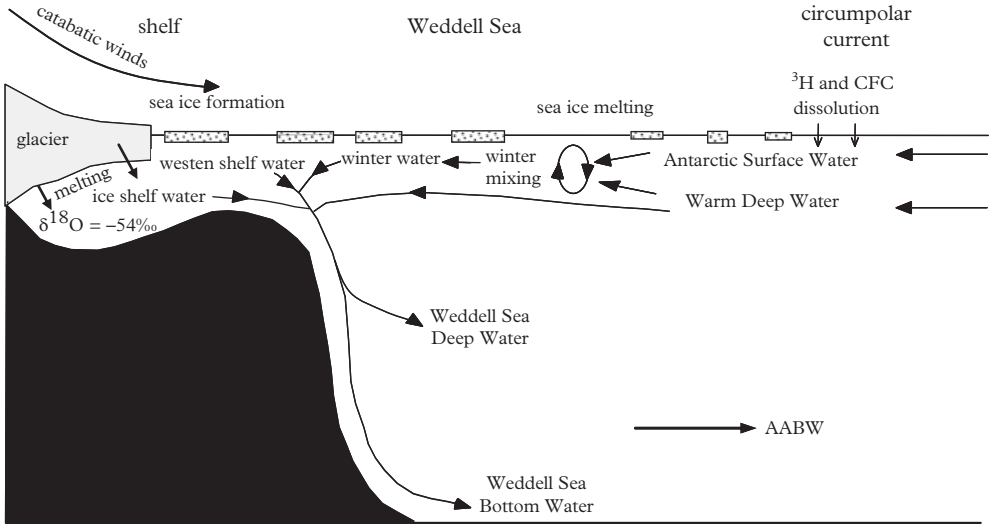

Figure 10.15 *Deep water formation in the Weddell Sea. The water penetrates into the Weddell Sea from the Antarctic Circumpolar Current: (1) the Antarctic Surface Water (AASW) has a low salinity due to sea-ice melting in summer ($S < 34.35$) and a variable temperature and (2) the Warm Deep Water (WDW, $\theta \sim +0.5°C$, everything is relative) which is found around 500 m deep and is a modified form of CDW. In winter, AASW is mixed with WDW and cooled to the freezing temperature of seawater (–1.84° C) to form Winter Water (WW). On the continental shelf, WW and WDW mix with Western Shelf Water (WSW). The WSW is more saline than the WDW due to sea-ice formation. Under the ice shelf, Ice Shelf Water (ISW) with a temperature ranging between –2.1 and –1.84° C (i.e., below the freezing temperature of seawater) reflects the input of Glacial Water (GW). Adapted from Wepperning et al. (1996)*

allowing it to store a large volume of water and to reach extreme densities. Under these circumstances, the water temperature should not be below –1.85°C, the equilibrium temperature between ice and seawater at atmospheric pressure.

In fact, the water on the Western shelf can reach temperatures lower than –2°C! These low temperatures are due to the melting of the ice shelf formed by the ice sheets flowing in the Weddell Sea (Fig. 10.16). This ice shelf sinks under its own weight in seawater. At the base of the ice shelf, the pressure induces a lowering of the equilibrium temperature between ice and seawater. In contact with the ice, seawater therefore reaches temperatures below –1.85°C. When this water is brought at the surface, it is supercooled (the ice shelf water). In addition, it has a low $\delta^{18}O$ inherited from the melting of ice shelf (the ice sheet has a very negative $\delta^{18}O$, because it is formed by snowfall over Antarctica, see Chapter 3). The respective contribution of the ice shelf melting and sea-ice formation can be determined from the $\delta^{18}O$ of seawater (Weiss et al., 1979).

The glacier is formed of fresh water like sea ice, but water from the glacier is highly depleted in ^{18}O compared to seawater and sea ice as it is formed from the snow that has fallen over Antarctica (Chapter 2). The very negative $\delta^{18}O$ of Glacial Water (GW) from the ice shelf imprints the Ice Shelf Water (ISW) and the Western Shelf Water (WSW). It reflects the contribution of atmospheric water and it allows an estimation that 0.3%

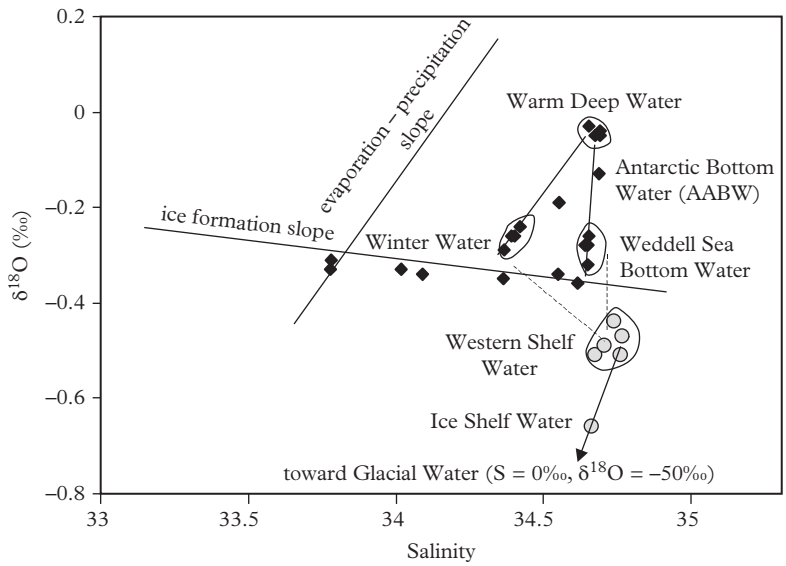

Figure 10.16 *Salinity–$\delta^{18}O$ diagram in the Weddell Sea. Black diamonds: samples with a temperature above –1.9°C. Gray rings: samples with a temperature below –1.9°C. Surface samples are plot on a straight line corresponding to sea ice formation and evaporation. The signature of the Western Plateau Water is marked by the addition of GW. After Weiss et al. (1979).*

of WSW is fresh water coming from glacier melting (see application exercise on the conservative mixing in Chapter 3).

The Weddel Sea Bottom Water (WSBW) is composed of 41% WSW, 40% Warm Deep Water (WDW, a modified form of the CDW) and 19% Winter Water. It fills the bottom of the Weddell Sea. Between the WSBW and the WDW, there is the typical AABW resulting from the mixing of the WSBW (64%) and the WDW (36%). This water leaves the Weddell Sea to spread on the bottom of the Atlantic seafloor, or take the Antarctic Circumpolar Current.

What is the rate of formation of AABW? A first estimate is based on the freshwater inputs related to the melting of the glacier. Indeed, the glacier advances regularly in the sea, providing 0.06 Sv of fresh water through the ice shelf water. These contributions must be balanced by the outflow of AABW, which contains 0.08% of GW (0.3% of GW in the WPW × 41% of WPW in the WSBW × 64% of WSBW in the AABW). This gives a flux of about 8 Sv of AABW.

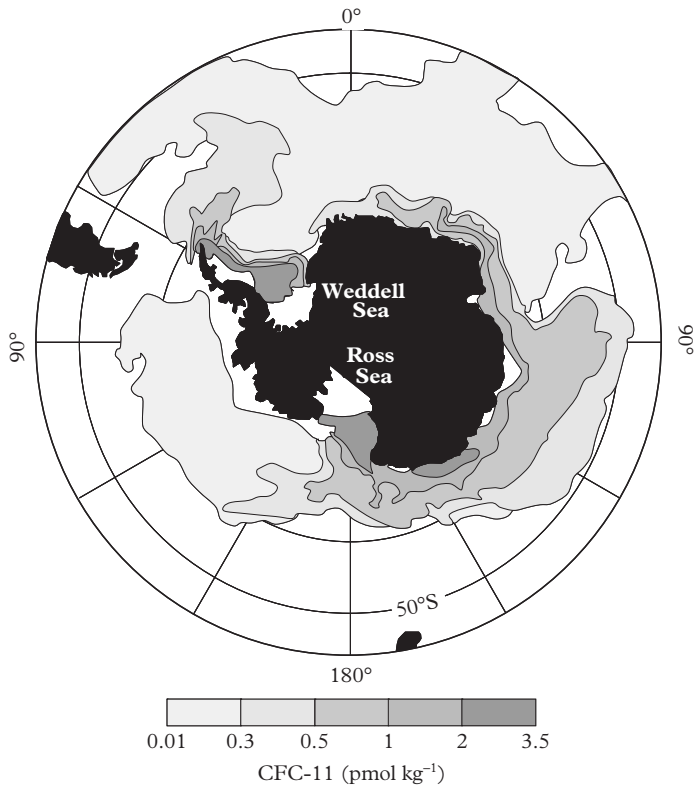

Figure 10.17 *CFCs in bottom waters around Antarctica. Concentration maxima mark of AABW formation areas. AABW flows along the Antarctica coast and eastward in the Circumpolar Current. After Orsi et al. (1999).*

This estimate concerns the deep water formation in the Weddell Sea only. An overview of the AABW formation around Antarctica is obtained with CFCs (Fig. 10.17): the Weddell Sea is not the only area of AABW formation: the Ross Sea and the Antarctic coast along the Bay of Enderby and the Terre Adélie also contribute to bottom waters (Orsi et al., 1999). In total, there are about 8–12 Sv of AABW formed around Antarctica.

10.6 Closure of the Meridional Overturning Circulation

The upwelling of dense deep water is made possible by the downward diffusion of lighter thermocline water. The average deep water upwelling velocity can be calculated with the ^{14}C model. Assuming that the deep water formation areas are restricted (Norwegian, Greenland and Labrador Seas in the northern hemisphere and Weddell and Ross Seas in the southern hemisphere) and that deep waters return to surface at the same speed over the whole ocean ($S = 3.6 \times 10^{14}$ m^2), we calculated the average upwelling velocity

$$w = F/S \sim 3 \text{ m y}^{-1}.$$

This speed is too low to be determined by direct physical measurements. By comparison, the average evaporation at the ocean surface is 1 m y^{-1} and Ekman pumping can be of the order of 10 m y^{-1}.

Taking $w = 3$ m y^{-1}, temperature and salinity profile modeling (Problem 4, Chapter 6) implies that $K_z \sim 1$ cm^2 s^{-1} in the deep ocean.

In fact, the upwelling rate is not the same everywhere. The local upwelling speed can be estimated from an advection–diffusion model calibrated by a vertical profile of ^{14}C, but this does not take into account horizontal aging of water masses. ^{228}Ra, which is produced in the sediment and which diffuses in deep water, was used to quantify eddy diffusion at the bottom of the ocean. However, despite its short half-life, there is an ambiguity between ^{228}Ra vertical diffusion from the sediment and ^{228}Ra lateral transport, because continental slope sediments are highly enriched in ^{232}Th (^{228}Ra parent isotope). Hopes are placed in ^{227}Ac, because his parent isotope (^{231}Pa) accumulates in deep sediments only (Problem 7). Unfortunately, its analysis is very difficult. Injections of artificial tracers show that vertical mixing increases strongly near rough topography due to the disturbances that it induces on the current flow and internal waves, in particular tidal waves (see Problem 4). The interplay between tidal waves and rough topography play a major role in vertical mixing (and hence the upwelling) of deep waters. Finally, methods combining measurements of the microstructures of the density gradient (see Chapter 6) and of the current speed allow K_z evaluation. It highlights the importance of vertical mixing in the Drake Passage, where the vertical diffusion coefficient can be from one to two orders of magnitude greater than the deep ocean average value (Fig. 10.18).

Compilation of density microstructure data suggests that the average diapycnal eddy diffusivity is of the order of 1 cm^2 s^{-1} below 1000 m in the deep ocean and of the order of 0.1 cm^2 s^{-1} above 1000 m in the thermocline (Waterhouse et al., 2014). So, deep

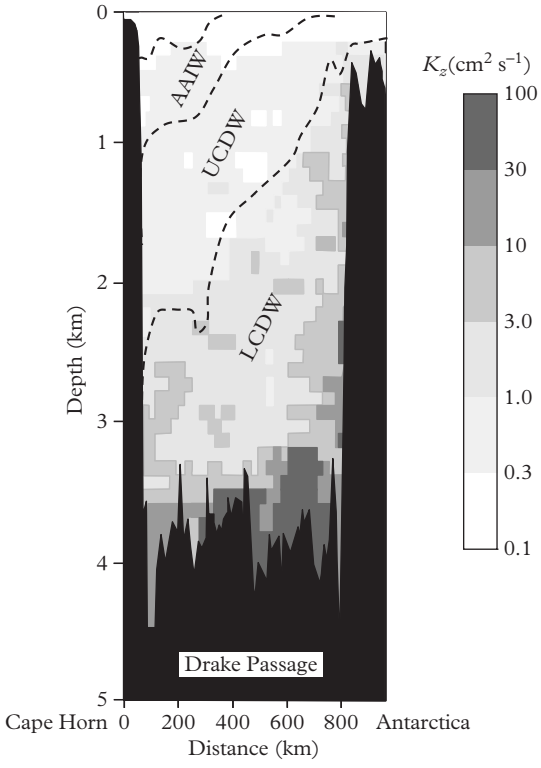

Figure 10.18 *Distribution of K_z in the Drake Passage. The topography and the strong horizontal current produce an intense mixing at the bottom and on the Antarctic slope. Modified from Naveira Garabato et al. (2004).*

water upwelling is possible and sufficient in the deep ocean, but the problem is to upwell the water through the thermocline where the diffusivity is 10 times too low! Remember that in Fig. 10.1, the oldest waters do not lay on the Pacific seafloor. Rather, they are stuck around 2000 m depth because they cannot make it through the thermocline and its low diffusivity. Upwelling through the thermocline is possible only in the Southern Ocean where steeply southward rising isopycnal surfaces connect the deep and the surface ocean (see Section 1.6 in Chapter 1).

Eventually, the formation of deep water in the Atlantic must be balanced by the upwelling and the return of the deep water arrived at the end of its trip in the deep Pacific dead-end. The exact route followed by these waters is still poorly understood. Three main routes have been proposed:

- the warm route, in which surface waters return to the South Atlantic through the Indonesian Straits and the Indian Ocean (Problem 8);
- the cold route, in which intermediate waters return through the Drake Passage. Data collected in the South Atlantic (see Chapter 4) show that around 870 m depth, intermediate water AAIW has an $\varepsilon_{Nd} = -6$ (Fig. 10.19). This ε_{Nd} is too high for surface or intermediate waters from the South Indian Ocean ($\varepsilon_{Nd} < -8$).

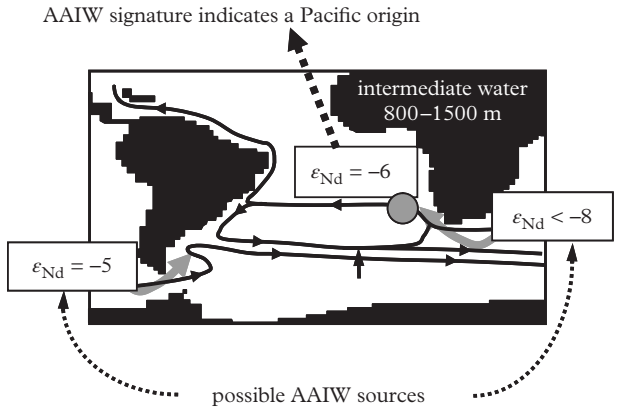

Figure 10.19 *Origin of the AAIW in South Atlantic witnessed by ε_{Nd}. Circulation models allow a Pacific or an Indian origin for the AAIW. The slightly negative ε_{Nd} of AAIW marks the presence of water of Pacific origin and suggests a return flow of the thermohaline circulation by the "cold route." After Jeandel (1993).*

It most likely reflects a Pacific origin of the water (the Pacific waters are overall more radiogenic than Indian waters, $\varepsilon_{Nd} \approx -5$). This ε_{Nd} corresponds to Pacific Water returning to the Atlantic through the cold route of the Drake Passage (Jeandel, 1993). This purely experimental result was later confirmed by numerical models.

- the "Tasman leakage" that passes south of Australia.

PROBLEMS

Problem 1: Deep water formation in Eastern Mediterranean Sea (Lascaratos et al., 1999)

There are several areas of deep water formation in the Mediterranean Sea (Fig. 10.20). In the Eastern Mediterranean Sea, deep waters are generally formed in the Adriatic Sea and intermediate waters in the Levantine Sea.

Hydrographic sections sampled in 1989 and 1995 in Eastern Mediterranean Sea show the changes of the properties of deep water masses (Fig. 10.21).

(a) Describe these changes and determine where the deep water formation took place to produce the 1989 and 1995 sections.

(b) Knowing that the 1988–1993 period has been extremely dry in the Mediterranean zone and that the 1992/1993 winter was particularly cold, suggest a scenario of deep water formation in 1995.

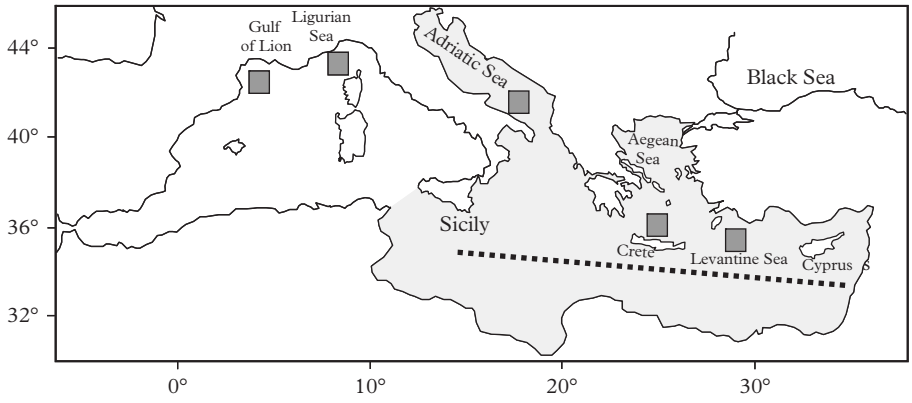

Figure 10.20 *Deep water formation areas in the Mediterranean Sea. Gray squares: possible areas of formation. Shaded area: Eastern Mediterranean Sea. Dotted line: hydrographic section.*

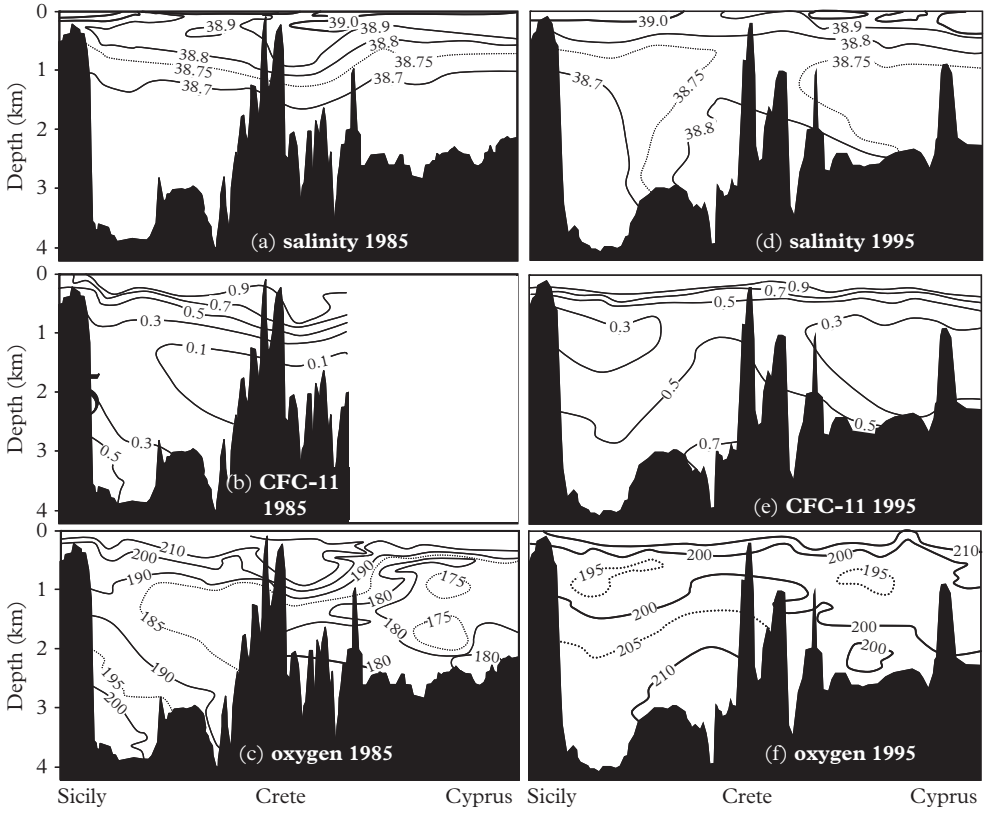

Figure 10.21 *Hydrographic sections of the Eastern Mediterranean: (a–c) 1985; (d–f) 1995. (a) and (d) Salinity; (b) and (e) CFC-11; (c) and (f) oxygen.*

Problem 2: The deep currents in the Brazil Basin (Hogg and Owens, 1999)

Buoys drifting at 2500 and 4000 m deep have been deployed in the Brazil Basin (South Atlantic, between Brazil and the mid-Atlantic ridge) for several years. At 2500 m deep, buoys dropped on the western boundary of the basin show a net southward motion. At 4000 m deep, buoys dropped on the western boundary of the basin show a net northward drift. Buoys dropped in the center of the basin (2500 or 4000 m) show zonal eastward or westward motions, but no meridian component.

(1) Which water masses flow along western boundary currents?
(2) Are the circulation highlighted by the buoys consistent the Stommel–Arons model?
(3) Using the results of Problem 4, propose an explanation for the difference between the Stommel–Arons model and the observed circulation.

Problem 3: CFC dissolution and water mass age (Smethie et al., 2002)

A sample collected in the deep Atlantic Ocean in 1990 has a CFC-11 concentration of 0.4×10^{-12} mol kg^{-1} and a CFC-12 concentration of 1.8×10^{-12} mol kg^{-1}. At the temperature of the sample, the solubility coefficients of CFC-11 and CFC-12 in seawater are $\alpha_{CFC11} = 20 \times 10^{-3}$ mol kg^{-1} atm^{-1} and $\alpha_{CFC12} = 49 \times 10^{-3}$ mol kg^{-1} atm^{-1}.

(1) Determine the partial pressures in CFC-11 and CFC-12 in the atmosphere in equilibrium with this sample. Compare the result with the evolution of the atmospheric concentrations (see Fig. 10.11).
(2) Determine the atmospheric CFC-11/CFC-12 ratio in equilibrium with this sample. When has the sample been in contact with the atmosphere for the last time?
(3) Explain the difference between the concentration-derived and the ratio-derived ages.

Problem 4: Vertical diffusion in the Brazil Basin (Ledwell et al., 2000)

Vertical (diapycnal) turbulent mixing is very important in the deep ocean, because it is the only mechanism that reduces the density of deep waters and thus that allows their upwelling. Turbulent mixing is estimated by injecting a SF_6 patch on a reference isopycnal surface around 4000 m depth in the Brazil Basin. Fourteen months after the injection, the dispersion of the tracer below and above the reference surface is measured:

- in the western part of basin which has a fairly flat seafloor located at 5000 m depth, most (95%) of the tracer is still within to ± 50 m around the reference surface;
- in the eastern part of the basin that has a rugged topography due to the presence of the mid-Atlantic ridge, most of the tracer (95%) is found up to 400 m above and below the reference surface.

(1) Determine the eddy diffusion coefficient in the eastern and western parts of the Brazil Basin.

(2) Discuss the impact of the topography on vertical mixing.

Problem 5: Nutrient origin in the deep ocean (Souza et al., 2012)

In the abyssal Atlantic Ocean ($z > 2000$ m), two water masses with distinct silicon signatures mix: NADW ($Si(OH)_4 < 20\,\mu M$ and $\delta^{30}Si = +1.7‰$) and AABW ($Si(OH)_4 = 120\,\mu M$ and $\delta^{30}Si = +1.2‰$).

(1) What is the origin of these distinct signatures?

(2) There is a tight linear correlation between $1/Si(OH)_4$ and the $\delta^{30}Si$ of seawater. What can you deduce from this correlation?

(3) By contrast, the nitrogen isotopic signature is constant throughout the abyssal Atlantic Ocean ($\delta^{15}N = +4.8‰$) despite a strong NO_3^- concentration gradient between NADW and AABW. Why?
Hint: Go back to Chapters 3 and 7.

Problem 6: Ventilation of the deep Arctic Ocean (Schlosser et al., 1997)

The Arctic Ocean has three major deep basins ($z > 2000$ m): the Nansen, Amundsen and Canada basins separated by oceanic ridges. In order to determine the water residence time in each of the basins, the $\Delta^{14}C$ of the dissolved inorganic carbon is measured in the deep waters of the three basins:

Nansen: $\Delta^{14}C = -85‰$
Amundsen: $\Delta^{14}C = -75‰$
Canada: $\Delta^{14}C = -106‰$
Assuming that prior to 1950, the Arctic surface waters had a $\Delta^{14}C$ of $-55‰$:

(1) Determine deep water residence time in the three basins.

(2) The waters of the deep Nansen and Canada basins contain no tritium while there is tritium in the deep Amundsen basin. Does it seem normal? Explain your reasoning.

Problem 7: The deep upwelling in the Pacific Ocean (Nozaki, 1984)

Actinium-227 (^{227}Ac) is used to determine the contribution of vertical eddy diffusion in the upwelling of deep water. ^{227}Ac is a radioactive isotope with a half-life of 21.8 y. It is produced by decay of ^{231}Pa. Considering the very low concentration of ^{231}Pa in seawater, it is assumed that most ^{227}Ac in seawater diffuses from the seafloor (deep sea sediments are enriched in ^{231}Pa). Measurements of ^{227}Ac on a vertical profile in the Pacific Ocean are given in Table 10.1.

Table 10.1 *^{227}Ac activity in the deep Pacific Ocean*

Depth (m)	**$\{^{227}Ac_{xs}\}$ (dpm m^{-3})**
4000	0.85
5000	1.2
6000	1.7

Note that $\{^{227}Ac_{xs}\}$ can be used in equations as a concentration.

(1) Assuming that ^{227}Ac is transported vertically by eddy diffusion only, write the differential equation describing the behavior of ^{227}Ac and use the data of Table 10.1 to determine K_z.

(2) Compare the vertical flux of ^{227}Ac generated by the turbulent diffusion with the advective flux produced by an upwelling speed of 3 m y^{-1}. Conclusion?

(3) In seawater, 99% of ^{227}Ac is dissolved and 1% of ^{227}Ac is scavenged on marine particles. Assuming that the average settling speed of these particles is 400 m y^{-1}, compare the particulate transport of ^{227}Ac to the vertical eddy diffusion transport. Conclusion?

Problem 8: The warm route (Jean-Baptiste et al., 2004b)

A fraction of the water carried in the Pacific Ocean by the thermohaline circulation returns to the Atlantic by the warm route in which warm Pacific water flows into the Indian Ocean through the Indonesian Straits. The sills of these straits reach 1500 m deep. The currents in these straits are highly variable leading to estimates ranging from 1.5 to 20 Sv. Tritium is used to obtain an average value of the warm route current.

In 1989, the average tritium concentration between surface and 1500 m depth was measured at the entrance (C_e = 0.662 TU) and at the exit (C_s = 0.466 TU) of the Indonesian Straits. It is estimated that the minimum concentration of tritium at the entrance of the Straits over time has evolved according to

$$C_e^t = e^{\lambda(1989-t)} \times \left(C_e^{1989} - \frac{C_e^{1989} - C_e^{1963}}{1989 - 1963} (1989 - t) \right),$$

with C_e^{1963} = 0 TU and C_e^{1989} = 0.663 TU. The first term on the right-hand side corrects the radioactive decay of the tritium and the second term represents the progressive arrival at the low latitude of waters which were enriched in tritium at high latitudes (there where it was deposited by precipitation) and which arrived through the thermocline.

(1) Neglecting tritium exchanges with the atmosphere, determine the transit time of the water in the Straits.

(2) Knowing that the Indonesian Straits cover an area of 2.2×10^6 km^2 at the level of the sea and 1.6×10^6 km^2 at 1500 m deep, determine the water flux that follows the warm route. The half-life of tritium is 12.4 y.

(3) The precipitation rate is $\rho_{\text{rain}} = 2000$ mm y^{-1}. The tritium concentration in precipitation (C_p) varied between 6 TU in 1973 and 2 TU in 1989. The evaporation rate is 1000 mm y^{-1}. Do exchanges with the atmosphere significantly affect the tritium budget in the Straits?

11

Ocean History and Climate Evolution

The ocean is a major and constantly evolving component of the Earth's **climate system**. To predict future climate changes, it is essential to reconstruct and understand past changes of the ocean behavior. Today's ocean is only one of the application fields of isotopic tracers. Isotopic tracers are also essential to reconstruct the history of the ocean. On one hand, radioactive isotopes provide the absolute chronology of geological events, which is the foundation on which the Earth's evolution study is built. On the other hand, stable and radiogenic isotopes record the environmental conditions prevailing during the formation of marine sediments. The message of the sediments is decrypted using relationships observed in the present ocean between the isotopic tracers and the oceanic parameters that we want to reconstruct. Tracers which allow these reconstructions are called **proxies**. As a tracer is generally sensitive to several environmental parameters, it is often essential to couple different tracers to deconvolute the effects of these parameters. The calibration of proxies is a very active field of marine geochemistry at the edge between the present and the past ocean. By combining information recorded in sediments with those recorded in the polar ice sheets (ice isotopes, air bubbles) and continental surfaces (pollen, tree rings, etc.), more or less accurate reconstructions of the evolution of the Earth's climate are obtained. A comprehensive ocean and climate history implies the ability to **date** precisely the various archives that are compared. Specific methods of sediment and sedimentary rock dating were presented in Chapter 9. In view of the diversity of the proxies, we present only a selection of results covering different aspects of the history of the ocean.

11.1 The Origin of the Ocean

The presence of water in the ocean seems so natural that no one imagines dry oceans. But has the ocean always existed? The solar system was formed by the collapse of a cloud of gas (mainly hydrogen and helium) and dusts on itself. The Sun has captured only 99.8% of the mass of this cloud. The remaining material formed a planetary disk whose chemical composition has rapidly evolved. Solar winds quickly pushed volatile elements (including water) toward the periphery of the disk, where they have formed the gaseous planets (Jupiter, Saturn, Uranus and Neptune). In the volatile-depleted central part of

Marine Geochemistry. First Edition. Matthieu Roy-Barman and Catherine Jeandel.

the disk, only mineral dusts remained. The accretion of these dusts led to the formation of small kilometer-size bodies whose agglomeration has produced the telluric planets (Mercury, Venus, Earth and Mars). If the terrestrial/Earth material was rather dry, how did water come back to Earth? The fall on Earth of comets (which are kilometer-size ice pieces rich in mineral dust) or of particular meteorites called carbonaceous chondrites (they are the most primitive material resulting from the agglomeration of the proto-solar nebula and they are rich in water) has been invoked. Hydrogen isotopes give a key argument. On Earth, water and hydrated minerals have a D/H ratio identical to the D/H ratio of carbonaceous chondrites and much lower than the D/H ratio of comets recently approached and visited by space probes (Fig. 11.1). This allows the conclusion that meteorites brought water to Earth. This meteoritic water was probably released as vapor due to the heat generated by the large meteor impacts that occurred during the formation of the Earth. This heat was such that the early Earth was probably covered by an ocean of . . . molten magma. There was no liquid water at the Earth's surface in these early days.

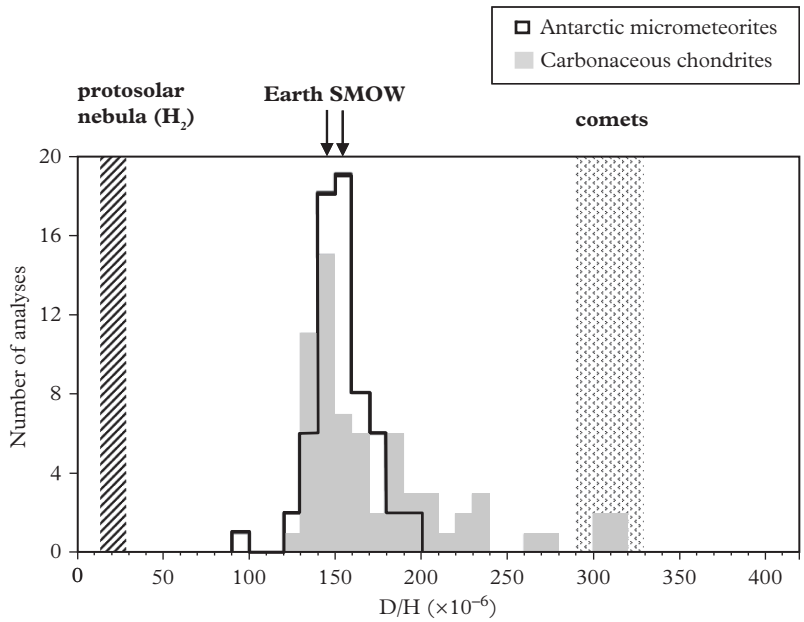

Figure 11.1 *Isotopic composition of hydrogen on Earth and in the solar system. The average isotopic composition of ocean water (SMOW) is similar to the Earth water as a whole. The average isotopic composition of the ocean is similar to the average isotopic compositions of carbonaceous chondrites and micrometeorites, highlighting their filiation. Comets have not contributed to the formation of the oceans. The water formed by the oxidation of hydrogen from the proto-solar nebula is not the main source of Earth's water. Modified after Robert (2001).*

In Greenland, 3.8 billion y old rocks formed by deposition of sediments in a marine environment prove the presence of an ocean 3.8 billion y ago. There is no direct evidence yet for an older ocean. However, isotopic analysis of zircons ($ZrSiO_4$, a mineral very resistant to weathering) suggests the presence of liquid water at the Earth surface before 3.8 billion y ago. Indeed, zircons crystallize from silicate magmas. They are so resistant that they can survive the destruction of their parent rock and be "inherited" in much younger rocks. Their great age is then betrayed by their dating, which is made possible due to their high uranium content. Zircons have been discovered that are 4.3–4.4 billion y old. The high $\delta^{18}O$ of some them indicates that they have crystallized from an ^{18}O-rich magma produced by melting of rocks that had been enriched in ^{18}O by interaction at low temperature with liquid water. Therefore, liquid water was probably present on Earth 150 million y after the formation of the Earth.

11.2 The First Traces of Life

The origin of life is closely linked to the presence of the ocean. The early Earth atmosphere was devoid of oxygen and ozone, so that the first living cells had to protect themselves from UV radiation in water. Although fossil records are abundant only since the beginning of the Paleozoic era (540 million y ago), we now know that life was present on Earth long before. The oldest known fossils (3.4 billion y) are stromatolites. Stromatolites are made of a superposition of submillimetric limestone sheets precipitated by the photosynthesis of bacterial films and they still exist today. Beyond 3.4 billion y, no fossil has been preserved, but it is, however, possible that life was already present. The oldest known sedimentary rocks (3.8 billion y) contain grains of graphite depleted in ^{13}C to ^{12}C and ^{12}C-rich carbonate. This isotopic fractionation between graphite and carbonate is similar to that seen today between organic carbon and biogenic carbonates. This has long been seen as a proof of the biological origin of this carbon (Mojzsis et al., 1996). However, recent experiments suggest that organic compounds formed abiotically in hydrothermal systems may have a $\delta^{13}C$ identical to that of the photosynthetic carbon.

11.3 The Rise of Oxygen

The appearance of life had considerable implications for the evolution of the Earth surface envelopes. The Earth's primitive atmosphere was probably rich in CO_2 and N_2 as are today those of Mars and Venus. The development of cyanobacteria producing O_2 by photosynthesis allowed the rise of O_2 in the atmosphere. Redox conditions in the ocean are closely related to the atmospheric O_2 content. Sulfur is an ideal tracer for these conditions because it has many oxidation degrees and S isotopes are fractionated during redox reactions. Today, in marine sediments, sulfate-reducing bacteria reduce

the sulfate ions dissolved in seawater to form sedimentary sulfides. These sulfides are strongly depleted in ^{34}S ($\delta^{34}S \approx -50‰$) compared to sulfate, due on one hand to the bacterial reduction ($\delta^{34}S \approx -15‰$) and on the other hand to the progressive reoxidation of sulfides ($\delta^{34}S \approx -35‰$), which is possible only with a sufficiently oxygenated seawater.

The isotopic compositions of marine sulfates and sulfides found in sedimentary rocks are used to reconstruct the evolution of the sulfur cycle in the ocean (Canfield, 1998). The $\delta^{34}S$ of dissolved sulfate is recorded by sulfate minerals (gypsum, anhydrite, barite) that precipitate quantitatively from seawater without fractionation in confined environments where intense evaporation raises salinity. The distribution of $\delta^{34}S$ in marine sulfides has evolved over the geological times (Fig 11.2):

(1) Prior to 2.2 billion y, the $\delta^{34}S$ of marine sulfide is similar the $\delta^{34}S$ of sulfate ions dissolved in seawater. This lack of fractionation implies that sulfate-reducing bacteria reduced all sulfate ions to sulfide because of the limited availability of sulfate in seawater (less than 0.2 mM compared to 28 mM today; Habitch et al., 2002). This implies a very low O_2 concentration in the ocean and the atmosphere (less than 1% of the current atmospheric content).

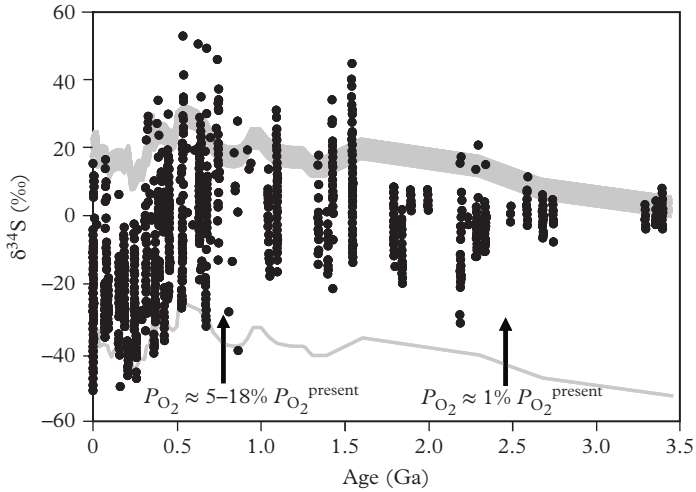

Figure 11.2 *Evolution of $\delta^{34}S$ in sedimentary sulfides over geologic times. The points correspond to marine sulfides. The upper gray band indicates the evolution of $\delta^{34}S$ of marine sulfate and the lower gray line simply represents the $\delta^{34}S$ of sulfide formed from marine sulfate with a fractionation of –50‰ (bacteria and reoxidation fractionation). Modified after Canfield (1998).*

(2) Between 2.2 billion y and 0.8 billion y, marine sulfides are depleted in ^{34}S with a range of $\delta^{34}S$ corresponding to the activity of sulfate-reducing bacteria not limited by the dissolved sulfate concentration but without sulfide reoxidation.

(3) Since 0.8 billion y, marine sulfides have a range of $\delta^{34}S$ equivalent to that of today's sediments. The O_2 content at the surface of the Earth has become sufficient (between 5 and 20% of the current atmospheric content) for the onset sulfide reoxidation.

A brilliant confirmation of these estimates was obtained with the isotopic signature that sulfur acquires in the atmosphere (Farquhar et al., 2007). Sulfur can undergo mass-independent isotopic fractionations during photochemical reactions in an oxygen- and ozone-free atmosphere (O_2 and O_3 inhibit these reactions by absorbing UV radiations). The isotopic analysis of marine sulfides and sulfates older than 2.2 billion y reveals that their sulfur had experienced mass-independent fractionations. This implies that before being incorporated in these minerals, sulfur had passed through an O_2-free and O_3-free atmosphere (Fig. 11.3). There is no more mass-independent fractionation in samples formed after 2.2 billion y due to the rise of O_2 and O_3 in the atmosphere. Difficulties related to the method are discussed in Problem 1.

The progressive oxygenation of the ocean, first in the surface waters and then in deep waters, had a considerable impact on the biosphere. First, oxygen is a poison for many

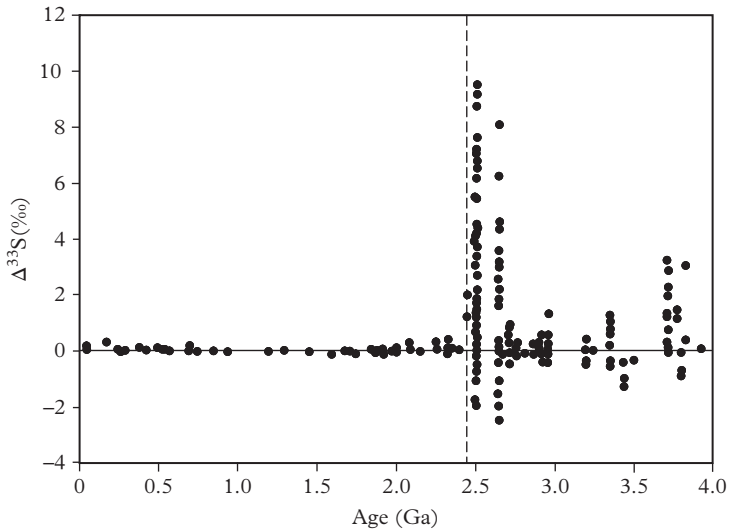

Figure 11.3 *Evolution of $\Delta^{33}S$ in sedimentary sulfides during the geologic times. Since 2.5 Ga, the increase of oxygen and ozone in the atmosphere prevents mass-independent fractionations. Modified from Farquhar et al. (2007).*

microbes. The ecological niches of anaerobic bacteria and archaebacteria were more and more reduced: they are now confined in reducing environments (anoxic sediments, cattle stomach, hydrothermal springs, etc.). Second, the oxygenation of the water has changed the availability of trace metals. Iron was present as soluble Fe^{2+} in the anoxic primitive ocean, but it became oxidized as very insoluble Fe^{3+} in oxic waters, resulting in an iron limitation of biological production. It is likely that the high-performance photon sensor system that allows *Prochlorococcus* to cope with Fe and N limitations (Chapter 7) dates from this time. Conversely, an element such as molybdenum (Mo), which was hardly available previously, became extremely soluble as oxyanions (Chapter 2). Today, Mo is involved in the protein that allows photosythetic algae to reduce NO_3^-. Ocean oxygenation thus triggered a faster development of eukaryotic phytoplankton (Problem 2).

11.4 Geological Sequestration of CO_2

The average temperature at the Earth's surface is highly dependent on the chemical composition of the atmosphere and the presence of greenhouse gases (see box "The natural greenhouse effect"). CO_2 was a major component of the Earth's primitive atmosphere and it played a key role in regulating the Earth's climate. 4.5 billion y ago, the Sun radiated 25% less energy than today. Without CO_2 and its strong greenhouse effect, the temperature at the Earth surface would have been below the freezing water temperature! Nevertheless, the occurrence of "Snowball Earth" periods during which the surface of the Earth would have been completely ice covered is well accepted today. For example, paleomagnetic and geologic data suggest that about 600 Ma ago, ice caps were present at the level of the sea in the equatorial zone.

The natural greenhouse effect

The Earth's surface is heated by solar radiation which consists mainly of visible light. The energy absorbed by the Earth's surface is re-emitted toward space as infrared radiation. In the absence of atmosphere, the average temperature at the Earth's surface would be to –18°C. The difference is related to the presence in the atmosphere of greenhouse gases such as H_2O (which is today the main greenhouse gas), CO_2, CH_4 and N_2O. These gases absorb infrared radiations and re-emit part of them toward the ground (Fig. 11.4). This recycling of energy maintains an average temperature of +15°C at the Earth's surface and makes it a habitable planet. It is a beneficial **natural greenhouse effect**. At the end of the chapter, we will describe the increase of the greenhouse gas concentrations related to human activities, resulting in an additional greenhouse effect which leads to a climate change.

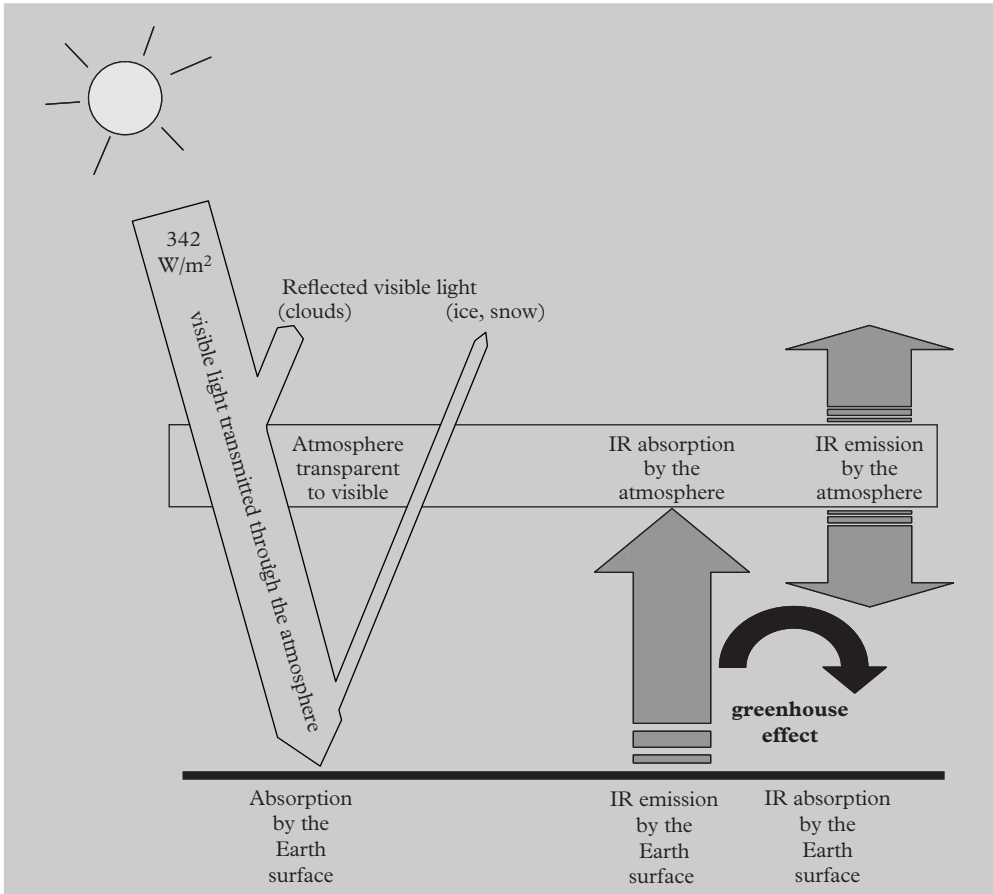

Figure 11.4 *Principle of the greenhouse effect.*

Little by little, the CO_2 has been trapped in limestones. This trapping involves the erosion of silicate rocks and the precipitation of $CaCO_3$. It can be summarized very simply:

(1) Weathering of volcanic rocks

$$\underset{\text{pyroxene}}{CaSiO_3} + \underset{\text{dissolved } CO_2}{CO_2} + \underset{\text{rain}}{H_2O} \rightarrow \underset{\text{dissolved species transported by the rivers}}{Ca^{2+} + HCO_3^- + HSiO_3^-}$$

(2) $CaCO_3$ precipitation in the ocean

$$Ca^{2+} + HCO_3^- + HSiO_3^- \rightarrow \underset{\text{solid}}{CaCO_3} + \underset{\text{solid}}{SiO_2} + H_2O.$$

Unlike the biological precipitation of $CaCO_3$ described in Chapter 8, which causes an increase in P_{CO_2}, here the $CaCO_3$ precipitation lowers P_{CO_2} and therefore facilitates the pumping of atmospheric CO_2 by the ocean. This is because the decrease of alkalinity related to Ca^{2+} consumption during $CaCO_3$ precipitation was preceded by an increase of alkalinity due to the release of dissolved Ca^{2+} by erosion.

Sequestration of CO_2 by erosion was not mentioned in Chapter 10 in the present carbon cycle because it is low on the short term (on the 100–1000 y timescale of the modern ocean). Instead, its long-term role is considerable as it balances the small but continuous degassing of CO_2 by volcanoes. Therefore, it controls the greenhouse effect on geological timescales. An increase in volcanism causes an increase of the atmospheric CO_2 content and of the greenhouse effect. This produces a warmer and more humid climate, promoting rock weathering. Finally, increased weathering of the igneous rocks causes a decrease of the atmospheric CO_2. Thus, on long timescales, the regulation of the greenhouse effect relies on the balance between the production of CO_2 by volcanism and its capture by the erosion and deposition as carbonates. The last "Snowball Earth" event on Earth is associated with to the fragmentation of the "Rodinia" supercontinent that produced high continental erosion 600 Ma ago (Donnadieu et al., 2004). When it is completely frozen, the Earth's surface reflects solar radiation very efficiently and it is very difficult to it warm up. The return to normal comes only after a very long period of volcanic CO_2 accumulation in the atmosphere that produces an intense greenhouse effect that triggers the thaw.

The marine Sr isotope composition brings constraints to the volcanism/erosion balance (see Chapter 4). Indeed, the Sr isotopic composition of seawater depends on the relative intensity of continental weathering which brings very radiogenic Sr (high $^{87}Sr/^{86}Sr$ ratio) and volcanism that brings non-radiogenic Sr (low $^{87}Sr/^{86}Sr$ ratio) via hydrothermal fluids. The evolution of the $^{87}Sr/^{86}Sr$ ratio over the last 540 million y illustrates some large variations in the Earth's climate (Fig. 11.5): the non-radiogenic Sr signature around 150 million y ago comes from the high hydrothermal inputs due to the strong seafloor spreading rate which occurred during this period. At that time, temperate climate plants and cold-blooded animals such as dinosaurs lived in Polar Regions which were devoid of ice caps. The average temperature at the Earth's surface was 14°C higher than today. The steady increase of the $^{87}Sr/^{86}Sr$ ratio during the last 40 million y is not due to a change of hydrothermal inputs because the seafloor spreading rate has remained stable during this period. It is attributed to the erosion of the Himalayas, formation of which began 40 million y ago by the collision between Tibet and Asia (the India–Tibet collision occurred 17 million y ago). During this period, there was a cooling of the climate that led to glaciations 6 million y ago. The resulting sea level variations have contributed to extreme conditions in the Mediterranean Sea (Problem 3).

Marine carbonates also provide information on the seawater temperature and the size of the polar caps with the oxygen isotopes. In particular, the opening of the Drake Passage 40 million y ago appears to be associated with the buildup of an ice cap over Antarctica following the isolation of Antarctica by the Antarctic Circumpolar Current.

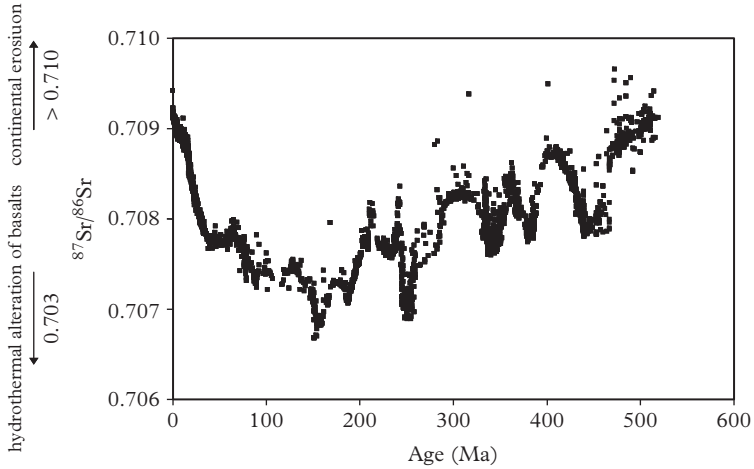

Figure 11.5 *Evolution of the isotopic composition of strontium in the Phanerozoic Ocean. The Phanerozoic times (0–543 Ma) are marked by the presence of abundant fossils in sedimentary rocks). The Sr residence time is much longer than the mixing time of the ocean, so that the $^{87}Sr/^{86}Sr$ ratio is uniform in the ocean and the analysis of a single marine fossil shell is sufficient to determine the $^{87}Sr/^{86}Sr$ ratio of the ocean at a given time. Modified after Veizer et al. (1999).*

11.5 The Closure of the Panama Isthmus

The erosion of the Himalayas and the Drake Passage opening alone cannot account for the appearance of glaciers in the northern hemisphere 6 million y ago and the cycles of glaciation which began around 3 million y ago. Continental drift and ocean circulation changes also had a major role. It was long suspected that the closure of the Panama Isthmus promoted a cooling of the climate by swerving to the Arctic seas the warm waters of the tropical Atlantic, which until then were transported into the Pacific by the trade winds. Nd isotopes allow clarification of the link between the isthmus closure and the establishment of glaciation in the northern hemisphere. Nd is highly enriched in the manganese crusts that grow at speeds of 1–15 mm My^{-1} in areas where there is no sedimentation. Each crust records the local ε_{Nd} of the deep water: unlike the $^{87}Sr/^{86}Sr$ ratio, the ε_{Nd} of seawater is heterogeneous in the ocean because the Nd residence time is much shorter than the mixing time of the ocean (see Chapter 4).

We compare the evolution of the ε_{Nd} in two Mn crusts sampled in the west of the Subtropical North Atlantic (Fig. 11.6). The end of the Pacific Intermediate Water inputs (marked by a radiogenic Nd, i.e., a high $^{143}Nd/^{144}Nd$ ratio) through the Panama seaway is marked by the decrease of the ε_{Nd} in the intermediate waters 5 million y ago. Since 3 million y, the intensification of the glaciations in the northern hemisphere (recorded by the $\delta^{18}O$ of foraminifera; see Section 11.6) accelerates the erosion of old shields which

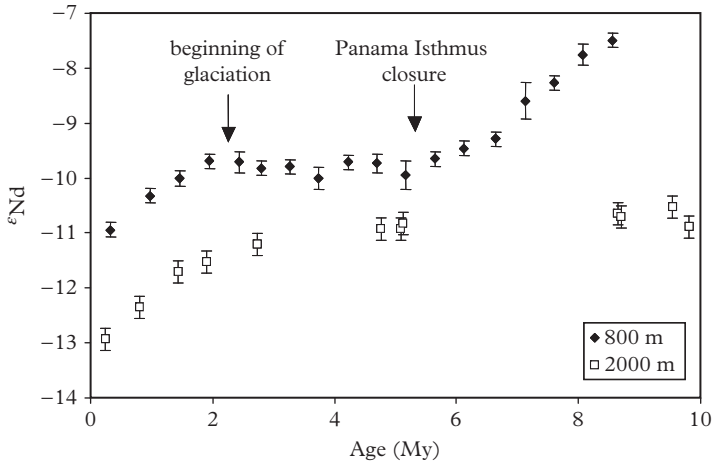

Figure 11.6 *Evolution of the Nd isotopic composition in Mn crusts from west of the Subtropical North Atlantic. Ages are estimated with ^{10}Be and the evolution of the $^{87}Sr/^{86}Sr$ ratio. At 800 m deep, the decline of the ε_{Nd} between 8 million y and 5 million y reflects the decrease and the end of the radiogenic Pacific Intermediate Water inputs through the Panama seaway. After a period of stability between 5 and 3 million y ago, the ε_{Nd} decreases at all depths. This decrease (which is visible across the Atlantic) is not due to the closure of Panama seaway but to the intensification of the glaciations in the northern hemisphere, which accelerates the erosion of old shields and injects very non-radiogenic Nd in the Atlantic Ocean. Modified after Burton et al. (1997) and Reynolds et al. (1999).*

injects very non-radiogenic Nd in the Atlantic Ocean. This example illustrates the possibilities (reconstruction of paleocirculations) and limits of the use of Nd isotopes in Mn nodules (ambiguity between circulation changes and changes of Nd inputs to the ocean).

It remains that the connection between the northward flow of warm water to the North Atlantic and the formation of ice caps is not straightforward: intuitively, the appearance of a paleo Gulf Stream should have warmed the northern hemisphere climate. However, this inflow of warm water in the North Atlantic Ocean could have initiated the buildup of ice sheets in the northern hemisphere by increasing the amount of moisture in the air and hence precipitations at high latitudes.

11.6 The Last Glaciation

We now live in a mild climate but the Cro-Magnon men who painted the Lascaux cave 18,000 y ago lived under much harsher climatic conditions. Glacial and interglacial periods have succeeded one another during the last 3 million y (Fig. 11.7). Their succession is reconstructed with the variation of $\delta^{18}O$ in benthic foraminifera, which depends on the

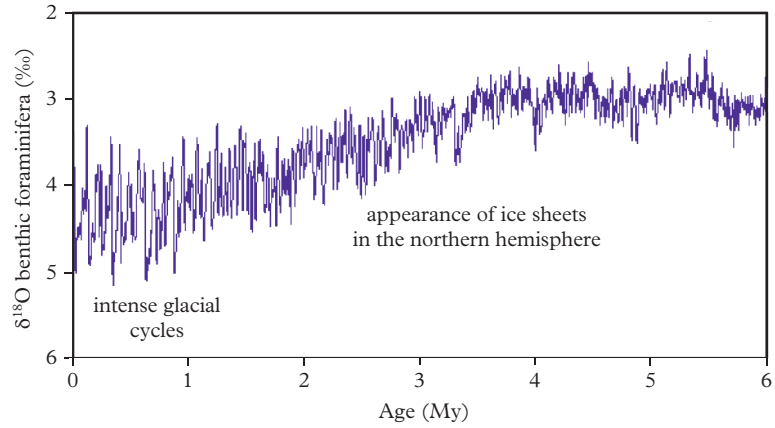

Figure 11.7 *Evolution of benthic foraminifera ^{18}O during the last 6 million y.*

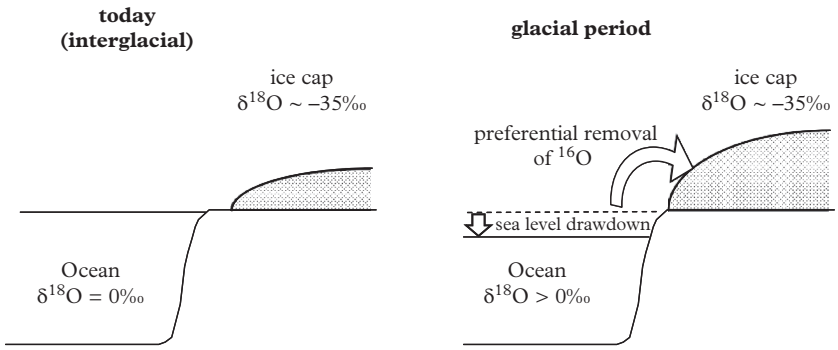

Figure 11.8 *Effect of growth of glaciers on the $\delta^{18}O$ of the ocean.*

$\delta^{18}O$ of seawater ($\delta^{18}O_{seawater}$) and seawater temperature (see Chapter 2). As, *a priori*, temperature should not change much in the deep ocean, the variations of the $\delta^{18}O$ of benthic foraminifera primarily reflects variations of $\delta^{18}O_{seawater}$. $\delta^{18}O_{seawater}$ depends of the amount of ice accumulated on the continents, because ice sheets are depleted in ^{18}O.

The growth of ice caps over continents produces a relative enrichment of the ocean in ^{18}O (Fig. 11.8). When the volume of the ice caps increases, the $\delta^{18}O$ of seawater and of benthic foraminifera also increases.

Application exercise: The $\delta^{18}O$ of the ocean during the Last Glacial Maximum

The Last Glacial Maximum (LGM) occurred 20,000 y ago. At that time, the sea level was 120 m below the current level. What was $\delta^{18}O$ of the ocean then?

Solution:

Today, the average ocean depth is 3800 m. During the LGM, 3% (= 120/3800) of the water that is currently in the ocean was on the continents in ice sheets. It is assumed that $\delta^{18}O_g$ of glaciers was –35‰. The present ocean ($\delta^{18}O_{po}$) result from the mixing of the glacial ocean ($\delta^{18}O_{go}$) and of the melted ice caps ($\delta^{18}O_{ic}$). Therefore,

$$100\% \times \delta^{18}O_{po} = 3\% \times \delta^{18}O_{ic} + 97\% \times \delta^{18}O_{go}.$$

It follows that

$$\delta^{18}O_{og} = -3/97 \times \delta^{18}O_g$$
$$= +1.08‰.$$

The $\delta^{18}O_{seawater}$ recorded in benthic foraminifera shows that, over the last 3 million y, our planet has experienced alternating warm and cold periods. These climatic variations correspond to cycles (known as Milankovitch cycles) with characteristic times determined by the orbital parameters of the Earth. These parameters determine the total amount of solar energy received by the Earth and its seasonal distribution (Fig. 11.9). However, if the astronomical factors give the tempo of climatic variations, they do not explain their high amplitude.

Eccentricity: The orbit of the Earth around the Sun is an ellipse called the ecliptic. Eccentricity gives the gap between the ellipse and a circular orbit. When eccentricity increases, the amount of solar energy received by the Earth increases. Eccentricity varies with pseudo-periods of 100,000 and 400,000 y.

Obliquity: The axis of Earth's rotation on itself is not perpendicular to the ecliptic. The inclination of this axis produces the seasons: the summer solstice occurs when the Earth's rotation axis at the North Pole points toward the Sun. Obliquity modulates the intensity of the seasons with a period of 41,000 y.

Precession of the equinoxes: At a given season, the Earth is not always at the same distance from the Sun. Today, the summer solstice occurs when the Earth is farthest from the Sun. 11,000 y ago, the summer solstice occurred when the Earth was at the closest from the Sun: warmer summers favored deglaciation. The precession of the equinoxes combined with the motion of the ecliptic produce two periods: 23,000–19,000 y.

Deep ice cores sampled in Antarctica and Greenland provide fundamental information on the climatic changes during the last glacial cycles. By drilling in ice caps, 740,000 y old ice cores were sampled. We saw in Chapter 3 that the $\delta^{18}O$ and the δD of the atmospheric precipitations (rain or snow) can be related to the local surface temperature of the deposition zone. By analyzing the $\delta^{18}O$ and the δD of ice cores and by applying to ancient periods the relationships observed today (Chapter 3, Fig. 3.7),

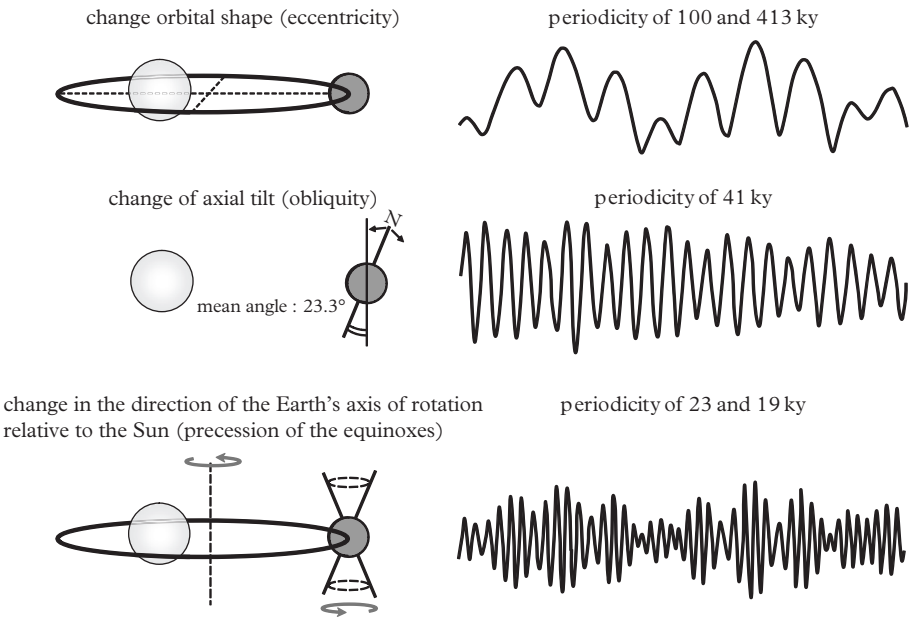

Figure 11.9 *Influence of astronomical parameters on the Earth's climate:*

we can determine the evolution of temperature in Antarctica and Greenland in the last cycles glacial (Fig. 11.10).

Application exercise: Variations of temperature in Antarctica

Using the calibration of the isotopic thermometer given in Chapter 3, determine the change in the average temperature of the air at the Dome C station between now and 20,000 y ago.

Solution:

20,000 y ago, the δD of the ice at Dome C was 40‰, lower than today's value (Fig. 11.10). The slope of the thermometer is 6‰/°C (Fig. 3.7). So, 20,000 y ago, the temperature at Dome C was 40/6 = 6.7°C lower than today.

The temperature variations recorded by the δD of ice at Dome C are synchronous to the variations of the ice sheets volume recorded by the $\delta^{18}O$ of benthic foraminifera: the presence of large ice sheets goes along with much colder air temperatures. These changes are accompanied by changes of the CO_2, CH_4 and N_2O content of the air bubbles entrapped in ice: during cold periods, the atmosphere is depleted in greenhouse gases (about 180 ppm of CO_2 during the LGM) while it is enriched in CO_2 during warm

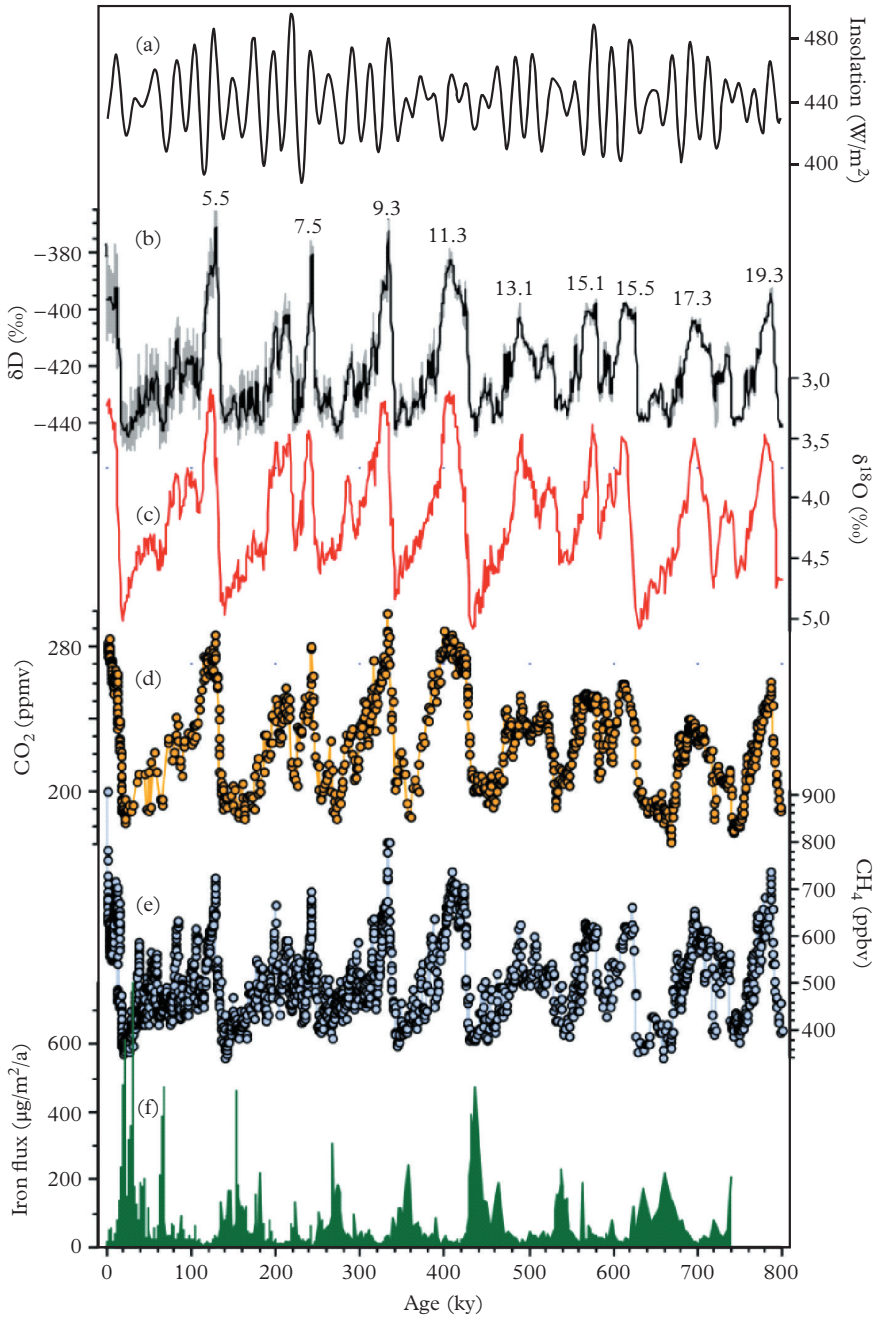

Figure 11.10 *Evolution of the climate parameters over 800,000 y. (a) Summer insolation at 65° N (its intensity directly affects the growth/melting of the ice caps that covered North America and Asia). (b) δD analyzed in the ice of the EPICA drilling at the Dome C site in Antarctica (the more negative the δD is, the lower the local temperature was). (c) $\delta^{18}O$ of benthic foraminifera (it gives the extension of the polar ice caps that accumulate ^{18}O-depleted water). (d) CO_2 concentration in air bubbles trapped in Antarctic ice (greenhouse gas). (e) CH_4 concentration in air bubbles trapped in Antarctic ice (greenhouse gas). (f) Atmospheric iron flux due to dust deposition in Antarctic ice (climate aridity and ocean fertilization). Modified after Barbante and Fischer (2010).*

periods (about 280 ppm of CO_2 during interglacial periods without anthropogenic perturbation). Thus, the greenhouse effect amplifies the astronomical forcings. The study of the present carbon cycle has taught us that the atmospheric CO_2 concentration is largely regulated by the ocean (Chapter 8). Isotope tracers in foraminifera shells allow us to glimpse why the ocean contained more carbon during the LGM than today.

By recording the $\delta^{13}C$ of deep water, benthic foraminiferal tests allow partial reconstruction of the chemical composition and origin of deep waters during the LGM. Indeed, we have seen that in the present Atlantic Ocean, PO_4^{3-} is a signature of the origin of the deep waters (Chapters 3 and 10). In addition, in today's ocean, there is a relationship between the $\delta^{13}C$ and the phosphate concentration of seawater (Chapter 3). North Atlantic Deep Water (NADW) is characterized by a low PO_4^{3-} and a positive $\delta^{13}C$, whereas Antarctic Bottom Water (AABW) is characterized by a high PO_4^{3-} content and a negative $\delta^{13}C$. The $CaCO_3$ test of some benthic foraminifera records the $\delta^{13}C$ of the deep water in which they grew. By analyzing foraminifera in sediments cored at different seafloor depths, it is possible to reconstruct a $\delta^{13}C$ hydrographic section of the Atlantic Ocean during the LGM. During this period, the contribution of the NADW was greatly reduced compared to today (Fig. 11.11). These results may be compared with those obtained with an independent tracer such as the neodymium isotopes (Problem 4).

The impact of these hydrological changes on the speed of the thermohaline circulation is estimated using the $\Delta^{14}C$ of foraminifera tests. The $\Delta^{14}C$ of a foraminifera test depends on its real age and on the $\Delta^{14}C$ of seawater when the test was formed. The $\Delta^{14}C$ difference between seawater and the atmosphere corresponds to the apparent age of seawater or reservoir age (for a definition, see Chapter 5). By comparing the $\Delta^{14}C$ of benthic and planktonic foraminifera tests of the same age (because these forams are collected at the same depth in the sediment core), it is possible to determine the age difference between the surface and the deep ocean. In the Atlantic Ocean, this difference was of 600 $\pm$ 250 y during the LGM while it is now about 400 $\pm$ 250 y. This suggests that the deep water ventilation was slower during the LGM than today.

The $^{231}Pa/^{230}Th$ of marine sediments could help in constraining the intensity of the ventilation of the Atlantic by the NADW independently of $\delta^{13}C$ and $\Delta^{14}C$. Today, the $^{231}Pa/^{230}Th$ ratio of Holocene marine sediment of the Atlantic is much lower than the production ratio of these nuclides in the water column because the marine particles falling through the water column quantitatively remove the ^{230}Th produced locally, but only 50% of the ^{231}Pa produced locally (see Chapter 4). The remaining ^{231}Pa is advected to the South Antarctic polar front where it is efficiently scavenged by the strong flux of diatom frustules that fall through the water column in this area. During the LGM, the $^{231}Pa/^{230}Th$ activity ratio of sediment located at 4000 m depth on Bermuda rise (North Atlantic) increased slightly while remaining lower than the production ratio, which suggests a slowdown (of 30%) of the NADW (Fig. 11.12). This result is consistent with the estimates based on $\Delta^{14}C$. On the other hand, a very strong increase in the $^{231}Pa/^{230}Th$ activity ratio occurs during the "H1" (for Heinrich 1) event. The H1 event is a strong iceberg discharge bringing enough excess fresh water to disrupt the formation of deep water. Concluding that, during H1, the $^{231}Pa/^{230}Th$ ratio sediment becomes equal to the production ratio suggests a total shutdown of the NADW production is tempting but

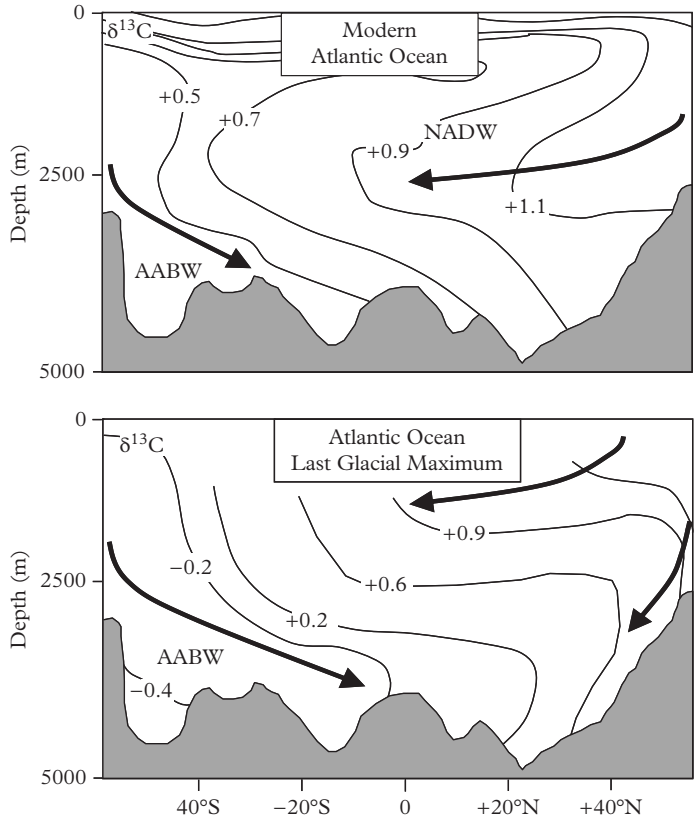

Figure 11.11 *Deep water circulation in the Atlantic Ocean. The $\delta^{13}C$ of seawater is used to determine the relative contributions of the NADW (positive $\delta^{13}C$) and the AABW (negative $\delta^{13}C$) in deep waters. (a) Hydrographic data for the modern Atlantic Ocean. (b) During the LGM, by analyzing the $\delta^{13}C$ benthic foraminifera from sediment cores collected at different depths. Today, the deep ocean is ventilated equally by the NADW and the AABW, during the LGM the NADW contribution was extremely reduced. Adapted from Duplessy (2004).*

premature in view of the current uncertainties on the impact of the composition of the particles on the binding of Pa–Th and those on the evolution of circulation in shallower waters.

In any event, a slowdown of the thermohaline circulation does not explain by itself an increase of the CO_2 storage by the ocean if it is not accompanied by a change in chemical composition of the ocean. The CO_2 absorption capacity of the ocean is linked to its content in carbonate ions (which neutralize CO_2) and thus its pH. The pH of the ocean can be determined from the $\delta^{11}B$ of foraminifera tests (Chapter 3). The $\delta^{11}B$ of benthic

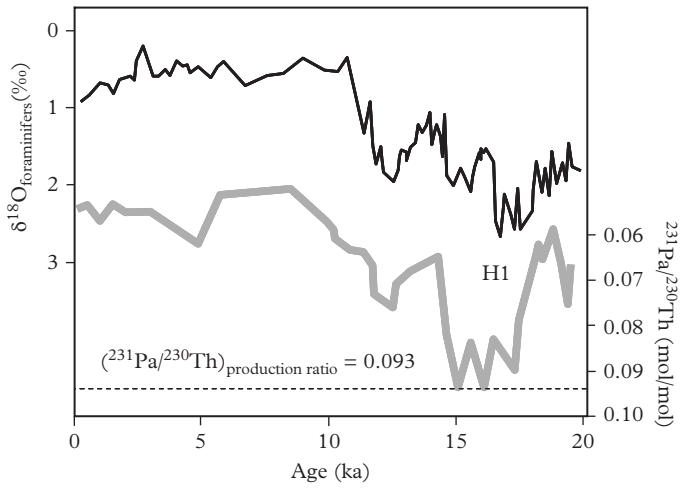

Figure 11.12 *Geochemical data on a North Atlantic core. Black curve: $\delta^{18}O$ of foraminifera (chronology). Gray curve: ^{231}Pa /^{230}Th activity ratio in marine sediments. Modified after McManus et al. (2004).*

foraminifera of the LGM is greater than current benthic foraminifera, suggesting that the pH of the ocean during the LGM was higher than today (Sanyal et al., 1995). The reason for this change is not clearly established. Today, the biological activity of large ocean areas is limited by the weakness of the iron inputs (see Chapter 7). It is possible that at the LGM, they were fertilized by high eolian dust inputs favored by a more arid climate than today, as shown by the strong dust deposits analyzed in Antarctic ice core during glacial periods (Fig. 11.10). Iron fertilization would also favor a better use of nutrients (Si and N) during the export of particulate organic carbon (see Problem 6 of Chapter 7). It remains that an increase of the biological pump driven by the Southern Ocean iron fertilization does not account for more than 50% of the decrease of atmospheric CO_2 observed between glacial and interglacial periods (see Problem 5). Recently, it was demonstrated that the intense production of dense and DIC-rich brines by sea-ice formation in the Southern Ocean produces a strong stratification of the deep ocean and a high DIC content that at last seems to account for the low CO_2 atmospheric content during the LGM (Bouttes et al., 2011).

The menu of Vikings (Arneborg et al., 1999)

At the end of the eleventh century, Eric the Red established Viking colonies in Greenland, which he so named to attract his compatriots with fake advertising. Nevertheless, the relatively mild climate during the "medieval warm period" across Europe allowed breeder populations gone with their livestock to settle in

Greenland. At the end of the sixteenth century, all the colonies in Greenland had disappeared. Historians hotly discuss the reasons for the departure of the Vikings: tough climatic conditions at the end of the medieval warm period, conflict with Eskimos, refusal or inability to use fishing?

Geochemistry provides clues for an answer. The analysis of collagen (a carbon-containing molecule that is the main constituent of bones) of human bones found by archaeologists shows an evolution of the $\delta^{13}C$ of the successive generations. The first generations have a $\delta^{13}C$ ($\sim -18.5 \pm 1.5‰$) identical to Swedish and Norwegian farmers who lived at the same time and who ate mainly agricultural products. Over the generations, the $\delta^{13}C$ of collagen declined to become identical ($\sim -15.5 \pm 1.0‰$) to the collagen of Eskimo populations that were their contemporaries and who only ate fish and seals. Thus, the abandonment of Greenland was not due to a refusal to use the resources of the sea.

11.7 El Niño Exacerbated by Human Activity?

Paleoreconstructions do not concern only very distant times. They can also fill the lack of instrumental data in the recent past. Considerable efforts have been deployed since the 1980s to understand and predict the El Niño phenomenon because of its major economic impacts (drought in Southeast Asia, torrential rains on the west coast of the United States and lack of fish for the Peruvian fishermen ...). In the tropical Pacific, trade winds drive surface water westward. These waters are warmed up during their journey and they accumulate on the east coast of Indonesia to form a "warm pool" of water. The warm pool induces the rise of warm and moist air, which leads to significant precipitation over the Western Pacific margin. During El Niño years, the intensity of the trade winds decreases, causing both an eastward shift of the warm pool and a warming of the surface waters in the East Pacific. The heavy rain area also shifts to the Eastern Pacific. El Niño does not occur regularly. Nevertheless, it is possible to predict its arrival almost a year in advance thanks to (i) data acquired by the buoy networks deployed along the equatorial Pacific and the regular temperature and salinity measurements over 1000 m depth by thermal probes dropped from merchant ships and satellites and (ii) ocean–atmosphere coupled models. Nevertheless, the network cannot reliably predict the intensity of El Niño. Instrumental data obtained over the past 50 y suggest a strengthening of the intensity and duration of El Niño events since 1976. Is this related to the global warming of the climate triggered by the increase of the greenhouse effect, or is it a transient phenomenon related to natural variations? The answer to this question (or at least part of it) is located in the coral of the Maiana Atoll in the western equatorial Pacific.

Just as tree rings can be counted on a trunk, aragonite layers filled each year by corals can be counted on a coral reef. By analyzing the $\delta^{18}O$ each of these layers, it is possible to reconstruct the evolution of El Niño events over time (Fig. 11.13). The $\delta^{18}O$ of the coral

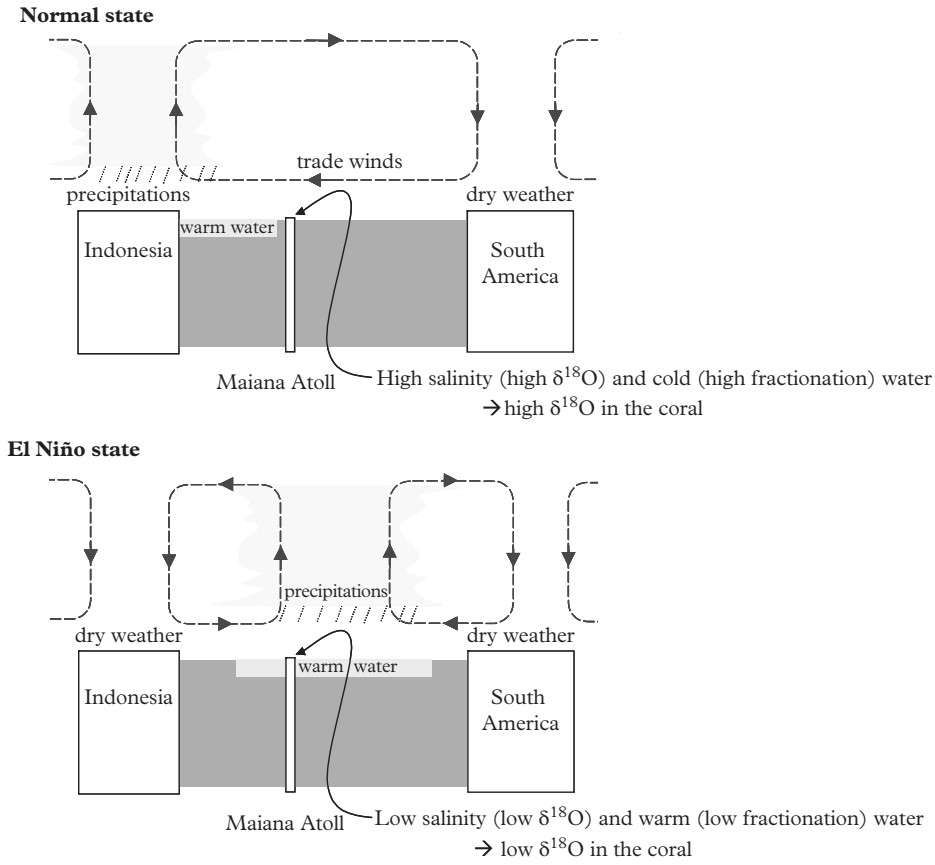

Figure 11.13 *Principle of recording of El Niño events by the $\delta^{18}O$ of the corals of the Maiana Atoll (equatorial Pacific).*

depends on the $\delta^{18}O$ and the temperature of the seawater in which it lives (Chapter 3). On the Maiana Atoll, seawater is warmer (displacement of warm pool at the level of the atoll) and less salty (heavy rains reduce the $\delta^{18}O$ of seawater, see Chapter 3) during El Niño years. The isotopic composition of the seawater and the temperature effect both contribute to produce coral with a very negative $\delta^{18}O$ during El Niño years.

The analysis of the $\delta^{18}O$ of coral back to 1850 shows that prolonged episodes of El Niño have not appeared recently (Fig. 11.14). In the late nineteenth century, El Niño periods of a dozen years occurred although there was no significant human impact at the time. However, the decrease of –3.5‰ of the average $\delta^{18}O$ of corals since 1976 appears to be unique over the studied period and is probably linked to anthropogenic perturbation. It reflects the increase in temperature (estimated at +0.6°C) and precipitation (salinity has decreased of about 0.8) in the area over the studied period.

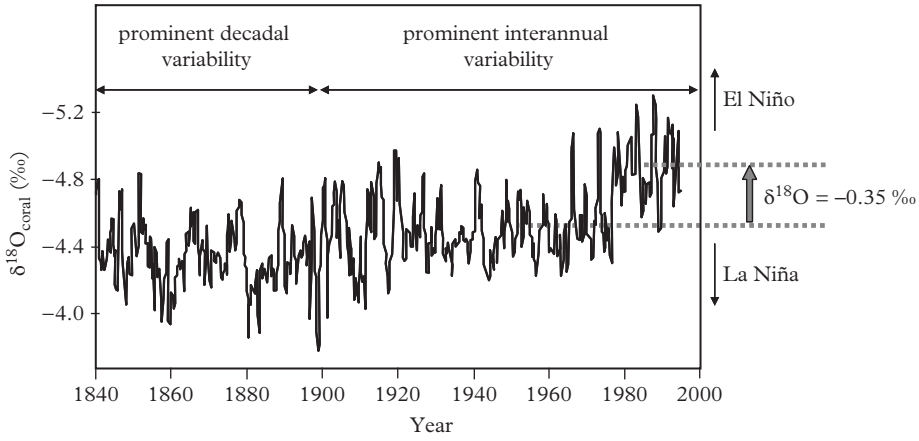

Figure 11.14 *Reconstruction of El Niño events since 1840 based on the $\delta^{18}O$ of the Maiana Atoll corals. The sharp decline of $\delta^{18}O$ since 1976 corresponds to a strong El Niño period. There is an increase of the variability between the nineteenth and the twenty-first century. Modified from Urban et al. (2000).*

11.8 The Climate of the Future and the Ocean

Since the end of the nineteenth century, there has been a marked increase of the Earth's average temperature (Fig. 11.15). Between 1850 and 2012, it has increased by 0.85°C (Stocker et al., 2013). Variation of natural forcings (orbital parameters of the Earth, intensity of solar activity, volcanic aerosols) explains no more than an increase of 0.2°C

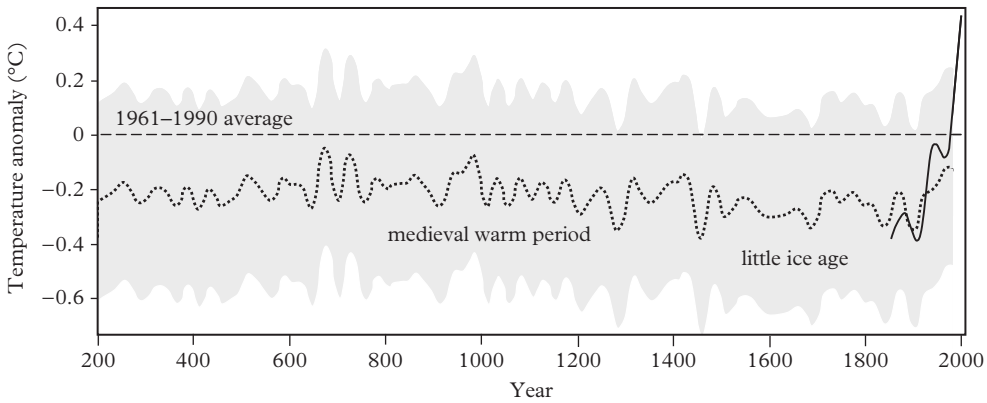

Figure 11.15 *Evolution of the global temperature of the Earth over the last 1800 y. All the curves represent temperature anomalies compared to the average instrumental data over 1961–1990. Dashed curve: average temperature anomaly estimated from proxies and smoothed over 40 y. Gray area: 95% confidence interval. Continuous curve: average based on the instrumental values (with smoothing over 40 y). Modified after Mann and Jones (2003).*

of the average temperature of the Earth (Problem 6). Taking into account the **additional greenhouse effect** linked to human activity is required to explain the observed temperature changes, as demonstrated by the work of the Intergovernmental Panel on Climate Change (IPCC). The cause is the massive emissions of greenhouse gases that are unbalancing the Earth's radiative budget (see the IPCC reports on this subject: www.ipcc.org).

Since the industrial revolution, the massive use of fossil fuels (coal, oil, natural gas) and deforestation have led to an exponential growth of the CO_2 released into the atmosphere (Fig. 11.16). In response, the atmospheric CO_2 content has increased from 280 ppmv before the industrial revolution to 400 ppmv (approximately) in 2014. We have seen in Chapter 8 that this increase represents only 55% of emissions, the remaining 45% having already been stored by the ocean and the accelerated growth of the continental biosphere. Other gases, much less abundant than CO_2, nevertheless play an important role because they absorb infrared radiation efficiently (Fig. 11.17):

- The methane concentration has more than doubled since the industrial revolution. Today 70% of the emissions are anthropogenic (biomass fires, fossil fuels combustion, emission from cattle and rice fields).
- Nitrous oxide is connected to denitrification in soil (in particular with the use of fertilizers) and in the ocean, as well as combustion in the air.
- CFCs are not present naturally in the atmosphere. Their production was stopped to preserve the stratospheric ozone layer but substitution products (halocarbons) have a significant greenhouse effect.

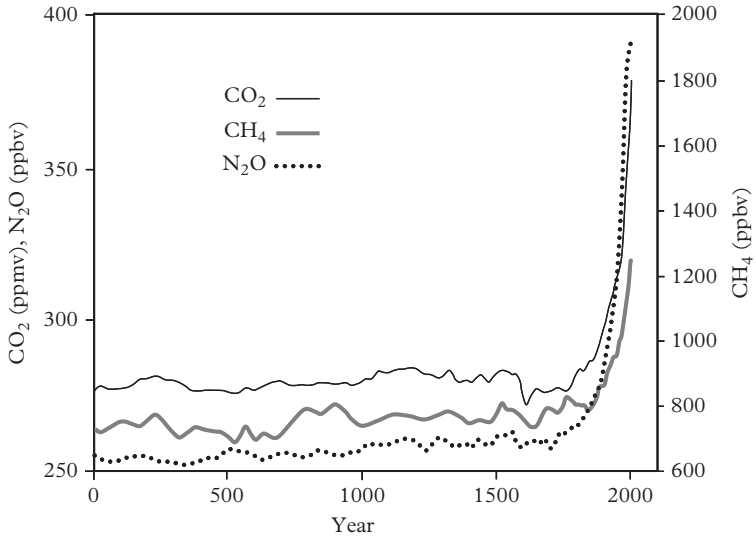

Figure 11.16 *Evolution of greenhouse gases for the last 2000 y. The increase since 1750 is due to human activity. Adapted from the answer to the frequently asked questions of the IPCC report (www.ipcc.org).*

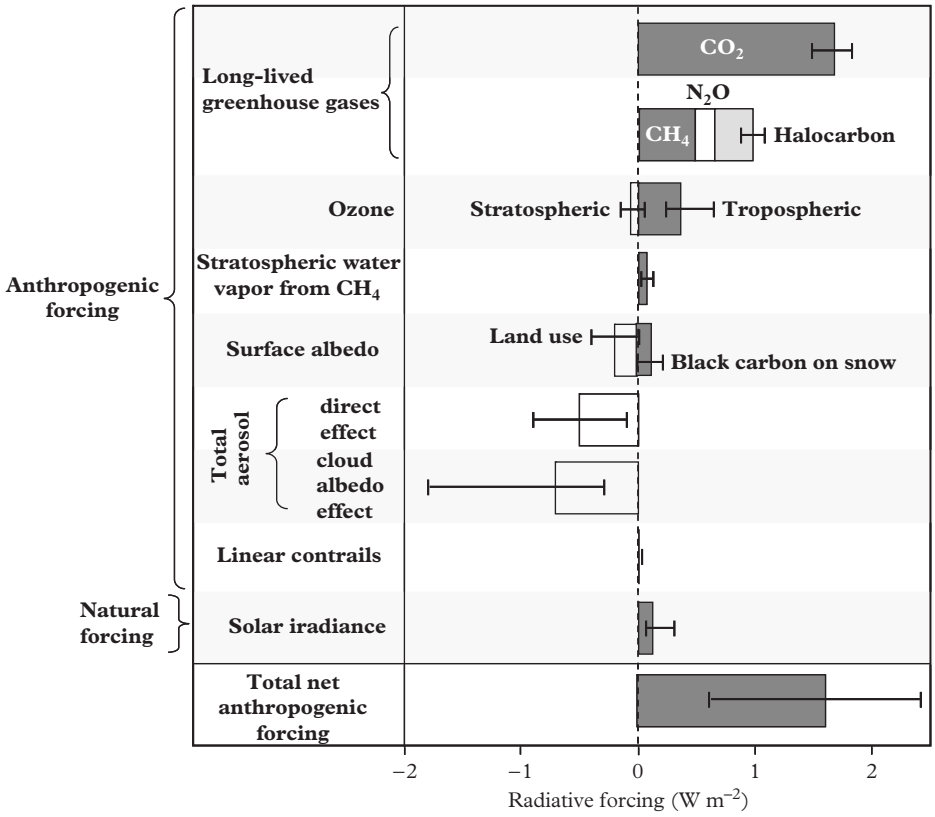

Figure 11.17 *Effect of natural and anthropogenic forcing on the radiative balance of the Earth between 1750 and 2011. The most important uncertainties relate to ozone and aerosols. Contrails are condensation trails produced by jet aircraft. Modified after the IPCC report (Stocker et al., 2013).*

Industrial activities (mineral processing and coal combustion) generate large quantities of aerosols in particular due to the emissions of sulfur compounds (SO_2). The role of these aerosols is twofold: (1) they scatter and reflect light which increases albedo and tends to cool the Earth; (2) they serve as condensation nuclei and promote the formation of clouds, which depending on their altitude may increase or reduce the greenhouse effect.

11.9 The Expected Consequences

The climatic consequences of human activities are frequently evaluated on the basis of a doubling of the atmospheric CO_2 content compared to the preindustrial situation.

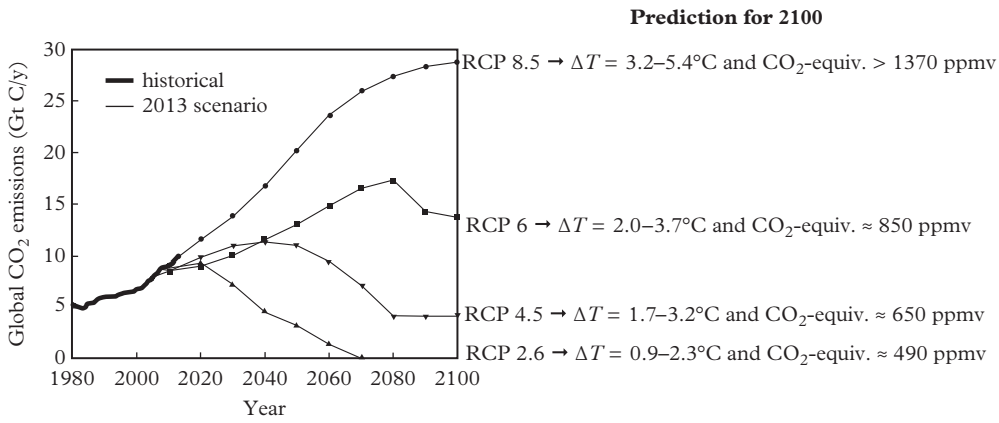

Figure 11.18 *Evolution of greenhouse gas (GHG) emissions and of temperature up to 2100 for different representative concentration pathways (RCPs). (a) Global CO_2 emissions required to achieve a radiative forcing of 2.6, 4.5, 6 and 8.5 W m^{-2}. RCP 8.5 corresponds to a "business as usual" scenario. By 2070, RCP 2.6 requires negative CO_2 emission (net CO_2 sequestration). (b) The ΔT values correspond to multi-model global minimum and maximum warming predicted for the scenarios of the twenty-first century. The projected CO_2-equivalent concentrations include GHG and short-lived aerosols emissions. RCP 2.6 is the only scenario with a high probability of maintaining the global warming below 2° C compared to the pre-industrial area. Modified after the IPCC report (Stocker et al., 2013).*

Taking into account all greenhouse gases, a situation equivalent to a doubling of CO_2 might be reached by 2030. What is then predicted by climate models (Fig. 11.18)?

If we take into account only the additional greenhouse effect directly linked to the human perturbation, the expected average global warming is of the order of 1.2°C. Without being negligible, such warming should not bring major changes: it is equivalent to the magnitude of global warming that we have known since the **little ice age.** The cold episode which extends from the sixteenth to the middle of the nineteenth century is probably linked to a period of low solar activity (observed since 1610 by Galileo Galilei). During the little ice age, the **Maunder Minimum** was a period of low solar activity which paradoxically corresponds to the reign of the king of France, Louis XIV, who built the Versailles Palace and who was called . . . the Roi Soleil (Sun King)!

However, this estimate does not take into account induced effects: the first one is that an increase in temperature induces an increase of water evaporation, of ice melting and of air moisture. This increase has various effects: (1) water is a greenhouse gas so that the moisture increase causes additional warming; (2) the melting of the ice decreases Earth's albedo, which promotes global warming; (3) the increase in humidity favors the formation of clouds that have varying effects depending on whether they are at low altitude (cooling effect) or high altitude (warming effect). The net effect of clouds is poorly constrained. When considering all these effects, all models predict an increase in the average temperature of the Earth from 2 to 5°C. This increase is significant: the average cooling

during the LGM compared to today was of the order of 4–5°C. The temperature change will not be homogeneous at the Earth's surface. It will be generally greater on the continents than on the ocean, because ocean surface temperature is buffered by mixing with the deep ocean. The Arctic Ocean is an exception because the sea-ice melting (surface reflecting light) replaced by free water (surface absorbing light) will cause a warming of the ocean (+6.5°C in the Arctic Ocean for an average warming at the surface of Earth of +2.2°C in RCP 6 scenario for example).

What are the foreseeable consequences of this increase?

(1) In the atmosphere, the increase in humidity and temperature must promote extreme events such as storms in mid-latitudes and cyclones at low latitudes. At high latitudes, the increase of the global temperature and the increase in air moisture must lead to an increase in precipitations.

(2) As a first step, this increase in precipitation may lead to an increase in the volume of the polar ice caps. Then, the increase in temperature must lead to melting of ice sheets and a decrease of their size. Observation of polar ice sheets by satellite indicates that the West Antarctic ice sheet is undergoing accelerated melting while the eastern part of Antarctica has gained a little mass due to an excess of precipitation. In Greenland, the accelerated ice melting in coastal areas is not balanced by the slight increase in mass due to precipitation in the center of the continent (Cazenave et al., 2008).

(3) The thermal expansion of seawater and the melting of the polar ice caps must produce an increase of the sea level. At the 2100 horizon and on the basis of the RCP 8.5, a rise of +40 to +80 cm compared to the 1980–1999 average is expected. This is +4 to +8 mm per year, which is little compared to the +10 to +40 mm per year of the last deglaciation. In a country like Bangladesh, where barely 10% of the territory is more than 1 m above sea level, the effect of mean sea level rise is amplified with the subsidence of the Ganges and Brahmaputra deltas. In addition to the increase of the average sea level, the expected increase of extreme events, such as tropical storms and cyclones (whose formation is directly due to the increase in the surface water temperature in the Bay of Bengal) will cause increased problems of flooding and erosion of the coasts (Karim and Mimura, 2008).

    Altimetric satellites show that over the past 15 y, the sea level has increased by an average of 3.1 mm per year (Fig. 11.19). This increase is mainly due to the thermal expansion of the surface ocean under the effect of global warming and the melting of the polar ice caps. While the increase in the sea level was essentially due to the thermal expansion up to 2003, the contribution of the ice cap melting has become predominant today.

(4) Even though it does not contribute to the increase of the sea level, the melting of the Arctic sea ice over the last 35 y is well demonstrated. It contributes to the accelerated global warming in this region compared to the world average. Over the same period, there is a smaller but statistically significant increase

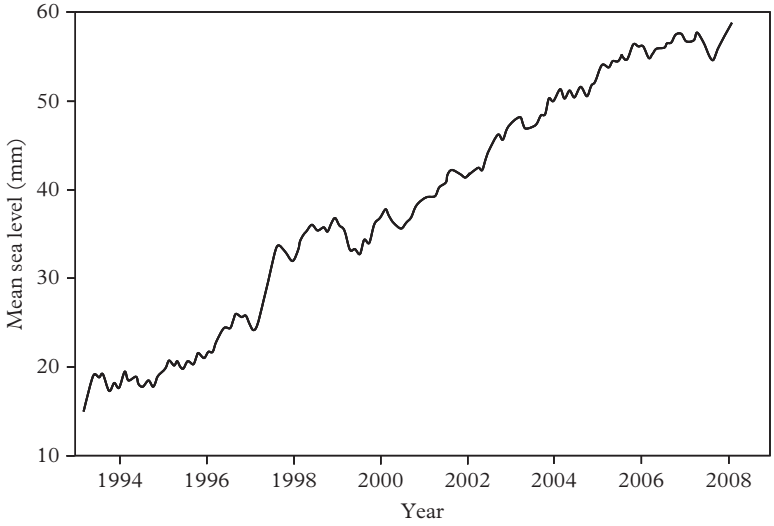

Figure 11.19 *Variation in the average sea level measured by satellite altimetry Cazenave et al. (2008).*

of the sea ice cover in Antarctic (Simmonds, 2015). An hypothetical explanation is that accelerated melting of the Antarctic ice sheet produces an influx of cool, fresh water near the surface of the ocean that could stabilize the water column and cut off the heat supply from the warmer Weddell Deep Water and Circumpolar Deep Water that would otherwise contribute to reduce the sea-ice cover.

(5) Paradoxically, this global warming could lead to a slowdown of the thermohaline circulation: warmer and less salty polar water would not be dense enough to sink at the bottom of the ocean. A reduction in North Atlantic thermohaline circulation would limit the northward trajectory of the Gulf Stream, substantially reducing the inputs of heat to Northern Europe. Models predict a slowdown in overturning circulation during the next century (from 20 ± 5 Sv today to 14 ± 5 Sv in 2140) but not a complete stop. Water transport across a long 26.5°N section measured between 2004 and 2014 shows a large intra- and interannual variation and a decline of the Atlantic meridional overturning circulation over the last decade. In the absence of longer time series, it is not possible to distinguish a possible anthropogenic influence from the natural variability (Srokosz and Bryden, 2015).

The consequences of the increase of CO_2 and climate warming on the biological pump are difficult to assess. For example, the physiological response of algae to a strong increase of P_{CO_2} is poorly known. Culture experiments under high P_{CO_2} show that the calcification rate of coccolithophorids decreases when P_{CO_2} increases (Fig. 11.20).

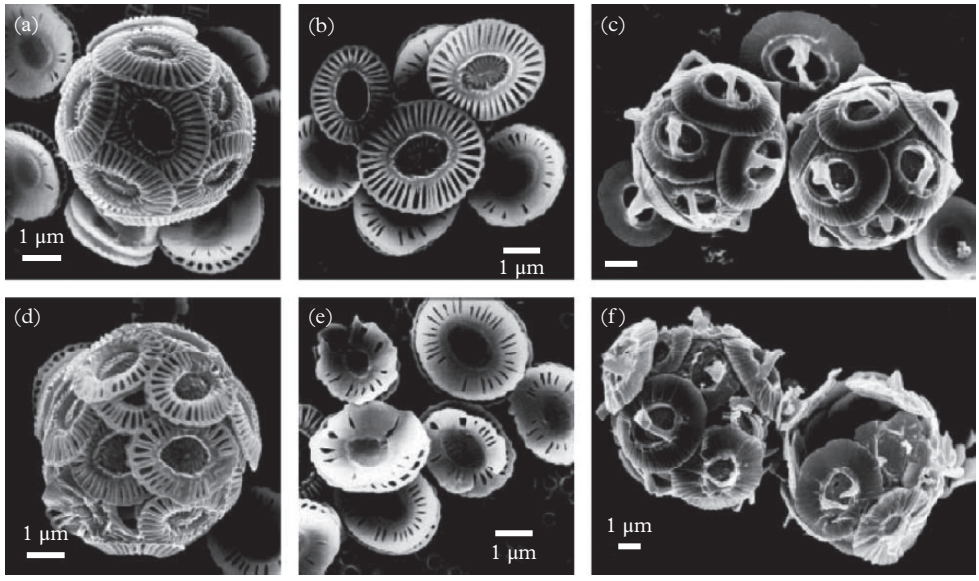

Figure 11.20 *Coccolithophorids grown under different partial pressure of CO_2. (a–c) Pre-anthropogenic level; (d–f) high P_{CO_2}. (a, b, d and e)* Emiliania huxleyi. *(c and f)* Gephyrocapsa oceanica . *It is clear that a high P_{CO_2} causes a poor calcification. Modified from Riebesell et al. (2000).*

These changes of calcification may have significant consequences on the biological pump. Zooplankton species (foraminifera, pteropods, etc.) seem also to be sensitive to these changes (Problem 7). Some corals regulate the pH of their internal calcifying fluid and hence reduce the effect of the seawater pH decrease (McCulloch et al., 2012).

Ocean models coupling physics and biology predict an overall decrease of the biological pump with local variations (Bopp et al, 2013):

(1) At low latitudes, the temperature increase and the salinity decrease of surface waters lead to an increase of the stratification. The supply of nutrients to the surface waters is then reduced, so a decrease of the biological production is expected. A similar reduction is visible during the El Niño phenomenon (Fig. 11.21).

(2) At high latitudes, shorter and less extensive coverage by sea ice must lead to a lengthening of the productive period. This trend has already been observed with the ocean color data collector since 1997 (Arrigo and van Dijken, 2011).

Systematic sampling of plankton over several decades with the "continuous plankton recorder" on merchant ships allows observation of the effects of climate change on phytoplankton and zooplankton in the Northeast Atlantic (Hayes et al., 2005). The response of the various groups and species of plankton to the warming of surface waters is extremely variable. However, there is an intensification of blooms in the cold waters

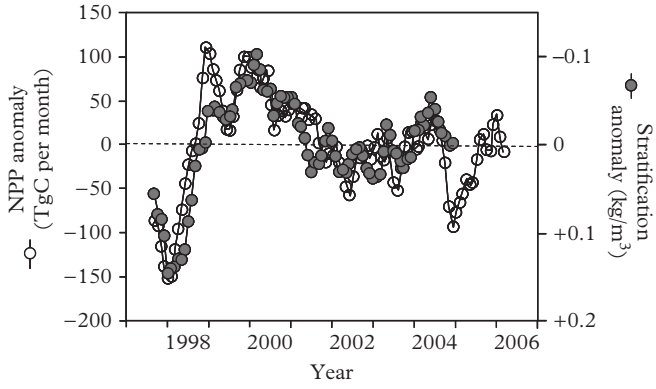

Figure 11.21 *Evolution joint net primary production and stratification in the Pacific Ocean between ~40° S and 40° N. The year 1998 was marked by a strong El Niño event. In 1999 and 2000 the reverse phenomenon (La Niña) occurred. Modified after Behrenfeld et al. (2006).*

and less intense blooms in warm and stratified waters, as predicted by the models. In addition, spring blooms occur earlier (as on continents). This can produce ecological disequilibrium since some zooplankton species are unable to advance their development peak as much as the phytoplankton on which they feed. For example, in 30 y, the *Calamus finmarchus* copepod advanced its development peak by 11 days while several phytoplankton species on which it feeds have advanced their own development by a month. There is also a migration of the ecosystem of temperate and warm waters toward high latitudes. For example, *Calamus trichoceros*, which did not occur further north than the South of England in the 1960s, is now found off the coast of Scotland. Cold water species have declined in parallel. Assembly of copepods changes have a direct impact for fish which feed on them and therefore on fishing. For example, despite overfishing, cod has been expanding in the North Sea in the 1980s because the arrival of large copepods has favored cod recruitment.

We may also fear a combination of global warming, overfishing and competition between species. For example, overfishing of sardines in the Benguela upwelling off the Namibia coast has led to a collapse of their population, so that the ecosystem is now dominated by jellyfish whose juvenile forms have no more predators. Other factors can promote jellyfish. Eutrophication of coastal areas promotes the development of photosynthetic bacteria and algae of small sizes (consumed by jellyfish) at the expense of the diatoms (more readily consumed by fish such as sardines). In addition, eutrophication of surface waters is accompanied by a low O_2 concentration which could be better tolerated by jellyfish than by fishes. In the North Atlantic, the period with abundant jellyfishes are associated with warmer waters. The underlying mechanisms remain to be determined, but this natural variability could prefigure the changes associated with the ocean warming (Richardson et al., 2009).

PROBLEMS

Problem 1: Sulfur isotopes and the Archean atmosphere (Ohmoto et al., 2006)

The presence, in terrestrial samples older than 2.4 billion y, of mass-independent fractionations of sulfur isotopes has been interpreted as evidence of the existence of an anoxic atmosphere (see Section 11.3). However, a recent study shows that 2.7–2.9 Gy old sedimentary rocks from Western Australia have sulfur isotopes with no trace of mass-independent fractionations. How can you explain this result?

Problem 2: Redox condition of the ocean in the Middle Proterozoic (Anbar, 2004)

We want to determine the redox conditions of the ocean during the Middle Proterozoic. For this, we use molybdenum (Mo) and its isotopic composition.

(1) First, we look at the chemical behavior Mo. The Mo concentration (~105 nmol kg^{-1}) is constant with depth in the open ocean and it does not vary significantly between the Atlantic Ocean and the Pacific Ocean. In the Black Sea, the Mo concentration is relatively high (60–70 nmol kg^{-1}) in surface waters. Below 100 m depth (in the presence of H_2S, see Problem 6 in Chapter 2), Mo concentration decreases rapidly (~5 nmol kg^{-1} below 500 m depth). At the pH of seawater, Mo is found as an oxyanion (MoO_4^{2-}) when pe > –4 and as molybdenite (MoS_2, a solid) when pe < –4. With this information, explain the chemical behavior of Mo in oxic and anoxic conditions.

(2) We now consider the isotopic composition of Mo. Molybdenum has only stable isotopes. The $^{97}Mo/^{95}Mo$ ratio is measured. The $\delta^{97/95}Mo$ notation represents the relative changes of the $^{97}Mo/^{95}Mo$ ratio (see Chapter 3).

The main Mo source to the ocean is the continental weathering. The main sinks are the sedimentation in the anoxic zones of the ocean and Mo uptake by iron and manganese nodules formed growing at the surface of the oxic sediments.

The following values are measured:

Samples	$\delta^{97/95}$Mo (‰)
Granite, basalt, molybdenite (Mo ore)	0 ± 0.4
Seawater (dissolved Mo)	$+1.6 \pm 0.6$
Fe–Mn crusts and nodules (oxic sediments)	-0.5 ± 0.2
Reducing sediments (Black Sea)	$+1.5 \pm 0.25$

What is the major process that fractionates Mo isotopes in seawater?

(3) Assuming that the Mo cycle is at steady state, estimate the percentage of Mo that is removed in oxic and anoxic regions of the ocean.

(4) The $\delta^{97/95}$Mo of extremely well-preserved reducing marine sediments from the Mid-Proterozoic is $+0.5 \pm 0.3$‰.

Assuming that the fractionation process of Mo and that the amplitude of the fractionation factor are the same as today, estimate the relative contributions of the oxidizing and reducing oceanic areas during the Mid-Proterozoic.

(5) Do these results support the hypothesis of an oxidized ocean or of a sulfide-rich ocean? During the Mid-Proterozoic, were the ocean redox conditions favorable to a limitation of the development of eukaryotic algae by Mo?

Problem 3: A dry Mediterranean Sea! (Flecker et al., 2002)

Six million y ago, the Mediterranean Sea experienced an unprecedented crisis. The presence of a 1 km thick salt layer (also called evaporites) in the Mediterranean sediments attests that, at the time, the Mediterranean Sea was completely dry. To understand the reasons of this drying, the strontium isotopic composition of marine carbonate deposited just before the crisis and of evaporites deposited during the crisis is analyzed. 10 million y ago, the $^{87}Sr/^{86}Sr$ ratio of Mediterranean marine carbonates was indistinguishable from the average value of the ocean. Just before the crisis, the $^{87}Sr/^{86}Sr$ ratio of marine carbonates was 0.70890. During the crisis, $^{87}Sr/^{86}Sr$ ratio of evaporites varies between 0.70890 (the oldest evaporites) and 0.70860 (the most recent evaporites). Around 6 million y ago, the $^{87}Sr/^{86}Sr$ ratio of the ocean (except the Mediterranean Sea) was of 0.70897 and the rivers feeding the Mediterranean Sea had an average $^{87}Sr/^{86}Sr$ ratio of 0.70800. What can you infer from these data on hydrological changes that produced the Messinian crisis?

Problem 4: Neodymium as a tracer of the glacial thermohaline circulation (Rutberg et al., 2000)

Different proxies are used to reconstruct the thermohaline circulation in the Atlantic during the last glacial period, but they sometimes give conflicting results. $\delta^{13}C$ data suggest a full stop of the NADW formation during the Last Glacial Maximum while the Pa–Th indicates a reduction of no more than 30% of the NADW flux. To obtain a proxy independent from the previous ones, manganese oxides are selectively dissolved in a sediment core and the isotopic composition of the Nd that they release is analyzed. Hence, it is possible to reconstruct the evolution of the Nd isotopic composition (ε_{Nd}) of the deep Atlantic waters during the last glacial period (points on the figure below). What causes the variations of ε_{Nd}? Are they in agreement with the $\delta^{13}C$ data (continuous line in Fig. 11.22)?

Problem 5: Iron fertilization and glacial CO_2 (Bopp et al., 2003)

Sophisticated numerical models estimate that, during the Last Glacial Maximum, the iron fertilization of the ocean by deposition of atmospheric dust would have increased the overall oceanic biological pump from 11.7 gigatons of carbon per year (interglacial value) to 12.4 gigatons of carbon per year (glacial value). What is the change in atmospheric P_{CO_2} induced by this enhanced biological pump? Suppose for simplicity that

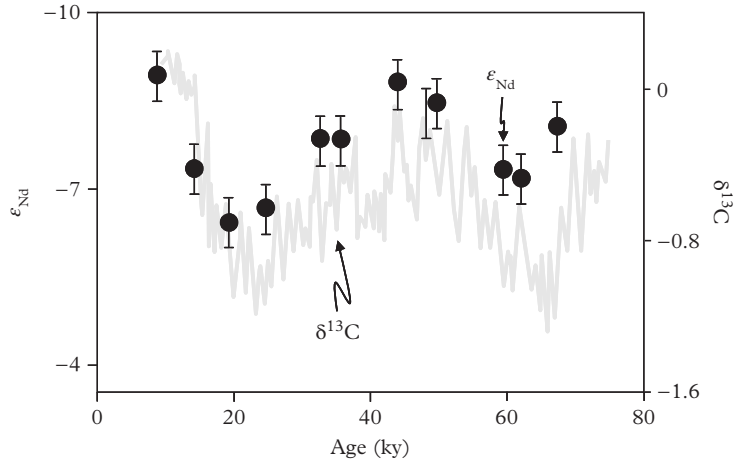

Figure 11.22 *$\delta^{13}C$ (gray curve) and ε_{Nd} (black dots) in a sediment core of the Atlantic Ocean.*

alkalinity remains constant and use a value of 10 for the Redfield ratio. Is this enough to explain the glacial-interglacial variations of the atmospheric P_{CO_2}?

Problem 6: Astronomical forcing and climate stability (Augustin et al., 2004)

Hydrogen isotopes measured in the Vostok ice core show that since 10,000 y, the Earth has experienced an interglacial period during which the climate has been remarkably

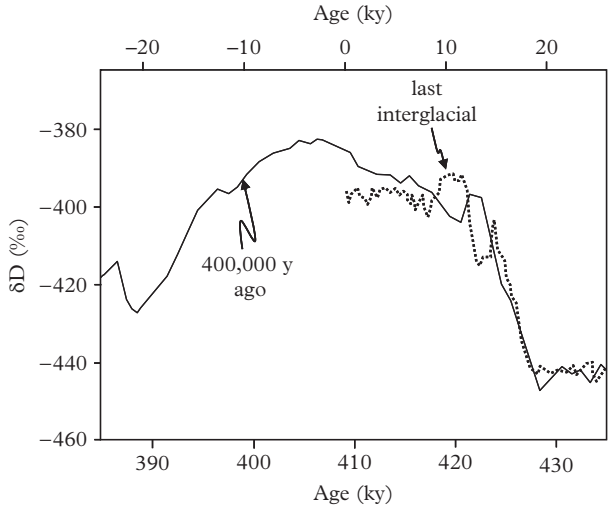

Figure 11.23 *δD of Antarctic ice during two interglacials. Dotted line: since 23,000 y. Continuous line: between 390,000 and 430,000 y. Modified after Augustin et al. (2004).*

stable compared to the previous interglacial periods (see Fig. 11.9). This is due to the low eccentricity of the Earth's orbit that produces a weak climatic forcing through equinox precession. According to you, at what period should we find an interglacial as stable as today? Figure 11.23 compares the δD of Antarctic ice since 23,000 y and between 390,000 and 430,000 y. Why should we compare the two periods? What can you conclude concerning climate stability in the future assuming that the anthropogenic perturbation can be mitigated?

Problem 7: Foraminifera's weight (Moy et al., 2009)

The weight of the Southern Ocean planktonic foraminifera tests has been determined for today's foraminifera collected in sediment traps, Holocene foraminifera collected in top core sediments and foraminifera that lived during the Last Glacial Maximum (LGM) collected deeper in the sediment core. For each period, 50 tests with sizes ranging from 300 to 355 mm are selected. The average weight of the tests is $18 \pm 5\,\mu g$ for present foraminifera, $24 \pm 3\,\mu g$ for Holocene foraminifera and $30 \pm 4\,\mu g$ for the foraminifera of the LGM. The deepest cores were collected under the lysocline, but for a given time period, there is no relationship between the weight of the foraminifera and the sampling depth. Explain the observed weight changes.

Problem solutions

1.1 (1) $\rho_{\text{Fram Strait}} = 1027.3$ kg m^{-3}. $\rho_{\text{Arctic Ocean}} < 1027.0$ kg m^{-3}.

(2) The Arctic surface water is very cold but it has a low density due to its very low salinity.

1.2 $\theta_{CDW} = f_{AAIW}\theta_{AAIW} + f_{NADW}\theta_{NADW} + f_{AABW}\theta_{AABW}$;
$S_{CDW} = f_{AAIW}S_{AAIW} + f_{NADW}S_{NADW} + f_{AABW}S_{AABW}$;
$f_{AAIW} + f_{NADW} + f_{AABW} = 1$;
from which we derive: f_{AAIW} : 18%, f_{NADW} : 24%, f_{AABW} : 56 %.

1.3 (1) The deepest buoy is below the Ekman layer and just follows the geostrophic current. The other buoys are driven by the sum of the Ekman drift and of the geostrophic current. By subtracting the lower buoy trajectory from the trajectories of the upper buoys, we obtain the Ekman drift.

(2) The buoy at 8 m drifts at 45° to the right of the wind. At depth, the direction of drift turns toward the right and the intensity of the drift decreases. This is the Ekman spiral.

1.4 From equation (1.13) and Figs. 1.15 and 1.16, upwelling: 70°S–55°S, 15°S–20°N and 50°N–65°N; downwelling: 50°S–20°S, 25°N–45°N and 70°N–80°N. Note that the sign of f changes with the hemisphere.

1.5 (1) upwelling of cold and deep water

(2) Toward the coast, the dynamic height decreases and the thermocline is uplifted.

(3) speed vector parallel to the lines of constant dynamic height. v_{max} at 41.8°N–125.5°W.

(4) 27 cm s^{-1}.

(5) Yes.

1.6 (1) Net transport: 0 Sv (Sverdrup transport balanced by the western boundary current.)

(2) 20 Sv.

(3) Northward net heat transport.

1.7 See the chapter.

2.1 93 Ma (equation 2.2)

2.2 0–50 m: oversaturation due to photosynthesis (chlorophyll maximum at 30 m). 60–150 m: undersaturation due to remineralization.

2.3 No, because the three measured points are not aligned in an S (conservative)–[In] diagram.

2.4 (1) the points form a straight line in a θ–S diagram, so it is a two-water mass mixing.

(2) no

(3) aragonite

(4) calcite dissolution → $(Sr/Ca)_{seawater} = 8.50$,
aragonite dissolution → $(Sr/Ca)_{seawater} = 8.63$.

(5) celestite dissolution → $(Sr/Ca)_{seawater} = 8.65$.

2.5 Between 0 and 100 m: O_2-rich water → Mn and Fe are oxidized as Mn^{4+} and Fe^{3+} (insoluble). Below 100 m: anoxic water → reduction of SO_4^{2-} to H_2S and of Mn^{4+} and Fe^{3+} (on the particles and sediment) into soluble Mn^{2+} and Fe^{2+}.

2.6 W: conservative. Co: particle reactive. Ni: non-limiting nutrient. Zn: limiting nutrient. Kr: rare gases. The increasing Kr concentration with depth is due to the temperature dependent solubility of Kr (temperature when water masses were in contact with the atmosphere).

2.7 (1) we call $[Fe_{available}]$ the concentration of iron not complexed by siderophores. From the course, at pH = 8, $[Fe^{3+}]/[Fe_{available}] = 10^{-20.7}$. So $[FeSid]/([Fe_{available}] \times [Sid]) = 10^{1.3}$. In addition, $[Fe_{available}] = [Sid] = 10^{-9}$ mol kg^{-1} – [FeSid]. Combining the two previous equations and solving, we obtain: $[Fe_{available}] = [Sid] = 0.2 \times 10^{-9}$ mol kg^{-1} and $[FeSid] = 0.8 \times 10^{-9}$ mol kg^{-1}. Most Fe is fixed by siderophores.

(2) Seawater is undersaturated with respect to $Fe_{available}$, iron hydroxides can dissolve spontaneously.

3.1 At the base (first 5 m): sea ice. At the top: snow ($\delta^{18}O \ll 0$). Between the two: mixture of snow and sea ice.

3.2 (1) Plotting the six samples in a $\delta^{13}C$ versus $1/[CO_2]$ diagram, there is a linear relationship (equation 3.10) corresponding to the oceanic air–gas exhaust mixing. $\delta^{13}C_{fuel} = -28‰$ (y-axis intercept), $\delta^{13}C_{oceanic\ air} = -7.5‰$ (ordinate for $1/[CO_2] = 1/370$ ppmv^{-1}).

(2) Respiration produces a signature ($\delta^{13}C_{breath} = -26‰$) distinct from exhaust gas.

3.3 Before 1950: Suess effect is not visible. After 1950: visible Suess effect.

3.4 (1) $\delta^{13}C$: Continental vegetation; $\delta^{18}O$: precipitations at mid-latitudes.

(2) Yes. The $\delta^{13}C$ of the contaminated water comes from oil, because runoff would also change the $\delta^{18}O$.

3.5 (1) $\delta^{13}C_f = \delta^{13}C_i + (\delta^{13}C_{organic\ matter} - \delta^{13}C_i)/DIC_f \times \Delta DIC$.

(2) $\delta^{13}C_f \approx \delta^{13}C_i - \Delta_{seawater-organic\ matter}/DIC \times R_{C/P} \times \Delta PO_4^{3-}$

3.6 The assimilable nitrogen concentration being zero in surface waters, the reaction is complete and there is no isotopic fractionation. As $\delta^{15}N_{trap}$ is different from $\delta^{15}N_{thermocline}$, there is dissolved N_2 fixation. Using equation (3.11b) and considering the nitrogen of the traps as a mixture between the thermocline nitrogen and N_2, we obtain: $f_{N_2} = 37\%$ in winter and 75% in summer.

3.7 Using equation (3.11b), we obtain: $f = 0\%$ upstream, 36% at the dumping site and 10% downstream.

3.8 (1) The dissolved Fe decreases while $\delta^{56}Fe_{dissolved}$ increases. There is biological uptake of Fe with light Fe preferential uptake.

(2) Before the bloom, $(Fe/Al)_{particles}$ is close (even lower) than $(Fe/Al)_{average\ crust}$ (= 0.2 mol mol^{-1}) → lithogenic particulate Fe with a heavy (crustal-like) $\delta^{56}Fe$. During the bloom, the high $(Fe/Al)_{particles}$ → most particulate Fe is biogenic in agreement with the low $\delta^{56}Fe$. However, the particulate Fe increase exceeds by far the dissolved Fe decrease, implying that an external input of Fe (of unknown signature) has occurred since the pre-bloom situation and makes any isotopic budget calculation very speculative.

3.9 (1) $\delta^{18}O = +13‰$ (Rayleigh distillation, equation 3.18 applied to O_2).

(2) $\delta^{18}O = 0‰$ (total reaction in microenvironments therefore not fractionation).

(3) The $\delta^{18}O$ value is intermediate. Therefore free bacteria and microenvironment bacteria are both active.

4.1 (1) Yes, the number of atoms remaining after seven half-lives is $N_0/2^7 = N_0/128$.

(2) 3 days ($N_0/2^{(7+3)} = N_0/1024$).

(3) Remaining activity = $(\ln(2)/T_{1/2}) \times (N_0/1024)$

4.2 (1) $t = -(\lambda_{14})^{-1} \times \ln((^{14}C/^{12}C)_{100cm}/(^{14}C/^{12}C)_{surface}) = 17{,}190$ y. It is assumed that when the foraminifer located now at 100 cm below the core top was alive, it had the same ($^{14}C/^{12}C$) ratio than the one deposited today at the top of the core.

(2) 58 mm ky^{-1}

4.3 (1) Plotting samples in a diagram $^{87}Sr/^{86}Sr$ versus 1/Sr, there is a linear relationship. There is therefore a conservative mixing between fresh water and seawater (equation 3.10).

(2) $^{87}Sr/^{86}Sr_{seawater} \approx 0.70912$.

(3) $[Sr]_{river} = 0.015$ ppm.

4.4 (1) $\varepsilon_{Nd}^{dust} = +6.5$.

(2) $f = 69\%$ (balance of concentrations), $f = 51\%$ (ε_{Nd} balance).

(3) hypothesis 2.

(4) seek for water mixing with a θ–S diagram.

4.5 (1) 1.134. The variation is small compared to the precision of the measurements. This is not a good chronometer.

(2) $\{^{238}U\}$ is constant over a few tens of thousands years. From the previous question, we consider that $\{^{234}U\}$ is also constant. $t \approx 1/\lambda_{230} \times \ln(1 - \{^{230}Th\}/\{^{234}U\})$. It follows that $t_1 = 7500$ y, $t_2 = 13,800$ y and $t_3 = 20,070$ y.

(3) U–Th ages are older than ^{14}C ages. In Problem 2, the deep foraminifer was in fact about 20,000 y old.

(4) Between 7500 y and 20,700 y ago, Earth's magnetic field was weaker than today. It allowed a stronger ^{14}C production and corals had higher in $^{14}C/^{12}C$ ratio than today. The ^{14}C ages of these old corals containing "a little too much ^{14}C" are too young.

4.6 $t = 13.4$ y.

4.7 $f_{Sellafield} = 10.4\%$, $f_{fallout} = 70.2\%$, $f_{military} = 19.4\%$.

5.1 (1) Production by cosmic rays is balanced by the radioactive decay: 112 atoms cm^2 $min^{-1} \times 4 \times \pi$ $(6400 \times 10^5$ cm$)^2 \times (60 \times 24 \times 365$ min $y^{-1}) = \lambda_{^{14}C} \times$ number of atoms. So that, number of ^{14}C atoms $= 2.5 \times 10^{30}$

(2) $^{14}C/^{12}C = 1.2 \times 10^{-12}$ mol mol^{-1}.

5.2 Conservation equation: $dC_d/dt = k_w(C_s - C_d) - \lambda C_d$. Taking $dt = 10$ y, $dC_d = C_{d(1981)} - C_{d(1971)}$ and $C_d = (C_{d(1981)} + C_{d(1971)})/2$ (average value), then $\tau_w = (k_w)^{-1} = 8$ y.

5.3 (1) $[Chl] = [Chl]_0 \times e^{\mu t}$

(2) Yes.

(3) $k_w = 0.0693$ $d^{-1} \rightarrow$ not negligible

(4) $d[Chl]/dt = (\mu - k_w)[Chl] + k_w[Chl]_0$

(5) $[Chl] = [Chl]_0 \times e^{(\mu - kw)t} + k_w[Chl]_0/(\mu - k_w) \times (1 - e^{(\mu - kw)t})$.

(6) Use the equation of question (5) to calculate [Chl] after 10 days for different values of μ: Chl] is multiplied by 10 when $\mu \approx 0.22$ d^{-1}.

5.4 (1) $k_w = 0.073$ y^{-1}.

(2) 15 μmol kg^{-1} y^{-1}.

5.5 (1) $\tau_{respiration} = 2000$–$4000$ y.

(2) Before the nuclear test period, newly formed DOC waters had a $\Delta^{14}C = -70$‰ (same value as the surface DIC). Assuming that $\Delta^{14}C_{average\ ocean}$ in the surface water ≈ -400‰ (intermediate value between new and old deep waters considered to represent most of the ocean): age of the DOC $= -1/\lambda_{14C} \ln((1-400‰)/(1-70‰)) = 3600$ y

5.6 (1) $\tau_w = 49$ y $\pm$ 79 y

(2) $\tau_w = 3.5$ y $\pm$ 3.5 y

(3) The second method gives a more accurate result.

5.7 (1) $k_w(C_0 - C) - \lambda C = 0$.

(2) See Chapter 4 and $\Delta t = -1/\lambda \times \ln(k_w/(k_w + \lambda))$.

(3) $k_w \gg \lambda$.

(4) When $k_w \ll \lambda$, Δt underestimates τ_w, because τ_w reflects the effect of disintegration and not circulation.

6.1 (1) SF_6 is larger and heavier than ^3He.

(2) 100 μm (for SF_6 and ^3He). $v_p(SF_6) = 793$ m y^{-1}, $v_p(^3He) = 1830$ m y^{-1}.

6.2 advection: 16 mmol m^{-3} y^{-1}, remineralization: 1 mmol m^{-3} y^{-1}, horizontal diffusion: 0.16 mmol m^{-3} y^{-1}, vertical diffusion: 0.05 mmol m^{-3} y^{-1}.

6.3 (1) $K_h = 1.6 \times 10^7$ cm^2 s^{-1}.

(2) $u = 25$ cm s^{-1}

6.4 (3) $\theta \approx (\theta_{5078} - \theta_{1000})e^{-w/K(z-1000)} - \theta_{5078}$.

(4) $w/K_z = 1.3 \times 10^{-3}$ m^{-1}.

(5) $K_z = 0.73$ cm^2 s^{-1}.

6.5 (1) $K_z \approx 0.12$ cm^2 s^{-1}

(2) $K_z \approx 4$ cm^2 s^{-1}.

(3) The stronger K_z in the Drake Passage is due to the perturbation of currents by the topography.

6.6 (1) over 12 days, $K_x \approx 4.8 \times 10^5$ cm^2 s^{-1} and over 42 days, $K_x \approx 6.7 \times 10^6$ cm^2 s^{-1}.

(2) K_x increases with the length scale.

7.1 (1) See the chapter.

(2) Spring bloom between 0 and 100 m, summer "bloom" in sub-surface (30–50 m).

7.2 (1) $GCP_{spring} = 2.9 \pm 1.3$ mmol O_2 m^{-3} d^{-1} and $GCP_{summer} = 0.6 \pm 2.1$ mmol O_2 m^{-3} d^{-1}.

(2) Converted to nitrogen with the Redfield ratio, it becomes: $GCP_{spring} = 25 \pm 11$ mmol N m^{-3} d^{-1} and $GCP_{summer} = 5 \pm 18$ mmol N m^{-3} d^{-1}, which is not significantly different from the PP.

(3) Spring: diatom (micro- and nanoplankton) dominates. Summer: easily remineralizable and less subject to limitations picoplankton dominates.

7.3 (1) Very strong stratification (no vertical mixing) and the cyclonic circulation is not due to the wind (no Ekman pumping) but to the shape of the basin.

(2) Input of nutrients by the rivers.

(3) Effect of the monsoon (wind reversal).

(4) South Pacific Ocean.

(5) It is on the western edge of the basin, but very warm water flowing from the Pacific through the Indonesian Straits blocks the upwelling.

7.4 In anticyclonic eddies, the deepening of the thermocline prevents nitrate upwelling, which promotes the N_2-fixing species.

7.5 (1) Fe input removes the limitation of organic matter production.

(2) $(Si/N)_{\text{Fe-repleted diatoms}} = 1.0$ and $(Si/N)_{\text{Fe-limited diatoms}} = 3.0$.

(3) Fe promotes a preferential assimilation of N compared to Si and therefore an N limitation rather than a Si limitation.

(4) With iron limitation, organic production is limited, but diatoms have heavier frustules so that export is more efficient (ballast effect).

7.6 (1) stronger wind

(2) more intense upwelling

(3) increased biological production

(4) increased biological production → increased remineralization in depth → $[O_2]$ decreases.

7.7 (1) An alga that grows rapidly increases the $\delta^{13}C$ of its environment that is not renewed quickly enough by molecular diffusion → the $\delta^{13}C$ of the alga increases.

(2) There was a decrease of the growth rate due to less abundant nutrients.

(3) Increase of the stratification.

(4) Suess effect.

(5) change of $\delta^{13}C_{atm} - 0.3‰$; change of $CO_{2atm} \rightarrow \approx -2‰$.

(6) very deep winter mixed layer → the Suess effect is not visible because too diluted → the initial approach remains valid.

8.1 See the chapter. On average over the year, the area is a CO_2 sink. It is an HNLC zone (non-limiting phosphate).

8.2 Sub-Antarctic zone and Southern Ocean: convection brings CO_2-rich deep waters at the ocean surface. Subtropical zone: CO_2 pumping by water cooling.

8.3

$$\frac{d\left[H^+\right]}{\left[H^+\right]} \approx \frac{d\,[CO_2]}{[CO_2]}\left(1 - \frac{2}{\zeta} \times \frac{CID}{\left[HCO_3^-\right]}\right)$$

In this case: $\frac{d\,[CO_2]}{[CO_2]} = +100\%$

$\zeta = 10$

$$\frac{CID}{\left[HCO_3^-\right]} \approx \frac{100\,\%}{90\,\%} \approx 1.1$$

Either $d[H^+]/[H^+] \approx 0.77$
If $pH_{280ppm} = -\log_{10}(10^{-8}) = +8$
then,
$pH_{560ppm} = -\log_{10}[(1 + 0.77) \times 10^{-8}] = +7.75$
The decline is therefore of 0.25 pH unit.

8.4 (1) We obtain: $\frac{d\left[CO_3^{2-}\right]}{\left[CO_3^{2-}\right]} \approx -\frac{d\,[CO_2]}{[CO_2]}\left(1 - \frac{4}{\zeta}\frac{CID}{\left[HCO_3^-\right]}\right)$
So that N. Atlantic: $CO_3^{2-} = 90\,\mu mol\ kg^{-1}$; tropical Atlantic: $CO_3^{2-} = 162\,\mu mol\ kg^{-1}$.

(2) The pteropods would live in a weakly supersaturated environment → no spontaneous dissolution but potential calcification problems.

8.5 No. In Paris, there is a quick mixing of ocean air and gas exhaust. Data collected over 10 y in Hawaii are affected by the mixing between oceanic air and fuel fossil but also by the exchange of CO_2 with the ocean.

8.6 (1) Ocean: 2.2 Gt C y^{-1}; continental biosphere: 1.6 Gt C y^{-1}.

(2) Applies only if the marine biosphere is steady state.

8.7 (1) O_2 corrected for remineralization with DIC and DIC itself corrected for the carbonate dissolution with alkalinity.

(2) Deep samples away from areas of rapid ventilation.

(4) The western boundary of the basin (see Chapter 10). From the surface to the bottom, C_{ant} = 108, 2, 17, 9 and 8 μmol kg^{-1}.

9.1 (1) τ_w = 1.4 h.

(2) $dC/dt = u dC/dx = -(k_w C + w_p/h \times C)$.

(3) $w_{p\_small\ particles}$ = 0.17 m d^{-1}, $w_{p\_medium\ particles}$ = 0.52 m d^{-1} and $w_{p\_large\ articles}$ = 0.88 m d^{-1}.

9.2 Advection: 86 km (1000 m trap) and 432 km (5000 m trap). Diffusion (equation 6.14): 42 km (1000 m trap) and 93 km (5000 m trap).

9.3 $C_{phytoplankton}$ = 89.2%, C_{DOC} = 5.1%, $C_{continental}$ = 5.7 %

9.4 Ra uptake at 200 m or mixture of Ra incorporated at the surface and in the deep Mediterranean Sea.

9.5 (1) Light limitation by under the ice.

(2) 88%.

(3) 133 mmol m^{-2} d^{-1} → strong overestimation.

9.6 (1) 1 cm (presence of $\{^{234}Th\}$ in excess to $\{^{238}U\}$ implies rapid input of recently deposited particulate matter).

(2) 0.88 cm^2 y^{-1}.

9.7 (1) sedimentation rate: 48 mm ky^{-1}.

10.1 (1) sinking of deep water (high salinity, CFC-rich and O_2 -rich) in the Aegean Sea.

(2) dry period → evaporation and salinity increase. Cooling of salted water → very dense water.

10.2 (1) NADW to 2500 m and AABW to 4000 m.

(2) No (see Fig. 10.10).

(3) The upwelling of deep water is not uniform but concentrated irregular topography.

10.3 (1) CFC-11: 20 μatm, CFC-12: 37 μatm, 1960–1965.

(2) 0.54. 1975–1990.

(3) The sample contains a small fraction (∼10%) of water that was equilibrated with the atmosphere around 1975–1990.

10.4 From equation (6.14), in the western part of the basin, $K_z = 0.5\ \text{cm}^2\ \text{s}^{-1}$ whereas in the eastern part $K_z = 7\ \text{cm}^2\ \text{s}^{-1}$.

10.5 (1) $\delta^{30}Si_{AABW} = \delta^{30}Si_{CDW}$ (Fig. 3.17). CDW fuels AABW formation and is Si-enriched by dissolution of opal formed in Si-replete surface waters with a relatively light $\delta^{30}Si$. $\delta^{30}Si_{NADW} \approx \delta^{30}Si_{AAIW/SAMW}$ (Fig. 3.17). SAMW/AAIW, intermediate waters of southern origin, flow through the thermocline to fuel low latitude surface/intermediate waters that will ultimately contribute to NADW formation. $\delta^{30}Si_{AABW} < \delta^{30}Si_{NADW}$ because SAMW/AAIW much less enriched in dissolved Si than AABW and this Si is supplied by dissolution of opal formed in Si-depleted surface waters with a heavy $\delta^{30}Si$.

(2) $Si(OH)_4$ behaves conservatively within the deep Atlantic. Particulate BSi dissolution is negligible, because there is little particulate BSi (opal) production and export from Si depleted surface waters. Opal cycling occurs mainly in the Southern Ocean that is not $Si(OH)_4$-limited (Fig. 7.13).

(3) Unlike $Si(OH)_4$, NO_3^- is completely depleted in the Atlantic surface waters → complete reaction → similar $\delta^{15}N$ during organic matter remineralization.

10.6 (1) Nansen: 169 y, Amundsen: 177 y, Canada: 468 y.

(2) Only the Amundsen basin has a relatively short residence time for a bit of tritium could enter.

10.7 (1) The differential equation is: $Kz\frac{\mathrm{d}^2C}{\mathrm{d}z^2} - \lambda C = 0$. By integrating, as for equation (6.33), and noting that far from the sediment, the ^{227}Ac concentration must tend toward 0, it follows that the ^{227}Ac vertical profile is therefore of the form: $C = C_0 e^{\sqrt{\lambda/K_z}z}$. K_z is determined with the result of two depths (5000 m and 6000 m): $K_z = \frac{\lambda(6000-5000)^2}{\left[\ln\left(\frac{1.2}{1.7}\right)\right]^2} = 2.6 \times 10^5 \text{m}^2/\text{y} \approx 80\ \text{cm}^2/\text{s}$

(2) and 3) diffusion dominates by far.

10.8 (1) The water exiting in 1989 arrived at the entrance of the Straits in 1981 ($C_e^{1981.3} \times e^{-\lambda(1989-1981.3)} = 0.663$) → $\Delta t = 7.7$ y.

(2) $F = 11.8$ Sv.

(3) In 1989, precipitations brought 4% (9×10^{12} TU y^{-1}) of tritium entering the Straits (2×10^{14} TU y^{-1}). In addition, part of the contribution of the precipitation is lost by evaporation. Trade with the atmosphere has little consequence on the estimation of question 2.

11.1 There was either an episode of high O_2 content in the atmosphere during Archean or these samples are all, for a reason which remains to be determined, derived from a source of sulfur with $\Delta^{33}S = 0$ (this signature in the Archean anyway and must correspond to a S source that has not transited through the atmosphere).

11.2 (1) Mo is soluble and conservative waters oxic; insoluble in reducing environment (see Chapter 2).

(2) Formation of crusts and nodules of Fe and Mn.

(3) 25%.

(4) 75%.

(5) More reducing the Proterozoic ocean, thus limiting possible Mo.

11.3 At the beginning of the crisis, the Sr has a purely marine signature. It shifts to a signature marked by the rivers, which is explained by a gradual reduction of the supply of seawater through the Gibraltar Strait.

11.4 The increase in ε_{Nd} shows an increased contribution of the AABW and disappearance of the NADW (see Fig. 4.7) in depth in accordance with $\delta^{13}C$.

11.5 Currently the biological pump maintains a difference of about 13% between the surface DIC (2000 μmol kg^{-1}) and the deep DIC (2300 μmol kg^{-1}). Fertilization will result in an increase of 6% of the biological pump, therefore, a decline of $13\% \times 6\% \approx 0.8\%$ of the surface DIC concentration. With a Revelle factor of 10, this decline of DIC corresponds to a 10% decrease of $P_{CO_2}^{atmosphere}$ (equation 8.15). For an atmosphere containing originally 280 ppmv CO_2, we obtain a decrease of –22 ppmv, which is much less than the –100 ppmv observed.

11.6 Without the anthropogenic perturbation, the climate would still remain stable 10,000 y before the next ice age.

11.7 Planktonic foraminifera weight is inversely proportional to the atmospheric CO_2 content, because the calcification rate decreases with the acidification level of surface waters.

Glossary

Abyssal plain the flat area of the deep ocean seafloor (between 4000 and 6000 m). It consists of basaltic oceanic crust (formed at mid-ocean ridges) covered with sediments.

Abyssal trench a deep (down to 11 km), long and narrow, underwater depression created by the oceanic crust when it sinks into the Earth's mantle in a subduction zone.

Activity number of disintegrations per unit of time produced by a radioactive isotope in a sample. Expressed in Becquerel (1 Bq = 1 disintegration per second), or in disintegration per minute (dpm)

Advection regular flow in given direction.

Alkalinity concentration of negative charges susceptible to neutralize the H^+ ion (to ensure the electro-neutrality of the solution)

Anthropogenic of human origin.

Anticyclonic which rotates clockwise in the northern hemisphere and counterclockwise in the southern hemisphere.

Autotrophic refers to a living being able to convert CO_2 into organic matter. Phytoplankton, like terrestrial plants uses light energy for this conversion (phototrophic). Some bacteria communities leaving around black smokers uses chemical energy (chemotrophic), because they live in the deep ocean, far from any source of light.

Benthos a set of species that make up the marine biomass living on the seafloor. It gives "benthic" as an adjective.

Biogeochemical cycle cyclic pathway of a chemical element at the Earth's surface, as it undergoes physical, chemical or biological processes.

Brunt–Väisälä frequency the number of oscillations per second of a water mass around its equilibrium depth when it returns to equilibrium after having being moved vertically out of equilibrium.

Carbonate the carbonate ion is CO_3^{2-}, but by extension carbonate also designates all the species that originate from the dissolution of CO_2 in water, which also includes the bicarbonate ion and dissolved CO_2 (carbonate system). Also refers to the solid $CaCO_3$ (calcium carbonate).

Chlorophyll one of the pigment from algae and autotrophic bacteria able to capture solar energy and to convert it into chemical energy.

Climate system all of the compartments of the planet who interact and play a role in the control of climate: atmosphere, ocean, biosphere, continental surfaces and ice.

Compensation depth depth below which a given mineral (e.g., carbonate) disappears from marine sediments because it is completely dissolved. The compensation depth

stands a few hundred meters below the lysocline. It also depends on the "rain rate" of the mineral from the ocean surface.

Conservative tracer parameter whose value changes only by mixing of water masses, when these water masses are isolated from the surface so that they cannot interact with the atmosphere (e.g., potential temperature or salinity).

Continental slope transition zone between the continental shelf (~100 m depth) and the abyssal plain (~4000 – 6000 m depth). It presents a slope generally between 1° and 5° but can be much more pronounced in the case of active margins as off the coast of the Chile.

Convection vertical mixing of water masses when the surface waters become denser than underlying waters.

Coriolis force not strictly speaking a force, but an acceleration term associated to Earth's rotation. As a result for an observer on Earth, the trajectory of water masses and air masses are generally not straight but they tend to be curved.

Continental shelf an extension of the continent covered by the sea. It has all the properties of a continent (same geological history). Usually covered with ~100 m of water, it may emerge during the glaciations. It can be very extended (1500 km wide for the Siberian plateau) or almost non-existent (Chilean coast)

Cyclonic that rotates counterclockwise in the northern hemisphere and clockwise in the southern hemisphere.

Decay constant the radioactive decay probability of atoms per unit of time. Its dimension is the inverse of a time (s^{-1}).

Denitrification chemical reaction (in this case a reduction) which converts nitrate (NO_3^-) into molecular nitrogen (N_2) or nitrogen monoxide (N_2O).

Density the density of a body is its mass divided by its volume. Seawater density depends on salinity, temperature and pressure. For surface seawater, it is approximately 1025 g m^{-3}. The density anomaly is the density expressed in kg m^{-3} minus 1000.

Diapycnal said of a transfer or motion that is perpendicular to surfaces of constant density.

Diffusion motion linked to random movements at microscopic (molecular diffusion) or macroscopic (turbulent diffusion) scale.

Dynamic height difference between the observed sea level and the level of the sea "at rest" (in the absence of forcings such as wind, evaporation, thermal expansion, precipitation, etc.).

Ekman layer the ocean surface layer directly affected by the effect of wind (around 50 m thick).

Ekman pumping vertical transport of seawater induced by wind. A cyclonic wind generates an upwelling (positive Ekman pumping). An anticyclonic wind forces surface water diving (negative Ekman pumping).

El Niño (or El Niño Southern Oscillation, ENSO) phenomenon returning irregularly with cycles of several years in which the decline of the trade wind intensity in the Pacific Ocean induces climatic disturbances in all the Pacific Ocean (drought in Indonesia, flooding in America, reduction of the equatorial upwelling, etc.) and beyond.

Euphotic layer the ocean surface layer where 99% of the sunlight is absorbed. Its thickness ranges from a few tens to 200 m depending on the water clarity.

Eutrophication increase in primary production because of the overabundance of nutrients. Remineralization of exported matter organic leads to a reduced oxygen concentration below the mixed layer.

Flux a quantity (of matter, of heat ...) flowing through a surface (which may be of unit size) per unit time, or a quantity (of matter, of heat ...) flowing in or out of a reservoir per unit time.

f-ratio the ratio of new production to primary production. It describes the efficiency of the vertical export of a biological system.

Greenhouse effect warming of the atmosphere due to greenhouse gases (water vapor, CO_2, CH_4, N_2O, O_3 and CFCs) that absorb infrared radiation emitted by the Earth's surface and re-emit a part toward the Earth's surface (creating warming).

Geoid theoretical surface corresponding to the surface of the ocean at rest (without wind, without evaporation/precipitation, without tides, etc.). At any point, the geoid is perpendicular to gravity. Because of the heterogeneous distribution of the masses in the Earth's mantle, the geoid height ranges from –60 to +100 m, but it is stable in time. The dynamic height of the ocean represents changes in the sea level of less than 1 m of amplitude which adds to the variation of the geoid.

Geostrophic current a current resulting from the equilibrium between the horizontal pressure gradient and the Coriolis force. This is the case of the main ocean currents (except in the equatorial zone where the Coriolis force vanishes).

Gyres refers to the great circular currents extending thousands of kilometers across different ocean basins. Created by the wind, they are anticyclonic at subtropical latitudes and cyclonic at subpolar latitudes.

Half-life also called period, it is the time required for half of an initial stock of radioactive atoms to disintegrate.

Heterotrophic refers to living beings needing to consume organic matter to develop, because they cannot directly use sunlight as an energy source.

Holocene the fourth and final epoch of the Neogene, one of the many interglacial periods of the Quaternary. It spans from 10,000 y ago to today. A current trend is to succeed to the Holocene with a new geological era: the Anthropocene, which expresses the role of the man on the climate.

Hyperbola of mixing form of the relationship between the concentration and isotopic tracer composition when two end-member are mixed in a conservative way in varying proportions (to obtain a mixing line, the isotopic composition must be plotted as a function of the inverse of the tracer concentration).

Isopycnal surface surfaces (and curves in oceanic sections) of equal density are called isopycnal surfaces. They are surfaces of preferential motion in the ocean.

Isotopes sets of the atoms that have the same atomic number but different mass (their neutron number differs). As they have the same number of electrons, isotopes of the same element have identical chemical properties.

Isotopic composition the abundance of the different isotopes of an element. Can also be used to refer to the isotope ratio.

Isotopic equilibrium state of two chemical phases/constituents that have constant isotopic compositions when they are in chemical equilibrium.

Isotopic exchange physical or chemical equilibrium between two phases in which the transfer of material is marked by a change in isotopic compositions.

Isotopic fractionation change of the isotopic composition of an element due to a (slight) difference in behavior of its isotopes during a physical, chemical or biological process.

Isotopic ratio the ratio of two isotopes of the same chemical element.

Kinetic that depends on the speed of physical or chemical reactions.

Limiting element chemical element or compound completely consumed by the biological activity so that its concentration becomes zero: its absence blocks the development of life.

Little ice age relatively cold period that extends from the end of the Renaissance to the nineteenth century. It is associated with a minimum of solar activity.

Lysocline depth below which water becomes undersaturated with respect to a mineral. Below the lysocline, this mineral dissolves spontaneously.

Mean lifetime inverse of the decay constant. It is the most probable lifetime (from the statistical point of view) of a radioactive isotope.

Medieval warm period warm period in Europe (between 800 and 1300 AD).

Metagenomic global study of the DNA collected in a given environment (like seawater).

Metaproteomic global study of the proteins collected in a given environment (like seawater).

Mixed layer the ocean surface layer stirred by the wind. It has constant physical and chemical characteristics (temperature, salinity, density).

Modal water layers of homogeneous water isolated from the surface by warming of surface water during spring: as they are denser than surface waters, they sink in the thermocline.

Nekton all living species that constitute "freely swimming" marine biomass.

Net community production part of the primary production of organic matter which is not destroyed by respiration. It is estimated from the oxygen concentration.

Non-conservative tracer a tracer whose concentration changes with physical, chemical or biological mechanisms other than water mass mixing.

North Atlantic oscillation (NAO) natural climate variation measured by the difference in pressure between the Azores and the Iceland, which intensity varies with cycles of several years. The NAO affects both the dynamics of the North Atlantic Ocean and the European climate. A high pressure difference (positive NAO Index) produced strong westerlies, relatively high ocean surface temperature and mild winters in Europe. A low differential pressure (negative NAO Index) produces opposite effects

pH expression of the H^+ ion concentration in a given solution ($pH = -\log[H^+]$).

Photosynthesis process by which plants capture solar energy and use it to transform the CO_2 and mineral salts dissolved organic matter.

Plankton a set of marine species which are "floating" marine biomass. It is divided in phytoplankton (vegetals), zooplankton (animals) but also bacterioplankton (bacteria).

Potential density the comparison of the density of two water masses has a meaning only if they are at the same depth (and therefore at the same pressure). It is the density recalculated for a reference pressure level (which is often atmospheric pressure).

Potential temperature when a water mass sinks to depth, it is compressed and its temperature increases. Water mass temperatures from different depths can be compared with the same reference, by using the potential temperature, which is the temperature that the water mass would have if it is brought adiabatically to the atmospheric pressure to remove the compressional heating effect.

Production the primary production refers to the organic matter photosynthesized in surface waters. It is the sum of the new production and regenerated production. New production: fraction of organic photosynthesized with nitrate (NO_3^-) as a source of nitrogen. Regenerated production: fraction of organic matter photosynthesized with ammonium ion (NH_4^+) as a nitrogen source. Exported production: fraction of the primary production exported to depth, below the photic layer.

Proterozoic geological period extending from 2.6 to 0.54 Ga (beginning of the Cambrian).

Proxy refers to a parameter (e.g., $\delta^{13}C$) recorded by a carrier phase (e.g., foraminiferal test) in an archive (e.g. sediment), to reconstruct another parameter of the natural system (dissolved phosphate in the deep waters).

Pumps (and counter-pumps) of CO_2 thermodynamic and biological processes that facilitate (or is opposed to) the penetration of CO_2 in seawater.

Pycnocline water layer in which the density varies strongly and often corresponding to the thermocline.

Radioactivity physical property of unstable isotopes. They are susceptible to disintegrate spontaneously by emitting radiation of type α, β or γ.

Radioactive disequilibrium characterizes a parent–daughter pair of radioactive isotopes in which the parent and daughter activities are different: the secular equilibrium is not reached.

Radiogenic Produced by radioactive decay: refers to the "daughter" isotope produced by disintegration.

Rayleigh distillation originally, it was a mechanism to separate two liquids (water/alcohol) by preferential evaporation and extraction of the most volatile one. By extension, it is a physical, chemical or biological process during which products are systematically separated from the reactants, which led to a rapid change of the isotopic composition of the products and reactants.

Redox refers to chemical reactions coupling oxidation (loss of electron) and reduction (gain of electrons).

Remineralization transformation of organic matter (made of mineral molecules by photosynthesis) in mineral molecules. More or less synonymous with respiration.

Reservoir age this is the "apparent" age of a radioactive tracer (as it is calculated from the radioactivity equation) when it is introduced into a reservoir.

Residence time the time required to build up the stock of an element/chemical compound in a reservoir that was originally free of this element/compound or to remove this element/compound from a reservoir that was originally filled with it.

Respiration first refers to oxygen consumption and CO_2 production accompanying consumption (oxidation) of organic matter, but applies also to the production of other mineral salts from the organic matter (synonym of remineralization).

Ridge (or mid-ocean ridge) an underwater volcanic mountain range. It is a boundary where two tectonic plates diverge from each other with creation of oceanic crust. Oceanic ridges are typically 2000 or 3000 m high.

Salinity represents the weight of solid residue (expressed in grams) when a kilogram of seawater is evaporated. It is now estimated from the electrical conductivity and the temperature of seawater.

Scavenging uptake of poorly soluble or insoluble metals on marine particles and their removal from the water column by the fall of particles.

SeaWiFS satellite equipped with sensors capable of determining the ocean color, which depends on the abundance of phytoplankton pigments at the ocean surface.

Secular equilibrium applies to a parent–daughter pair of two radioactive isotopes. When the daughter has a shorter period than the parent, the secular equilibrium is reached when the decay rate of the daughter (daughter activity) is equal its production rate the parent decay (parent activity). The amount of daughter isotope is then constant and determined by the decay rate of the parent isotope.

Sink process (other than transport by a current) destroying/removing a tracer from a reservoir.

Source process (other than transport by a current) producing/introducing a tracer in a reservoir.

Stratification under the effect of gravity, the ocean density increases with depth, the lightest water being at the surface and densest ones always being in the deep ocean. Warming of surface water by the sun strongly contributes to the stable stratification of surface waters.

Subduction of the isopycnal surface sinking of dense water under light surface water, along isopycnal surfaces which initiates the modal water formation.

Suess effect change of the carbon isotopic composition ($\delta^{13}C$, $\Delta^{14}C$) of the atmosphere, ocean and biosphere due to the combustion of coal and oil.

Sverdrup transport Meridian transport of water masses that is proportional to the wind curl.

Thermocline water layer in which there is a strong vertical gradient of temperature. The permanent thermocline is the transition between the warm surface waters and the deep cold waters. It extends roughly from 200 to about 1000 m. In summer, surface water warming creates a seasonal thermocline that is destroyed in winter.

Thermodynamics that which relates or which depends on the flow of energy.

Thermodynamic equilibrium state of a physical or chemical reaction when the quantities of products and reactants do not vary any longer.

Thermohaline that depends on the heat and salt content.

Time constant for a process affecting an element with a first-order kinetics, it is the probability per unit time that the element goes through this process. The time constant multiplied by the element concentration is a flux.

Tracer chemical element, isotope or parameter such as temperature which allows a process in the ocean to be followed (traced).

Transform faults boundary between two tectonic plates along which the two plates slide horizontally.

Transient said of anthropogenic tracers which are injected into the natural system over a short time period.

Transport the average speed of a current multiplied by the depth of the current or the current flux divided by the width of the current.

Turbidity the cloudiness of a liquid due to the presence of suspended particles that absorb, scatter or reflect light.

Turbulence complex physical mechanism causing random (and difficult to model) motions in a fluid.

Ventilation when a water mass is at the ocean surface, its oxygen content is at equilibrium with the atmosphere. If, subsequently, this water mass quit the surface, it refills the deep ocean with oxygen by renewing oxygen depleted waters.

Volatile which easily evaporates under temperature and pressure conditions common at the Earth's surface.

Vorticity defined as the curl of the speed, it is used to estimate the spinning motion of a fluid. Water masses and air masses have a planetary vorticity due to the Earth's rotation around its axis and a relative vorticity corresponding to a rotation in a coordinate system fixed relative to the Earth (a swirl motion for example). The total vorticity is the sum of the planetary vorticity and of the relative vorticity. The potential vorticity is the ratio between the total vorticity of a water mass and its thickness. Away from the ocean borders, the potential vorticity is a conservative property.

Water mass large water volume with fairly homogeneous properties (temperature, salinity, etc.) indicating a common origin.

References

Abe K., 2004. Cadmium distribution in the Western Pacific. In *Global environmental change in the ocean and on land* (ed. M. Shiyomi, H. Kawahata, H. Koizumi, A. Tsuda, and Y. Awaya), pp. 189–203. TERRAPUB.

Abraham E. R., Law C. S., Boyd P. W., Lavender S. J., Maldonado M. T., and Bowle A., 2000. Importance of stirring during the development of an iron-fertilized phytoplankton bloom. Nature 407, 727–730.

Albarède F., 1995. *Introduction to geochemical modeling*. Cambridge University Press.

Alibo D. S., Nozaki Y., and Jeandel C., 1999. Indium and yttrium in North Atlantic and Mediterranean waters: comparison to the Pacific data. Geochim. Cosmochim. Acta 63, 1991–1999.

Allègre C. J., 2008. *Isotope geology*. Cambridge University Press.

Alleman L., 1997. Apport des isotopes stables du plomb au suivi des traces métalliques en Méditerranée et en Atlantique Nord. Ph.D. Thesis, University of Aix-Marseille III, France.

Altabet M. A. and François R., 1994. The use of nitrogen isotopic ratio for reconstruction of the past changes in surface ocean nutrients utilization. In *Carbon cycling in the glacial ocean: constraints on the ocean's role on the global change*, Vol. 117 (ed. R. Zhan), pp. 281–306. Springer-Verlag.

Anbar A. D., 2004. Molybdenum stable isotopes: observations, interpretations and directions. Rev. Mineral. Geochem. 55, 429–454.

Anbar A. D., Creaser R. A., Papanastassiou D. A., and Wasserburg G. J., 1992. Rhenium in seawater: confirmation of a generally conservative behavior. Geochim. Cosmochim. Acta 56, 4099–4103.

Anderson R. F., Fleisher M. Q., Biscaye P. E., Kumar N., Ditrich B., Kubik P., and Suter M., 1994. Anomalous boundary scavenging in the Middle Atlantic Bight: evidence from ^{230}Th, ^{231}Pa, ^{10}Be and ^{210}Pb. Deep Sea Res. II 41, 537–561.

Andersson P. S., Wasserburg G. J., and Ingri J., 1992. The source and transport of Sr and Nd isotopes in the Baltic Sea. Earth Planet. Sci. Lett. 113, 459–472.

Andrié C. and Merlivat, L., 1988. Tritium in the western Mediterranean Sea during 1981 *Phycemed* cruise. Deep Sea Res. 35, 247–267.

Andrié C., Rhein M., Freudenthal S., and Plan O., 2002. CFC time series in the deep water masses of the western tropical Atlantic. Deep Sea Res. 49, 281–304.

Andrié C., Ternon J.-F., Messias M.-J., Memery L., and Bourlès B., 1998. Chlorofluoromethane distributions and deep circulation in the deep equatorial atlantic during january-march 1993. Deep Sea Res. 45, 903–930.

Arneborg J., J. H., Lynnerup N., Nielsen H. L., Rud N., and Sveinbjörnsdóttir A. E., 1999. Change of diet of the Greenland Vikings determined from stable carbon isotope analysis and ^{14}C dating of their bones. Radiocarbon 41, 157–168.

Arraes-Mescoff R., Coppola L., Roy-Barman M., Souhaut M., Tachikawa K., Jeandel C., Sempéré R., and Yoro C., 2001. The behavior of Al, Mn, Ba, Sr, REE and Th isotopes during in vitro bacterial degradation of large marine particles. Mar. Chem. 73, 1–19.

Arrigo K. R. and van Dijken G. L., 2011. Secular trends in Arctic Ocean net primary production. J. Geophys. Res. Oceans 116(C9).

Augustin L., Barbante C., Barnes P. R., Barnola J. M., Bigler M., Castellano E., Cattani O., Chappellaz J., Dahl-Jensen D., Delmonte B., and Dreyfus G., 2004. Eight glacial cycles from an Antarctic ice core. Nature 429, 623–628.

Bacon M. P., Huh C.-H., Fleer A. P., and Deuser W. G., 1985. Seasonality in the flux of natural radionuclides and plutonium in the deep Sargasso Sea. Deep Sea Res. 32, 273–286.

Bange H. W., Wajih S., Naqvi A., and Codispoti L. A., 2005. The nitrogen cycle in the Arabian Sea. Prog. Oceanogr. 65, 145–158.

Barbante C. and Fischer H., 2010. Climate of the last million years: new insights from EPICA and other records. Quaternary Sci. Rev. 29, 1–7.

Bard E., Hamelin B., Fairbanks R. G., and Zindler A., 1990. Calibration of the ^{14}C timescale over the past 30,000 years using mass spectrometric U–Th ages from Barbados corals. Nature 345, 405–410.

Barth J. A., Pierce S. D., and Smith R. L., 2000. A separating coastal upwelling jet at Cape Blanco, Oregon and its connection to the California Current System. Deep Sea Res. II 47, 783–810.

Barth S., 1998. $^{11}B/^{10}B$ variations of dissolved boron in a freshwater–seawater mixing plume (Elbe estuary, North Sea). Mar. Chem. 62, 1–14.

Baskaran M., Swarzenski P. W., and Porcelli D., 2004. Role of colloidal material in the removal of ^{234}Th in the Canada Basin of the Arctic Ocean. Deep Sea Res. 50, 1353—1373.

Bates N. R., Best M. H. P., Neely K., Garley R., Dickson A. G., and Johnson R. J., 2012. Detecting anthropogenic carbon dioxide uptake and ocean acidification in the North Atlantic Ocean. Biogeosciences 9, 2509–2522.

Battle M., Bender M. L., Tans P. P., White J. W. C., Ellis J. T., Conway T., and Francey R. J., 2000. Global carbon sinks and their variability inferred from atmospheric O_2 and $\delta^{13}C$. Science 287, 2467–2470.

Beauvais S., Pedrotti M. L., Villa E., and Lemée R., 2003. Transparent exopolymer particle (TEP) dynamics in relation to trophic and hydrological conditions in the NW Mediterranean Sea. Mar. Ecol. Prog. Ser. 262, 97–109.

Behrenfeld M. J., O'Malley R. T., Siegel D. A., McClain C. R., Sarmiento J. L., Feldman G. C., Milligan A. J., Falkowski P. G., Letelier R. M., and Boss E. S., 2006. Climate-driven trends in contemporary ocean productivity. Nature 444, 752–755.

Beining P. and Roether W., 1996. Temporal evolution of CFC-11 and CFC-12 concentrations in the ocean interior. J. Geophys. Res. 101, 16455–16464.

Benner R. and Amon R. M. 2015. The size-reactivity continuum of major bioelements in the ocean. Annu. Rev. Mar. Sci. 7, 185–205.

Bender M. L., 1990. The $\delta^{18}O$ of dissolved O_2 in seawater: a unique tracer of circulation and respiration in the deep-sea. J. Geophys. Res. 95, 22243–22252.

Biller, S. J., Berube, P. M., Lindell, D., and Chisholm, S. W., 2015. Prochlorococcus: the structure and function of collective diversity. Nature Reviews Microbiology 13, 13–27.

Blain S., Tréguer P., Belviso S., Bucciarelli E., Denis M., Desabre S., Fiala M., Martin-Jézéque l. V., Le Fèvre J., Mayzaud P., Marty J.-C., and Razouls S., 2001. A biogeochemical study of the island mass effect in the context of the iron hypothesis: Kerguelen Islands, Southern Ocean. Deep Sea Res. I 48, 163–187.

Bopp L., Kohfeld K. E., Le Quére C., and Aumont O., 2003. Dust impact on marine biota and atmospheric CO_2 during glacial periods. Paleoceanography 18, DOI: 10.1029/2002PA000810.

Bopp L., Resplandy L., Orr J. C., Doney S. C., Dunne J. P., Gehlen M., Halloran P., Heinze C., Ilyina T., Séférian R., and Tjiputra J., 2013. Multiple stressors of ocean ecosystems in the 21st century: projections with CMIP5 models. Biogeosciences 10, 6225–6245.

Bouttes N., Paillard D., Roche D. M., Brovkin V., and Bopp L., 2011. Last Glacial Maximum CO_2 and $\delta^{13}C$ successfully reconciled. Geophys. Res. Lett. 38, L02705.

Braungardt C. B., Achterberg E. P., Elbaz-Poulichet F., and Morley N. H., 2003. Metal geochemistry in a mine-polluted estuarin system in Spain. Appl. Geochem. 18, 1757–1771.

Broecker W. S. and Maier-Reimer E., 1992. The influence of air and sea exchange on the carbon isotope distribution in the sea. Global Biogeochem. Cycles 6, 315–320.

Broecker W. S. and Peng T. H., 1982. *Tracers in the sea*. Lamont-Doherty Geological Observatory, Columbia University.

Broecker W. S. and Peng T. H., 1998. *Greenhouse puzzles*. 2nd ed. Eldigio Press.

Broecker W. S., Blanton S., Smethie Jr. M., and Ostlund G., 1991. Radiocarbon decay and oxygen utilization in the deep Atlantic Ocean. Global Biogeochem. Cycles 5, 87–117.

Buesseler K. O., Jayne S. R., Fisher N. S., Rypina I. I., Baumann H., Baumann Z., Breier C. F., Douglass E. M., George J., Macdonald A. M., Miyamoto H., Nishikawa J., Pike S. M., and Yoshida S., 2012. Fukushima-derived radionuclides in the ocean and biota off Japan. Proc. Natl. Acad. Sci. 109, 5984-5988.

Bruland K. W. and Lohan M. C., 2003. Controls of trace metals in seawater. In *Treatise on geochemistry*, Vol. 6 (ed. K. Turekian), pp. 23–47. Elsevier.

Brum J. R., Schenck R. O., and Sullivan, M. B., 2013. Global morphological analysis of marine viruses shows minimal regional variation and dominance of non-tailed viruses. ISME J. 7, 1738–1751.

Burkhardt S., Amorosa G., Riebesell U., and Sultermeyer D., 2001. CO_2 and HCO_3^- uptake in marine diatoms to different CO_2 concentrations. Limnol. Oceanogr. 46, 1378–1391.

Burton K. W., Ling H.-F., and O'Nions R. K., 1997. Closure of the Central American isthmus and its impact on North Atlantic deepwater circulation. Nature 386, 382–385.

Caldeira K., Archer D., Barry J. P., Bellerby R. G., Brewer P. G., Cao L., Dickson A. G., Doney S. C., Elderfield H., Fabry V. J., and Feely R. A., 2007. Comment on "'Modern-age buildup of CO_2 and its effects on seawater acidity and salinity"' by Hugo A. Loaiciga. Geophys. Res. Lett. 34, DOI: 10.1029/2006GL027288.

Canfield D. E., 1998. A new model for proterozoic ocean chemistry. Nature 396, 450–453.

Caschetto S. and Wollast R., 1977. Vertical distribution of dissolved aluminum in the mediterranean sea. Mar. Chem 7, 141–155.

Cazenave A., Lombard A., and Llovel W., 2008. Present-day sea level rise: a synthesis. C. R. Geosci. 340, 761–770.

Chereskin T. K., 1995. Direct evidence for an Ekman balance in the California Current. J. Geophys. Res. 100, 18261–18269.

Choi M. S., Francois R., Sims K., Bacon M. P., Brown-Leger S., Fleer A. P., Ball L., Schneider D., and Pichat S., 2001. Rapid determination of ^{230}Th and ^{231}Pa in seawater by desolvated micro-nebulisation inductively comupled mass spectrometry. Mar. Chem. 76, 99–112.

Chou L. and Wollast R., 1997. Biogeochemical behavior and mass balance of dissolved aluminum in the western Mediterranean Sea. Deep Sea Res. 44, 741–768.

Coale K. H. and Bruland K. W., 1987. Oceanic stratified euphotic zone as elucidated by ^{234}Th:^{238}U disequilibria. Limnol. Oceanogr. 32, 189–200.

Conway T. M. and John S. G., 2014. Quantification of dissolved iron sources to the North Atlantic Ocean. Nature 511, 212–215.

Coppin-Montégu G., 1996. *Chimie de l'eau de mer*. Paris: Institut Océanographique.

Coppola L., Roy-Barman M., Wassmann P., Mulsow S., and Jeandel C., 2002. Calibration of sediment traps and particulate organic carbon export using ^{234}Th in the Barents Sea. Mar. Chem. 80, 11—26.

Cózar A., Echevarría F., González-Gordillo J. I., Irigoien X., Úbeda B., Hernández-León S., Palma Á. T., Navarro S., García-de-Lomas J., Ruiz A., and Fernández-de-Puelles M. L., 2014. Plastic debris in the open ocean. Proc. Natl. Acad. Sci. 111, 10239–10244.

Craig H. and Hayward T., 1987. Oxygen supersaturation in the ocean: biological versus physical contributions. Science 235, 199–202.

Cullen J. T., Rosenthal Y., and Falkowski P. G., 2001. The effect of anthropogenic CO_2 on the carbon isotope composition of marine phytoplankton. Limnol. Oceanogr. 46, 996–998.

Cummins R. C., Finnegan S., Fike D. A., Eiler J. M., and Fischer W. W., 2014. Carbonate clumped isotope constraints on Silurian ocean temperature and seawater $\delta^{18}O$. Geochim. Cosmochim. Acta 140, 241–258.

Dandonneau Y. and Jeandel C., 1998. Le cycle océanique du carbone: la machine thermodynamique et la jungle biologique. Pour la Science, special issue on "Les Humeurs de l'Océan".

Dandonneau Y. and Le Bouteillier A., 1992. A simple and rapid device for measuring planktonic primary production by in situ sampling, and ^{14}C injection and incubation. Deep Sea Res. 39, 795–803.

Davis C. S. and McGillicuddy Jr D. J., 2006. Transatlantic abundance of the N_2-fixing colonial cyanobacterium Trichodesmium. Science 312, 1517–1520.

De La Rocha C. L., Brzezinski M. A., and DeNiro M. J. 1997. Fractionation of silicon isotopes by marine diatoms during biogenic silica formation. Geochim. Cosmochim. Acta 61, 5051–5056.

De Villiers S., 1999. Seawater strontium and Sr/Ca variability in the Pacific and Atlantic Ocean. Earth Planet. Sci. Lett. 171, 623–634.

Deleersnijder E., Campin J.-M., and Delhez E. J. M. 2001. The concept of age in marine modelling. I. Theory and preliminary model results. J. Mar. Syst. 28, 229–267.

Dickson B., 1997. From the Labrador Sea to global change. Nature 386, 649–650.

Dilling L. and Alldredge A., 2000. Fragmentation of marine snow by swimming macrozooplankton: a new process impacting carbon cycling in the sea. Deep Sea Res. 47, 1227–1245.

Doney S. C., Jenkins W. J., and Ostlung H. G., 1993. A tritium budget for the North Atlantic. J Geophys. Res. 98, 18069–18081.

Donnadieu Y., Goddéris Y., Ramstein G., Nédélec A., and Meert J., 2004. A "snowball Earth" climate triggered by continental break-up through changes in runoff. Nature 428, 303–306.

Druffel E. R. M., Williams P. M., Bauer J. E., and Ertel J. R., 1992. Cycling of dissolved and particulate organic matter in the open ocean. J. Geophys. Res. 97, 15639–15659.

Duce R. A., Liss P. S., Merrill J. T., Atlas E. L., Buat-Ménard P., Hicks B. B., Miller J. M., Prospero J. M., Arimoto R., Church T. M., Ellis W., Galloway J. N., Hansen L., Jickells T. D., Knap A. H., Reinhardt K. H., Schneider B., Soudine A., Tokos J. J., Tsunogai S., Wollast R., and Zhou M., 1991. The atmospheric input of trace species to the world ocean. Global Biogeochem. Cycles 5, 193–259.

Duplessy J.-C., 2004. La circulation globale de l'océan et ses variations dans le passé. C. R. Geosci. 336, 657–666.

Dutta K., Bhushan R., and Somayajulu B. L. K., 2007. Rapid vertical mixing rates in deep waters of the Andaman Basin. Sci. Total Environ. 384, 401–408.

Edmond J. M., Measures C., McDuff R. E., Chan L. H., Collier R., Grant B., Gordon L. I., and Corliss J. B., 1979. Ridge crest hydrothermal activity and the balances of the major and minor elements in the ocean: the Galapagous data. Earth Planet. Sci. Lett. 46, 1–18.

Ellwood M. J., Hutchins D. A., Lohan M. C., Milne A., Nasemann P., Nodder S. D., Sander S. G., Strzepek R., Wilhelm S. W., and Boyd, P. W., 2015. Iron stable isotopes track pelagic iron cycling during a subtropical phytoplankton bloom. Proc. Natl. Acad. Sci. 112, E15–E20.

Emerson S. and Hedges J., 2008. *Chemical oceanography and the marine carbon cycle.* Cambridge University Press.

Epstein S., Buchsbaum R., Lowenstam H. A., and Urey H. C., 1953. Revised carbonate–water isotopic temperature scale. GSA Bull. 64, 1315–1326.

Fairbanks R. G., Mortlock R. A., Chiu T.-C., Cao L., Kaplan A., Guilderson T. P., Fairbanks T. W., Bloom A. L., Grootes P. M., and Nadeau M.-J., 2005. Radiocarbon calibration curve spanning 0 to 50,000 years BP based on paired $^{230}Th/^{234}U/^{238}U$ and ^{14}C dates on pristine corals. Quaternary Sci. Rev. 24, 1781–1796.

Farquhar J., Peters M., Johnston D. T., Masterson A., Wiechert U., and Kaufman A. J., 2007. Isotopic evidence for Mesoarchaean anoxia and changing atmospheric sulphur chemistry. 449, 706–709.

Flecker R., de Villiers S., and Ellam R. M., 2002. Modelling the effect of evaporation on the salinity–$^{87}Sr/^{86}Sr$ relationship in modern and ancient marginal-marine systems: the Mediterranean Messinian Salinity Crisis. Earth Planet.Sci. Lett. 203, 221–233.

Forero M. G., Hobson K. A., Bortolotti G. R., Donazar J. A., Bertellotti M., and Blanco G., 2002. Food ressource utilisation by the Magellanic penguin evaluated through stable-isotope analysis: segregation by sex and age and influence on offspring quality. Mar. Ecol. Prog. Ser. 234, 289–299.

François R., Altabet M. A., Goericke R., McCorkle D. C., Brunet C., and Poisson A., 1993. Changes in the $\delta^{13}C$ of surface water particulate organic matter across the subtropical convergence in the SW Indian Ocean. Global Biogeochem. Cycles 7, 627–644.

François, R., Frank, M., Rutgers van der Loeff, M. M., and Bacon, M. P., 2004. ^{230}Th normalization: an essential tool for interpreting sedimentary fluxes during the late Quaternary. Paleoceanography 19(1).

Freudenthal S. and Andrié C., 2002. The arrival of a "new" Labrador Sea Water signal in the tropical Atlantic in 1996. Geophys. Res. Lett. 29.

Friedli H., Lötscher H., Oeschger H., Siegenthaler U., and Stauffer B., 1986. Ice core record of the $^{13}C/^{12}C$ ratio of atmospheric CO_2 in the past two centuries. Nature 324, 237–238.

Fripiat F., Cavagna A. J., Dehairs F., Brauwere A. D., André L., and Cardinal D. 2012. Processes controlling the Si-isotopic composition in the Southern Ocean and application for paleoceanography. Biogeosciences 9, 2443–2457.

Garabato, A. C. N., Polzin, K. L., King, B. A., Heywood, K. J., & Visbeck, M., 2004. Widespread intense turbulent mixing in the Southern Ocean. Science 303, 210–213.

Gary S. F., Lozier M. S., Biastoch A. and Böning C. W., 2012. Reconciling tracer and float observations of the export pathways of Labrador Sea Water. Geophys. Res. Lett., 39, L24606.

Georg R. B., West A. J., Basu A. R., and Halliday A. N., 2009. Silicon fluxes and isotope composition of direct groundwater discharge into the Bay of Bengal and the effect on the global ocean silicon isotope budget. Earth Planet. Sci. Lett. 283, 67–74.

Grasse P., Ehlert C., and Frank M., 2013. The influence of water mass mixing on the dissolved Si isotope composition in the Eastern Equatorial Pacific. Earth Planet. Sci. Lett. 380, 60–71.

Guidi L., Chaffron S., Bittner L., Eveillard D., Larhlimi A., Roux S.,... and Gorski G., 2016. Plankton networks driving carbon export in the oligotrophic ocean. Nature 532, 465–470.

Guieu C., Roy-Barman M., Leblond N., Jeandel C., Souhaut M., Le Cann B., Dufour A., and Bournot C., 2005. Vertical particle flux in the North-East Atlantic Ocean (POMME experiment). J. Geophys. Res. 110, DOI: 10.1029/2004JC002672.

Habitch K. S., Gabe M., Thamdrup B., Berg P., and Canfield D. E., 2002. Calibration of sulfate levels in the archean ocean. Science 298, 2372–2374.

Halkin D. and Rossby T., 1985. The structure and transport of the Gulf Stream at 73 W. J. Phys. Oceanogr. 15, 1439–1452.

Hamelin B., Ferrand J. L., Alleman L., Nicolas E., and Veron A., 1997. Isotopic evidence of pollutant lead transport from North America to the Subtropical North Atlantic Gyre. Geochim. Cosmochim. Acta 61, 4423–4428.

Hansell D. A. and Carlson C. A., 1998. Deep-ocean gradients in the concentration of dissolved organic carbon. Nature 395, 263–266.

Hatta M., Measures C. I., Wu J., Roshan S., Fitzsimmons J. N., Sedwick P., and Morton P., 2014. An overview of dissolved Fe and Mn distributions during the 2010–2011 US GEOTRACES north Atlantic cruises: GEOTRACES GA03. Deep Sea Res. II 116, 117–129.

Hattenrath-Lehmann T. K., Marcoval M. A., Berry D. L., Fire S., Wang Z., Morton S. L., and Gobler C. J., 2013. The emergence of *Dinophysis acuminata* blooms and DSP toxins in shellfish in New York waters. Harmful Algae 26, 33–44.

Hautala S. L., Roemmich D. H., and Schmitz Jr. W. J., 1994. Is the North Pacific in Sverdrup balance along 24°N? J. Geophys. Res. 99, 16041–16052.

Hayes C. T., Anderson R. F., Jaccard S. L., François R., Fleisher M. Q., Soon M., and Gersonde R. 2013. A new perspective on boundary scavenging in the North Pacific Ocean. Earth Planet. Sci. Lett. 369, 86–97.

Hayes C. T., Anderson R. F., Fleisher M. Q., Huang K. F., Robinson L. F., Lu Y., Cheng H., Edwards R. L., and Moran S. B., 2014. ^{230}Th and ^{231}Pa on GEOTRACES GA03, the US GEOTRACES North Atlantic transect, and implications for modern and paleoceanographic chemical fluxes. Deep Sea Res. II 116, 29–41.

Hayes G. C., Richardson A. J., and Robinson C., 2005. Climate change and marine plankton. Trends Ecol Evol. 20, 337–344.

Hedges J. I., Baldock J. A., Gélinas Y., Lee C., Peterson M. L., and Wakeham S. G., 2002. The biochemical and elemental compositions of marine plankton: a NMR perspective. Mar. Chem. 78, 47–63.

Hellerman S. and Rosenstein M., 1983. Normal monthly wind stress over the world ocean with error estimate. J. Phys. Oceanogr. 13, 1093–1104.

Hendricks M. B., Bender M., and Barnett B., 2004. Net and gross O_2 production in the Southern Ocean from measurements of biological O_2 saturation and its triple isotope composition. Deep Sea Res. I 51, 1541—1561.

Hensen C., Pfeifer K., Wenzhöfer F., Volbers A., Schulz S., Romero O., and Seiter K., 2004. Fluxes at the benthic boundary layer—A global view from the South Atlantic. In *The South Atlantic in the Late Quaternary* (ed. G. Wefer, S. Mulitza, and C. Rühlemann). Springer.

Hobson K. A., Blight L. K., and Arcese P., 2015. Human-induced long-term shifts in gull diet from marine to terrestrial sources in North America's coastal Pacific: more evidence from more isotopes (δ^2H, δ^{34}S). Environ. Sci. Technol. 49, 10834–10840.

Hogg N. G. and Owens W. B., 1999. Direct measurement of the deep circulation within the Brasil basin. Deep Sea Res. 46, 335–353.

Holm E., Aakorg A., Ballestra S., and Dalghaard H., 1986. Origin and isotopic ratios of plutonium in the Barents and Greenlan Seas. Earth Planet. Sci. lett. 79, 27–32.

Honeyman B. D. and Santschi P. H., 1989. A Brownian-pumping model for trace metal scavenging: evidence from Th isotopes. J. Mar. Res. 47, 950–995.

Hutchins D. A. and Bruland K. W., 1998. Iron-limited diatom growth andSi:N uptake ratios in a coastal upwelling regime. Nature 393, 561–564.

IOC, SCOR and IAPSO, 2010. The international thermodynamic equation of seawater—2010: calculation and use of thermodynamic properties. Intergovernmental Oceanographic

Commission, Manuals and Guides No. 56. UNESCO. http://www.teos-10.org/pubs/TEOS-10_Manual.pdf

Jahnke R. A. and Jahnke D. B., 2000. Rates of C, N, P and Si recycling and denitrification at the US Mid-Atlantic continental slope depocenter. Deep Sea Res. I 47, 1405–1428.

Jarman W. M., Hobson K. H., Sydeman W. J., Bacon C. E., and McLaren E. B., 1996. Influence of trophic position abd feeding location on contaminant levels in the Gulf of the Farallones food web revealed by stable isotope analysis. Environ. Sci. Technol. 30, 654–660.

Jean-Baptiste P. and Poisson A., 2000. Gas transfer experiment on a lake (Kerguelen Islands) using ^{3}He and SF_6. J. Geophys. Res. 105, 1177–1186.

Jean-Baptiste P., Fourre E., Metzl N., Ternon J. F., and Poisson A., 2004a. Red Sea deep water circulation and ventilation rate deduced from the ^{3}He and ^{14}C tracer fields. J. Mar. Syst. 48, 37–50.

Jean-Baptiste P., Jenkins W. J., Dutay J. C., Fourré E., Leboucher V., and Fieux M., 2004b. Temporally integrated estimate of the Indonesian throughflow using tritium. Geophys. Res. Lett. 31, DOI: 10.1029/2004GL020854.

Jeandel C., 1993. Concentration and isotopic composition of neodymium in the South Atlantic Ocean. Earth Planet. Sci. Lett. 117, 581–591.

Jeandel C., 1998. Les particules marines. Pour la Science, special issue on "Les Humeurs de l'Océan".

Jeandel C., Arsouze T., Lacan F., Têchiné P., and Dutay J.-C., 2007. Isotopic Nd compositions and concentrations of the lithogenic inputs into the ocean: a compilation, with an emphasis on the margins. Chem. Geol. 239, 156–164.

Jeffries M. O., Shaw R. A., Morris K., Veazey A. L., and Krouse H. R., 1994. Crystal structure, stable isotopes (δ^{18}O) and development of sea ice in the Ross, Amundsen and Bellinghausen seas, Antarctica. J. Geophys. Res. 99, 985–995.

Johnson K. S., Coale K. H., Berelson W. M., and Gordon R. M., 1996. On the formation of the manganese maximum in the oxygen minimum. Geochim. Cosmochim. Acta 60, 1291–1299.

Jouzel J., Alley R. B., Cuffey K. M., Dansgaard W., Grootes P., Hoffmann G., Johnsen S. J., Koster R. D., Peel D., Shuman A., Stievenard M., Stuiver M., and White J., 1997. The variability of temperature reconstruction from water isotopes in ice cores. J. Geophys. Res. 102, 26471–26487.

Karim M. F. and Mimura N. 2008. Impact of climate change and sea-level rise on cyclonic storm surge floods in Bangladesh. Global Environ. Change 18, 490–500.

Karl D., Letelier R., Tupas L., Dore J., Christian J., and Hebel D. 1997. The role of nitrogen fixation in biogeochemical cycling in the subtropical North Pacific Ocean. Nature 386, 533–538.

Karner M. B., DeLong E. F., and Karl D. M. 2001. Archaeal dominance in the mesopelagic zone of the Pacific Ocean. Nature 409, 507–510.

Key R. M., Quay P., Jones G. A., Schneider R. J., McNichol A., and Reden K. F. V., 1996. WOCE AMS Radiocarbon I: Pacific Ocean Results; P6, P16, & P17. Radiocarbon 38, 425–518.

Khatiwala S. P., Fairbanks R. G., and Houghton R. W., 1999. Freshwater sources to the coastal ocean off northeastern North America: evidence from $H_2{}^{18}O/H_2{}^{16}O$. J. Geophys. Res. 104, 18241–18255.

Könneke M., Bernhard A. E., José R., Walker C. B., Waterbury J. B., and Stahl D. A., 2005. Isolation of an autotrophic ammonia-oxidizing marine archaeon. Nature 437, 543–546.

Kovaltsov G. A., Mishev A., and Usoskin I. G., 2012. A new model of cosmogenic production of radiocarbon 14C in the atmosphere. Earth Planet. Sci. Lett. 337–338, 114–120.

Ku T. L., Kusakabe M., Measure C. I., Southon J. R., Cusimano G., Vogel J. S., Nelson D. E., and Nakaya S., 1990. Beryllium isotope distribution in the western North Atlantic: a comparison to the Pacific. Deep Sea Res. 37, 795–808.

Kusakabe M., Ku T. L., Southon J. R., Vogel J. S., Nelson D. E., Measure C. I., and Nozaki Y., 1987. Distribution of ^{10}Be and ^{9}Be in the Pacific Ocean. Earth Planet. Sci. Lett. 82, 231–240.

Labatut M., Lacan F., Pradoux C., Chmeleff J., Radic A., Murray J. W., Poitrasson F., Johansen A. M., and Thil F., 2014. Iron sources and dissolved–particulate interactions in the seawater of the Western Equatorial Pacific, iron isotope perspectives. Global Biogeochem. Cycles 28, 1044–1065.

Lacan F. and Jeandel C., 2005. Neodymium isotopes as a new tool for quantifying exchange fluxes at the continent-ocean interface. Earth Planet. Sci. Lett. 232, 245–257.

Lascaratos A., Roether W., Nittis K., and Klein B., 1999. Recent changes in deep water formation and spreading in the eastern Mediterranean Sea: a review. Prog. Oceanogr. 44, 5–36.

Ledwell J. R., Montgomety E. T., Polzin K. L., St Laurent L. C., Schmitt R. W., and Toole J. M., 2000. Evidence for enhanced mixing over rough topography in the abyssal ocean. Nature 403, 179–182.

Ledwell, J. R., Watson, A. J., and Law, C. S. (1993). Evidence for slow mixing across the pycnocline from an open-ocean tracer-release experiment. Nature, 364 701–703.

Ledwell J. R., Watson A. J., and Laws C. S., 1998. Mixing of a tracer in the pycnocline. J. Geophys. Res. 108, 21499–21529.

Lee B.-S., Bullister J. L., Murray J. W., and Sonnerup R. E., 2002. Anthropogenic chlorofluorocarbons in the Black Sea and the Sea of Marmara. Deep Sea Res. 49, 895–913.

Lee C., Wakeham S., and Arnosti C., 2004a. Particulate organic matter in the sea: the composition conundrum. AMBIO 33, 565–575.

Lee S.-Y., Huh C.-A., Su C.-C., and You C.-F., 2004b. Sedimentation in the Southern Okinawa Trough: enhanced particle scavenging and teleconnection between the Equatorial Pacific and western Pacific margins. Deep Sea Res. 51, 1769–1780.

Legeleux F. and Reyss J.-L., 1996. ^{228}Ra/^{226}Ra activity in oceanic settling particles: implications regarding the use of barium as a proxy of paleoproductivity reconstruction. Deep Sea Res. I 43, 1857–1863.

Lehahn Y., d'Ovidio F., Lévy M., and Heifetz E., 2007. Stirring of the northeast Atlantic spring bloom: a Lagrangian analysis based on multisatellite data. J. Geophys. Res. 112, DOI: 10.1029/2006JC003927.

Le Quéré C., Peters G. P., Andres R. J., Andrew R. M., Boden T., Ciais P., Friedlingstein P., Houghton R. A., Marland G., Moriarty R., and Sitch, S., 2013. Global carbon budget 2013. Earth Syst. Sci. Data Discuss. 6, 689–760.

Li Y.-H., 1991. Distribution patterns of elements in the ocean: a synthesis. Geochim. Cosmochim. Acta 55, 3224–3252.

Lindsley B. K., Ren L., Dunbar R. B., and Howe S. S., 2000. El Nino Southern Oscillation (ENSO) and decadal scale climate variability at 10°N in the Eastern Pacific from 1893 to 1994: a coral-based reconstruction from Cliperton Atoll. Paleoceanography 15, 322–335.

Little S. H., Vance D., Walker-Brown C., and Landing W. M., 2014. The oceanic mass balance of copper and zinc isotopes, investigated by analysis of their inputs, and outputs to ferromanganese oxide sediments. Geochim. Cosmochim. Acta 125, 673–693.

Liu K.-K. and Kaplan I. R., 1989. The eastern tropical Pacific as a source of ^{15}N-enriched nitrate in seawater off southern California. Limnol. Oceanogr. 34, 820–830.

Lombard F., Guidi L., and Kiørboe, T., 2013. Effect of type and concentration of ballasting particles on sinking rate of marine snow produced by the appendicularian *Oikopleura dioica*. PLoS One 8, e75676.

Lynch-Stieglitz J., Stocker T. F., Broecker W. S., and Fairbanks R. G., 1995. The influence of sea-air exchange on the isotopic composition of oceanic carbon: observation and modeling. Global Biogeochem. Cycles 9, 653–655.

Mann M. E. and Jones P. D., 2003. Global surface temperatures over the past two millennia. Geophys. Res. Lett. 30, DOI: 10.1029/2003GL017814.

Marshall J. and Speer K., 2012. Closure of the meridional overturning circulation through Southern Ocean upwelling. Nat. Geosci. 5, 171–180.

Martin J. H., Knauer G. A., Karl D. M., and Broenkow W. W., 1987. VERTEX, carbon cycling in the northeast Pacific. Deep Sea Res. 34, 267–285.

Matsumoto K., 2007. Radiocarbon-based circulation age of the world oceans. J. Geophys. Res. 112, DOI: 10.1029/2007JC004095.

Matsumoto K. and Key R. M., 2004. Natural radiocarbon distribution in the deep ocean. In *Global environmental change in the ocean and on land* (ed. M. Shiyomi, H. Kawahata, H. Koizumi, A. Tsuda, and Y. Awaya), pp. 45–58. TERRAPUB.

McCave I. N., Hall I. R., Antia A. N., Chou L., Dehairs F., Lampitt R. S., Thomsen L., van Weering T. C. E., and Wollast R., 2001. Distribution, composition and flux of particulate material over the European margin at 471–501N. Deep Sea Res. 48, 3107–3139.

McCulloch M., Trotter J., Montagna P., Falter J., Dunbar R., Freiwald A., Försterra G., Correa M. L., Maier C., Rüggeberg A., and Taviani M., 2012. Resilience of cold-water scleractinian corals to ocean acidification: boron isotopic systematics of pH and saturation state up-regulation. Geochim. Cosmochim. Acta 87, 21–34.

McManus J. F., Francois R., Gherardi J.-M., Keigwin L. D., and Brown-Leger S., 2004. Collapse and rapid resumption of Atlantic meridian circulation linked to deglacial climate changes. Nature 428, 834–837.

Medina-Bellver J. I., Marín P., Delgado A., Rodríguez-Sánchez A., Reyes E., Ramos J. L., and Marqués S., 2005. Evidence forin situcrude oil biodegradation after the *Prestige* oil spill. Appl. Microbiol. 7, 773–779.

Metzl N., Brunet C., Jabaud-Jan A., Poisson A., and Schauer B., 2006. Summer and winter air–sea CO_2 fluxes in the Southern Ocean. Deep Sea Res. I 53, 1548–1563.

Millero F. J., 1998. Solubility of Fe(III) in seawater. Earth Planet. Sci. Lett. 154, 323–329.

Milliman J. D. and Meade R. H., 1983. World-wide delivery of river sediment to the oceans. J. Geol. 91, 1–21.

Mojzsis S. J., Arrhenius G., McKeegan K. D., Harrison T. M., Nutman A. P., and Friend C. R. L., 1996. Evidence for life on Earth before 3,800 million years ago. Nature 384, 55–59.

Mollenhauer G., Schneider R. R., Muller P. J., Spiess V., and Wefer G., 2002. Glacial/interglacial variability in the Benguela upwelling system: spatial distribution and budgets of organic carbon accumulation. Global Biogeochem. Cycles 16, DOI: 10.1029/2001GB001488.

Montoya J. P. 1994. Nitrogen isotope fractionation in the modern ocean: implication for the sedimentary record. In *Carbon cycling in the glacial ocean: constraints on the ocean's role on the global change*, Vol. 117 (ed. R. Zhan), pp. 257–279. Springer-Verlag.

Moore W. S., 1996. Large groundwater inputs to coastal waters revealed by ^{226}Ra enrichments. Nature 380, 612–614.

Moy A. D., Howard W. R., Bray S. G., and Trull T. W., 2009. Reduced calcification in modern Southern Ocean planktonic foraminifera. Nat. Geosci. 2, 276–280.

Munk W. H., 1950. On the wind-driven ocean circulation. J. Meteorol. 7, 80–93.

Munk W. H., 1966. Abyssal recipes. Deep Sea Res. 13, 707–730.

Naveira Garabato A. C., Polzin K. L., King B. A., Heywood K. J., and Visbeck M., 2004. Widespread intense turbulent mixing in the Southern Ocean. Science 303, 210–210.

Neretin L. N., Pohl C., Jost G., Leipe T., and Pollehne F., 2003. Manganese cycling in the Gotland Deep, Baltic Sea. Mar. Chem. 82, 125–143.

Not F., Siano R., Kooistra W. H., Simon N., Vaulot D., and Probert I., 2012. Diversity and ecology of eukaryotic marine phytoplankton. Adv. Bot. Res. 64, 1–53.

Nozaki Y., 1984. Excess ^{227}Ac in deep ocean water. Nature 310, 486–488.

Nozaki Y., 1997. A fresh look at element distribution in the North Pacific Ocean. Eos Trans. AGU 78, 221.

Nozaki Y., Yamada M., Nakanishi T., Nagaya Y., Nakamura K., Shitashima K., and Tsbota H., 1998. The distribution of radionuclides and some trace metals in the water columns of the Japan and Bonin trenches. Oceanol. Acta 21, 469–484.

Ohmoto H., Watanabe Y., Ikemi H., Poulson S. R., and Taylor B. E., 2006. Sulphur isotope evidence for an oxic Archaean atmosphere. Nature 442, 908–911.

Okubo A., Obata H., Nozaki Y., Yamamoto Y., and Minami H., 2004. ^{230}Th in the Andaman Sea: rapid deep-sea renewal. Geophys. Res. Lett. 31, L22306.

Open University. 1989. *Ocean circulation*. Pergamon Press.

Orr J. C., Fabry V. J., Aumont O., Bopp L., Doney S. C., Feely R. A., Gnanadesikan A., Gruber N., Ishida A., Joos F., and Key R. M., 2005. Anthropogenic ocean acidification over the twentyfirst century and its impact on calcifying organisms. Nature 437, 681–686.

Orsi A. H., Johnson G. C., and Bullister J. L., 1999. Circulation, mixing and production of Antarctic Bottom Water. Prog. Oceanogr. 43, 55–109.

Östlund H. and Rooth C., 1990. The North Atlantic tritium and radiocarbon transients 1972–1983. J. Geophys. Res. 95, 20147–20165.

Palter J. B., Lozier M. S., and Barber R. T., 2005. The effect of advection on the nutrient reservoir in the North Atlanctic subtropical gyre. Nature 437, 687–692.

Papucci C., Charmasson S., Delfanti R., Gasco C., Mitchell P., and Sanchez-Cabeza J. A., 1996. Time evolution and levels of man-made radioactivity in the Mediterranean Sea. In *Radionucleides in the oceans: inputs and inventories* (ed. P. Guéguéniat, P. Germain, and H. Métivier). Les Editions de Physique.

Partensky F., Hess W. R., and Vaulot D., 1999. *Prochlorococcus*, a marine photosynthetic prokaryote of global significance. Microbiol. Mol. Biol. Rev. 63, 106–127.

Pfeifer K., Hensen C., Adler M., Wenzhöfer F., Weber B., and Schultz H. D., 2002. Modeling of subsurface calcite dissolution, including the respiration and reoxidation processes of marine sediments in the region of equatorial upwelling off Gabon. Geochim. Cosmochim. Acta 66, 4247–4259.

Pickart R. S., Hogg N. G., and Smethie W. R., 1989. Determining the strength of the deep boundary current using the chlorofluoromethane ratio. J. Phys. Oceanogr. 19, 940–951.

Piepgras D. J. and Wasserburg G. J., 1985. Strontium and neodymium isotopes in hot springs on the East Pacific Rise and Guaymas Basin. Earth Planet. Sci. Lett. 72, 341–356.

Quay P. D., Tilbrook B., and Wong C. S., 1992. Oceanic uptake of fossil fuel CO_2: carbon-13 evidence. Science 256, 74–79.

Quinby-Hunt M. S. and Turekian K. K., 1983. Distribution of elements in seawater. Eos Trans. AGU 64, 130–131.

Radic A., Lacan F., and Murray J. W., 2011. Isotopic composition of dissolved iron in the equatorial Pacific Ocean: new constraints for the oceanic iron cycle. Earth Planet. Sci. Lett. 306, 1–10.

Rea D. K., 1994. The paleoclimatic record provided by eolian deposition in the deep sea: the geologic history of wind. Rev. Geophys. 32, 159–195.

Reynolds B. C., Frank M., and O'Nions R. K., 1999. Nd- and Pb-isotope time series from Atlantic ferromanganese crusts: implications for changes in provenance and paleocirculation over the last 8 Myr. Earth Planet. Sci. Lett. 173, 381–396.

Richardson A. J., Bakun A., Hays G. C., and Gibbons M. J., 2009. The jellyfish joyride: causes, consequences and management responses to a more gelatinous future. Trends Ecol. Evol. 24, 312–322.

Ridgwell A. and Zeebe R. E., 2005. The role of the global carbonate cycle in the regulation and evolution of the Earth system. Earth Planet. Sci. Lett. 234, 299–315.

Riebesell U., Zondervan I., Rost B., Tortell P. D., Zeebe R. E., and Morel F. M., 2000. Reduced calcification of marine plankton in response to increased atmospheric CO_2. Nature 407, 364–367.

Rio M. H., Guinehut S., and Larnicol G., 2011. New CNES-CLS09 global mean dynamic topography computed from the combination of GRACE data, altimetry, and in situ measurements. J. Geophys. Res. 116, C07018.

Robert F., 2001. The origin of water on Earth. Science 293, 1056–1058.

Rost B., Riebesell U., Burkhardt S., and Sültemeyer D., 2003. Carbon acquisition of bloom-forming marine phytoplankton. Limnol. Oceanogr. 48, 55–67.

Roy-Barman M., Chen J. H., and Wasserburg G. J., 1996. ^{230}Th–^{232}Th systematics in the Central Pacific Ocean: the sources and the fates of thorium. Earth Planet. Sci. Lett. 139, 351–363.

Rutberg R. L., Hemming S. R., and Goldstein S. L., 2000. Deep water flux to the glacial Southern Ocean inferred from neodymium isotope ratios. Nature 405, 935–938.

Sabine C., Feely R. A., Gruber N., Key R. M., Lee K., Bullister J. L., Wanninkhof R., Wong C., Wallace D. W., Tilbrook B., and Millero F. J., 2004. The oceanic sink for anthropogenic CO_2. Science 305, 367–371.

Saito M. A., McIlvin M. R., Moran D. M., Goepfert T. J., DiTullio G. R., Post A. F., and Lamborg C. H., 2014. Multiple nutrient stresses at intersecting Pacific Ocean biomes detected by protein biomarkers. Science 345, 1173–1177.

Salter I., Lampitt R. S., Sanders R., Poulton A., Kemp A. E. S., Boorman B., Saw K., and Pearce R., 2007. Estimating carbon, silica and diatom export from a naturally fertilised phytoplankton bloom in the Southern Ocean using PELAGRA: a novel drifting sediment trap. Deep Sea Res. 54, 2233–2259.

Sanyal A., Hemming N. G., Hanson N. H., and Broecker W. S., 1995. Evidence for higher pH in the glacial ocean from boron isotopes in foraninifera. Nature 373, 234–236.

Sarmiento J. L. and Gruber N., 2002. Sinks for anthropogenic carbon. Phys. Today 55, 30–36.

Sarmiento J. L., Gruber N., Brzezinski M. A. J. P., and Dunne M. A., 2004. High-latitude controls of thermocline nutrients and low latitude biological productivity. Nature 247, 56–60.

Schell D. M., 2000. Declining carrying capacity in the Bering Sea: isotopic evidence from whale baleen. Limnol. Oceanogr. 45, 459–462.

Schell D. M., 2001. Carbon isotope ratio variations in Bering Sea biota: the role of anthropogenic carbon dioxide. Limnol. Oceanogr. 46, 999–1000.

Schlosser P., Bullister J. L., Fine R., Jenkins W. J., Key R., Lupton J., Roether W., and Smethie Jr. W. M. 2001. Transformation and age of water masses. In *Ocean circulation and climate* (ed. G. Siedler, J. Church, and J. Gould), pp. 431–452. Academic Press.

Schlosser P., Kromer B., Ekwurzel B., Bönisch G., McNichol A., Schneider R., von Reden K., Ostlund H. G., and Swift J. H., 1997. The first trans-Arctic ^{14}C section: comparison of the mean ages of the deep waters in the Eurasian and Canadian basins of the Arctic Ocean. Nucl. Instrum. Methods Phys. Res. B 123, 431–437.

Schmidt S., van Weering T. C. E., Reyss J.-L., and van Beek P., 2002. Seasonal deposition and reworking at the sediment-water interface on the northwestern Iberian margin. Prog. Oceanogr. 52, 331–348.

Schmitz W. J., 1995. On the interbasin-scale thermohaline circulation. Rev. Geophys. 33, 151–173.

Siedler G., Church J., and Gould J. 2001. *Ocean circulation and climate: observing and modelling the global ocean*. Academic Press

Siegel D. A., Fields E., and Buesseler K. O., 2008. A bottom-up view of the biological pump: modeling source funnels above ocean sediment traps. Deep Sea Res. 55, 108–127.

Simmonds I., 2015. Comparing and contrasting the behaviour of Arctic and Antarctic sea ice over the 35 year period 1979–2013. Ann. Glaciol. 56, 18–28.

Smethie Jr. W. M., Fine R. A., Putzka A., and Jones E. P., 2002. Tracing the flow of North Atlantic Deep Water using chlorofluorocarbon. J. Geophys. Res. 105, 14297–14323.

Smith J. N., Moran S. B., and Macdonald R. W., 2003. Shelf–basin interactions in the Arctic Ocean based on ^{210}Pb and Ra isotope tracer distributions. Deep Sea Res. I 50, 397–416.

Souza G. F., Reynolds B. C., Rickli J., Frank M., Saito M. A., Gerringa L. J. and Bourdon B., 2012. Southern Ocean control of silicon stable isotope distribution in the deep Atlantic Ocean. Global Biogeochem. Cycles 26(2) DOI: 10.1029/2011GB004141.

Srokosz M. A. and Bryden H. L., 2015. Observing the Atlantic Meridional Overturning Circulation yields a decade of inevitable surprises. Science 348, 1255575.

Stemmann L., Gorsky G., Marty J.-C., Picheral M., and Miquel J.-C., 2002. Four-year study of large-particle vertical distribution (0–1000 m) in the NW Mediterranean in relation to hydrology, phytoplankton, and vertical flux. Deep Sea Res. II 49, 2143–2162.

Stemmann S., Jackson G. A., and Ianson D., 2004. A vertical model of particle size distributions and fluxes in the midwater column that includes biological and physical processes. Part I: model formulation. Deep Sea Res. 51, 865–884.

Stewart R. H., 2004. *Introduction to physical oceanography*. Texas A & M University.

Stocker T. F., Qin D., Plattner G. K., Tignor M., Allen S. K., Boschung J., Nauels A., Xia Y., Bex B., and Midgley, P. M., 2013. Climate change 2013: the physical science basis. Intergovernmental Panel on Climate Change, Working Group I Contribution to the IPCC Fifth Assessment Report (AR5).

Stommel H. and Arons A. B., 1960. On the abyssal circulation of the world ocean. I. Stationary planetary flow patterns on a sphere. Deep Sea Res. 6, 140–154.

Stommel H., Arons A. B., and Faller A. J., 1958. Some examples of stationary planetary flow patterns in bounded basins. Tellus 10, 179–187.

Stramma L., Schmidtko S., Levin L. A., and Johnson G. C., 2010. Ocean oxygen minima expansions and their biological impacts. Deep Sea Res. 57, 587–595.

Stuiver M., Reimer P. J., and Braziunas T. F., 1998. High-precision radiocarbon age calibration for terrestrial and marine samples. Radiocarbon 40, 1127–1151.

Sudre J., Maes C., and Garçon V., 2013. On the global estimates of geostrophic and Ekman surface currents. Limnol. Oceanogr. 3, 1–20.

Suttle C. A., 2007. Marine viruses: major players in the global ecosystem. Nat. Rev. Microbiol. 5, 801–812.

Sutton J. N., Varela D. E., Brzezinski M. A., and Beucher C. P., 2013. Species-dependent silicon isotope fractionation by marine diatoms. Geochim. Cosmochim. Acta 104, 300–309.

Sweeney C., Gloor E., Jacobson A. R., Key R. M., McKinley G., Sarmiento J. L., and Wanninkhof R., 2007. Constraining global air–sea gas exchange for CO_2 with recent bomb ^{14}C measurements. Global Biogeochem. Cycles 21, GB2015.

Tachikawa K., Jeandel C., and Roy-Barman M., 1999. A new approach to Nd residence time in the ocean: the role of atmospheric inputs. Earth Planet. Sci. Lett. 170, 433–446.

Takahashi T., Broecker W. S., and Langer S., 1985. Redfield ratios based on chemical data from isopycnal surfaces. J. Geophys. Res. 90, 6907–6924.

Takahashi T., Sutherland S. C., Wanninkhof R., Sweeney C., Feely R. A., Chipman D. W., Hales B., Friederich G., Chavez F., Sabine C., and Watson A., 2009. Climatological mean and decadal change in surface ocean pCO_2, and net sea–air CO_2 flux over the global oceans. Deep Sea Res. II 56, 554–577.

Taylor S. R. and McLennan S. M., 1995. The geochemical evolution of the continental crust. Rev. Geophys. 33, 241–265.

Thiemens M. H. and Shaheen R., 2013. Mass independent isotopic composition of terrestrial and extraterrestrial materials. Treatise on Geochemistry. The Atmosphere.

Thill A., Moustier S., Garnier J.-M., Estournel C., Naudin J.-J., and Bottero J.-Y., 2001. Evolution of particle size and concentration in the Rhone River mixing zone: influence of salt flocculation. Continental Shelf Res. 21, 2127–2140.

Thomas H., Bozec Y., Elkalay K., and de Baar H. J. W., 2004. Enhanced open ocean storage of CO_2 from shelf sea pumping. Science 304, 1005–1008.

Thomson J., Green D. R. H., van Calsteren P. Richter T. O., and van Weering T. C. E., 2006. Holocene sediment deposition on a NE Atlantic transect including Feni Drift quantified by radiocarbon and ^{230}Th excess methods. Earth Planet. Sci. Lett. 242, 170–185.

Tyrell T., 1999. The relative influence of nitrogen to phosphorus on oceanic primary production. Nature 400, 525–531

Tomczak M. and Godfrey J. S., 2003. *Regional oceanography: an introduction*. Delhi: Daya Publishing House.

Touratier F. and Goyet C., 2004. Applying the new TrOCA approach to assess the distribution of anthropogenic CO_2 in the Atlantic Ocean. J. Mar. Syst. 46, 181–197.

Tsurushima N., Nojiri Y., Imai K., and Watanabe S., 2002. Seasonal variations of carbon dioxide system and nutrients in the surface mixed layer at station KNOT (44°N, 155°E) in the subarctic western North Pacific. Deep Sea Res. II 49, 5377–5394.

Turcotte D. L. and Schubert G., 2014. *Geodynamics*. Cambridge University Press.

Urban F. E., Cole J. E., and Overpeck J. T., 2000. Influence of mean climate change on climate variability from a 155-year tropical Pacific coral record. Nature 407, 989–993.

Urey H. C., 1947. The thermodynamic properties of isotopic substances. J Chem. Soc., 562–581.

Van Beek P. and Reyss J. L., 2001. ^{226}Ra in marine barite: new constraints on supported ^{226}Ra. Earth Planet. Sci. Lett. 187, 147–161.

Van Dover C. L., Grassle J. F., Fry B., Garritt R. H., and Starczak V. R., 1992. Stable isotope evidence for entry of seawage-derived organic material into a deep-sea food web. Nature 360, 153–156.

Vázquez-Rodriguez M., Touratier F., Lo Monaco C., Waugh D., Padin X. A., Bellerby R., Goyet C., Metzl N., Rios A., and Perez F., 2009. Anthropogenic carbon distributions in the Atlantic Ocean: data-based estimates from the Arctic to the Antarctic. Biogeosciences 6, 439–451.

Veizer J., Ala D., Azmy K., Bruckschen P., Buhl D., Bruhn F., Carden G. A. F., Diener A., Ebneth S., Godderis Y., Jasper T., Korte C., Pawellek F., Podlaha O. G., and Strauss H., 1999. ^{87}Sr/^{86}Sr, δ^{13}C and δ^{18}O evolution of Phanerozoic seawater. Chem. Geol. 161, 59–88.

Verdugo P., Alldredge A. L., Azam F., Kirchman D. L., Passow U., and Santschi P. H., 2004. The oceanic gel phase: a bridge in the DOM–POM continuum. Mar. Chem. 92, 67—85.

Warner M. J. and Weiss R. F., 1985. Solubilities of chlorofluorocarbons 11 and 12 in water and seawater. Deep Sea Res. I 32, 1485–1497.

Waterhouse A. F., MacKinnon J. A., Nash J. D., Alford M. H., Kunze E., Simmons H. L., Polzin K. L., St. Laurent L. C., Sun O. M., Pinkel R., and Talley, L. D., 2014. Global patterns of diapycnal mixing from measurements of the turbulent dissipation rate. J. Phys. Oceanogr. 44, 1854–1872.

Watson A. J., Ledwell J. R., Messias M. J., King B. A., Mackay N., Meredith M. P., Mills B., and Garabato A. C. N., 2013. Rapid cross-density ocean mixing at mid depths in Drake Passage measured by tracer release. Nature 501, 408–413.

Weinbauer M. G., 2004. Ecology of prokaryotic viruses. FEMS Microbiol. Rev. 28, 127–181.

Weiss R. F., Ostlund H. G., and Craig H., 1979. Geochemical studies of the Weddell Sea. Deep Sea Res. 26, 1093–1120.

Wepperning R., Schlosser P., Khatiwala S., and Fairbanks R. G., 1996. Isotope data from Ice Station Weddell: implications for deep water formation in the Weddell Sea. J. Geophys. Res. 101, 25723–25739.

Widory D. and Javoy M., 2003. The carbon isotope composition of atmospheric CO_2 in Paris. Earth Planet. Sci. Lett. 215, 289–298.

Witter A. E., Hutchins D. A., Butler A., and Luther III G. W., 2000. Determination of conditional stability constants and kinetic constants for strong model Fe-binding ligands in seawater. Mar. Chem. 69, 1–17.

Yamaguchi A., Watanabe Y., Ishida H., Harimoto T., Furusawa K., Suzuki S., Ishizaka J., Ikeda T., and Mac Takahashi M., 2002. Structure and size distribution of plankton communities down to the greater depths in the western North Pacific Ocean. Deep Sea Res. II 49, 5513–5529.

Yemenicioglu S., Erdogan S., and Tugrul S., 2006. Distribution of dissolved forms of iron and manganese in the Black Sea. Deep Sea Res. II 53, 1842–1855.

Young J. R., Davis S. A., Brown P. R., and Mann S., 1999. Coccolith ultrastructure and biomineralization. J. Struct. Biol. 126, 195–215.

Index

A

Acidification 244, 261–263, 294
Actinium 86, 144, 328
Activity 134–135, 143–146, 159
Advection 184–186, 197–198, 204–205
Alkalinity 72, 238–241, 252, 260, 296
Ammonium (ion) 214–215
Amorphous silica 59, 208, 225, 268, 292
Anoxia 76, 293, 295
Antarctic Bottom Water (AABW) 9–12, 55, 303, 320–323, 345
Antarctic Circumpolar Current 14, 205, 322
Antarctic Intermediate Water (AAIW) 9–12, 55, 140, 226
Anthropogenic perturbation 345, 349, 361
Arabian Sea 76–77, 233
Aragonite 73–74, 88, 145, 263
Arctic Ocean 18, 42, 44–45, 204, 314–328
Artificial fertilization 179, 205
Atlantic Ocean 3–4, 8–10, 13–14, 56, 89, 260, 264, 289, 303, 315, 319, 327, 328, 340, 346
Autotrophic 58, 207–208, 215, 268

B

Bacteria 53, 58–59, 65, 74, 76, 104, 110, 126–128, 206–207, 210–217, 225, 233, 293, 333–336
Ballast 276
Baltic Sea 159, 275
Barents Sea 145, 161, 300
Barite 145, 280, 300
Benthic chamber 295–296
Benthos 206
Beryllium-10 150
Biogenic 280
Biogeochemical cycles 49, 50–60
Biological activity 53, 59–62, 206, 224–225, 268, 276, 347
Bioturbation 152, 201–203, 292–293, 295, 297, 301
Black Sea 76, 78, 88–89, 233, 295
Bloom 214, 225, 231, 356–357
Boron 72, 83, 111–112, 117–118
Boundary exchange 289–290
Boundary scavenging 287–289
Brunt–Väisälä frequency 192

C

Calcite 73–74, 88, 103–104, 252
Calcium carbonate 73–74, 268, 276
Carbon 56–59, 70–75, 83, 278
Carbon cycle 206, 235, 237, 241, 246, 260
Carbon dioxide 57–59, 62–64, 70–72, 241–243, 253, 293, 351–353
Carbon-14 147–154, 159–161, 173–175, 179–181, 217–218, 246–256, 279, 300–307, 314–316, 323, 328, 345
Carbonate counter-pump 241
Chemotrophic 212–213
chlorofluorocarbons (CFCs) 62, 64, 169–170, 180, 310–316, 322–323, 326–327
chlorophyll 179–180, 205, 207, 213–214, 221–224, 232
Clay 111–112, 266, 291
Climate change 233, 331, 336, 351, 356
Climate system 331
Coccolithophorids 208, 211–212, 355–356
Compensation depth of carbonate 73–74, 280, 291
Complexation 81, 90
Conservative tracer 9, 13, 66, 68, 102, 117, 196
Convection 7–8, 41, 169, 308–314
Coral 99, 102, 126, 149, 160–61, 173, 263, 348
Coriolis force 16–20, 26–28, 35, 38, 41, 43, 309–310, 312, 316
Curl 22–25, 31–32, 34, 37–38, 223

D

Dating of sediments 297–298, 301
Decay chains 135, 143–146, 170–171
Decay constant 130, 132, 165
Denitrification 77, 110, 229, 294, 351
Density 2, 5–9, 18, 22, 45, 192, 275–277
Density anomaly 5–6, 9
Deuterium 103
Diagenesis 280, 292–295
Diapycnal 8, 323
Diatoms 59, 90, 112, 208, 211–212, 217, 225, 229, 233, 273, 291–292, 320, 357
Dissolved silica 56–59, 113, 225–226
Dole effect 97–98
Downwelling 21–22, 24, 45, 258
Dynamic height or dynamic topography 22, 26–28, 30, 41, 45, 47

E

Eddies 36, 38–39, 155, 184, 192–193, 223, 233
Eddy diffusion 191–194, 197–198, 200, 202, 205, 323, 328–329
Ekman drift 23–24, 34, 36, 42
Ekman layer 23–25, 34, 36, 40
Ekman pumping 21–25, 34, 37, 221–223
El niño 223, 348–350, 356–357
Estuary 51–52, 78, 117–118
Eutrophication 229, 357
Exported production 214–215, 233, 278

F

Fecal pellet 81, 109, 128, 271, 273, 280
Fermentation 293
Flux 14, 61, 163–166, 183–194, 237
Food chain 60, 107–110, 210, 278
Foraminifer 103, 112, 159, 209–211, 216, 271, 297, 339–347, 361
Fractionation (isotopic) 93–114, 120–122
f-ratio 217, 219, 233

G

Gas 52, 62–64, 245–251, 336, 344, 351
Geoid 21, 27
Geostrophic currents 26–31, 45–47
Grazing 179–180, 210, 214, 217, 276
Green tide 229–230
Greenhouse effect 295, 336–338, 345, 348, 351–353
Greenland 14, 101, 139–141, 149, 169, 333, 342–343, 347–348, 354
Greenland Sea 303, 305, 311–312, 314, 323
Gulf Stream 13–15, 18, 30–31, 37–39, 42–43, 142, 195, 303, 313, 340, 355
Gyre 5, 13, 18, 21–23, 30–42, 127, 204, 216–217, 221–223, 233, 254–256, 268, 278

H

Half-life 131–132, 134, 138, 143, 145–146
Helium 83, 129, 138, 142–143, 147, 161, 172–173, 331
Heterotrophic 58–59, 208, 210, 212, 234, 239, 278
HNLC (area) 179, 223–225, 253, 259
Holocene 345, 361
Hydrocarbon 126, 213, 267
Hydrogen isotopes 101, 103, 110, 332, 360
Hydrothermal 114, 137, 139, 143, 172–173, 207–208, 212–213, 333

I

Ice 3, 14, 18, 41–43, 95–96, 99–105, 118, 125, 149–150, 300–301, 303, 320–322, 336–347, 353–356, 360–361
Iceberg 292, 345
Indian Ocean 10, 13, 140, 181, 227, 272, 304–305, 324
Indium 85, 87
Interstitial fluid 201–202, 292–294
Iron 52–54, 79, 81–84, 90, 179–180, 213, 217, 223–225, 233, 253, 259, 293–294, 344, 347, 359
Iron isotopes 112–115, 128, 205
Isopycnal surface 5–8, 29, 38–40, 46, 68–70, 200, 256, 324, 327
Isotope exchange 96–97, 103, 137, 140, 265, 290
Isotope ratio 92–93, 171
Isotopes 91–159

K

Kerguelen Islands 224
Kinetics 164–165, 168, 175–176, 179–181, 235, 279
Kuroshio 13–14, 47, 155, 289

L

Labile 74, 214, 267, 269, 278
Labrador Sea 12, 102, 140, 303, 305, 312, 314, 323
Last Glacial Maximum 149, 341, 346, 359, 361
Lead 51–52, 82, 138, 141–147, 288
Limitation of the biological activity 59, 68, 213–214, 217, 223–229, 233, 336, 359
Lithogenic 61, 114, 138–140, 144, 151, 266, 268–269, 280, 291–292
Little ice age 350, 353
Lysocline 73–74, 240, 280, 295, 361

M

Manganese 78–79, 81
Marine particles 53, 61, 79, 90, 139–152, 167–168, 176–178, 200, 259, 265–301
Marine snow 215, 271, 273, 275–276
Marmara Sea 180
Medieval warm period 347–348, 350
Mediterranean water 11, 65
Mesoscale 193, 200, 223
Metagenomic 215
Metaproteomic 217
Methane 213, 293, 295, 351
Mixed layer 7–8, 20, 41, 191, 199, 213, 220–223, 245–251
Mixing 6–13, 38, 42–43, 52, 65–66, 69, 115–120, 314–315, 323–324
Modal water 38–39, 225–226
Molecular diffusion 95, 106, 186–191, 245–247

N

Nekton 206
Neodymium 138–141, 160, 289–290, 339–340, 359
Nepheloid layer 272–273
Net community production 219–221, 231
New production 214–215, 216–219, 221
Nitrate 52, 58–59, 77, 108–110, 121–123, 204, 213–219, 228–230

Nitrogen fixation 108–109, 127, 207, 214–217, 224–225, 228–229
North Atlantic Deep Water (NADW) 9–12, 42, 55, 258, 260, 302–305
North Atlantic oscillation (NAO) 312
Norwegian Sea 41–42, 140, 305, 311, 314
Nuclear tests 148, 151–154, 161, 167, 174, 254
Nutrient 57–61, 67–68, 78–80, 213–217, 223–229

O

Ocean color 221–223, 233
Oil spill 126
Organic matter (dissolved) 74, 180–181, 214–215, 300
Organic matter (particulate) 65, 74, 212–215, 268, 278, 300, 306
Oxidation and reduction 53, 58, 74–81, 176–177, 292–295, 333–335
Oxygen 40, 55–59, 63–70

P

Pacific Ocean 4, 10–14, 40–42, 56–57, 141, 204, 216, 254, 279, 281–283, 286–287, 289–290, 306
pe 76–79
pH 70–72, 76–79, 82, 111–112, 253, 294, 356
Photic layer 6–7, 58, 213, 215, 217
Photosynthesis 56–59, 75–76, 97–98, 103, 106–107, 206–207, 214, 221–222, 239–241, 263, 333
Phytoplankton 58–59, 74, 106, 207–208, 210, 212–217, 222–223, 356–357
Pigment 207, 222, 271
Piston velocity 188, 191, 203, 220, 246–247
Plankton 58–59, 74, 109, 206–217, 222–223, 229–231, 270, 356–357
Plutonium 151–152, 161, 167
POC 74, 227, 278–279, 287, 294, 300, 308
Porosity 201–202, 292, 295
Potential temperature 4, 6, 9–12, 54, 204
Primary production 214–223, 274, 295–296, 357
Prochlorococcus 207–208, 215, 217, 336
Production, *see* exported production, net community production, new production, primary production, regenerated production
Protactinium 132, 144–147, 202, 288–289, 317, 345–347
Proterozoic 358–359
Proxy 331
Pump (CO_2) 214–215, 241–243, 244, 251, 259
Pycnocline 8

R

Radioactive disequilibrium 134–135, 145–147, 170, 281–284
Radioactivity 129–159
Radiogenic isotopes 136–143
Radiolarian 59, 209, 211, 216, 291–292
Radium 130, 144–145, 195–199, 204, 300
Radon 144–145, 147, 170–171
Rayleigh distillation 100, 121–125
Recirculation 38, 312–314, 317
Red Sea 172–175, 247, 272
Redox 75–78, 86, 88, 333
Regenerated production 214–215, 218–220
Remineralization 59–61, 65–69, 72, 75–76, 107, 214, 229, 239–241, 274, 278–280, 292, 294–295
Reservoir age 177–179, 306, 345
Residence time 51, 53–54, 61, 165–166, 177, 179
Respiration: *see* Remineralization
Revelle factor 244, 249, 251, 261
Ross Sea 269, 323

S

Salinity 2–7, 9–12, 41–42, 45, 50–54, 102, 117–118, 303, 320–321, 326, 348–349, 356
Sargasso Sea 284–285
Saturation horizon 73
Scavenging 61, 167–168, 281–289, 317
Sea ice 3, 41–42, 102, 125, 150–152, 300, 303, 320–321, 347, 354–356
SeaWiFS 222, 224, 232
Secular equilibrium 133–135, 143–146, 160
Sediment 51–53, 60–62, 73, 77–79, 110, 114, 138, 143–147, 201–203, 212, 291–298
Sediment trap 221, 270–274, 278, 284–285
Sedimentation rate 135, 150, 203, 291–293, 297–298, 319
Shadow zone 39–40
Solubility (of gas) 62–65, 70, 191, 227, 236, 241
Solubility product 73
Source minus sink 163
Southern Ocean 10, 18, 29, 36, 112–113, 223–226, 237, 289, 292, 303–305, 320–324, 347, 355
Spallation 147, 151
Spring bloom 214, 357
Stagnant film 189–191, 203, 220, 245–247
Stokes law 275–277
Stratification 6–8, 42, 44, 192, 277, 347, 356–357
Strontium 59, 87–88, 137–139, 159, 297, 338–339, 359
Subduction (isopycnal surface) 39
Suess (effect) 104, 108
Sulfate 53, 58–59, 88, 110, 294, 333–335
Sulfide 53, 110, 212, 230, 294, 334–335, 359
Sulfur hexafluoride 180, 199–201, 203, 327
Sulfur isotopes 94, 110–111, 127, 335–336

T
Terrigenous 266
Thermocline 2, 7–8, 21–22, 26, 28–31, 36–41, 68–69, 175, 199–201, 221–226, 254–257, 259–260, 323–324
Thermohaline circulation 42–43, 60–61, 150, 302–330, 346–347, 355, 359
Thorium 143–147, 280–287, 298, 301, 318–320
Time constant 164–165, 167–170, 177, 190, 248–251
Trace metals 78–82, 87–88, 268–269, 289–290, 335–336
Tracer 9, 13, 49, 54, 55, 65–70, 92–93
Trade winds 3–4, 18, 21, 23, 40–41, 43–44, 222–223, 339–340, 348–349
Transport 20–21, 23, 26, 34–37, 46
Trichodesmium 108, 207–208, 216, 225, 228, 233
Tritium 143, 151–154, 161, 179, 308, 328–330
Turbulence 178, 184, 190–201, 302

U
Upwelling 21–26, 32, 41–42, 45, 47, 58, 213, 215, 222–223, 225, 291–292, 310–314, 323–324
Uranium 79, 143–147, 160, 280, 333

V
Ventilation 38–39, 172–175, 255–257, 308–309, 311–312, 314–316, 319–320, 328–329, 345–346
Vorticity 31–34, 39, 313–314

W
Water mass 5–6, 9–13, 38–39, 55
Weddell Sea 42, 118, 320–323
Western boundary current 13, 34–37, 48, 310–318, 327
Wind stress 18–21

Z
Zooplankton 58–59, 74, 108–109, 206, 209, 211–217, 229–230, 271–274, 356–357